Impact of Physical Properties of Silica on the Reaction Kinetics of Silica Supported Metallocenes and Polyethylene Morphology

Muhammad Ahsan Bashir

N°d'ordre NNT : **2016 LYSE1253**

THESE de DOCTORAT DE L'UNIVERSITE DE LYON
opérée au sein de
l'Université Claude Bernard Lyon 1

Ecole Doctorale N° ED206
(Chimie de Lyon)

Spécialité de doctorat : **Polyolefins Reaction Engineering**
Discipline : (Chemical Engineering)

Soutenue publiquement le 29/11/2016, par :

Muhammad Ahsan Bashir

Impact of Physical Properties of Silica Supported Metallocenes on their Ethylene Polymerisation Kinetics and Polyethylene Properties

Devant le jury composé de :

Fongarland, Pascal
Directeur/ Laboratoire de Génie des Procédés Catalytiques (Président)

Paredes Martínez, Beatriz
Professor/Universidad Rey Juan Carlos, Spain (Rapporteur)

Ribeiro, Maria do Rosario Gomes
Professor/ Instituto Superior Técnico, Universidade de Lisboa (Rapporteur)

Severn, John
Principal Scientist, DSM, Geleen, The Netherlands (Examinateur)

Mckenna, Timothy
Directeur/ Laboratory of Chemistry, Catalysis, Polymers and Process (Directeur de these)

UNIVERSITE CLAUDE BERNARD - LYON 1

Président de l'Université	**M. le Professeur Frédéric FLEURY**
Président du Conseil Académique	M. le Professeur Hamda BEN HADID
Vice-président du Conseil d'Administration	M. le Professeur Didier REVEL
Vice-président du Conseil Formation et Vie Universitaire	M. le Professeur Philippe CHEVALIER
Vice-président de la Commission Recherche	M. Fabrice VALLÉE
Directrice Générale des Services	Mme Dominique MARCHAND

COMPOSANTES SANTE

Faculté de Médecine Lyon Est – Claude Bernard	Directeur : M. le Professeur G.RODE
Faculté de Médecine et de Maïeutique Lyon Sud – Charles Mérieux	Directeur : Mme la Professeure C. BURILLON
Faculté d'Odontologie	Directeur : M. le Professeur D. BOURGEOIS
Institut des Sciences Pharmaceutiques et Biologiques	Directeur : Mme la Professeure C. VINCIGUERRA
Institut des Sciences et Techniques de la Réadaptation	Directeur : M. X. PERROT
Département de formation et Centre de Recherche en Biologie Humaine	Directeur : Mme la Professeure A-M. SCHOTT

COMPOSANTES ET DEPARTEMENTS DE SCIENCES ET TECHNOLOGIE

Faculté des Sciences et Technologies	Directeur : M. F. DE MARCHI
Département Biologie	Directeur : M. le Professeur F. THEVENARD
Département Chimie Biochimie	Directeur : Mme C. FELIX
Département GEP	Directeur : M. Hassan HAMMOURI
Département Informatique	Directeur : M. le Professeur S. AKKOUCHE
Département Mathématiques	Directeur : M. le Professeur G. TOMANOV
Département Mécanique	Directeur : M. le Professeur H. BEN HADID
Département Physique	Directeur : M. le Professeur J-C PLENET
UFR Sciences et Techniques des Activités Physiques et Sportives	Directeur : M. Y.VANPOULLE
Observatoire des Sciences de l'Univers de Lyon	Directeur : M. B. GUIDERDONI
Polytech Lyon	Directeur : M. le Professeur E.PERRIN
Ecole Supérieure de Chimie Physique Electronique	Directeur : M. G. PIGNAULT
Institut Universitaire de Technologie de Lyon 1	Directeur : M. le Professeur C. VITON
Ecole Supérieure du Professorat et de l'Education	Directeur : M. le Professeur A. MOUGNIOTTE
Institut de Science Financière et d'Assurances	Directeur : M. N. LEBOISNE

Abstract

Polyolefins account for more than half of the world's plastic production and about 80% of these polyolefins are commercially produced with heterogeneous olefin polymerization catalysts such as Phillips, Ziegler-Natta and metallocenes. Trouble-free plant operation due to low fouling of the reactor or other plant equipment, relatively stable catalytic activity, good polymer morphology and high polymer bulk densities can be achieved by employing heterogeneous olefin polymerization catalysts. On the other hand, heterogenization of the olefin polymerization catalysts lead to drastic reduction in their activities and broadening of the polymer molar mass distribution which is undesirable in some cases because it can influence the processability and mechanical properties of the polyolefin grade. Various explanations have been proposed in the open literature to explain these effects of catalyst immobilization which mainly include existence of diffusion resistance to (co)-monomer(s) transport at the active sites during polymerization and the change of the active site(s) behavior due to immobilization leading to multiple site types on the final supported catalyst. Nevertheless, both of these explanations have a connection with the physical properties (e.g., particle size, surface area, pore volume, pore diameter etc.) of the support because the support can impact the nature of the final active species formed on it, dispersion of the active species throughout the support particles and, last but not the least, the intraparticle diffusion of (co)-monomer(s) during polymerization. Metallocenes are considered as single-site catalysts and any changes in the nature of the active site(s) upon their immobilization on a support or during the course of polymerization due to mass transfer resistance can be detected from the broadening of polyolefin molar mass distribution.

Therefore, the present work is an attempt to study the effects of physical properties of silica supported metallocenes on their ethylene polymerization kinetics as well as on the morphology of the produced polyethylene. For this purpose, the surface chemistry of the used commercial silica supports was fixed by dehyroxylating all of them at 600 °C, whereas, the final metal loadings of the supported catalysts were nearly kept constant by preparing them under identical conditions. Furthermore, slurry and gas phase polymerization protocols along with the used aluminum alkyl scavenger (which can also induce chemical effects on the catalytic behavior of supported metallocenes) were also fixed by testing different polymerization protocols and scavengers. Such systematic study has allowed us to attribute the observed differences in the reaction kinetics of the supported metallocenes, explicitly, to the differences in the physical parameters of the silica

supports and, consequently, to the existence of diffusion resistance to (co)-monomer(s) transport at the active site(s) during the course of polymerization.

Résumé

Les polyolefins représentent plus de la moitié de la production mondiale de plastiques et 80% de ces polymères sont produits avec des catalyseurs hétérogènes de type Phillips, Ziegler-Natta et métallocènes. En effet, un bon fonctionnement des unités du fait d'un faible encrassement du réacteur ou des autres équipements de l'unité, une activité stable, une bonne morphologie particulaire des polymères et un une densité apparente élevée sont obtenus en utilisant des catalyseurs hétérogènes. D'un autre côté l'hétérogénéisation d'un catalyseur s'accompagne d'une diminution de l'activité et d'un élargissement de la distribution de masses molaires qui est parfois non désiré car cela peut influencer l'aptitude à la transformation et les propriétés mécaniques des polyoléfines. Plusieurs explications ont été avancées dans la littérature afin d'expliquer l'effet de l'immobilisation d'un catalyseur ce qui inclut la résistance diffusionnelle au transport du (des) (co)-monomère(s) vers le site actif et la modification du comportement du catalyseur conduisant à plusieurs espèces actives. Néanmoins l'ensemble de ces explications est en connexion avec les propriétés physiques du support (tailles des particules, surface spécifique, volume poreux, diamètre des pores…) car ce dernier peut en effet impacter la nature des espèces actives ainsi que leur dispersion et la diffusion des monomères. Les catalyseurs métallocène sont considérés comme mono-site et tout changement dans la nature du site actif au cours de son immobilisation et toute résistance au transfert de matière peuvent être détectés par un élargissement de la distribution des masses molaires.

Le présent travail a pour objet d'étudier les effets des propriétés physiques des catalyseurs métallocènes supportés sur silice concernant la cinétique de polymérisation et les caractéristiques des polymères produits. Pour cela le traitement thermique de la silice a été fixé à 600°C afin de contrôler son état de surface tandis que la quantité de catalyseur supporté a été gardée autant que possible constante. De plus les protocoles de polymérisation en phases suspension et gaz ont été fixés après avoir évalué différentes conditions de polymérisation et différents composés alkylaluminium. Cette étude systématique a permis d'attribuer les différences observées en termes de cinétique de réaction des catalyseurs métallocènes à la différence des paramètres physiques des silices utilisées comme support et par conséquent à la résistance diffusionnelle au transport du (des) (co)-monomère(s) au(x) site(s) actif(s) durant la polymérisation.

Acknowledgements

The current PhD thesis is a combined effort from me and several people in my personal and professional life. At first, the person to whom I would like to say Thanks and give credit is Dr. Timothy McKenna who considered me suitable for this project and provided the opportunity to learn from him. While his professional guidance will serve as a roadmap for my career, his kind and flexible nature encouraged me to excel and work with an open mind. This Phd work was co-catalyzed by Dr. Christophe Boisson to whom I owe a huge Thanks. It has been a great experience to be in long meetings with him and benefit from his expert opinion in almost all the chemistry related issues of this work. Dr. Vincent Monteil, who read consistently and thoroughly all my quarterly project reports besides providing his valuable comments on the thesis, also deserves a big Thanks from me and I really appreciate his contribution in this work.

In addition, I am extremely Thankful to Dr. Vasileios Kanellopoulos and Dr. Mohammad Al-Haj Ali from Borealis Polymers Oy, Finland, for aiding me in getting this opportunity and for their guidance in the modelling work performed within the scope of this project.

I would also like to pay my Regards and Special Thanks to the Polyolefins consortium of Dutch Polymer Institute (DPI) and more specifically to Dr. John Severn, Dr. John Walzer, Dr. Nick Friederichs, Dr. Jeff Brinen and Dr. Michael Bartke whose input in this Phd work greatly helped in shaping it and can be considered nothing less than an invaluable expert opinion. Gratefully, I would also like to acknowledge the financial help from DPI for this work.

During more than 500 experiments conducted in this thesis, most of the help came from Dr. Sébastian Norsic along with Pierre Yves Dugas, Dr. Olivier Boyron, Dr. Kai Szeto, Dr. Cherif Larabi, Dr. Nicolas Merle, Dr. Dominique Sauter and Nesrine Cherni. I would like to say Thanks to these people also for their kind help during different experiments. This acknowledgement may not be complete without mentioning the kind help of Manel Taam who has been aiding all the important (but the most irritating) HT-SEC, DSC and NMR analysis of this work in a highly professional way. I am really Thankful for her help and guidance not in laboratory but normal life matters also where I felt difficulty with my ‘niveau de langue française’.

The company of Manel Taam, Dr. Ana Carolina, Dr. Solmaz Ariyafar and Aaron Jose Cancelas Sanz in the room we used to share in C2P2 is unforgettable in any sense and I would like to say Merci to them for their support and company during this work. In addition, I am also thankful to Dominique Sauter (especially, for the time he spent in cutting silica samples for SEM-EDX), Islem Belaid, Fabiana, Ali Rida, and everyone else in the laboratory for their support and companionship.

Finally, I am immensely Thankful to my Parents, Wife, Brothers, Sisters and Friends (who make my world) from the depth of my heart for their encouragement in this thesis as well as throughout my life. For the rest of my personal and professional life, I will need the same from them. Without them it may have not been that easy.

This research forms part of the research programme of the Dutch Polymer Institute (DPI), project#753.

Dedicated to my Parents, Wife and Daughters

Table of Contents

Chapter 1 : Literature Review

1. Introduction to Polyolefins 1
1.1. Polyolefin Production Processes 3
1.1.1. High Pressure Process (Radical Polymerization) 3
1.1.2. Low pressure processes (Catalytic Polymerization) 4
2. Olefin Polymerization Catalysts 6
2.1. Ziegler-Natta catalysts 7
2.2. Phillips or Chromium Catalyst 8
2.3. Metallocene Catalysts 9
3. Heterogeneous Catalysts 14
3.1. Synthesis Methods for Heterogeneous Metallocenes 14
3.1.1. Physical adsorption supporting methods 15
3.1.2. Chemical Tethering Methods 21
4. Types of Co-catalysts 22
4.1. Aluminum Alkyls (AlR_3) 23
4.2. Aluminoxane 23
4.3. Boranes & Borates 27
4.4. Activating Supports 28
5. Types of Supports for Heterogeneous Metallocenes 29
5.1. Magnesium Dichloride 31
5.2. Clays 32
5.3. Zeolites and Mesoporous Materials 33
5.4. γ-Alumina 33
5.5. Silica 34
5.5.1. Surface Chemistry and Thermal Treatment of Silica 35
5.5.2. Role of Surface Chemistry in Supporting Metallocene or Co-catalyst 37
5.5.3. Impact of Physical Properties of Silica 39
5.6. Other Supports 65
6. Mechanism of Olefin Polymerization with Fundamental Model 66
7. Polymer Particle Growth 70
7.1. Solid Core Model 70
7.2. Polymer Flow Model (PFM) 71
7.3. MultiGrain Model (MGM) 72
8. Conclusion 73
9. References 75
Appendix 1 89

Chapter 2: Effect of Silica Dehydroxylation Temperature on the Grafting of MAO and Metallocene Activity

1. Introduction ---- 94
2. Experimental Section ---- 97
2.1. Materials ---- 97
2.2. Drying of MAO ---- 97
2.3. Catalyst Synthesis ---- 97
2.4. Polymerization Procedure ---- 98
2.5. Pressure Curve Fitting and Conversion into Ethylene Mass ---- 100
2.6. Silica, SMAO and Catalyst Characterization ---- 101
2.7. Polymer Characterization ---- 102
3. Results and Discussion ---- 103
3.1. DRIFT Analysis of Silica, Dried MAO, SMAO and Supported Metallocene Catalysts ---- 104
3.2. Solid State NMR Analysis of Dried MAO and SMAO samples ---- 106
3.3. Catalyst Evaluation ---- 115
3.4. Crystallinity and Molecular Masses of PE Samples ---- 120
4. Conclusion ---- 121
5. References ---- 122
Appendix 1 ---- 127

Chapter 3: The Effect of Polymerization Protocol on Catalyst Leaching in Slurry Phase Ethylene Polymerization

1. Introduction 133
2. Experimental Section 137
2.1. Materials 137
2.2. Supported Catalyst Synthesis 137
2.3. Polymerization Protocols 137
2.3.1. Method one for slurry polymerization (MSP-1) 138
2.3.2. Method two for slurry polymerization (MSP-2) 138
2.4. Catalyst Characterization 138
2.5. Polymer Characterization 139
3. Results and Discussion 140
3.1. Effect of pre-contact between TEA and supported catalyst in slurry polymerization 140
3.2. Effect of pre-contact between TIBA and supported catalyst in slurry polymerization 151
3.3. Effect of TOA concentration on the activity of supported catalyst 162
3.4. Comparison of the effect of different alkyl aluminums on the reaction kinetics of silica supported $(n\text{-BuCp})_2ZrCl_2$/MAO catalyst and the polymer PSD 165

3.5. Impact of Butylated Hydroxytoluene (BHT-H) on the reaction kinetics of silica supported (n-BuCp)$_2$ZrCl$_2$/MAO catalyst 169
4. Conclusion 177
5. References 179
Appendix 1 182

Chapter 4: The Effect of Particle Size and Porosity of Silica Supported Metallocene/MAO Catalysts on their Slurry Phase Ethylene Polymerization Kinetics and Polymer Properties

1. Introduction 184
2. Experimental section 186
2.1. Materials 186
2.2. Silica Sieving 186
2.3. Catalyst Synthesis Procedure 187
2.4. Polymerization Reactor 187
2.4.1. Method one for Slurry Polymerization (MSP-1) 188
2.4.2. Method two for Slurry Polymerization (MSP-2) 188
2.5. Silica and Catalysts Characterization 188
2.6. Polymer Characterization 189
3. Results & Discussion 191
3.1. Pore structure of silica supports and catalyst particles 191
3.1. Slurry Phase Ethylene Homopolymerisations and Ethylene/1-Hexene Copolymerisations with Reference Full Batch Catalysts 200
3.2. Effect of Silica Support Particle Size in Slurry Phase Ethylene Homopolymerisations and Ethylene/1-Hexene Copolymerisation 211
3.2.1. Effect of Particle Size studied with Grace 948 Silica Based Catalysts 211
3.2.2. Effect of Particle Size Studied with PQMS 1732 Silica Based Catalysts 220
3.2.3. Effect of Particle Studied with PQMS 3040 Silica Based Catalysts 234
3.3. Slurry Phase Ethylene Polymerizations with Silica Supported THI/MAO catalyst ... 244
3.4. Conclusion from Particle Size Study 252
3.5. Effect of Pore Volume, Pore Diameter and Surface Area of the Silica Supports on the Catalytic Activity, Molecular Properties and Physical Properties of Polyethylene 254
3.6. Conclusion from the Effect of Porosity Study 266
4. References 267
Appendix-1 270

Chapter 5: The Effect of Particle Size and Porosity of Silica Supported Metallocene/MAO Catalysts on their Gas Phase Ethylene Polymerization Kinetics and Polymer Properties

1. Introduction **271**
2. Experimental Section **272**
2.1. Polymerization Protocol 272
3. Results and Discussion **273**
3.1. Gas Phase Ethylene Homopolymerisations and Ethylene/1-Hexene Copolymerisations with Reference Catalysts Supported on Full Batch of Silica 273
3.2. Effect of Silica Support Particle Size in Gas Phase Ethylene Homopolymerisations and Ethylene/1-Hexene Copolymerization 282
3.2.1. Effect of Silica Particle Size Studied with Grace 948 Based Catalysts 282
3.2.2. Effect of Silica Particle Size Studied with PQMS 3040 Based Catalysts 288
3.2.3. Effect of Silica Particle Size Studied with PQMS 1732 Based Catalysts 292
3.2.4. Effect of Silica Support Particle Size Studied with THI/MAO and $(n\text{-}BuCp)_2ZrCl_2$/MAO supported Catalysts 298
3.3 Conclusion from the Silica Support Particle Size Study in Gas Phase Polymerizations .. **322**
3.4. Effect of Porosity of Silica Supported Metallocene/MAO Catalysts on their Activity, Molecular and Physical Properties of Polyethylene 324
3.5. Conclusions from the Effect of Porosity of the Supported Metallocene/MAO Catalysts on their Activity, Molecular and Physical Properties of Polyethylene **333**
4. References **335**
Appendix 1 ..... **337**
Conclusion & Perspectives **341**

CHAPTER 1

LITERATURE REVIEW

Contents

1. Introduction to Polyolefins 1
1.1. Polyolefin Production Processes 3
1.1.1. High Pressure Process (Radical Polymerization) 3
1.1.2. Low pressure processes (Catalytic Polymerization) 4
2. Olefin Polymerization Catalysts 6
2.1. Ziegler-Natta catalysts 7
2.2. Phillips or Chromium Catalyst 8
2.3. Metallocene Catalysts 9
3. Heterogeneous Catalysts 14
3.1. Synthesis Methods for Heterogeneous Metallocenes 14
3.1.1. Physical adsorption supporting methods 15
3.1.2. Chemical Tethering Methods 21
4. Types of Co-catalysts 22
4.1. Aluminum Alkyls (AlR_3) 23
4.2. Aluminoxane 23
4.3. Boranes & Borates 27
4.4. Activating Supports 28
5. Types of Supports for Heterogeneous Metallocenes 29
5.1. Magnesium Dichloride 31
5.2. Clays 32
5.3. Zeolites and Mesoporous Materials 33
5.4. γ-Alumina 33
5.5. Silica 34
5.5.1. Surface Chemistry and Thermal Treatment of Silica 35
5.5.2. Role of Surface Chemistry in Supporting Metallocene or Co-catalyst 37
5.5.3. Impact of Physical Properties of Silica 39
5.6. Other Supports 65
6. Mechanism of Olefin Polymerization with Fundamental Model 66
7. Polymer Particle Growth 70
7.1. Solid Core Model 70
7.2. Polymer Flow Model (PFM) 71
7.3. MultiGrain Model (MGM) 72
8. Conclusion 73
9. References 75
APPENDIX 1 89

1. Introduction to Polyolefins

Polyolefins is a generic name given to the homopolymers of lighter olefins like ethylene and propylene and their copolymers with higher α-olefins (e.g., 1-butene, 1-hexene, 1-octene etc). Polyethylene (PE) and polypropylene (PP) are the most well-known polyolefins which is a generic term that include not just homopolymers of ethylene or of propylene, but also linear low density polyethylene, low density polyethylene, high impact polypropylene etc. These polymers are composed only of carbon and hydrogen atoms which can have different arrangements around the backbone. Despite their apparently simple structure, properties of these materials can be tailored in such a way that one can either replace an ultra-rigid thermoset or a high performance elastomer. In addition, cleaner life-cycle of production, processing, application and recycling compared with other materials has made these materials well-suited for packaging and other disposables, appliances, electronics, communication, agriculture, construction, automotive etc. All these factors, simplicity, properties and cost, are what has led to production volumes on the order of 150 million tons in 2015, which was nearly half of the global polymer production. Recently, accrued interest in topics such as sustainable development and green chemistry have led to the development of even more advanced polyolefins, which can be considered as both sustainable and green plastics.[1,2] It is not hard to imagine that such advances in polyolefins would have never been possible if the polyolefin catalysts and reaction engineering aspects had not been developed simultaneously.

The most important ethylene-based Polyolefins include low density polyethylene (LDPE), linear low density polyethylene (LLDPE) and high density polyethylene (HDPE), as shown in **Figure 1** schematically. Note that the density ranges shown can vary among different sources. Polyethylenes with densities lower than 0.915 $g.cm^{-3}$ are sometimes called ultra-low-density polyethylene (ULDPE) or very-low-density polyethylene (VLDPE). LDPE has the highest amount of short and long chain branching, whereas HDPE shows mostly linear structure. LLDPE can be obtained from the copolymerization of ethylene with higher α-olefins (e.g., 1-hexene) and contains short chain branches (SCB).[3]

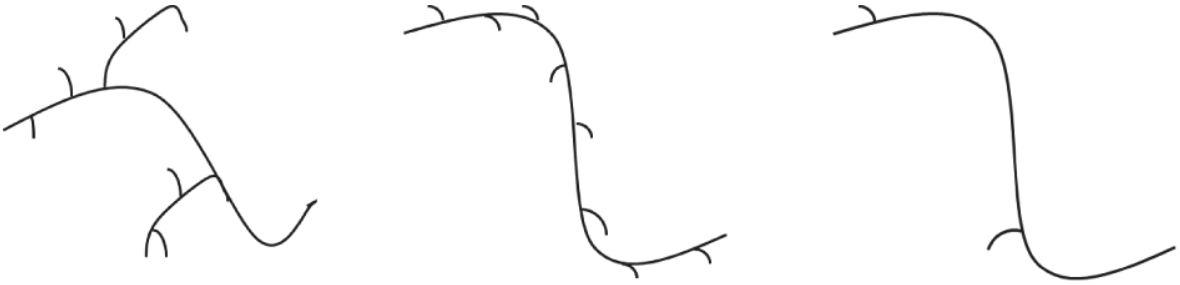

LDPE,
0.910 to 0.940 g.cm^{-3}

LLDPE/VLDPE
0.915-0.940/0.88- 0.915 g.cm^{-3}

HDPE
0.941-0.970 g.cm^{-3}

Figure 1. Polyethylene classification according to branching and density.

Polypropylene (PP) is based upon propylene as monomer and represents one third of the world-wide production of polyolefins. The asymmetrical nature of propylene leads to different stereochemical microstructures (tacticity) of PP, as shown in **Figure 2**. The orientation of the methyl group of propylene unit in the resulting polymer can significantly influence the crystallization of the polymer and thus the physical and mechanical properties of PP. Atactic polypropylene (aPP) is amorphous due to its random arrangement of methyl groups. The two other PP grades, namely isotactic PP (iPP) and syndiotactic PP (sPP), are of commercial importance due to their semicrystalline nature which provides them high melting temperatures. iPP holds the major market share mainly due to the fact that it is produced with (relatively) inexpensive heterogeneous Ziegler-Natta (ZN) catalysts (and to a much less extent with metallocenes), whereas sPP which can only be produced with specific (post-) metallocenes, which have lower activities and make for a more expensive process. There is, therefore, a much lower demand for sPP than for iPP.[3]

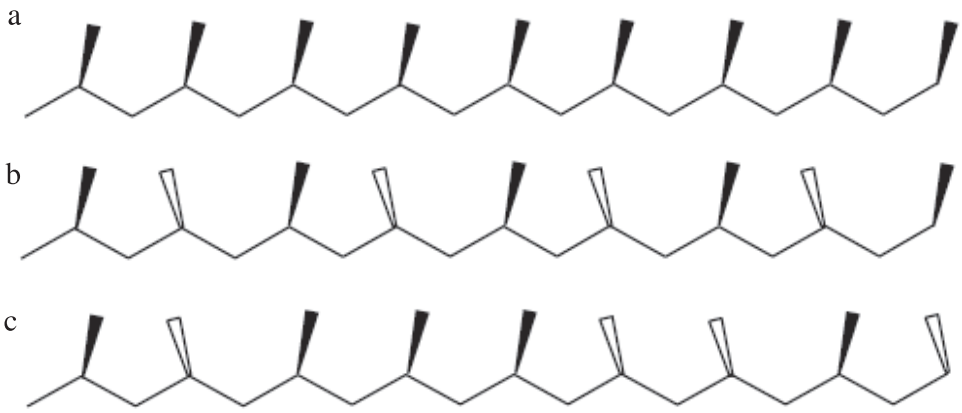

Figure 2. Main types of polypropylene (a) isotactic, (b) syndiotactic, and (c) atactic.[3]

1.1. Polyolefin Production Processes

Just as for any other polymer, both the production process and the chemistry employed can have a strong impact on the physical and chemical properties of polyolefins. Since no single process can produce all commercially important grades of polyolefins a variety of production processes, catalysts and free radical initiators exist. These production processes can be divided into two broader classes as shown in **Figure 3**. Some of these processes will be described briefly here. For a detailed discussion the potential reader is suggested to read Chapter 4 of Soares and McKenna.[4] Furthermore, focus will be placed on PE processes employing supported catalysts, as these are the objects of interest in this thesis. Free radical, solution and PP processes are mentioned in passing to give the reader a rapid idea of similarities and differences with the processes of interest.

1.1.1. High Pressure Process (Radical Polymerization)

This process is used to produce LDPE since its development by ICI in 1933. Tubular or autoclave reactor geometries are generally used with the operating temperatures in the range of 150 to 350 °C while the pressure can vary between 1200 to 3500 bar. Benefits of this process include production of long chain branched LDPE which has useful processing properties and possibility to copolymerize a variety of polar monomers with ethylene. Commercial plants of this process are owned by Sabic, LyondelBasell and ExxonMobil.

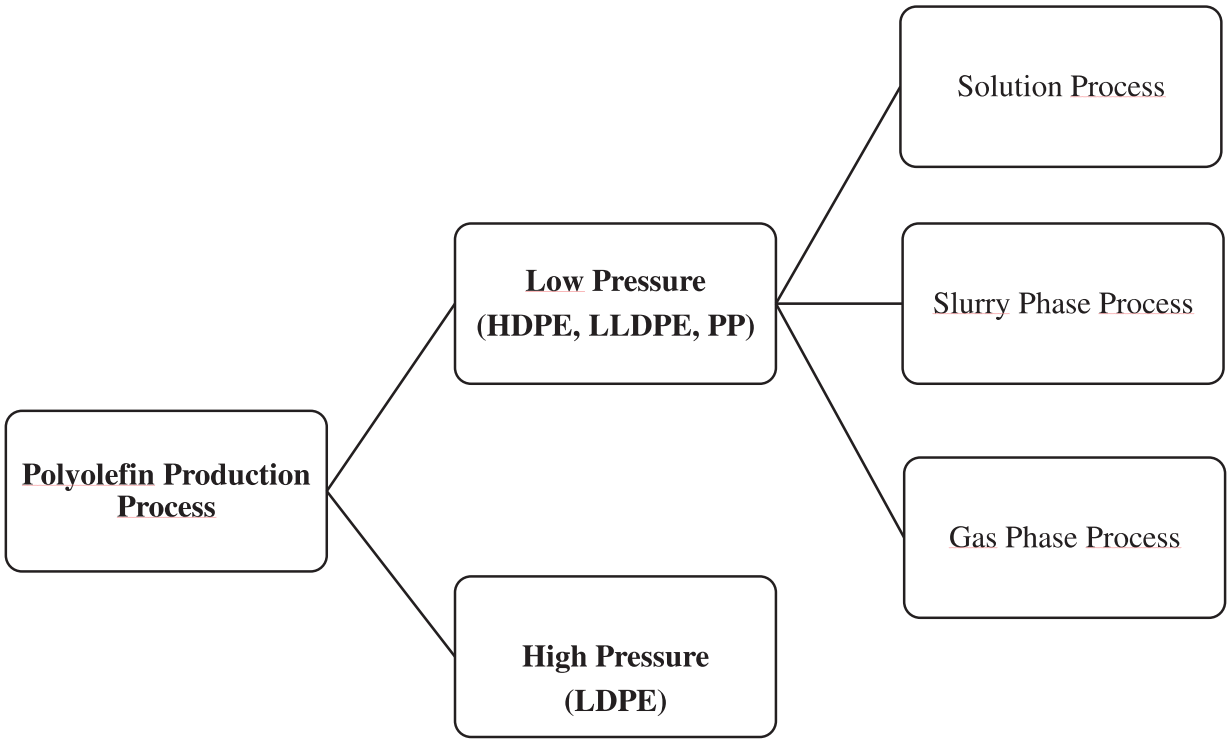

Figure 3. Classification of commercial polyolefin production processes.

1.1.2. Low pressure processes (Catalytic Polymerization)

Solution, slurry and gas phase processes constitute the class of low pressure processes. 80 % of the world-wide polyolefin production is carried out with these processes because of their energy efficiency and easy operation which is attributable to the development of high activity olefin polymerization catalysts.

Solution process refers to the polymerization in liquid phase with reactor temperatures in the range of ~140 °C to 250 °C so that the produced polyolefin remains dissolved in the reactor diluent. Autoclave, and to a lesser extent tubular loop reactors are used for this purpose. Reactor volumes are in the range of 3 to 15 m^3 and the typical residence times are in the range of 1 to 20 minutes. The fact that the reaction is carried in an homogeneous phase and that the catalysts are unsupported and dissolved in the solvent means there is no mass transfer resistance. This, coupled with the high temperature needed to keep the polymer in solution means that the polymerizations are quite rapid.

This process is commonly used for the production of different PE grades (e.g., ethylene/1-octene copolymers) with soluble metallocene and ZN catalysts, while ethylene-propylene-diene (EPDM) rubbers are also produced with this process usually by employing soluble vanadium-based ZN or titanium-based post-metallocene catalysts. EPDM is polymerized at a lower temperature due to its amorphous nature. Molar masses of the products produced with this process are generally low due to high reactor temperature. Different commercial technologies employing this process include Dowlex from Dow Chemical, DSM Compact Process from DSM (now owned by Borealis) and Sclairtech and Advanced Sclairtech (AST) processes by Nova Chemicals.[4]

Slurry processes employ a heterogeneous catalyst, and the reactor can operate in two (liquid and solid) or three (i.e., gas, liquid and solid) phases. Polymerization occurs inside solid supported catalyst/polymer particles which are suspended in a suitable inert diluent. Reactors are generally followed by flashing units where the absorbed diluent is desorbed from the polyolefin grade and recycled into the process. Reactors of choice are loop reactors or, increasingly less frequently, autoclaves. Typical reactor temperatures range between 75 to 100 °C and reactor pressures vary from about 8 to 65 bar depending upon the diluent used, reactor configuration and polyolefin grade being produced. Most commonly employed reactor diluents are linear alkanes like supercritical propane, or subcritical isobutane and hexane. Residence times of the slurry inside the reactor can vary from 45 minutes to 5 hours depending upon reactor type and number of reactors. In addition to PP (where the diluent is liquefied monomer), HDPE and MDPE are commonly produced with this process. Chevero Phillips Chemical (CP Chem), Mitsui, LyondellBasel, Borealis and INEOS have their own slurry process technologies with the Phillips loop process from CP Chem being the most widely used process for PE.[4]

Gas phase processes are also multiphase processes. Typically, heterogeneous catalysts are used along with gaseous inerts, hydrogen and (co)-monomer(s). Depending upon the reactor configuration, the catalyst/polymer particles remain suspended in the gas phase by a fluidizing gas, mechanical stirring (mostly in the case of PP) or both. Fluidized Bed Reactors (FBR) are the only reactors used to make PE in the gas phase. PP can be made in FBRs, continuous (vertical) stirred tank reactors (CSTR) and horizontal stirred bed reactors (HSBR). A fourth reactor type, the Spherizone riser-downer reactor from LyondelBasell is also used. Gas phase reactors generally operate in the range of 70 to 110 °C, and pressures of 20 to 25 bars depending upon process

technology. Residence time of the particles inside one reactor can be from 1.5 to 3 hours, and the reactor operation can be either in dry (no liquefied inert condensing agent used) or condensed mode (a liquefied inert condensing agent used to improve heat transfer inside the reactor). Reactor volumes can vary from 50 to 150 m^3.[4] The companies which have their own gas phase licensed technologies include Univation Technologies, LyondellBasell, INEOS and Mitsui.

The Borstar process from Borealis is a mixed-phase process since it employs a mix of slurry loop(s) and FBR to produce a complete range of PE (Borstar PE) and PP (Borstar PP) products. The benefit of using slurry loop(s) is that catalyst particles can be pre-polymerized at mild conditions in order to have a good morphology and the effects of particle overheating can be minimized. Higher hydrogen concentrations are achievable in this process since propane used as the diluent has very low solubility in polyethylene and therefore, a broad range of low molar mass PEs can be obtained without any fears of reactor fouling. Use of FBR allows one to achieve higher comonomer contents inside the polyethylene without risking issues related to solubility and allows this process to produce PE grades with densities in the range of 0.92 to 0.96 $g.cm^{-3}$. While the slurry loop(s) run at 85 °C and 65 to 80 bar pressure the FBR operates at 80 °C and 20 bar pressure.

2. Olefin Polymerization Catalysts

Market demand for polyolefins has steadily increased since they first appeared in the 1930s. The variety of properties and applications possible with polyolefins is huge, and includes products with properties ranging from ultra-rigid thermosets to high-performance elastomers. What is really fascinating from a scientific point of view is that all these properties can be obtained from molecules that contain only carbon and hydrogen. As we mentioned above, this is due to the innovative use of processes and catalysts.

Transition metal-based catalysts, which have been modernized over a period of more than half a century in such a way that they provide thorough molecular control of the polymerization process, are the key reason for this apparent but fascinating contradiction. Although the importance of appropriate process and process conditions cannot be neglected but if one combines a proper catalyst with them it is possible to produce polyolefin materials with precise and tunable chain microstructures and molar mass distributions which then translates into the desired material and

product properties.[5] Therefore, it is of interest to have an overview of the variety of olefin polymerization catalysts, their specific features and the level of commercial usage.

2.1. Ziegler-Natta catalysts

Ziegler-Natta (ZN) catalysts are formed by the interaction of main group metal alkyls with halides or other derivatives of transitions metals of Groups 4 - 8 of the periodic table. In the metal alkyl component of the ZN catalysts, the metal atom belongs to group 1 - 3 of the periodic table.[6,7] The metal alkyl component is also known as activator or co-catalyst, whereas, the transition metal halide or other derivative part is most of the times referred to as catalyst or, perhaps more accurately, as pre-catalyst because alone it is inactive in olefin polymerization. In this work we will refer to it as catalyst. Interaction of catalyst and co-catalyst enables the generation of species which are active for olefin polymerization and generally referred to as active sites. The co-catalyst alkylates and reduces the transition metal center of the catalyst to produce the active site and therefore, active site generation is considered to be a two-step process. Trimethylaluminum (TMA), triethylaluminum (TEA) and diethylaluminum chloride (DAEC) are some of the preferred co-catalysts for ZN catalysts. Both, homogeneous and heterogeneous forms of ZN catalysts can be found in commercial applications, but we will focus on supported catalysts.[7,8]

As mentioned above, supported, or heterogeneous ZN catalysts are used commercially in slurry and gas phase processes, and dominate the polyolefins industry from last 50 years due to their ferocious productivity and a relatively low production cost (on the order of tens of euros per kg of catalyst). $TiCl_4$ supported on $MgCl_2$ is the most general form of heterogeneous catalyst for polyolefin production, and there are various synthesis routes for these catalysts in order to guarantee high activity, good molar mass control, better comonomer incorporation, stereoselectivity, and polymer morphology.[9] ZN catalysts are generally divided into different generations. Soares[7] has divided them in four generations, whereas Chadwick et al.,[9] classified them in five generations. Without going into too much detail, ZN catalysts of the earlier generations were based on $TiCl_3$ catalysts activated with DAEC and $TiCl_3$ modified with donors to enhance the stereoselectivity. Later generations are based $TiCl_4$ supported on $MgCl_2$. Further improvements include chemical modification of the supports, better internal and external donors, and in certain cases better morphology control to help reduce or eliminate the need for palletization. Each generation showed gains in terms of property control and productivity. With current ZN catalyst

systems, it is possible to make tens, or even hunderds of kilograms of polymer per gram of catalyst (with high stereoregularity in the case of PP catalysts). Major steps in the development of electron donors for heterogeneous ZN catalyst are shown in **Table 1**.

Table 1. Major steps in the developments of electron donors for ZN catalysts.[7]

Internal donor	External donor	Isotacticity index (%)
Aromatic monoesters (EB)	-	60
Aromatic monoesters (EB)	Aromatic monoesters (EB) (methyl p-toluate)	95
Aromatic diesters (DIBP)	Silanes (NPTMS)	97-99
Diethers (1,3-diether)	-	97-99

2.2. Phillips or Chromium Catalyst

Phillips or Chromium catalysts were discovered by J. Paul Hogan and Robert L. Banks at the Philips Petroleum company in the last half of 1951,[10] more or less at the same time when Karl Ziegler disseminated his results about Ziegler catalysts. A common Chromium catalyst is made by supporting Chromium (Cr) (III) hydroxide on silica or aluminosilicate followed by calcination in dry air at high temperatures. Generally speaking, they are classified into two main families: (i) those based upon chromium oxide known as Phillips type; and (ii) the one based upon organochromium compounds. However, a third class can also be made if one considers organosilylchromate catalysts as a separated group.[9] They are different from ZN catalysts in the following respects:

- They do not need an aluminum alkyl cocatalyst to form the required metal-carbon bond. They are first pre-activated by calcination at temperatures in the range of 200 - 900 °C. During thermal activation, the Cr species attaches to silica by reactions with the surface silanols in the temperature range of 200 - 300 °C. Further rise in temperature (i.e., > 500 °C) removes the neighboring silanols.[7] During this step of activation, the Cr (III) is converted into Cr (VI) which itself is not active in olefin polymerization and must be further reduced to the lower oxidation, i.e., most probably Cr (II) in order to be able to polymerise ethylene. This transformation of Cr (VI) to Cr (II) happens inside the reactor when it comes in contact with ethylene monomer and is the typical route applied in commercial plants using this catalyst.

- Polymerization activity, MWD of the polymer and Long Chain Branching (LCB) inside the polymer are significantly influenced by the calcination temperature and procedure.
- Since MWD is affected by the support porosity and pore volume, hydrogen is not an effective chain transfer agent for this catalyst.
- Long induction periods are very common during polymerizations with this type of catalyst.[7,9]

Phillips catalysts are mainly employed in the commercial production of HDPE which, after 50 years of their development, still amounts to one third of the total HDPE production. In general, there poor capability to incorporate higher α-olefins makes them unsuitable for LLDPE production. MWDs of the HDPE produced with Phillips catalysts are very broad with molar mass dispersities (Đ) easily approaching 10 or even higher (e.g., 65 reported by McDaniel[10]) which can be controlled by changing support properties or thermal activation step. Such a high Đ value also indicates that there are numerous active sites taking part during polymerization. An important feature of the HDPE produced via Phillips catalyst is the existence of LCB in them which provides excellent melt strength to these resins. Various companies including LyondelBasell, W.R. Grace, INEOS Silica, PQ Corporation and Univation Technologies are producing these catalysts with different compositions on commercial scale. Industrially, these catalysts are used by Chevron Phillips in slurry loop process and by Union Carbide in its gas phase process for the production of HDPE. An exhaustive review describing in detail the specific features of Phillips catalysts, reaction mechanism and polymer properties can be found in the work of McDaniel.[10,11]

2.3. Metallocene Catalysts

Transition metal atom sandwiched between two cyclopentadienyl (Cp) or cyclopentadienyl-derivative rings, as depicted in **Figure 4**, are known as metallocenes[7] and in the field of olefin polymers their structure was uncovered by Ernst O. Fischer and Geoffrey Wilkinson in 1952 for which both of them were awarded with the Nobel Prize in 1973.[12] The transition metal atom usually belongs to Group 4, and most often it is Zirconium (Zr) leading to Zirconocenes, Titanium (Ti) leading to Titanocenes and Hafnium (Hf) leading to Hafnocenes. Metallocenes are soluble in hydrocarbons and show only one type of active site upon activation. The first application of metallocenes in olefin polymerization dates back to ‘50s when Breslow[13] and Natta[14] independently activated Cp_2TiCl_2 with mixed aluminum alkyl halides ($AlXR_2$) in homogeneous polymerization

but with poor activities towards ethylene.[7,15,16] Significantly enhanced activities of metallocenes (i.e., about 10000 times higher than their activities with $AlXR_2$) were only made possible after the discovery of methylaluminoxane (MAO) by Sinn and Kaminsky,[17-19] almost three decades after the results reported by Breslow[13] and Natta[14]. This discovery of MAO re-ignited the scientific research in the field of metallocene catalysis. Homogeneous metallocenes can be many more times as active as established Ziegler-Natta catalysts due to the fact that a high percentage of metal is active e.g., one of the record setting metallocenes in terms of ethylene polymerization activity is the bridged bis(fluroenyl) complex which produced 300 tons of polyethylene per gram Zirconium per hour.[15,20]

The reactivity of these catalysts towards olefins can be tailored by variations in the electronic and steric environment around the transition metal which has enabled the production of polyolefins with reasonably well-controlled molar mass distribution (ideally with a Flory distribution having molar mass dispersity (Đ) = 2) and polymer microstructure (e.g., comonomer content and distribution, SCB, LCB and polymer tacticity).[12] Molar mass of the polyethylenes produced with metallocene catalysts can vary in a wide range of 18000 to 1.5 million $g.mole^{-1}$. Reactor temperature, metallocene/ethylene ratio and hydrogen amount injected into the reactor can be used as molar mass control handles.[20] Various classes of metallocenes have now been developed and, just to name few, ansa-metallocenes is one of those classes in which the two Cp rings are connected through bridges of different types which alter the ligand-metal-ligand angle (commonly known as the bite-angle).[7] Half Sandwiched or Constrained Geometry Catalysts (CGC) are another type of metallocenes in which there is only one Cp ring, as shown in **Figure 4c**. They represent a class of metallocenes with high reactivity ratios for α-olefin incorporation during their copolymerizations with ethylene because the absence of one Cp ring facilitates monomer access to the active site, along with other factors like different electronic environment around the active metal center. Infinite possibilities exist for the combination of different ligands in CGC and other metallocene compounds.[7,16,21] Generally speaking, Zirconocenes with various ligand geometries can be considered as the most studied academically and applied industrially metallocenes because they show higher activities than Hafnocenes or Titanocenes. Rapid deactivation of Titanocenes above 50 °C, probably due to the reduction of Ti(IV) to Ti(III), makes them the least productive metallocenes.[22]

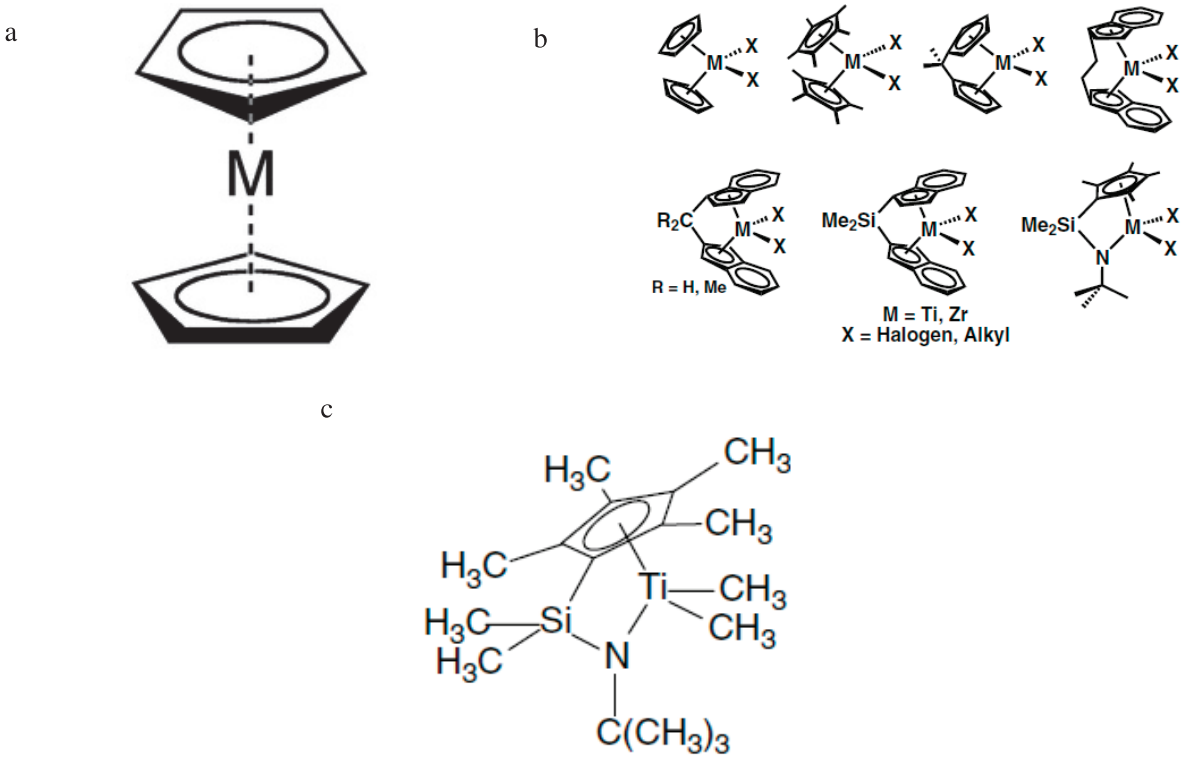

Figure 4. Schematic presentation of metallocene catalysts (a,b) and CGC (c).

Metallocene catalysts are generally known as 'Single-site' catalysts as they produce polyolefins of Đ = 2. While there might be advantages to narrow MWDs, this lower Đ value can make the metallocene-polyolefins difficult to process (especially at higher molecular weights) in comparison to those obtained with ZN or Philips catalysts which possess broader MWDs. The reason for this is the absence of low molecular weight polymer fraction in high MW metallocene polymers. This low MW fraction acts as a lubricant and enhances the shear thinning property of the polyolefins, corresponds to higher critical shear rates at the onset of melt fracture, higher flowability in the molten state under high shear rates (which is very important in melt extrusion) and high zero-shear viscosities (which is required and beneficial in blow molding processes).[7,16] Various approaches have been developed industrially to enhance the processability of metallocenes based polyolefins which include blending of polymers produced by different catalysts, multireactor technology, and the use of tandem catalysts (i.e. catalysts with more than one type of active site) which have components with varying comonomer incorporation abilities, stereoselectivities, hydrogen responses and chain walking abilities in one reactor. This third strategy has led to a new generation

of catalysts generally known as mixed catalysts, hybrid catalysts or multisite catalysts which have been tested either in homogeneous or in heterogeneous forms.[1] Metallocenes are widely employed in such multisite catalysts which clearly sheds light on their industrial importance. For example, there are many patents on this topic, including a number of them applied to the Phillips Loop Slurry Process[23-27]. The interested reader can also find a detailed discussion of the industrial use of multisite metallocenes catalysts in the work of Markus et al.[1] Going back to the point of low Đ value, it should be mentioned here that metallocenes have actually proved to be effective models for mechanistic studies of heterogeneous ZN catalysts[16] which allows us to suggest that low Đ values help in understanding the behavior of active sites by kinetic studies.

Among different activators or co-catalysts (like aluminum alkyls, borates, fluoroarylalanes, trityl and ammonium borate and aluminate salts etc.[28]) for metallocenes, MAO and its different modified forms seem to be the most widely used, both in research and production. While metallocenes are used to a lesser extent than ZN catalysts, the fact that in 2010 over 5 million tons of polyolefins, especially different grades of polyethylene, were produced commercially by using MAO as an activator points to the fact that this is still an important market.[18]

It should be noted that without a co-catalyst metallocenes are inactive in olefin polymerization and the co-catalyst is often more expensive than the metallocene.[28] MAO consists of alternate arrangements of aluminum and oxygen atoms while the free valances are saturated by methyl substituents. The basic structural unit of MAO is considered to be $[Al_4O_3Me_6]$ as investigated and proposed by Sinn[29] and Barron.[30] Since the aluminum atoms are coordinatively unsaturated, agglomeration of the structural units lead to clusters and cages of MAO. Solutions of MAO, in the simplest form, consists of two different components: trimethylaluminum (TMA) which is partially free and bound with the second polymer MAO fraction whose chemical notation is either written as $[\text{-Al}(CH_3)\text{O-}]_n$ or as $[Al(CH_3)_{1.4-1.5}O_{0.75-0.80}]_n$. While research is still underway to know the exact structure of MAO, consensus of the scientific society seems to be converging on cage structure with 4-coordinated aluminum (Al) and 3-coordinated oxygen (O) centers. However, the proposals of nano-tube like structures,[31] linear chains and cyclic ring structures of MAO are also not uncommon.[28] The molar mass of MAO can apparently vary between 700 (corresponding to 12 aluminum atoms)[29,32] to 18000 $g.mole^{-1}$ (corresponding to aggregates of 150 to 200 aluminum atoms)[33] and its solubility in aromatic solvents is higher than in aliphatic hydrocarbons.[18,28] The

most recent and extensive work of Linnolahti et al.,[34] employed small angle neutron scattering (SANS) and pulsed field gradient spin echo (PFG-SE) NMR measurements to suggest that molar mass of polymeric MAO is about 1800 ± 100 g.mole^{-1} corresponding to about 30 aluminum atoms per MAO polymer, whereas the hydrodynamic radius is 12.0 ± 0.3 Å. When used in solution process to activate the metallocenes, the Al/transition-metal ratios appear generally to be on the order of 10^3-10^4/, with some studies reporting ratios of over 300000/1.[34,35] Such high amounts of MAO are needed to shield the active sites from each other and avoid any bimolecular deactivation.[7]

Some homogeneous or soluble metallocene/MAO catalysts have found industrial applications in solution processes (e.g., Dow ELITE, Nova Surpass, Exxon EXACT)[36] where the operating conditions such that the whole reaction mixture remains in liquid phase.[16] However, the high cost of the co-catalyst along with high required amounts, difficulty of injecting them into the existing slurry and gas phase reactors, low processability and poor polymer morphology inhibited their direct use in existing slurry and gas phase processes. However, progress in supporting or immobilizing the metallocene/MAO catalysts on suitable carriers (or supports) like silica, alumina, alumina-silica etc., has allowed us to overcome most of these problems cited above in recent years, allowing this type of catalyst to be used as 'drop-in-technology'; i.e. as new catalysts that be used in an existing polyolefin plant without any significant structural changes being needed.[16,28,37]

However, it turns out that heterogeneous or supported metallocene/MAO catalysts are not as active as their homogeneous analogs, perhaps due to different side reactions that might depend on the method of supporting. In addition, leaching of the supported catalyst that can cause reactor fouling is another operational problem. Continued industrial and academic research has partially mitigated these issues by providing better understanding about the interactions of catalysts and/or co-catalyst with various supports. As mentioned above, this has led to the use of a significant amount of metallocenes in commercial processes, either as individual catalysts or as a component of a multisite supported catalysts.[1,16,24,37] Despite this progress, there still remains a number of important points that need to be investigated in terms of improving the supporting process, understand how it influences the performance of the catalyst, and even how the characteristics of the support influence the polymerization.

3. Heterogeneous Catalysts

In the context of our work, the term heterogeneous catalysts refer to a catalyst which is either chemically fixed or physically dispersed on solid material, referred to as a support or carrier. For example, silica is used as a support for numerous organometallic catalysts. People often refer to silica or other supports as being inert, but this is not strictly speaking true. Silica shows reactivity towards the catalysts/co-catalysts and thus can alter the nature of the active sites, even if it does not take part directly in ethylene polymerization. On the other hand, if the catalyst is not supported on an inert carrier and dissolves in the reaction medium (e.g., diluents used in olefin polymerization processes) it is termed as homogeneous catalyst. In the polyolefins industry, about 80 % of the total production is done using slurry and gas phase reactors which use heterogeneous organometallic catalysts. If they are well synthesized, one obtains minimal reactor fouling with heterogeneous catalysts, and a final product with high bulk density which, of course, is essential in storage and transportation of the polyolefins.[7,16] However, they tend to be less well-defined than similar homogeneous catalysts, undoubtedly because the act of supporting them creates poorly understood interactions between carrier and site. All-in-all, this means that homogeneous (or molecular) catalysts are chemically better defined, activate at lower temperatures, have higher selectivities than their heterogeneous analogs. It is also less complicated to perform rational catalyst development using structure-property relationships with homogeneous catalysts due to their well-defined active sites.[38]

Readers interested in the finer details of site structure and types, and current methods used to support active sites to see the work of Collins et al.,[39] Waymouth et al.,[40] Theopold et al., et al.,[41,42] Severn et al.,[16] McDaniel,[10,11] and Hlatky [43]. In the coming subsections, we will briefly describe the methods used to heterogenize metallocenes.

3.1. Synthesis Methods for Heterogeneous Metallocenes

Several methods have been developed in the open literature for preparing heterogeneous or supported metallocene catalysts. In the next sections, we will use the term supported metallocenes instead of heterogeneous metallocenes. Each method involves a certain level of complexity and provides supported metallocenes with specific advantages. Generally, most of the methods used for supporting metallocenes fall into two broad categories;[15,22,44]

1- Physical adsorption supporting methods
    a. Support/Metallocene/Co-catalyst
    b. Support/Co-catalyst/Metallocene
    c. (Metallocene + Co-catalyst)/Support
2- Chemical tethering methods
    a. Support/Functionalized Metallocene/Co-catalyst
    b. Metallocene Generation on the Support

3.1.1. Physical adsorption supporting methods

Synthesis methods included in this class provide supported metallocenes where the bonding between the support and the catalyst or co-catalyst is not very strong. Although, some of these methods have found successful industrial implementation and provide supported metallocenes with commercially operable activities, selectivities etc., the inherent problems of low activities as compared to their homogeneous analogs, catalyst leaching, multisite behavior etc., are still being investigated and improved. As we shall see, when these methods are preferred it is probably due to their simplicity leading to low production costs, rather than the efficiency of tethering the site to the support.

3.1.1.1. Support/Metallocene/Co-catalyst

In this method, the metallocene dissolved in a suitable solvent (e.g., toluene) is contacted with the solid support. The functional groups (e.g., hydroxyl groups (OH) in the case of silica and alumina) available on the support react with the metallocene and fix it on either coordinatively or covalently, as shown in **Scheme 1a** for silica as a model support. Hydrochloric acid (HCl), which is a poison for metallocenes, may be generated during this step (when zirconocene dichlorides are used) due to the reaction between OH groups present on the support and the zirconocene. The amount and type of functional groups present on the support surface are a strong function of the temperature and time given during the dehydroxylation process. Last step in this catalyst supporting method consists of adding co-catalyst (e.g., MAO dissolved in toluene) to this supported metallocene which coordinatively attaches with the metallocene and generates the active species (see **Scheme 1a**). Washing steps are commonly applied after the metallocene fixation and co-catalyst impregnation. The actual number of washing steps, the volume and type of hydrocarbon used, and the preparation temperature vary significantly in the literature. This method of supported metallocene synthesis is

not preferred because, in the case of silica supports for example, it is still difficult to predict which concentration and type of OH groups are sufficient for preparing a catalyst of desired traits with a given metallocene. The local steric environment of the metallocenes can also be influenced by close contact to the support surface and that's why successful examples of post-metallocenes grafted and activated by this method are rare.[45] Furthermore, the generation of HCl which can deactivate other metallocene molecules in the mixture along with the formation of bidentate species (see **Scheme 1b**) during catalyst synthesis can reduce significantly the activity of such supported metallocenes in olefin polymerization.[16]

a

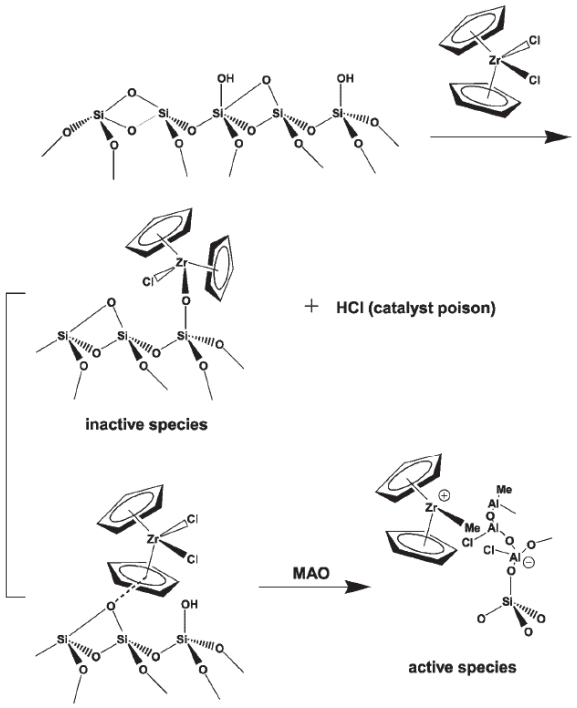

b

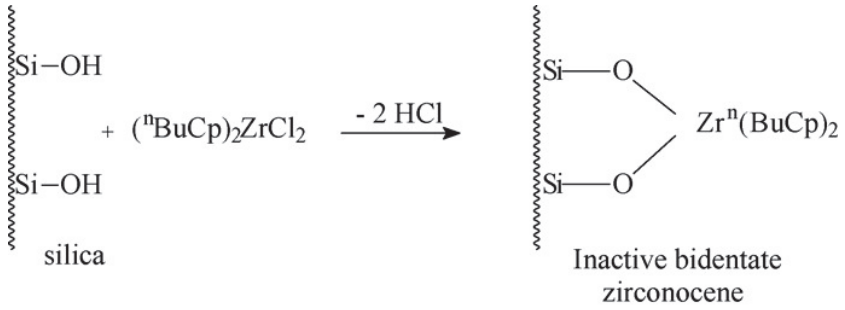

Scheme 1. (a) Synthesis of silica supported metallocene catalyst by the method 1a.[44] (b) Generation of inactive bidentate zirconocene during the method 1a.[46]

With silica as a support, dos Santos et al.,[47-49] studied this catalyst synthesis method extensively by varying silica dehydroxylation temperature from room temperature to 450 °C, contact time between the support and metallocene and the solvents from non-polar to polar. Higher silica dehydroxyalation temperatures decreased the catalyst loadings but increased the catalytic activity in ethylene polymerizations with MAO as co-catalyst, whereas higher impregnation temperatures (i.e. the temperature at which metallocene and MAO were supported in the steps described before) and longer contact times led to higher metal contents of the final supported catalyst but reduced the overall activity of $(n\text{-BuCp})_2ZrCl_2$/silica catalysts. Two different zirconocene species were found on the silica surface, as shown in **Figure 5**. Here it is species **I** that is assumed to form an active site with MAO, presumably by metathesis of the surface Si-O-M bond, while **II** is believed to be inactive probably due to steric and electronic arrangements. Severn et al.,[16] proposed that metathesis of the surface Si-O-M bond can lead to the onset of catalyst leaching from the silica surface. Collins et al.,[50] also studied this method of preparing supported metallocenes and reported that the reaction between coordination sphere of $rac\text{-Et(Ind)}_2ZrCl_2$ and one or two OH groups of silica surface can decompose the metallocene and liberate bis(indenyl)-ethane in the grafting solvent. Detailed reviews by Severn et al.[16] and Soares et al.[44] provide an overview of the research groups who utilized this method of supporting metallocenes and arrived at conclusions similar to those discussed above.

A modification of this catalyst synthesis method has been used by some authors in which the co-catalyst is not supported, rather it is fed separately into the reactor which leads to a one-step catalyst synthesis method but does not guarantee the removal of said disadvantages of this method unless surface chemistry of the support does not allow such deactivation reactions.[44]

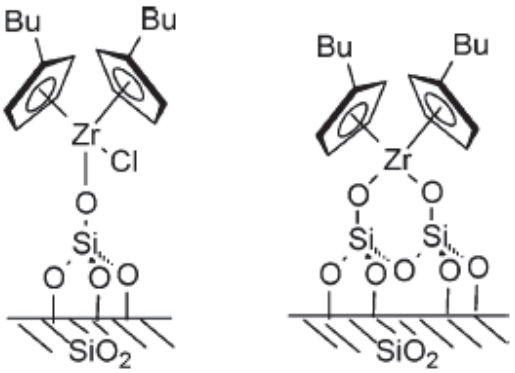

Figure 5. Two species present on silica supported $(n\text{-}BuCp)_2ZrCl_2$ catalyst.[16]

3.1.1.2. Support/Co-catalyst/Metallocene

In this method, first disclosed by Welborn[51] and Takashi[52] using silica as support, the support is first impregnated with the co-catalyst followed by washing and drying steps. A metallocene in solution is added in a second step where the support impregnated with the co-catalyst (i.e., the product of first step) is suspended in a hydrocarbon to form a slurry. Washing and drying steps are applied again and the final product is the supported catalyst. The reaction and drying temperatures and contact time of both the steps can vary along with the number of washing steps employed at the end of each step. In the case of silica and γ-alumina supports, the hydroxyl groups act as the fixation sites for the co-catalyst e.g., trimethyl aluminum (TMA) in MAO, whereas the absorbed MAO coordinates with the metallocene to form the active species. MAO supported on different silica (SMAO) is also available commercially and one can directly support metallocene on such a commercial SMAO. If an aluminum alkyl (e.g., triethyl aluminum (TEA), triisobutyl aluminum (TIBA) etc.) is used as a co-catalyst, this method does not always provide an active supported metallocene. Generally, more aluminum alkyls and MAO must be added to the reactor, where they can act as additional activators and scavengers. Conversely, hydrated silica added to the aluminum alkyl solutions, which led to in-situ generation of MAO on the supports (by the reaction of adsorbed water and the aluminum alkyl as shown in **Figure 6b**), followed by metallocene addition has also been tested and provided catalysts of reasonable activities.[53-57]

A major benefit of this method is the avoidance of metallocene decomposition or deactivation by direct interaction with the functional groups of the support surface. The work of dos Santos et al.,[58]

showed that those OH groups which do not react with the TMA present in a given batch of MAO are shielded by the bulky MAO molecules. It is generally assumed that in this case the MAO physisorbs on the support. This method is also suitable in cases where pre-contact between the metallocene and the co-catalyst leads to over-reduction or deactivation of the catalyst.[45] A great deal of research by various groups has shown that the efficiency of the final supported catalyst can be improved by orders of magnitude by correctly choosing the heat treatment during co-catalyst (i.e., usually MAO) impregnation on the support (i.e., silica in most cases), duration of contact between the support and the co-catalyst and chemical modifications of the co-catalyst after (as well as before) immobilization.[15,16,22,45] Alternatively, one can also chemically modify the inorganic oxide supports with various inorganic, organic or organometallic compounds in order to: (i) remove the surface OH groups; (ii) generate a more uniform surface species; (iii) add an additional functional group; or (iv) alter the electronic properties such as the number and nature of Lewis and Brønsted acidic sites of the support.[46,59-63] For these reasons, this method of supporting metallocences has become among the most widely used academically and industrially.

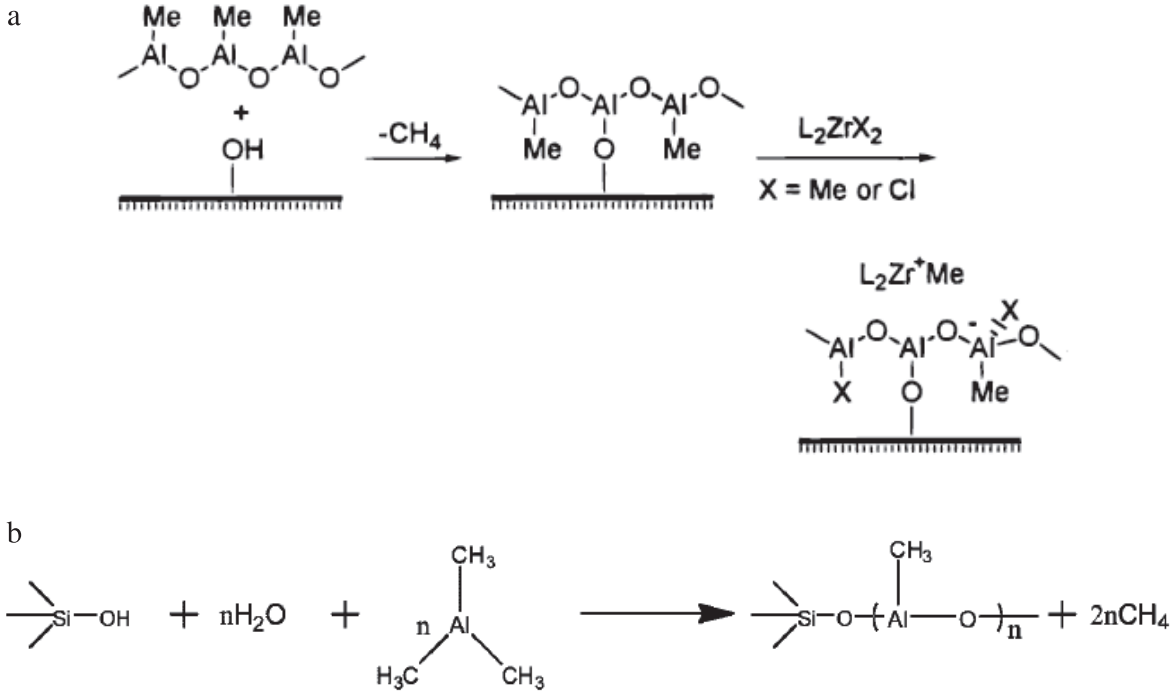

Figure 6. MAO immobilization on support surface followed by coordination with metallocene (a)[28], in-situ MAO generation by the reaction of water adsorbed on the silica support with TMA (b).[44]

3.1.1.3. (Metallocene + Co-catalyst)/Support

Mixing a metallocene and co-catalyst (i.e., mostly MAO) in a suitable solvent prior to their addition on a solid support has become one of the most frequently utilized method of preparing supported metallocenes. This approach allows for a reduction in the production cost of supported metallocenes because it has a limited number of time consuming steps, uses less solvent than most methods and generates fewer byproducts. Furthermore, in instances where the combination of catalyst and cocatalyst permits it, dissolving the two species in one pot can lead to better activation of some metallocenes since there are no diffusion limitations and fewer byproducts that can interfere with catalyst activity in solution. These are problems that can occur if the activation occurs directly on a support. It should also be noted that some complexes can deactivate upon pre-contact with co-catalyst, so the scope of this method is limited. [44,45]

Just as with the previous strategies, various modifications proposed for this method have also led to substantial increments in the activity and stereoselectivity of the metallocenes. For instance, increasing the time MAO and $Me_2Si(2\text{-}Me,4\text{-}PhInd)_2ZrCl_2$ are contacted in solution without exposure to light prior to its addition on silica support has been reported to double the activity in comparison to that of a supported catalyst derived from immediate contact.[64] MAO can be used to pacify the silica surface before adding the solution of metallocene/co-catalyst. This has led to increased stereoselectivity, and can be considered as a hybrid route of method **1b** and **1c**.[65] Chemical modification of the support surface prior to the addition of metallocene/co-catalyst solution has also been reported to enhance the activity of the final supported catalyst. As an example, Speca[66] fluorinated a silica support with $[NH_4][X]$ (X = F, SiF_6, PF_6 or BF_4) before supporting metallocene/MAO solution which led to a three times enhancement in the activity for propylene polymerization.

An important advancement in the supported catalyst synthesis methods is the development of **'incipient wetness method'** which allows commercial plants to save production costs by reducing the amount of the solvents used and byproducts produced. [45,67-69] In this technique the pores of the support are filled in a controlled manner with the solvent containing either metallocene/co-catalyst mixture or only MAO (or a solution of metallocene can be fed to co-catalyst/support i.e., (method **1b**)). The total volume of the solution of active ingredients is typically 100 – 150 % of the pore volume of the bare support (although occasionally the solution volume can exceed 150 % of the

total pore volume in order to shift from mud-point to slurry state)[72.] Capillary forces draw the solution into the pores of the support leading (in principle) to uniform dispersion of the active ingredients throughout the solid porous particles. [45,67-69]

Finally, it is important to mention here that the solvents used during supported catalyst synthesis cannot be completely removed even after vacuum drying the final catalyst at different temperatures, inert gas flow rates etc. The amount of residual toluene, for example, can vary from ~1 to ~30 wt% of the final catalyst depending upon the drying condition employed.[45]

3.1.2. Chemical Tethering Methods

Silica supported metallocenes prepared by the physical adsorption methods described in the previous section can be prone to leaching; in other words, the extraction or desorption of the metallocene or metallocene/co-catalyst species from the solid support. Desorbed metallocenes are generally soluble in the reactor diluent and can polymerize in that phase in the presence of separately added co-catalyst (or if the metallocene and co-catalyst together have desorbed they do not need a separately added co-catalyst for starting solution polymerization). This phenomenon is undesirable since it causes reactor fouling and, consequently, heat transfer problems. Clearly, it is more of a concern in slurry phase reactors than in gas phase olefin polymerization reactors. Major reasons for leaching, other than poor fixation on the support, include solubility of catalyst and/or co-catalyst in the reaction medium and interaction of the co-catalysts (like MAO) with other aluminum alkyls (e.g., TEA, TIBA etc.) that are added to the reactor as scavengers. TIBA is known to modify MAO and increase its solubility in commonly used industrial alkane diluents. High TIBA concentrations or prolonged contact between the supported catalyst and TIBA due to poor mixing can lead to reactor fouling. Chemical tethering of metallocene on the supports can provide a means to covalently attach the complex with the carrier and hence, decreases the chances of catalyst leaching. However, such methods of supported metallocene synthesis are not preferred industrially due to the number and complexity of the involved steps which leads to higher production costs than those prepared with physical adsorption methods. Furthermore, highly oxophilic nature of Group 4 metallocenes combined with fact that the steric and electronic environments of such catalysts are always different from their homogeneous analogs (which may lead to significantly different active sites) are important issues associated with these synthesis methods.[16,44]

Due to a number of variables playing crucial role along with the fact that the sequence of reagent addition can also impact the performance of the final supported metallocenes, no universal method has been developed which gives supported metallocenes of all the required traits. Considerable research needs to be conducted if one wants to optimize a particular metallocene.

4. Types of Co-catalysts

As we have seen in the previous sections, metallocenes need an activator or co-catalyst to convert into an active olefin polymerization catalyst no matter whether they are in homo- or heterogeneous form. Fundamental understanding of the single-site catalysts and major technological developments have been greatly helped by the discoveries of new and more effective co-catalysts. Generally, the cost of a co-catalyst (which are mainly organometallic compounds of Group 13) for Group 4 metallocenes is higher than the cost of the catalyst which is another driving force for the development of new more effective but cheap co-catalysts. Generally, the co-catalyst activates the metallocenes by extracting one or more of their non-cyclopentadienyl ligands and creating an ion-pair in which the transition metal center of metallocene becomes the cation, whereas, the co-catalyst becomes anion may influence the polymerization process and properties of the obtained polymer. Possible relationships between the catalyst and co-catalysts in metal catalyzed olefin polymerizations are illustrated in **Figure 7**.[28] Different types of co-catalysts have been developed since the discovery of metallocenes as catalysts for olefin polymerizations and a short overview of these co-catalysts will be helpful for understanding their differences.

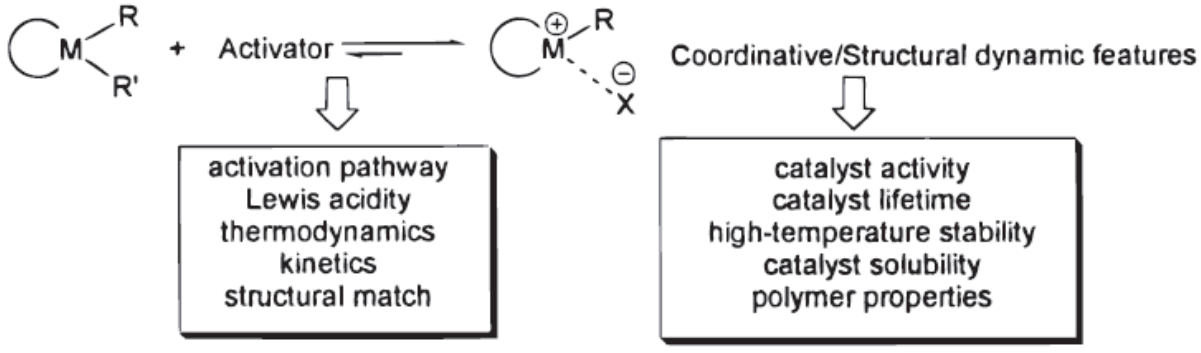

Figure 7. Illustration of possible relationships between the catalysts and co-catalysts used in metal catalyzed olefin polymerizations.[28]

4.1. Aluminum Alkyls (AlR_3)

The use of AlR_3, and more specifically their mono-halide derivatives, as co-catalysts for metallocenes dates back to late 1950s when Breslow[13] first showed that Cp_2TiCl_2 was active (although the activity was relatively low) in homogeneous ethylene polymerization with diethylaluminum chloride (DAEC) as a co-catalyst. Eisch et al.,[70] provided a strong evidence that the active component of Cp_2TiCl_2 + DAEC mixture is a positively charged Cp_2TiMe^+ species which is counter balanced by the $AlCl_4^-$ (i.e., both form an ion-pair). Such an ion-pair is formed by Ti-Cl/Al-Me ligand exchange and subsequent abstraction of Cl^{-1} by the Lewis acidic Al center.

Supported metallocenes prepared on different supports and with different methods have been tested in olefin polymerizations with AlR_3 or $AlEt_nCl_{3-n}$ as co-catalysts by different authors.[71-73] It has been shown that in addition to the relatively low activity of these systems as compared to their homogeneous analogs, the single-site nature of the metallocenes was also affected by the used co-catalyst. Soga et al.,[71] showed that silica supported metallocenes, when activated with AlR_3, are negligibly active in comparison to the propylene polymerization activities of the same metallocene supported on alumina or $MgCl_2$. In conclusion, metallocenes activated by AlR_3 (e.g., TEA, TIBA, ToA etc.) do not show high activities in ethylene polymerizations which is attributed to the side reactions such as alkyl and H-exchange as well as the reduction of Ti in titanocenes to lower oxidation states. All of these side reactions cause rapid deactivation of metallocenes activated with AlR_3. Nevertheless, their low cost as compared to other co-catalysts still allowed them to play other roles inside the reactor (e.g., reactor scavengers are usually AlR_3) and be investigated in the development of new or better co-catalysts e.g., TEA is used in developing activating supports whereas TIBA is used in the preparation of modified MAO.

4.2. Aluminoxane

As indicated by their name, the atomic structure contains aluminum and oxygen in addition to carbon and hydrogen. These oligomeric compounds are generally produced by the controlled hydrolysis of aluminum alkyls (AlR_3) and are usually represented as -Al(R)-O-, where R represents methyl, ethyl, t-butyl etc., depending upon the AlR_3 used as reactant. These compounds are known to be active for polymerization of the monomers like oxiranes as early as 1960s.[28] However, Kaminsky and Sinn[74,75] showed that methyl aluminoxane (MAO) is a very effective co-catalyst for olefin polymerization metallocene catalysts and can sometimes lead to metallocene activities

higher than those of traditional ZN catalysts in homogeneous olefin polymerizations.[12,18] Since then, no other aluminoxane family member (like ethylaluminoxane (EAO) or t-butylaluminoxane (tBAO)) has been found to be a better co-catalyst for metallocenes than MAO, so we will focus our discussion on this latter compound.

MAO is produced by the controlled reaction of trimethyl aluminum (TMA) with water, and consists of alternate arrangements of aluminum and oxygen atoms while the free valances are saturated by methyl substituents. The basic structural unit of MAO is considered to be $[Al_4O_3Me_6]$ as proposed by Sinn[29] and Barron.[30] The aluminum atoms are unsaturated in the unit structure, which leads to agglomeration of the molecules that can then form cages or clusters of MAO. As discussed above, in their simplest form solutions of MAO consist of two different components: residual trimethylaluminum (TMA) and a polymer MAO fraction whose chemical notation is either written as $[\text{-Al}(CH_3)\text{O-}]_n$ or as $[Al(CH_3)_{1.4-1.5}O_{0.75-0.80}]_n$. While research is still underway to know the exact structure of MAO, consensus of the scientific society seems to be converging on cage structure with 4-coordinated aluminum (Al) and 3-coordinated oxygen (O) centers based upon various characterization studies.[76] However, nano-tube like structures,[31] linear chains and cyclic ring structures of MAO are also thought to exist (see **Figure 8**).[28] Structures **1** and **2** contain three coordinate Al atoms which are difficult to observe as one needs to hinder the oligomerization by bulky ligands. Therefore, ladder-like structures resulting from the stacking of linear chains have been proposed. A variety of structures might be generated by different stacking mechanisms e.g., structure **3** with four membered rings and structure **4** with more relaxed hexagonal rings with partially three-coordinated Al center. Structure **5** is less favorable because stacking by bridging methyl (Me) groups is less likely due to superiority of O in bridging. In contrast to the stacking of linear structures, if cyclic structures stack they give rise to cage like structure i.e., 3D-shape **6** in **Figure 8**. Sinn et al.,[29] proposed the three dimensional (3D) cage like structure based on the structural similarities between MAO and t-butylaluminoxanes[77] which are isolable and characterizable by X-ray crystallography (structure **9** in **Figure 8**). In structure **6**, CH_3/Al ratio is about 1.5 which is in good agreement with the work of Imhoff et al.,[78] who used ^{1}H NMR to characterize MAO and TMA. Further support to structure **6** came from multinuclear NMR investigations of MAO.[79] Most recently, Collins et al.,[80] used mass spectroscopy to characterize MAO and suggested that their results support cage like or extended shapes such as nanotubes. Another recent work by Harder et al.,[76] analyzed MAO by using cryo-TEM to study the dried MAO

samples of different ages and showed that MAO molecules exist as clusters whose size depend upon age of the sample.

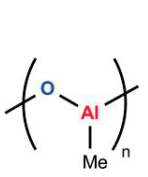

1- Linear Chains

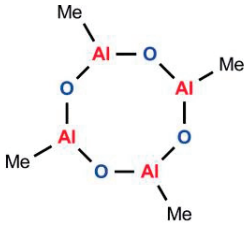

2- Cyclic Rings

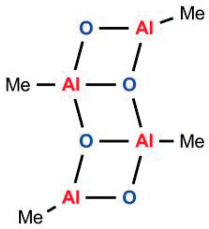

3- Square Ladder Like

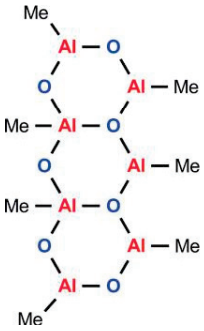

4- Cyclic Ladder Like

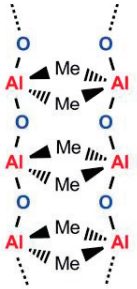

5- Bridged Ladder Like

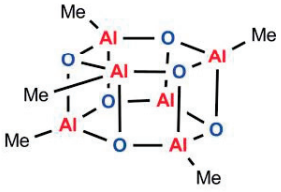

6- 3D Cage

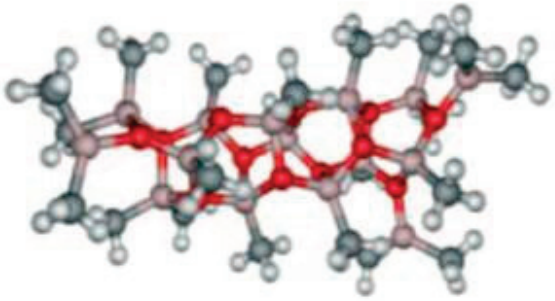

7- Chiral (2, 1) nanotubes

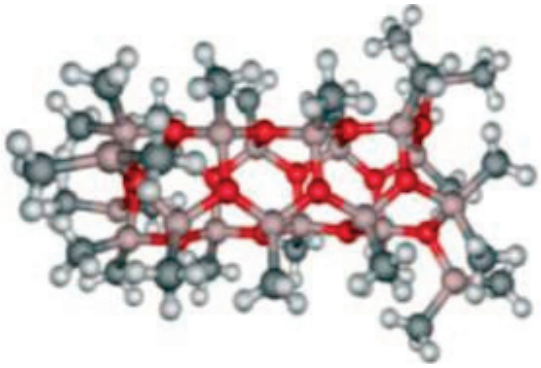

8- Armchair (2, 2) nanotubes

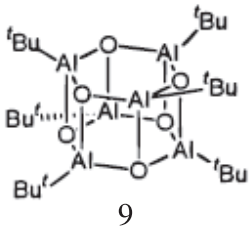

9

Figure 8. Different proposed structures of MAO reproduced after permission from the publishers.[28,31,81]

Difficulty in determining the exact MAO structure stems from the fact that dynamic equilibria exist between different oligomeric structures of MAO and the unreacted TMA (due to partial hydrolysis) which exists both as associated and free TMA. In addition, this complex melange of various oligomeric molecules varies in composition with time and temperature which can lead to reproducibility issues.[76] The molar mass of MAO varies between 700 (corresponding to 12 aluminum atoms)[29,32] and 18000 g.mole^{-1} (corresponding to aggregates of 150 to 200 aluminum atoms),[33] and its solubility in aromatic solvents is higher than in aliphatic hydrocarbons.[18,28] Recently, Linnolahti et al.,[34] employed small angle neutron scattering (SANS) and pulsed field gradient spin echo (PFG-SE) NMR measurements to suggest that molar mass of polymeric MAO is about 1800 ± 100 g.mole^{-1} corresponding to about 30 aluminum atoms per MAO polymer, and that its hydrodynamic radius is 12.0 ± 0.3 Å. When used in a solution process to activate the metallocenes, the Al/transition-metal ratios are on the order of 10^3-10^4/1, with some studies also reporting this ratio to be over 300000/1 in that specific work.[34,35] Such high amounts of MAO are needed to shield the active sites from each other and avoid any bimolecular deactivation.[7]

Free TMA present in MAO reduces the activity of metallocenes activated with this co-catalyst, and several studies have shown that increased TMA content decreases the activity as well as molar mass of the produced polyolefin.[82,83] Metallocenes with MAO appear to be activated by one of two mechanisms: 1) abstraction of either a methyl or a chloride from the metallocene molecule by a Lewis acid site of MAO; or 2) transfer of an $AlMe_2^+$ from MAO to the metallocene catalyst.[81,84,85] Linnolahti et al.,[34,84] showed that although both the activation mechanisms are feasible, the second mechanism where $AlMe_2^+$ cleaves from MAO and transfers to the metallocene catalyst is more favorable. Their results are further supported by the study of Collins et al.[80]

The addition of AlR_3 compounds (like TEA, TIBA etc.) are reported to increase the solubility of MAO in alkane diluents as well as the activity of a metallocene activated with MAO. This effect has been attributed to the fact that the AlR_3 compounds trap free TMA in MAO through Al-alkyl scrambling. TIBA has been found to be better free-TMA-trapping agent than TEA due to the fact that mixed alkyl dimers are generated when bulkier AlR_3 is added. These mixed alkyl dimers and bulkier AlR_3 are known to not to deactivate the cationic metallocene species and therefore, leads to higher activities. Furthermore, the presence of bulkier AlR_3 complexes could also lead to Me/R exchange with Me groups in the alumoxane clusters and thus, modify the MAO which shows lesser

tendency to aggregate with cationic metallocene species and therefore, enhances the activity. Akzo-Nobel sells modified MAO (MMAO) which is basically TIBA modified MAO.[81]

MAO it is relatively expensive and dangerous, so development of other co-catalysts or activating systems is an active area of research. For a detailed overview of this complex co-catalyst we suggest the recent review of Harder et al.[81]

4.3. Boranes & Borates

Compounds of Group 13 bearing pentafluorinated aryl ligands when combined with aluminum alkyls are also known to be efficient co-catalysts for Group 4 halogenated metallocenes in olefin polymerization. In the case of pre-alkylated metallocenes, compounds of Group 13 bearing pentafluorinated aryl ligands can be used without aluminum alkyls to activate the metallocenes. They coordinate weakly with the metallocenes which provides two benefits: i) the activity of metallocenes in the presence of Boranes and Borates as co-catalysts is similar to their activities in the presence of MAO as a co-catalyst under identical conditions and ii) efficient activation of metallocenes needs lower amount of these co-catalysts (generally stoichiometric amounts are used) as compared to MAO amount required which makes them competitive with aluminoxane co-catalyst despite their higher prices than MAO. The discrete nature of these co-catalysts has allowed complete understanding of their behavior due to the possibility to characterize them unambiguously.[16]

Supporting boranes and borates is no less difficult than immobilizing aluminoxane based co-catalysts, since the boron bearing family is highly sensitive to impurities e.g., silica dehydroxylated at 800 °C can have enough hydroxyl groups to deactivate zirconocenes. Silica or alumina supports pacified with compounds like AlR_3, butyllithium or butylethyl magnesium followed by reaction with BrC_6F_5, NH_4F, hexamethyldisilazane or chlorosilianes have been shown to very effective supports for the immobilization of metallocene/borate or borane mixtures (i.e., metallocene pre-activated with borane or borate) as the supported catalysts showed high activities in olefin polymerizations. In addition, constrained - geometry catalysts (CGC) (such as $Me_2Si(N\text{-}t\text{-}Bu)(C_5Me_4)TiMe_2$) supported in the same way also showed good activities.[86] Most of the polymers produced showed narrow molar mass distributions with other molecular and physical properties also comparable to those of the polyolefins produced with supported metallocene/MAO catalysts.

For a detailed overview the reader is suggested to read Chivers et al.,[87] Severn et al.,[16] Eugene et al.,[28] and Lynch et al.[86]

4.4. Activating Supports

All the co-catalysts described above have at least one thing in common: they need to be supported on a suitable carrier if one needs to utilize their dangerously beautiful chemistry in low pressure industrial olefin polymerization reactors. In addition, the immobilization process can have its own effects on the performance of the co-catalysts. Furthermore, the activation process of metallocenes with all of the above mentioned co-catalysts clearly indicates that each of them should be a strong enough Lewis acid so that it can extract alkyl or chloride ligands of the catalyst and create an active species (although there are other requirements but for the sake of simplicity we can consider Lewis acidity as the major requirement). With the aim of overcoming all these problems, work on rendering the support sufficiently acidic that it can directly activate the metallocene has been undertaken. Soga et al.,[59,71,73] showed that metallocenes can be activated with AlR_3 impregnated γ-alumina and magnesium dichloride supports in propylene polymerization without the need of additional co-catalyst but the obtained activities were lower than their homogeneous analogs. In contrast, metallocenes supported on AlR_3 impregnated silica were inactive. The authors attributed this observation to different Lewis acidities of the used supports (as silica has the lowest Lewis acidity as compared to that of γ-alumina and magnesium dichloride). First Spitz et al.[88], then Boisson et al.,[89-91] proposed activating support which have acidic sites based on aluminum and fluorine, where fluorine is linked directly to the aluminum using relatively simple synthesis strategy. This approach of using activating supports is a promising one, and it is likely that one day they will be found extensively in commercial applications.

The above discussion shows that the choice of a right co-catalyst for a given metallocene depends upon the level of trade-off one can do between the catalytic activity and other molecular properties (e.g., MWD, Đ, CCD, comonomer content) of the obtained polyolefin. It should also be noted that the behavior of a given co-catalyst can change significantly after immobilization on the supports which poses further challenge in the selection of co-catalysts and their industrial implementation. At present, MAO seems to be the most efficient co-catalyst for metallocenes utilized in the commercial processes despite its complex structure and high cost. We will therefore focus exclusively on MAO as a co-catalyst in the rest of this document.

5. Types of Supports for Heterogeneous Metallocenes

The material used for supporting metallocenes has a crucial role in keeping the performance of the final supported metallocene more or less similar to, if not perfectly, to its homogeneous analog. By performance of the metallocene, we mean its polymerization activity, comonomer incorporation and seteroselectivity which are all, inevitably, affected by the process of heterogenisation. In addition to good polymer morphology of the final product, increased bulk density, low catalyst deactivation during polymerization and avoiding reactor fouling are the main purpose of supporting metallocenes is to reduce the catalyst to co-catalyst ratio which normally varies between 10^3-10^4/1 when MAO is used as the co-catalyst. Other benefits of supported metallocenes include increment in the molar masses of the obtained polyolefins, slightly broadened MWD of the polymer (Đ ~ 2-5)[92] which facilitates processability of that specific grade, nevertheless at the cost of poor mechanical properties and production of multisite catalysts to produce polyolefin grades of tailored MWD and chemical composition distribution (CCD).[7] Broadening of the MWD is often attributed to the interactions between metallocene and the support which, consequently, generates an active species different from that formed in the case of the homogeneous analog. It should be noted that the characterization of the supported active species is difficult particularly due to low catalyst loadings, so a great deal of this type of information remains in the speculative domain.

It is easy to imagine that using different supports will confer different advantages and disadvantages when supporting metallocenes. It has been 40 years since the disclosure of the U.S. patent 4161462 in 1976 where the inventors showed that 1,2-polybutadiene can be used as a support for Cp_2TiCl_2. Ever since, different materials used for supporting metallocenes include inorganic oxides like silica and alumina, zeolites (which are aluminosilicates), mesoporous silicates, magnesium dichloride, clays, layered double hydroxides (LDH) and polymers.[16,36,43,92-95]

The most widely used support seems to be silica due to its low cost, ease of handling and good reactivity towards the metallocences and co-catalysts due to the presence of various hydroxyl groups on its surface and interior. Prior to short description of other support materials and then focusing on silica, let us briefly discuss the fragmentation step which is an essential and inevitable step during olefin polymerization with catalysts supported on silica and other inorganic oxide supports. Note that in the case of polymer supported metallocenes, fragmentation step is assumed to be absent.

In general, the inorganic oxide support materials have two structural levels i.e., the nano sized microparticles (or micrograins) which combine to form the bigger particles of diameters typically in the range of 10 – 100 µm usually termed as the macroparticles (or macrograins). These macroparticles are highly porous with surface areas on the order of several hundred square meters per gram of the support. Upon impregnation with metallocenes and/or co-catalysts the active species are assumed to be evenly distributed throughout the macroparticles. As soon as these supported catalyst particles are injected into the reactor containing the reactive species, polymer starts to accumulate within the pores of the macroparticles due to polymerization at the active sites. At this point, such polymerizing catalyst particles are generally termed as growing catalyst/polymer particles. Accumulation of the polymer inside pores generate hydraulic stresses and at a certain point where the physical bonds holding the micrograins are unable to bear the hydraulic stresses generated by the formed polymer, the so-called phenomenon of 'Particle Fragmentation' starts.

Fragmentation of the growing catalyst/polymer particles is an extremely important phase of particle growth because it helps to expose those active sites which are buried under the formed polymer layer and, consequently, facilitates the access of the reactive species (i.e., monomers, scavenger, hydrogen etc.) to the active sites. Note that in the case of $MgCl_2$ supported ZN catalysts the fragmentation step can create new active sites since they are integrated into the support material. However, in the case of silica supported metallocenes the active sites are located on the surface, as discussed before in the section of synthesis methods for heterogeneous metallocenes. By the end of this fragmentation step, the original bi-phasic support material (i.e., the pore space and solid particle) is converted into tri-phasic mixture containing catalyst-impregnated solid fragments of the support material, a continuous polymer phase embedding these catalyst-impregnated solid fragments and the porous space through which the reactants are transported. Ideally, one catalyst particle should generate one polymer particle which will continue to grow by expansion due to polymer formation at the active sites. The different steps of particle fragmentation are schematically shown in **Figure 9**.

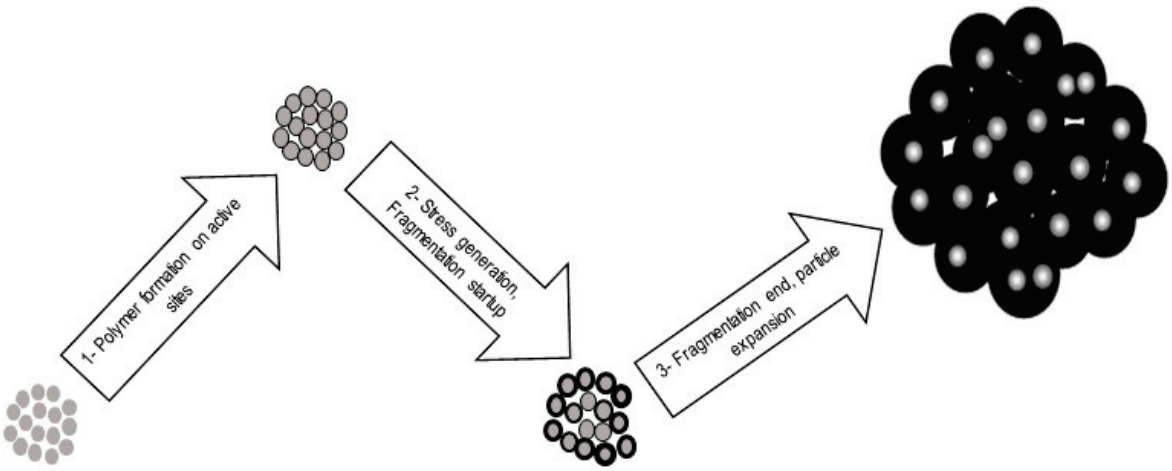

Figure 9. Schematic representation of particle fragmenation and growth inside the reactor. Gray portion depicts catalyst particles and the black color shows polymer formed.

Different proposals exist on how this critical step of particle fragmentation occurs but the most widely accepted for silica supported catalyst particles is that the polymer layer is first formed on the outermost easily accessible particle surface leading to higher inward stresses due to polymer formation and therefore, the fragmentation proceeds from outside towards the center of the particle. Typically, the time span of fragmentation completion is several tens of seconds for silica supported catalysts.[96,97] If the support material is weak, fine polymer particles (i.e., particles with diameters below 200 μm) can be generated due to uncontrolled fragmentation step which are detrimental for industrial reactors. On the other hand, too strong support material can lead to pore blockage with polymer and, consequently, low or no catalytic activity. Therefore, one has to select a support material carefully so that both of these problems can be avoided. Nevertheless, adjustment of reactor conditions, addition of certain comonomers and inert condensing agents into the reactor have also been shown to be helpful in controlling the fragmentation step, especially during the gas phase process where heat transfer control is generally problematic.[97]

All the support materials discussed here have different properties including the matrix strength or fragility leading to difference in the fragmentation step and therefore, the metallocenes supported on them behave differently under similar reaction conditions.

5.1. Magnesium Dichloride

Magnesium dichloride ($MgCl_2$) is the support material used extensively in the polyolefins industry for ZN catalysts, it is also an option for supporting metallocenes. Some difficulties of using $MgCl_2$

stem from challenges related to the lack of strong "fixation sites" for metallocenes (or co-catalyst like MAO) due to the absence of silanols groups or anything similar. Nevertheless, porous $MgCl_2$ supported zirconocenes can be obtained by partial dealcoholation of a $MgCl_2$.3EtOH adduct followed by reaction with MAO or common alkyl aluminum(AlR_3)/zirconocene mixture.[98] Sivaram et al.,[99] reported a very stable kinetic profile Cp_2TiCl_2 supported on $MgCl_2$ which otherwise decays rapidly. Guan et al.,[100] impregnated $MgCl_2$ with MAO using a cross-linking agent followed by pre-contacting with rac-Et$(Ind)_2ZrCl_2$ metallocene just before injection into the reactor. Severn et al.,[101] showed that metallocenes and other single-site catalysts can be immobilized and efficiently activated by supporting them on $MgCl_2/AlR_n(OEt)_{3-n}$ supports which were prepared by the reaction of $MgCl_2$/EtOH adducts with aluminum alkyls. In their case, no MAO or other co-catalysts (like borate) were used in polymerizations with these catalysts which was another differentiating feature of this work. In addition, the kinetic profiles were very stable, in agreement with the work of Sivaram et al.,[99] which the authors attributed to the stabilizing effect of $MgCl_2$ support. Polymer properties were similar to those produced with homogeneous or silica supported metallocenes under identical conditions. However, the global activities (~ 300 kgPE.moleTi^{-1}.h^{-1}.bar^{-1}) were 1-2 orders of magnitude lower than those obtained with homogeneous metallocene/MAO catalysts.[102]

It is safe to say that $MgCl_2$ is a reasonably good support for metallocenes but the problems associated with low catalyst activity, challenges in keeping good particle morphology (with respect to silica-supported catalysts), and poor fixation of catalyst or MAO due to the absence of silanol groups all contribute to the fact that it is still not a popular commercial support for metallocenes.[100]

5.2. Clays

A clay is usually composed of natural clay minerals as the main constituents and most of the clays are ion exchanging layered compounds.[103] Those which have been extensively studied as supports for metallocene catalysts include montmorillonite, hectorite, vermiculite, hydrotalcitite, smectite, mica, kaolin etc.[16,43] Numerous studies have looked at activating the clay supports through various chemical modifications.[103-106] This proved to be quite challenging as the poorly understood MAO structure made it difficult to react with the clays, as well as the fact that the activation mechanism of metallocenes is still not perfectly understood, so it is difficult to rationally design the system. Reactor fouling problems due to improper fixation of MAO with silanol (SiOH) deficient clays,

especially the montmorillonite (MMT) family,[107] were also observed. Other studies investigated the preparation of polyolefin/clay nanocomposites by in-situ olefin polymerization.[107-109]

These problems, and the fact that the synthesis of clay supports is quite complicated means that they are not used in commercial processes.[110]

5.3. Zeolites and Mesoporous Materials

Crystalline aluminosilicates with structural units composed of three dimensional tetrahedral arrangements of Al^{3+} or Si^{4+} (MO4; M = Al or Si) are referred to as Zeolites. Unlike the case of amorphous silica where the pore size distributions are sometimes broad, the pore structure of Zeolites supports is well defined, with a narrow pore size distribution.[16,43,93]

It is interesting to note that pore dimensions and well-connected pore structure of Zeolite supports can impact the molecular weight and comonomer incorporation of the supported metallocene/co-catalyst system as shown by the Woo et al.,[121-124] One can deduce from the work of these groups and others that the concentration of Al embedded inside the zeolite structure is the determining factor in the performance of these materials as metallocene supports in olefin polymerization.[111,112]

Despite certain potentially interesting characteristics, the complex surface chemistry of these materials lead to numerous interactions between the support and the catalyst/co-catalyst mixture which, consequently, further complicates the characterization and identification of the active sites.[16,43,93] The overall activities of the catalysts on Zeolite supports were found to be less than their homogeneous analogs for a number of reasons, not the least of which is that they are too strong to fragment (we will see below that this is an essential step in olefin polymerization). We will not discuss these points further, but developments regarding these materials as supports for metallocenes the interested reader can read the work of Riberio et al.,[93] Soares et al.,[44] Zhiqiang et al.,[113] and the relatively older work of Severn et al.[16]

5.4. γ-Alumina

The form of alumina which is of interest in polyolefins industry as a catalyst support is γ-alumina (γ-Al_2O_3) which is a metastable member of binary aluminum oxide family and is produced by heating hydrated aluminum hydroxide ($Al(OH)_3$). On the untreated or hydroxylated alumina surface, three different types of hydroxyl (OH) groups are present, and these can be used to anchor the metallocene molecules. One can also generate Lewis acidic sites on the surface of γ-Al_2O_3

either by partial or complete dehydroxylation due to coordinatively unsaturated Al sites which can be used as activation sites for the metallocenes.[16,114]

Polymer morphology obtained with alumina supported catalysts was found to be very poor when compared with the morphology of polymers produced with silica supported metallocenes i.e. slurry process polymer particles, produced with the former supported catalysts, had an irregular shape with a broad particle size distribution accompanied by a very low bulk density (0.1 to 0.2 g/cm^3). [115] The most probable reasons for this poor morphology with alumina supported catalysts could be the poor morphology of the alumina support itself (as highlighted by the authors that particle size and morphology control during silica synthesis is easier and more developed than in the case of sol-gel based aluminas) along with other factors like uncontrolled fragmentation during reaction start-up due to higher activities. A review of the literature points to the fact that although alumina supported catalysts have higher activities than the same catalysts supported on silica, significant problems of poor polymer morphology and leaching[115,116,117] mean that silicas are still the supports of choice in the industry at the current time.

5.5. Silica

The use of silica as a support in olefin polymerization dates back to 1950s and remains today in the top position among the support materials used as catalyst supports in the polyolefins industry. As discussed above, it is considered as inert in terms of polymerization, but is reactive with metallocenes and co-catalysts due to the presence of various types of hydroxyl groups and siloxane groups. Interactions between the silica and components of the active sites can have a significant influence on the productivity, comonomer incorporation, stereoselectivity of the supported metallocenes, as well as on the molar mass distribution of the polyolefins. The physical properties of silica support, which can be altered to varying degrees during silica synthesis, can also play a vital role in determining the final performance of metallocenes and/or co-catalysts supported on silica in olefin polymerization. As we will point out below, little systematic work has been done to understand the impact of the geometric factors of the supports on the polymerization and polymers made with metallocenes.

Key properties of silica supports which can be immensely influential on the kinetic behavior of the heterogeneous metallocene and on the properties of the final polyolefin grade are:

- Chemical properties and surface chemistry (number and type of surface species e.g., silanol, silyl-ether and Lewis and/or Brønsted acid sites).
- Physical properties (e.g., Particle size, pore volume, pore size and pore size distribution, surface area).
- External and internal pore structure (i.e., the manufacturing method of silica)
- Mechanical properties of silica (i.e., friability which refers to strength of silica matrix against internal stresses which generate upon, for example, polymer accumulation during polymerization and attrition).

In the present work, different silicas have been employed to analyze the impact of their physical properties on the catalytic performance of metallocenes supported on them in ethylene polymerization. These silicas have been obtained from different suppliers and therefore, show different internal and external morphologies (as we shall see in the next chapters) and therefore, a brief discussion about silica manufacturing is provided in the **Appendix** of this chapter.

5.5.1. Surface Chemistry and Thermal Treatment of Silica

Amorphous silica surface is saturated in silanol groups in its fully hydroxylated and unmodified form. Three distinct types of silanol groups (SiOH) present on silica surface along with siloxane group (-Si-O-Si-) are schematically presented in **Figure 10**. As indicated by the name, isolated groups are single silanols, whereas the vicinal silanols are bridged by the hydrogen bonds and are also known as bridged silanols. In addition to silanols and oxygen bound siloxanes, water is also structurally bound inside the silica skeleton and in very fine ultramicropores with diameter less than a nanometere i.e. internal silanol groups.[118] Untreated amorphous silica surface is ideal for the adsorption of water molecules either through hydrogen bonding with silanols or by physical adsorption.

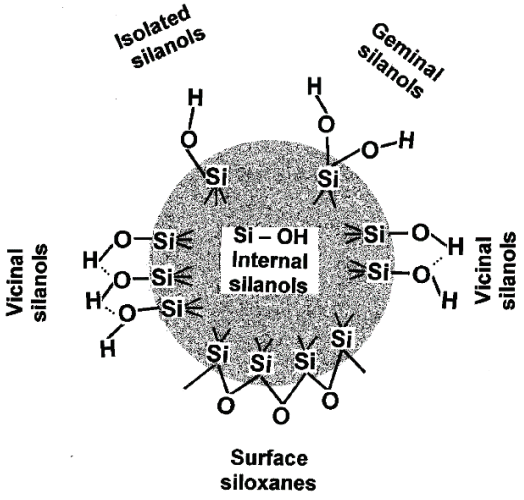

Figure 10. Schematic representation of different silanol groups present on silica. Siloxane groups are also shown. [118]

Calcination or dehydroxylation is required to get rid of adsorbed water and the most of the silanol groups since they are poisons for metallocenes. Calcination refers to the thermal treatment where the support material is fixed or fluidized in an oven, multiple hearth furnaces or rotary oven. The fluid phase may consist of air or inert gas or a combination of these two where calcination is done by air while cooling is performed under inert gas atmosphere. Heating, calcination and cooling are three steps which have their own distinct time and temperature ramps, hold time and temperature as well as optional agitation, and all of these parameters are set in such a way that particle sintering is avoided during the whole process.[45] On the other hand, dehydroxylation is generally done under vacuum without any inert or air flow. It has two steps of heating and cooling whose time and temperature ramps and hold times can also differ.

During thermal treatment of silica different physical and chemical phenomenon may occur. The physically adsorbed and hydrogen bonded water generally desorbs in the temperature ranges of 25-105 °C and 105-180 °C, respectively. Upper limit values of these temperature ranges for water removal are generally attributed to the micropores in silica which can retain water up to 180 °C.[118] As the temperature is ramped above 180 °C, surface siloxanes (i.e., silyl ether) can be produced due to the condensation of adjacent vicinal silanol groups. For typical silica, isolated silanols and siloxane groups remain on the silica surface above 400 °C, as we shall see in the next chapter. The final hydroxyl group density depends on the temperature and time used during the thermal

treatment but usually stays between 1-5 OH.nm^{-2}. It is important to mention here that calcination can also alter the pore volume and pore size distribution e.g., increased calcination temperatures have been reported to decrease the pore volume and surface area of the support. Furthermore, one can also modify the silica surface with different compounds like chloro- or alkoxy-silanes or disilazanes for specific applications in metallocene heterogenization.[45]

5.5.2. Role of Surface Chemistry in Supporting Metallocene or Co-catalyst

From the previous discussion, it can be concluded that the main aim of all the different methods for the surface treatment of silica is to generate an immobilization surface which does not poison the metallocene or the co-catalyst, and allow the final supported metallocene to behave as similarly as possible to its homogeneous analog. Silanol, siloxane and other functional groups in the case of modified silicas act as fixation sites for metallocenes or the co-catalysts. However, the optimized values of these silica surface functionalities are rarely available in the open literature due to the fact that different metallocenes and co-catalysts have different sensitivity towards them. MAO can contain different amounts of TMA, and MAO itself it evolves with time. Furthermore, MAO obtained from different suppliers can also have differences in terms of composition because it will have been produced under different conditions (i.e., time and temperatures, washing, solvent type, solvent amount etc.). Moreover, the conditions used during the catalyst heterogenization step can depend on the method chosen (as discussed in the previous sections), and these too can impact the MAO. Finally, one can find different silica supports with broadly varying physical properties.[16,92]

In the search of suitable silica dehydroxylation temperature for metallocenes supported on unmodified silica, dos Santos et al.,[47] supported (n-BuCp)$_2$ZrCl$_2$ on Grace 948 silica dehydroxylated in the temperature range of 27-450 °C. Metallocene fixation on silica was done at room temperature for 30 min in toluene followed by 12 washings of toluene and vacuum drying for 4 h. MAO or TMA (both 10 wt% separate toluene solutions) was added separately into the reactor in order to have Al/Zr molar ratio of 100-5000, and the slurry polymerizations were done at 70 °C with only 1 bar ethylene pressure. Metallocene supported on silica heat treated at room temperature showed the lowest activity despite its highest Zr loading (~0.48 wt%), whereas those dehydroxylated between 200-450 °C afforded 0.12-0.22 wt% Zr and showed higher activities than the former one. Higher metal loading at lower silica dehydroxylation temperature was attributed to the presence of more hydroxyl groups on the silica surface. Overall, the relationship between

catalytic activity and silica dehydroxylation temperature was not clear over the whole temperature range. It was deduced that with this method of catalyst preparation, higher Si-OH concentration on silica surface (i.e., low dehydroxylation temperatures) can cause deactivation of metallocene species due to the formation of inactive bidentate species.

Using the same zirconocene, van Greiken et al.,[119] studied the effect of silica dehydroxylation temperature on the catalytic activity using different supports in the temperature range of 200 to 600 °C. Their method of catalyst synthesis involved supporting a pre-mixed solution of MAO (30 wt% toluene solution) and $(n\text{-BuCp})_2ZrCl_2$ on the dehydroxylated silica in toluene slurry at room temperature for 3 h. The targeted Al/Zr molar ratio on the final catalyst was 170. The final supported catalysts were not washed, and the catalysts were dried under vacuum. Ethylene homopolymerizations were done at 70 °C, and an ethylene pressure of 1.2 bar for 30 min in the presence of TIBA (i.e., Al_{TIBA}/Zr molar ratio = 800). Total Al content of the final silica supported catalysts was observed to decrease with increasing dehydroxylation temperature which is in agreement with the decreasing silica hydroxyl concentration at higher heat treatment temperatures. The average activities of the catalysts (in $gPE.molZr^{-1}.h^{-1}.bar^{-1}$) increased slightly when the silica calcination temperature was raised from 200 to 400 °C, whereas it remained virtually constant for silica calcined at 400 °C and 600 °C. Once again, no clear conclusion was obtained about the dependence of catalytic activity on silica dehydroxylation temperature. MWD of the obtained polyethylenes was found to be unaffected by the changes in silica dehydroxylation temperature which indicated that similar active species were formed on the final catalyst irrespective of the hydroxyl concentration. It should be noted that with the catalyst synthesis method employed in this study, it is difficult to predict whether the surface hydroxyl groups first react with metallocene or MAO. Most probably, free TMA present in MAO reacts with the surface hydroxyl group while the activated complex (i.e., pre-mixed metallocene/MAO) physically adsorbs on the silica particles.

Another study related to the effect of silica dehydroxylation temperature on the catalytic activity of $(n\text{-BuCp})_2ZrCl_2$ was reported by Atiqullah et al.,[46] who calcined commercial ES-70 silica in the temperature range of 250 to 800 °C. The calcined silicas were functionalized by $n\text{-BuSnCl}_3$ at 130°C before impregnation of the particles with MAO and grafting of the zirconocene at room temperature. These steps were followed by vacuum drying of the catalysts at 55 °C. Once again no clear trend was observed and the catalytic activity (in $kgPE.mol^{-1}Zr.bar^{-1}.h^{-1}$) decreased from

250°C to 450°C and then increased up to 800°C, with the lowest activity at 450°C and the highest at 250°C. Other work related to the effect of silica dehydroxylation temperature on the catalytic activity of supported metallocences in olefin polymerization involves catalysts different from (n-BuCp)$_2$ZrCl$_2$ and therefore, reports different results.[50,120]

Since MAO is used as the co-catalyst in this study, along with different metallocenes, but mainly (n-BuCp)$_2$ZrCl$_2$, it seems that silica dehydroxylation should be done at a temperature higher than 400 °C (preferably but not necessarily 600 °C) so that only isolated silanols and siloxanes are expected on the silica surface. This should provide (n-BuCp)$_2$ZrCl$_2$/MAO-supported catalysts with reasonable activities in ethylene polymerization if the following supporting methods are followed:[16,44]

1- Impregnation of MAO on silica using toluene as solvent at 60-100 °C with subsequent washing with warm toluene and drying under vacuum. Free TMA present in MAO can pacify the silica surface by reacting with isolated silanols and siloxanes. Metallocene grafted on such silica modified with MAO (SMAO) followed by washing and vacuum drying in the temperature range of 60-100 °C are reasonably active in slurry and gas phase ethylene homopolymerizations and copolymerizations with higher α-olefins. Note that the activity units used by different authors are also different due to which it is difficult to provide a range of expected activity.
2- Mixing the metallocene catalyst and MAO in a toluene solution to activate the catalyst in homogeneous phase following incipient wetness method and then impregnating the silica support with this activated catalyst at 50-100 °C followed by vacuum drying in the same temperature range. This method consumes less time and solvents providing silica supported metallocene/MAO catalysts with reasonably good activities in ethylene homopolymerizations and copolymerizations with higher α-olefins. Fixation of the activated catalyst on silica surface is unclear since it is difficult to analyze that the surface silanol and siloxane groups have reacted either co-catalyst or metallocene.

5.5.3. Impact of Physical Properties of Silica

Physical properties of silica supports are as crucial as its surface properties are since they impact the distribution of the catalyst and co-catalyst throughout the solid particles during catalyst synthesis, (co)-monomer(s) diffusion during the course of polymerization, molar mass of the

polyolefin and, last but not the least, crystallization process of nascent polyolefin chains within the porous support. Despite their significance, the impact of physical properties of silica supports on the performance of metallocenes supported on them in ethylene (co)-polymerization processes (i.e., slurry, gas or bulk processes) is not as well explored as the impact of chemical or surface properties on silica support on the reaction kinetics of supported metallocenes in olefin polymerization, as will be shown in this section.

5.5.3.1. Effect of Silica Particle Size

The size of the silica support particles is an important physical property for a number of reasons of which its impact on heat transfer and mass transfer are two of the most important. If we talk about heat transfer it is reasonably well accepted that resistance to heat transfer (i.e. particle overheating) is greater for large catalyst particles than small ones. This is because the heat generated is proportional to the volume of the particle (i.e. the number of active sites it contains) and the heat removed is proportional to the surface area. The surface per unit volume varies as one over the radius, so it is harder to remove the heat from big, fresh catalyst particles than small ones. It is also well-known that the resistance to heat transfer decreases as the reaction progresses because the number of active sites in the particle remains the same or diminishes via deactivation, whereas the surface area increases as polymer accumulates in the particle. Thus it is quite possible that very large catalyst particles will heat up more than small ones, and thus find themselves at a higher temperature in the same reactor than small ones.

Mass transfer is a bit more complex and considered to be more important in large catalyst particles than smaller ones for fresh catalysts. The reason for this is the same logic as for heat transfer: big particles contain more active sites, but have a lower surface to volume ratio so it is harder to supply larger catalyst particles with the monomer they need to function at full potential. The characteristic time for diffusion to occur inside a catalyst particle is equal to the diffusivity divided by the square of the particle radius. Thus, if we have a particle with a radius of 10 microns, and one with a radius of 20 microns, it will take four times longer for a molecule of ethylene to diffuse from the surface to the center of the larger particle. It is, therefore, more likely that mass transfer resistance will occur in larger catalyst particles; i.e. larger particles will be undersupplied with monomer so polymerize more slowly than smaller ones. Moreover, gradients of concentration (i.e. lower

monomer concentration at the center than the outside) mean that we will have gradients of MWD inside the particle in certain cases.

While a great deal of modelling has been done on this point, very little experimental work has been published on the impact of particle size, despite its importance. Fink et al.,[121-123] performed slurry phase homopolymerizations of propylene in toluene at 2 bar and 40 °C for different particle diameters; all other parameters were kept constant. Silica support particle size (or diameter) was varied in the range of 10 to 80 µm. rac-$Me_2Si[IndR_2]_2ZrCl_2$ was mixed with MAO solution in toluene prior to its fixation on dehydroxylated silica, followed by stirring at a specific temperature and then washing and finally vacuum drying. However, due to a patent application filed at that time, the authors gave no information about the silica dehydroxylation temperature and catalyst synthesis temperature. TIBA was used as the scavenger in slurry reactions and the propylene pressure for polymerization was. SEM-EDX analysis of the catalyst particles showed that MAO was uniformly distributed throughout the smaller catalyst particles, whereas core-shell distribution was observed for bigger catalyst particles which lead to higher MAO concentrations at the surface than at the particle center.

Homopolymerization rate profiles with the catalysts of different sizes clearly showed that the smaller the catalyst particle size the higher the instantaneous activity, and the shorter the induction period. An induction period of about 40 minutes was observed in the case of polymerization conducted with 80 µm catalyst, whereas for the catalyst of 10 µm diameter this induction period was negligible. In order to have a further insight into the effect of particle size, the authors conducted reactions of very short time (i.e., 1 minute), intermediate time (i.e., 20 minutes) and long times of 90 minutes followed by microtoming of the polymer particles and analysis by SEM. This cross-sectional analysis of the polymer particles clearly showed the presence of polypropylene layer around the particle surface until the first 20 minutes of reaction time for all the particles of different sizes. After 90 minutes, the catalyst particles of 35 µm and 50 µm were found to be completely filled with polymer with no big fragments of silica support whereas the polymer particles produced with 80 µm catalyst still contained unfragmented silica core.

Based on these results the authors proposed that the initial polypropylene film formed around the catalyst surface acts as a barrier to monomer transport inside the particle leading to the induction period and as the reaction goes on more and more polymer is formed which consequently fragments

the catalyst particles making easier the monomer transport at the active sites and therefore, causes disappearance of the induction period in the kinetic profiles. DSC results of the obtained polymer samples showed that the crystallinity of the polypropylene formed during first 6 minutes of reaction time was higher than that of the polymer formed after 20 minutes of reaction time and after 20 minutes it remained unchanged. In the case of 80 µm catalyst particles, the core-shell distribution of Al suggested that the core of the catalyst particles did not take part in the reaction and therefore, appeared as unfragmented silica core in the microtommed polymer particles even after 90 minutes of polymerization. These observations also suggested that the particle fragmentation starts from the outer surface and moves towards the particle center.

Weight average molar mass (M_w) of the polypropylene produced with smaller and more active catalyst particles (e.g., 35 µm catalyst) was 450000 $g.mole^{-1}$, higher than that of the polypropylene produced with bigger (80 µm catalyst), less active catalyst particles, which was found to be 250000 $g.mole^{-1}$. Overall, the Mw values didn't show significant dependence on polymerization time. Dispersity of the molar masses was not significantly affected by the catalyst particle size as it remained in the range of 2.2 to 4.0 and did not show a trend with respect to polymerization time and/or particle size. The lower mass of the polymer produced with bigger catalyst particles was attributed by the authors to the variations in the spatial distribution of Al in bigger catalyst particles which have higher Al content on the outer surface that might have led to increased chain transfer reactions at the particle surface than at the interior of the particle where MAO was present in lower concentrations. On the other hand, smaller catalyst particles showed uniform Al distribution which lead to higher activity and higher molar masses probably due to lower chain transfer reactions. This work also provides a good example about the existence of mass transfer resistance during early stages of olefin polymerization but it should be noted that the monomer pressure used in polymerization was significantly lower than those employed industrially and Floyd et al.,[124] predicted, by using MGM, that the mass transfer resistance in slurry phase olefin polymerizations will be higher at lower monomer pressures than at higher ones.

In a more recent work, Tisse et al.,[125,126] also analyzed the impact of the size of a silica support on the reaction kinetics and molar mass distribution of homo- and copolymers. A master batch of the commercial silica was sieved in fractions ranging from 36 to 100 µm. Each sieved fraction was used to support rac-$Et(Ind)_2ZrCl_2$ either by first converting the sieved fraction into an activating

support or by impregnating it with MAO. The two commercial silica supports used were SP9_446 and Grace 948 which have very similar pore volumes of about 1.8 $mL.g^{-1}$, but the surface area and pore diameters are significantly different (i.e., SP9_446 has surface area of 520 $m^2.g^{-1}$ and pore diameter of 13.1 nm whereas Grace 948 has surface area of 290 $m^2.g^{-1}$ and pore diameter of 23.2 nm). Elemental analysis showed very similar metal loadings on all the catalysts, suggesting that any observed effects of support size on the catalytic activity should be due to physical properties of the support, rather than to an uneven distribution of active sites. EDX analysis of the catalyst particles showed uniform Al and F distribution throughout the surface and interior of the particles in the case of activating supports (SMAO support particles could not be analyzed by EDX). Slurry phase homo- and ethylene/1-hexene copolymerizations with TIBA as scavenger showed that, for both support types, the smaller the particle size of the silica support, the higher the catalytic activity, and the faster the polymerizations reached their maximum activity. However, with this metallocene, the molar masses of the homo- and copolymers remained unaaffected by the changes in support particle size.

The visibly significant differences in the kinetic profiles of catalysts of different sizes allowed the authors to attribute these differences to the existence of higher mass transfer resistance in the case of bigger catalyst particles as compared to that in the case of smaller catalyst particles. On the other hand, since the molar masses of the polymers and their dispersity were practically identical, the authors also suggested that the observed difference in the kinetic profiles of different sized catalyst particles cannot be solely due to the presence of mass transfer resistance as if there exists mass transfer resistance in larger particles then they should produce polymers with low molar mass as well as their molar mass distributions should be broader than the ones produced with smaller sized catalyst particles. It was also shown by Tisse et al.,[125,126] that the fine particles appearing in the full silica batch come from the smallest particles present in the full silica batch and are not the result of uncontrolled particle fragmentation or particle sintering. Finally, one important point which needs to be highlighted here is that in all the polymerizations, SMAO based catalysts were pre-contacted for 10 minutes with TIBA prior to their injection into the reactor. As it will be shown in the coming chapters, this pre-contact between the SMAO based catalyst and TIBA can lead to catalyst leaching which can cause homogeneous and heterogeneous polymerizations going in parallel. This point was not addressed by the authors.

More recently, Tioni et al.,[127] used sieved fractions of Grace 948 silica and supported MAO on each sieved fraction which was dehydroxylated at 200 °C prior to the fixation of $(n\text{-BuCp})_2ZrCl_2$. The resulting supported catalysts also showed that the smaller particles were more active in comparison to their bigger counterparts in gas phase ethylene/1-butene copolymerizations (at 80 °C, 6 bar ethylene and 0.25 bar 1-butene pressure). The differences in catalytic activities of smaller and bigger catalyst particles were attributed to the higher level of mass transfer resistance in bigger diameter particles as compared to that in the smaller sized particles.

5.5.3.2. Effect of Silica Porosity

Porosity is a general term which refers to the physical properties of silica like pore size, pore size distribution, pore volume and surface area collectively. Mercury intrusion and nitrogen adsorption porosimetery are two most common analytical techniques employed to estimate silica porosity. While mercury porosimetery provides information about average particle size, density, macropores, average pore volume, the nitrogen porosimetery provides more information about micro-, meso- and macroporosity levels. Most of the earlier works related to silica supported metallocene/MAO catalysts employed nitrogen adsorption porosimetery for the estimation of the surface area, average pore volume, average pore diameter, pore size and pore volume distributions of the silica supports and the final supported catalysts. Among different available methods, Brunauer–Emmett–Teller (BET) theory is most commonly used to estimate the specific surface area of silica supports and the supported catalysts, whereas the average pore volume and pore size distribution of a given sample are preferably estimated by employing Barrett-Joyner-Halenda (BJH) method. By using BET specific surface area and BJH average pore volume, one can estimate the average pore diameter by using the simple relationship of pore diameter = (4×pore volume)/specific surface area. Desorption branch of the nitrogen porosimetery isotherm is generally preferred in the estimation of pore size because of its smoothness as compared to the adsorption branch.

Just like particle size, silica support porosity also plays its role during the synthesis of supported catalysts as well as during olefin polymerization process. Depending upon the method of catalyst synthesis and molecular dimensions it can have a strong influence on the distribution of catalyst and/or co-catalyst inside the support particles. It should be noted that pore morphology is typically divided into three families depending upon the pore size. Micropores are those pores with a

diametere less than 2 nm, mesopores have diameters from 4-200 nm, and macropores have diameters greater than 100 nm (0,1 μm).[128] It is claimed that the mesoporosity has the strongest influence on catalyst performance for silica-supported catalysts.[96]

Soga et al.,[129-131] analyzed the impact of the pore diameter of the mesoporous silica supports on the catalytic activities of ethylene homopolymerization with Cp_2ZrCl_2 catalyst and propylene homopolymerizations with rac-ethylenebis(indenyl) zirconium dichloride (rac-$Et(Ind)_2ZrCl_2$) in slurry process. The basic idea behind the work of these authors was to separate methylaluminoxane (MAO) on mesoporous MCM-41 silica of different pore sizes, and use the MAO impregnated supports in olefin polymerizations to assess the impact of support pore size on catalytic activity, polymer physical and molecular properties and the number of active species taking part in polymerization. The word 'separate' was used by the authors because it is believed that MAO is a mixture of several oligomers which would allow different oligomers to enter pores of different sizes. As a comparison, the authors also used silica gels and silicalite as supports. Before impregnating the supports, they were all treated with trimethylchlorosilane in order to consume the silanol groups present on each silica. This silylation of the supports allowed the MAO to physically absorb on the silica surfaces.

The pore diameter of the silicalite support was the lowest with the value of 0.56 nm, and that of MCM-41 supports varied systematically from 1.8 to 3.5 nm whereas the silica gels had pore diameters in the range of 7.2 to 29.3 nm. MAO was supported on each silylated silica at room temperature followed by decantation, and triple washing with toluene and vacuum drying at room temperature. The Al content of the decanted liquid and MAO impregnated silica (SMAO) samples was analyzed by ICP-AES. The results showed that the silicalite support afforded the lowest Al content, presumably because it had the smallest pore diameter, whereas the MCM-41 supports attained almost same amounts of Al, varying over a very narrow range of 5.56 to 5.71 wt% and the same Al content was also noticed on the silica gels.

Ethylene homopolymerizations performed for 30 minutes at 40°C in toluene. It was observed that the activity of the supported Cp_2ZrCl_2/SMAO catalysts were correlated with the pore diameters of the supports in each experiment. When the pore diameter of the support was too low, like for silicalite supported catalyst, the catalytic activity was minimal. In the case of the catalysts supported on MCM-41, the activity increased with increasing pore diameter, and showed a

maximum value for the catalyst supported on 2.5 nm pore diameter MCM-41 silica followed by a decrease in activity on further increase in support pore diameter. In case of silica gel supported catalysts, activity was higher for the catalyst supported on the gel with the smallest pore diameters. Note, of course, that the smallest pores in the silica gel are much larger than the largest pores in the MCM-41, so this is coherent with the results using the latter support. Molar mass dispersity of the polyethylene samples produced with MCM-41 based catalysts was very similar in a narrow range of 2.9 to 3.7. The presence of mass transfer resistance to monomer transport at the active sites was proposed to explain the higher molar mass dispersity values in comparison to those of the polyethylene samples produced in homogeneous polymerizations. Note that the ethylene pressure used in the reactions was not mentioned and the Al/Zr molar ratios of the final catalysts were in the range of 70-90. In addition, trace amounts of leaching were also noticed by the authors.

Similar results are reported by the authors for propylene homopolymerizations[130,131] with rac-$Et(Ind)_2ZrCl_2$ supported on the same SMAO samples with different pore diameters but with the Al/Zr ratios fixed at 40. It is important to mention here that in case of propylene polymerizations, the zirconocene was added to a toluene suspension of SMAO samples followed by 1 h stirring at the room temperature before addition of 7 L of propylene into the reactor and reaction start-up at 40 °C. It should also be highlighted here that no information was provided about the PSD of all the silica used. This information is important because, as we shall see in coming chapters, it is easy to compare the effect of one physical property of the silica supported catalyst on the catalytic activities (and on the properties the polymer produced) only if the other physical and chemical properties of the supports are kept (reasonably) constant. In addition, the different silica types used in this work (i.e., silicalite, MCM-41 and silica gel) have different pore structures e.g., regular arrays of uniform and uni-directional pores are present in MCM-41 silica, whereas, the pore structure of silica gel is not that uniform and may contain various diffusional paths for the species like co-catalyst, catalyst and monomer(s). These differences in the pore structure of silica supports could have a significant effet on the distribution of active species throughout the particles during catalyst synthesis. An uneven distribution of active species could in turn impact the fragmentation of the support and subsequently, the expansion of catalyst/polymer particles.

Silveira et al.,[132] used two metallocenes (Cp_2ZrCl_2 and $(n\text{-}BuCp)_2ZrCl_2$) in the ratio of 1:3 to study the impact of textural properties of various supports on the supported catalytic activity in ethylene

homopolymerization, and on the molecular and physical properties of the final HDPE. The supports used included a variety of materials ranging from conventional Grace 956 silica, pure alumina, various alumino-silicates like MCM-41, SBA-15, MCM-22 and non-conventional supports like chrysotile and ITQ-2. According to the authors, ITQ-2 is described as a delaminated zeolite, whereas, chrysotile is a kind of natural nano-fibriform mineral, containing silica and brucita and both of them have never been used as catalyst supports in olefin polymerization. In all the supported catalysts, Cp_2ZrCl_2 was first reacted with the supports (dehydroxyalted at 450 °C) followed by the fixation of $(n\text{-}BuCp)_2ZrCl_2$ at room temperature. Slurry phase ethylene polymerizations were conducted at 60 °C for half an hour in a 0.3 L pyrex glass reactor with toluene as a diluent and ethylene pressure of 1 bar. It should be noted that rather than supporting MAO on the catalyst it was fed separately into the reactor in such a way that Al/Zr molar ratio was set to 1000 in all the reactions. Before evaluating the catalysts, the authors conducted leaching tests on the catalysts and found that the leached Zr content varied between 0.1 to 0.5 wt% of the supported Zr content. Leaching was shown to be highest (0.5 wt%) in the case of Grace 956 silica and lowest (0.1 wt%) in the case of alumina supported catalyst.

Within a given class of support material, catalytic activities were found to be higher for the catalysts with larger pore diameters. The authors attributed this effect to the easy fixation of metallocenes within larger pores, along with easy access of MAO and monomer to the supported metallocene. The smallest pore diameters were found to be of the catalysts supported on ITQ-2 (1.4 nm) and MCM-22 (1.9 nm). The catalysts made from these materials showed the lowest activities. According to the authors, this was probably due to the fixation of the used metallocenes on the external surface of the particles which made them more prone to deactivation.

With respect to size of the support particles, it was found that, within the same class of support material, smaller catalyst particles showed higher average activities than their bigger counterparts despite differences in their metal loadings which is in agreement with the results of Fink et al.,[121] and Tisse et al.[125,126] discussed above. When the average activities of all the supported catalysts were compared, regardless of whether they were on an alumino-silicate or pure silica support, no clear trend was established in terms of the impact of particle size or pore diameter. It should be kept in mind here that different support materials will have different physical characteristics (e.g. resistance to fragmentation), as well as differences in the surface groups. For instance, alumina is

known to have an amphoteric character due to the presence of both Lewis acidic and basic sites on its surface. In the case of molar mass, the results obtained showed that the average molecular weight decreased with increasing pore diameter. The authors attributed this to a phenomenon called extrusion polymerization in which the polymer being formed is continuously moved away from the active sites and extruded out of the pores leading to reduction in chain transfer reactions. It is important to mention that no kinetic rate profiles of the reactions were shown by the authors which would have been helpful for the reader to see differences in catalyst activation due to varying pore diameters of the used supports.

In another work from the same group,[133] three different commercial silicas of W.R. Grace (i.e., Grace 948, Grace 955, Grace 956) along with two xerogel silicas and one aerogel silica prepared in-house were used to study effects of textural properties of the silica supports on the catalytic activity and polymer properties. Same hybrid catalysts were prepared by using Cp_2ZrCl_2 and $(n\text{-}BuCp)_2ZrCl_2$ in 1 to 3 ratio under exactly the same conditions as described in the previous paragraph. The polymerization procedure and conditions were also kept similar to those used in the previously discussed work.[132] Based on half hour reactions, it was found that the catalysts supported on W.R. Grace silicas showed highest activities while the lowest activities were observed for the two xerogel based catalysts; with activities from the aerogel supported catalyst being between the two. When the activity (in $kgPE.moleZr^{-1}.h^{-1}$) is plotted against pore diameter of each catalyst, there was a trend as shown in **Figure 11**. However, a closer look at **Figure 11** reveals that among the catalysts supported on three W.R. Grace silicas, the highest activity is shown by the catalyst with the lowest pore diameter i.e., the one supported on Grace 948 silica. The authors attributed low activities of the catalysts with low pore diameters to the possibility of the formation of inactive bidentate species which is significantly high if the support pore diameter is below 10 nm (i.e., 100 Å) because at such low pore sizes the negative surface curvature keeps the silanol groups very close to each other which favors the formation of hydrogen bonds between them and, consequently, hinders their removal during heat treatment. It should be noted that the two metallocenes were supported on the naked silicas bearing isolated silanols only and, therefore, this explanation seems reasonable. In addition, the same explanation seems equally applicable to the results discussed in the previous paragraph. When plotted against the particle size of each supported catalyst, the average activity decreased with increasing the catalyst particle size. Based on the molar masses of the produced polyethylene samples, the authors concluded that the molar mass increased

with increasing the pore diameter of the final hybrid catalyst. Once again no kinetic profiles were provided by the authors. Based on these two works [132,133] it can be concluded that trends observed for low pore diameter catalysts can be attributed to the increased possibility of the formation of inactive bidentate species (due to close proximity of the silanol groups on surface) and no treatment of the used silicas with an appropriate co-catalyst like MAO prior to metallocene grafting which can also avoid the formation of bidentate species. Furthermore, the particle sizes of the used supports were also significantly different.

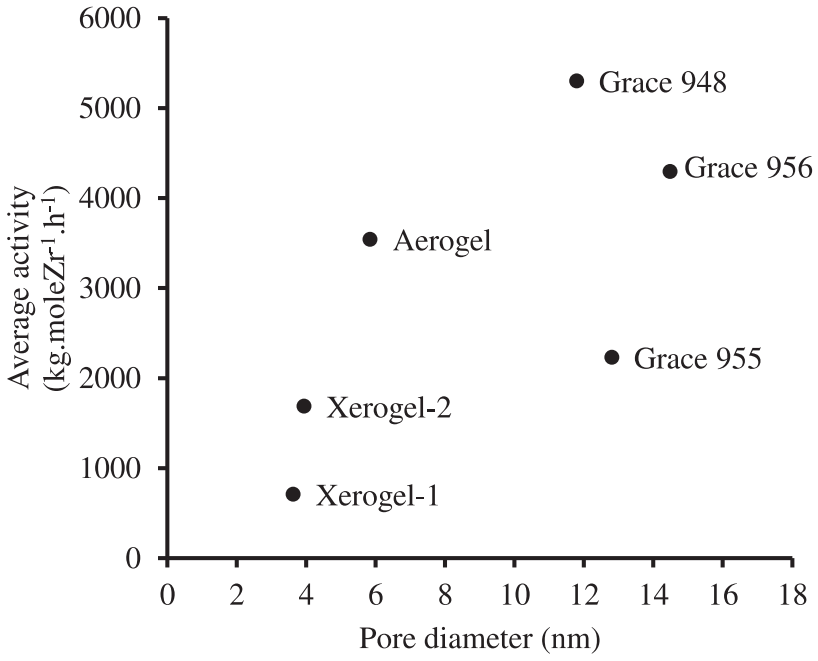

Figure 11. Dependence of the average catalytic activity on the pore diameter of the final supported catalyst. Data obtained from Figure 8 of dos Santos et al.[133]

Jongsomjit et al.,[134] analyzed the impact of pore size of pure silica and silica-Alumina (Si-Al) support on the activity of rac-Et(Ind)$_2$ZrCl$_2$ in slurry phase ethylene/1-octene copolymerization at 70°C and 3.4 bar ethylene pressure. The two pure silica supports used had unimodal pore size distribution with one support having average pore diameter of 13.7 nm and a pore volume of 1.50 mL.g^{-1} whereas the second silica support had a pore diameter of 33.8 nm with pore volume of 0.26

1.50 mL.g^{-1}. The third Si-Al mixed support had a bimodal distribution of pore size with the average pore diameter of small pores equal to 3.8 nm and that of larger pores equal to 33.6 nm. The pore volume of Si-Al mixed support was 0.30 mL.g^{-1}. Modified methylaluminoxane after drying under vacuum (i.e., dMMAO) was supported on all the used supports and the metallocene complexed with TMA in a toluene solution was added into the reactor separately. The silica support with the largest pore diameter had the highest Al content of 18.9 wt% after dMMAO impregnation step, in contrast to the other two supports which attained very similar Al content of about 12 wt%. SEM-EDX analysis of the dMMAO treated silica particles showed that Al was evenly distributed on each silica surface but no cross-sectional analysis of these particles was presented in order to show the Al distribution inside the support particles.

During very short time copolymerization reactions, the $[Al]_{dMMAO}/[Zr]$ ratio was kept constant at 1135 which is almost three orders of magnitude higher than those used in this work. Their results show that highest catalytic activities were obtained with the catalyst supported on the silica with the largest pore diameter, whereas, the one supported on Si-Al mixed support was the least active and the one supported on smallest pore diameter pure silica showed intermediate activity. The authors proposed that due to higher dMMAO loading of the silica support with the largest pore diameter, the concentration of active sites was higher on that catalyst as compared to the other silica support with the lower pore diameter and lower dMMAO loading. In the case of Si-Al mixed support based catalyst, Thermal Gravimetric Analysis (TGA) revealed that the interaction of dMMAO with the support surface was significantly stronger than in the case of two other pure silica supports which, consequently, led to the reduced activity of the final supported catalyst. It is important to mention here that a co-catalyst bound strongly with the support cannot lead to a highly active metallocene catalyst due to its inability to interact with the metallocene.[134] Comonomer content of the polymer produced with the catalyst supported on smallest pore diameter was found to be the highest. Overall, the authors did not attribute the observed differences in catalytic activities purely to the physical properties of the silica supports. In addition, no information is provided by the authors about the particle size of the used silica supports since it is also an important physical property of the silica supports used in heterogeneous catalysis.

Using exactly the same catalyst synthesis procedure and copolymerization conditions, the same group[135] analyzed the effect of pore size of MCM-41 mesoporous silica supports on the activity of

the same metallocene (i.e., rac-Et$(Ind)_2ZrCl_2$). Once again, dMMAO was used as the co-catalyst. One of the MCM-41 silica supports used in this study possess unimodal pore size distribution with small pores having an average diameter equal to 2 nm. The other MCM-41 supports have a bimodal pore size distribution with large and small pores with the average pore diameters of 5 and 6 nm. The unimodal support has specific surface area of 864 $m^2.g^{-1}$ which is 2 times the specific surface area of the two other bimodal supports. All the silica supports contained 27 wt% of Al after impregnation with dMMAO at room temperature. As in the previous study,[134] copolymerization reactions of very short times (i.e., in the range of 27 to 186 seconds) indicate that the catalyst supported on the silica with bimodal pore size distribution (those having both small and large pores and smaller surface area) are more active (approximately 30%) than the one supported on silica with unimodal pore size distribution (i.e., the silica having higher surface area and small pore size). The authors proposed that although the smaller pore size leads to higher surface area and better dispersion of the co-catalyst and catalyst, mass transfer resistance to monomer(s) transport within the pores at the reaction start-up and during the course of polymerization is higher which leads to the low activity of the final supported catalyst.

On the other hand, the support with bimodal pore size distribution provides the benefit of good active sites' distribution (due to small pores) and reduced mass transfer resistance to monomer(s) transport (due to large pores) which leads to higher catalytic activities. In contrast to this explanation based on support geometry, TGA analysis of the three dMMAO/silica support catalyst revealed that the interaction of dMMAO with the unimodal small pore sized MCM-41 silica supported was significantly stronger than its interaction with bimodal large pore sized MCM-41 supports. This observation provided an explanation to the differences in the observed catalytic activities based on the chemical differences in the catalysts prepared with small and large pore diameter silica supports (as the stronger interaction of the co-catalyst with the small pore sized silica support reduces its ability to activate the catalyst molecules in comparison to a silica support which has larger pore diameter but weaker interaction with the co-catalyst).

Furthermore, the polydispersity of the molar mass distribution of the copolymers produced with larger and bimodal pores was about 2 times higher than that of the copolymer produced with catalyst supported on small sized unimodal silica support which also indicates the differences in the nature of the active sites in the final catalysts and supplements the idea that the observed

differences in catalytic activities of these catalysts are probably due to chemical reasons. Once again, there is a lack of information about the particle size (and distribution) of the used MCM-41 supports. Furthermore, it is important to highlight here that the weaker interaction of dMMAO with larger pore diameter supports might have also caused leaching of the co-catalyst from the support into the reactor diluent (i.e., toluene) and there is a chance that the higher activities observed with these catalysts could be the result of homogeneous polymerization occurring in parallel to heterogeneous polymerization. However, the authors ruled out this possibility by saying that leaching, if present, was negligible. However, it should be noted that the activity differences observed with these catalysts was about 30% for the very short reaction times, which is not nothing but insignificant.

Tisse et al.,[126] evaluated the impact of silica support porosity and particle size distribution of silica supports on the activity of supported rac-Et(Ind)$_2$ZrCl$_2$ metallocene. This work used two types of activation processes for rac-Et(Ind)$_2$ZrCl$_2$; i) activating supports having aluminum (Al) and fluoride (F) species attached on them which gives enough acidity to the supports so that they can activate the metallocene for olefin polymerization[90] ii) silicas impregnated with MAO (SMAO) in order to have variety and correlate the observed trends with the type and size of activator used in addition to the support properties. All the supported catalysts were prepared on commercial silicas. The pore volumes of the silica supports varied in the range of 1 to 3.2 mL.g^{-1} with the corresponding pore diameters within 3.7 nm to 40.0 nm range, and the corresponding surface areas of these silica laid in the range of 290 to 800 m^2.g^{-1}. Slurry phase ethylene homo & copolymerizations with 1-hexene were conducted at 80 °C in a 2 L reactor with 6 wt% ethylene in heptane and, where applicable, 2.44 wt% 1-hexene in heptane. No information about the metal loadings was provided for the catalysts based on full batches of silica supports, however, for activating supports the Zr/support ratio was kept constant at 0.4 wt% of Zr, whereas, in case of SMAO the targeted amount of final Al content on each support was 15 wt% and that of Zr loading was 2 wt% which is significantly high.

Although the authors concluded that based on the polymerization activities (of both types of activated catalysts), no clear trend could be established between the catalytic activity and support properties like the pore volume, pore diameter and surface area. **Figure 12** shows their tabular data in graphical form and correlates the pore volume and pore diameter of each support with the

reported average activity and surface activity (obtained by dividing the reported average activity with the corresponding reported surface area of the support because the surface area of final catalysts is not given by the authors). It can be noticed in **Figure 12a & b** that both the average activities and surface activities show a maximum value close to a pore volume of 2 $mL.g^{-1}$ after which they decrease and remain almost constant. When plotted against pore diameters, a more or less similar trend can be noticed with initial rise in activities with a maximum at about 25 nm followed by decreasing activities on further increase in pore diameter up to 40 nm (see **Figure 12c & d)**. One can see two peaks in **Figure 12c & d** but for the sake of simplicity we can neglect the initial peak at about 13 nm. These graphs at least provide some idea that pore volume and pore diameter of the silica supported catalyst are very important physical parameters and have to be optimized in such a way that the catalyst neither becomes totally inactive (e.g., see the first point in **Figure 12a & d**) or its activity is the lowest within the selected range. To supplement these observations, **Figure 12e** shows the activity vs pore diameter graph of Soga et al.,[129] which also shows similar dependence of catalytic activity of the same metallocene supported on different silica in slurry phase ethylene polymerization at different conditions. The most probable explanation for this type of dependence of catalytic activity on the pore volume and pore diameter of the silica supports is that, once inside reactor, fragmentation of the supported catalyst with low pore volume will occur faster than that of a catalyst with higher pore volume (assuming similar metal loadings and same support fragility) which leads to higher activities of low pore volume (and diameter) catalysts. However, we should note that no comparison of the kinetic profiles of such catalysts was provided by both the authors along with the fact that Tisse et al.,[126] used silicas from various manufacturers which may have been made with different production processes and therefore, should have different pore structures and fragility levels.

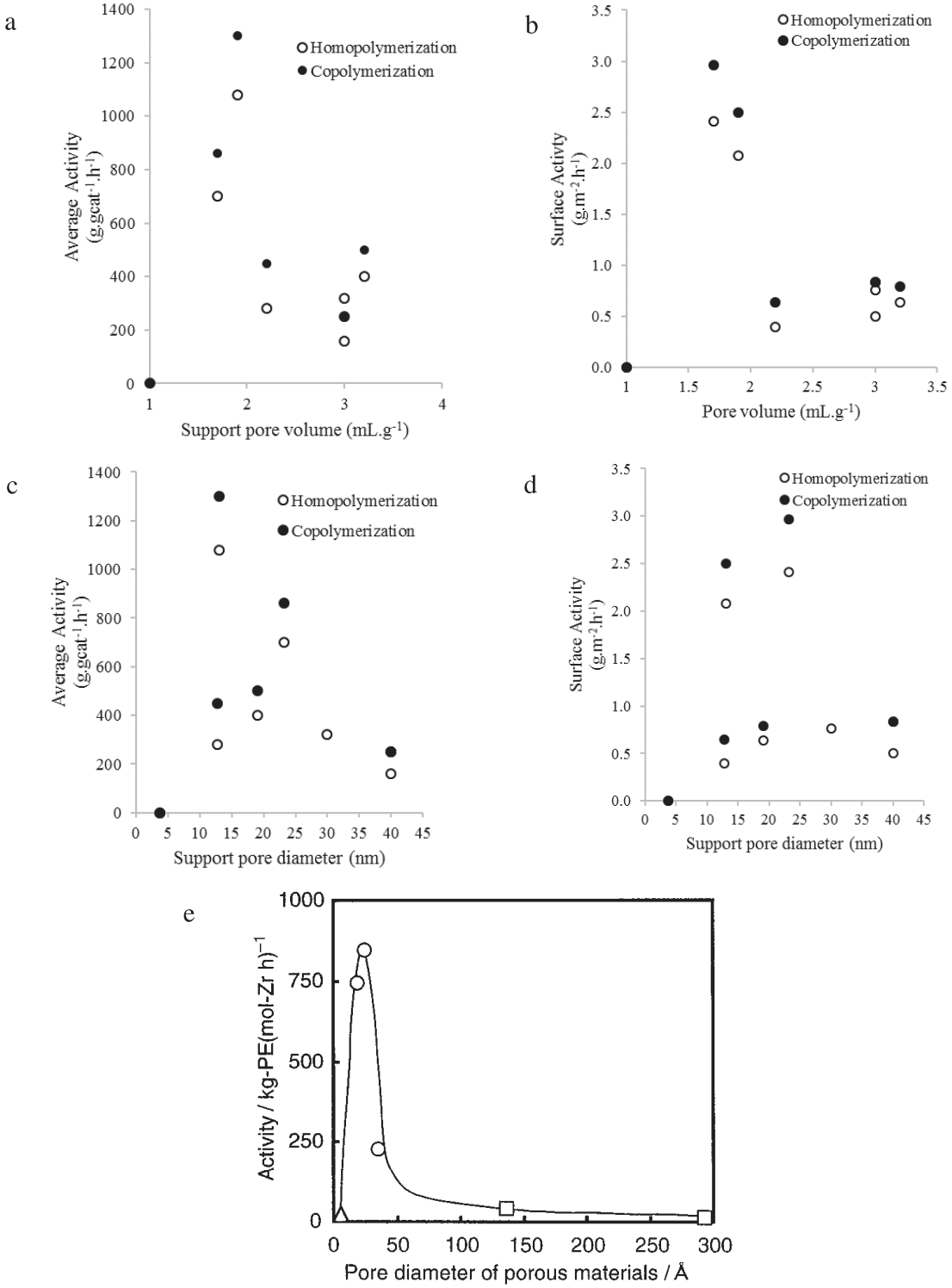

Figure 12. Graphical presentation of the experimental data reported by Tisse et al.,[126] on average activities, pore volumes and pore diameters of the activating support based catalysts (a-d). The data of Soga et al.,[129] presented with permission in 'e'.

The above mentioned research work employed slurry phase polymerizations. Gas phase ethylene polymerization studies focused on investigating the impact of support's physical properties on the reaction kinetics of silica supported metallocenes and the polymer produced thereof are rather scarce in the open literature. The work of Kumkaew et al.,[136] is one of the few available examples where the authors have made an attempt to analyze the impact of pore diameter of mesoporous molecular sieves on the reaction kinetics of supported $(n\text{-BuCp})_2ZrCl_2$ catalyst in gas phase ethylene homo and ethylene/1-hexene copolymerizations. Various molecular sieves with pore diameters in a broad range of 2.6 to 25 nm were used to first support MAO at room temperature for 12 h, followed by the grafting of $(n\text{-BuCp})_2ZrCl_2$ at room temperature for 4 h, after which vacuum drying at room temperature for several hours provided the free flowing supported catalysts. It should be noted that no washing step was employed during any stage of the catalyst synthesis and since the MAO was supported before the metallocenes fixation these catalysts fall in the "category of SMAO based catalysts". One silicalite support (which is basically an aluminium-free pentasil-type zeolite) of pore diameter equal to 0.54 nm and one silica-gel support of pore diameter equal to 16 nm was also used in order to have variety and compare the performance of mesoporous molecular sieves based catalysts with the catalysts supported on these ones. Gas phase homo- and copolymerizations were performed in a 1 L reactor using dried NaCl as a seeded in the temperature range of 50 to 100 °C and at different pressures by using TIBA as a scavenger for 2 h.

The authors started their investigations by first analyzing the impact of Al/Zr molar ratio of the supported catalyst on the catalytic activity and found that by increasing this ratio of the supported catalyst from 100 to 170 the average activity increased about 6 times and therefore, fixed the Al/Zr molar ratio of all other catalysts used to analyse the impact of catalyst pore diameter to 170. In addition to Al/Zr ratio, it is also shown by the authors that the amount of TIBA utilized as a scavenger can also have a strong effect on the kinetic profile of the supported catalyst i.e., low amount of TIBA allows the catalyst to activate and then deactivate faster whereas higher TIBA concentration leads to longer the induction periods which can last up to 40 minutes before the catalyst starts to show some activity. By fixing the TIBA content in the reactor to 0.6 mmole per liter and Al/Zr molar ratio of the catalysts to 170, the gas phase polymerizations showed that the catalysts with the smaller pore diameter attained higher instantaneous and average activities in comparison to the catalysts with larger pore diameter. However, the lowest pore diameter catalyst

based on silicalite showed very low activity which the authors attributed to the inability of MAO diffusion into its pores of 0.54 nm.

The same dependence of the catalytic activity on its pore diameter was also noticed for copolymerization reactions. The instantaneous activity profiles of the catalysts also showed distinct differences based on their pore diameters i.e., the catalyst with smaller pore diameter showed relatively faster activation and took less time to achieve its peak activity after which it should continuous deactivation, whereas, the catalyst with larger pore diameter showed broad kinetic profiles in which it showed relatively slower activation and took more time to reach the peak activity followed by continuous deactivation. This difference in the kinetic profiles was more pronounced at higher reaction temperatures than at the lower ones. Average molar mass dispersity of the polyethylene samples was close to 2.5 and the molar masses along with their dispersities did not show any specific trend with the pore diameter of the used silica supports. It is important to mention here that the particle sizes of the used supports were not kept constant in this study e.g., the catalyst with pore diameter of 2.6 nm had particles in the range of 100 to 300 µm whereas the one with pore diameter of 5.8 nm had fibrous particle structure with sizes in the range of 20 to 50 µm. For other supported catalysts no information was provided by the authors about their particle sizes.

In the extension of the same work, Kumkaew et al.,[137] studied the effect of support pore diameter on the incorporation of 1-hexene into polyethylene at different temperatures and 1-hexene concentrations by employing different polymer characterization techniques like Temperature Rising Elution Fractionation (TREF) along with conventional DSC and HT-SEC. TREF analysis provided information about 1-hexene content of the LLDPE sample and the number of active sites involved in the reaction. The focus of this work was only on molecular sieves supported MAO and $(n\text{-BuCp})_2ZrCl_2$ catalyst and one silicalite support. Catalyst synthesis procedure was kept similar to that used in the previous work.[136] Pore diameters of the catalyst were varied systematically from 2.5 nm to 20 nm for molecular sieve supports with the lowest pore volume of 0.6 $cm^3.g^{-1}$ corresponding to 2.5 nm diameter catalyst and highest pore volume of 1.6 $cm^3.g^{-1}$ corresponding to the support with the widest pore of 20 nm. The effect of increasing initial 1-hexene concentration inside reactor was studied only with the most active catalyst of 2.5 nm pore diameter. The results obtained showed that the catalytic activities were higher if the initial concentration of 1-hexene

inside the reactor was below 12 mole.m^{-3} whereas initial 1-hexene concentrations in excess of 18 mole.m^{-3} reduced the instantaneous activity to such an extent that the polymer yields were lower than those obtained in homopolymerizations. By ruling out the presence of any mass transfer resistance at higher 1-hexene concentrations, the authors attributed this behavior to the increase in gas phase temperature inside the reactor during the polymerization process at lower initial 1-hexene concentrations which indicates heat accumulation inside the reactor and poor heat removal from the reactor.

TREF results of the copolymer samples obtained by using catalysts of pore diameters in the range of 2.6 to 20 nm showed at least two distinct peaks, one in the temperature range of 55 to 70 °C and the second one at about 98 °C. With increasing catalyst pore diameter, the low temperature peak (i.e., in the range of 55 to 70 °C) became dominant indicating enhanced 1-hexene incorporation and reduced formation of homopolymer (note that the activity decreased with increasing the catalyst pore diameter). The presence of minimum two distinct peaks in TREF results also indicated that there were at least two types of active sites from which one site was mainly producing homopolymer corresponding to the peak at 98 °C and the other site(s) were responsible for producing LLDPE corresponding to low temperature peaks. Based on these results, the authors suggested that the nature of active sites formed on a supported catalyst can be effected by its pore size. Since the catalyst with smaller pore diameters showed high amounts of homopolymer in comparison to those with bigger pores, the authors suggested that the confined (i.e., small) pore size probably effects the structure of supported MAO and, consequently, the nature of interactions between MAO and $(n\text{-BuCp})_2ZrCl_2$ which leads to active species that produces higher amounts of homopolymer. As the support pore size is increased this effect of confined space reduces leading to a different type of active site which incorporates higher 1-hexene.

Experiments of different reaction times but constant 1-hexene initial concentration showed that the produced polymer had a higher homopolymer fraction during the first 30 minutes and as the reaction time increased up to 2 h the homopolymer fraction decreased significantly whereas the copolymer fraction seemed to be affected slightly by variations in the reaction time. The authors suggested that either the homopolymerization sites transform to copolymerization sites with reaction time or the homopolymerization sites deactivate faster than the copolymerization sites over the reaction period.

In another series of experiments with the catalyst of 2.5 nm pore diameter, TREF analysis of the polymer samples showed that by keeping the catalyst pore diameter constant but increasing the initial 1-hexene concentration inside the reactor can also change the active sites in such a way that no homopolymer is produced at high 1-hexene concentrations of 47.2 mole.m^3 whereas at intermediate 1-hexene concentrations of 18.5 to 25.8 mole.m^3 the fraction of the homopolymer inside the final polymer sample dominates the copolymer fraction just like at low 1-hexene initial concentrations. These observations confirmed that the quantity of 1-hexene present inside the reactor, and at the active sites, can alter the behavior of active sites present in a supported metallocene/MAO catalyst. This trend was also obvious in the molar dispersity values which showed an increase from 2.5 to 4.0 with increasing 1-hexene concentrations from 0 to 47.2 mole.m^3. DSC analysis of the obtained polymer samples were also found to be coherent with those of TREF analysis and indicated that as the catalyst pore diameter increased multiple crystallization peaks start to appear at low temperatures due to increased 1-hexene incorporation, as discussed before.

Recently, Tioni et al.,[138] studied the impact of silica support on the evolution of thermal properties of polyethylene by conducting very short time reactions in a specially designed stop flow reactor. Grace 948 silica supported (n-BuCp)$_2$ZrCl$_2$ and rac-Et(Ind)$_2$ZrCl$_2$ catalysts were prepared by first impregnating the silica with MAO followed by metallocene grafting. Gas phase ethylene homo- and ethylene/1-butene copolymerizations were conducted for the time as short as 0.3 seconds at 9 bar ethylene pressure and at 80 °C. The results obtained indicated that the polyethylene produced during very early stages of polymerization (i.e., after 0.3 seconds) is mainly amorphous with melting temperature at about 118 °C and as the reaction continues up to 180 seconds the crystalline polymer fraction becomes significant leading to a melting temperature of 131 °C. Polyethylene crystallization peaks also showed similar dependence on the polymerization time. The authors attributed this observation to the pore confinement effect which perturbs the crystallization of nascent polymer chains and as the reaction time goes on such an effect of the pores is vanished due to the fragmentation of the support.

All the above mentioned studies were focused on supported metallocene catalysts. Support porosity plays an important role in silica supported Phillips catalysts. McDaniel[96] systematically studied the impact of silica support pore volume, pore diameter, surface area and support fragility on i) the

activity of chromium (Cr) and metallocene catalysts in slurry phase ethylene polymerization and ii) molecular properties (i.e., molar mass, long chain branching and melt index) of the polyethylene samples produced from these supported catalysts. Various series of silicas prepared in-house and obtained from commercial sources were used to prepare the catalysts so that at least one physical property of the support was kept constant in order to analyze the impact of the other physical properties of the support on catalytic activity and molecular properties of the produced polyethylene. Chromia-silica-titania catalysts of various pore volumes and pore diameters were prepared by immersing the hydrogel in liquids of different surface tensions and then drying at 110°C. Liquids with higher surface tension (like water) give low pore volume to the final silica support as compared to those with low surface tension (like isopentyl alcohol). This is due to the fact that higher surface tension forms a meniscus that pulls strongly on the pore walls. The surface area of these catalysts remained fairly constant around 400 $m^2.g^{-1}$ whereas the pore volume increased systematically from 0.7 $mL.g^{-1}$ to 3.3 $mL.g^{-1}$ and, consequently, the pore diameter increased from 5.6 to 26.4 nm. Slurry phase ethylene polymerizations with these catalysts were performed in a 2.2 L reactor at 105°C in 1.2 L iso-butane as diluent for about 1 h at 37.9 bar ethylene pressure. The results showed that the catalytic activity increased with increasing pore volume up to 2 $mL.g^{-1}$ and pore diameter of about 18 nm after which it began to plateau. The melt flow index of the produced polymer samples reduced with increasing pore volume and pore diameter of the catalysts indicating that the molar mass of the polyethylene produced with higher pore volume chromia-silica-titania catalysts was lower than that of the polyethylene produced with lower pore volume catalysts.

These trends were confirmed by using another silica-chromia-titania catalyst with a pore volume of 3.3 $mL.g^{-1}$ which was then mechanically pressed with different pressures from zero to 483 MPa in order to produce catalysts of lower pore volumes. The activity of these catalysts and the molecular properties of the polyethylene samples produced with them showed dependence on the pore volumes and pore diameters which was similar to the case discussed in the previous paragraph i.e., the catalytic activity increased with pore volume and pore diameter of the catalyst whereas the molar mass decreased with increasing pore volume and pore diameters. Similarly, long chain branching (LCB) also decreased with increasing catalyst pore volumes and pore diameters. The author suggested two reasons for this behavior of chromia-silica-titania catalysts which are i) the higher pore diameter facilitates the egress or extrusion of the ‘semi-molten’ polyethylene from the

pores present in the interior of the support fragment and ii) higher pore volume of the support indicates that it has low strength which leads to higher extent of fragmentation of such catalysts as compared to those which have lower pore volume and are less fragile.

The effect of catalyst surface area on the catalytic activity and molecular properties of the polyethylene samples was analyzed by using another series of silica. These silicas were prepared from commercial silica sols of particle sizes varying in the range of 7 to 85 nm whose hydrogels were then impregnated to have 0.4 $Cr.nm^{-2}$ followed by drying with liquids of different surface tensions in order to have varying pore volumes and pore diameters also (e.g., three catalysts with same surface of 325 $m^2.g^{-1}$ were prepared with pore volumes of 1.6, 0.7 and 0.4 $mL.g^{-1}$). The surface area of the final catalysts varied in a fairly broad range of 35 $m^2.g^{-1}$ to 325 $m^2.g^{-1}$. The basic structure of these silicas could be imagined as agglomerated primary particles of different sizes which make these silicas different from reinforced silicas prepared by coalescence studied separately by the author. Polymerization results with these catalysts indicated that the variations in surface area has almost no impact on the catalytic activity and polymer properties which suggests that the size of the primary particles or the radius of curvature has no impact on the catalyst performance and polyethylene properties. However, if one considers the red circles in **Figure 13**, it can be seen that at a constant pore volume the catalysts with lower surface area showed higher activities and lower molar masses. Since the pore volumes are kept constant, catalysts with lower surface area possess wider pores than those with higher surface area (as Average pore diameter = (4×Pore volume)/Surface area). Note that the constant pore volume indicates that the number of connections between primary particles (i.e., the coordination number which relates to strength of the silica matrix) is also constant. These wider pores facilitate the extrusion of the polymer being formed within them during the polymerization and therefore, leads to higher activities and lower molar mass polymer samples produced with these Cr/silica catalysts. This observation is in good agreement with the one based on first series of catalysts used in this work (see previous paragraphs).

To support further these observations, the author estimated mathematically the silica support strength by changing the surface areas and pore diameters at constant pore volume. Each silica was assumed to have cubic close packing and the fragmentation of the silica was assumed to be from surface to the center since forces generated due to polymer formation at the exterior surface of the catalyst particles are not balanced which lead to inward direction of fragmentation. Based on the

results of these mathematical calculations, it was suggested that at a constant pore volume the higher surface area (with small pores) silica have higher strength than the low surface area silica (with wide pores). These mathematical estimations were found to be in good correlation with the experimental determination of pore volume shrinkage of the same silica supports upon using water and n-propyl alcohol as hydrogel liquids. Note that these two liquids have very different surface tensions which lead to significant differences in the force applied by the liquid meniscus on the primary silica particles. The results showed that silica sols with smaller primary particle size (i.e., high surface area) attained higher pore volumes than those with bigger primary particle size (i.e., low surface area) for both the pore liquids indicating that the smaller primary particle silicas showed higher resistance to shrinkage than the bigger primary particle silicas (which is an indirect way of their strength assessment). Of course, while drying of these silicas the direction of force applied is opposite to that applied by the polymer accumulation in these pores but these experiments provide a good understanding of silica strength. However, it should be kept in mind that in case of bigger pore diameters there are fairly enough chances that the egress of the polymer being formed is higher than that in the case of smaller pore diameters leading to different rates and extents of particle fragmentation in narrow and wide pore silicas (making again a contradiction with the results just discussed and also highlighted by the author).

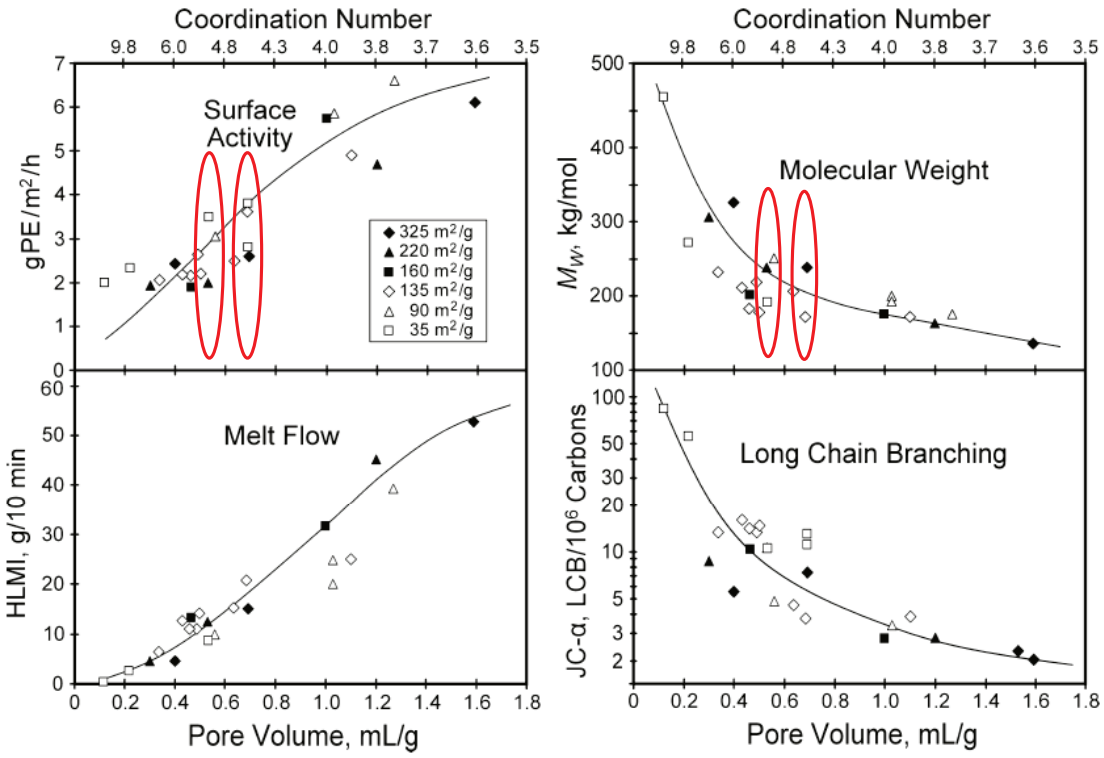

Figure 13. Effect of physical properties of Cr/silica catalysts made from colloidal particles that were varied in size to produce catalysts of widely differing surface areas but similar structure. Reproduced with permission from the work of McDaniel.[96] Red circles are added for the ease of reader.

Another important physical property of the silica supports is their fragility or strength. McDaniel[96] used commercial silicas under the name of Sylox from W.R. Grace whose surface areas were systematically varied by using secondary reinforcement process. Various methods of increasing the silica strength include coalescence by Oswald ripening (or alkaline aging), sintering and hydrothermal treatment (or steaming). Still another method of reinforcing precipitated silica (as opposed to gelled silica) network exists which involves secondary deposition of silica onto an existing silica structure.[96] Depending upon the severity of conditions used in these methods, different levels of coalescence and, therefore of silica strength can be achieved. The surface areas of these commercial silica supported catalysts varied in the range of 257 to 105 $m^2.g^{-1}$ whereas the pore volume kept almost constant and the pore diameters increased with decreasing surface area of the support. In addition to catalysts supported on Sylox silicas, additional Cr/silica catalysts were supported on reinforced silica by using the process of alkaline aging which gave final pore volumes

of the catalysts around 1.6 $mL.g^{-1}$. The effect of reinforcement of the silica support on the polymerization activity, MFI, molar mass of the polyethylene samples and LCB is shown in **Figure 14**. According to the author, plotting these results with respect to pore diameter provided better presentation rather than using surface area on the x-axis. It can be noticed that the surface activity increased with increasing the pore diameter up to 20 nm after which it began to plateau and on further increasing the pore diameter above 60 nm the surface activity decreased. Note that the increase in pore diameter represents loss of surface area due to coalescence which indicates increase in silica strength. This increase in catalytic activity with increasing pore diameter was attributed to enhanced egress of the polymer formed in the pores. Plateau and decrease in surface activity after certain pore diameter values were attributed to too strong silica support which couldn't fragment. At low pore diameters the molar mass of the produced polymers was higher due to low activities but then starts to increase after a minimum at about 20 nm due to drop in activities after passing through the maximum. The behavior of polyethylene melt flow is in-line with that of molar mass and can be explained by combining the LCB behavior with that of molar mass. In addition, the MWD distribution of the polyethylene samples showed bimodality at very low and very large pore diameters which indicated that two types of polymer were formed whose relative contribution depends on the catalyst porosity and its structure.

Other supports including aluminophosphates, aluminas and clays were also investigated with Cr catalysts, and showed similar effects of the physical properties of the catalyst supports on the activity and polymer properties discussed above. Based on the results of Cr/aluminophosphate catalyst, the author concluded that it is the mesoporosity which influences strongly the catalytic activity and the polymer properties.

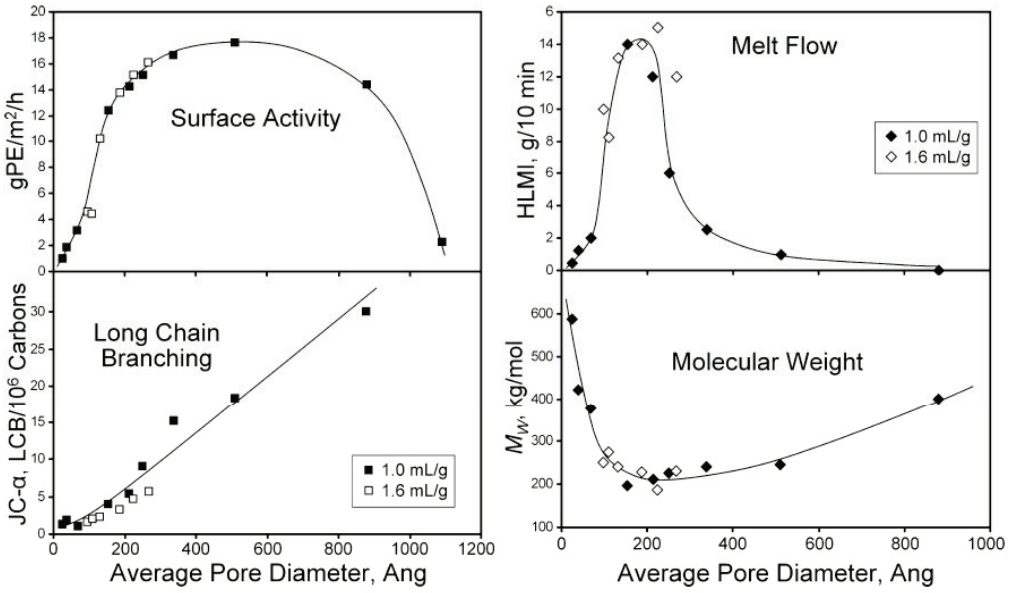

Figure 14. Effect of silica support reinforcement on the activity of Cr/silica catalysts in ethylene polymerization. Reproduced from McDaniel[96] with permission.

Finally, the author used a (2-(η-5-cyclopentadienyl)-2(η-5-fluorenyl)hex-5-ene zirconium dichloride) metallocene catalyst activated by acidic aluminas of pore volumes in the range of 0.45 to 1.38 mL.g^{-1}, corresponding to pore diameters in the range of 18.2 to 6.3 nm, to confirm that the discussion above is applicable to single-site catalysts also. Note that the surface area of acidic alumina supports remained almost constant. Slurry phase ethylene/1-hexene copolymerizations were conducted to evaluate these catalysts. Similar trends were observed i.e., the catalytic activity and melt flow index of polymer samples increased with increasing pore volume and pore diameters.

It is important to mention here that no information was provided about the kinetic profiles and PSD of the supports or PSD of the final catalysts in any of the cases discussed above. Both the kinetic profiles and catalyst PSD can provide very important information about the existence of mass transfer resistance during olefin polymerization via supported catalysts which the author rules out in conclusion. Furthermore, the information about the distribution of the active species throughout the supported catalyst particles (usually obtained by SEM-EDX on microtommed catalyst particles) is another important information which can be linked to surface activity. Unfortunately, this information is also missing in this work. Previously published work of McDaniel reported more or less similar results.[139-142]

5.6. Other Supports

A significant number of studies have been devoted to the development of supported metallocenes using organic supports which are generally linear or cross-linked polystyrene (PS) or polysiloxane-based polymers. These supports were expected to provide various benefits over the traditional inorganic supports described in the previous sections e.g., i) they offer a flexible surface and surrounding for the supported metallocence unlike inorganic supports which are relatively rigid causing partial shielding of the active species and also effects the confirmation of active species leading to reduced stereoselectivity during ethylene/higher α-olefin copolymerizations, ii) (co)-monomer(s) diffusion resistance was expected to be less in organic supports since the support itself can swell by the (co)-monomer(s), iii) functionalization of organic supports is easier than inorganic ones and iv) in case of low activities organic residues are expected to have less impact on the properties of the polyolefin grade than that of the inorganic residues. However, these benefits have been partially obtained by the metallocenes supported on organic supports since fragmentation of such supports does not happen in a way similar to that of organic supports which led to their low activities and inhomogeneties in the produced polyolefin properties. The review articles of Müllen et al.,[95] and Cramail et al.,[94] along with the book chapter of Klapper and Fink[143] can be consulted to have a detailed overview of the state-of-art in these supports.

Highly dispersible layered double hydroxides (AMO−LDHs) is another recently developed class of crystalline solid supports having high surface area has been developed by O'Hare et al.[36] Layered double hydroxides (LDHs) are the compounds containing brucite-like layers with general chemical composition $[M_{1-x}M'_x(OH)_2]^{y+}[A^{n-}_{y/n}]\cdot zH_2O$, where M is typically a divalent cation such as Mg^{2+} and M' is typically a trivalent cation such as Al^{3+}, A = anions, although many other metal combinations are possible. Metallocenes supported on such carriers already impregnated with a co-catalyst like MAO are shown to provide reasonable activities in slurry phase ethylene homopolymerizations with polymer molar mass dispersities around 3.5.

Still another class of support materials is metal-organic frameworks (MOFs) show great potential as carriers for metallocenes since they can be tuned on molecular level.[144]

Based upon the discussion made in this section it can be concluded that although all the discussed support materials show specific pros and cons, silica seems to the most commonly tested and applied industrially as it provides benefits of low costs in conjunction with tunable surface

chemistry and particle properties which lead to final supported metallocenes of commercial interest.

6. Mechanism of Olefin Polymerization with Fundamental Model

Despite the existence of many different types of active sites, co-catalysts etc., it appears that there is a general consensus on the 'basic mechanism' which governs the main steps of olefin polymerization with organometallic catalysts. Soares[7] proposed a 'fundamental model' which describes some of the well-established steps. It should be noted, however, that some important phenomena like the effect of hydrogen and co-monomer on the catalytic activity of organometallic catalysts are not described by the fundamental model. We will discuss the mechanisms of such effects where appropriate. **Figure 15** shows schematically the major reactions described by fundamental model i.e., catalyst activation by a co-catalyst, chain initiation and propagation. A general notation has been used in this figure where, L indicates a ligand (e.g., Cp ring in metalloecenes, Cl atoms for ZN catalysts), A denotes the transition metal active center and X represents halogens, commonly chlorine atoms. AlR_3, where R is generally an alkyl, denotes the co-catalyst which, when contacted with catalyst, extracts two halogens and transfers one alkyl group to the catalyst. The resulting positively charged metal atom is called active site and the negatively charged co-catalyst ($AlR_2X_2^-$) is a non-coordinating anion which is required to stabilize the catalyst. The electron deficient active metal center is now ready to initiate the polymerization by interacting with the π-electrons in the double bond of the olefins, and as soon as an olefin monomer approaches the active site it is inserted and chain growth is initiated (**Figure 15b**). Further monomer insertion steps lead to chain propagation (see **Figure 15c**) and growth of the polyolefin chain. Despite the fact that it is not always possible to quantify the difference between the reaction rate constants for chain initiation (i.e., the first monomer insertion) and propagation steps, they are conventionally assigned with different rate constants.

a) Catalyst activation with co-catalyst

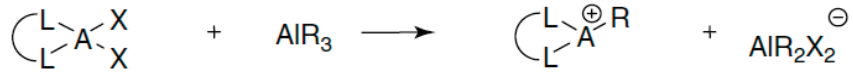

b) Chain initiation

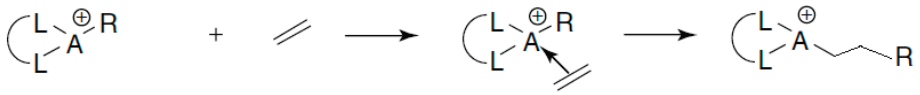

c) Chain propagation

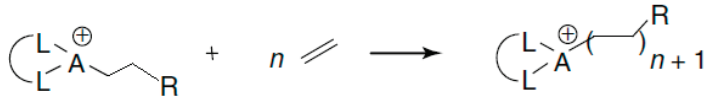

d) Chain transfer to hydrogen

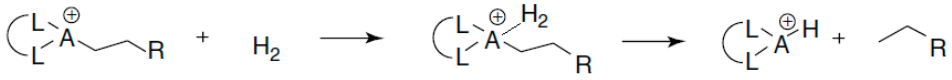

e) Initiation of metal-hydride site

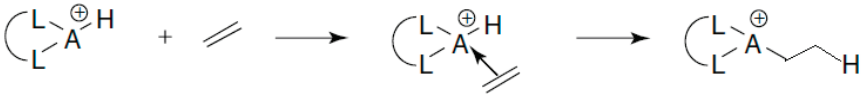

f) β-H elimination

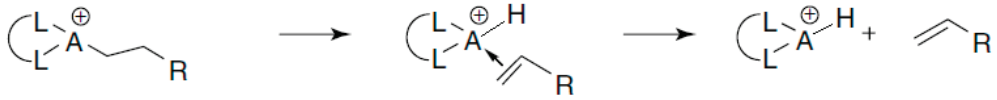

g) β-methyl elimination

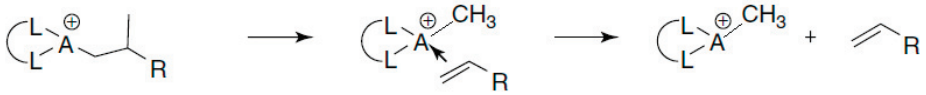

h) Formation of LCB by re-insertion of macromonomer

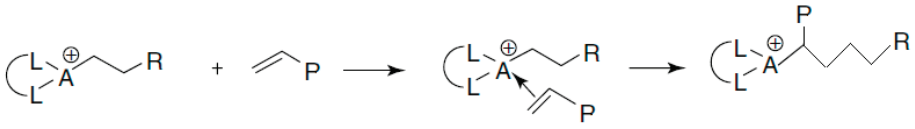

i) Chain transfer to ethylene

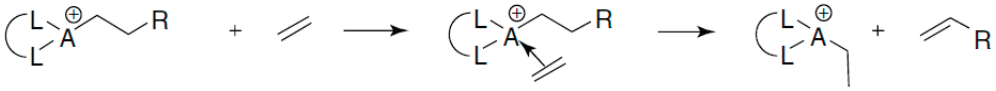

j) Chain transfer to aluminum

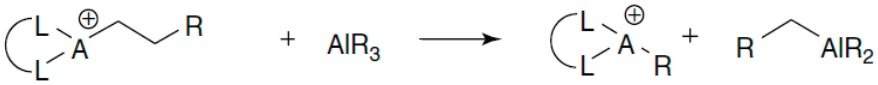

Figure 15. Mechanism of coordination polymerization with organometallic catalysts. Reproduced with permission from Soares et al.[7]

Hydrogen is the most common chain transfer agent for ZN, metallocene and other single-site catalysts, and it is commonly used to control the molecular weight. Note that one exception is that in the case of Phillips or Chromium catalysts, calcination temperature of the catalyst and support type are used to control polymer molar mass instead of by using hydrogen as a chain transfer agent. **Figure 15d** shows the mechanism of chain transfer to hydrogen which produces metal-hydride bond and a dead polymer chain. The metal-hydride bond is active and can lead to other polymerization mechanisms, as shown in **Figure 15e**. Note that the active species formed in **Figure 15e** differs from the one produced in **Figure 15b** by the presence of hydrogen atom at the end.

Another well-known chain termination mechanism leading to vinyl-terminated chains in ethylene polymerization and vinylidene-terminated chains in propylene polymerization (depending upon the catalyst used for propylene polymerization) is β-H elimination shown in **Figure 15f**. The reactivity of vinyl-terminated chains is higher than that of vinylidene terminated ones, with the former more likely to produce Long Chain Branching (LCB) with a suitable catalyst. If the catalyst allows, vinyl-terminated polypropylene macromonomers are produced by the mechanism shown in **Figure 15g,** generally termed as β-methyl elimination and such macromonomers can be reinserted into the growing polymer chain to form LCB (see **Figure 15h** for mechanism).

Chain transfer to monomer is yet another mechanism by which the growing polyolefin chain can terminate and produce one vinyl-terminated dead chain (in ethylene polymerization) along with an alive chain of length 1 as shown by **Figure 15i**. Finally, the co-catalyst molecule can also act as a chain transfer agent in addition to playing the role of alkylating and reducing agent for the catalyst (see **Figure 15j**).

In the case of polymerization with multiple monomers, the steps just described for the homopolymerization (**Figure 16**) remain valid. With a given catalyst/co-catalyst system, the rates at which propagation and chain transfer reactions occur during copolymerizations depend upon the monomer type being added to polymer backbone and at the chain end. Interaction of the incoming monomer with the last inserted monomer into the polymer chain can affect the polymerization rate. The model which describes this mechanism is generally known as copolymerization terminal model with each involved step having a different propagation rate and is elaborated in **Figure 16** for ethylene/1-butene copolymerization. Similarly, the rates of other chain transfer reactions like

β-hydride elimination, transfer to hydrogen, monomer and co-catalyst may also be altered by the chain-end type.

It is important to mention that a unique reaction (or kinetic) rate constant can be assigned for each polymerization step described above. However, for ZN catalysts which involve multiple active sites, one needs to assign rate constants for each family of active sites and each polymerization step.

Finally, the detailed discussion about other important reaction mechanisms used to explain stereo- and regioselectivity in propylene polymerization, comonomer effect, hydrogen effect and catalyst/co-catalyst ratio effect on catalyst behavior during olefin polymerization with organometallic catalysts can be found elsewhere.[7,145-147] Mathematical modelling of olefin polymerization kinetics with various organometallic catalysts and comprehensive examples is very nicely explained by Soares elsewhere.[37]

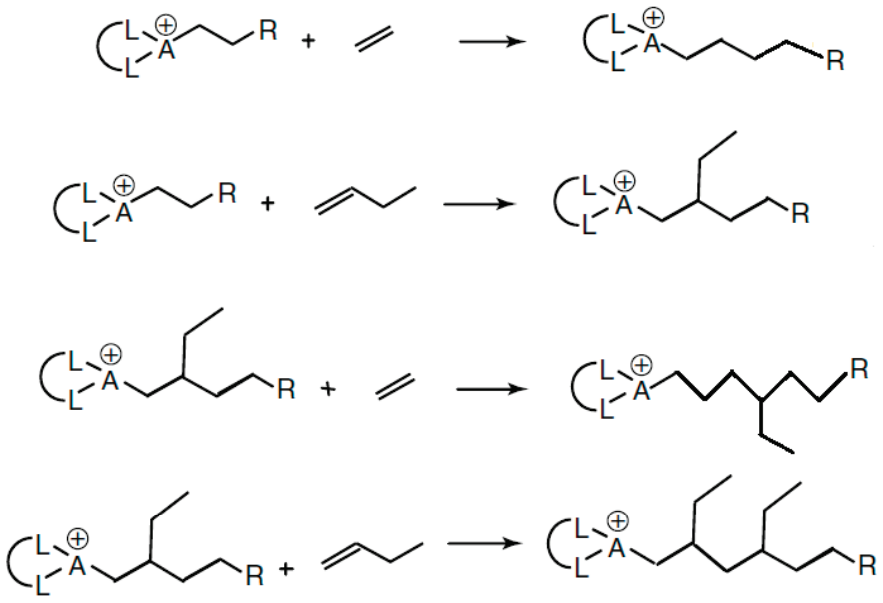

Figure 16. Terminal model of copolymerization for ethylene/1-butene. Reproduced with permission from Soares et al.[7]

7. Polymer Particle Growth

Despite the many benefits of heterogneization, supported metallocenes can have low activities, stereoselectivities, and unexpectedly broad MWD uncharacteristic of single-site catalysts. Process modelling is an effective tool for understanding and eventually predicting such behaviour. When dealing with heteroegenous catalysts, it is however necessary to have a kinetic model (previous secton), and a model describing heat and mass transfer in the catalyst particles, as well as linking any changes in the physical structure of the catalyst to the "chemistry". Since the catalyst particles are (relatively) rapidly transformed into growing polymer particles, one needs to have particle growth model. The term polyolefin particle growth generally refers to the conversion of a supported olefin polymerization catalyst particle into a polyolefin particle upon injection into the reactor containing (co)-monomer(s) and other inert species. However, this conversion from catalyst to polyolefin particle is not straight forward and involves different steps which can be generalized as; i) diffusion of reactive and inert species at the active sites leading to polymerization within the pores (if the support is porous) ii) pore filling by the polymer formed with in the pores iii) fragmentation of the pores and/or the whole particle and iv) continued diffusion of reactive and inert species at the active sites through the polymer layer and inherent pores or the ones created due to fragmentation leading to continued particle growth over the reaction period. Parallel to these mass transfer steps, polymerization generates heat and needs to be continuously dissipated from the growing polyolefin particles and, subsequently, from the reactor. Therefore, the polyolefin particle growth presents a coupled heat and mass transfer problem.

Different research groups have developed various approaches to model olefin polymerization over supported catalysts. All of these approaches can be classified into three general classes of physical models and differentiate from each other on the basis of treatment of the fragmentation step (see **Figure 17**).

7.1. Solid Core Model

The first and simplest model proposed by Begley[148] assumes that the no fragmentation of the solid support occurs and the polymer grows over the periphery of the solid particles which does not allow this model to predict stable polymerization rates because of increased transport length due to polymer accumulation. Later on it was shown by Shmeal et al.,[149] and Nagel et al.,[150] that this model cannot predict the experimentally observed polymerization rates and broadness of MWDs.

Due to the basic contradiction between this model and reality where fragmentation does occur this model was abandoned.

7.2. Polymer Flow Model (PFM)

In PFM, the solid supported catalyst particle fragments into numerous fractions which remain entrained in the formed polyolefin layers and therefore, produces a pseudo-homogeneous phase which, in addition to catalyst fragments and polymer, contains pore space. Mass and heat transfer occurs through this homogeneous polymeric particle. This model was developed by Shmeal and co-workers[149] whereas, it was further modified by numerous authors.[151-159]

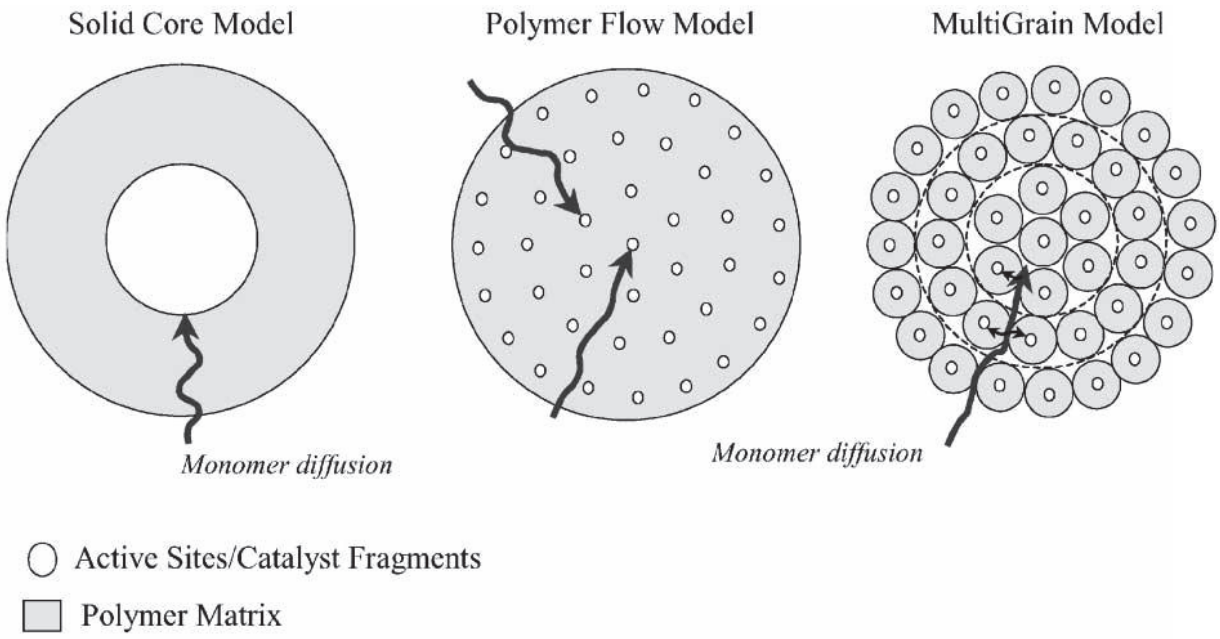

Figure 17. Three classes of polyolefin growth models described in the open literature. Reproduced from McKenna et al.,[156] with permission.

By employing this model, various researchers have shown that inter-particle diffusion monomer resistance can lead to low activity of supported olefin polymerization catalysts, broadening of polymer MWD and CCD. Accurate estimation of effective mass and heat transfer parameters with in the growing particle is the key for getting reliable results from this model. Limitations of this model are often attributed to the fact that it does not consider the fragmentation step explicitly and the heterogeneous nature of the growing polymer particle. However, the assumption of pseudo-

homogeneous polymer particle renders this model to be mathematically simple and therefore, preferable in certain cases.

7.3. MultiGrain Model (MGM)

MGM is an extended form of PFM in which the particle fragmentation has been explicitly taken into account. The solid catalyst particle is assumed to consist of micrograins on which the active sites are fixed and as the polymerization starts the polymer layer is formed on each of these particles. All of these growing micrograins agglomerate to form macrograin which refers to the growing polymer particle. Microparticles are assumed to be of the same radius and therefore, experience similar concentration and temperature gradients. As each layer of the micrograin grows, it pushes the micrograin layer next to it and the macrograin grows in size (see **Figure 17**). This model was developed by Nagel et al.,[150] and then extended by Laurence and Chiovetta[160] to include fragmentation step. Chiovetta et al.,[161-167] further refined this model by proposing various modifications. The MGM was used extensively to model polyolefin particle growth in slurry, gas and bulk phase ethylene and propylene homo- and copolymerization processes and to explain the issues related to the existence of mass transfer resistance during early and later stages of olefin polymerization processes along with broadening of molar mass distribution due to intraparticle diffusion resistance as well as other issues. [124,168-172] Although electron microscopy studies[173] on polymer particles obtained from ZN catalysts have shown the existence of primary and secondary structures, no real improvements have been made with this model except for better estimation of reaction kinetics. Finally, the extensive review article from McKenna et al.,[156] provides a comparison of different models used to study polyolefin particle growth.

8. Conclusion

Supported olefin polymerization catalysts are the heart of industrial polyolefin production plants using low pressure catalytic process technology. At present, Ziegler-Natta and chromium catalysts dominate the polyolefins industry primarily due to their low cost and ability to produce polyolefins of different properties. However, the lack of understanding about their multisite nature has triggered the development of other well-defined olefin polymerization catalysts like metallocenes, tandem catalysts, late transition metal catalysts etc., among which metallocenes present an attractive class of catalysts with reasonable olefin, and in particular ethylene, polymerization activities and behave like single-site catalysts. In parallel, co-catalyst development has also seen new achievements with the discovery of methylaluminoxane (MAO), Borates, activating supports etc., among whom MAO being the most widely used co-catalyst for metallocenes regardless of the fact that its a complex, poorly understood and dangerous molecule. Activation of metallocenes with MAO is more efficient as compared to their activation with other co-catalysts leading to metallocene/MAO catalysts of considerable activities. In addition, MAO serves the purpose of scavenger which other co-catalysts are incapable of.

Since low pressure catalytic processes for polyolefins production require supported catalysts, last 50 years have also seen a significant amount of research focused on the development of new support materials. Nevertheless, silica appears to be a still better option as a support material, in particular for the metallocenes due to its low cost, ease of physical property (e.g., particle size, fragility and porosity) tailoring and better affinity towards metallocenes as well as the co-catalysts (like MAO) due to the presence of surface hydroxyl groups.

While the polyolefins industry employing silica supported metallocene/MAO catalysts is still growing in volume, the effect of support's physical properties on; i) the immobilization of metallocene/MAO catalysts, ii) the performance of these supported catalysts during polymerization and iii) the properties (e.g., molar mass distribution (MWD), chemical composition distribution (CCD) etc.,) of the polyolefin grade is not well-explored and therefore, remains a subject of research. Among various physical properties of the silica supported metallocene catalysts investigated in the open literature, particle size appears to be the one of interest. Although the research has shown that supported catalyst particles of different size have different instantaneous activities during olefin polymerization, the physical reason why these particles behave differently

has not seen consensus. Similarly, one may find hard to conclude from the studies devoted to the investigation of the impact of other physical properties (like pore volume, pore diameter, surface area etc.,) of, in particular, silica supported metallocene/MAO catalysts. The most probable reasons for the lack of agreement on this topic of significant importance is the difference of catalyst synthesis methods employed, variety of supports used with vastly different chemical and physical properties, inability to keep other physical properties constant while analyzing the impact of one property on the catalyst behavior and, last but not the least, using conditions which are not industrially relevant.

Therefore, in this work we aim to find the underlying reasons which can be attributed to the variation in ethylene polymerization kinetics as well as in the properties of the obtained polyethylene grade upon changing the physical properties of the used supported olefin polymerization catalysts. For this purpose, metallocene catalysts are selected mainly thanks to their single-site behavior which allows us to separate, where possible, the chemical effects of the supported catalyst from the physical ones. MAO has been used as a co-catalyst due to the fact that metallocenes activated by this compound have fairly high activities in ethylene polymerization. Both, slurry and gas phase ethylene homo- and ethylene/1-hexene copolymerizations, have been conducted at conditions of industrial relevance in order to affirm that the observed effects of support properties remain the same in both type of processes. Commercial silicas have been used in this work as support for metallocene/MAO catalysts. Particle size of the silica support, while keeping other physical properties constant, was varied by sieving the full batch of the used silica. Each sieved fraction was then dehydroxylated prior to its impregnation with the metallocene/MAO catalyst. Similarly, when studying the impact of changes in support porosity on catalyst performance and polymer properties, the support particle size was kept constant. Different polymer characterization techniques have been employed to analyze the polymer properties. Finally, the observed changes in reaction kinetics and polyethylene properties due to the changes made in the physical properties of the supported catalysts are explained based upon physical reasons.

9. References

1. Markus Stürzel, Mihan, S, Rolf Mülhaupt, From Multisite Polymerization Catalysis to Sustainable Materials and All-Polyolefin Composites, Chem. Rev., **2016**, 116, 1398-1433.

2. Qiao, J, Guo, M, Wang, L, Liu, D, Zhang, X, Yu, L, Song, W, Liu, Y, Recent advances in polyolefin technology, Polym. Chem., **2011**, 2, 1611-1623.

3. Soares, J B P, McKenna, T F L., Introduction to Polyolefins, In Polyolefin Reaction Engineering, Wiley-VCH Verlag GmbH & Co. KGaA, **2012**.

4. Soares, J B P, McKenna, T F L., Polyolefin Reactors and Processes, In Polyolefin Reaction Engineering, Wiley-VCH Verlag GmbH & Co. KGaA, **2012**.

5. Gahleitner, M, Severn, J R., Designing Polymer Properties, In Tailor-Made Polymers, Wiley-VCH Verlag GmbH & Co. KGaA, **2008**.

6. Fred W.Billmeyer., Ionic and Coordination Chain (Addition) Polymerization, In Textbook of Polymer Science, 3 ed.; Wiley Interscience, New York, **1984**.

7. Soares, J B P, McKenna, T F L., Polymerization Catalysis and Mechanism, In Polyolefin Reaction Engineering, Wiley-VCH Verlag GmbH & Co. KGaA, **2012**.

8. Gambarotta, S, Vanadium-based Ziegler–Natta: challenges, promises, problems, Coordination Chemistry Reviews., **2003**, 237, 229-243.

9. Chadwick, J C, Garoff, T, Severn, J R., Traditional Heterogeneous Catalysts, In Tailor-Made Polymers, Wiley-VCH Verlag GmbH & Co. KGaA, **2008**.

10. McDaniel, M P., Chapter 3 - A Review of the Phillips Supported Chromium Catalyst and Its Commercial Use for Ethylene Polymerization, In Advances in Catalysis, Volume 53 ed.; Eds. C.G.a.H. Bruce., Academic Press, **2010**.

11. McDaniel, M P., Review of the Phillips Chromium Catalyst for Ethylene Polymerization, In Handbook of Heterogeneous Catalysis, Wiley-VCH Verlag GmbH & Co. KGaA, **2008**.

12. Kaminsky, W, Highly active metallocene catalysts for olefin polymerization, J. Chem. Soc. , Dalton Trans., **1998**, 1413-1418.

13. Breslow, D S, Newburg, N R, Bis-(cyclopentadienyl)-titanium dichloride-alkylaluminum complexes as catalysts for the polymerization of ethylene, J. Am. Chem. Soc., **1957**, 79, 5072-5073.

14. Natta, G, Pino, P, Mazzanti, G, Giannini, U, A crystallizable organometallic complex containing titanium and aluminum, J. Am. Chem. Soc., **1957**, 79, 2975-2976.

15. Alt, G, The heterogenization of homogeneous metallocene catalysts for olefin polymerization, J. Chem. Soc. , Dalton Trans., **1999**, 1703-1710.

16. Severn, J R, Chadwick, J C, Duchateau, R, Friederichs, N, "Bound but Not Gagged" Immobilizing Single-Site α-Olefin Polymerization Catalysts, Chem. Rev., **2005**, 105, 4073-4147.

17. Kaminsky, W, Kopf, J, Sinn, H, Vollmer, H J, Extrem verzerrte Bindungswinkel bei Organozirconium-Verbindungen, die gegen Ethylen aktiv sind, Angewandte Chemie., **1976**, 88, 688-689.

18. Kaminsky, W, Discovery of Methylaluminoxane as Cocatalyst for Olefin Polymerization, Macromolecules., **2012**, 45, 3289-3297.

19. Sinn, H, Kaminsky, W., Ziegler-Natta Catalysis, In Advances in Organometallic Chemistry, Volume 18 ed.; Eds. F.G.A. Stone and Robert West., Academic Press, **1980**.

20. Kaminsky, W, Production of Polyolefins by Metallocene Catalysts and Their Recycling by Pyrolysis, Macromol. Symp., **2016**, 360, 10-22.

21. Coates, G W, Precise Control of Polyolefin Stereochemistry Using Single-Site Metal Catalysts, Chem. Rev., **2000**, 100, 1223-1252.

22. Severn, J R, Chadwick, J C, Immobilisation of homogeneous olefin polymerisation catalysts. Factors influencing activity and stability, Dalton Trans., **2013**, 42, 8979-8987.

23. Jayaratne, K. C.; Jensen, M. D.; Yang, Q. Polymerization catalysts and process for producing bimodal polymers in a single reactor. WO2007037836A3, **2007**.

24. Martin, J. L.; Thorn, M. G.; Mcdaniel, M. P.; Jensen, M. D.; Yang, Q.; Deslauriers, P. J.; Kertok, M. E. Polymerization catalysts and process for producing bimodal polymers in a single reactor. US7312283B2, **2007**.

25. Yang, Q.; Jayaratne, K. C.; Jensen, M. D.; Mcdaniel, M. P.; Martin, J. L.; Thorn, M. G.; Lanier, J. T.; Crain, T. R. Dual metallocene catalysts for polymerization of bimodal polymers. US7619047B2, **2007**.

26. Masino, A. P.; Murray, R. E.; Yang, Q.; Secora, S. J.; Jayaratne, K. C.; Beaulieu, W. B.; Ding, E.; Glass, G. L.; Solenberger, A. L.; Cymbaluk, T. H. Dual metallocene catalyst systems for decreasing melt index and increasing polymer production rates. WO2011002497 A1, **2011**.

27. Ding, E.; Yang, Q.; Yu, Y.; GUATNEY, L. W.; ASKEW, J. B. Metallocene and half sandwich dual catalyst systems for producing broad molecular weight distribution polymers. WO2014052364A1, **2014**.

28. Chen, E Y-X, Marks, T J, Cocatalysts for Metal-Catalyzed Olefin Polymerization:Activators, Activation Processes, and Structure-Activity Relationships, Chem. Rev., **2000**, 100, 1391-1434.

29. Sinn, H, Proposals for structure and effect of methylalumoxane based on mass balances and phase separation experiments, Macromol. Symp., **1995**, 97, 27-52.

30. Koide, Y, Bott, S G, Barron, A R, Alumoxanes as Cocatalysts in the Palladium-Catalyzed Copolymerization of Carbon Monoxide and Ethylene: Genesis of a Structure-Activity Relationship, Organometallics., **1996**, 15, 2213-2226.

31. Linnolahti, M, Severn, J, Pakkanen, T, Formation of Nanotubular Methylaluminoxanes and the Nature of the Active Species in Single-Site α-Olefin Polymerization Catalysis, Angewandte Chemie International Edition., **2008**, 47, 9279-9283.

32. Ystenes, M, Eilertsen, J L, Liu, J, Ott, M, Rytter, E, Stovneng, J A, Experimental and theoretical investigations of the structure of methylaluminoxane (MAO) cocatalysts for olefin polymerization, J. Polym. Sci. A Polym. Chem., **2000**, 38, 3106-3127.

33. Babushkin, D E, Brintzinger, H H, Activation of Dimethyl Zirconocene by Methylaluminoxane (MAO)Size Estimate for Me-MAO- Anions by Pulsed Field-Gradient NMR, J. Am. Chem. Soc., **2002**, 124, 12869-12873.

34. Ghiotto, F, Pateraki, C, Tanskanen, J, Severn, J R, Luehmann, N, Kusmin, A, Stellbrink, J, Linnolahti, M, Bochmann, M, Probing the Structure of Methylalumoxane (MAO) by a Combined Chemical, Spectroscopic, Neutron Scattering, and Computational Approach, Organometallics., **2013**, 32, 3354-3362.

35. Matsui, S, Mitani, M, Saito, J, Tohi, Y, Makio, H, Matsukawa, N, Takagi, Y, Tsuru, K, Nitabaru, M, Nakano, T, Tanaka, H, Kashiwa, N, Fujita, T, A Family of Zirconium Complexes Having Two Phenoxy-Imine Chelate Ligands for Olefin Polymerization, J. Am. Chem. Soc., **2001**, 123, 6847-6856.

36. Buffet, J C, Wanna, N, Arnold, T A Q, Gibson, E K, Wells, P P, Wang, Q, Tantirungrotechai, J, O'Hare, D, Highly Tunable Catalyst Supports for Single-Site Ethylene Polymerization, Chem. Mater., **2015**, 27, 1495-1501.

37. Soares, J B P, McKenna, T F L., Polymerization Kinetics, In Polyolefin Reaction Engineering, Wiley-VCH Verlag GmbH & Co. KGaA, **2012**.

38. Copéret, C, Comas-Vives, A, Conley, M P, Estes, D P, Fedorov, A, Mougel, V, Nagae, H, Nunez-Zarur, F, Zhizhko, P A, Surface Organometallic and Coordination Chemistry toward Single-Site Heterogeneous Catalysts: Strategies, Methods, Structures, and Activities, Chem. Rev., **2016**, 116, 323-421.

39. Collins, R A, Russell, A F, Mountford, P, Group 4 metal complexes for homogeneous olefin polymerisation: a short tutorial review, Applied Petrochemical Research., **2015**, 5, 153-171.

40. McKnight, A L, Waymouth, R M, Group 4 ansa-Cyclopentadienyl-Amido Catalysts for Olefin Polymerization, Chem. Rev., **1998**, 98, 2587-2598.

41. Theopold, K H, Heintz, R A, Noh, S K, Thomas, B J., Homogeneous Chromium Catalysts for Olefin Polymerization, In Homogeneous Transition Metal Catalyzed Reactions, 230 ed.; American Chemical Society, **1992**.

42. Theopold, K H, Homogeneous Chromium Catalysts for Olefin Polymerization, Eur. J. Inorg. Chem., **1998**, 1998, 15-24.

43. Hlatky, G G, Heterogeneous Single-Site Catalysts for Olefin Polymerization, Chem. Rev., **2000**, 100, 1347-1376.

44. Choi, Y, Soares, J B, Supported single-site catalysts for slurry and gas-phase olefin polymerisation, The Canadian Journal of Chemical Engineering., **2012**, 90, 646-671.

45. Severn, J R., Methylaluminoxane (MAO), Silica and a Complex: The "Holy Trinity" of Supported Single-Site Catalyst, In Tailor-Made Polymers, Wiley-VCH Verlag GmbH & Co. KGaA, **2008**.

46. Atiqullah, M, Akhtar, M N, Moman, A A, Abu-Raqabah, A H, Palackal, S J, Al-Muallem, H A, Hamed, O M, Influence of silica calcination temperature on the performance of supported catalyst SiO2-nBuSnCl3/MAO/(nBuCp)2ZrCl2 polymerizing ethylene without separately feeding the MAO cocatalyst, Applied Catalysis A: General., **2007**, 320, 134-143.

47. dos Santos, J H Z, Krug, C, da Rosa, M B, Stedile, F C, Dupont, J, de Camargo Forte, M, The effect of silica dehydroxylation temperature on the activity of SiO2-supported zirconocene catalysts, Journal of Molecular Catalysis A: Chemical., **1999**, 139, 199-207.

48. dos Santos, J H Z, Larentis, A, da Rosa, M B, Krug, C, Baumvol, I J R, Dupont, J, Stedile, F C, de Camargo Forte, M, Optimization of a silica supported bis(butylcyclopentadienyl)-zirconium dichloride catalyst for ethylene polymerization, Macromol. Chem. Phys., **1999**, 200, 751-757.

49. dos Santos, J H Z, Dorneles, S, Stedile, F C, Dupont, J, de Camargo Forte, M M, Baumvol, I J R, Silica supported zirconocenes and Al-based cocatalysts: surface metal loading and catalytic activity, Macromol. Chem. Phys., **1997**, 198, 3529-3537.

50. Collins, S, Kelly, W M, Holden, D A, Polymerization of propylene using supported, chiral, ansa-metallocene catalysts: production of polypropylene with narrow molecular weight distributions, Macromolecules., **1992**, 25, 1780-1785.

51. Welborn, H. C. Supported polymerization catalyst. US4808561A, **1989**.

52. Takahashi, T. Process for producing ethylene copolymers. US5026797A, **1991**.

53. Chang, M. Olefin polymerization catalyst from trialkylaluminum mixture, silica gel and a metallocene. US5006500A, **1991**.

54. Chang, M. Method for preparing a silica gel supported metallocene-alumoxane catalyst. US5086025A, **1992**.

55. Chang, M. Supported catalyst for 1-olefin(s) (co)polymerization. US5238892A, **1993**.

56. Simplicio, L M T, Costa, F G, Boaventura, J S, Sales, E A, Brandao, S T, Study of some parameters on the zirconocene immobilization over silica, Journal of Molecular Catalysis A: Chemical., **2004**, 216, 45-50.

57. Lee, D H, Shin, S Y, Lee, D H, Ethylene polymerization with metallocene and trimethylaluminumtreated silica, Macromol. Symp., **1995**, 97, 195-203.

58. Haag, M C, Krug, C, Dupont, J, de Galland, G B, dos Santos, J H Z, Uozumi, T, Sano, T, Soga, K, Effects of Al/Zr ratio on ethylene–propylene copolymerization with supported-zirconocene catalysts, Journal of Molecular Catalysis A: Chemical., **2001**, 169, 275-287.

59. Soga, K, Shiono, T, Kim, H J, Activation of SiO2-supported zirconocene catalysts by common trialkylaluminiums, Makromol. Chem., **1993**, 194, 3499-3504.

60. Chao, C, Pratchayawutthirat, W, Praserthdam, P, Shiono, T, Rempel, G L, Copolymerization of Ethylene and Propylene Using Silicon Tetrachloride-Modified Silica/MAO with Et[Ind]2ZrCl2 Metallocene Catalyst, Macromol. Rapid Commun., **2002**, 23, 672-675.

61. Jongsomjit, B, Kaewkrajang, P, Wanke, S E, Praserthdam, P, A Comparative Study of Ethylene/α-Olefin Copolymerization with Silane-Modified Silica-Supported MAO Using Zirconocene Catalysts, Catalysis Letters., **2004**, 94, 205-208.

62. Atiqullah, M, Anantawaraskul, S, Emwas, A H, Al-Harthi, M A, Hussain, I, Ul-Hamid, A, Hossaen, A, Silica-supported (nBuCp)2ZrCl2: effect of catalyst active center distribution on ethylene-1-hexene copolymerization, Polym. Int., **2014**, 63, 955-972.

63. Akhtar, M N, Atiqullah, M, Moman, A A, Abu-Raqabah, A H, Ahmed, N, Supported (nBuCp)2ZrCl2 Catalysts: Effects of Selected Lewis Acid Organotin Silica Surface Modifiers on Ethylene Polymerization, Macromolecular Reaction Engineering., **2008**, 2, 339-349.

64. Fraaije, V. D.; Bachmann, B. D.; Winter, A. D. Supported catalyst system, process for production of the same and the use thereof for the polymerization of olefins. EP0780402A1, **1997**.

65. Paczkowski, N. S.; Winter, A.; Langhauser, F. Metallocene catalysts, their synthesis and their use for the polymerization of olefins. US7169864 B2, **2007**.

66. Speca, A. N. Highly active supported catalyst compositions. WO2000012565 A1, **2000**.

67. Kamfjord, T, Wester, T S, Rytter, E, Supported metallocene catalysts prepared by impregnation of MAO modified silica by a metallocene/monomer solution, Macromol. Rapid Commun., **1998**, 19, 505-509.

68. Moroz, B L, Semikolenova, N V, Nosov, A V, Zakharov, V A, Nagy, S, O'Reilly, N J, Silica-supported zirconocene catalysts: Preparation, characterization and activity in ethylene polymerization, Journal of Molecular Catalysis A: Chemical., **1998**, 130, 121-129.

69. Rytter, E, Ott, M, Supported Metallocene Catalysts Prepared by Impregnation of Silica with Metallocene/Aluminoxane/1-Hexene Solutions, Macromol. Rapid Commun., **2001**, 22, 1427-1431.

70. Eisch, J J, Piotrowski, A M, Brownstein, S K, Gabe, E J, Lee, F L, Organometallic compounds of Group III. Part 41. Direct observation of the initial insertion of an unsaturated hydrocarbon into the titanium-carbon bond of the soluble Ziegler polymerization catalyst Cp2TiCl2-MeAlCl2, J. Am. Chem. Soc., **1985**, 107, 7219-7221.

71. Kaminaka, M, Soga, K, Polymerization of propene with the catalyst systems composed of Al2O3- or MgCl2-supported Et[IndH4]2ZrCl2 and AlR3 (R = CH3, C2H5), Makromol. Chem. , Rapid Commun., **1991**, 12, 367-372.

72. Slotfeldt-Ellingsen, D, Dahl, I M, Ellestad, O H, Heterogenization of homogeneous catalysts I. EPR study of (n-C5H5)2TiCl2/(C2H5)nAlCl3-n (n = 1, 2, 3) supported on silica gel, Journal of Molecular Catalysis., **1980**, 9, 423-434.

73. Kaminaka, M, Soga, K, Polymerization of propene with catalyst systems composed of Al2O3 or MgCl2-supported zirconocene and Al(CH3)3, Polymer., **1992**, 33, 1105-1107.

74. Sinn, H, Kaminsky, W, Vollmer, H J, Woldt, R, "Lebende Polymere" bei Ziegler-Katalysatoren extremer Produktivitat, Angewandte Chemie., **1980**, 92, 396-402.

75. Kaminsky, W, Miri, M, Sinn, H, Rüdiger Woldt, Bis(cyclopentadienyl)zirkon-verbindungen und aluminoxan als Ziegler-Katalysatoren für die polymerisation und copolymerisation von olefinen, Makromol. Chem. , Rapid Commun., **1983**, 4, 417-421.

76. Zijlstra, H S, Stuart, M C A, Harder, S, Structural Investigation of Methylalumoxane Using Transmission Electron Microscopy, Macromolecules., **2015**, 48, 5116-5119.

77. Mason, M R, Smith, J M, Bott, S G, Barron, A R, Hydrolysis of tri-tert-butylaluminum: the first structural characterization of alkylalumoxanes [(R2Al)2O]n and (RAlO)n, J. Am. Chem. Soc., **1993**, 115, 4971-4984.

78. Imhoff, D W, Simeral, L S, Sangokoya, S A, Peel, J H, Characterization of Methylaluminoxanes and Determination of Trimethylaluminum Using Proton NMR, Organometallics., **1998**, 17, 1941-1945.

79. Babushkin, D E, Semikolenova, N V, Panchenko, V N, Sobolev, A P, Zakharov, V A, Talsi, E P, Multinuclear NMR investigation of methylaluminoxane, Macromol. Chem. Phys., **1997**, 198, 3845-3854.

80. Trefz, T K, Henderson, M A, Wang, M Y, Collins, S, McIndoe, J S, Mass Spectrometric Characterization of Methylaluminoxane, Organometallics., **2013**, 32, 3149-3152.

81. Zijlstra, H S, Harder, S, Methylalumoxane-History, Production, Properties, and Applications, Eur. J. Inorg. Chem., **2015**, 2015, 19-43.

82. Chien, J C W, Wang, B P, Metallocene-methylaluminoxane catalysts for olefin polymerization. I. Trimethylaluminum as coactivator, J. Polym. Sci. A Polym. Chem., **1988**, 26, 3089-3102.

83. Tritto, I, Donetti, R, Sacchi, M C, Locatelli, P, Zannoni, G, Dimethylzirconocene-Methylaluminoxane Catalyst for Olefin Polymerization: NMR Study of Reaction Equilibria, Macromolecules., **1997**, 30, 1247-1252.

84. Hirvi, J T, Bochmann, M, Severn, J R, Linnolahti, M, Formation of Octameric Methylaluminoxanes by Hydrolysis of Trimethylaluminum and the Mechanisms of Catalyst Activation in Single-Site α-Olefin Polymerization Catalysis, ChemPhysChem., **2014**, 15, 2732-2742.

85. Luo, L.; Sangokoya, S. A.; Wu, X.; Diefenbach, S. P.; Kneale, B. Aluminoxane Catalyst Activators Derived From Dialkylaluminum Cation Precursor Agents, Processes For Making Same, And Use Thereof In Catalysts And Polymerization Of Olefins. US20090062492A1, **2009**.

86. Hlatky, G G, Lynch, M W., Perfluoroaryl Group 13 Activated Catalysts on Inorganic Oxides, In Tailor-Made Polymers, Wiley-VCH Verlag GmbH & Co. KGaA, **2008**.

87. Piers, W E, Chivers, T, Pentafluorophenylboranes: from obscurity to applications, Chem. Soc. Rev., **1997**, 26, 345-354.

88. Malinge, J.; Saudemont, T.; Spitz, R. Solid catalyst compound for polymerization of olefins. US6057258A, **1998**.

89. Prades, F.; Boisson, C.; Spitz, R.; Razavi, A. Activating supports for metallocene catalysis. 7759271B2, **2005**.

90. Prades, F, Broyer, J P, Belaid, I, Boyron, O, Miserque, O, Spitz, R, Boisson, C, Borate and MAO Free Activating Supports for Metallocene Complexes, ACS Catal., **2013**, 3, 2288-2293.

91. Prades, F.; Spitz, R.; Boisson, C.; Sirol, S.; Razavi, A. Transition metal complexes supported on activating fluorinated support. WO2007014889 A1, **2007**.

92. Ribeiro, M R, Deffieux, A, Portela, M F, Supported Metallocene Complexes for Ethylene and Propylene Polymerizations: Preparation and Activity, Ind. Eng. Chem. Res., **1997**, 36, 1224-1237.

93. Campos, J M, Lourenco, J P, Cramail, H, Ribeiro, M R, Nanostructured silica materials in olefin polymerisation: From catalytic behaviour to polymer characteristics, Progress in Polymer Science., **2012**, 37, 1764-1804.

94. Heurtefeu, B, Cécile Bouilhac, Éric Cloute, Taton, D, Deffieux, A, Cramail, H, Polymer support of "single-site" catalysts for heterogeneous olefin polymerization, Progress in Polymer Science., **2011**, 36, 89-126.

95. Klapper, M, Joe, D, Nietzel, S, Krumpfer, J W, Müllen, K, Olefin Polymerization with Supported Catalysts as an Exercise in Nanotechnology, Chem. Mater., **2014**, 26, 802-819.

96. Mcdaniel, M P, Influence of Catalyst Porosity on Ethylene Polymerization, ACS Catal., **2011**, 1, 1394-1407.

97. Soares, J B P, McKenna, T F L., Particle Growth and Single Particle Modeling, In Polyolefin Reaction Engineering, Wiley-VCH Verlag GmbH & Co. KGaA, **2012**.

98. Sacchetti, M.; Pasquali, S.; Govoni, G. Components and catalysts for the polymerization of olefins. US5698487A, **1997**.

99. Satyanarayana, G, Sivaram, S, An unusually stable supported bis(cyclopentadienyl)titanium dichloride-trialkylaluminum catalyst system for ethylene polymerization, Macromolecules., **1993**, 26, 4712-4714.

100. Guan, Z, Zheng, Y, Jiao, S, Spherical MgCl2-supported MAO pre-catalysts: preparation, characterization and activity in ethylene polymerization, Journal of Molecular Catalysis A: Chemical., **2002**, 188, 123-131.

101. Severn, J R, Chadwick, J C, MAO-Free Activation of Metallocenes and other Single-Site Catalysts for Ethylene Polymerization using Spherical Supports based on MgCl2, Macromol. Rapid Commun., **2004**, 25, 1024-1028.

102. Saito, J, Mitani, M, Matsui, S, Tohi, Y, Makio, H, Nakano, T, Tanaka, H, Kashiwa, N, Fujita, T, A New Titanium Complex Having Two Phenoxy-Imine Chelate Ligands for Ethylene Polymerization, Macromol. Chem. Phys., **2002**, 203, 59-65.

103. Suga, Y.; Maruyama, Y.; Isobe, E.; Suzuki, T.; Shimizu, F. Catalyst for polymerizing an olefin and method for producing an olefin polymer. US5308811A, **1994**.

104. Suga, Y.; Uehara, Y.; Maruyama, Y.; Isobe, E.; Ishihama, Y.; Sagae, T. Catalyst for polymerizing an olefin and method for polymerizing the olefin. US5928982A, **1999**.

105. Kurokawa, H, Morita, S, Matsuda, M, Suzuki, H, Ohshima, M a, Miura, H, Polymerization of ethylene using zirconocenes supported on swellable cation-exchanged fluorotetrasilicic mica, Applied Catalysis A: General., **2009**, 360, 192-198.

106. Weiss, K, Wirth-Pfeifer, C, Hofmann, M, Botzenhardt, S, Lang, H, Br++ning, K, Meichel, E, Polymerisation of ethylene or propylene with heterogeneous metallocene catalysts on clay minerals, Journal of Molecular Catalysis A: Chemical., **2002**, 182-183, 143-149.

107. Maneshi, A, Soares, J B P, Simon, L C, Polyethylene/Clay Nanocomposites Made with Metallocenes Supported on Different Organoclays, Macromol. Chem. Phys., **2011**, 212, 216-228.

108. Dong-ho Lee and Hyuk-soo Kim and Keun-byoung Yoon and Kyung Eun Min and Kwan Ho Seo and Seok Kyun Noh, Polyethylene/MMT nanocomposites prepared by in situ polymerization using supported catalyst systems, Science and Technology of Advanced Materials., **2005**, 6, 457.

109. Maneshi, A, Soares, J B P, Simon, L C, An Efficient In Situ Polymerization Method for the Production of Polyethylene/Clay Nanocomposites: Effect of Polymerization Conditions on Particle Morphology, Macromol. Chem. Phys., **2011**, 212, 2017-2028.

110. Tayano, T, Uchino, H, Sagae, T, Ohta, S, Kitade, S, Satake, H, Murata, M, Locating the active sites of metallocene catalysts supported on acid-treated montmorillonite, Journal of Molecular Catalysis A: Chemical., **2016**, 420, 228-236.

111. Michelotti, M, Arribas, G, Bronco, S, Altomare, A, Effect of the zeolite HY-support on the monoalkene polymerization by group IV metallocenes, Journal of Molecular Catalysis A: Chemical., **2000**, 152, 167-177.

112. Costa Vaya, V I, Belelli, P G, dos Santos, J H Z, Ferreira, M L, Damiani, D E, Influence of Acidic Support in Metallocene Catalysts for Ethylene Polymerization, Journal of Catalysis., **2001**, 204, 1-10.

113. Qi Meizho, Fu Zhisheng, Fan Zhiqiang, Immobilization of Metallocene Catalysts, Progress in Chemistry., **2014**, 26, 737-748.

114. Stalzer, M M, Delferro, M, Marks, T J, Supported Single-Site Organometallic Catalysts for the Synthesis of High-Performance Polyolefins, Catalysis Letters., **2015**, 145, 3-14.

115. Harrison, D, Coulter, I M, Wang, S, Nistala, S, Kuntz, B A, Pigeon, M, Tian, J, Collins, S, Olefin polymerization using supported metallocene catalysts: development of high activity catalysts for use in slurry and gas phase ethylene polymerizations, Journal of Molecular Catalysis A: Chemical., **1998**, 128, 65-77.

116. Maria De Fatima V.Marques, Moacir de Alcantara, Alumina as support for metallocene catalyst in ethylene polymerization, J. Polym. Sci. A Polym. Chem., **2004**, 42, 9-21.

117. Turunen, J P J, Venäläinen, T, Suvanto, S, Pakkanen, T T, Novel use of mesoporous aluminas as supports for Cp2ZrCl2 and Cp*ZrMe3: Ethylene polymerization and formation of polyethylene nanofibers, J. Polym. Sci. A Polym. Chem., **2007**, 45, 4002-4012.

118. Zhuravlev, L T, The surface chemistry of amorphous silica. Zhuravlev model, Colloids and Surfaces A: Physicochemical and Engineering Aspects., **2000**, 173, 1-38.

119. Van Grieken, R, Carrero, A, Suarez, I, Paredes, B, Ethylene polymerization over supported MAO/(nBuCp)2ZrCl2 catalysts: Influence of support properties, European Polymer Journal., **2007**, 43, 1267-1277.

120. Smit, M, Zheng, X, Loos, J, Chadwick, J C, Koning, C E, Effects of methylaluminoxane immobilization on silica on the performance of zirconocene catalysts in propylene polymerization, J. Polym. Sci. A Polym. Chem., **2005**, 43, 2734-2748.

121. Fink, G, Steinmetz, B, Zechlin, J, Przybyla, C, Tesche, B, Propene Polymerization with Silica-Supported Metallocene/MAO Catalysts, Chem. Rev., **2000**, 100, 1377-1390.

122. Goretzki, R, Fink, G, Tesche, B, Steinmetz, B, Rieger, R, Uzick, W, Unusual ethylene polymerization results with metallocene catalysts supported on silica, J. Polym. Sci. A Polym. Chem., **1999**, 37, 677-682.

123. Steinmetz, B, Tesche, B, Przybyla, C, Zechlin, J, Fink, G, Polypropylene growth on silica-supported metallocene catalysts: A microscopic study to explain kinetic behavior especially in early polymerization stages, Acta Polym., **1997**, 48, 392-399.

124. Floyd, S, Heiskanen, T, Taylor, T W, Mann, G E, Ray, W H, Polymerization of olefins through heterogeneous catalysis. VI. Effect of particle heat and mass transfer on polymerization behavior and polymer properties, J. Appl. Polym. Sci., **1987**, 33, 1021-1065.

125. Tisse, V F, Prades, F, Briquel, R, Boisson, C, McKenna, T F L, Role of Silica Properties in the Polymerisation of Ethylene Using Supported Metallocene Catalysts, Macromol. Chem. Phys., **2010**, 211, 91-102.

126. Tisse, V F, Briquel, R M, McKenna, T F L, Influence of Silica Support Size on the Polymerisation of Ethylene Using a Supported Metallocene Catalyst, Macromol. Symp., **2009**, 285, 45-51.

127. Tioni, E, Broyer, J P, Monteil, V, McKenna, T, Influence of Reaction Conditions on Catalyst Behavior during the Early Stages of Gas Phase Ethylene Homo- and Copolymerization, Ind. Eng. Chem. Res., **2012**, 51, 14673-14684.

128. Webb, S W, Weist, E L, Chiovetta, M G, Laurence, R L, Conner, W C, Morphological influences in the gas phase polymerization of ethylene by silica supported chromium oxide catalysts, The Canadian Journal of Chemical Engineering., **1991**, 69, 665-681.

129. Sano, T, Doi, K, Hagimoto, H, Wang, Z, Uozumi, T, Soga, K, Adsorptive separation of methylalumoxane by mesoporous molecular sieve MCM-41, Chem. Commun., **1999**, 733-734.

130. Sano, T, Hagimoto, H, Sumiya, S, Naito, Y, Oumi, Y, Uozumi, T, Soga, K, Application of porous inorganic materials to adsorptive separation of methylalumoxane used as co-catalyst in olefin polymerization, Microporous and Mesoporous Materials., **2001**, 44–45, 557-564.

131. Sano, T, Hagimoto, H, Jin, J, Oumi, Y, Uozumi, T, Soga, K, Influences of methylaluminoxane separated by porous inorganic materials on the isospecific polymerization of propylene, Macromol. Rapid Commun., **2000**, 21, 1191-1195.

132. Silveira, F, Petry, C F, Pozebon, D, Pergher, S B, Detoni, C, Stedile, F C, dos Santos, J H Z, Supported metallocene on mesoporous materials, Applied Catalysis A: General., **2007**, 333, 96-106.

133. Silveira, F, Pires, G P, Petry, C F, Pozebon, D, Stedile, F C, Santos, J H Z, Rigacci, A, Effect of the silica texture on grafting metallocene catalysts, Journal of Molecular Catalysis A: Chemical., **2007**, 265, 167-176.

134. Wongwaiwattanakul, P, Jongsomjit, B, Copolymerization of ethylene/1-octene via different pore sized silica-based-supported zirconocene/dMMAO catalysts, Catalysis Communications., **2008**, 10, 118-122.

135. Bunchongturakarn, S, Jongsomjit, B, Praserthdam, P, Impact of bimodal pore MCM-41-supported zirconocene/dMMAO catalyst on copolymerization of ethylene/1-octene, Catalysis Communications., **2008**, 9, 789-795.

136. Kumkaew, P, Wanke, S E, Praserthdam, P, Danumah, C, Kaliaguine, S, Gas-phase ethylene polymerization using zirconocene supported on mesoporous molecular sieves, J. Appl. Polym. Sci., **2003**, 87, 1161-1177.

137. Kumkaew, P, Wu, L, Praserthdam, P, Wanke, S E, Rates and product properties of polyethylene produced by copolymerization of 1-hexene and ethylene in the gas phase with (n-BuCp)2ZrCl2 on supports with different pore sizes, Polymer., **2003**, 44, 4791-4803.

138. Tioni, E, Monteil, V, McKenna, T, Morphological Interpretation of the Evolution of the Thermal Properties of Polyethylene during the Fragmentation of Silica Supported Metallocene Catalysts, Macromolecules., **2013**, 46, 335-343.

139. Mcdaniel, M P, Fracturing silica-based catalysts during ethylene polymerization, J. Polym. Sci. Polym. Chem. Ed., **1981**, 19, 1967-1976.

140. Mcdaniel, M P, Rohlfing, D C, Benham, E A, Long Chain Branching in Polyethylene from the Phillips Chromium Catalyst, Polymer Reaction Engineering., **2003**, 11, 101-132.

141. Mcdaniel, M P, Collins, K S, The influence of porosity on the Phillips Cr/silica catalyst 2. Polyethylene elasticity, J. Polym. Sci. A Polym. Chem., **2009**, 47, 845-865.

142. McDaniel, M P, Influence of porosity on PE molecular weight from the Phillips Cr/silica catalyst, Journal of Catalysis., **2009**, 261, 34-49.

143. Klapper, M, Fink, G., Polymeric Supported Catalysts, In Tailor-Made Polymers, Wiley-VCH Verlag GmbH & Co. KGaA, **2008**.

144. Comito, R J, Fritzsching, K J, Sundell, B J, Schmidt-Rohr, K, Dincâ, M, Single-Site Heterogeneous Catalysts for Olefin Polymerization Enabled by Cation Exchange in a Metal-Organic Framework, J. Am. Chem. Soc., **2016**, 138, 10232-10237.

145. Soga, K, Shiono, T, Ziegler-Natta catalysts for olefin polymerizations, Progress in Polymer Science., **1997**, 22, 1503-1546.

146. Galli, P, Vecellio, G, Technology: driving force behind innovation and growth of polyolefins, Progress in Polymer Science., **2001**, 26, 1287-1336.

147. Hamielec, A E, Soares, J B P, Polymerization reaction engineering-Metallocene catalysts, Progress in Polymer Science., **1996**, 21, 651-706.

148. Begley, J W, The role of diffusion in propylene polymerization, J. Polym. Sci. A-1 Polym. Chem., **1966**, 4, 319-336.

149. Schmeal, W R, Street, J R, Polymerization in expanding catalyst particles, AIChE J., **1971**, 17, 1188-1197.

150. Nagel, E J, Kirillov, V A, Ray, W H, Prediction of Molecular Weight Distributions for High-Density Polyolefins, Ind. Eng. Chem. Prod. Res. Dev., **1980**, 19, 372-379.

151. Galvan, R, Tirrell, M, Molecular weight distribution predictions for heterogeneous Ziegler-Natta polymerization using a two-site model, Chemical Engineering Science., **1986**, 41, 2385-2393.

152. Kanellopoulos, V, Dompazis, G, Gustafsson, B, Kiparissides, C, Comprehensive Analysis of Single-Particle Growth in Heterogeneous Olefin Polymerization: The Random-Pore Polymeric Flow Model, Ind. Eng. Chem. Res., **2004**, 43, 5166-5180.

153. Kittilsen, P, Svendsen, H, McKenna, T F, Modeling of transfer phenomena on heterogeneous Ziegler catalysts. IV. Convection effects in gas phase processes, Chemical Engineering Science., **2001**, 56, 3997-4005.

154. McKenna, T F, Dupuy, J, Spitz, R, Modeling of transfer phenomena on heterogeneous Ziegler catalysts: Differences between theory and experiment in olefin polymerization (an introduction), J. Appl. Polym. Sci., **1995**, 57, 371-384.

155. McKenna, T F, Dupuy, J, Spitz, R, Modeling of transfer phenomena on heterogeneous Ziegler catalysts. III. Modeling of intraparticle mass transfer resistance, J. Appl. Polym. Sci., **1997**, 63, 315-322.

156. McKenna, T F, Soares, J B P, Single particle modelling for olefin polymerization on supported catalysts: A review and proposals for future developments, Chemical Engineering Science., **2001**, 56, 3931-3949.

157. Parasu Veera, U, Mass transport models for a single particle in gas-phase propylene polymerisation, Chemical Engineering Science., **2003**, 58, 1765-1775.

158. Singh, D, Merrill, R P, Molecular Weight Distribution of Polyethylene Produced by Ziegler-Natta Catalysts, Macromolecules., **1971**, 4, 599-604.

159. Yiagopoulos, A, Yiannoulakis, H, Dimos, V, Kiparissides, C, Heat and mass transfer phenomena during the early growth of a catalyst particle in gas-phase olefin polymerization : the effect of prepolymerization temperature and time, Chemical Engineering Science., **2001**, 56, 3979-3995.

160. Chiovetta, M G, Laurence, R L, Polymer reaction engineering. Influence of reaction engineering on polymer properties., Acta Polym., **1985**, 36, 346.

161. Estenoz, D A, Chiovetta, M G, A structural model for the catalytic polymerization of ethylene using chromium catalysts. Part I: Description and solution, Polym Eng Sci., **1996**, 36, 2208-2228.

162. Estenoz, D A, Chiovetta, M G, A structural model for the catalytic polymerization of ethylene using chromium catalysts. Part II: Thermal effects, Polym Eng Sci., **1996**, 36, 2229-2240.

163. Estenoz, D A, Chiovetta, M G, Olefin polymerization using supported metallocene catalysts: Process representation scheme and mathematical model, J. Appl. Polym. Sci., **2001**, 81, 285-311.

164. Ferrero, M A, Chiovetta, M G, Catalyst fragmentation during propylene polymerization: Part I. The effects of grain size and structure, Polym Eng Sci., **1987**, 27, 1436-1447.

165. Ferrero, M A, Chiovetta, M G, Catalyst fragmentation during propylene polymerization: Part II. Microparticle diffusion and reaction effects, Polym Eng Sci., **1987**, 27, 1448-1460.

166. Ferrero, M A, Chiovetta, M G, Catalyst fragmentation during propylene polymerization. III: Bulk polymerization process simulation, Polym Eng Sci., **1991**, 31, 886-903.

167. Ferrero, M A, Chiovetta, M G, Effects of catalyst fragmentation during propylene polymerization. IV: Comparison between gas phase and bulk polymerization processes, Polym Eng Sci., **1991**, 31, 904-911.

168. Floyd, S, Choi, K Y, Taylor, T W, Ray, W H, Polymerization of olefins through heterogeneous catalysis. III. Polymer particle modelling with an analysis of intraparticle heat and mass transfer effects, J. Appl. Polym. Sci., **1986**, 32, 2935-2960.

169. Floyd, S, Heiskanen, T, Taylor, T W, Mann, G E, Ray, W H, Polymerization of olefins through heterogeneous catalysis. VI. Effect of particle heat and mass transfer on polymerization behavior and polymer properties, J. Appl. Polym. Sci., **1987**, 33, 1021-1065.

170. Hutchinson, R A, Ray, W H, Polymerization of olefins through heterogeneous catalysis. VII. Particle ignition and extinction phenomena, J. Appl. Polym. Sci., **1987**, 34, 657-676.

171. Hutchinson, R A, Ray, W H, Polymerization of olefins through heterogeneous catalysis. VIII. Monomer sorption effects, J. Appl. Polym. Sci., **1990**, 41, 51-81.

172. Hutchinson, R A, Chen, C M, Ray, W H, Polymerization of olefins through heterogeneous catalysis X: Modeling of particle growth and morphology, J. Appl. Polym. Sci., **1992**, 44, 1389-1414.

173. Noristi, L, Marchetti, E, Baruzzi, G, Sgarzi, P, Investigation on the particle growth mechanism in propylene polymerization with MgCl2-supported ziegler–*N*atta catalysts, J. Polym. Sci. A Polym. Chem., **1994**, 32, 3047-3059.

APPENDIX 1

CHAPTER 1

A. Silica Synthesis

In a typical process, sodium silicate is reacted with a mineral acid e.g., sulfuric acid which yield siliconhydroxide and sodium sulfate. Condensation of silicon hydroxide forms polysilic acid units, whose continued condensation leads to the formation of a polymer of composition very similar to that of silica. The degree of polymerization can be increased by increasing the solution concentration and, more importantly, the acidity. The end product of this step is called a hydrosol, which is transparent and contains micelles of diameters in the range of 1-3 nm. The size of these micelles can be adjusted by controlling solution pH (larger micelles are obtained at higher pH).

In the next step, referred to as gelation, hydrosol is gelled to form a three dimensional (3D) network created by the formation of hydrogen bonds between the surface hydroxyl groups of micelles. At the start of this step, the solution pH is around 10 which is then reduced by acid addition. In addition to pH, mixing and reaction temperature also impact the rate of gelation. The gel obtained in this step is generally referred to as hydrogel. Mass fractional dimension is increased in this step by treating the gel at appropriate pH and temperature. The gel gets stronger due to dissolution and re-precipitation of the smaller particles on and in between the bigger ones. While the strength of the hydrogel is increased in this step, the surface area decreases due to Ostwald-ripening. This stage provides tailoring option for a metallocene catalyst support; it should have enough strength to withstand forces applied during catalyst synthesis and handling, but it should be fragile enough that it fragments under a reasonable applied stress. In other words, one can adjust the friability of the final silica support in this step. An illustration of this step is presented in **Figure S1**.

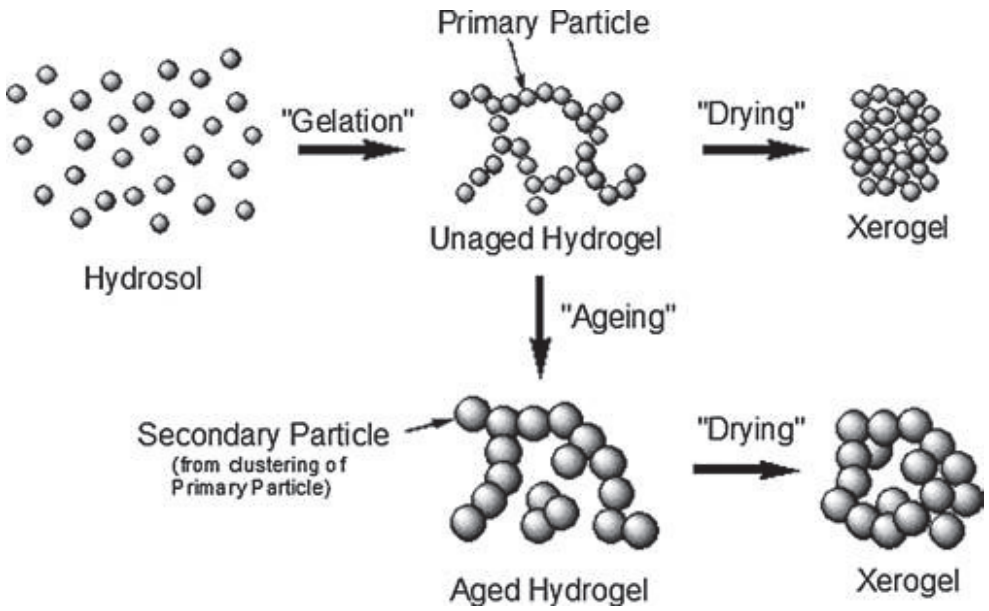

Figure S1. A schematic presentation of the ageing step during silica synthesis. Reproduced with permission from Severn et al.[45]

Washings applied to the hydrogel after the ageing process are of substantial importance as dissolved salts can affect the thermal and electrical properties of the final silica if they are not properly removed. The melting point of silica is a function of residual sodium oxide that is left in silica after neutralization and washing i.e., higher amounts of residual sodium oxide can reduce the melting temperature of silica which is of importance in high temperature processes. Surface acidity can also be impacted by the increased amounts of residual salts in silica which, consequently, impact the coordination capacity of the silica support. At this point if Al^{3+} ions are doped into the silica, its surface acidity is impacted significantly. Sodium and sulfate residues in the final silica product are attributed to poor washing of hydrogel, whereas water supply used is blamed for calcium, magnesium and soda residues. Aluminum, titanium and iron present in the final silica are passed on by the sand used to make silicates. Special care is taken in removing polyolefin catalyst poisons from the silica supports which can increase the production cost since several washing steps may be introduced to achieve the specified purity level.

Finally, the hardened and washed hydrogel is dried and during this step the pore volume of the hydrogel reduces significantly due to shrinkage of silica particles and removal of the liquid present in the hydrogel. The pore volume of the hydrogel is somewhere between 4-5 $mL.g^{-1}$ which is then reduced to 2-3 $mL.g^{-1}$ after drying. Mean pore diameters of the final support varies between 10 -

30 nm. As a rule of thumb, if the desired silica is to possess large porosity the drying is done at a faster rate than it is done for a silica to be of lesser porosity. Surface tension of water is higher and therefore, hydrocarbons are sometimes preferable than water because they cause lower pore volume shrinkage than water upon drying.[10,11,96] For this purpose, an aqueous solution of the hydrogel can be exchanged with a light hydrocarbon through emulsification step. Distillation of the solution under supercritical conditions is also employed sometimes to avoid the shrinkage effects.[45]

Silica used for metallocenes can be either irregularly formed granulates or spherical particles. The granulates arise from the grinding the filter cake obtained after the drying process and sieving or air separation can be used to obtain granulates of different particle sizes. Spherical shape provides high bulk density and therefore, most of the silica employed industrially consists of reasonably round particle as shown in **Figure S2**. Spray-drying or emulsification of a silica sol in an immiscible liquid (as said before also) can be used to obtain particles of spherical geometry.

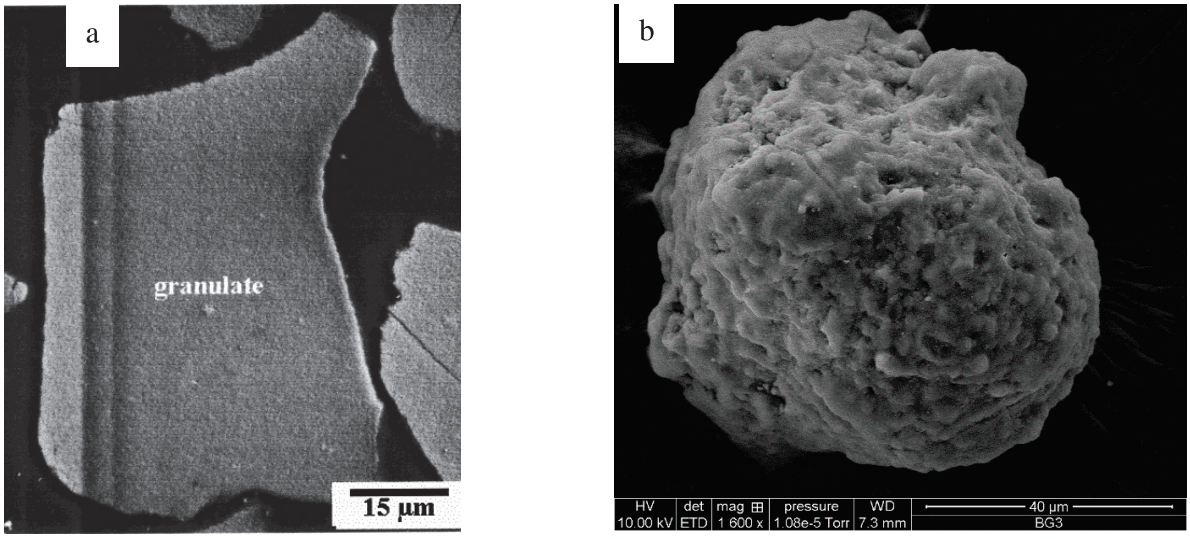

Figure S2. Comparison of granulate[121] (a) and spherical silica (b) particle morphology.

In the former procedure, silica granulates typically in the size range of 10-100 µm are re-dispersed in a mineral acid followed by drying using a standard spray-drying procedure in which the wet slurry is sprayed through a nozzle into a countercurrent of dry gas. This procedure is efficient enough and in a very short time fine silica powder in the size range of 10-100 µm can be obtained. In the second method of preparing spherical silica particles, the silica sol is first emulsified in an immiscible non-polar liquid by stirring, dropping etc., followed by the droplets being formed into

gelled beads of silica hydrogel. Drop size and sol viscosity are used to control the particle size of the gelled silica beads.[121]

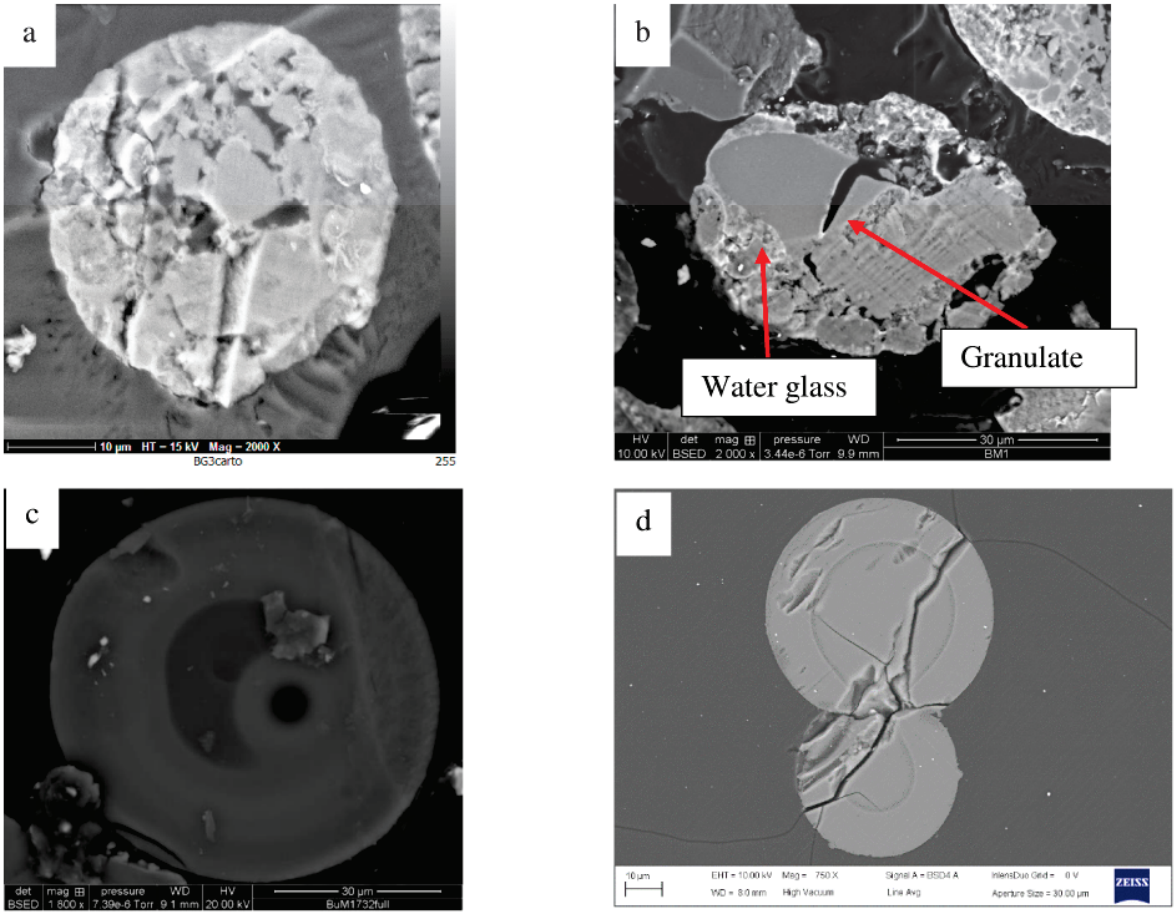

Figure S3. Comparison of the cross-sectional images of two commercial silicas used in this work. Grace 948 (a,b) and PQMS 1732 (c,d).

The differences between internal and external morphologies of two commercial silicas are shown in **Figure S3** where it is evident that both of them have been converted into spherical particles by a different method. Grace 948 silica seems to be spray dried since the interstitial voids which span throughout the particle surface and interior along with the fact that silica granulates and water glass also apparent in the cross-sectional images (see **Figure S3a, b**). Water glass is basically an alkali metal silicate which acts as glue for the silica granulates. Interstitial voids are tailored carefully since their non-uniform distribution inside the particles can affect the friability of the spherical silica particles. On the other hand, cross-sectional SEM images of PQMS1732 silica particles show

very uniform and well-connected porous structure without any interstitial voids or water glass which provides evidence that this silica has not been spray-dried and may have been emulsified in an immiscible liquid prior to drying. Note that the cracks shown in (see **Figure S3d**) are due to diamond knife as we shall see in the coming chapters also that this silica does not show any interstitial voids.[45,121] Such differences in the porous structure as well porosity of the silica supports can influence, at first, catalyst/co-catalyst dispersion throughout the individual particles and, secondly, diffusion of (co)-monomer(s) which generally diffuse inwards from the surface of the silica supported metallocenes, as we shall see in the coming chapters.

CHAPTER 2

Effect of Silica Dehydroxylation Temperature on the Grafting of MAO and Metallocene Activity

Contents

1. INTRODUCTION ---- 94
2. EXPERIMENTAL SECTION ---- 97
2.1. Materials ---- 97
2.2. Drying of MAO ---- 97
2.3. Catalyst Synthesis ---- 97
2.4. Polymerization Procedure ---- 98
2.5. Pressure Curve Fitting and Conversion into Ethylene Mass ---- 100
2.6. Silica, SMAO and Catalyst Characterization ---- 101
2.7. Polymer Characterization ---- 102
3. RESULTS AND DISCUSSION ---- 103
3.1. DRIFT Analysis of Silica, Dried MAO, SMAO and Supported Metallocene Catalysts 104
3.2. Solid State NMR Analysis of Dried MAO and SMAO samples ---- 106
3.3. Catalyst Evaluation ---- 115
3.4. Crystallinity and Molecular Masses of PE Samples ---- 120
4. CONCLUSION ---- 121
5. REFERENCES ---- 122
APPENDIX 1 ---- 127

1. Introduction

Amorphous silica is one of the most widely investigated and commonly used catalyst supports in the polyolefins industry. Metallocenes are anchored on pure, or methylaluminoxane (MAO)-modified amorphous silica to prepare supported (or heterogeneous) catalysts, which are then employed in slurry or gas phase processes to produce different grades of polyolefins.[1] The benefits of using supported metallocenes as opposed to homogenous catalysts include the ease of their injection and removal of the final product in solid form, reduced catalyst decay rates during polymerization[2] and the reduction of the risk of polymer film formation on the reactor walls which can in turn lead to poor heat removal from the reactor. A well-designed supported catalyst should offer good morphology control, high productivity, and ultimately economic gains. One of the keys to obtaining these advantages is fine control of the surface chemistry of the support, and the procedure used to produce the MAO activated silica support (SMAO). Recent progress in deciphering MAO structure and its impact on the mechanism of metallocene activation leads us to believe that the cationic species $[AlMe_2]^+$ plays an important role in the activation process.[3,4] It is important to investigate the impact of the grafting of MAO on silica on the performance of this activator.

It is well-known that geminal, vicinal and isolated hydroxyl groups (OH), known collectively as silanols, and water can be found on the surface of untreated silica particles (**Scheme 1**). Furthermore, it has also been well established in the open literature that the surface concentration of these OH groups can be reduced by heating the silica, leaving only isolated silanol and siloxane (Si-O-Si) bridges at temperatures above 500°C.[5-11] On the other hand, it is difficult to know a priori what type and concentration of silanol groups are optimal in terms of activating a given metallocene precursor. Depending on the size and shape of the metallocene, one needs to minimize the steric hindrance to the incoming catalyst precursor or co-catalyst molecule, to prevent bimolecular deactivation, and promote the generation of the active metallocenium cation, all of which contribute in determining the activity and performance of the catalyst. For example, $(n\text{-}BuCp)_2ZrCl_2$ is one of the metallocenes that has found its application in industrial as well as academic research,[12-14] yet only a few researchers have studied the effect of silica dehydroxylation temperature on its activity.[7,9,11,15] Based on these studies, it is difficult to draw clear conclusion on what, if any relationship exists between the silica dehydroxylation temperature and the catalytic activity, i.e. whether or not a

decrease in the concentration of OH groups on the silica surface helps to increase supported catalyst's activity. Since it has been shown[1,15] that different synthesis methods give different activities of the silica supported metallocenes, the most probable reason for this lack of clarity seems to be that different catalyst synthesis procedures were used in the previously cited studies, as discussed briefly in the next paragraph.

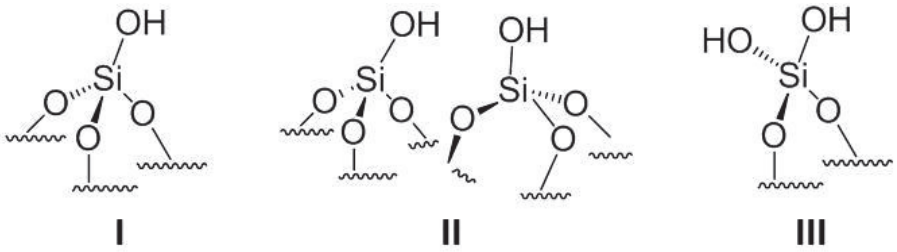

Scheme 1. Schematic representation of Isolated (I), Vicinal (II) and Geminal (III) silanol groups on the surface of silica.

Santos et al.,[7] analyzed the effect of silica dehydroxylation temperature on the metal loading on silica, catalytic activity in slurry ethylene polymerizations, the molecular weight distribution and crystallinity of the obtained polyethylenes. The catalysts were prepared by grafting $(n\text{-}BuCp)_2ZrCl_2$ on Grace 948 silica dehydroxylated in the temperature range of 27 °C to 450 °C. MAO (10 wt% toluene solution) was added separately into the reactor in order to obtain Al/Zr molar ratio in the range of 100-5000, and the polymerizations were done at only 1 bar ethylene pressure. Using the same zirconocene, van Greiken et al.,[11] studied the effect of silica dehydroxylation temperature (in the range of 200 to 600 °C) on the catalytic activity by grafting a pre-mixed solution of MAO (30wt% toluene solution) and $(n\text{-}BuCp)_2ZrCl_2$ on the dehydroxylated silica in toluene slurry at room temperature for 3h. Another study dedicated to the effect of silica dehydroxylation temperature on the catalytic activity of $(n\text{-}BuCp)_2ZrCl_2$ was reported by Atiqullah et al.,[9] who calcined the commercial ES-70 silica in the temperature range of 250 to 800 °C. The calcined silica were functionalized by $n\text{-}BuSnCl_3$ at 130 °C before impregnation with MAO and grafting of the zirconocene at room temperature. Based on all of these studies, it is difficult to identify a single silanol concentration which provides maximum catalytic activity for the silica supported $(n\text{-}BuCp)_2ZrCl_2$ in ethylene homopolymerization at conditions of industrial relevance and the reason due to which silica dehydroxylation temperature affects the catalytic activity. Furthermore, keeping in view the fact that MAO has a significant effect on the catalytic performance of supported $(n\text{-}BuCp)_2ZrCl_2$, the effect of varying silanol

concentration on the nature of Aluminium species generated after the interaction of MAO with silica cannot be understood based on the above mentioned studies. Other works related to the influence of silica dehydroxylation temperature on the catalytic activity of supported metallocences in olefin polymerization involves catalysts different from $(n\text{-}BuCp)_2ZrCl_2$ and therefore, reports different results.[16,17]

The present study aims to investigate the influence of silica dehydroxylation temperature on i) the type(s) of Aluminium specie(s) generated on the silica surface after impregnating MAO on silica dehydroxylated in the temperature range of 200 to 600 °C (i.e., by preparing SMAO) and ii) the catalytic performance of the active species generated on the surface of these SMAO samples after grafting the $(n\text{-}BuCp)_2ZrCl_2$ metallocene in ethylene homopolymerizations. In order to achieve this, an optimized incipient wetness method is used to make SMAO samples and the final supported catalysts. The catalysts are then evaluated in, both, slurry and gas phase ethylene homopolymerizations at conditions of industrial relevance. The benefit of using SMAO supported metallocene is twofold i.e., it allows to study the interactions between hydroxyl groups of silica and the MAO molecule and the leaching of the catalyst during polymerization is supressed ensuring heterogeneous catalysis. In addition, Diffuse Reflectance Fourier Transform Infrared Spectroscopy (FT-IR-DRIFT) analysis of the SMAO and of the catalysts (SMAO-$(n\text{-}BuCp)_2ZrCl_2$) coupled with a Solid State Nuclear Magnetic Resonance (SS NMR) characterization of SMAO are reported. The results are used to provide unique information on the nature of chemical species formed on the surface of silica after impregnation of MAO which subsequently influences the catalytic activity of the resulting supported metallocene catalyst. Furthermore, this study will allow us to fix a single dehydroxylation temperature for all the silica supports used in this work which, indirectly, means that we will be able to fix the surface chemistry of the supports. This means that the observed differences in the behaviour of supported catalysts can be attributed to the differences in physical parameters of the carrier.

2. Experimental Section

2.1. Materials

Grace 948 silica with a surface area of 290 m^2 g^{-1}, average particle diameter of 58 µm and a pore volume of 1.7 mL g^{-1} was used as the catalyst support. $(n\text{-}BuCp)_2ZrCl_2$ was obtained from Sigma-Aldrich. Triethylaluminium (TEA) and triisobutylaluminium (TIBA) were used as received from SGS and Witco Corporation, respectively. The MAO solution 30 wt% in toluene used in this study was supplied by Albemarle with the following characteristics: 13.6 wt% Al, 5.24 wt% $AlMe_3$, gas/Al = 1.65. n-heptane used in catalyst synthesis and as a diluent in slurry polymerizations were dried on 3 Å molecular sieves.

Ethylene (purity 99.95%) was purchased from Air Liquide (Paris, France) and passed through three different purification columns before use: a first one filled with reduced BASF R3-16 catalyst (CuO on alumina), a second one filled with molecular sieves (13X, 3A, Sigma-Aldrich), and a last one filled with Selexsorb COS (Alcoa).

2.2. Drying of MAO

White powder of dried MAO was obtained by first evaporating toluene from 30 wt% MAO commercial solution. Subsequently, the powder was dried under a dynamic vacuum of 10^{-3} to 10^{-5} mbar for 4 h at 80 °C. The dried MAO was then stored in a glove box.

2.3. Catalyst Synthesis

For silica dehydroxylation, 3 g of Grace 948 silica were taken in a Schlenk tube and heated under dynamic vacuum of 10^{-3} to 10^{-5} mbar following the profiles shown in **Figure S1**. The profiles for 450°C and 600°C are similar except the maximum temperatures. For 200°C profile, silica was heated at 130°C for 1h in order to remove all the adsorbed water whereas for the other two profiles this was achieved by heating for 2 h at 200°C. A time of 4h was given at maximum temperature under vacuum for all profiles. After dehydroxylation, silica was kept in the glove box.

The silica impregnated with MAO, named hereafter as SMAO, was prepared as follows. 2 g of dehydroxylated silica were placed in a three neck round bottom flask in the glove box under Argon. An amount of pure dry toluene equal to the pore volume of silica i.e., 1.7 ml g^{-1} was mixed with 3.5 ml of 30 wt% MAO solution in a separate vial at room temperature under argon and left for 30 min. This solution of MAO in toluene was then added to the silica drop-wise which wetted the silica completely. Then this thick slurry was heated at 80°C for 4h without any stirring under argon and the evaporating toluene was refluxed with the help of a

condenser. At the end of this process, the mixture was once washed with heptane and then dried under static vacuum at 80°C. Dried SMAO, a free flowing white powder, was stored in glove box.

Supported metallocene catalysts were synthesized by adding 2 g of SMAO in the three neck round bottom flask and adding a 10 mL solution of $(n\text{-}BuCp)_2ZrCl_2$ (by aiming Al/Zr molar ratio of 150 in the final catalyst) in toluene drop-wise at room temperature under argon. The volume of toluene solution was just enough to completely fill the pores. The slurry was then heated for 1h at 50°C followed by one heptane wash and vacuum drying at 50°C for few hours. Finally, a free flowing catalyst was obtained which was then stored in a glove box.

2.4. Polymerization Procedure

Polymerization runs were carried out in a spherical laboratory scale 2.5 L semi-batch reactor which can be operated both in slurry and gas phases. The reactor set-up used here is shown in **Figure 1**. Ethylene is supplied from a cylinder (1) and passes through the purification columns (2) before being stored in a separate cylinder (3) referred to as Ballast, which in turn supplies ethylene to the reactor during polymerizations. The spherical reactor (6) is equipped with a water circulation jacket through which the reactor temperature is varied by circulating hot or cold water (8). The rotational speed of the stirrer is controlled by the external unit (4). For injecting liquids like diluent for slurry polymerizations or scavenger during gas phase polymerizations, a separate valve (10) is used which is also used to vent the reactor at the end of polymerization time. A catalyst injection cartridge (5) could also be used depending upon the polymerization protocol used which is connected with ballast while injecting the catalyst into the reactor under high pressure. A thermocouple and a pressure sensor present inside the reactor provide internal temperature and pressure data which is then recorded by the software in computer (7). Similarly, the reactor bath temperature and ballast pressure are also recorded by the same software. In case where hydrogen is needed, a separate ballast (9) connected to the reactor can be used.

The reactor was conditioned for at least 1h at 80ºC with a minimum of three argon-vacuum cycles, and then cooled down to the room temperature. For slurry polymerizations, 500 mL of dry heptane containing 30 to 40 mg of catalyst and 1 mL of a 1 M solution of triethyl aluminium (TEA) or triisobutyl aluminium (TIBA) were added under argon into the reactor at room temperature. The reactor was then heated to the reaction temperature of 80ºC under continuous stirring at 400 rpm. Ethylene was injected and maintained at 8 bar pressure once

the desired reaction temperature was achieved. Consumption of ethylene was recorded by the pressure drop in an ethylene cylinder equipped with a pressure gauge.

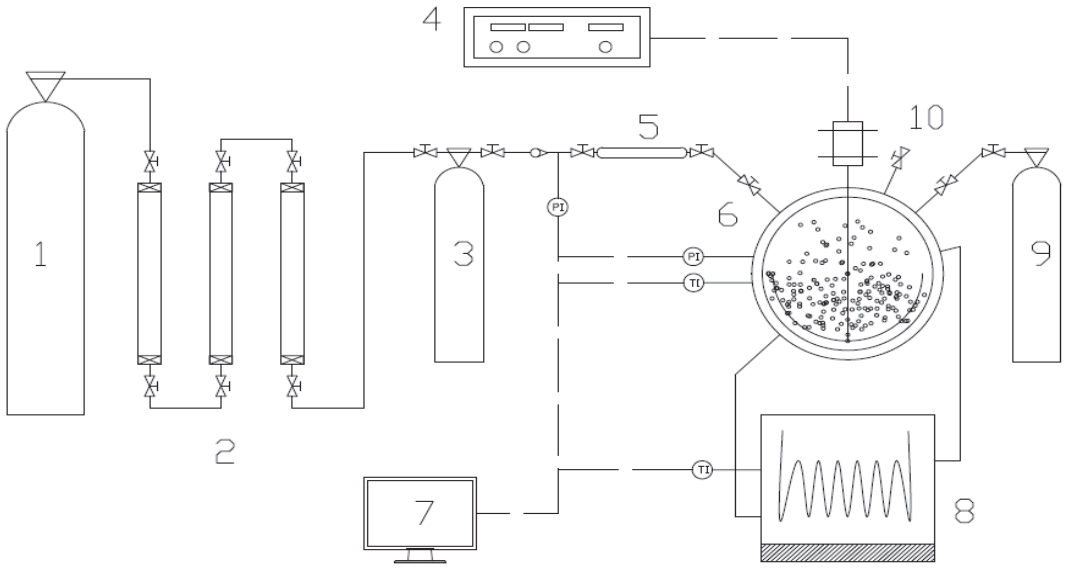

Figure 1. Schematic presentation of the reactor set-up.

For gas phase polymerizations, 30 g of dry sodium chloride (NaCl) was used as seed bed. The salt was dried twice at 400ºC for 4 h under vacuum of 10^{-3} mbar in order to remove all the adsorbed water. In order to prepare the seed bed, 30 g of dried NaCl were mixed with 15 to 18 mg of catalyst in a 100 mL flask inside glovebox and then transferred into the reactor under argon pressure. 1 mL of 1 M heptane solution of TIBA was then added into the reactor under argon flow at 70ºC. Then reactor temperature was then raised up to 80ºC. Ethylene was injected into the reactor once the desired reaction temperature was achieved under continuous stirring at 400 rpm. The reactions were stopped by venting the gaseous ethylene through reactor exhaust and cooling the reactor to 20ºC. The obtained polyethylene powder was then poured into a beaker of water where the salt was dissolved in water during overnight stirring at room temperature.

Reaction time was 1 h for slurry polymerizations and 2 h for gas phase polymerizations unless otherwise mentioned.

2.5. Pressure Curve Fitting and Conversion into Ethylene Mass

The pressure drop of ethylene inside the ballast attached to the reactor during polymerization run was recorded by a recorder attached to the computer, and a typical curve is shown in **Figure 2**. This pressure data was smoothed by fitting it to the Equation-1 which is termed as Logistics function in Origin Pro8 commercial software.

$$P = A_2 + \frac{(A_1 - A_2)}{\left(1 + \left(\frac{t}{t_0}\right)^p\right)} \quad (1)$$

Where, P is the pressure calculated in bar, A_1, A_2, p are adjustable model parameters and t_0 represent the central value of time axis. Other than the presented case, the R^2 values were about 0.999 which indicates excellent fitting results.

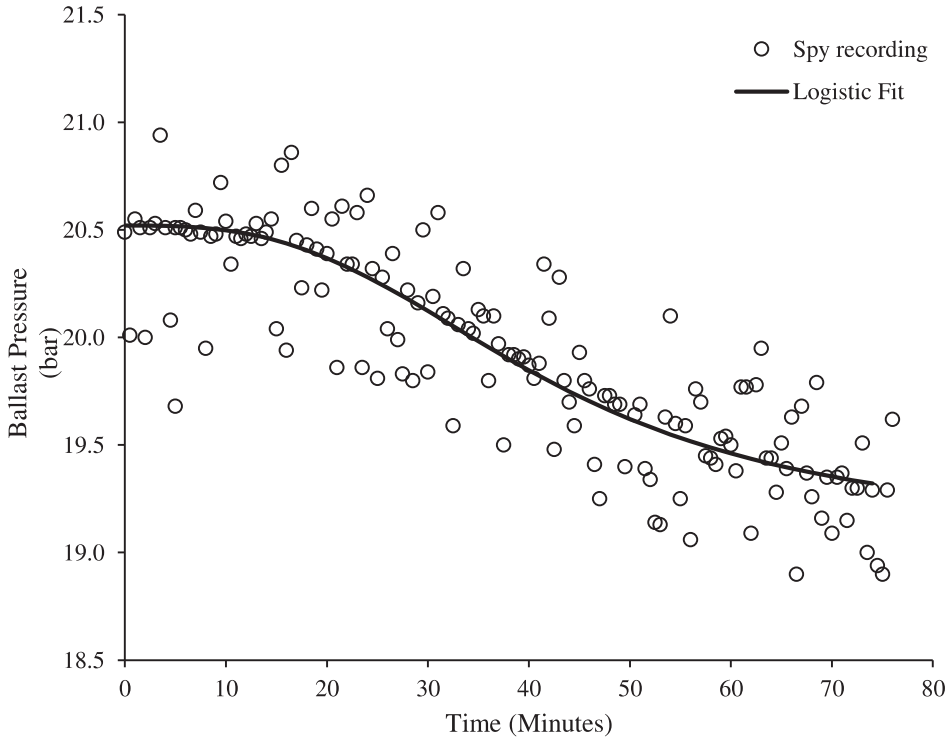

Figure 2. Comparison of ballast pressure recorded by the recorder (spy) during polymerization and its fitting with Logistic equation.

The fitted pressure curves were then used to calculate the ethylene mass (M_{Eth}) by employing Equation-2 for which volume (V_B) and temperature of ballast (T_B) were set to 5 L and 20 °C. Activity of the catalysts was then estimated by using this M_{Eth} value.[56]

$$M_{Eth} = V_B \times P \times (a + b + c) \quad (2)$$

where,

$$a = (1.256 - 0.004505 \times T_B + 0.0000109 \times T_B^2)$$

$$b = (0.0052 - 0.00001495 \times T_B - 0.0000001244 \times T_B^2) \times P$$

$$c = (0.0003252 - 0.00000732 \times T_B + 0.00000004195 \times T_B^2) \times P^2$$

2.6. Silica, SMAO and Catalyst Characterization

Al and Zr content of the final catalysts were then obtained by Inductively Coupled Plasma-Atomic Emission Spectroscopy (ICP-AES) at Mikroanalytisches Labor Pascher, Germany.

Diffuse Reflectance Fourier Transform Infrared spectroscopy (FT-IR-DRIFT) was used to characterise the as-received Grace 948 silica, the silica dehydroxylated at different temperatures, and MAO impregnated silica (SMAO) prepared by using silica dehyroxylated at different temperatures and the final catalysts. A few milligrams of each sample were added in a DRIFT cell equipped with CaF_2 windows within a glove box. For dried MAO, the sample was mixed with dry KBr (10wt%). IR spectra were recorded on a Nicolet 6700 FT-IR spectrometer. Typically, 64 scans were accumulated for each spectrum (resolution 4 cm^{-1}).

Solid-state NMR spectra were acquired on a Bruker Avance III 800 spectrometer (^{1}H: 800.13 MHz, ^{27}Al: 208.50 MHz). For ^{1}H experiments, the spinning frequency was 20 kHz, the recycle delay was 5 s and 128 scans were collected using a 90° pulse excitation of 2.25 μs. The ^{27}Al MAS NMR spectra at 18.8 T were acquired at a spinning frequency of 20 kHz, using central transition –selective Hahn echo sequence. The D-HMQC experiments were set up with a ^{27}Al spin echo selective to the central transition, with pulses of 8 and 16 μs, with ^{1}H π/2 pulse of 3.3 μs on either side of the ^{27}Al π pulse. The number of scans for each t1 increment was set to 1280. The dipolar recoupling scheme ($SR4^2_1$) was applied for 600 μs.[18] Two-dimensional (2D) ^{1}H-^{1}H Double Quantum Magic-Angle Spinning spectra were performed at 20 kHz spinning speed using the $R12_2^5$ symmetry-based recoupling scheme[19] applied for 133 μs at RF field strength of 65 kHz. The recycling delay was set to 2 s and 16 transients were added for each of the 100 t1 increments. The ^{27}Al MQMAS spectra were collected using the Z-filter sequence,[20] which consists of two hard pulses of 3.5 and 1.3 μs at an RF field of 90 kHz, for triple-quantum excitation and reconversion, respectively, followed by a soft pulse of 6 μs at an RF field of 15 kHz. The t1 step was set to the MAS period.

Chemical shifts were given in ppm with respect to TMS as external reference for ^{1}H NMR, and to $Al(H_2O)_6^{3+}$ for ^{27}Al NMR. The NMR-analysed samples are dried MAO, SMAO-200°C, SMAO-450°C and SMAO-600°C. Samples were prepared under strictly inert conditions in an argon-filled glovebox by packing into ZrO_2 rotors closed with Kel-F caps.

2.7. Polymer Characterization

High Temperature Size Exclusion Chromatography (HT-SEC) analyses were performed using a Viscotek system (from Malvern Instruments) equipped with three columns (PLgel Olexis 300 mm x 7 mm I. D. from Agilent Technologies). 200 µL of sample solutions with a concentration of 5 mg mL^{-1} were eluted in 1,2,4-trichlorobenzene using a flow rate of 1 mL min^{-1} at 150°C. The mobile phase was stabilized with 2,6-di(tert-butyl)-4-methylphenol (200 mg L^{-1}). Online detection was performed with a differential refractive index detector and a dual light scattering detector (LALS and RALS) for absolute molar mass measurement. The OmniSEC 5.02 software was used for calculations.

Thermal characterizations were performed with a differential scanning calorimetry, Mettler Toledo DSC 1, equipped with an auto-sampler and a 120 thermocouple sensor. The temperature and the heat flow of the equipment were calibrated with an indium standard. All samples were accurately weighed (between 5 to 10 mg) and sealed in aluminium pans. They were heated from -20 °C to 180 °C at 10 °C.min^{-1} with an empty aluminium pan as reference. Two successive heating and cooling were performed and only the second run was considered. Dry nitrogen with a flow rate set at 50 mL.min^{-1} was used as the purge gas. The melting temperature (T_m) was measured at the top of the endothermic peak. The STAR^e thermal analysis software is used to calculate the melting temperature and the crystallinity (χ) of the polymers: $\chi = \Delta H_f / \Delta H_{f0}$ where ΔH_f (J.g^{-1}) is the melting heat of the sample and ΔH_{f0} (= 293 J.g^{-1}) the melting heat of a 100 % crystalline polyethylene.[21]

3. Results and Discussion

The manner in which supported catalysts (metallocene or other) are prepared will obviously have an impact on the quantity and nature of the active species, and this in turn have an effect on the kinetic performance of the catalyst in the polymerization process, molecular and physical properties of the final polymer product. As we mentioned above, various routes for the preparation of silica-supported metallocenes have been presented in the literature, and each synthesis procedure has specific advantages.[7,9,11,15,22,23] Supporting MAO on dehydroxylated silica before grafting the metallocene is one of the most common methods discussed in the open literature. However, the role of the dehydroxylation temperature of silica on the grafting of MAO, which in turn impacts the performance of the catalyst, has not been clearly explained.

In the present work three SMAO/$(n\text{-BuCp})_2ZrCl_2$ catalysts were prepared using the Grace 948 silica treated respectively at 200°C, 450°C or 600°C. The dehydroxylation of silica was followed by the impregnation of a toluene solution of 30 wt% MAO (Albemarle) for 4 h at 80°C. The chemical formula of the MAO can be determined from the analysis provided by the supplier (see experimental part). In agreement with the work of Imhoff et al.,[24] the formula of MAO can be represented as $(Al(CH_3)_{1.42}O_{0.79})_n$ and free trimethylaluminium (TMA, representing14.4% of Al). The final product of this step was a white free flowing powder named as SMAO-200°C, SMAO-450°C or SMAO-600°C depending upon the silica dehydroxylation temperature used. The activation of $(n\text{-BuCp})_2ZrCl_2$ on each SMAO i.e., SMAO-200°C, SMAO-450°C and SMAO-600°C was carried out by first mixing the toluene solution of metallocene with SMAO followed by heating at 50°C for 1h under Argon without any stirring. One wash of heptane was applied at the end of reaction time at 50°C, and the mixture was then dried under vacuum at 50°C. The final catalyst was a free flowing light green powder, which will be referred, hereafter, as n-BuCp-200°C, n-BuCp-450°C and n-BuCp-600°C depending upon the silica dehydroxylation temperature used.

The elemental analysis of these catalysts by ICP-AES is presented in **Table 1**. The aluminium content of the final catalysts decreased with the increase of the silica dehydroxylation temperature. The Al/Zr molar ratio was close to the targeted ratio of 150 based on a full impregnation of the MAO and of the metallocene complex when the silica was thermally treated at 450 and 600°C. Surprisingly, the Zr content for the n-BuCp-200°C catalysts was lower than expected. It can be assumed that the supported activator SMAO-200°C displays lower amount of activating sites leading to a lower grafting of the

metallocene. We can thus suppose that the nature of the silanol groups on silica support, which is controlled by the thermal treatment of the silica, impacts the structure of the supported MAO and consequently its ability to react with a metallocene precursor. DRIFT and SS-NMR analyses of SMAO were performed for characterizing the SMAO and provided some information regarding the difference of reactivity between MAO and the Grace 948 silica treated, respectively, at 200°C, 450°C or 600°C.

Table 1. Elemental analysis of the supported catalysts prepared by using different silica dehydroxylation temperatures.

Silica T(°C)	**Al (wt%)**	**Zr (wt%)**	**Al moles**	**Zr moles**	**Al/Zr**
200	16.24	0.11	6.02E-03	1.21E-05	499
450	13.45	0.29	4.99E-03	3.18E-05	157
600	11.40	0.26	4.23E-03	2.85E-05	148

3.1. DRIFT Analysis of Silica, Dried MAO, SMAO and Supported Metallocene Catalysts

Silica surface hydroxyl (OH) groups are characterized as isolated silanol (**scheme 1**, **I**), vicinal silanol (**scheme 1, II**) and geminal silanol (**scheme 1, III**). These silanol groups act as fixation sites for the cocatalysts or metallocenes depending upon the method of catalyst synthesis and their concentrations decrease with an increase in silica dehydroxylation temperature. DRIFT is an essential analytical tool for analysing different type of chemical species present on silica surface and it has been used extensively to characterize different species present or generated on the silica surface before and after dehydroxylation, impregnation with MAO and metallocene grafting.[5-8,25,26] The DRIFT spectra of 600 °C dehydroxylated Grace 948 silica, SMAO-600°C and n-BuCp-600°C are compared in **Figure 3** (See also **Figures S2** and **S3** in supporting information for silica treated at 200°C and 450°C, respectively). It can be observed that, in addition to isolated silanol groups (peak at 3736 cm^{-1}), vicinal OH groups (peak at 3661 cm^{-1} and 3536 cm^{-1}) are also present after heat treatment at 200°C,[7] whereas, only isolated silanol groups remain on silica after treatment at 450°C and 600°C. Broad bands at 1870 cm^{-1} and 1632 cm^{-1} are overtones and result from combination of intense Si-O fundamental modes. These results are in good agreement with available literature data.[5-8]

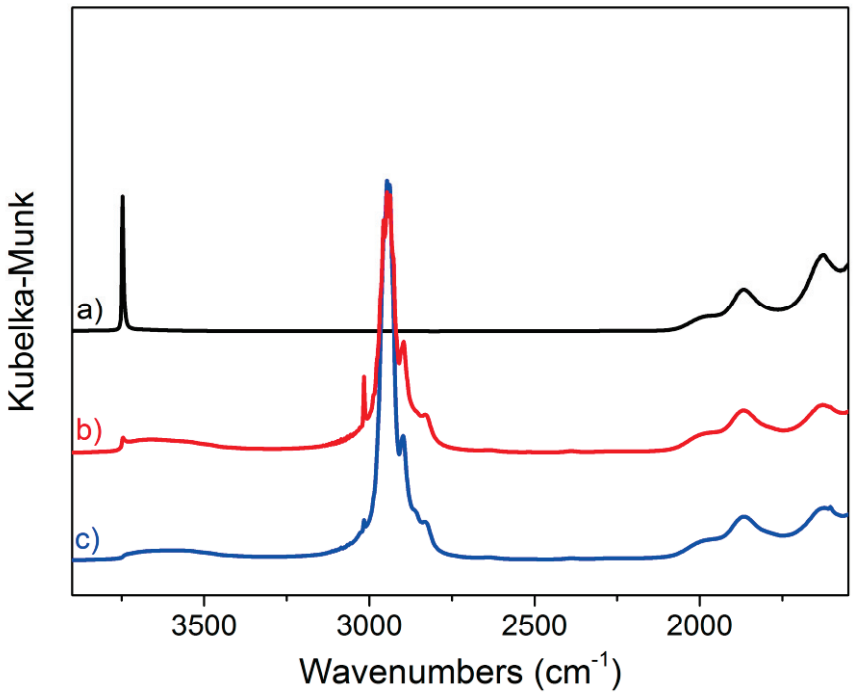

Figure 3. DRIFT spectra of silica-600°C (a), after reaction of MAO (SMAO-600°C) (b), after activation of $(n\text{-BuCp})_2ZrCl_2$ (n-BuCp-600°C) (c).

After impregnation of each silica with MAO, new peaks appear, especially in the range of 3100 to 2700 cm^{-1} due to the reaction of MAO with different silanol groups present on silica. Since, MAO is a mixture of oligomeric MAO and TMA,[6,27] it has been suggested that, depending on the dehydroxylation temperature, silanol (Si-OH) or siloxane (Si-O-Si) groups of silica react with TMA, whereas MAO is physically adsorbed on the surface.[6,7,10] The reaction of TMA with OH groups generate -Si-O-Al-(CH_3) species, whereas, -Si-CH_3 moieties are produced by the reaction of Al-CH_3 species with Si-O-Si siloxane groups.[6,27] For SMAO-200°C and SMAO-450°C, isolated silanols are totally consumed by reaction with MAO in contrast to SMAO-600°C as indicated by a small band at 3745 cm^{-1} in **Figure 3** characteristic of isolated silanols. This peak totally disappeared after metallocene grafting. Hydrogen bonded OH groups can be observed in all the SMAO samples in the range of 3680 to 3660 cm^{-1}.

Methyl groups of MAO can be observed in the region of 3000 to 2800 cm^{-1} with υ_a and υ_s of the terminal methyl groups in the range of 3050-2018 cm^{-1} and 2950-2750 cm^{-1}.[5,6] In case of SMAO-450°C and SMAO-600°C, very similar peaks can be observed at 2957, 2947, 2940 and 2900 cm^{-1} that can be attributed to the stretching vibrations of methyl groups in Al-CH_3 species or Si-CH_3 species. Distinction between the two species (i.e., Al-CH_3 or Si-CH_3) based on DRIFT spectra is difficult because the stretching vibrations of methyl groups in both the

species are very similar, [6,27] however, Bianchini and Panchenko et al.,[5,6] attributed the peak at 2960 cm^{-1} to the presence of Si-CH_3 species. The DRIFT spectra of SMAO samples show the presence of this peak in SMAO-450°C and SMAO-600°C at 2957 cm^{-1}, whereas, no such peak is present in the SMAO-200°C sample. This is due to the fact that reactive siloxane bonds (Si-O-Si) are formed only at higher dehydroxylation temperatures. DRIFT spectrum of SMAO-200°C (i.e., Figure S2) showed peaks at 2949 and 2900 cm^{-1} due to the stretching vibrations of methyl groups in Al-CH_3 species.[5,6] In addition, the DRIFT spectrum of dried MAO (**Figure S4**) showed peaks at 2947, 2937 and 2895 cm^{-1} for the stretching vibrations of methyl groups in Al-CH_3 species. This analysis confirms the assignment of peaks observed in the same region for SMAO. In summary DRIFT analyses of dehydroxylated silica, SMAO and supported metallocene showed that the nature of surface species is influenced by the reactivity of silanol and siloxane bonds which depends on the thermal treatment of silica.

DRIFT spectra of the final supported catalysts i.e., after grafting the metallocene on SMAO samples are also shown **Figure 3**, **Figure S2** and **Figure S3**. It is important to mention that characteristic absorption peaks of the aromatic and alkyl groups present in the (n-$BuCp)_2ZrCl_2$ molecule appear in the same region as that of MAO molecule i.e., 3100-2800 cm^{-1} (C-H stretching) and 1500-1300 cm^{-1} (methyl and methylene deformation modes).[7] Therefore, it is difficult to differentiate between the DRIFT peaks coming from metallocene, MAO and toluene molecules. However, the peak at 1602 cm^{-1} can be attributed to -C=C- stretching of the Cp ring, whereas, the one at 1494 cm^{-1} can be attributed to bending vibrations $\delta(CH_3)$ of the butyl substituent of the Cp ligand[25,28] and appears in the DRIFT spectra of all the final supported catalysts only. The stretching vibrations at 3016 cm^{-1} have been attributed to the Cp ring by Bianchini et al.,[5] This peak was also observed in our spectra, however, it should be noticed that residual toluene shows the same vibration (see SMAO spectra in **Figure 3**, **Figure S2** and **Figure S3**).

3.2. Solid State NMR Analysis of Dried MAO and SMAO samples

Liquid-state NMR studies on MAO and aluminoxanes have been previously reported in the literature.[29-31] In particular, given the possibility to determine the coordination number of aluminum alkyl from their chemical shift, ^{27}Al should be the most adequate tool to determine the structural features with MAO.[32,33] However, ^{27}Al being a quadrupolar nucleus (S=5/2), the broad line width encountered in non-highly symmetrical environments prevents any detailed analysis. On the other hand, solid state NMR provides access to additional

spectroscopic parameters other than chemical shift. Namely, it is possible to determine quadrupolar coupling constants that are characteristic for given structural types. One can also benefit from high resolution techniques such as MQMAS to disentangle complex 1D spectra (vide infra). Indeed, a few studies on MAO and molecular models have been performed, with mixed conclusions regarding the actual MAO structure.[34,35] It is therefore of interest to perform more detailed studies involving state of the art NMR methodology focused on structural investigations on MAO and to its grafting on silica. In the present study, we used high field NMR, combined to high resolution method MQMAS for quadrupolar nuclei, as well as homo- and heteronuclear correlations to determine the main features of MAO and its silica-supported version along with the grafting reaction pathways. It should be taken into account that we will be studying materials (dried MAO and SMAO) that have been subjected to vacuum treatment. Thus in the case of dried MAO studied here, its composition differs from that of commercial MAO solutions, where $AlMe_3$ (either free or bound) is present in the samples. Indeed, the vacuum treatment causes $AlMe_3$ elimination from the product (**Figure S5**).

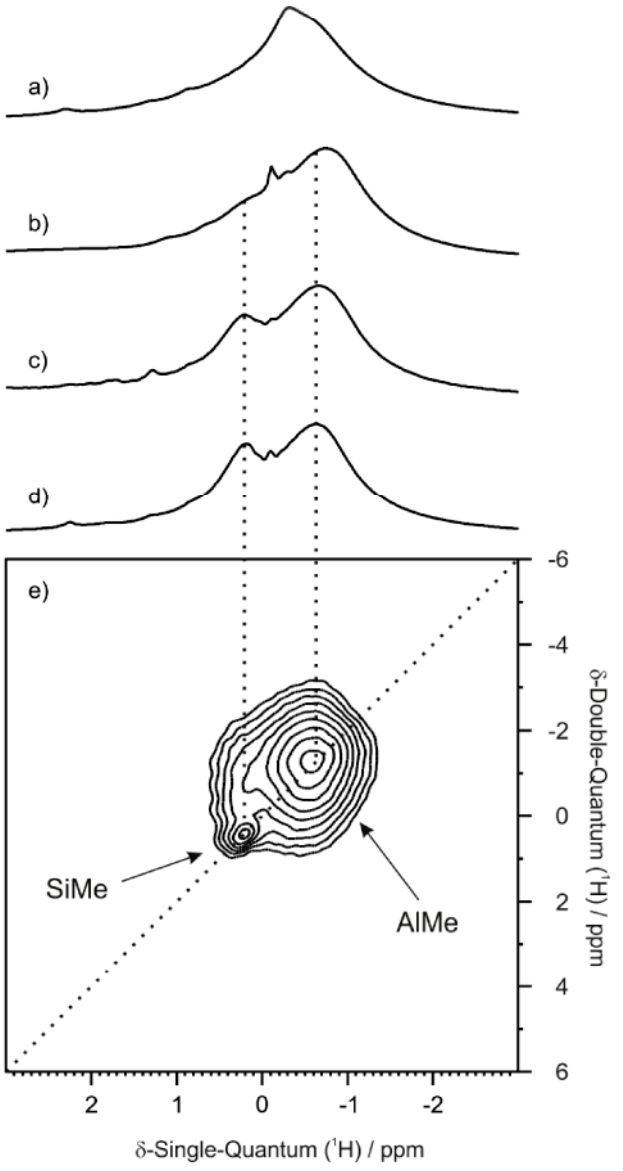

Figure 4. ^{1}H MAS NMR spectra of a) dried MAO, b) SMAO-200°C, c) SMAO-450°C and d) SMAO-600°C; e) ^{1}H-^{1}H DQ MAS NMR spectrum of SMAO-600°C (18.8 T, spinning speed 20 kHz)

^{1}H MAS NMR spectra of dried MAO and supported MAO (SMAO-200°C, SMAO-450°C and SMAO-600°C) feature signals expected for Al-Me groups at a chemical shift (CS) of about -0.7 ppm (**Figure 4a-d**). A slight shift is observed in the position of the Al-Me signal upon grafting, from -0.4 ppm in dried MAO to about -0.7 ppm in the supported MAOs. Furthermore, when comparing spectra of SMAO-200°C and SMAO-600°C, one notices the increase of the 0.2 ppm signal assigned to Si-Me protons. This is in line with infrared studies described above. These groups arise from reaction of Al-Me with strained siloxane bridges, the proportion of which increases with silica dehydroxylation temperature (**Scheme 2**).

Proximities between protons within a solid can be determined using ^{1}H-^{1}H Two-Dimensional (2D) Double-Quantum MAS NMR spectroscopy (DQ MAS), which relies on homonuclear dipolar recoupling methods.[36] The DQ MAS spectrum of SMAO-600°C (**Figure 4e**) shows that the Si-Me groups are close to some of the Al-Me moieties, as expected from the postulated reaction mechanism. This is highly reminiscent of the surface chemistry of $AlMe_3$, where similar spectra are obtained (See **Figure S6** in Supporting Information for comparison).[37,38] This demonstrates that grafting of MAO occurs not only via Al-Me protonolysis, but also from Si-O-Si opening, which results in spatially close Si-Me and Al-Me groups (**Scheme 2**).

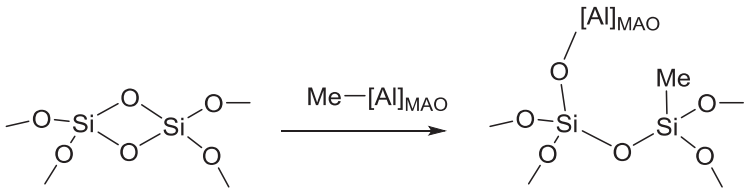

Scheme 2. Reaction of MAO with strained siloxanes

A further confirmation of proton signal assignment was brought by the ^{1}H-^{27}Al D-HMQC spectrum.[39] This technique probes the spatial proximity of heteronuclear pairs, within a given sphere radius. Using a short recoupling delay thus provides selective information on close spin pairs (below 4 to 5 Å). In the case of SMAO-600°C, the observed correlation with the ^{27}Al dimension (**Figure 5**) only concerns the -0.7 ppm ^{1}H signal, which confirms its assignment to Al-CH_3 group. Accordingly, no cross-peak is observed for the Si-Me site.

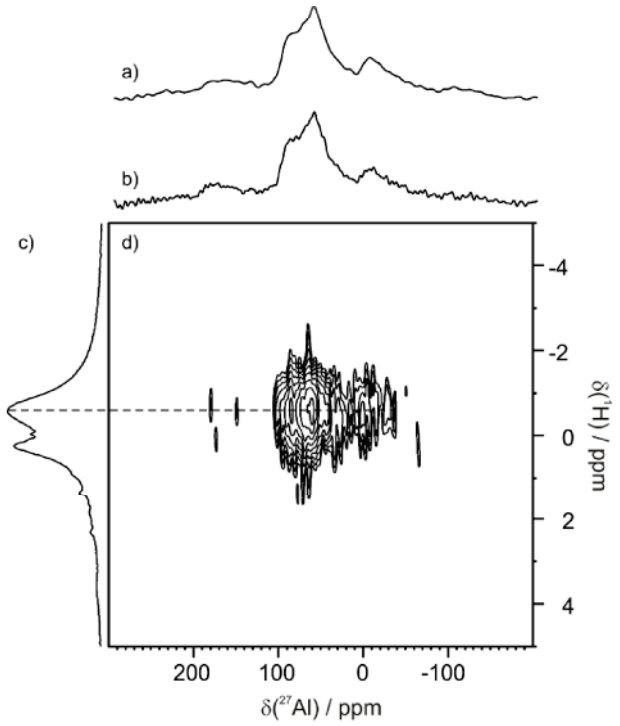

Figure 5. SMAO-600°C: a) ^{27}Al Hahn-echo, b) ^{1}H-filtered ^{27}Al D-HMQC, c) ^{1}H and d) 2D ^{1}H-^{27}Al D-HMQC MAS NMR spectra (18.8 T, spinning speed 20 kHz)

The ^{27}Al Hahn echo MAS NMR spectra of dried MAO and supported MAO (**Figure 6a-c**) are composed of a broad resonance as a consequence of a large second-order quadrupolar interaction, not averaged under MAS conditions. In an initial stage, the spectra look similar, with a featureless signal [20-110 ppm], most probably resulting from the overlapping of several Al sites. The observed CS values are in line with those reported by Talsi, of about 110 ppm.[29] In order to get a more precise insight into the dried MAO structure, we resorted to the 2D high resolution method MQ MAS.[40] The molecular sample of dried MAO affords a spectrum with good signal-to-noise ratio, which is rather complex and features peculiar line shapes due to large quadrupolar coupling associated with significant chemical shift anisotropy. This combination leads to a large number of highly distorted spinning side bands in the isotropic dimension (δ_1(^{27}Al)). This is reported in the literature in extreme cases such as ^{93}Nb MQ MAS NMR spectra of specific inorganic materials.[41,42] Remarkably, in the present case, the distortion is such that it can result in the quasi-negligible intensity of the isotropic signal, with maximized intensity in the spinning side bands. The position of the isotropic signals was unambiguously determined by recording the MQ MAS spectrum at 2 different spinning speed (**Figure S7**). Thus, three main sites emerge from the high resolution

spectrum: a) the major site (site A, **Figure 6**) features a chemical shift of 100 ppm, with a large quadrupolar coupling, of about 18 MHz (calculated from the position and width of the isotropic signal in the 2D spectrum);[43] b) a second site of lesser intensity (site B, **Figure 6**) resonates at 119 ppm, with also quadrupolar coupling above 18.5 MHz, similar to that of site A; c) a third site appears as a minor component at 69 ppm, with a broadening dominated by chemical shift distribution, and no apparent quadrupolar broadening (Site C, **Figure 6**). These parameters have been successfully used to simulate the CS lines on the MQ MAS spectrum (**Figure S8**). The reader's attention is drawn on the fact that in the case of spectra featuring quadrupolar lineshapes (like in the present cases), the isotropic chemical shift is not located in the center of the central transition signal, but on its lower frequency end.

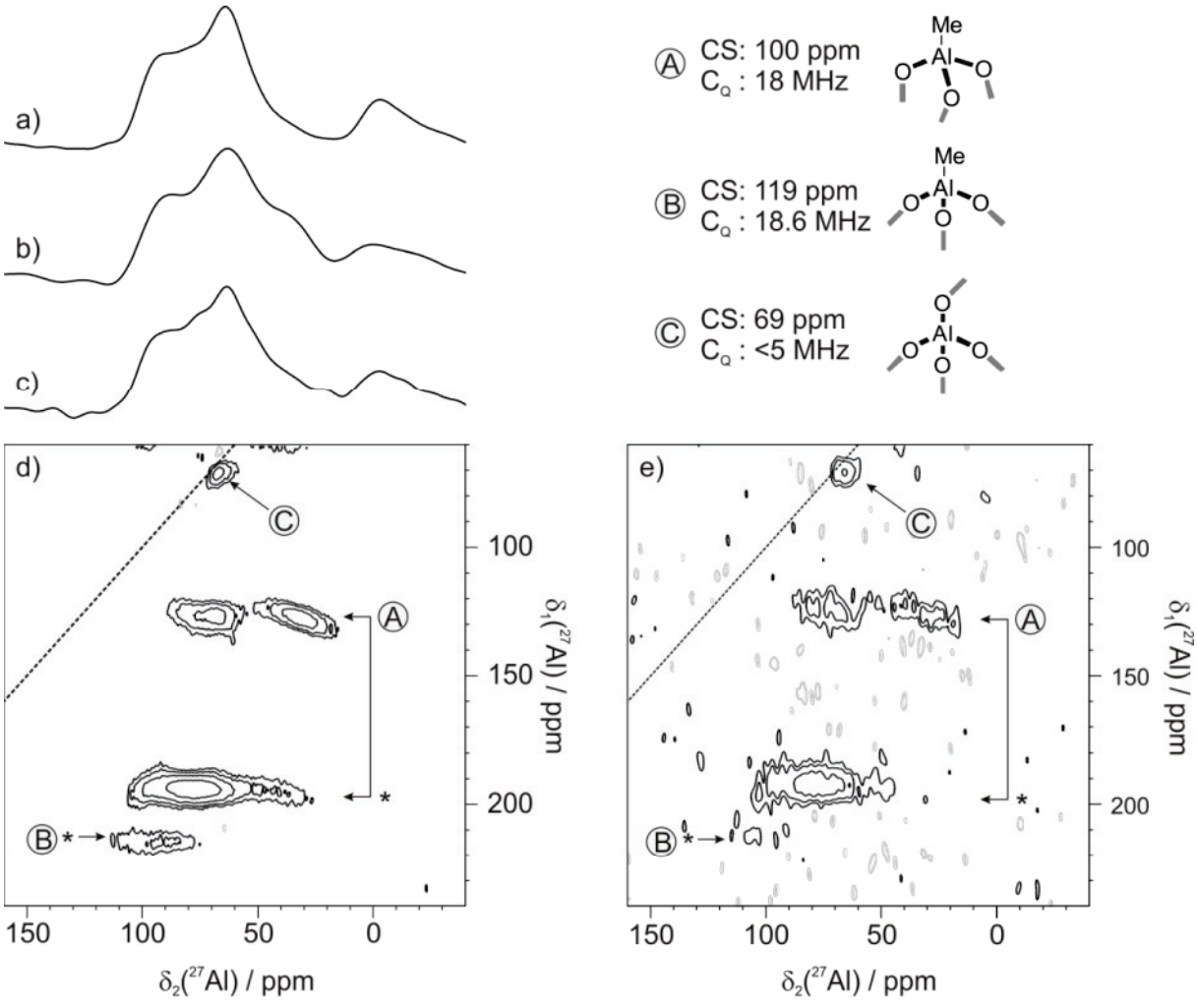

Figure 6. ^{27}Al Hahn Echo MAS spectrum of a) MAO, b) SMAO-200°C and c) SMAO-600°C, and ^{27}Al MQ MAS spectrum of d) MAO and e) SMAO-600°C (18.8 T, spinning speed 20 kHz); On spectrum d), the B species is evidenced by its rotation band at 215 ppm in the isotropic dimension, while the chemical shift band expected at 146 ppm is not observed due large anisotropic interactions associated with inhomogeneous MQ excitation conditions. Asterisks designate spinning side bands.

Thus, sites A and B feature rather similar chemical shift and quadrupolar coupling constant. The well-admitted main structural type within MAO is tetracoordinated $Al(Me)O_3$. Molecular species with similar aluminum coordination sphere indeed give rise to CS in the 120-80 ppm range, which is in agreement with both observed values for A and B.[30,44] The quadrupolar coupling constant is in the same range to that of MAO-related molecular species (where $Al(Me)O_3$ display a C_Q value of 17.5 MHz[35]) and of electronically comparable surface monohydride on tetra-coordinated aluminum ($Al(H)(O)_3$) which features a C_Q value of about 15 MHz.[45] However, the rather well-separated lines for A and B in the MQ MAS and the lack of CS and C_Q distribution are indicative of two slightly but definitively distinct types of environments. Interestingly, the IFPEN theory group recently studied the structure of "pure" MAO cages, composed of $[AlOMe]_n$ units (with a 1:1 Al:Me ratio) arranged in either square or hexagonal faces, and computed the corresponding ^1H and ^{27}Al NMR chemical shifts.[46] They correlated the local environment of aluminum atoms in terms of nature of edge-sharing faces with ^{27}Al chemical shift. Based on this, we propose that site A (CS of about 100 ppm) is on the edge of 1 square and 2 hexagonal faces (calculated range: 103-109 ppm) and that site B (CS of about 119 ppm) is on the edge of 2 square and 1 hexagonal faces (calculated range: 111-120 ppm). This is depicted on **Figure 7**, which features as an example a cage structure involving 8 Al atoms. This is the first experimental evidence of the topology and structure of MAO-cages that have been postulated by DFT calculations.

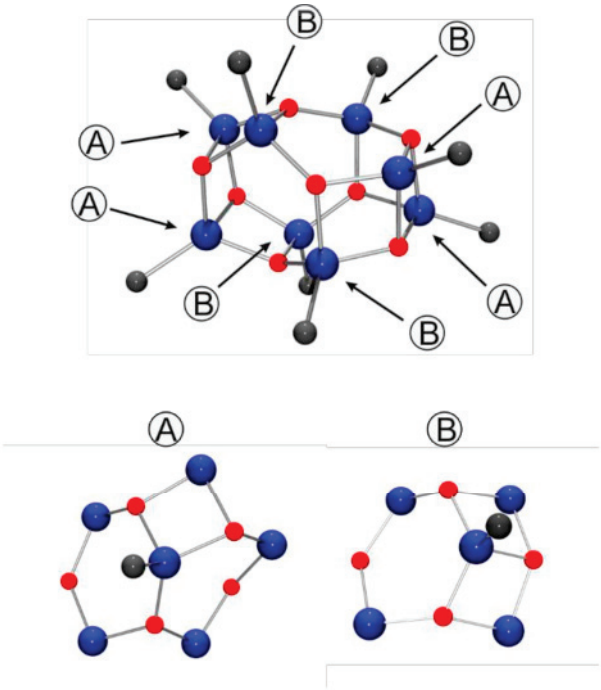

Figure 7. Example of [$(AlMeO)_8$] MAO-cage and the two A and B structures

Regarding site C, the low CS and C_Q values plead for a purely oxygenated coordination sphere, of the $Al(O)_4$ type.[47] Most specifically, the low C_Q (less than 5 MHz) rules out the hypothesis of $AlMeO_3$ sites on the edge of 3 hexagonal faces (calculated CS of 90 ppm). The low quantity of these sites may be an indication that they result from decomposition by hydrolysis or oxidation, although one cannot rule out that they are "buried" aluminum centers from larger structures within MAO.

Unfortunately, unambiguous determination of the proportions of these sites (and thus assessment of the oligomers' average size based on DFT-calculated models) is out of reach, due to both inhomogeneous site excitation for MQ MAS, to strong line shape overlapping of 1D spectra and to the occurrence of spectral components with fairly similar features (CS and C_Q). Furthermore, due to intrinsic NMR limitations, we cannot rule out the presence of aluminum centers featuring higher C_Q, as was proposed in several MAO models,[34,35] or observed for silica-supported aluminum alkyls.[48] This means that bis- or tris-alkyl species such as $[Al(O)_nMe_m]$ (n,m= 2 or 3) that have been postulated in the literature may have escaped detection under our experimental conditions, and that we may not be observing all the aluminum centers present in the dried MAO sample. In particular, we did not observe oxygen-bound TMA in the above described spectra. This is a species postulated in the MAO structure that would give rise to signals in the 185-170 ppm range.[32,49]

These elements can help to determine for the dried MAO a range of possible structure with various nuclearity. Indeed, in reference 45, the most stable $(AlOMe)_n$ structures have been determined by theoretical calculations. It appears that for value 'n' above 13, the number of hexagonal faces increases, while the number of square faces is constant. Thus, from there on, the quantity of Al sitting on 3 hexagonal faces increases constantly with the nuclearity of the cages. Such Al centers give rise to an NMR signal expected at 90 ppm, which is not observed in the present case. On the other hand, below n=12, the proportion of such sites is low (only 2 out of 10 and 2 out of 11 respectively for $(AlOMe)_{10}$ and $(AlOMe)_{11}$), below the detection limit of MQ MAS. Along the same line, the 'n' values less than 6 can be excluded based on high proportion of square faces. Thus, we propose that the nuclearity of the $(AlOMe)_n$ is most probably between 6 and 12. This is much lower than reported values.[50] This discrepancy may be due to the thermal treatment of MAO upon its drying, that affects the size of the cage. On the other hand, one can also propose that as NMR is sensitive to local parameters, as it gives evidence for low nuclearity, the larger MAO sizes determined in solution would be the result of aggregates formation by clustering of smaller entities.

The MQ MAS NMR spectrum of SMAO-600°C was recorded (**Figure 6e**). It features overall similar signals to that of dried MAO described above. This indicates that the structures present in the dried MAO are found in this material, obtained from reaction of MAO solution with silica followed by mild (80°C) thermal treatment under vacuum. In spite of the low signal-to-noise ratio due to the low Al concentration in the silica-supported sample, it appears that the B sites are preferentially consumed upon grafting (see **Figure S9** for the comparison of the isotropic projections of dried MAO and SMAO-600°C). However, further discussion is not possible at this stage.

In conclusion, both DRIFT and SS-NMR analysis of SMAO highlighted that the concentration and the nature of silanol and siloxane groups impact the reaction of MAO with silica. The analysis of SMAO obtained from silica thermally treated at elevated temperature (450-600 °C) showed the presence of Si-Me groups formed by opening of strained siloxane moieties. Thus, for silica treated at 200 °C the MAO reacts only with the silanol while for silica treated at higher temperature the MAO reacts first with the silanol and subsequently the surface Al-Me function opens siloxane moieties leading possibly to the formation of vicinal $Si\text{-}CH_3$ sites. We can reasonably assume that the way the MAO reacts with silica impact the structure of the activator and thus, the number of activating sites leading to different Zr content after impregnation of the metallocene precursor (see **Table 1**). Another important

issue concerns the actual nature of the MAO compound that reacts with the silica surface. Indeed, MAO solution consists of a mixture of polymeric MAO fraction $(Al(CH_3)_{1.42}O_{0.79})_n$ and free trimethylaluminium (TMA). It is well accepted that the TMA reacts preferentially with silica due to its smaller size and its higher reactivity. However, we cannot rule out direct reaction of polymeric MAO, especially, with silica treated at low temperature (200°C) where a sub-stoichiometric amount of TMA (related to Si-OH concentration) was introduced. The nature of the aluminum species that reacts can obviously impact the number of activating site on SMAO. It appears that a thermal treatment of silica at elevated temperature leading to a lower concentration of silanol group (isolated silanol) favored the grafting of the metallocene $(n\text{-}BuCp)_2ZrCl_2$. However, further discussion is not possible at this stage. Another observation is the fact that the structure of SMAO is close to that of dried MAO, namely consisting of cage structures.

3.3. Catalyst Evaluation

This part of the work describes the impact of silica thermal treatment on the catalytic efficiency of the SMAO/$(n\text{-}BuCp)_2ZrCl_2$ in, both, slurry and gas phase homopolymerizations. The effect of the silica dehydroxylation temperature on the catalytic activity was evaluated at 80 °C in slurry and gas phase ethylene homopolymerization at pressures of 8 and 11 bar of ethylene, respectively. Two different alkylaluminium compounds i.e., TEA and TIBA were used in slurry reactions to see how the catalysts behave in the presence of different scavengers, and to confirm that the silica dehydroxylation temperature has a similar effect on the catalytic activity independently of the specific alkylaluminium or scavenger. It should be noted that the concentration of both the scavengers was 2 $mmol.L^{-1}$ for the slurry phase reactions and 1 mmol of alkylaluminium was injected in a 2.5 L reactor for the gas phase polymerizations.

Figure 8a and **b** show that in slurry phase reactions the catalytic activity increased with increasing the silica dehydroxylation temperature for both of the alkylaluminiums. However, the kinetic profiles obtained with TEA and TIBA show some differences. Stable kinetic profiles with slow activation and almost no decay in catalytic activity over a polymerization time of 1 h can be observed when TEA was used as a scavenger. Contrary to this, fast activation followed by slight deactivation in the similar overall reaction time (i.e., 1h) can be observed when TIBA was used in the reaction as a scavenger (compare **Figure 8a** with **b**). In addition, higher average activities (or productivities) were obtained when TIBA was used as scavenger, as shown in **Figure S10** of the supporting information. As discussed previously by

Tisse et al.[51], the lower activity observed in the presence of TEA can be ascribed to the formation of the hetero-bimetallic dormant species $[(nBu\text{-}Cp)_2Zr(\mu R_2)AlR_2]^+$ because the stability of the Zr/Al dormant species increases as the size of 'R' group decreases (i.e., size: Et < i-Bu).[52,53] Moreover, the morphology of PE produced in all of these reactions was very similar showing spherical particles (**Figure S11**) and the bulk densities of the PE samples (presented in **Table 2**) also indicate that the polymerization occurred on the solid support.

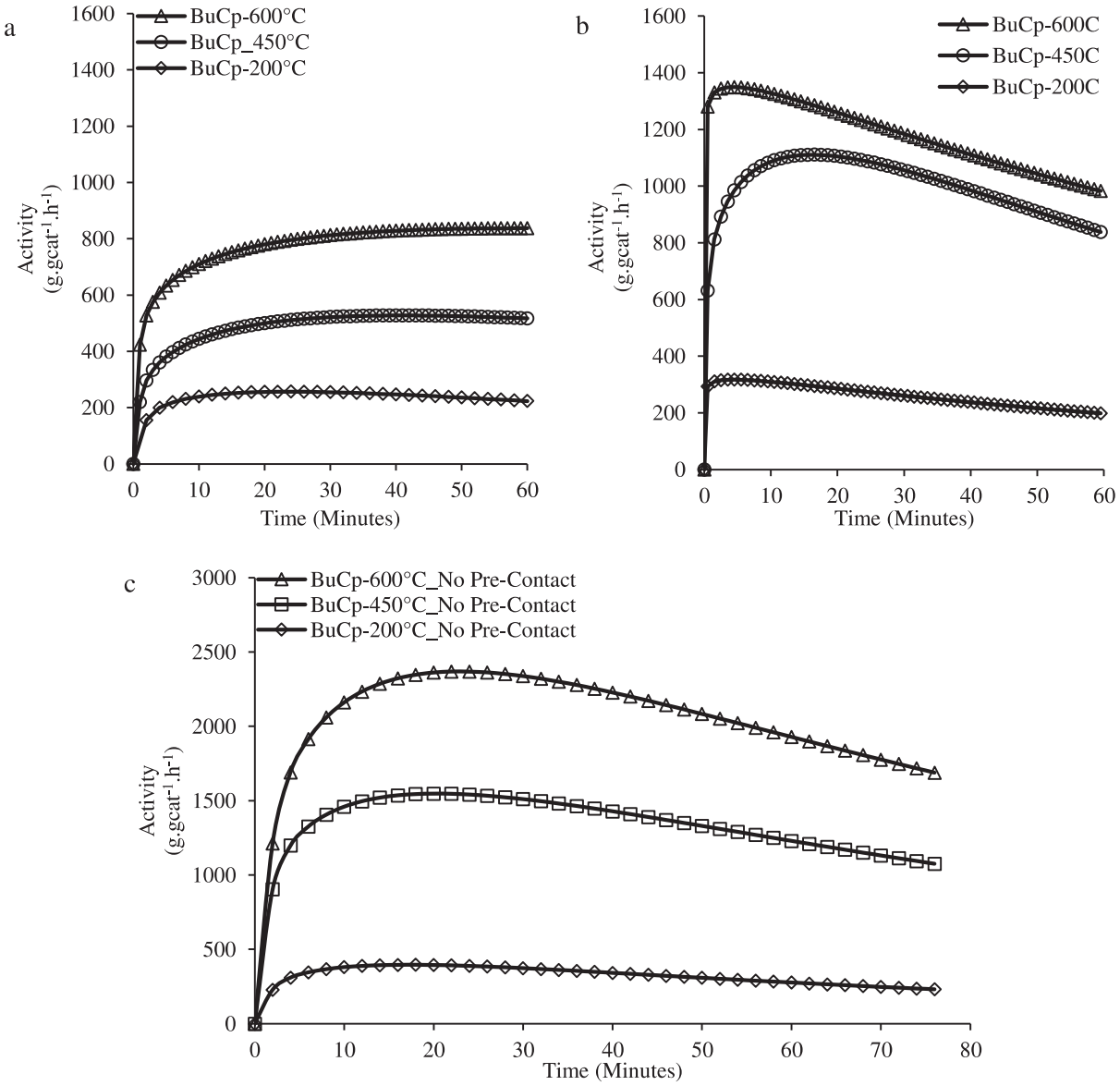

Figure 8. Comparison of slurry phase homopolymerization kinetic profiles of catalysts prepared with different silica dehydroxylation temperature using (a) TEA as scavenger, (b) TIBA as scavenger and (c) TIBA as scavenger but at 10 bar ethylene pressure and after purification of ethylene columns by avoiding any pre-contact of catalyst with TIBA.

Table 2. Comparison of catalytic activity and bulk densities of polymers produced in slurry and gas phase reactions. T denotes the silica dehydroxylation temperature.

T (°C)	Al/Zr	Average Activity, Slurry Phase, TEA	Average Activity, Slurry Phase, TIBA	Average Activity, Gas Phase, TIBA	Bulk Density ,Slurry Phase [c]	Bulk Density ,Gas Phase [c]
200	499	227[a] (206364)[b]	257[a] (233636) [b]	223[a] (202727) [b]	0.46	0.40
450	157	475[a] (163793)[b]	981[a] (338276) [b]	728[a] (251035) [b]	0.34	0.32
600	148	855[a] (328846) [b]	1162[a] (446923) [b]	990[a] (380769) [b]	0.38	0.34
200	-	-	352[a*] (320273) [b*]	-	-	-
450	-	-	1390[a*] (479310) [b*]	-	-	-
600	-	-	2180[a*] (838462) [b*]	-	-	-

[a)] Average activity in g $gcat^{-1}$ h^{-1}, [b)] Average activity in g gZr^{-1} h^{-1}, [c)] Bulk density in g cm^{-3}, * Reactions done by using injection cartridge.

At this point it is important to mention that a thin film formation around the reactor stirrer was also noticed at the end of these reactions, which indicated catalyst leaching due to prolonged pre-contact between the supported catalysts and scavenger containing reactor diluent (see polymerization procedure). Therefore, few more reactions were performed by injecting the catalysts with an injection cartridge into the reactor containing diluent plus scavenger (2 $mmole.L^{-1}$) at 80 °C. This allowed us to avoid prolonged pre-contact between the supported catalysts and the scavenger and thus, catalyst leaching. These polymerizations were done at 10 bar ethylene pressure for 1 h 15 minutes. The obtained catalytic activity profiles are shown in **Figure 8c** where it can be seen that the effect of silica dehydroxylation temperature remained the same as that shown in **Figure 8a** and **b**. However, the lower instantaneous activities and higher deactivation rates of the catalysts shown in **Figure 8b** as compared to those shown in **Figure 8c** can be attributed to higher ethylene pressure used as well as the absence of any catalyst leaching in the latter case. Furthermore, ethylene purification columns were also regenerated when the reactions shown in **Figure 8c** were conducted. In the next chapter we will discuss in more detail about the impact the of slurry phase polymerization protocol on catalyst leaching from silica supported metallocenes and reactor fouling.

For gas phase process where catalyst leaching is not an issue, polymerizations were run only using TIBA since no difference was observed in the molecular or physical properties of PE produced by using TEA in slurry polymerizations other than rise in intrinsic catalytic activity.

The kinetic profiles of gas phase polymerizations, shown in **Figure 9,** have a different shape than the shape of slurry polymerization kinetic profiles with the same alkylaluminium, showing first a gradual increase in the activity and then deactivation. Each catalyst reached its maximum activity in a different time. For example, the SMAO-200°C catalyst took 22 minutes, whereas, SMAO-600°C catalyst took 38 minutes to reach its maximum activity. A number of polymerizations were done to confirm these observations and the results are shown in **Figure S12** of the supporting information. It should be noted that the catalytic activity in g $gcat^{-1}$ h^{-1} increased with increasing silica dehydroxylation temperature. Considering the wt% of Zr for the different catalysts it appears that the most efficient catalysts was the one obtained with SMAO-600°C. In addition, the obtained polymers showed similar molecular and physical characteristics, as shown in **Tables 3** of the next section, despite of different silica thermal treatments. This result is of high importance because it shows that whatever the initial thermal treatment of silica the same active species are formed which only differ by their concentration.

The effect of silica thermal treatment on the catalyst performance is, thus, twofold; i) it controls the percentage of co-catalytically active Aluminium species on SMAO leading to different concentrations of zirconocene in the final catalysts (i.e., lower zirconium content on catalyst prepared with SMAO-200°C than those prepared with SMAO-450°C or SMAO-600°C) and ii) it impacts the percentage of active Zr (C* = [Zr*]/[Zr]), since the higher catalytic activity was observed for n-BuCp-600°C catalyst (both in per g of catalyst and per mol of Zr).

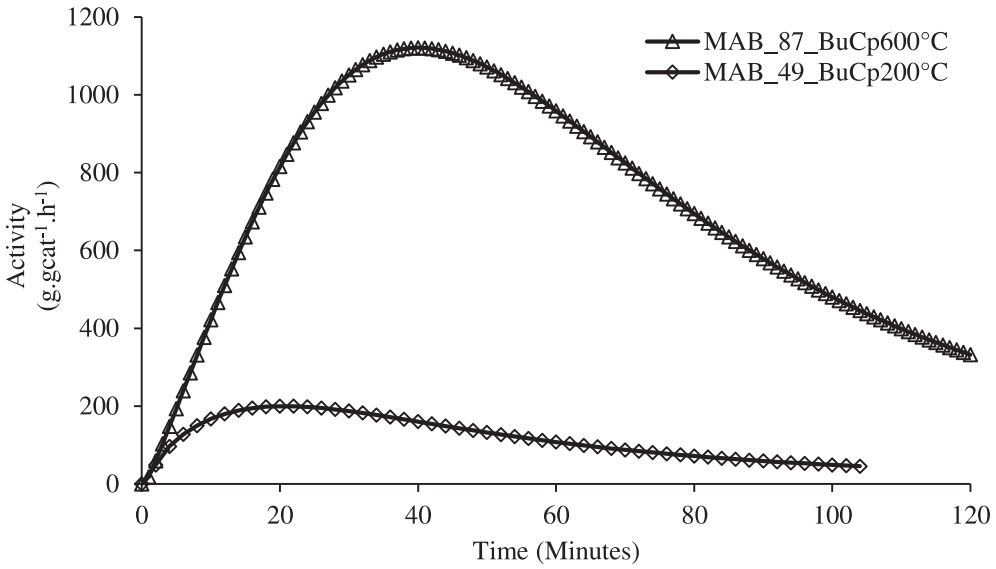

Figure 9. Comparison of gas phase homopolymerization kinetic profiles of catalysts prepared with different silica dehydroxylation temperature.

The difference of catalyst activation (as shown by the kinetic profiles) in slurry and gas phase polymerizations has also been observed by Kumkaew et al.,[54] who used similar silica supported and mesoporous molecular sieves supported $(nBuCp)_2ZrCl_2$ catalyst with similar Al/Zr molar ratios. Kumkaew et al.,[54] showed that the broadening of the kinetic profile in gas phase homo- and co-polymerizations with 1-hexene is related to the amount of triisobutyl aluminium (TIBA) and increased amounts of TIBA (e.g., 1 mmol) causes large induction periods (e.g., 40 min at 14 bar ethylene pressure), broadens the kinetic profile by increasing the time to reach maximum activity. On the other hand, slurry homopolymerization kinetic profiles with the same silica supported catalysts did not show induction period and were stable. It should be noted that in the present study, similar behaviour has been observed for both the slurry and gas phase ethylene homopolymerizations using the same catalyst. However, it is obvious from the **Figure 9** that in present work, no induction period of 40 min by using 1mmol TIBA in gas phase polymerizations is present in any of the used catalysts.

In another work from the same group[55], effect of different alkylaluminium compounds including TIBA on gas phase ethylene homo and copolymerizations has been evaluated using $(n\text{-}BuCp)_2ZrCl_2$/MAO supported on polymeric supports. In the work of Hammawa et al.,[55] the kinetic profile obtained at highest TIBA reactor concentration i.e., 0.59 mmol in a 2 L reactor was very similar (i.e., in shape and time required to reach the maximum activity of 900 g $gcat^{-1}$ h^{-1} approximately) to what is shown in **Figure 9** for the catalyst prepared with SMAO-600°C. In the case of gas phase polymerization, the initial local concentration of

TIBA can be very high in the catalyst particles due to the low vapour pressure of this alkylaluminium which can certainly impact the initiation of the polymerization. Actually, a high local concentration of AlR_3 favours the formation of a dormant metallocenium-ion/TIBA complex in the initial stages of polymerization which is activated with time due to TIBA depletion. Fragmentation of the silica support, which does not happen in polymeric supports, can also help to access more active sites to TIBA in the initial stages of gas phase polymerization and formation of dormant metallocenium-ion/TIBA complex. In case of slurry phase polymerization, the presence of diluent probably dilutes TIBA on catalyst active sites and therefore, activation of catalyst is fast.

3.4. Crystallinity and Molecular Masses of PE Samples

The average molecular weights, polydispersity (Đ) and crystallinity of the PE samples produced in slurry and gas phase polymerizations are shown in **Table 3,** and do not show any specific correlation with the silica dehydroxylation temperature. The polydispersity is close to the theoretical value of 2 for all samples, as expected of a single-site catalyst, thereby suggesting that the catalyst synthesis procedure does not lead to a multiplicity of active sites. In other words, the fact that the same polyethylene was produced regardless of the thermal treatment of silica and of the phase in which the reaction was performed tells us that the same active species were formed on the support. Thus, the dehydroxylation of silica appears to mainly impact the efficiency of the SMAO activator, i.e. the percentage of co-catalytically active aluminium site.

Table 3. MWD and crystallinity of slurry and gas phase PE samples.

	Slurry Phase			Gas Phase		
Catalyst	**M_w[a)] g mol^{-1}**	**Đ[a)]**	**Crystallinity[b] (%wt)**	**M_w[a)] g mol^{-1}**	**Đ[a)]**	**Crystallinity[b)] (%wt)**
Cat-200°C	122100	2.2	65	143000	2.2	63
Cat-450°C	123600	2.3	66	119000	2.4	68
Cat-600°C	125600	2.2	63	127500	2.2	68

[a)] Determined by high temperature SEC using triple detection. [b)] Determined by DSC

4. Conclusion

The concentration and the nature of silanol (Si-OH) groups on the surface of silica support is an important chemical property of silica and significantly affects the catalytic activity of supported $(n\text{-BuCp})_2ZrCl_2$ metallocene complex in ethylene homopolymerizations. Increasing the dehydroxylation temperature from 200°C to 600°C decreases the OH concentration of silica and only isolated silanol groups remain on Grace 948 silica at 600°C. After impregnation of the silica with MAO the aluminium content of these silica (dehydroxylated at different temperatures) decreased with increase in dehydroxylation temperature. DRIFT and SS-NMR analysis showed that the grafting of MAO was impacted by the nature and the concentration of silanol groups on the silica surface. MAO reacted on silica dehydroxylated at high temperature (i.e., ≥ 450°C) with both silanol and siloxane groups which was evidenced by the formation of Si-Me. In addition, the presence of $Al(Me)O_3$ sites in different configuration was evidenced for the first time by SS-NMR in the present work. Consequently, the final supported metallocene catalysts showed a higher content of zirconium at elevated dehydroxylation temperature (450-600°C). The intrinsic and average activity of $(n\text{-BuCp})_2ZrCl_2$ supported on MAO impregnated silica (SMAO) in ethylene homopolymerizations was observed to increase with increasing silica dehydroxylation temperature from 200 to 600°C, both in slurry and gas phase processes. Furthermore, no significant effect of silica dehydroxylation temperature was observed on the MWD and crystallinity of the polyethylene produced both in slurry and gas phase polymerizations. Thus, whatever the thermal treatment of silica is, the same active species are formed but more active sites are generated when silica was thermally treated at high temperature. Finally, this study suggests that $(n\text{-BuCp})_2ZrCl_2$ supported on 600 °C dehydroxylated silica will provide reasonable activity in slurry and gas phase ethylene polymerizations when TIBA is used as a scavenger.

5. References

1. Severn, J R., Methylaluminoxane (MAO), Silica and a Complex: The Holy Trinity of Supported Single-Site Catalyst, In Tailor-Made Polymers, Eds. J.R. Severn, J.C. Chadwick., Wiley-VCH Verlag GmbH & Co. KGaA, Weinheim, **2008**.

2. Markus Stürzel, Mihan, S, Rolf Mülhaupt, From Multisite Polymerization Catalysis to Sustainable Materials and All-Polyolefin Composites, Chem. Rev., **2016**, 116, 1398-1433.

3. Ghiotto, F, Pateraki, C, Tanskanen, J, Severn, J R, Luehmann, N, Kusmin, A, Stellbrink, J, Linnolahti, M, Bochmann, M, Probing the Structure of Methylalumoxane (MAO) by a Combined Chemical, Spectroscopic, Neutron Scattering, and Computational Approach, Organometallics., **2013**, 32, 3354-3362.

4. Hirvi, J T, Bochmann, M, Severn, J R, Linnolahti, M, Formation of Octameric Methylaluminoxanes by Hydrolysis of Trimethylaluminum and the Mechanisms of Catalyst Activation in Single-Site α-Olefin Polymerization Catalysis, ChemPhysChem., **2014**, 15, 2732-2742.

5. Bianchini, D, dos Santos, J H Z, Uozumi, T, Sano, T, Characterization of MAO-modified silicas, Journal of Molecular Catalysis A: Chemical., **2002**, 185, 223-235.

6. Panchenko, V N, Semikolenova, N V, Danilova, I G, Paukshtis, E A, Zakharov, V A, IRS study of ethylene polymerization catalyst SiO2/methylaluminoxane/zirconocene, Journal of Molecular Catalysis A: Chemical., **1999**, 142, 27-37.

7. dos Santos, J H Z, Krug, C, da Rosa, M B, Stedile, F C, Dupont, J, de Camargo Forte, M, The effect of silica dehydroxylation temperature on the activity of SiO2-supported zirconocene catalysts, Journal of Molecular Catalysis A: Chemical., **1999**, 139, 199-207.

8. Bianchini, D, Stedile, F C, dos Santos, J H Z, Effect of MAO silica surface loading on (nBuCp)2ZrCl2 anchoring, on catalyst activity and on polymer properties, Applied Catalysis A: General., **2004**, 261, 57-67.

9. Atiqullah, M, Akhtar, M N, Moman, A A, Abu-Raqabah, A H, Palackal, S J, Al-Muallem, H A, Hamed, O M, Influence of silica calcination temperature on the performance of supported catalyst SiO2/BuSnCl3/MAO/(nBuCp)2ZrCl2 polymerizing ethylene without separately feeding the MAO cocatalyst, Applied Catalysis A: General., **2007**, 320, 134-143.

10. Low, M J D, Severdia, A G, Chan, J, Reactive silica: XV. Some properties of solids prepared by the reaction of trimethylaluminum with silica, Journal of Catalysis., **1981**, 69, 384-391.

11. van Grieken, R, Carrero, A, Suarez, I, Paredes, B, Ethylene polymerization over supported MAO/(nBuCp)2ZrCl2 catalysts: Influence of support properties, European Polymer Journal., **2007**, 43, 1267-1277.

12. Kou, B, McAuley, K B, Hsu, C C, Bacon, D W, Yao, K Z, Gas-Phase Ethylene/Hexene Copolymerization with Metallocene Catalyst in a Laboratory-Scale Reactor, Ind. Eng. Chem. Res., **2005**, 44, 2443-2450.

13. Paredes, B, Grieken, R v, Carrero, A, Suarez, I, Soares, J B P, Ethylene/1-Hexene Copolymers Produced with MAO/(nBuCp)2ZrCl2 Supported on SBA-15 Materials with Different Pore Sizes, Macromol. Chem. Phys., **2011**, 212, 1590-1599.

14. Zhou, J M, Li, N H, Bu, N Y, Lynch, D T, Wanke, S E, Gas-phase ethylene polymerization over polymer-supported metallocene catalysts, J. Appl. Polym. Sci., **2003**, 90, 1319-1330.

15. Hlatky, G G, Heterogeneous Single-Site Catalysts for Olefin Polymerization, Chem. Rev., **2000**, 100, 1347-1376.

16. Bun-Yeoul Lee; Jae-Seung Oh Method for producing supported metallocene catalyst and olefin polymerization process using the same. US6469113 B1, **1999**.

17. Smit, M, Zheng, X, Loos, J, Chadwick, J C, Koning, C E, Effects of methylaluminoxane immobilization on silica on the performance of zirconocene catalysts in propylene polymerization, J. Polym. Sci. A Polym. Chem., **2005**, 43, 2734-2748.

18. Brinkmann, A, Kentgens, A P M, Proton-Selective 17O−1H Distance Measurements in Fast Magic-Angle-Spinning Solid-State NMR Spectroscopy for the Determination of Hydrogen Bond Lengths, J. Am. Chem. Soc., **2006**, 128, 14758-14759.

19. Carravetta, M, Eden, M, Zhao, X, Brinkmann, A, Levitt, M H, Symmetry principles for the design of radiofrequency pulse sequences in the nuclear magnetic resonance of rotating solids, Chemical Physics Letters., **2000**, 321, 205-215.

20. Amoureux, J P, Fernandez, C, Steuernagel, S, ZFiltering in MQMAS NMR, Journal of Magnetic Resonance, Series A., **1996**, 123, 116-118.

21. B. Wunderlich. Thermal Analysis, Academic Press Inc, San Diego, 1990.

22. Tailor-Made Polymers: Via Immobilization of Alpha-Olefin Polymerization Catalysts, Wiley-VCH Verlag GmbH & Co. KGaA, Weinheim, 2008.

23. Severn, J R, Chadwick, J C, Duchateau, R, Friederichs, N, 'Bound but Not Gagged' Immobilizing Single-Site α-Olefin Polymerization Catalysts, Chem. Rev., **2005**, 105, 4073-4147.

24. Imhoff, D W, Simeral, L S, Sangokoya, S A, Peel, J H, Characterization of Methylaluminoxanes and Determination of Trimethylaluminum Using Proton NMR, Organometallics., **1998**, 17, 1941-1945.

25. Jezequel, M, Dufaud, V, Ruiz-Garcia, M J, Carrillo-Hermosilla, F, Neugebauer, U, Niccolai, G P, Lefebvre, F, Bayard, F, Corker, J, Fiddy, S, Evans, J, Broyer, J P, Malinge, J, Basset, J M, Supported Metallocene Catalysts by Surface Organometallic Chemistry. Synthesis, Characterization, and Reactivity in Ethylene Polymerization of Oxide-Supported Mono- and Biscyclopentadienyl Zirconium Alkyl Complexes:

Establishment of Structure/Reactivity Relationships, J. Am. Chem. Soc., **2001**, 123, 3520-3540.

26. Panchenko, V N, Echevkaya, L G, Zakharov, V A, Matsko, M A, Influence of triisobutylaluminum on the polymerization of ethylene by SiO2-supported ansa-zirconocene catalysts, Applied Catalysis A: General., **2011**, 404, 47-53.

27. Tritto, I, Mealares, C, Sacchi, M C, Locatelli, P, Methylaluminoxane: NMR analysis, cryoscopic measurements and cocatalytic ability in ethylene polymerization, Macromol. Chem. Phys., **1997**, 198, 3963-3977.

28. Britcher, L, Rahiala, H, Hakala, K, Mikkola, P, Rosenholm, J B, Preparation, Characterization, and Activity of Silica Supported Metallocene Catalysts, Chem. Mater., **2004**, 16, 5713-5720.

29. Babushkin, D E, Semikolenova, N V, Panchenko, V N, Sobolev, A P, Zakharov, V A, Talsi, E P, Multinuclear NMR investigation of methylaluminoxane, Macromol. Chem. Phys., **1997**, 198, 3845-3854.

30. Mason, M R, Smith, J M, Bott, S G, Barron, A R, Hydrolysis of tri-tert-butylaluminum: the first structural characterization of alkylalumoxanes [(R2Al)2O]n and (RAlO)n, J. Am. Chem. Soc., **1993**, 115, 4971-4984.

31. Harlan, C J, Mason, M R, Barron, A R, Tert-Butylaluminum Hydroxides and Oxides: Structural Relationship between Alkylalumoxanes and Alumina Gels, Organometallics., **1994**, 13, 2957-2969.

32. Benn, R, Rufinska, A, Lehmkuhl, H, Janssen, E, Kruger, C, 27AI-NMR Spectroscopy: A Probe for Three-, Four-, Five-, and Sixfold Coordinated Al Atoms in Organoaluminum Compounds, Angew. Chem. Int. Ed. Engl., **1983**, 22, 779-780.

33. Benn, R, Janssen, E, Lehmkuhl, H, Rufinska, A, 27Al-NMR-Spektroskopie zur Charakterisierung von Organoaluminium-Verbindungen, Journal of Organometallic Chemistry., **1987**, 333, 155-168.

34. Bryant, P L, Harwell, C R, Mrse, A A, Emery, E F, Gan, Z, Caldwell, T, Reyes, A P, Kuhns, P, Hoyt, D W, Simeral, L S, Hall, R W, Butler, L G, Structural Characterization of MAO and Related Aluminum Complexes. 1. Solid-State 27Al NMR with Comparison to EFG Tensors from ab Initio Molecular Orbital Calculations, J. Am. Chem. Soc., **2001**, 123, 12009-12017.

35. Wu, F J, Simeral, L S, Mrse, A A, Eilertsen, J L, Negureanu, L, Gan, Z, Fronczek, F R, Hall, R W, Butler, L G, Structural Characterization of Al10O6iBu16(μ-H)2, a High Aluminum Content Cluster: Further Studies of Methylaluminoxane (MAO) and Related Aluminum Complexes, Inorg. Chem., **2007**, 46, 44-47.

36. Schnell, I, Brown, S P, Low, H Y, Ishida, H, Spiess, H W, An Investigation of Hydrogen Bonding in Benzoxazine Dimers by Fast Magic-Angle Spinning and Double-Quantum 1H NMR Spectroscopy, J. Am. Chem. Soc., **1998**, 120, 11784-11795.

37. Anwander, R, Palm, C, Groeger, O, Engelhardt, G, Formation of Lewis Acidic Support Materials via Chemisorption of Trimethylaluminum on Mesoporous Silicate MCM-41, Organometallics., **1998**, 17, 2027-2036.

38. Li, J, DiVerdi, J A, Maciel, G E, Chemistry of the Silica Surface: Liquid–Solid Reactions of Silica Gel with Trimethylaluminum, J. Am. Chem. Soc., **2006**, 128, 17093-17101.

39. Trebosc, J, Hu, B, Amoureux, J P, Gan, Z, Through-space R3-HETCOR experiments between spin-1/2 and half-integer quadrupolar nuclei in solid-state NMR, Journal of Magnetic Resonance., **2007**, 186, 220-227.

40. Frydman, L, Harwood, J S, Isotropic Spectra of Half-Integer Quadrupolar Spins from Bidimensional Magic-Angle Spinning NMR, J. Am. Chem. Soc., **1995**, 117, 5367-5368.

41. Hung, I, Trebosc, J, Hoatson, G L, Vold, R L, Amoureux, J P, Gan, Z, Q-shear transformation for MQMAS and STMAS NMR spectra, Journal of Magnetic Resonance., **2009**, 201, 81-86.

42. Wang, X, Adhikari, J, Smith, L J, An Investigation of Distortions of the Dion–Jacobson Phase RbSr2Nb3O10 and Its Acid-Exchanged Form with 93Nb Solid State NMR and DFT Calculations, J. Phys. Chem. C., **2009**, 113, 17548-17559.

43. J.P.Amoureux, M P., Advances in MQMAS NMR, In Encyclopedia of Nuclear Magnetic Resonance, Eds. R.K.H. D.M.Grant., John Wiley, Chichester, **2002**; Vol. 9.

44. Obrey, S J, Bott, S G, Barron, A R, A Lewis Base Promoted Alkyl/Alkoxide Ligand Redistribution: Reaction of [Me2Al(μ-OCPh3)]2 with THF, Organometallics., **2001**, 20, 5119-5124.

45. Mazoyer, E, Trebosc, J, Baudouin, A, Boyron, O, Pelletier, J, Basset, J M, Vitorino, M J, Nicholas, C P, Gauvin, R M, Taoufik, M, Delevoye, L, Heteronuclear NMR Correlations To Probe the Local Structure of Catalytically Active Surface Aluminum Hydride Species on γ-Alumina, Angewandte Chemie International Edition., **2010**, 49, 9854-9858.

46. Boudene, Z, De Bruin, T, Toulhoat, H, Raybaud, P, A QSPR Investigation of Thermal Stability of [Al(CH3)O]n Oligomers in Methylaluminoxane Solution: The Identification of a Geometry-Based Descriptor, Organometallics., **2012**, 31, 8312-8322.

47. Mackenzie, K, Smith, M., Preface, In Pergamon Materials Series Multinuclear Solid-State NMR of Inorganic Materials, Volume 6 ed.; Eds. J.D.M. Kenneth., Pergamon, **2002**.

48. Kerber, R N, Kermagoret, A, Callens, E, Florian, P, Massiot, D, Lesage, A, Coperet, C, Delbecq, F, Rozanska, X, Sautet, P, Nature and Structure of Aluminum Surface Sites Grafted on Silica from a Combination of High-Field Aluminum-27 Solid-State NMR Spectroscopy and First-Principles Calculations, J. Am. Chem. Soc., **2012**, 134, 6767-6775.

49. Benn, R, Janssen, E, Lehmkuhl, H, Rufinska, A, Koordinations-Komplexe Lewis-basischer Dialkylaluminiumalkoxide mit Trialkylaluminium, Journal of Organometallic Chemistry., **1987**, 333, 169-180.

50. Zijlstra, H S, Harder, S, Methylalumoxane-History, Production, Properties, and Applications, Eur. J. Inorg. Chem., **2015**, 2015, 2.

51. Tisse, V F, Boisson, C, McKenna, T F L, Activation and Deactivation of the Polymerization of Ethylene over rac-EtInd2ZrCl2 and (nBuCp)2ZrCl2 on an Activating Silica Support, Macromol. Chem. Phys., **2014**, 215, 1358-1369.

52. Bochmann, M, Lancaster, S J, Monomer–Dimer Equilibria in Homo- and Heterodinuclear Cationic Alkylzirconium Complexes and Their Role in Polymerization Catalysis, Angew. Chem. Int. Ed. Engl., **1994**, 33, 1634-1637.

53. Song, F, Cannon, R D, Bochmann, M, Zirconocene-Catalyzed Propene Polymerization:A Quenched-Flow Kinetic Study, J. Am. Chem. Soc., **2003**, 125, 7641-7653.

54. Kumkaew, P, Wanke, S E, Praserthdam, P, Danumah, C, Kaliaguine, S, Gas-phase ethylene polymerization using zirconocene supported on mesoporous molecular sieves, J. Appl. Polym. Sci., **2003**, 87, 1161-1177.

55. Hammawa, H, Mannan, T M, Lynch, D T, Wanke, S E, Effects of aluminum alkyls on ethylene/1-hexene polymerization with supported metallocene/MAO catalysts in the gas phase, J. Appl. Polym. Sci., **2004**, 92, 3549-3560.

56. Michel-Florin B. (1977). Copolymers Ethylene Hexene-1: Synthese, Caracterisation, Etude de quelques proprietes. Phd Thesis, Université Claude Bernard, Lyon 1, France.

APPENDIX 1

CHAPTER 2

Effect of Support Dehydroxylation Temperature on the Grafting of MAO and Ethylene Polymerization

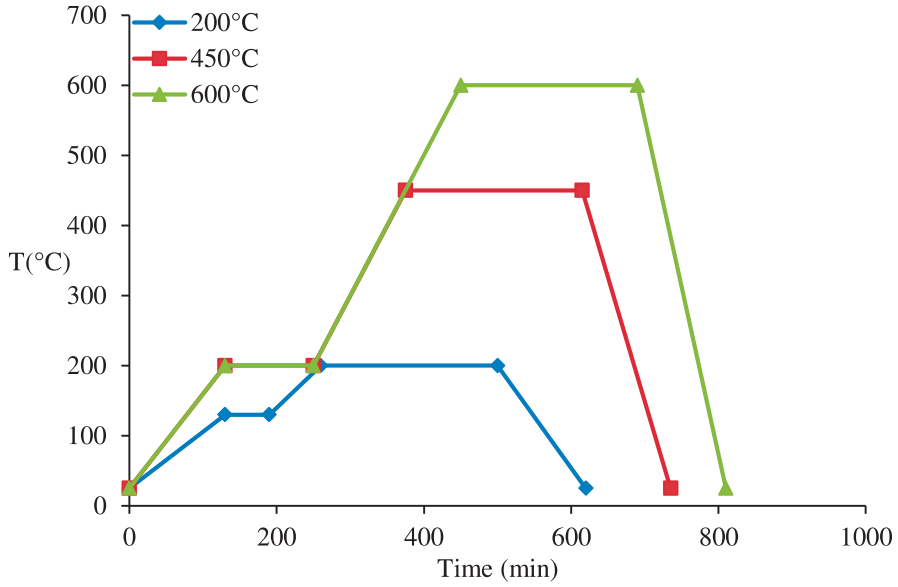

Figure S1. Temperature profiles used for silica dehydroxylation.

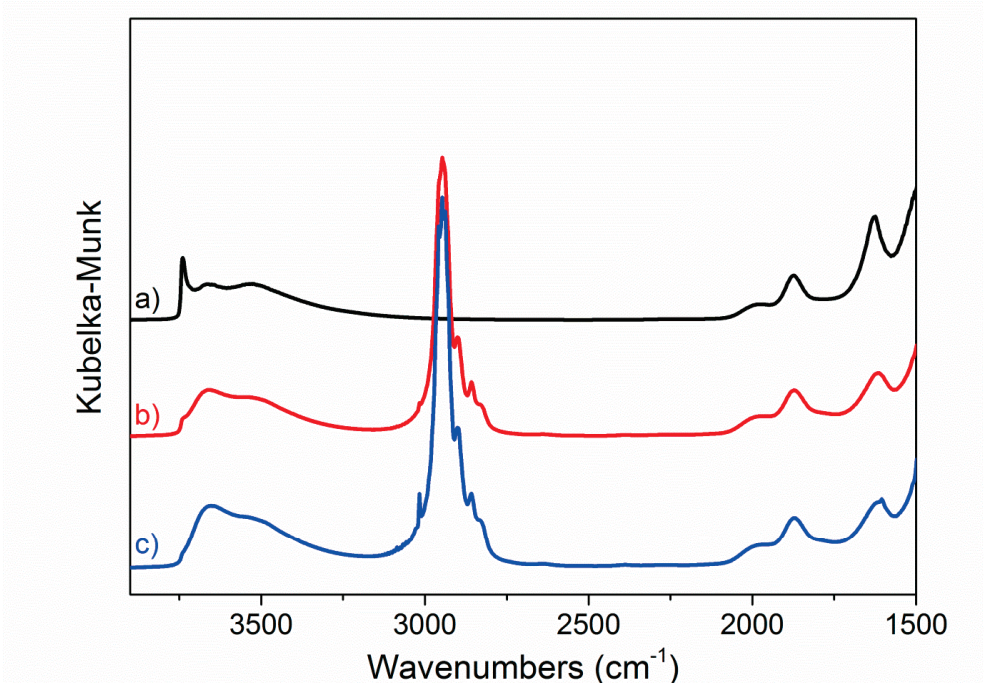

Figure S2. DRIFT spectra of silica-200°C (a), after reaction of MAO (SMAO-200°C) (b), after activation of $(n\text{-BuCp})_2ZrCl_2$ (n-BuCp-200°C) (c).

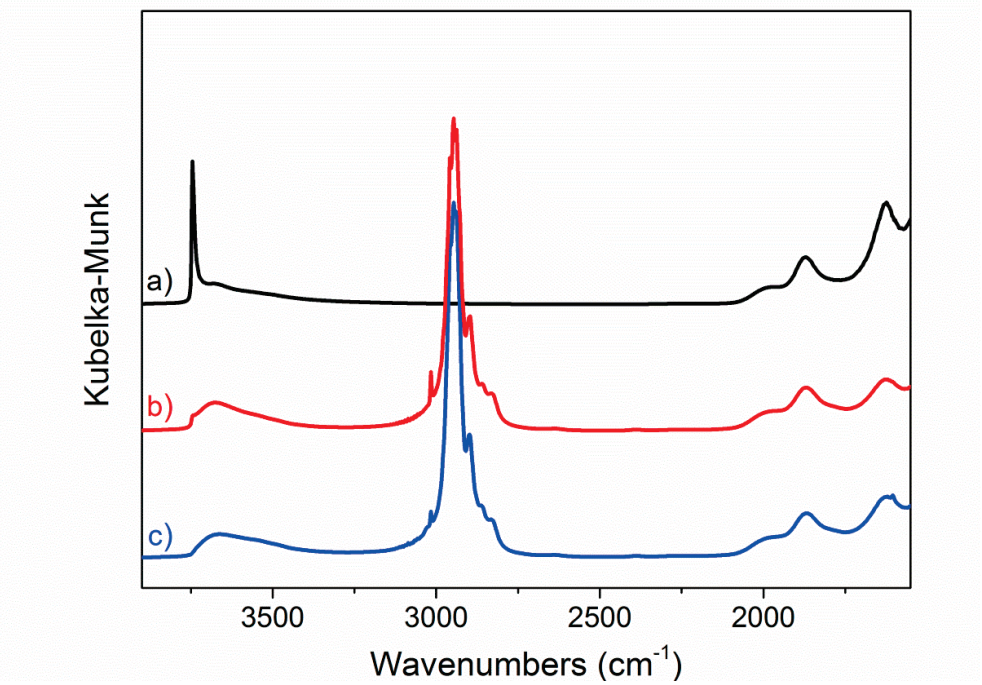

Figure S3. DRIFT spectra of silica-450°C (a), after reaction of MAO (SMAO-450°C) (b), after activation of $(n\text{-BuCp})_2ZrCl_2$ (n-BuCp-450°C) (c).

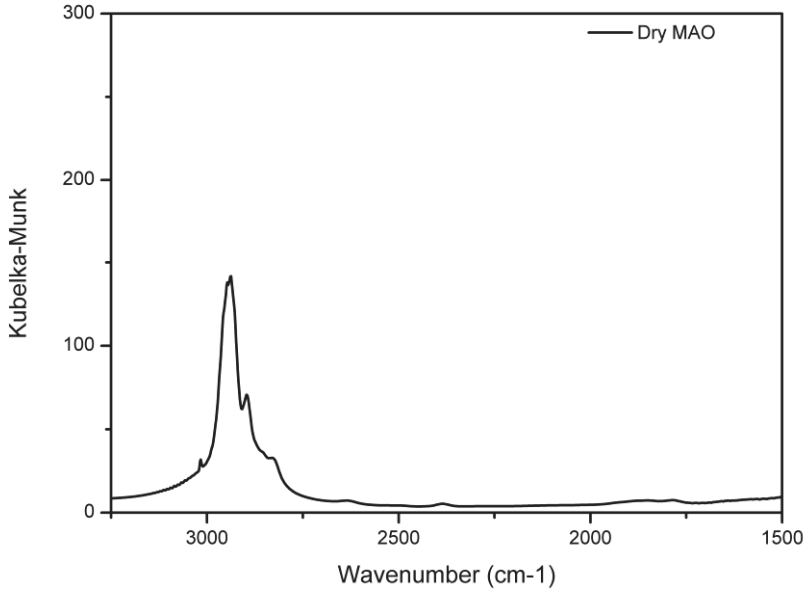

Figure S4. DRIFT spectrum of MAO dried at 100°C.

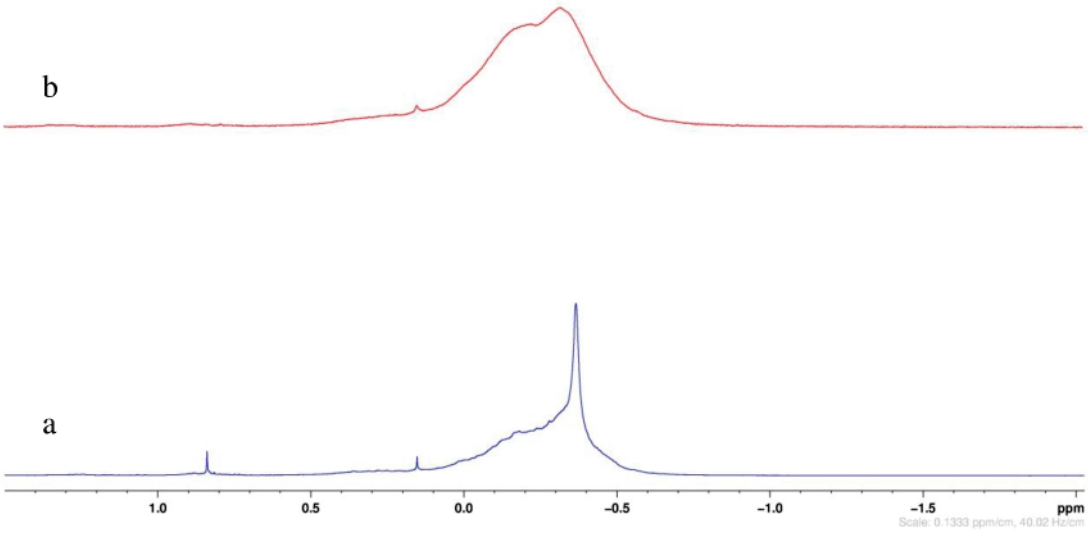

Figure S5. ^{1}H proton NMR spectrum of 30wt%MAO solution (a) and dried MAO obtained by heating the 30wt% MAO solution at 80°C under vacuum for 4h (b). Benezene was used to as solvent for both the NMR spectra.

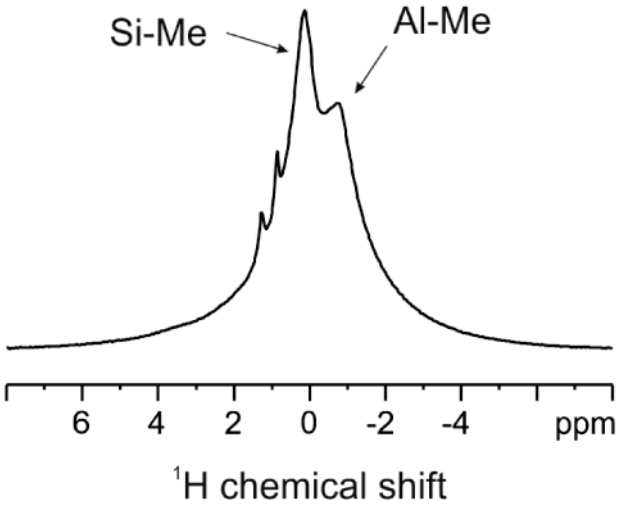

Figure S6. ^{1}H MAS NMR spectrum of $AlMe_3$ grafted on $SiO_{2\text{-}600}$ (18.8 T, at spinning speed 20 kHz).

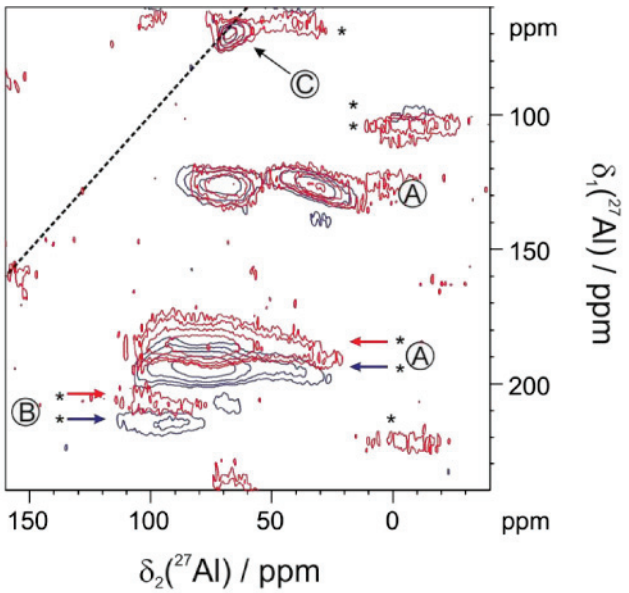

Figure S7. ^{27}Al MQ MAS spectrum of MAO (18.8 T), at spinning speed 20 kHz (blue) and 18 kHz (red); asterisks designate spinning side bands.

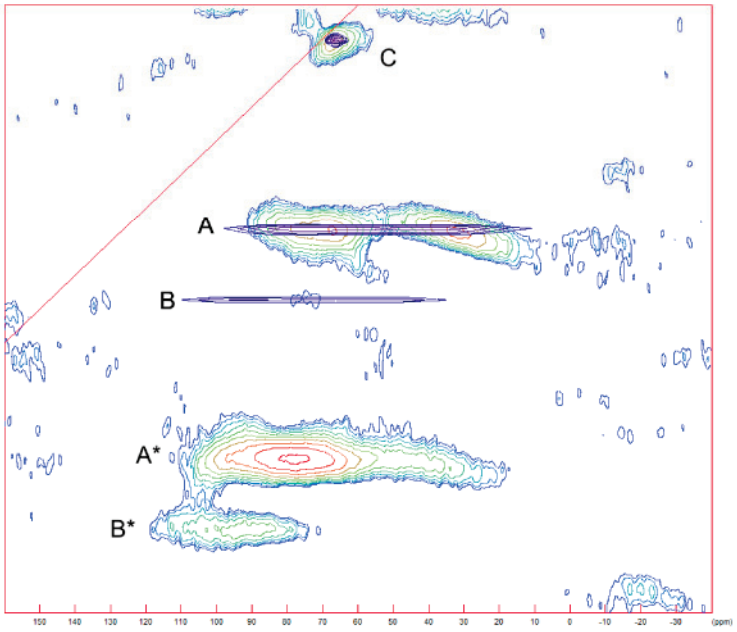

Figure S8. ^{27}Al MQ MAS spectrum of MAO (18.8 T), at spinning speed 20 kHz with simulated CS resonances. A: CS=100 ppm, C_Q=18 MHz; B: CS=119 ppm, C_Q=18.6 MHz; C: CS=69 ppm, C_Q<5 MHz. Asterix designate spinning side bands.

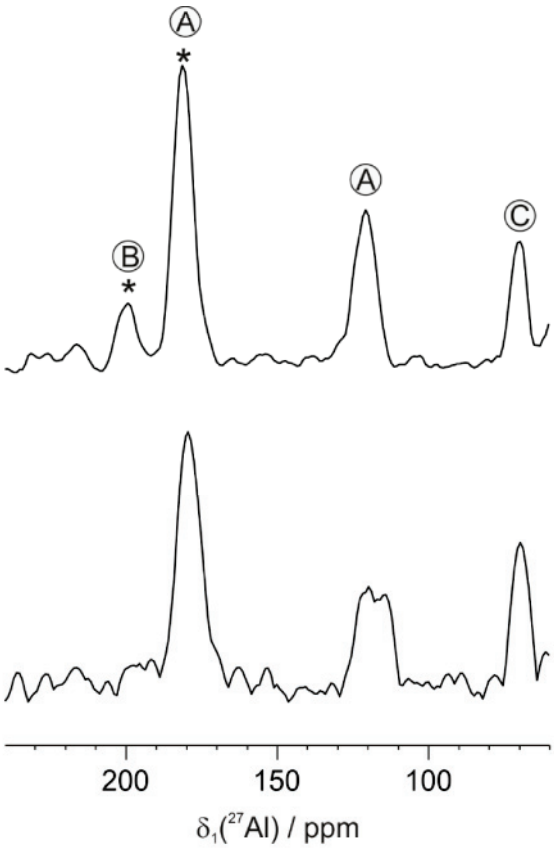

Figure S9. ^{27}Al MQ MAS isotropic projections of dried MAO (top) and SMAO-600 (bottom) (18.8 T). Asterisks designate spinning side bands.

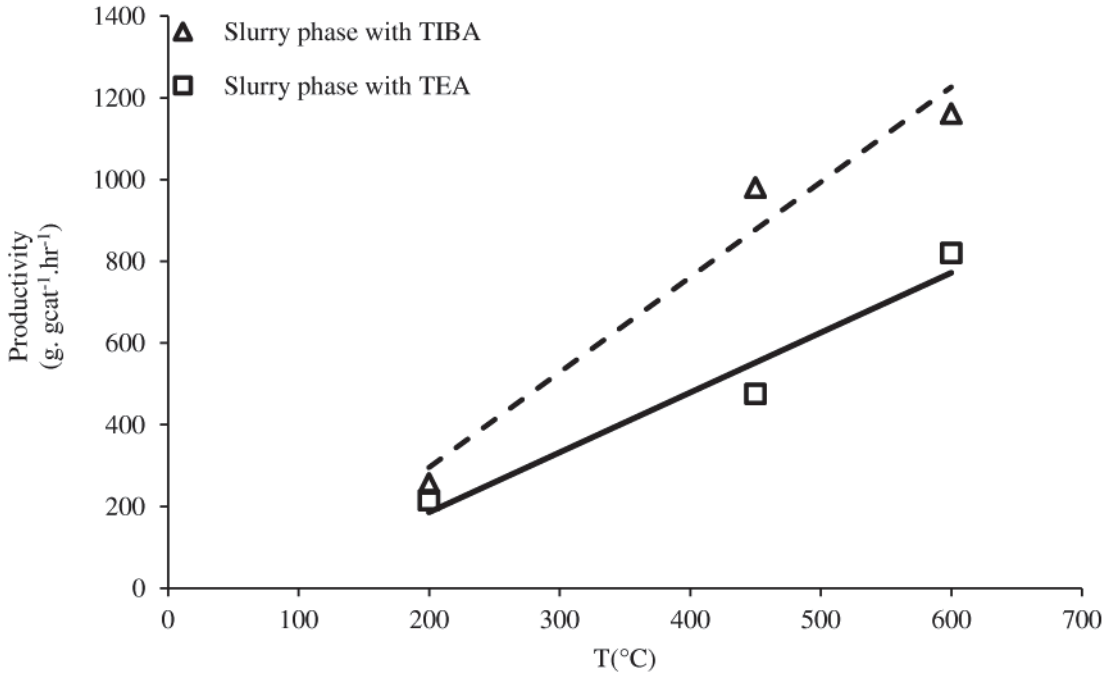

Figure S10. Average activities (or productivity) of the catalysts with different silica dehydroxylation temperatures in the presences of different scavenger in slurry polymerizations.

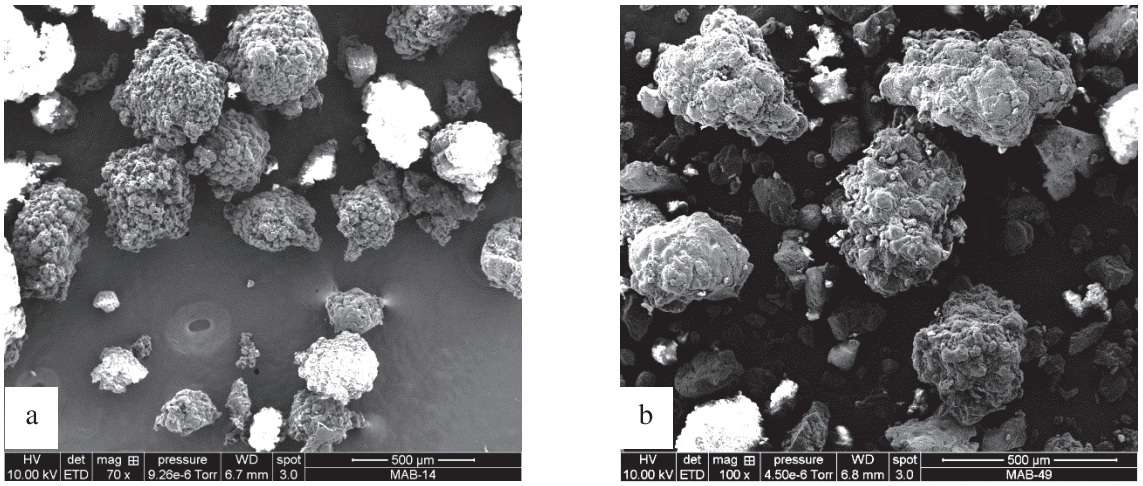

Figure S11. Comparison of polyethylene morphology produced in slurry (a) and gas phase (b) polymerizations using catalysts shown in Table 1.

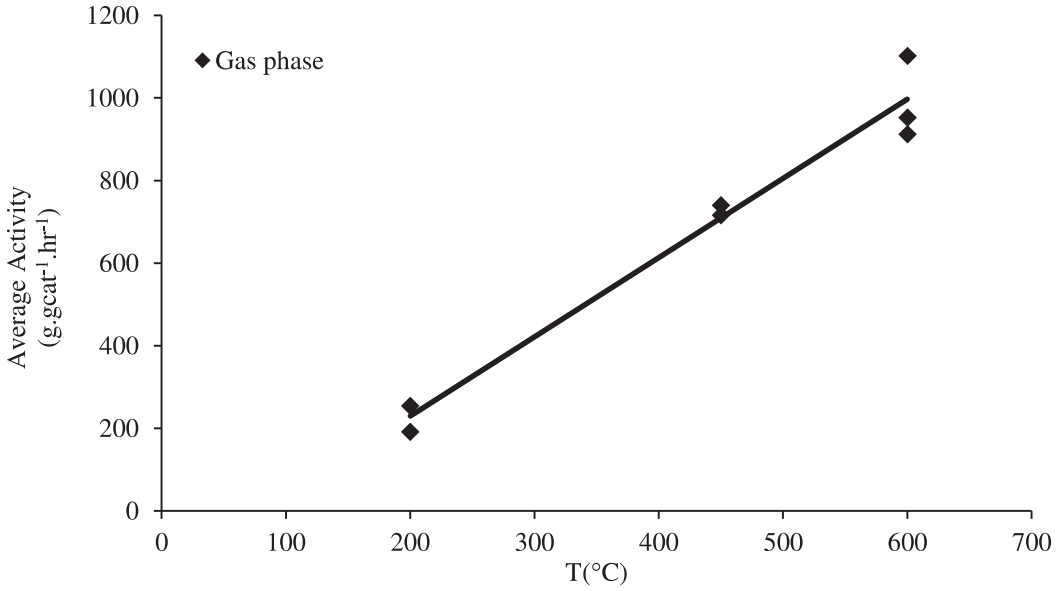

Figure S12. Comparison and reproducibility of catalysts average activity (or productivity) in gas phase homopolymerizations.

CHAPTER 3

The Effect of Polymerization Protocol on Catalyst Leaching in Slurry Phase Ethylene Polymerization

Contents

1. Introduction 133

2. Experimental Section 137

2.1. Materials 137

2.2. Supported Catalyst Synthesis 137

2.3. Polymerization Protocols 137

2.3.1. Method one for slurry polymerization (MSP-1) 138

2.3.2. Method two for slurry polymerization (MSP-2) 138

2.4. Catalyst Characterization 138

2.5. Polymer Characterization 139

3. Results and Discussion 140

3.1. Effect of pre-contact between TEA and supported catalyst in slurry polymerization 140

3.2. Effect of pre-contact between TIBA and supported catalyst in slurry polymerization 151

3.3. Effect of TOA concentration on the activity of supported catalyst 162

3.4. Comparison of the effect of different aluminum alkyls on the reaction kinetics of silica supported $(n\text{-BuCp})_2ZrCl_2$/MAO catalyst and the polymer PSD 164

3.5. Impact of Butylated Hydroxytoluene (BHT-H) on the reaction kinetics of silica supported $(n\text{-BuCp})_2ZrCl_2$/MAO catalyst 168

4. Conclusion 177

5. References 179

APPENDIX 1 182

1. Introduction

Metallocene catalysts, which are generally composed of a transition metal sandwiched between two cyclopentadienyl or cyclopentadienyl-derivative rings, represent a versatile group of organometallic catalysts suitable for olefin(s) polymerization. In comparison to polyolefins produced by conventional Ziegler-Natta or Phillips catalysts, polyolefins from metallocene catalysts show narrower molar mass distribution with a polydispersity index close to 2, better defined microstructures due to controlled comonomer incorporation that is independent of molar masses, comparable mechanical properties and better clarity which make metallocenes industrially attractive catalysts.[1-5] This statement can be better understood if one considers that about 5 million tons of LLDPE produced worldwide in 2009 were based on single-site catalysts which are often metallocenes.[6]

Metallocenes can be used to polymerize olefins in both homogenous or heterogeneous forms (i.e., supported on a carrier like silica, alumina etc.). The major benefits of using supported metallocenes are that they can be dropped into existing commercial reactors without significant process changes, they require reduced amounts of co-catalysts (like methylaluminoxane (MAO)), they reduce the chances of reactor fouling and cause greater ease of handling than polyolefins produced with homogeneous catalysts.[7] On the other hand, supported metallocenes show reduced catalytic activity (perhaps due to diffusion limitations), as well as deactivation of some of the sites during synthesis of the supported catalyst. Most commonly used methods for supporting metallocene on a carrier are related to the absorption of the molecular catalyst during its activation via the formation of an ion pair and include:[8]

i) Anchoring the metallocene pre-catalyst to the support by reacting the metal center with a functional group of the support. This method is not common because of the difficulties in predicting how the support functional groups will interact with the pre-catalyst (e.g., the interaction of various silanol groups of amorphous silica support with the metallocenes is not well-understood) and how the resultant species interact with the co-catalyst molecule.[8] Deactivation of metallocenes by the formation of bidentate species is also known to occur with this procedure.

ii) First treating the support with the co-catalyst (e.g., Methylaluminoxane (MAO) and/or other aluminum alkyls such as triethylaluminium (TEA), triisobutylaluminium (TIBA)

etc.) to obtain a certain amount of the co-catalyst on the support. The metallocene is then fixed on to this co-catalyst pre-treated support by the ionic interactions in the second step. This method is the most frequently applied method both in academia and industry to prepare supported metallocenes.[8]

iii) Mixing the metallocene and co-catalyst (e.g., MAO) in a suitable solvent like toluene and then grafting this solution of activated metallocene onto the support surface. The advantages of this method include better activation of the metal center due to contact between the catalyst and co-catalyst in homogenous form and low amount of solvents used.[8,9]

In conjunction with the type of the support and how it is conditioned, each of the above mentioned methods for supported metallocene synthesis can significantly effect the catalytic activity of heterogeneous metallocenes in olefin polymerization.[8]

Despite the various benefits obtained by supported metallocenes, reactor fouling (i.e., the formation of polyolefin film around the reactor walls and/or stirrer or other plant equipment) can still occur with these catalysts, especially in slurry phase polymerization reactors. Desorption, or leaching, of the metallocene molecule, co-catalyst or metallocene/co-catalyst active species from the support can initiate homogeneous polymerization in the diluent, thereby causing reactor fouling.[1,7,8,10,11] Different methods proposed in the open literature to overcome this problem of leaching include attempts to fix the metallocene covalently with the support via functional group of the ansa or cyclic ligand,[12-14] and the consecutive-combined method where the ligands of desired metallocene are first chemically bonded to the silica support and then the transition metal is inserted to create the metallocene complex on the silica surface.[9,15,16] However, these methods do not improve the yields of the supported metallocenes drastically, but do require additional steps during the synthesis procedure which makes them economically less attractive.[9] Therefore, most academic and industrial research commonly employs one of the above mentioned three supporting methods.

In addition to the discrepancies in catalyst synthesis methods, the major cause of catalyst leaching from the support is the interaction of supported MAO (the main focus of the current discussion) and metallocenes with the common aluminum alkyls (e.g., triethyl aluminum (TEA), tri isobutylaluminum (TIBA) etc.) which are added in the inert diluent of the slurry reactors either as co-catalysts or scavengers. The work of Sacchi et al.,[17] compares the impact of MAO and TIBA on

the leaching of silica-supported metallocenes (i.e., Cp_2ZrCl_2, $(Ind)_2ZrCl_2$, rac-$Et(Ind)_2ZrCl_2$) which were prepared by either supporting the metallocene directly on the silica support or by first impregnating the silica with MAO to prepare SMAO and then supporting the metallocene on SMAO. Their data suggests that in case of pre-contacting the SMAO-supported zirconocene with MAO solution in toluene, about 18 wt% of the originally supported zirconocene was leached into the solution, whereas only 1.2 wt% of it was desorbed into the solution when the same catalyst was pre-contacted with TIBA as co-catalyst. Similarly, the work of Semikolenova et al., [18] also showed that interaction of MAO or TIBA with the silica-supported metallocenes (prepared by using different synthesis methods) led to catalyst leaching under polymerization conditions. About 50 to 60 wt% of the supported metallocene was found to leach when silica/MAO/Cp_2ZrMe_2 or silica/TEA/Cp_2ZrMe_2 catalysts were contacted with MAO solution at 70 °C for 30 minutes, whereas pre-contacting with TIBA at the same conditions caused 20 wt% loss in the zirconocene content of the same catalysts. Ernst et al.,[19] reported 15 to 24 mole% desorption of the zirconocene from silica/MAO/$Me_2Si(2\text{-Me-Ind})_2ZrCl_2$ and silica/MAO/$Me_2Si(2\text{-Me-4-Ph-Ind})_2ZrCl_2$ catalysts when contacted with TIBA.

In another study, Panchenko et al.,[11] showed that contacting heptane solution of TIBA with SMAO-supported rac-$Me_2Si(Ind)_2ZrCl_2$ can leach 15 to 40 wt% of Al and 50 to 60 wt% of Zr from the supported metallocene which leads to both homogeneous and heterogeneous polymerizations and bimodality in the molar mass distribution of the polyethylene produced via slurry phase reaction. Furthermore, it is also proposed that the interaction of TIBA with the silica surface bound MAO modifies the MAO in such a way that it becomes more soluble in aliphatic hydrocarbons and behaves like modified MAO (MMAO). It is important to mention here that all of the above mentioned studies are more focused on showing that significant leaching occurs regardless of the method of catalyst synthesis employed; they do not explore the impact of polymerization protocol on the catalyst leaching or the ways to reduce it. In fact, there appears to be very few, if any, such studies in the open literature.

Other commonly used scavengers in olefin polymerizations include compounds which are product of the reaction between aluminum alkyls and simple phenols or substituted phenols.[20-29] These scavengers have been used mainly in homogeneous olefin polymerizations and termed as ‘non-interacting’ scrubbing agents. However, to the best of our knowledge these compounds have not

been tested in slurry phase polymerizations employing silica-supported metallocene/MAO systems. Therefore, the question remains as to whether or not catalyst leaching and consequently reactor fouling, occurs with these scavengers (based on the reaction products of aluminum alkyls and simple phenols or substituted phenols) in aliphatic diluents commonly used in commercial processes.

In general, it is believed that either diluents like toluene in which co-catalysts and metallocenes have high solubility, or high Al/Zr molar ratios (greater than 200:1) in the case of aliphatic diluents are the reasons for catalyst leaching. On the other hand, it appears that at lower Al/Zr ratios (on the order of 50-200:1), the metallocene/MAO catalysts are insoluble in common commercial aliphatic hydrocarbons.[30] Therefore, we aim to determine whether or not leaching of silica-supported metallocene/MAO catalysts with Al/Zr molar ratios close to 150 occurs in slurry phase ethylene polymerizations conducted in heptane. We considered different polymerization protocols and types of aluminum alkyl used as scavenger. Furthermore, the impact of the scavengers based on the reaction between common aluminum alkyls and the substituted phenol 2,6-Di-tert-butyl-4-methylphenol (commonly known as butylated hydroxytoluene; BHT-H) on catalyst leaching and reactor fouling is also analyzed. Consequently, this study is a crucial part of the present thesis because if the supported catalyst leaches out from the silica then one cannot analyze the effect of the physical properties of silica support on the reaction kinetics and morphology of the polyethylene produced since purely heterogeneous catalysis cannot be guaranteed.

2. Experimental Section

2.1. Materials

Two commercial silica have been used in this study as catalyst support. The first one is Grace 948 silica with a surface area of 290 m^2 g^{-1}, average particle diameter of 59 µm and a pore volume of 1.7 mL g^{-1}. The second is PQMS 3040 silica with a surface area of 420 m^2 g^{-1}, average particle diameter of 45µm and a pore volume of 3.0 mL g^{-1}. 30 wt% methylaluminoxane (MAO) solution (5.24 wt% TMA) in toluene was obtained from Albermarle, and the $(n\text{-}BuCp)_2ZrCl_2$ precatalyst from Sigma-Aldrich, and both were used as received. Triethyl aluminum (TEA), Triisobutyl aluminum (TIBA) and Trioctyl aluminum (TOA) were used as received from SGS, Witco Corporation and Schering AG, respectively. 2,6-Di-tert-butyl-4-methylphenol purchased from Sigma Aldrich was sublimed at room temperature and then dissolved in dry heptane to prepare 1 M stock solution. Dried heptane was used as diluent for slurry polymerizations. Ethylene (purity 99.95%) was purchased from Air Liquide (Paris, France) and passed through three different purification columns before use: a first one filled with reduced BASF R3-16 catalyst (CuO on alumina), a second one filled with molecular sieves (13X, 3A, Sigma-Aldrich), and a final one filled with Selexsorb COS (Alcoa).

2.2. Supported Catalyst Synthesis

The first step of catalyst synthesis method involves mixing the metallocene with MAO (30 wt% toluene solution) in dry toluene at room temperature. This solution was kept at room temperature inside the glove box for 1 h in order to have better catalyst activation and the volume of toluene used was about 150 % in excess of the pore volume of the used silica. Each silica used was dehydroxylated at 600 °C prior to its impregnation with the metallocene/MAO mixture. The solution of $(n\text{-}BuCp)_2ZrCl_2$ and MAO was then added drop wise to the weighed amount of silica (generally 2 g) in a three neck round bottom flask inside a glove box. The slurry was then heated at 50°C for 1 h outside the glove box followed by vacuum drying at 75°C for few hours. The final catalyst was a free flowing powder which was then stored in a glove box.

2.3. Polymerization Protocols

Polymerization runs were carried out in a spherical laboratory scale 2.5 L semi-batch reactor which can be operated both in slurry and gas phases. The detailed reactor set-up has been described in the

previous chapter. The reactor was conditioned for at least 2 h at 80 ºC with a minimum of three argon-vacuum cycles, and then cooled down to the room temperature.

2.3.1. Method one for slurry polymerization (MSP-1)

Two methods of catalyst injection into reactor were used during slurry phase homopolymerizations. In the first method, referred to hereafter as Method for Slurry Polymerization 1 (MSP-1), 20 to 25 mg of catalyst and 1 mL of a 1M TEA or TIBA or TOA solution in heptane were added to 500 mL of pure dried heptane under argon. This mixture (i.e., supported catalyst + scavenger + 500 mL heptane) was then injected into the reactor at room temperature under argon pressure followed by reactor heating to 80ºC under constant stirring at 450 revolutions per minute (rpm). Ethylene was then injected and maintained at 8 bar once the desired reaction temperature was achieved. Consumption of ethylene was recorded by the pressure drop in an ethylene cylinder equipped with a pressure gauge.

2.3.2. Method two for slurry polymerization (MSP-2)

In the second method of catalyst injection in slurry polymerizations, referred to hereafter as Method two for Slurry Polymerization (MSP-2), 25 to 30 mg of each catalyst were added to an injection cartridge with 5 mL of pure dried heptane inside the glove box. The injection cartridge was then attached to the reactor. 500 mL of pure dried heptane containing 1 mL of 1 M TEA or TIBA or TOA solution was injected separately into reactor under argon pressure, after which the reactor temperature was raised to 80 °C under constant stirring at 400 rpm. The mixture in the cartridge (i.e., the catalyst in 5 mL heptane) was then injected into the reactor under ethylene pressure at 80 °C and then the ethylene pressure was maintained at 8 bar throughout the reaction. Consumption of ethylene was recorded by the pressure drop in an ethylene cylinder equipped with a pressure gauge. It is important to highlight here that the major difference between these two methods is that MSP-2 does not entail any pre-contact between the scavenger and catalyst prior to polymerization, whereas MSP-1 does.

All the reactions were of 1 hour and 15 minutes unless otherwise mentioned.

2.4. Catalyst Characterization

Al and Zr content of the final catalysts were obtained by Inductively Coupled Plasma-Atomic Emission Spectroscopy (ICP-AES) at Mikroanalytisches Labor Pascher, Germany. Al and silicone

(Si) mapping of the catalysts was performed by Scanning Electron Microscope coupled with Energy Dispersive X-ray (SEM-EDX) at Centre Technologique des Microstructures Université Claude Bernard Lyon 1, Lyon, France.

2.5. Polymer Characterization

High temperature Size Exclusion Chromatography (HT-SEC) analyses were performed using a Viscotek system (from Malvern Instruments) equipped with three columns (PLgel Olexis 300 mm x 7 mm I. D. from Agilent Technologies). 200 µL of sample solutions with a concentration of 5 mg mL^{-1} were eluted in 1,2,4-trichlorobenzene using a flow rate of 1 mL min^{-1} at 150°C. The mobile phase was stabilized with 2,6-di(tert-butyl)-4-methylphenol (200 mg L^{-1}). The OmniSEC software was used for data acquisition and data analysis. Online detection was performed with a differential refractive index detector and a dual light scattering detector (LALS and RALS) for absolute molar mass measurement. The OmniSEC 5.02 software was used for calculations.

Malvern Mastersizer 3000 was used for the measurement of particle size distribution (PSD) of silica supports in water with the specially designed Hydro unit whereas for polymer particles a dry module was used for the measurement. Equation-1 was used to calculate the span of the PSD curves.

$$\text{Span} = \frac{d_{90} - d_{10}}{d_{50}} \quad (1)$$

Where,

d_{10} = diameter value (in µm) possessed by of 10 vol% of the particles present in the measured sample

d_{50} = diameter value (in µm) possessed by of 50 vol% of the particles present in the measured sample

d_{90} = diameter value (in µm) possessed by of 90 vol% of the particles present in the measured sample

3. Results and Discussion

Elemental analysis of the final catalysts is shown in **Table 1**. It can be seen here that all the catalysts obtained had very similar metal loadings, and the Al to Zr molar ratio is very close to the targeted value of 150 during the catalyst synthesis as mentioned in the experimental part.

Table 1. Elemental characterization of the catalysts by ICP-AES.

Catalyst	Al (wt%)	Zr (wt%)	Al/Zr Molar Ratio
$(n\text{-}BuCp)_2ZrCl_2$/MAO/Grace 948	14.0	0.31	153
$(n\text{-}BuCp)_2ZrCl_2$/MAO/PQMS3040	12.3	0.30	139

3.1. Effect of pre-contact between TEA and supported catalyst in slurry polymerization

As described above in the polymerization section, the two polymerization protocols used in this study differ from each other as to whether the catalyst and the scavenger are pre-contacted (MSP-1) or not (MSP-2) before the polymerization begins. **Figure 1** and **Figure 2** show the effect of pre-contacting the $(n\text{-}BuCp)_2ZrCl_2$/MAO/Grace948 and $(n\text{-}BuCp)_2ZrCl_2$/MAO/PQMS3040 supported catalysts with TEA, respectively. It can be seen that pre-contacting each catalyst with TEA reduced the instantaneous catalytic activity as compared to that attained when there was no pre-contact between them. In the case of Grace 948 based catalyst, the activation behavior remains very similar in two polymerization protocols (i.e., compare first 5 minutes of reaction time in **Figure 1**), whereas, for the catalyst supported on PQMS3040 silica the activation is delayed by pre-contacting the catalyst with TEA (i.e., compare first 5 minutes of reaction time in **Figure 2**). It is also evident that the effect of pre-contacting is more pronounced in the case of catalyst supported on PMS3040 silica where the catalyst productivity is reduced by almost 50%, whereas, this decrease is approximately 30% in the case of catalyst supported on Grace 948 silica (see **Figure 3**).

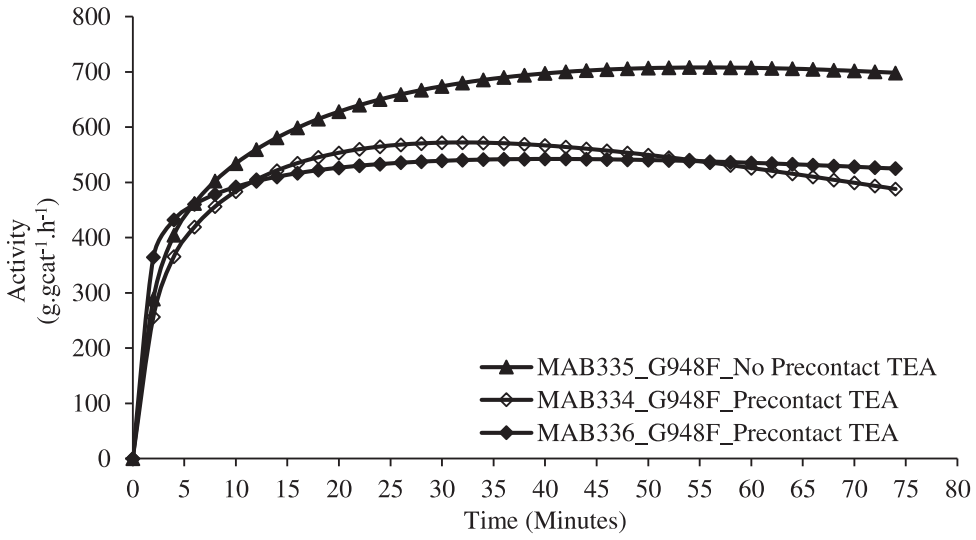

Figure 1. Effect of pre-contact between Grace 948 based catalyst and TEA in slurry phase polymerizations.

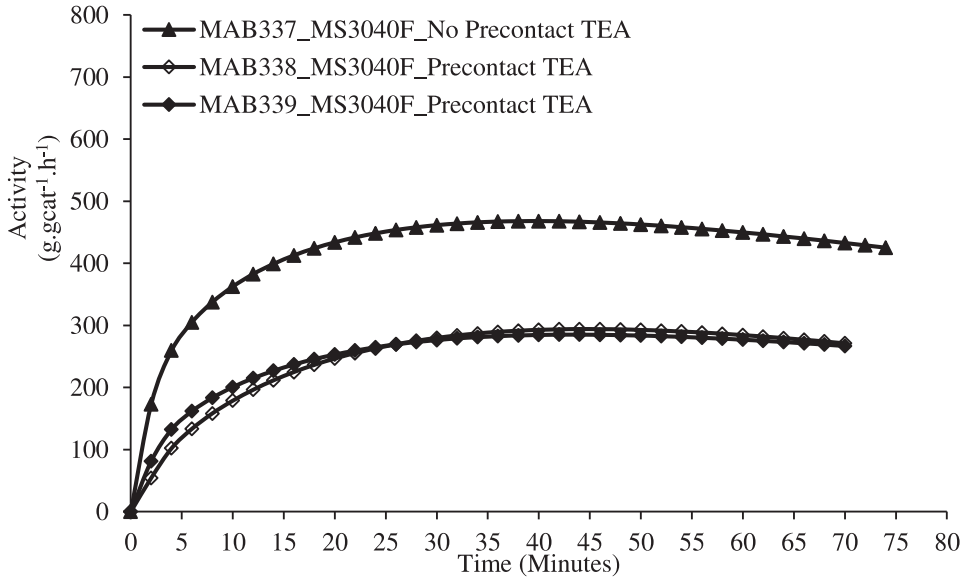

Figure 2. Effect of pre-contact between PQMS3040 based catalyst and TEA in slurry phase polymerizations.

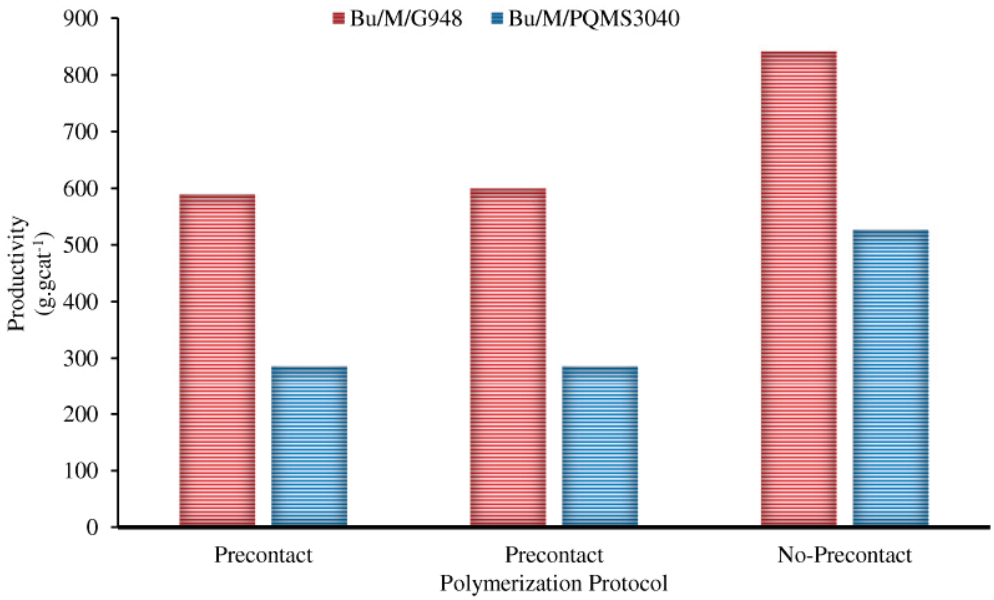

Figure 3. Effect of polymerization protocol on the productivity of catalyst for the reaction time of 1 hour 15 minutes.

The effect of two polymerization protocols on the reactor fouling was also observed and the condition of the reactor and its contents at the end of some of the representative polymerizations is shown in **Figure 4**. A white colored polymer film formed around the reactor wall is visible in **Figure 4a**, whereas, no such film is present on the reactor wall in **Figure 4b**. This supports the idea that pre-contacting the supported catalyst with TEA is correlated with the leaching of supported $(n\text{-BuCp})_2ZrCl_2$/MAO complex from the silica support, which remained active in the continuous phase and produced polyethylene that was deposited (at least partially) on the reactor walls as an indication of reactor fouling. On the other hand, no pre-contact between the catalyst and TEA (i.e., MSP-2) led to heterogeneous catalysis without any leaching where the polyethylene was formed on the supported catalyst particles leading to no reactor fouling as shown by the clean reactor walls in **Figure 4b** at the end of reaction. It should be noted that the same behavior was noticed for Grace 948 based catalyst but for the sake of brevity **Figure 4** only shows reactor condition at the end of reaction with PQMS 3040 based catalyst. Morphology of the obtained HDPE samples is shown in **Figure S1(a-c)** of the Appendix which shows spherical particles in both cases because the thin film formed around the reactor wall was not collected with the whole MSP-1 sample. These results clearly indicate that the polymerization protocol can significantly affect the reaction kinetics of

silica supported metallocene/MAO complex as well as the fact that catalyst leaching can be avoided by selecting an appropriate polymerization protocol.

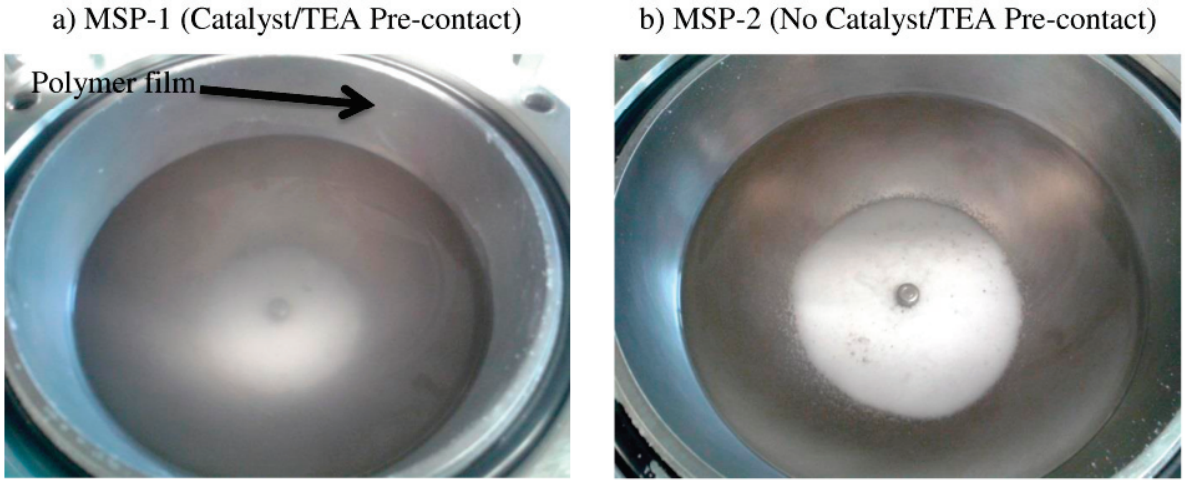

Figure 4. Effect of polymerization protocols on reactor fouling a) MAB-339 and b) MAB-337. White colored PE film can be noticed on the reactor walls at the end of polymerization with MSP-1 protocol, whereas, no such film can be noticed on the reactor walls at the end of polymerization with MSP-2 protocol.

As stated above, the major difference between the two protocols is the pre-contact, or absence thereof between the supported catalyst and the TEA. In both cases the TEA is well dispersed in the slurry phase, however in the case of MSP-1, the supported catalyst particles are exposed to the TEA in solution for a much longer period of time (approximately 10 minutes starting from catalyst injection into 500 mL heptane containing scavenger followed by injection into the reactor and until the reactor is heated to the reaction temperature and ethylene injection). This allows the active sites, especially those close to the exterior of the silica particles to eventually be dissolved in the heptane and diffuse out of the particles. The lower instantaneous polymerization rate obtained with the MSP-1 protocol (i.e., upon pre-contacting the supported catalyst with TEA) can be attributed to the fact that pre-contact of TEA with the supported (n-BuCp)$_2$ZrCl$_2$/MAO catalyst causes the generation of heterobimetallic species $[L_2M(\mu\text{-}R)_2AlR_2]^+$, both in the reaction milieu where there is leached catalyst, and inside the supported catalyst. It is well-known that this species is very stable

when it is generated via TEA, and decreases the activity of metallocenes in olefin polymerizations.[31,32]

On the other hand, in MSP-2 protocol, despite the fact that the TEA is well dispersed in the diluent before the polymerization (as in MSP-1), there is no catalyst until the ethylene is injected. The diluent therefore comes in contact essentially at the same time the ethylene is injected and polymerization can begin. Upon injection the Al/Zr ratio inside the particles will be lower at the active sites than is the case with MSP-1, thus giving us a very different reaction rate. In addition, polymer forms immediately at the exterior of the particles, provoking mass transfer limitations for both ethylene and TEA, but given that the TEA is bulkier, it will diffuse more slowly through the surface pores to the interior, thereby maintaining low Al/Zr ratios inside the particles, but still acting as a scavenger outside. Furthermore, polymer layer will rapidly cover accessible sites, thereby preventing leaching and consequently reducing the possibility of reactor fouling. The fraction of heterobimetallic species formed will therefore be lower with MSP-2 than MSP-1, leading to faster reactions.

Molecular weight distribution (MWD) curves of the HDPE samples via two polymerization protocols are shown in **Figure 5** and the values of weight average molar mass (M_w) and dispersity of molar mass (Đ) are shown in **Table 2**. No significant effect of either polymerization protocol is obvious on the MWD or Đ values of the HDPE samples which indicates that the active sites which produced polymer remain similar in both polymerization protocols. In addition, the melting temperatures of the HDPE samples also remain unaffected by the polymerization protocol.

However, the bulk density of the HDPE decreased when the supported catalysts were pre-contacted with TEA with only 1% reduction in the case of polyethylene produced by Grace 948 supported catalyst, and 13% reduction in the case of polyethylene produced by PQMS3040 supported catalyst. This observation is also attributable to the poor morphology of the homogenously formed polyethylene due to the leaching of active metallocene/MAO complex from both the silica supports. It should be recalled that one of the various benefits of supporting metallocenes on silica is the higher bulk density of the polyolefins produced by using such catalysts (as compared to polyolefin bulk density produced from their homogeneous analogs) due to support replication phenomenon and this benefit of supported catalysts is lost if the supported active species leaches away from the support leading to poor polymer morphology and a decrease bulk density.

Table 2. Weight average molar mass (M_w), polydispersity index (Đ), bulk density and melting temperature (T_m) of HDPE samples produced with MSP-1 and MSP-2 polymerization protocols.

Catalyst Support	Sample Name	Catalyst/TEA Pre-Contact	M_w (g. mole^{-1})	Đ	Bulk Density (g. mL^{-1})	T_m (°C)
Grace 948	MAB335	No	155 000	2.4	0.38	135.7
Grace 948	MAB334	Yes	175 000	2.4	0.37	134.5
Grace 948	MAB336	Yes	175 000	2.4	0.37	135.2
PQMS3040	MAB337	No	165 000	2.4	0.39	135.7
PQMS3040	MAB338	Yes	175 000	2.3	0.34	135.3
PQMS3040	MAB339	Yes	180 000	2.4	0.34	135.2

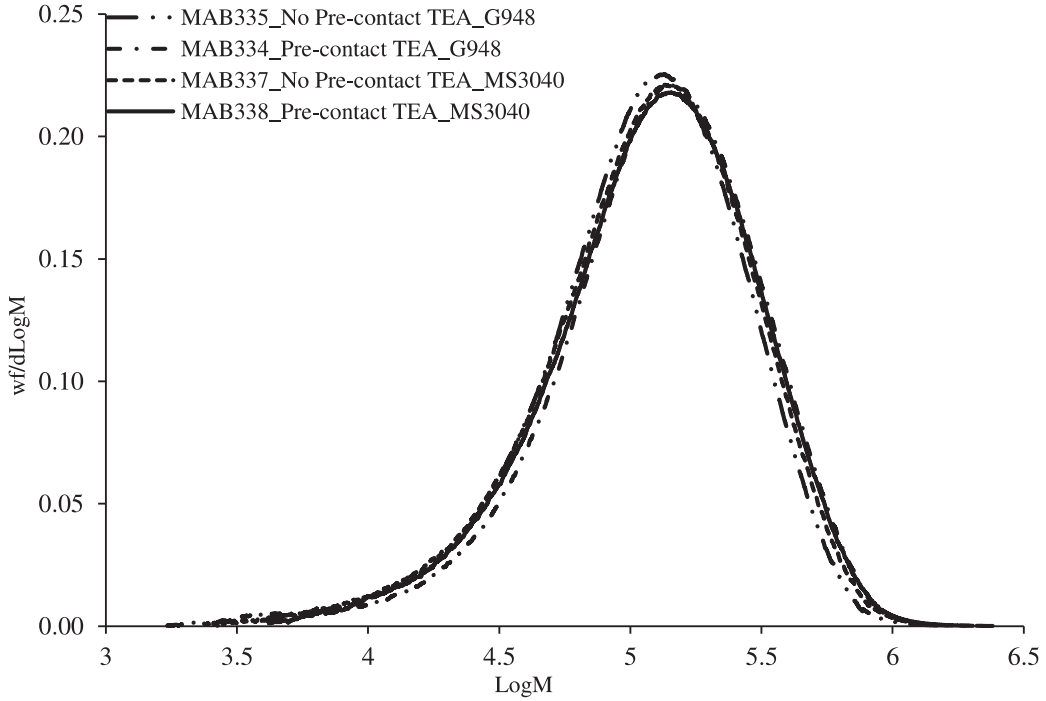

Figure 5. Effect of pre-contacting the two different silica supported catalysts with TEA on the MWD of HDPE produced in slurry phase homopolymerizations.

The particle size distributions (PSD) of the silica supports and the HDPE samples produced by the two polymerization protocols are compared in **Figure 6** and **Figure 7**. It should be noted that in case of HDPE samples produced by using MSP-1 protocol the PSD measurements correspond only to the powder recovered and not to the polymer film formed on the reactor walls (see **Figure 4a**). The PSD of Grace 948 silica and PQMS 3040 silica show clear differences in the amount of particles smaller than 30 µm, whereas the d_{50} values of both the silica are not very different i.e., d_{50} for Grace 948 is 59 µm whereas the d_{50} value for PQMS3040 silica is 45 µm. All the HDPE samples

replicate the morphology of their respective support on which they were produced. In the case of HDPE samples produced by using Grace 948 silica as catalyst support, the polymer PSD clearly shift towards larger particle size when there was no pre-contact between the catalyst and TEA which can be attributed to the higher productivity with MSP-2 as compared to that in MSP-1. In addition, a closer look on the PSD curves of Grace 948 silica based samples shows differences in the amount of fine particles (i.e., the polymer particles with diameter ≤ 200 μm) generated during the two polymerization protocol. Pre-contact between the Grace 948 silica supported catalyst and TEA generated more fine particles in the HDPE sample as compared to the fine particles generated without any pre-contact between them (see inset of **Figure 6**). This observation supports the slight difference (i.e., only 1%) noted in the bulk density values of the HDPE samples produced by the two different polymerization protocols shown in **Table 2** i.e., the higher the fine particles are in the sample the higher is the mass per unit volume of the bulk of PE sample.

On the other hand, PSD curves of the HDPE samples produced from PQMS3040 based catalyst shows opposite trend with respect to the amount of fine particles i.e., less fines are present in the HDPE samples produced by MSP-1 as compared to the fines present in HDPE samples prepared from MSP-2 polymerization protocol. This observation supports the bulk density values (see **Table 2**) for HDPE samples produced by using PQMS3040 based catalyst i.e., the lower bulk density of HDPE samples produced by using PQMS3040 supported catalyst is due to less number of fine particles. Overall, these results indicate that the catalyst supported on PQMS3040 silica leaches more as compared to that supported on Grace 948 silica, probably, due to the larger pore volume of the former support as compared to the later one.

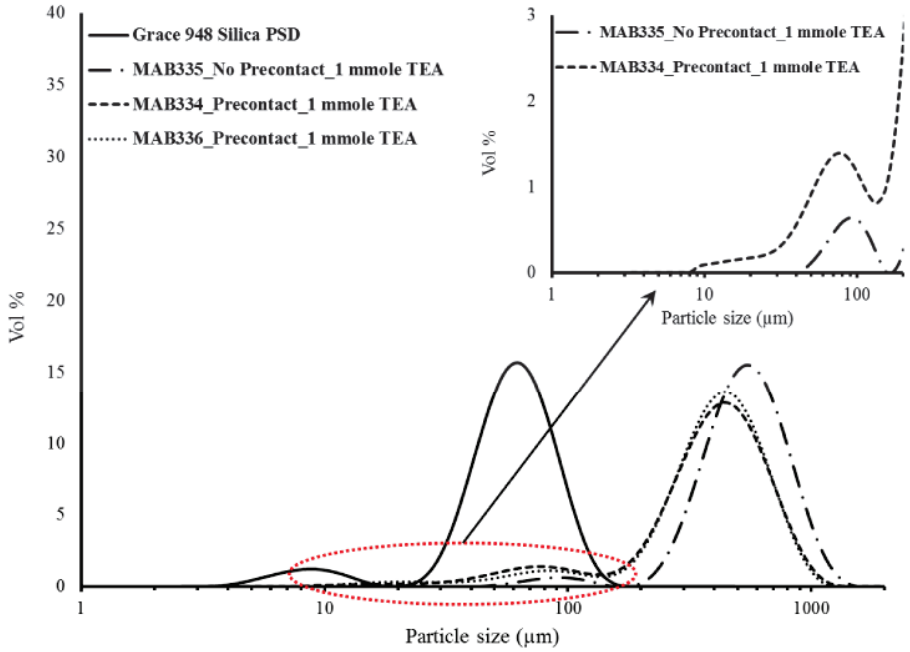

Figure 6. Effect of polymerization protocol on the PSD of HDPE produced by using Grace 948 as catalyst support. Span of MAB335 = 0.95, span of MAB334 = 1.45 and span of MAB336 = 1.31.

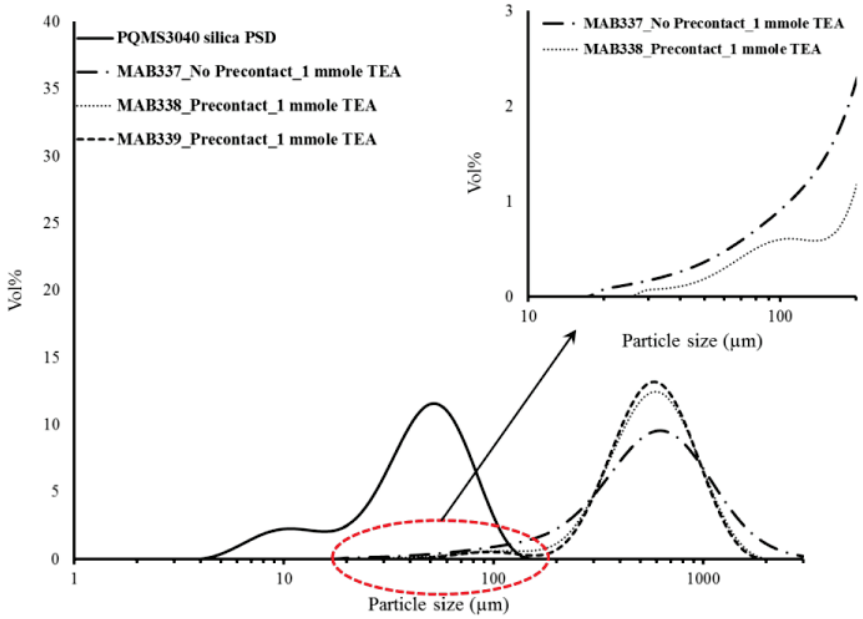

Figure 7. Effect of polymerization protocol on the PSD of HDPE produced by using Grace 948 as catalyst support. Span of MAB337 = 1.88, span of MAB338 = 1.30 and span of MAB339 = 1.26.

The benefit of polymerization protocol without any pre-contact with the aluminum alkyl allows one to analyze the impact the higher concentrations of aluminum alkyl on the polymerization

kinetics, molecular properties and morphology of the produced polyethylene sample by ensuring purely heterogeneous catalysis. **Figure 8** shows the effect of increasing TEA concentration inside reactor with MSP-2 on the kinetic profiles of ethylene homopolymerizations with Grace 948 supported (n-BuCp)$_2$ZrCl$_2$/MAO catalyst. A decrease in the instantaneous activity can be noticed with increasing TEA concentration inside the reactor. The importance of using TEA as a scavenger is also shown in **Figure 8** where the rate profile of the run without any TEA shows rapid deactivation of the catalyst after 10 minutes of reaction. It is important to mention here that no reactor fouling at all was observed in these reactions, as shown also by **Figure S1(d)** of the Appendix which shows spherical HDPE particles at 12 mmole.L^{-1} concentration of TEA. This means that all the polymerization occurred on the supported catalyst particles.

The reason for decrease in the catalytic activity by increasing TEA concentration inside reactor is probably the same as discussed in the previous paragraphs which points towards the generation of a dormant heterobimetallic species [L$_2$M(μ-R)$_2$AlR$_2$]$^+$ formed by interaction between supported (n-BuCp)$_2$ZrCl$_2$/MAO catalyst and TEA. It is easy to understand that the generation of this dormant and stable cationic species is more probable at higher TEA concentrations. A similar impact of increasing TEA reactor concentration on the kinetics of (n-BuCp)$_2$ZrCl$_2$ supported on activating silica support in slurry phase ethylene/1-hexene copolymerization was observed by Tisse et al.[32] In other words, one can also say that TEA acts as a catalyst poison for the silica supported metallocene when added in large excess into the slurry phase ethylene polymerization reactor. This is a further evidence of our proposed explanation for the increase in activity with MSP-2 discussed above. MWD of the HDPE samples and melting temperature seem to be unaffected by TEA concentration as shown by **Figure 9** and **Table 3**. Molar mass dispersity of these samples remained in a close range of 2.4 to 2.8 which shows that single site behavior of the silica supported (n-BuCp)$_2$ZrCl$_2$/MAO is also not affected by increasing TEA concentration inside reactor.

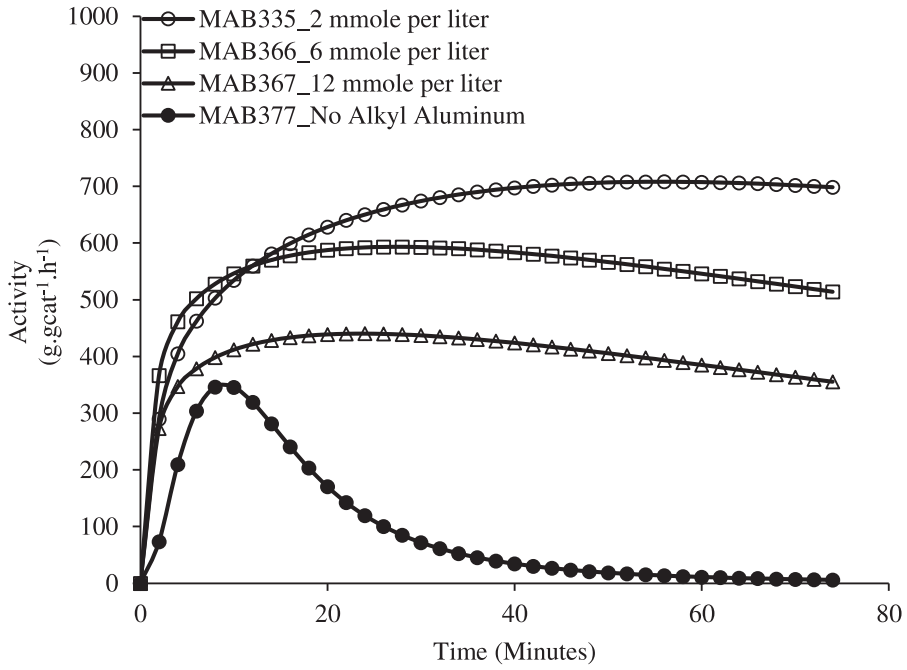

Figure 8. Effect of TEA concentration inside reactor on the instantaneous activity of silica supported (n-BuCp)$_2$ZrCl$_2$/MAO in ethylene homopolymerization with MSP-2.

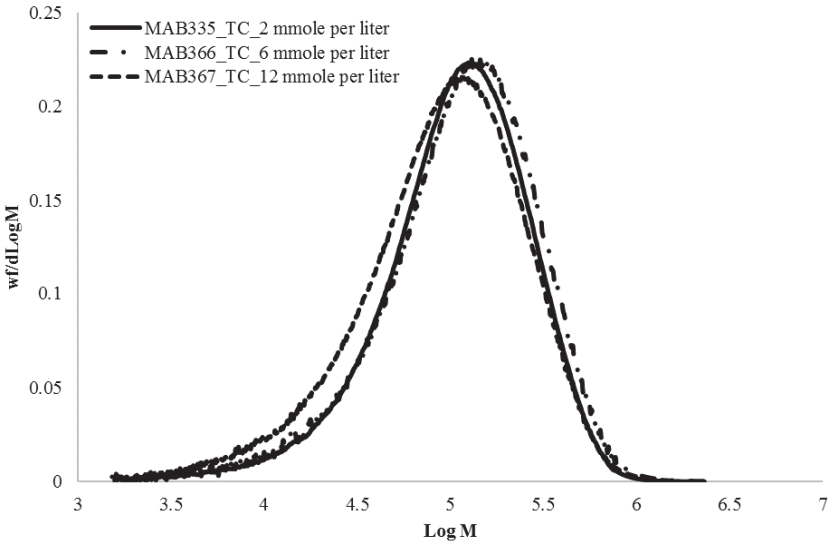

Figure 9. Effect of TEA concentration inside reactor on the MWD of HDPE samples.

Table 3. Weight average molar mass (M_w), polydispersity index (Đ) and melting temperature (T_m) of HDPE samples produced by changing TEA concentration in reactor diluent. C_{TEA} refers to TEA concentration.

Sample Name	C_{TEA} (mmole. L^{-1})	M_w (g. $mole^{-1}$)	Đ	T_m (°C)
MAB335	2	155 000	2.4	135.7
MAB366	6	154 000	2.7	136.5
MAB367	12	140 000	2.8	135.8

In addition to influencing the reaction rate, the TEA concentration seems to effect the particle size distribution and bulk density of the polyethylene as shown by **Figure 10**. All the polymer samples replicate the support morphology indicating that there was no catalyst leaching with this polymerization protocol despite adding more TEA into the reactor. An important observation evident in **Figure 10** is that the concentration of fine particles (i.e., the particles with diameter ≤ 200 µm) increased with increasing TEA concentration inside reactor e.g., almost 15% rise in the concentration of 104 µm particles can be observed while going from 2 to 12 mmole TEA per liter of reactor diluent. This increase in the concentration of fine particles increases the bulk density of the polyethylene sample as shown in the inset of **Figure 10**. Therefore, increased TEA content inside reactor can be detrimental to reactor operation due to excessive generation of fines. The most probable reason for increase in fines concentration with increasing TEA content is that the small catalyst particles probably get more influenced by the higher TEA concentration as it is easier for TEA to diffuse in smaller catalyst particles than in the bigger ones. Based on these results it is easy to imagine the impact of increased TEA content inside a gas phase reactor although it is out of the scope of the present study. Another observation from **Figure 10** is the shift of PSD curves towards larger particle size at lower TEA content which is directly attributable to increased productivity at lower TEA concentration inside reactor. In addition, broadening of polymer PSD curve with increasing TEA content is also visible from the span values (see caption of **Figure 10**).

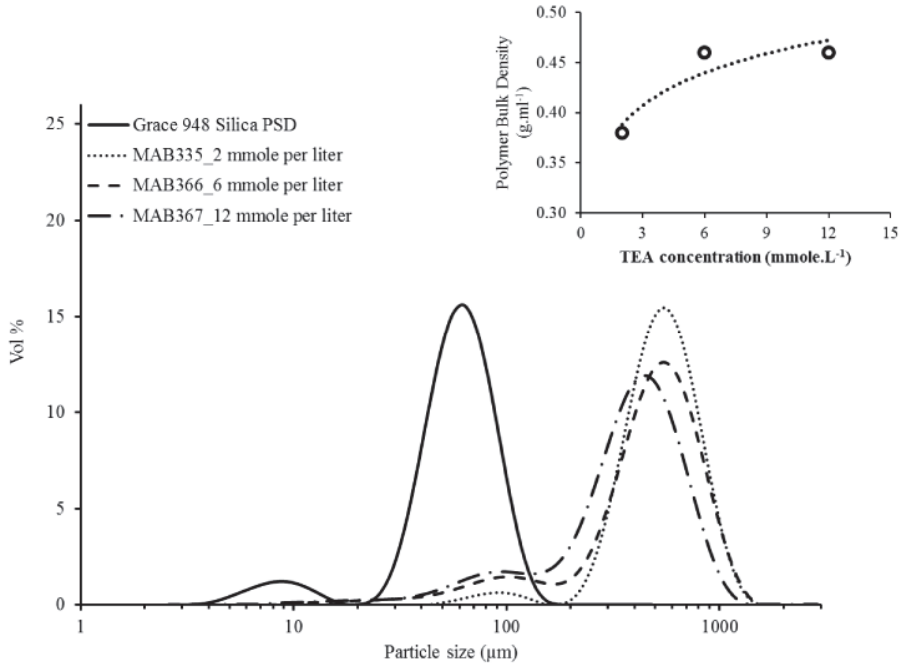

Figure 10. Effect of TEA concentration inside reactor on the PSD of HDPE produced in slurry phase polymerizations. Span of MAB335 PSD curve = 0.95, MAB366 PSD curve = 1.46 and MAB367 PSD curve = 1.48. Bulk density values are average values of minimum two measurements for one sample and in case of multiple samples they represent the average of those samples also.

3.2. Effect of pre-contact between TIBA and supported catalyst in slurry polymerization

Figure 11 and **Figure 12** show the comparison of the kinetic profiles obtained by using two different protocols for the catalyst supported on Grace 948 and PQMS3040 silica, respectively. In contrast to what is shown in the previous section, it can be observed that the instantaneous polymerization rate is higher for MSP-1 (i.e. pre-contacted with TIBA) than with MSP-2 (no pre-contact with TIBA). While the maximum rate of polymerization was higher in the case of pre-contact with TIBA, the rate decay (i.e. deactivation) was less significant with MSP-2.

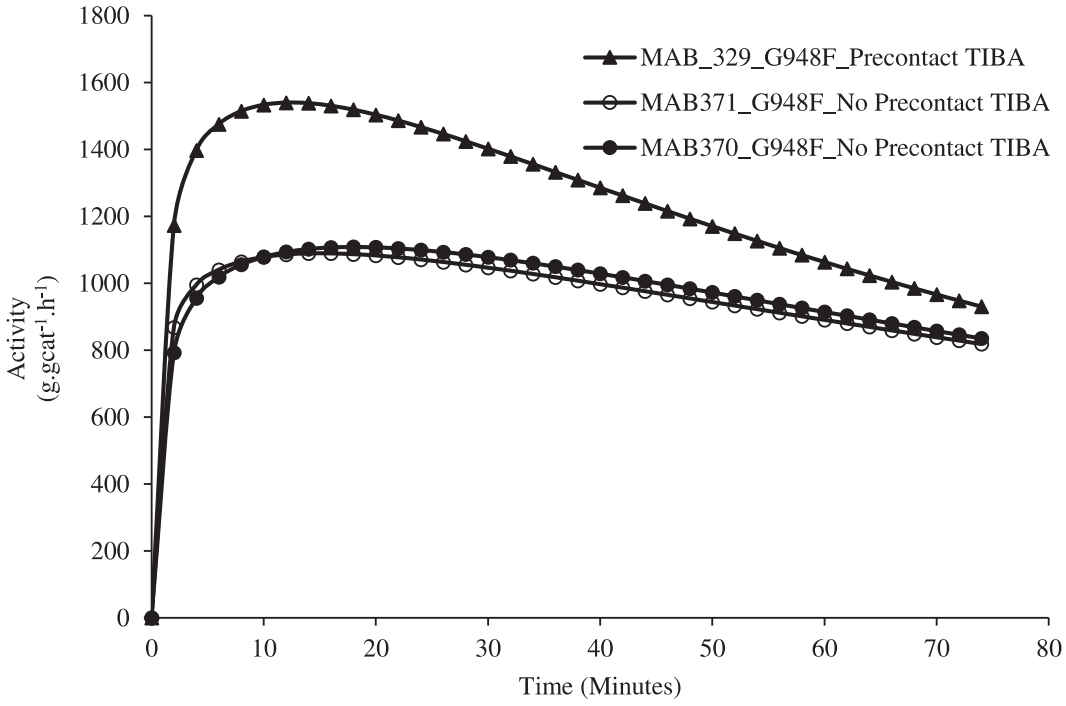

Figure 11. Kinetic profiles obtained with Grace 948 catalyst.

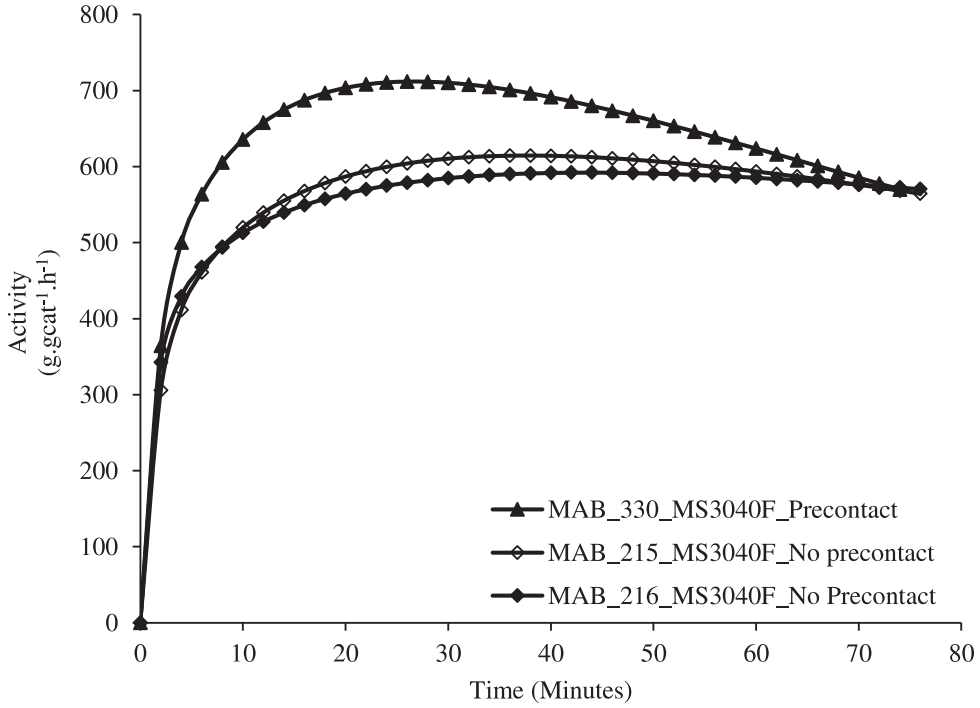

Figure 12. Kinetic profiles obtained with PQMS3040 catalyst.

Furthermore, the reactor condition at the end of reaction and morphology of the polyethylene samples produced with both the polymerization protocols was very different. As we saw above when TEA was used as the aluminum alkyl, using MSP-1 and the Grace 948-supported catalyst led to extensive reactor fouling (c.f. **Figure 13a**), the formation and film-like polymer chunks and/or agglomerates of polyethylene, and virtually no well-defined granules that we would expect if the reaction proceeded ideally (see **Figure 13b**). Similarly, reactor fouling was also observed with MSP-1 when PQMS3040 based catalyst was used (see **Figure 13c**) but the polymer morphology was somewhat better than that obtained with Grace 948-supported catalyst, with some spherical particles being obtained (see **Figure 13d**). On the other hand, when polymerizations were conducted without pre-contacting TIBA and the supported catalyst (i.e., with MSP-2) no reactor fouling was observed in any of the polymerizations conducted by both the catalysts (see **Figure 13e**) and the obtained polymer particles possessed spherical shape indicating purely heterogeneous catalysis (see **Figure 13f** and **Figure S2(a, b)**).

The presence of reactor fouling in the case of polymerizations done with the MSP-1 protocol explains the higher activities obtained with the two catalysts as compared to their activities obtained with MSP-2 protocol. It has been shown in the literature by various authors[7,8,11,18] that pre-contacting the supported metallocenes with aluminum alkyl like TIBA causes the desorption or leaching of the metallocene/MAO activated complex from the support which leads to homogenous polymerization in the diluent. The amount of zirconocene and aluminum desorbed into the diluent depends on the type of diluent, catalyst supporting method, properties of the support used and the conditions used during the leaching experiments with some of the studies[18] reporting 10-18 wt% of supported zirconocene desorbed into the diluent while others[19] reported 15-24 wt% of zirconocene leached into the diluent upon contact with TIBA. Panchenko et al.,[11] showed that the pre-contact of TIBA with MAO-modified silica-supported metallocene can leach 15-40 wt% of aluminum and 50-60 wt% of the zirconocene from the supported catalyst. This leached metallocene is active in polymerization if MAO is also present in the diluent, as shown by Kaminsky et al.[10,33] Therefore, the higher instantaneous activities showed by the two silica supported (n-BuCp)$_2$ZrCl$_2$/MAO catalysts when pre-contacted with TIBA, as compared to the case when there is no pre-contact, is likely due to the leaching of (n-BuCp)$_2$ZrCl$_2$/MAO from the support leading to homogenous polymerization in the diluent causing reactor fouling (as well as the heterogeneous polymerization which occurred due to the part of (n-BuCp)$_2$ZrCl$_2$/MAO remained on silica).

In contrast to the previously discussed case of TEA pre-contacting with the same supported catalysts (where, although catalyst leaching occurred, the activity of the catalysts after pre-contacting was less than in the absence of any pre-contact), the increase of activity by pre-contacting TIBA with supported $(n\text{-BuCp})_2ZrCl_2$/MAO catalyst can be explained by the fact that: i) the stability of heterobimetallic species $[L_2M(\mu\text{-}R)_2AlR_2]^+$ formed by the presence of TIBA is less than that formed by the presence of TEA[31] and ii) TIBA interacts with MAO and partially replaces the Al-Me groups of MAO with Al-^{i}Bu groups which converts MAO into modified MAO (MMAO) which is better cocatalyst for metallocenes and has higher solubility in heptane then MAO.[11,34,35] In case of no pre-contact between the supported catalysts and TIBA there was no leaching of the active species into the diluent which lead to purely heterogeneous catalysis, absence of any reactor fouling and provided kinetic profiles with less catalyst deactivation as compared to the deactivation observed in MSP-1 protocol.

Figure 13. Reactor fouling caused by the polymerization protocol MSP-1 (a-d) and the absence of reactor fouling in the case of MSP-2 protocol (e,f).

Effect of pre-contacting TIBA with silica supported (n-BuCp)$_2$ZrCl$_2$/MAO on the MWD of HDPE produced in slurry phase process is shown in **Figure 14** where it is clear that the HDPE produced by pre-contacting the supported metallocene with TIBA has higher molar mass than that produced without any pre-contact between the supported catalyst and TIBA. Presence of the homogeneous polymerization is also evident from the dispersity of molar masses and bulk density values shown in **Table 4**, both of which decreased when the supported catalyst was pre-contact with TIBA. Note

that polyethylene produced with single-site catalysts via homogeneous polymerization shows Đ values close to 2. The melting temperature of the HDPE samples remained uninfluenced by the polymerization protocols.

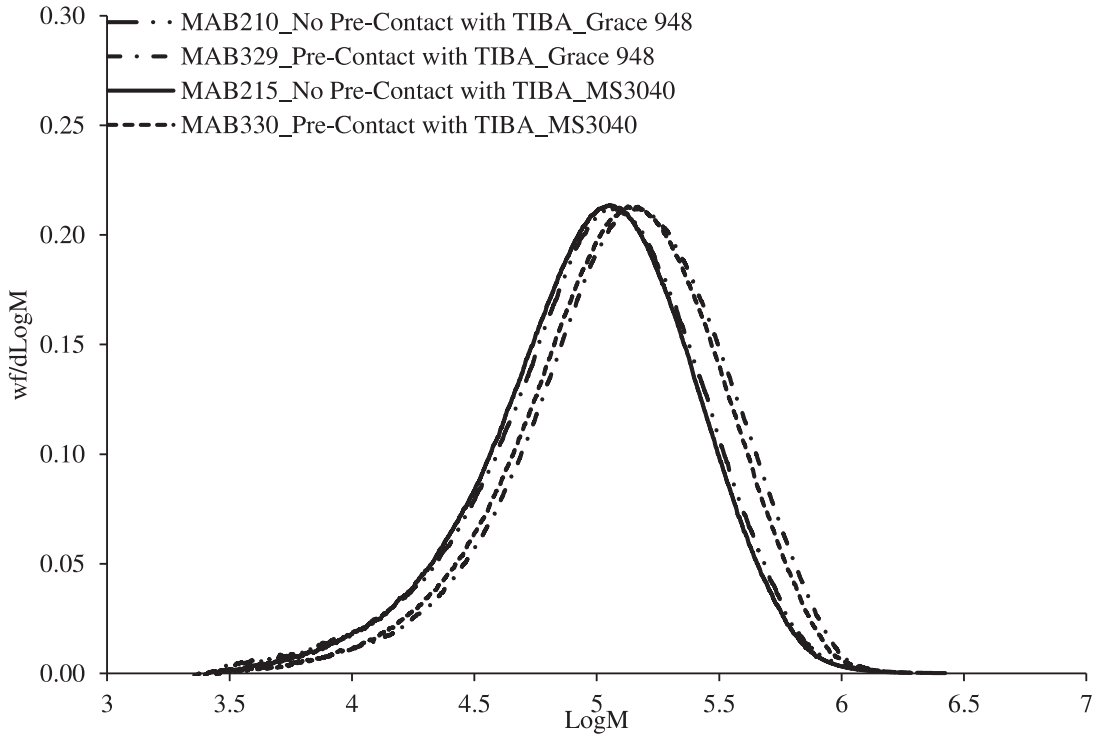

Figure 14. Effect of pre-contacting the two different silica supported catalysts with TIBA on the MWD of HDPE produced in slurry phase homopolymerizations.

Table 4. Weight average molar mass (M_w), polydispersity index (Đ), bulk density and melting temperature (T_m) of HDPE samples produced with MSP-1 and MSP-2 polymerization protocols.

Catalyst Support	Sample Name	Catalyst/TIBA Pre-Contact	M_w (g/mole)	Đ	Bulk density (g/ml)	T_m (°C)
Grace 948	MAB370	No	153 000	2.8	0.37	134.2
Grace 948	MAB371	No	156 000	2.8	0.38	-
Grace 948	MAB329	Yes	190 000	2.4	0.23	134.2
PQMS3040	MAB215	No	140 000	2.7	0.34	134.5
PQMS3040	MAB216	No	130 000	2.6	0.35	135.3
PQMS3040	MAB330	Yes	175 000	2.4	0.23	134.7

The particle size distribution (PSD) of the polymer samples obtained by pre-contacting the supported catalyst with TIBA is not possible because of the film and agglomerates like morphology whereas the PSD of the HDPE samples obtained by MSP-2 method is compared in **Figure 15**. It can be noticed that both the HDPE samples replicate the respective support morphologies, and the amount of fines present in both the polymer samples is very similar. The PSD curve of the polymer sample produced with PQMS3040 silica supported catalyst is broader than that of the HDPE sample produced with Grace 948 based catalyst, despite the fact that PQMS3040 based catalyst has lower activity than the one supported on Grace 948 silica. This observation is in agreement with the bulk density values shown in **Table 4** for the respective HDPE samples which shows higher bulk density for the HDPE sample produced from Grace 948 based catalyst. Therefore, it can be suggested that the HDPE particles produced from Grace 948 based catalyst are more compact and dense than those prepared from PQMS3040 based silica.

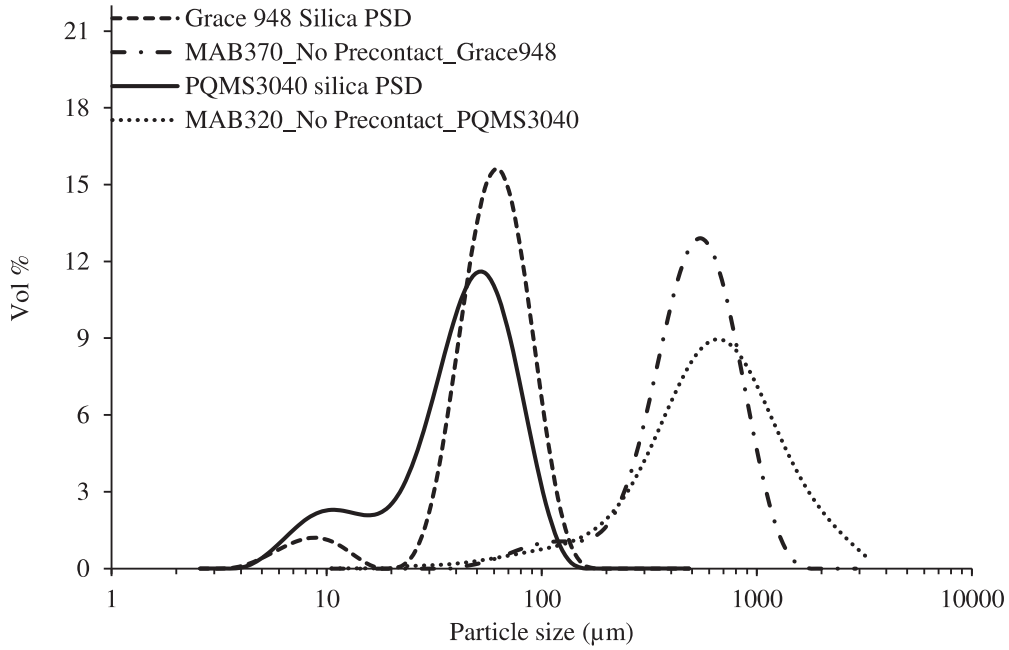

Figure 15. PSD of HDPE samples produced by MSP-2. Grace 948 indicates that the catalyst support used was silica Grace 948 and PQMS 3040 shows that the silica used for this support was PQMS3040.

The effect of increasing TIBA concentration on the reaction kinetics of Grace 948 supported (n-BuCp)$_2$ZrCl$_2$/MAO catalyst is shown in **Figure 16**. In agreement with the observations made in the previous TEA section, increasing concentration of TIBA inside reactor decreases the instantaneous polymerization rate and productivity of silica supported (n-BuCp)$_2$ZrCl$_2$/MAO catalyst which can be attributed to the formation of dormant and stable heterobimetallic species $[L_2M(\mu\text{-}R)_2AlR_2]^+$ due to the contact between supported (n-BuCp)$_2$ZrCl$_2$/MAO catalyst and TIBA. If one compares the effect of increasing aluminum alkyl concentration from 2 to 12 mmole per liter of reactor diluent, it can be noticed that there is 36% reduction in the productivity of the catalyst when TEA was used as a scavenger whereas this loss in productivity is 29% in case of TIBA (productivity comparison not shown here) which can be attributed the difference in the stability of heterobimetallic species $[L_2M(\mu\text{-}R)_2AlR_2]^+$ generated by the contact between the supported metallocene and respective aluminum alkyl (i.e., the bulkier the alkyl group of aluminum alkyl the lower is the stability of this heterobimetallic species and therefore, the lesser the impact of aluminum alkyl concentration on the catalytic activity of supported metallocene).

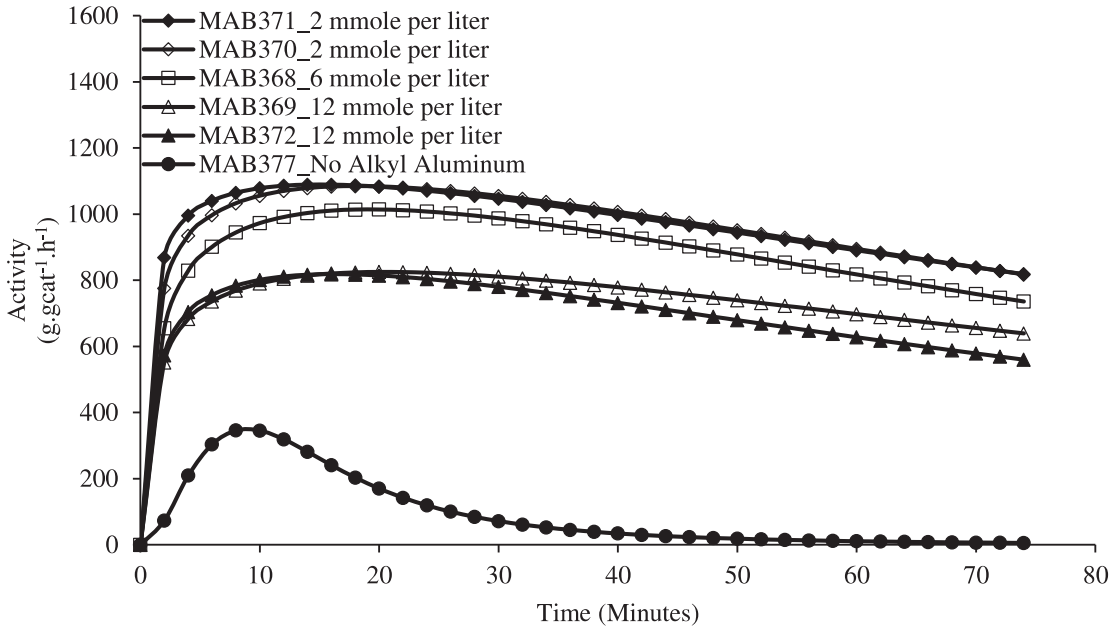

Figure 16. Effect of TIBA concentration inside reactor on the instantaneous activity of Grace 948 supported $(n\text{-BuCp})_2ZrCl_2$/MAO catalyst.

MWD curves of the HDPE samples produced by using different TIBA concentrations inside the reactor are shown in **Figure 17** which seem to be insensitive to TIBA concentration inside the reactor suggesting that no transfer to aluminum occurred and the same is also true for the melting temperature of the polymer samples presented in **Table 5**. Polydispersity indices for all of these HDPE samples remained in the range of 2.5 to 2.8 which indicates that the single site nature of the metallocene is not strongly influenced by the TIBA content inside the slurry phase reactor.

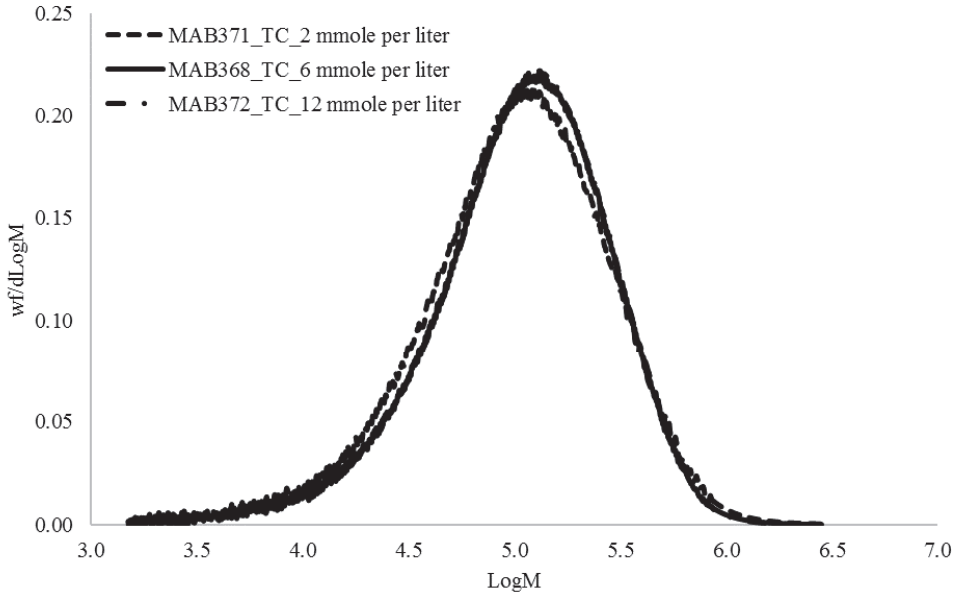

Figure 17. Effect of reactor concentration of TIBA on MWD of HDPE produced by using Grace 948 based $(n\text{-}BuCp)_2ZrCl_2$/MAO catalyst.

Table 5. Weight average molar mass (M_w), polydispersity index (Đ) and melting temperature (T_m) of HDPE samples produced by changing TIBA concentration in reactor diluent. C_{TIBA} indicates TIBA concentration.

Sample Name	C_{TIBA} (mmole. L^{-1})	Mw (g. $mole^{-1}$)	PDI	Tm (°C)
MAB371	2	156 000	2.8	135.3
MAB368	6	157 000	2.8	135.8
MAB372	12	158 000	2.7	135.8

The effect of varying TIBA concentration inside reactor on the PSD and concentration of fines in the obtained HDPE samples is shown in **Figure 18**. In all the polymerizations, support shape replication by the polymer particles is evident. In line with observations made for increasing TEA content inside the reactor, increasing TIBA concentration also causes an increase in the volume fraction of fine particles generated during polymerization using same silica support and reaction conditions e.g., the volume fraction of 104 µm diameter particles increase from 1.02 % to 2.14 % which corresponds to 52 % rise in their concentration when the TIBA content inside reactor is increased from 2 to 12 mmole per liter of the reactor diluent. Further evidence for this is presented in **Figure S2(c, d)** of the Appendix where one can see fine particles in the full batch of HDPE

sample produced at 12 mmole.L^{-1} TIBA concentration. This observation, once again, suggests that the small catalyst particles are probably more influenced by the higher TIBA concentration whose diffusion in such particles should be easier as compared to that in the bigger ones. Higher fractions of fines appear to be correlated with higher values of the polymer bulk density (see the inset **Figure 18**) which is also in agreement with the observation made in the previous section of TEA. The span of the PSD curves is also shown in **Figure 18** which increases systematically with increasing TIBA concentration inside reactor and clearly indicates the broadening of the PSD curve with increasing TIBA content in slurry reactor. Furthermore, the bulk density of the HDPE samples produced with TIBA is lower than that of the samples produced with TEA which can be attributed to higher catalytic activities observed in when TIBA was used a scavenger.

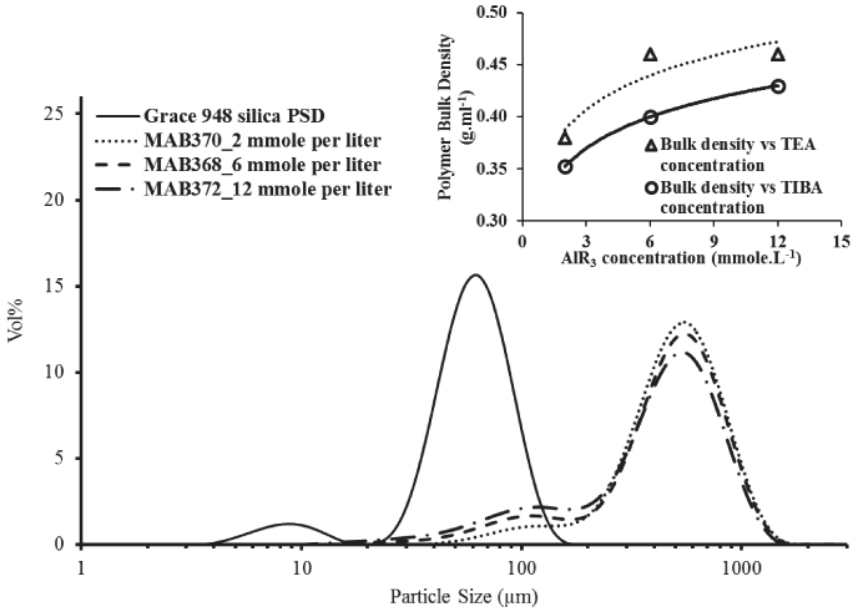

Figure 18. Effect of TIBA concentration inside reactor on PSD and bulk density of HDPE produced. Span for MAB370 = 1.30, span for MAB368 = 1.50 and span for MAB372 = 1.60. Bulk density values are average values of minimum two measurements per sample and in case of multiple samples they represent the average of those samples also.

3.3. Effect of TOA concentration on the activity of supported catalyst

Since it has been established in the previous sections that pre-contacting the supported catalyst with aluminum alkyls will lead to reactor fouling due to catalyst leaching and it is better to avoid any pre-contact between the two species, for this reason the impact of trioctyl aluminum (TOA) on the catalytic activity was studied only by MSP-2 i.e., by avoiding any pre-contact between the aluminum alkyl and the supported catalyst. In contrast to the observations made for the effect of TEA and TIBA reactor concentration on the kinetic profiles of silica-supported (n-$BuCp)_2ZrCl_2$/MAO catalyst, the instantaneous activity of the catalyst increased slightly by increasing TOA concentration inside reactor as shown in **Figure 19**. Rates of polymerization are on a par with those seen with equivalent quantities of TIBA, and higher than those observed with TEA. It is also important to mention here that no reactor fouling was observed in these reactions (see **Figure S2e** of the Appendix). This observation can be attributed to the bulkier structure of TOA as compared to TEA and TIBA which probably reduces the diffusivity of TOA and also the stability of the heterobimetallic species $[L_2M(\mu\text{-}R)_2AlR_2]^+$ formed by the interaction of TOA with supported catalyst is less than that formed by the interaction of smaller aluminum alkyls with the same supported catalyst.[31] The concentration of TOA in the reactor diluent does not affect the MWD and melting temperature of the HDPE as shown in **Table 6**.

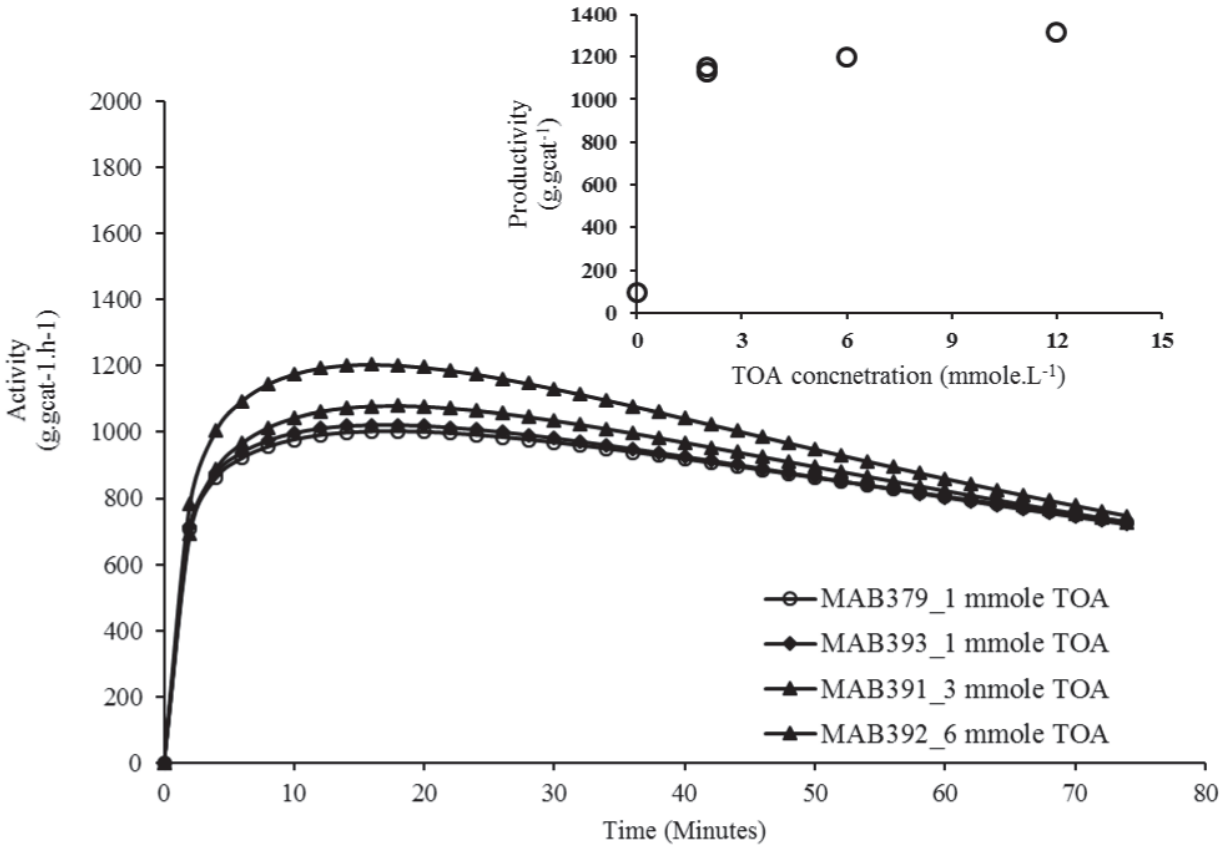

Figure 19. Effect of TOA concentration inside reactor on the instantaneous activity of silica supported (n-BuCp)$_2$ZrCl$_2$/MAO catalyst. Productivity calculated based on polymer powder recovered at the end of each 1 h 15 min reaction.

Table 6. Weight average molar mass (M_w), polydispersity index (Đ) and melting temperature (T_m) of HDPE samples produced by changing TOA concentration in reactor diluent. C_{TOA} indicates the concentration of TOA used.

Sample Name	C_{TOA} (mmole.L^{-1})	Mw (g.mole^{-1})	PDI	Tm (°C)
MAB379	2	140 000	2.2	135.2
MAB393	2	141 000	2.4	134.8
MAB391	6	140 000	2.4	135.8
MAB392	12	160 000	2.5	136.1

PSD and bulk density of the HDPE samples produced by varying TOA concentration inside reactor is shown in **Figure 20**. Due to similar instantaneous reaction rate the effect of TOA concentration on the polymer PSD and, especially, on the concentration of fines is not considerable. However,

there is a small increment in the concentration of fines with increasing TOA concentration as indicated by the span values also which is in agreement with the observations made when TEA and TIBA were used as scavengers. Bulk density of the polymer samples increases with increase in TOA concentration and attains similar values as in the case of TIBA but lower than those in the case of TEA (see inset of **Figure 20**) which can be attributed to higher polymerization rates in case of TOA then in the case of TEA.

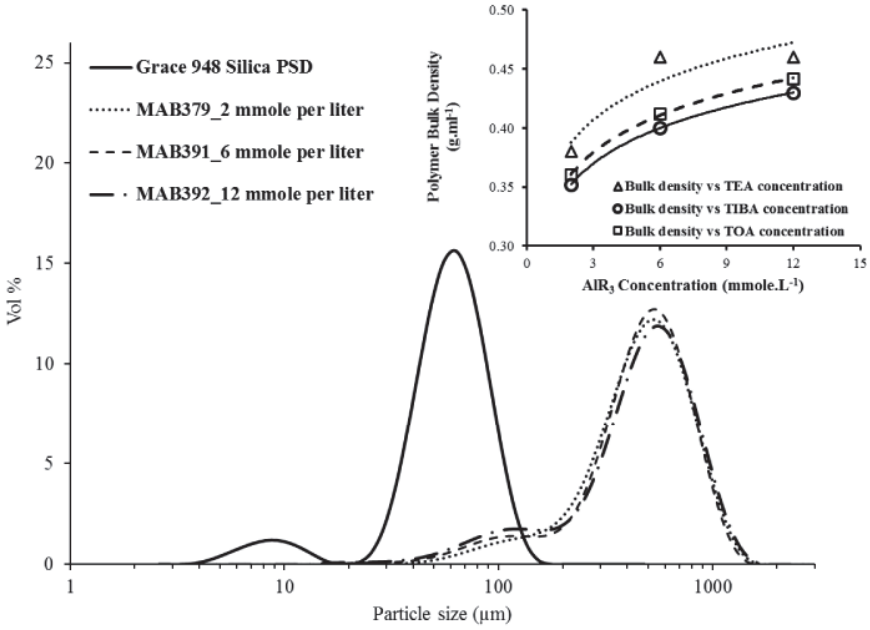

Figure 20. Effect of TOA concentration inside reactor on PSD and bulk density of HDPE produced. Span for MAB379 = 1.34, span for MAB391 = 1.43 and span for MAB392 = 1.52. Bulk density values are average values of minimum two measurements per sample and in case of multiple samples they represent the average of those samples also.

3.4. Comparison of the effect of different aluminum alkyls on the reaction kinetics of silica supported (n-BuCp)$_2$ZrCl$_2$/MAO catalyst and the polymer PSD

At this point it is of interest to compare the effect of the nature and concentration of different common aluminum alkyls used in this study on the reaction kinetics of silica supported (n-BuCp)$_2$ZrCl$_2$/MAO catalyst and the PSD of the produced polyethylene in slurry phase ethylene polymerization. Note that the MWD and melting temperatures of the HDPE samples were unaffected by the nature and concentration of aluminum alkyls and therefore, does not need to be

compared. **Figure 21** presents the polymerization rate profiles obtained by using different types and concentrations of aluminum alkyls, as well as comparative profiles showing the percentage difference between the instantaneous polymerization rates. It can be noticed that at concentrations higher than 2 mmole of aluminum alkyl per liter of the reactor diluent, highest instantaneous activity of Grace 948 silica supported $(n\text{-}BuCp)_2ZrCl_2$/MAO catalyst can be obtained by using TOA as a scavenger, whereas, at 2 mmole of aluminum alkyl per liter the highest instantaneous activity can be obtained by using TIBA.

However, with in the range of 2 to 6 mmole per liter of reactor diluent the difference between the instantaneous activities of TIBA and TOA scavenged polymerizations is approximately 10 % (see solid lines in **Figure 21b** and **Figure 21d**) which suggests that one can switch between these two scavengers without huge loss or gain in the polymerization activity of silica supported $(n\text{-}BuCp)_2ZrCl_2$/MAO catalyst and the polymer properties since scavenger concentration does not seem to affect any of the molecular properties of polyethylene. TEA, which is the smallest of the aluminum alkyls studied here, has the strongest negative impact on the rates (i.e. increasing the concentration of TEA leads to greater reductions in the reaction rate than equivalent increases of TIBA or TOA). In addition, the stability of the heterobimetallic species formed by the interaction of these aluminum alkyls with the activated metalloence/MAO system decreases with increase in the size of their alkyl ligand and explains why higher concentrations of TOA in the reaction medium of the slurry reactor does not reduce the catalytic activity of the studied metallocene/MAO system.

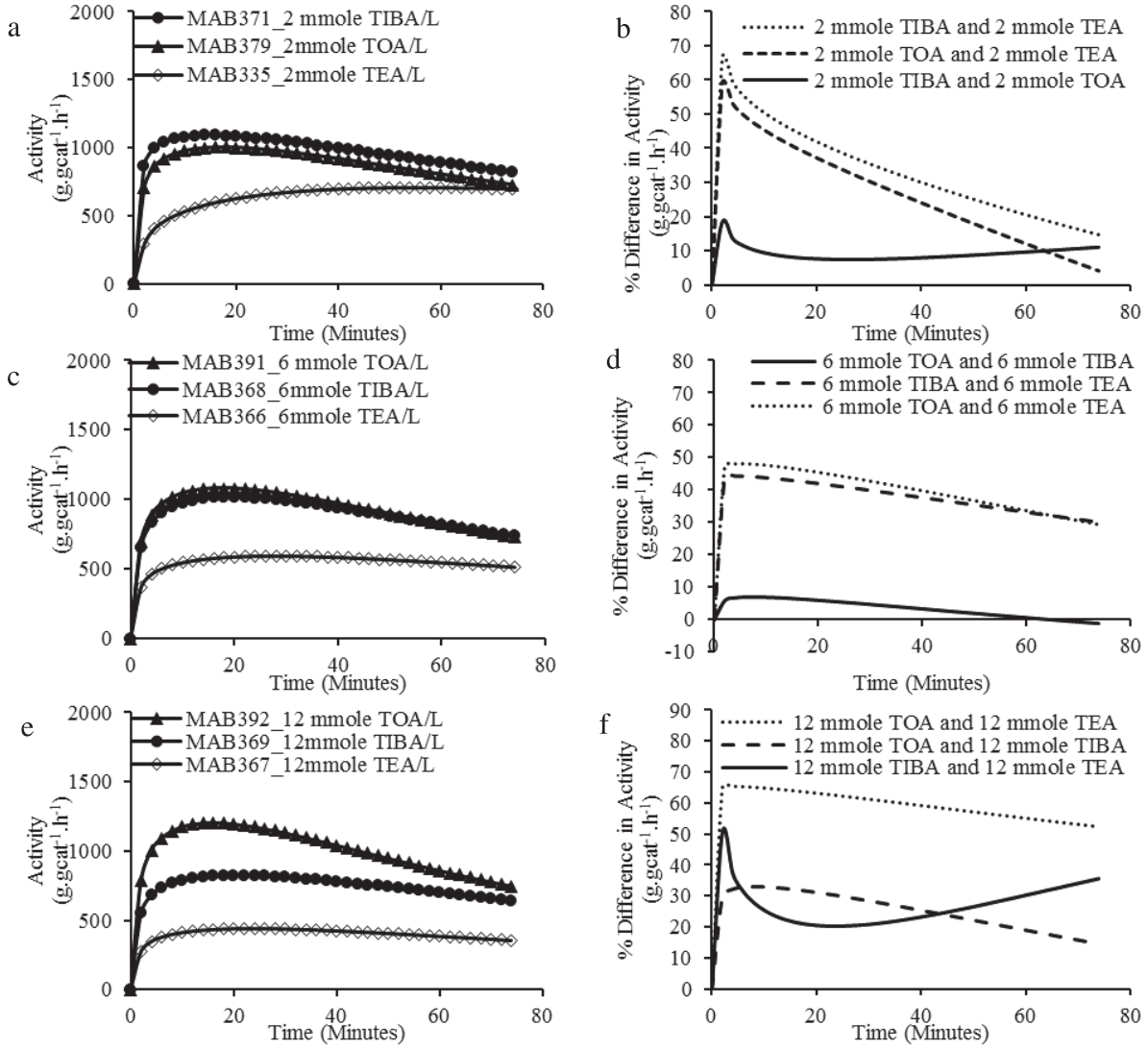

Figure 21. Comparison of the effect of different aluminum alkyls on the reaction kinetics of ethylene slurry phase homopolymerization using silica supported (n-BuCp)$_2$ZrCl$_2$/MAO catalyst. Activity profiles are shown in a, c & e whereas the relative differences in activities are shown in b, d & f.

The impact of the concentration of aluminum alkyl scavengers on the PSD of the obtained HDPE samples is compared in **Figure 22.** It can be seen from this figure that concentration of fine particles increases with increasing the concentration of each aluminum alkyl. In addition, it can also be noticed that the peak below 200 µm broadens towards smaller particle sizes with increasing concentrations of aluminum alkyls which causes broadening of the PSD span of the respective HDPE sample. On the other hand, catalytic activity decreased at higher concentrations of TEA and TIBA.

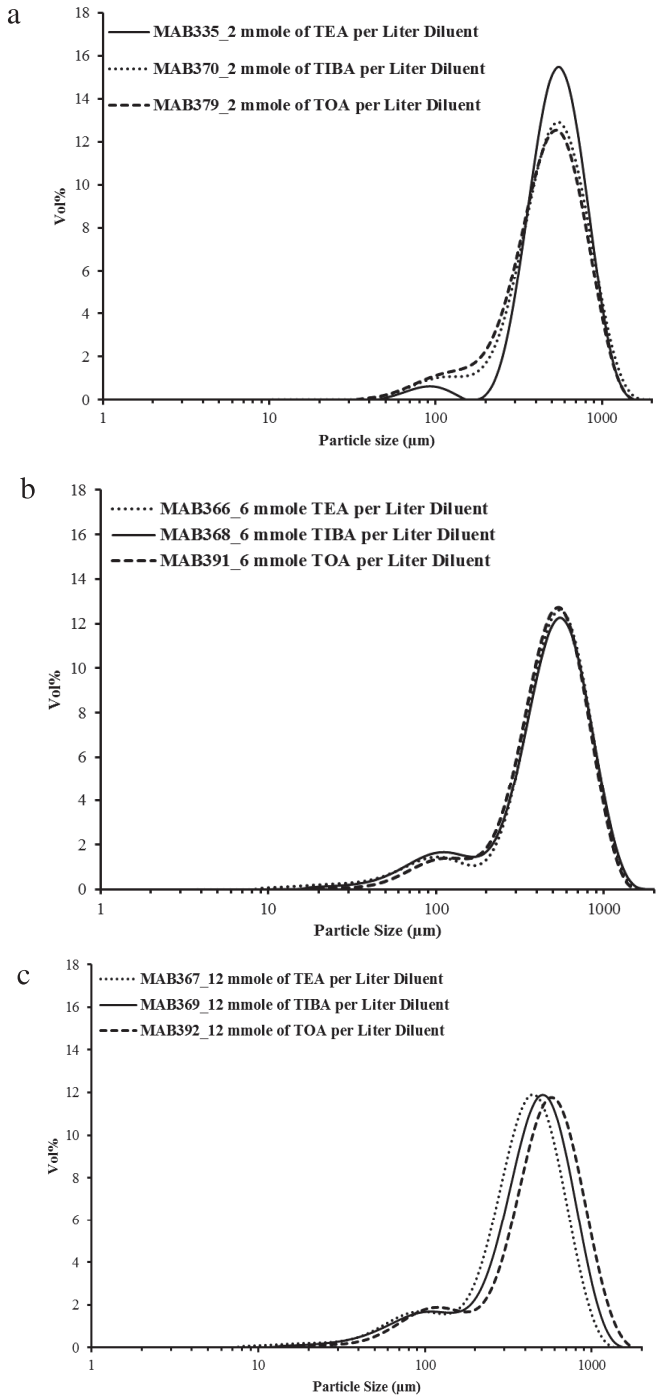

Figure 22. Comparison of the effect of different aluminum alkyls on the PSD of HDPE produced by slurry process using Grace 948 silica supported $(n\text{-BuCp})_2ZrCl_2$/MAO catalyst.

The most probable reason for this behavior is the higher diffusivity of smaller aluminum alkyls (i.e., TEA and TIBA) in heptane as well as inside the small catalyst particles as compared to that in bigger catalyst particles leading to i) reduction in the overall catalytic activity (since the smaller

catalyst particles in a given catalyst batch are more active than their bigger counterparts as we shall see in the coming chapters) as well as ii) an increase in the concentration of fine particles. The size of TOA molecule is relatively bigger than the molecular sizes of TEA and TIBA and therefore, its diffusion in heptane as well as inside the catalyst particles should be slower as compared to that of smaller aluminum alkyls leading to its similar effect on the concentration of fine particles but different effect on the overall catalytic activity which is further related to the low stability of heterobimetalic ion generated upon the interaction of TOA with the supported metallocene. Nevertheless, one can also argue that these fine particles are coming due to aluminum alkyl left unreacted in the reaction mixture and finally appears as alumina particles in the final PSD of the polymer. The shift of PSD curves shown in **Figure 22c** towards larger particle diameters is in agreement with the catalytic activity trend observed with the three aluminum alkyls at 12 mmole of each scavenger per liter of reactor diluent.

3.5. Impact of Butylated Hydroxytoluene (BHT-H) on the reaction kinetics of silica supported (n-BuCp)$_2$ZrCl$_2$/MAO catalyst

The effect of adding BHT-H into the reaction mixture was also studied by i) pre-contacting the aluminum alkyl (AlR_3) + BHT-H + heptane mixture with the supported catalyst and ii) by avoiding any pre-contact between the catalyst and AlR_3 + BHT-H + heptane mixture i.e., by injecting the catalyst into the reactor containing the AlR_3 + BHT-H + heptane mixture using an injection cartridge at the reaction temperature and pressure. The AlR_3 + BHT-H + heptane mixture was prepared by first adding the desired amount of AlR_3 to heptane under argon, and then adding the desired amount of BHT-H to that solution. A 1M stock solution of BHT-H in heptane was used in all reactions. Note that the temperature and pressure of these polymerizations were kept the same to the conditions used in the previous polymerizations. All reactions are of 1 h 15 minutes reaction time.

When TEA and TOA were used as aluminum alkyl, it was found that the impact of pre-contacting the silica supported catalyst with AlR_3 + BHT-H + heptane mixture on the reaction kinetics, reactor fouling and polyethylene morphology was very similar to that observed in the case when the supported catalyst was pre-contacted with the AlR_3 + heptane mixture discussed above. It can be seen in **Figure 23a** and **Figure 23c** (for TEA and TOA respectively) that reactor fouling, and poorly controlled morphologies were found for these systems (see also **Figure S2 (f, g)** of the Appendix). This suggests that both homogenous and heterogeneous modes of polymerization occurred in these

reactions as well. On the other hand, the presence of BHT-H in the TEA or TOA + heptane mixture increased the instantaneous activity of the catalyst with respect to the activity observed for the analogous reactions without BHT-H. The effect of BHT-H concentration on the reaction kinetics is also shown in **Figure 23a**, where it can be seen that equal concentrations of BHT-H and TEA lead to a kinetic profile which was similar in shape to that when BHT-H was not used, but also made the catalyst more active as compared to the reactions where only TEA was used as scavenger. When the concentration of BHT-H was more than two times the concentration of TEA, the catalytic activity was highest and showed similar shape as in the case of TIBA and TOA i.e., decay in the rate profile after reaching a maximum in the instantaneous activity. Similar rate profiles have also been observed by Reddy et al.,[27] who used isolated $AlMe(BHT)_2$ as a scavenger in Zirconocene catalyzed ethylene slurry polymerization. Note that $AlMe(BHT)_2$ is product of equimolar reaction between trimethyl aluminum (TMA) and BHT-H and we will discuss these reactions in the coming paragraphs.

Surprisingly, absolutely no reactor fouling occurred when TIBA + BHT-H + heptane mixture was pre-contacted with the silica supported $(n\text{-}BuCp)_2ZrCl_2$/MAO catalyst as shown by the polymer morphology (see **Figure 23b** and **Figure S2h** of the Appendix) and the absence of any polymer film formation around the reactor walls or stirrer (not shown here). The rate profiles in **Figure 23b** show that during the first 40 minutes of reaction time, pre-contacting the supported catalyst with TIBA + BHT-H + heptane mixture provided higher instantaneous activities (e.g., 32 % difference can be noted at 10 minutes of reaction time) than was observed in the reaction where only TIBA was used. Due to continuous decay after reaching the maximum catalytic activity, the instantaneous polymerization rates in the presence and absence of BHT-H become very similar after the first 40 minutes of reaction. Two replicate kinetic profiles shown in **Figure 23b** indicate that these reactions are reasonably well-reproducible.

It is rather well-known that aluminum alkyls react readily with simple phenols to give phenoxide compounds which are bridged through the oxygen atom, whereas, the reaction of the same aluminum alkyls with substituted or sterically hindered phenols such as BHT-H under similar conditions yields compounds of the type $AlR_2(BHT)$ and $AlR(BHT)_2$ (where R = ethyl or Butyl group), which are monomeric in nature. According to Ittel et al.,[24] the chemical reaction between 1 equivalent of TEA and 2 or more equivalents of BHT-H yields a mixture of TEA, $AlEt_2BHT$ and

$AlEtBHT_2$ which are in dynamic equilibrium, whereas, the same reaction between 1 equivalent of TIBA and 2 equivalents of BHT-H leads to complete consumption of TIBA and yields only the Al(i-Bu)BHT_2 species; i.e., there is no dynamic equilibrium between the TIBA and Al(i-Bu)BHT_2. $AlEtBHT_2$ was shown to be reactive with t-BuOH whereas no discussion was made about the reactivity of Al-R bond in Al(i-Bu)BHT_2. Later on it was shown by different authors[23,25-29] that $AlMeBHT_2$ (which is a product of the reaction of trimethyl aluminum (TMA) with BHT-H similar to the reaction of TEA with BHT-H) can be used as a 'non-interacting' scavenger or scrubbing agent for metallocene catalyzed olefin slurry polymerization due to its reactive nature (just like $AlEtBHT_2$) as discussed by Ittel et al.[24]

The results observed in our work where pre-contact between the silica supported catalyst and AlR_3 + BHT-H + heptane mixture lead to reactor fouling when TEA or TOA were used can be explained using the preceding concept. The presence of TEA + $AlEt_2BHT$ + $AlEtBHT_2$ (due to the reaction between TEA and BHT-H) mixture in heptane causes catalyst leaching from the support due to the interactions between TEA, $AlEt_2BHT$ and the supported (n-BuCp)$_2ZrCl_2$/MAO catalyst which consequently leads to reactor fouling. The same explanation can be considered valid for the system involving TOA as reactor fouling was observed in that case also. On the other hand, the reaction of TIBA with BHT-H leads to complete transformation of TIBA into Al(i-Bu)BHT_2, and since no fouling was observed in the reactions when the catalyst was pre-contacted with the TIBA + BHT-H + heptane mixture (see **Figure 23b**) it is reasonable to assume that Al(i-Bu)BHT_2 does not interact with the supported metallocene and therefore no catalyst leaching occurs. Furthermore, the fast decay of the catalytic activity shown in **Figure 23b** as compared to the decay in the kinetic profiles shown in **Figure 23a** and **Figure 23c** clearly suggests that the substituted aluminum alkyls formed after the reactions of TEA and TOA with BHT-H are more reactive with the impurities inside the reactor as compared to Al(i-Bu)BHT_2. These results clearly indicate that only Al(i-Bu)BHT_2 can be used as a 'non-interacting' scavenger for supported metallocenes whereas other similar species generated by the reaction of TEA or TOA with BHT-H generate species which interact with the supported metallocene and lead to catalyst leaching from the silica support.

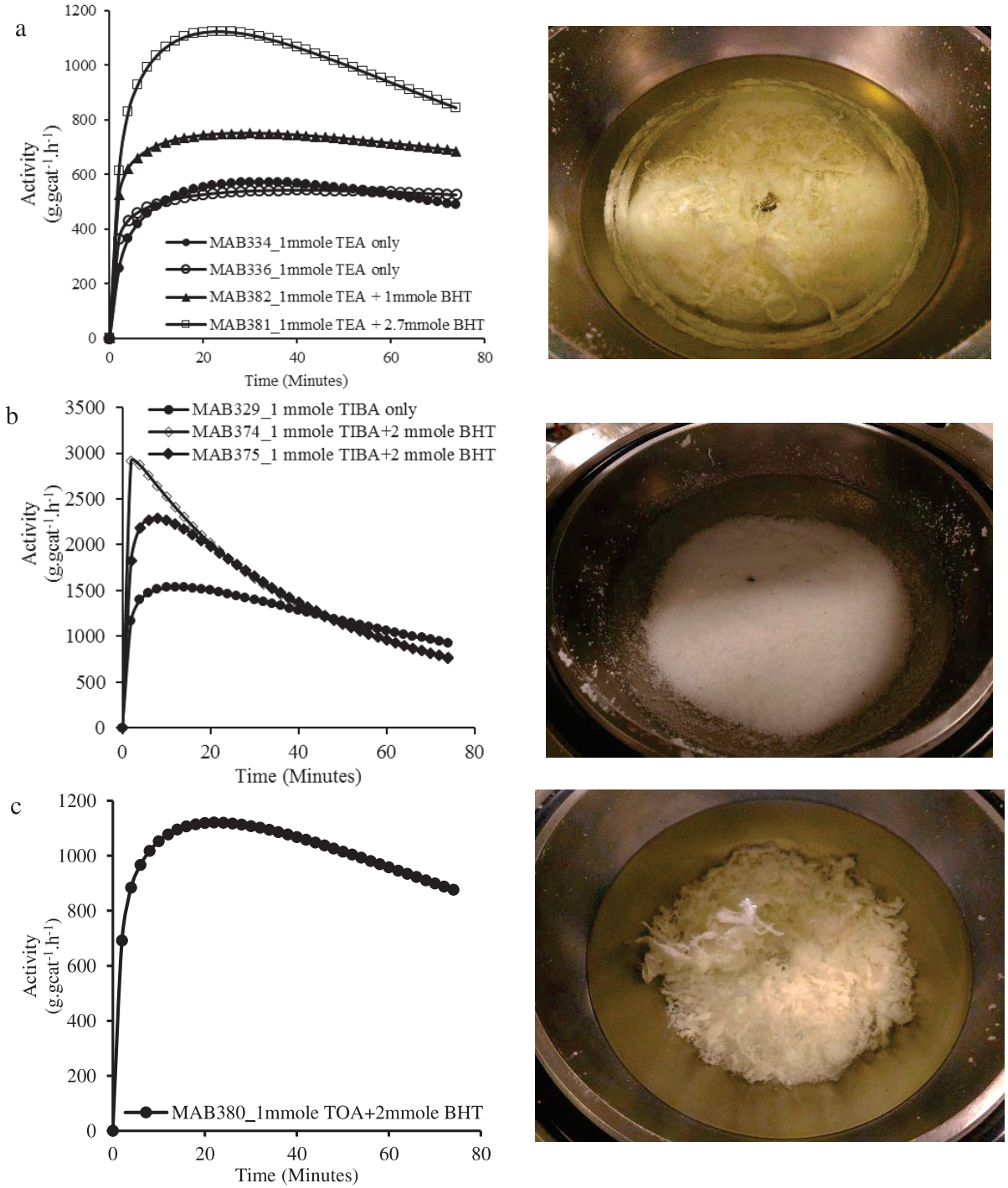

Figure 23. Effect of pre-contacting the aluminum alkyl + BHT-H + heptane mixture with the silica supported $(n\text{-BuCp})_2ZrCl_2$/MAO catalyst on reaction kinetics of slurry phase ethylene homopolymerization, reactor fouling and polyethylene morphology.

Ethylene homopolymerizations were also conducted by avoiding any pre-contact between the silica supported $(n\text{-BuCp})_2ZrCl_2$/MAO and AlR_3 + BHT-H + heptane mixture i.e., by using MSP-2. The rate profiles of ethylene homopolymerization in slurry phase obtained with and without BHT-H in the AlR_3 + heptane mixture using MSP-2 are shown in **Figure 24**. The trend of instantaneous activity is TIBA > TOA > TEA when no BHT-H was used. However, adding BHT-H led to similar rate profiles for all three aluminum alkyl. Note that absolutely no reactor fouling occurred in these reactions, indicating that purely heterogeneous catalysis occurred and confirming once again that avoiding any pre-contact between the supported catalyst and scavenger prohibits catalyst leaching from the support. Similarity in the kinetic profiles after the addition of BHT-H to AlR_3 + heptane mixtures can be attributed to the similar species formed after the reaction between the used AlR_3 and BHT-H as discussed in the previous paragraph. However, more deactivation in the reactions conducted by using TIBA + BHT-H in comparison to the reactions where TEA or TOA + BHT-H were used can be attributed to the complete consumption of TIBA by BHT-H whereas in case of other aluminum alkyls a dynamic equilibrium exists between the AlR_3, AlR_2BHT and $AlRBHT_2$ species (with R = Ethyl or Octyl) which probably allows for better scavenging of the impurities and, more importantly, alkylation of the supported zirconocene since the common aluminum alkyls are known to re-activate the deactivated sites by alkylating them. These results clearly indicate that the lower the amount of AlR_3 in the diluent, the faster the catalyst activation is and the higher the instantaneous polymerization and catalyst deactivation rates.

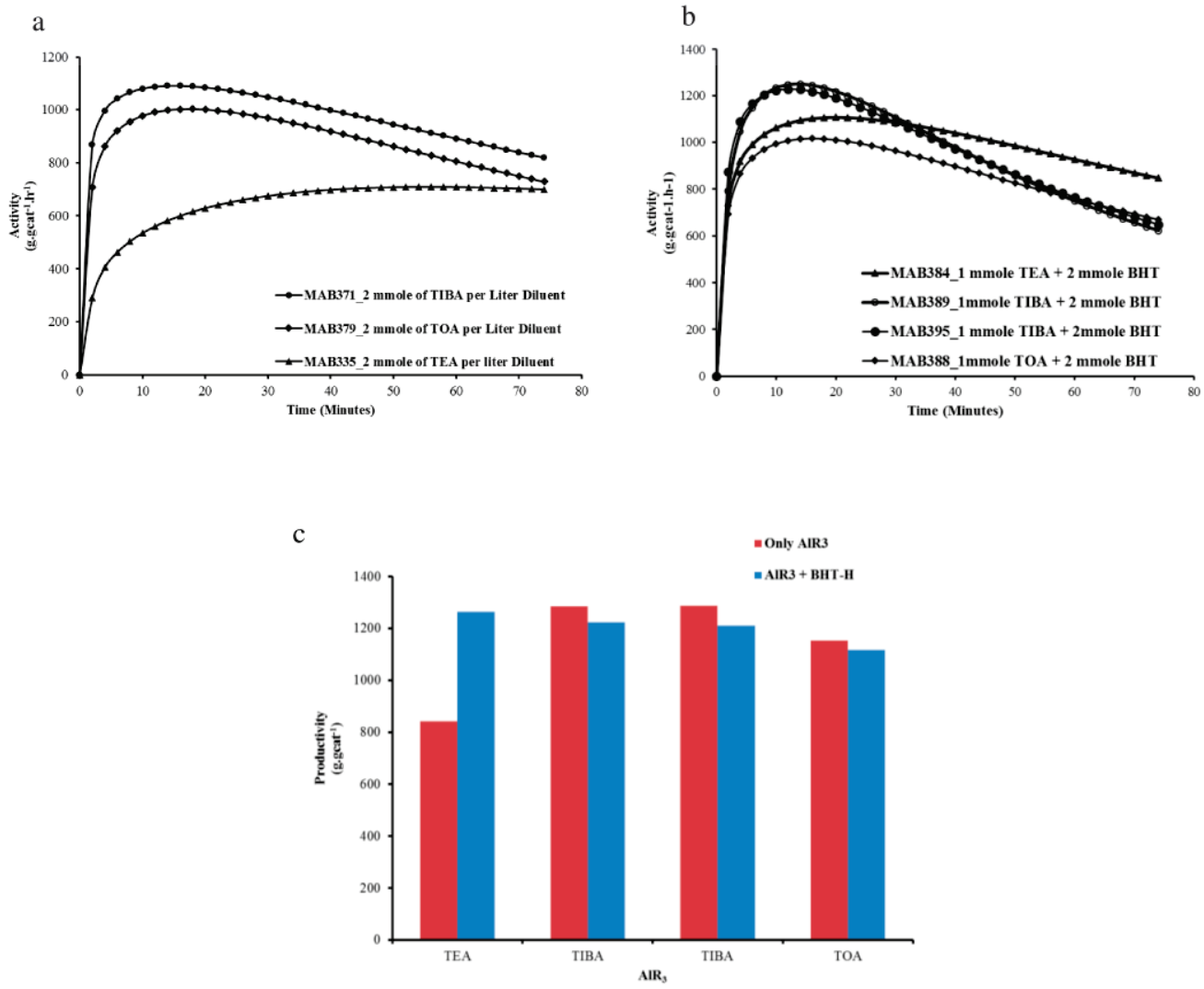

Figure 24. Comparison of the kinetic profiles obtained without using BHT-H (a) and with BHT-H heptane (b). Polymerization method used is MSP-2 i.e., no pre-contact between the supported catalyst and AlR_3 + heptane or AlR_3 + BHT-H + heptane mixture. Productivity of the supported catalyst with and without BHT-H is shown in c.

A comparison of the catalyst productivity (calculated from the polymer recovered at the reaction end) with and without BHT-H is also shown in **Figure 24c** which indicates that the addition of BHT-H is most effective when TEA is present in the reactor diluent giving approximately 35% rise in the catalyst productivity (for exactly equal polymerization time of 1 hour 15 minutes) which is non-trivial as compared to the other cases. Also, it can be seen that the catalyst productivity is almost independent of the aluminum alkyl used if BHT-H is added in the reactor diluent which can

be attributed to the formation of similar species due to the chemical reaction between the aluminum alkyl and BHT-H. MWD and melting temperatures of the HDPE samples do not seem to be changed when BHT-H is added along with the aluminum alkyls, as shown in **Figure 25** and **Table 7**.

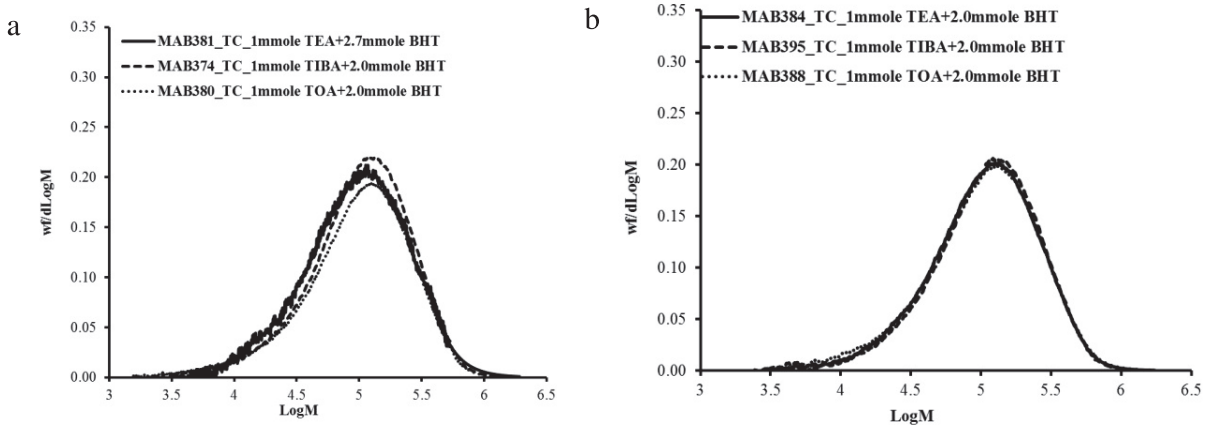

Figure 25. Effect of BHT-H and polymerization protocol on the MWD of HDPE produced in slurry phase polymerizations. Pre-contact between the supported catalyst and AlR_3+BHT-H+Heptane mixture (a) and no pre-contact between the supported catalyst and AlR_3+BHT-H+Heptane mixture (b).

Table 7. Weight average molar mass (M_w), polydispersity index (Đ) and melting temperature (T_m) of HDPE samples produced by using BHT-H the in reactor diluent as scavenger. C_{AlR3} indicates concentration of the aluminum alkyl used.

Sample Name	AlR_3 used	C_{AlR3} (mmole/500ml Heptane)	Pre-contact	Reactor fouling	Mw ($g.mole^{-1}$)	Đ	T_m (°C)
MAB381	TEA	2.7	Yes	Yes	145 000	2.2	136.5
MAB382	TEA	1.0	Yes	Yes	165 000	2.2	-
MAB374	TIBA	2.0	Yes	No	148 000	2.5	134.5
MAB375	TIBA	2.0	Yes	No	142 000	2.1	135.2
MAB380	TOA	2.0	Yes	Yes	144 000	2.8	136.2
MAB384	TEA	2.0	No	No	148 000	2.3	135.2
MAB389	TIBA	2.0	No	No	164 000	2.3	135.8
MAB395	TIBA	2.0	No	No	150 000	2.3	135.7
MAB388	TOA	2.0	No	No	150 000	2.4	135.8

The effect of the use of BHT-H in the reactor diluent on the polymer PSD is shown in **Figure 26** where it can be noticed that for TIBA or TOA + BHT-H systems the polymer PSD is more or less

the same to that case when only the respective AlR_3 was used which can be attributed to similarity in the catalytic activities and productivities. Good reproducibility of the experiments is also evident in **Figure 26c**. In case of TEA + BHT-H system (**Figure 26a**), there is a clear rise in the volume fraction of 200 µm particles and a shift of polymer PSD towards bigger particle size which is also attributable to the gain in catalytic productivity by using BHT-H than by using only the pure TEA.

The effect of pre-contact between the supported catalyst and TIBA + BHT-H + heptane mixture on the polymer PSD is compared with the case where there was no pre-contact between the two (i.e., the supported catalyst and TIBA + BHT-H + heptane mixture) is shown in **Figure 26c**. The noticeable differences between the PSD curves are that in case of pre-contact there is no distinct peak of particles below 200 microns and the presence of a small volume fraction of particles bigger than 1500 microns whereas in the case of no pre-contact a distinct peak representing particles below 200 microns is always present. Once again these differences can be attributed to the differences in catalytic productivity which was about 2000 $g.gcat^{-1}$ in the pre-contact case and about 1300 $g.gcat^{-1}$ without pre-contacting which corresponds to 35 % difference. **Figure 26d** shows that the amount of fine polymer particles generated by adding BHT-H into TIBA containing heptane is equivalent to the amount of fines generated when pure TIBA concentration in the reactor diluent was 6 mmole per liter because of the similar catalytic activities obtained in the two cases.

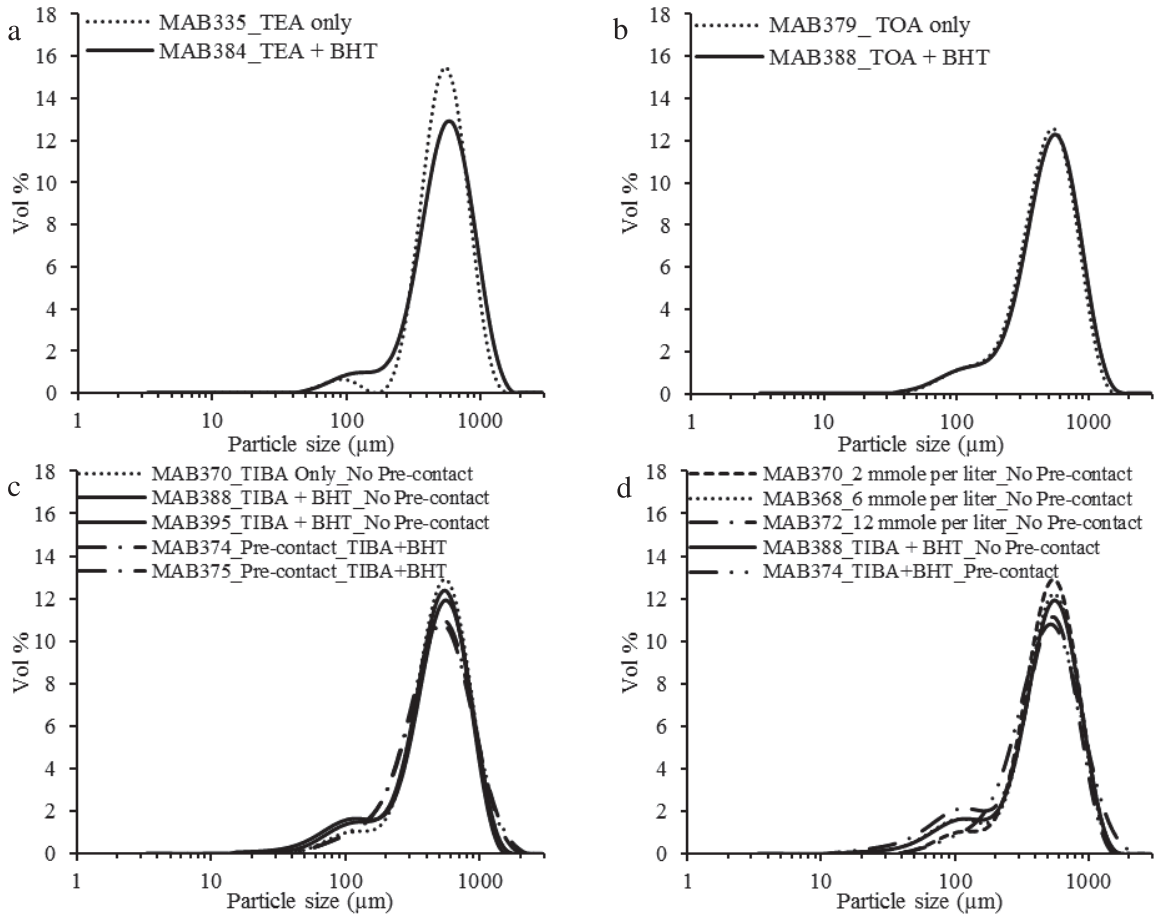

Figure 26. Comparison of polymer PSD with and without BHT-H in the reactor diluent containing the AlR_3.

4. Conclusion

In ethylene polymerization via silica supported metallocene/MAO complex the used polymerization protocol can significantly affect the kinetic profile of the reaction, morphology of the polyethylene produced and reactor fouling. The results obtained in this section clearly demonstrate that catalyst leaching will happen if an aluminum alkyl (e.g., TEA, TIBA or TOA) is pre-contacted with the silica supported metallocene consequently leading to poor morphology of the polymer and reactor fouling due to homogeneous polymerization occurring parallel to heterogeneous reaction. On the other hand, one can get rid of these problems in slurry phase ethylene polymerizations by avoiding any pre-contact between the silica supported metallocene/MAO complex and the used aluminum alkyl scavenger. Kinetic profiles of silica supported $(n\text{-BuCp})_2ZrCl_2$/MAO complex are also altered by the polymerization protocol in such a way that: i) when TEA is pre-contacted with the catalyst there is a reduction in the instantaneous reaction rate (and productivity) as compared to that when there is no pre-contact between the catalyst and TEA and ii) when TIBA is pre-contacted with the catalyst there is an increment in the instantaneous reaction rate (and productivity) as compared to that when there is no pre-contact between the catalyst and TIBA.

Both of these effects of pre-contacting the silica supported $(n\text{-BuCp})_2ZrCl_2$/MAO with aluminum alkyls are explainable based on the stability of the heterobimetallic species $[L_2M(\mu\text{-}R)_2AlR_2]^+$ formed and the impact of the aluminum alkyl on the structure of MAO i.e., increased activities in the case of pre-contacting silica supported $(n\text{-BuCp})_2ZrCl_2$/MAO with TIBA are attributable to the fact that the heterobimetallic species $[L_2M(\mu\text{-}R)_2AlR_2]^+$ formed is less stable than that formed by the presence of TEA as well as to the fact that interaction of TIBA with MAO converts it into modified MAO (MMAO) which is known to be more soluble in aliphatic hydrocarbons and more active than MAO in ethylene polymerizations. PSD of HDPE samples produced with MSP-2 protocol showed that with increasing aluminum alkyl content in the reactor the concentration of fine particles increases. This observation is probably due to the fact that diffusivity of aluminum alkyls in smaller catalyst particles is higher than in the bigger ones which reduces the activity of smaller catalyst particles and therefore, the concentration of fine particles increase in the final polyethylene batch.

When BHT-H is added into the reactor diluent containing one of the aluminum alkyls used in this work, it's only TIBA which is completely consumed by the reaction with BHT-H so that the resulting species do not interact with the silica supported $(n\text{-BuCp})_2ZrCl_2$/MAO catalyst leading to no catalyst leaching and, consequently, no reactor fouling independent of the polymerization protocols used in this work. On the other hand, such a complete consumption of TIBA by the BHT-H causes rapid catalyst deactivation during ethylene homopolymerization while partial consumption of TEA and TOA by BHT-H reduces the catalyst deactivation and provides catalytic activities with MSP-2 protocol similar to those obtained by using TIBA as scavenger.

Finally, the results obtained in this section clearly suggest that if ethylene polymerization is following both the homogeneous and heterogeneous paths than one cannot study the impact of physical properties of the silica support on the reaction kinetics and morphology of polyethylene as we shall see in the next chapter.

5. References

1. Casas, E, van Grieken, R, Escola, J M, Polymerization of ethylene with (nBuCp)2ZrCl2 supported over mesoporous SBA-15 functionalized with sulfonic acid groups, Applied Catalysis A: General., **2012**, 437-438, 44-52.

2. Jungling, S, Koltzenburg, S, Mulhaupt, R, Propene homo- and copolymerization using homogeneous and supported metallocene catalysts based on Me2Si(2-Me-Benz[e]Ind)2ZrCl2, J. Polym. Sci. A Polym. Chem., **1997**, 35, 1-8.

3. Kaminsky, W, Külper, K, Niedoba, S, Olefin polymerization with highly active soluble zirconium compounds using aluminoxane as co-catalyst, Makromolekulare Chemie. Macromolecular Symposia., **1986**, 3, 377-387.

4. Sperber, O, Kaminsky, W, Synthesis of Long-Chain Branched Comp-Structured Polyethylene from Ethylene by Tandem Action of Two Single-Site Catalysts, Macromolecules., **2003**, 36, 9014-9019.

5. Ostoja Starzewski, K A, Xin, B S, Steinhauser, N, Schweer, J, Benet-Buchholz, J, Donor–Acceptor Metallocene Catalysts for the Production of UHMW-PE: Pushing the Selectivity for Chain Growth to Its Limits, Angewandte Chemie International Edition., **2006**, 45, 1799-1803.

6. Baier, M C, Zuideveld, M A, Mecking, S, Post-Metallocenes in the Industrial Production of Polyolefins, Angew. Chem. Int. Ed., **2014**, 53, 9722-9744.

7. Turunen, J P J, Pakkanen, T T, Suppression of metallocene catalyst leaching by the removal of free trimethylaluminum from methylaluminoxane, J. Appl. Polym. Sci., **2006**, 100, 4632-4635.

8. Severn, J R, Chadwick, J C, Duchateau, R, Friederichs, N, "Bound but Not Gagged" Immobilizing Single-Site α-Olefin Polymerization Catalysts, Chem. Rev., **2005**, 105, 4073-4147.

9. Choi, Y, Soares, J B P, Supported single-site catalysts for slurry and gas-phase olefin polymerisation, Can. J. Chem. Eng., **2012**, 90, 646-671.

10. Kaminsky, W, Strübel, C, Hydrogen transfer reactions of supported metallocene catalysts, Journal of Molecular Catalysis A: Chemical., **1998**, 128, 191-200.

11. Panchenko, V N, Echevkaya, L G, Zakharov, V A, Matsko, M A, Influence of triisobutylaluminum on the polymerization of ethylene by SiO2-supported ansa-zirconocene catalysts, Applied Catalysis A: General., **2011**, 404, 47-53.

12. Kristen, M, Supported metallocene catalysts with MAO and boron activators, Topics in Catalysis., **1999**, 7, 89-95.

13. Suzuki, N, Asami, H, Nakamura, T, Huhn, T, Fukuoka, A, Ichikawa, M, Saburi, M, Wakatsuki, Y, Immobilization of a C_2-Symmetric ansa-Zirconocene Complex on Silica Surfaces Using a Si-Cl Anchor: Catalysts for Isospecific Propene Polymerization, Chemistry Letters., **1999**, 28, 341-342.

14. Uusitalo, A M, Pakkanen, T T, Iskola, E I, Immobilization of metal chloride complexes of titanium, zirconium, and hafnium on a cyclopentadienyl surface of silica for ethylene polymerization, Journal of Molecular Catalysis A: Chemical., **2002**, 177, 179-194.

15. Soga, K, Kim, H J, Shiono, T, Highly isospecific SiO2-supported zirconocene catalyst activated by ordinary alkylaluminiums, Macromol. Rapid Commun., **1994**, 15, 139-143.

16. Soga, K, Kim, H J, Shiono, T, Polymerization of propene with highly isospecific. SiO2-supported zirconocene catalysts activated with common alkylaluminiums, Macromol. Chem. Phys., **1994**, 195, 3347-3360.

17. Sacchi, M C, Zucchi, D, Tritto, I, Locatelli, P, Dall'Occo, T, Silica-supported metallocenes: stereochemical comparison between homogeneous and heterogeneous catalysis, Macromol. Rapid Commun., **1995**, 16, 581-590.

18. Semikolenova, N V, Zakharov, V A, On the interaction of supported zirconocene catalysts with alkylaluminium co-catalysts, Macromol. Chem. Phys., **1997**, 198, 2889-2897.

19. E.Ernst, J R P D., The Impact of the Cocatalyst on the Polymerisation Behaviour of Supported Metallocenes, In Metalorganic Catalysts for Synthesis and Polymerization, Eds. K. Walter., Springer Berlin Heidelberg, **1999**.

20. Mole, T, Organoaluminium compounds. X. Formation of dimethylaluminium alkoxides and phenoxides, Aust. J. Chem., **1966**, 19, 373-379.

21. Skowronska-Ptasinska, M, Starowieyski, K B, Pasynkiewicz, S, Carewska, M, Phenoxyaluminium compounds : VII. Reactions of organoaluminium compounds with hindered phenols, Journal of Organometallic Chemistry., **1978**, 160, 403-409.

22. Starowieyski, K B, Pasynkiewicz, S, Skowroñska-Ptasiñska, M, Phenoxyaluminium compounds IV. syntheses and structures of monomeric (2,6-DI-t-Butyl-4-methylphenoxy)aluminium compounds, Journal of Organometallic Chemistry., **1975**, 90, C43-C44.

23. Healy, M D, Wierda, D A, Barron, A R, Sterically crowded aryloxide compounds of aluminum, Organometallics., **1988**, 7, 2543-2548.

24. Shreve, A P, Mulhaupt, R, Fultz, W, Calabrese, J, Robbins, W, Ittel, S D, Sterically hindered aryloxide-substituted alkylaluminum compounds, Organometallics., **1988**, 7, 409-416.

25. Vollmerhaus, R, Rahim, M, Tomaszewski, R, Xin, S, Taylor, N J, Collins, S, Ethylene Polymerization Using β-Diketimine Complexes of Zirconium, Organometallics., **2000**, 19, 2161-2169.

26. Williams, V C, Dai, C, Li, Z, Collins, S, Piers, W E, Clegg, W, Elsegood, M R J, Marder, T B, Activation of [Cp2ZrMe2] with New Perfluoroaryl Diboranes: Solution Chemistry and Ethylene Polymerization Behavior in the Presence of MeAl(BHT)2, Angewandte Chemie International Edition., **1999**, 38, 3695-3698.

27. Reddy, S S, Shashidhar, G, Sivaram, S, Role of trimethylaluminum on the zirconocene-methylaluminoxane-catalyzed polymerization of ethylene, Macromolecules., **1993**, 26, 1180-1182.

28. Williams, V C, Irvine, G J, Piers, W E, Li, Z, Collins, S, Clegg, W, Elsegood, M R J, Marder, T B, Novel Trityl Activators with New Weakly Coordinating Anions Derived from C6F4-1,2-[B(C6F5)2]2: Synthesis, Structures, and Olefin Polymerization Behavior, Organometallics., **2000**, 19, 1619-1621.

29. Busico, V, Cipullo, R, Pellecchia, R, Talarico, G, Razavi, A, Hafnocenes and MAO: Beware of Trimethylaluminum!, Macromolecules., **2009**, 42, 1789-1791.

30. Hlatky, G G, Heterogeneous Single-Site Catalysts for Olefin Polymerization, Chem. Rev., **2000**, 100, 1347-1376.

31. Kleinschmidt, R, van der Leek, Y, Reffke, M, Fink, G, Kinetics and mechanistic insight into propylene polymerization with different metallocenes and various aluminium alkyls as cocatalysts, Journal of Molecular Catalysis A: Chemical., **1999**, 148, 29-41.

32. Tisse, V F, Boisson, C, McKenna, T F L, Activation and Deactivation of the Polymerization of Ethylene over rac-EtInd2ZrCl2 and (nBuCp)2ZrCl2 on an Activating Silica Support, Macromol. Chem. Phys., **2014**, 215, 1358-1369.

33. Kaminsky, W, Winkelbach, H, Influence of supported metallocene catalysts on polymer tacticity, Topics in Catalysis., **1999**, 7, 61-67.

34. Bryliakov, K P, Semikolenova, N V, Panchenko, V N, Zakharov, V A, Brintzinger, H H, Talsi, E P, Activation of rac-Me2Si(ind)2ZrCl2 by Methylalumoxane Modified by Aluminum Alkyls: An EPR Spin-Probe, 1H NMR, and Polymerization Study, Macromol. Chem. Phys., **2006**, 207, 327-335.

35. Babushkin, D E, Panchenko, V N, Timofeeva, M N, Zakharov, V A, Brintzinger, H H, Novel Zirconocene Hydride Complexes in Homogeneous and in SiO2-Supported Olefin-Polymerization Catalysts Modified with Diisobutylaluminum Hydride or Triisobutylaluminum, Macromol. Chem. Phys., **2008**, 209, 1210-1219.

APPENDIX 1

CHAPTER 3

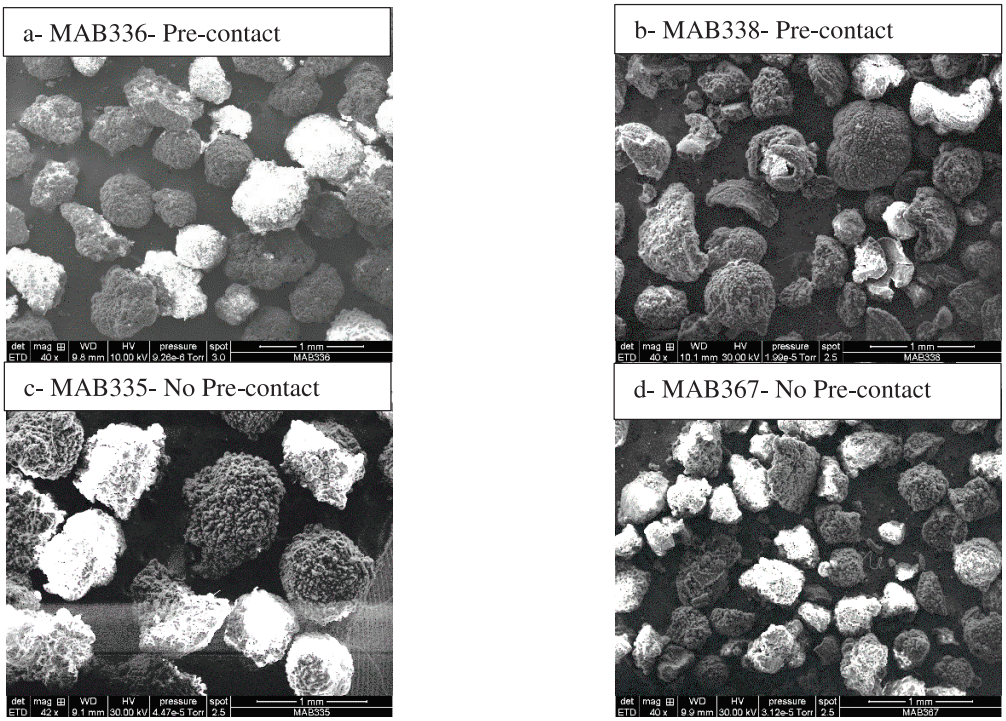

Figure S1: SEM micrographs of HDPE samples produced by MSP-1 (a,b) and MSP-2 (c,d) using TEA.

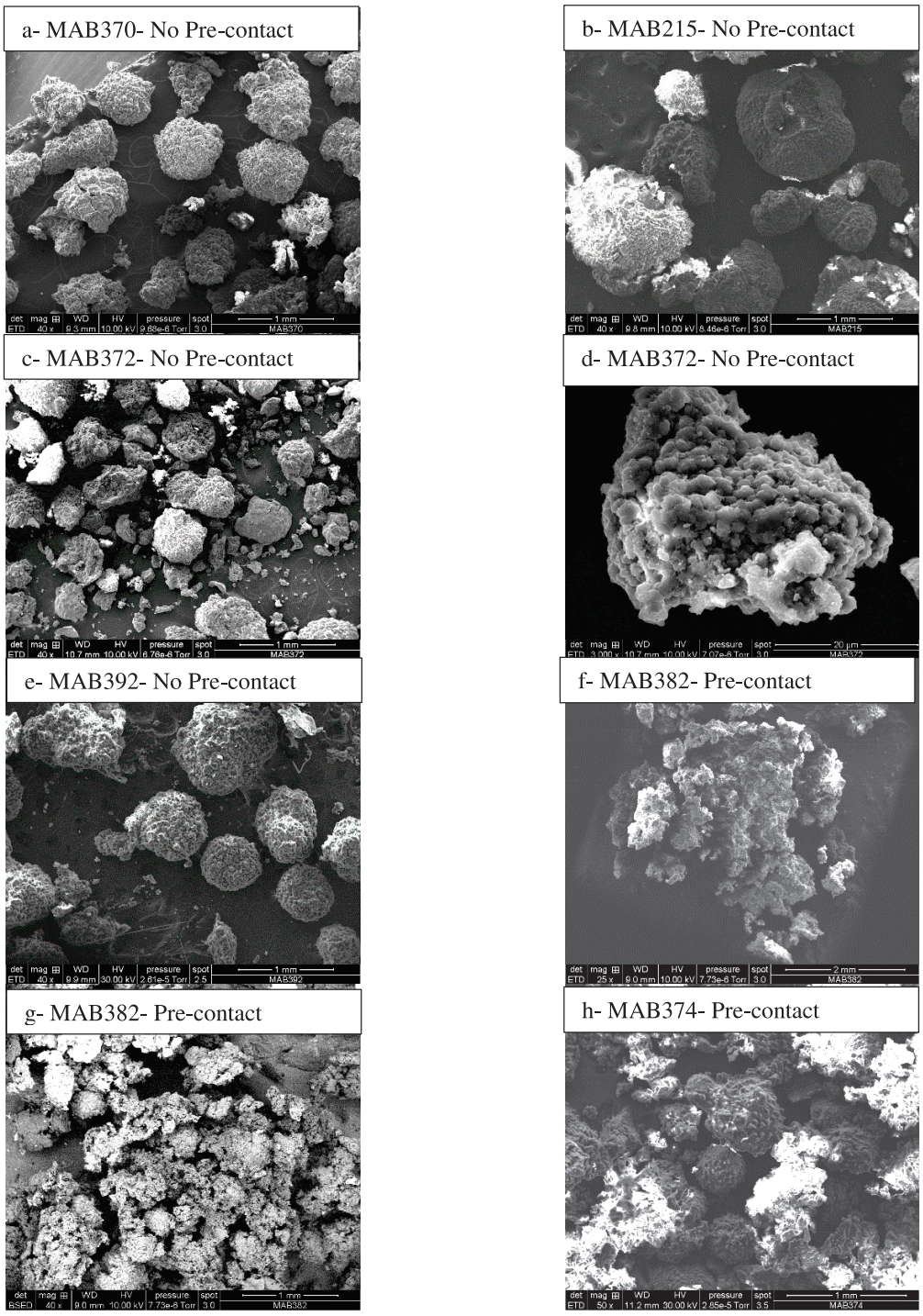

Figure S2: SEM micrographs of HDPE samples produced by MSP-2 using 2 mmole TIBA.L^{-1} (a,b), 12 mmole TIBA.L^{-1} showing the presence of fine particles (c,d), 12 mmole TOA.L^{-1} showing the presence of fine particles (e), Pre-contact with TEA+BHT-H (f,g) and Pre-contact with TIBA+BHT-H (h).

CHAPTER 4

The Effect of Particle Size and Porosity of Silica Supported Metallocene/MAO Catalysts on their Slurry Phase Ethylene Polymerization Kinetics and Polymer Properties

Contents

1. Introduction 184

2. Experimental section 186

2.1. Materials 186

2.2. Silica Sieving 186

2.3. Catalyst Synthesis Procedure 187

2.4. Polymerization Reactor 187

2.4.1. Method one for Slurry Polymerization (MSP-1) 188

2.4.2. Method two for Slurry Polymerization (MSP-2) 188

2.5. Silica and Catalysts Characterization 188

2.6. Polymer Characterization 189

3. Results & Discussion 191

3.1. Pore structure of silica supports and catalyst particles 191

3.1. Slurry Phase Ethylene Homopolymerisations and Ethylene/1-Hexene Copolymerisations with Reference Full Batch Catalysts 200

3.2. Effect of Silica Support Particle Size in Slurry Phase Ethylene Homopolymerisations and Ethylene/1-Hexene Copolymerisation 211

3.2.1. Effect of Particle Size studied with Grace 948 Silica Based Catalysts 211

3.2.2. Effect of Particle Size Studied with PQMS 1732 Silica Based Catalysts 220

3.2.3. Effect of Particle Studied with PQMS 3040 Silica Based Catalysts 233

3.3. Slurry Phase Ethylene Polymerizations with Silica Supported THI/MAO catalyst ... 243

3.4. Conclusion from Particle Size Study 251

3.5. Effect of Pore Volume, Pore Diameter and Surface Area of the Silica Supports on the Catalytic Activity, Molecular Properties and Physical Properties of Polyethylene 253

3.6. Conclusion from the Effect of Porosity Study 265

4. References 266

APPENDIX-1 269

1. Introduction

A significant amount of polyethylene (PE) is produced via slurry phase polymerization process which employs a solid heterogeneous catalyst (for most of PE grades) suspended in an inert diluent typically C_3 to C_6 alkane. Gaseous monomers and hydrogen are continuously bubbled through the inert diluent while the higher α-olefin co-monomers are added as liquid to the reactor in the case of copolymerizaitons. Major benefit of this process is the better heat transfer control, both on the growing polymer particle and reactor level. Good heat transfer control leads to higher specific reaction rates which finally translates into shorter reactor residence times, reactor volumes and faster grade changes with less off-spec material. On the other hand, slurry phase process is expensive since it involves purchase, purification, removal and recycling of the inert diluent. Slurry phase reactors are more prone to reactor fouling as either the amorphous polymer part can easily dissolve into the reactor diluent or the catalyst can leach from the support leading to homogeneous polymerization. Out of the autoclave and loop reactor configuration, the most efficient and common reactor geometry for industrial slurry phase processes is the second one due to the fact that it provides higher heat transfer area thanks to its higher surface to volume ratios which can reach up to 100 $m^2.m^{-3}$.[1]

Physical properties of silica supported metallocenes (i.e., particle size and porosity) are of considerable importance in slurry phase ethylene polymerization process since diffusion resistance to (co)-monomer(s) transport at the active sites can be high, especially during the start of polymerization causing slow catalyst activation as well as, for example, broadness of polymer molar mass distribution. It should be noted here that monomer diffusion resistance is not an issue for only very high activity heterogeneous catalyst rather low to moderately active supported catalysts can also suffer from its consequences. Furthermore, it has a more pronounced effect on the catalyst performance at low reactor pressures.[2] As a result, some studies have been conducted to investigate the effect of size and porosity of the silica supported catalysts on their instantaneous polymerization rates in laboratory scale slurry phase reactors and on the produced polyethylene grade. Nevertheless, as discussed in Chapter 1, mixed conclusions have been reported in the open literature due to very different catalyst synthesis procedures and polymerization conditions used in such studies. Silica supports prepared by different synthesis methods adds another level of complexity in those results. Since a detailed literature review has already been provided in the first chapter, we will only mention a few points briefly here, and refer the reader to chapter 1 for the more general discussion.

In chapter 1, we mentioned that in a previous study from our research group, Tisse et al.,[3] analyzed the impact of silica support PSD on the reaction kinetics and molar mass distribution of the homo and copolymer samples of rac-Et(Ind)$_2$ZrCl$_2$ supported on different sized silica particles from a master batch. They showed that there are visibly significant differences in the kinetic profiles of catalysts of different sizes. They also proposed that since the molar masses of the polymers and their dispersity were practically identical, regardless of the particle size, the observed difference in the kinetic profiles of different sized catalyst particles cannot be solely due to the presence of mass transfer resistance. Two important points should be made here about this work. The first is that in all the polymerizations, SMAO based catalysts were pre-contacted for 10 minutes with TIBA prior to their injection into the reactor. As shown in the previous Chapter 3, this pre-contact between the SMAO based catalyst and TIBA can lead to catalyst leaching which can cause homogeneous and heterogeneous polymerizations going in parallel. This point was not addressed by the authors. The second point is that the authors did not consider the possibility that this behaviour could be caused by the underlying "chemistry" of the catalyst itself.

The focus of the current chapter is silica supported metallocene/MAO catalysts in which the used metallocenes were pre-activated with MAO prior to their grafting on the silica supports. The first part of this chapter investigates the effect of catalyst particle diameter on its instantaneous activity in slurry phase ethylene homo- and copolymerizations with 1-hexene at 80 °C and on the polymer properties produced thereof. Different ethylene pressures have been used while keeping scavenger concentration of 2 mmole.L^{-1} unless otherwise mentioned. In the second part of this chapter we will discuss the impact of pore diameter, pore volume and the surface area of the supported metallocene/MAO catalysts on their instantaneous activities in ethylene polymerizations as well as on polyethylene properties.

2. Experimental section

2.1. Materials

Three commercial silica were used in this study whose physical characteristics are shown in Table **1**. $(n\text{-BuCp})_2ZrCl_2$ was obtained from Sigma-Aldrich. Triethylaluminium (TEA) and triisobutylaluminium (TIBA) were used as received from SGS and Witco Corporation, respectively. The MAO solution 30 wt% in toluene used in this study was supplied by Albemarle with the following characteristics: 13.6 wt% Al, 5.24 wt% $AlMe_3$, gas/Al = 1.65. n-heptane used in catalyst synthesis and as a diluent in slurry polymerizations were dried on 3 Å molecular sieves.

Table 1. Physical properties of as-received commercial silica used in this work measured with nitrogen porosimetery.

Silica Trade Name	**A_s (m^2/g)**	**P_v (ml/g)**	**P_d (Å)**	**d_{50} (µm)**
Grace 948	290	1.7	232	60
PQ MS3040	420	3.0	300	45
PQ MS1732	536	1.4	101	128

Ethylene (purity 99.95%) was purchased from Air Liquide (Paris, France) and passed through three different purification columns before use: a first one filled with reduced BASF R3-16 catalyst (CuO on alumina), a second one filled with molecular sieves (13X, 3A, Sigma-Aldrich), and a last one filled with Selexsorb COS (Alcoa).

2.2. Silica Sieving

For obtaining silica with varying particle sizes, full batch of each commercial silica was sieved according to **Scheme 1** where pan refers to the smallest fraction obtained after the last sieve in series.

Scheme 1. Sieving scheme of each commercial silica.

2.3. Catalyst Synthesis Procedure

Incipient wetness method is used to prepare all the catalysts used in this work i.e., whether the full silica based catalyst is considered or a catalyst based on a sieved fraction of silica. Each silica was dehydroxylated at 600°C under dynamic vacuum of 10^{-3} to 10^{-5} mbar prior to its impregnation with the metallocene + MAO mixture. In the first step, a weighed amount of (n-BuCp)$_2$ZrCl$_2$ was mixed with dry toluene and MAO (30 wt% toluene solution) and left for 1h at the room temperature inside the glove box. The amounts of (n-BuCp)$_2$ZrCl$_2$ and MAO were selected by aiming Al/Zr molar of 150 in the final catalysts whereas the volume of toluene used was in 150% excess of the pore volume of the used silica support. More precisely, the amount of MAO solution used was 1.77 mL.g^{-1} for each catalyst. In the second step, the (n-BuCp)$_2$ZrCl$_2$ + Toluene + MAO mixture was added to the weighed amount of silica dropwise followed by heating at 50 °C for 1 h without any stirring. In the third step, the supported catalyst was dried under vacuum at 75 °C, without applying any wash, for 2-3 h and then stored inside the glovebox.

2.4. Polymerization Reactor

Polymerization runs were carried out in a spherical laboratory scale 2.5 L semi-batch reactor which can be operated both in slurry and gas phases. The detailed reactor set-up has been described in **Chapter 2**. The reactor was conditioned for at least 2 h at 80 ºC with a minimum of three argon-vacuum cycles, and then cooled down to the room temperature. Two different polymerization protocols were used for slurry phase reactions which are described below.

2.4.1. Method one for Slurry Polymerization (MSP-1)

As shown in detail in the previous **Chapter 3**, that this polymerization protocol leads to significant catalyst leaching and reactor fouling, therefore this reaction procedure was used only in few polymerization runs whose results will be compared with those obtained by following the Method two for slurry polymerization (MSP-2) described next.

In this method, referred to hereafter as, Method one for slurry polymerization (MSP-1), 20 to 25 mg of catalyst and 1 mL of 1 M TIBA solution in heptane were added to 500 mL of pure dried heptane under argon. This mixture (i.e., supported catalyst + scavenger + 500 mL heptane) was then injected into the reactor at room temperature under argon pressure followed by reactor heating to 80ºC under constant stirring at 450 revolutions per minute (rpm). Ethylene was then injected and maintained at 8 bar once the desired reaction temperature was achieved. Consumption of ethylene was recorded by the pressure drop in an ethylene cylinder equipped with a pressure gauge.

2.4.2. Method two for Slurry Polymerization (MSP-2)

This polymerization protocol has been adopted as the main polymerization method due to the fact that it helps to avoid catalyst leaching from the silica support, as shown in the previous chapter. For each polymerization run, 25 to 30 mg of catalyst were added to an injection cartridge with 5 mL of pure dried toluene inside the glove box. The injection cartridge was then attached to the reactor after which three cycles of vacuum and argon were made. 500 mL of pure dried heptane containing 1 mL of 1 M TIBA solution was injected into reactor under argon pressure after which the reactor temperature was raised to 80 °C under constant stirring at 450 rpm. Catalyst + 5 mL heptane mixture inside injection cartridge was then injected into the reactor under ethylene pressure at 80 °C and then ethylene pressure was maintained at the desired pressure throughout the reaction. Consumption of ethylene was recorded by the pressure drop in an ethylene cylinder equipped with a pressure gauge. At the end of reaction time, ethylene was vented from the reactor along with reactor cooling to room temperature. The slurry containing polyethylene was then filtered followed by polymer drying under vacuum at 50 °C. Reaction time was 1 h 15 minutes for all the reactions unless otherwise mentioned.

2.5. Silica and Catalysts Characterization

Al and Zr content of the final catalysts were then obtained by Inductively Coupled Plasma-Atomic Emission Spectroscopy (ICP-AES) at Mikroanalytisches Labor Pascher, Germany.

Diffuse Reflectance Fourier Transform Infrared spectroscopy (FT-IR-DRIFT) was used to characterise the as-received silica, the dehydroxylated silica. A few milligrams of each sample were added in a special air tight sample holder in glove box and the spectra were recorded using Thermo Scientific Nicolet™ iS™50 spectrometer.

Mercury porosimetery of the full batch as received silica was performed by Delft Solid Solutions, The Netherlands, and each sample was degassed in vacuum at 200 °C for 16 h prior to the analysis which was performed in a Micromeritics Autopore 9505 analyzer. The weight loss obtained upon pre-treatment was recorded and the dry sample weight was used in the calculations.

Nitrogen adsorption/desorption isotherms of silica and silica supported final catalysts were obtained in a Micromeritics ASAP 2020 V3.04 H unit at -196 °C. All the silica samples were degassed for 4 h at 200 °C, whereas the supported catalysts were not degassed prior to the measurements since the used silica supports were thermally treated at 600 °C and the catalysts were dried at 75 °C for few hours before their storage in the glove box. Specific surface area(s) (A_s) were determined by the Brunauer–Emmett–Teller equation. Desorption branch of Barrett–Joyner–Halenda (BJH) method which employed Halsey standards was used to estimate the mesopore size and distribution and pore volume of all the samples. For t-plot measurements, Harkins and Jura Equation was used.

2.6. Polymer Characterization

High Temperature Size Exclusion Chromatography (HT-SEC) analyses were performed using a Viscotek system (from Malvern Instruments) equipped with three columns (PLgel Olexis 300 mm x 7 mm I. D. from Agilent Technologies). 200 µL of sample solutions with a concentration of 4 mg mL^{-1} were eluted in 1,2,4-trichlorobenzene using a flow rate of 1 mL min^{-1} at 150 °C. The mobile phase was stabilized with 2,6-di(tert-butyl)-4-methylphenol (200 mg L^{-1}). The OmniSEC software was used for data acquisition and data analysis. Online detection was performed with a differential refractive index detector and a dual light scattering detector (LALS and RALS) for absolute molar mass measurement.

Thermal characterizations were performed with a differential scanning calorimetry, Mettler Toledo DSC 1, equipped with an auto-sampler and a 120 thermocouple sensor. The temperature and the heat flow of the equipment were calibrated with an indium standard. All samples were accurately weighed (between 5 to 10 mg) and sealed in aluminium pans. They were heated from -20 °C to 180 °C at 10 °C.min^{-1} with an empty aluminium pan as reference. Two

successive heating and cooling were performed and only the second run was considered. Dry nitrogen with a flow rate set at 50 mL.min^{-1} was used as the purge gas. The melting temperature (T_m) was measured at the top of the endothermic peak. The STAR^e thermal analysis software is used to calculate the melting temperature and the crystallinity (χ) of the polymers: $\chi = \Delta H_f / \Delta H_{f0}$ where ΔH_f (J.g^{-1}) is the melting heat of the sample and ΔH_{f0} (= 293 J.g^{-1}) the melting heat of a 100 % crystalline polyethylene.

A Malvern Mastersizer 3000 was used to determine the particle size distribution (PSD) of silica and the PE samples. Water was used only for the PSD measurement of silica using a Hydro unit of Malvern Mastersizer 3000.

Nuclear Magnetic Resonance (NMR) characterization was performed on a Bruker Avance III 400 spectrometer operating at 400 MHz for ^{1}H and 100.6 MHz for ^{13}C NMR. The spectra of ^{13}C NMR were obtained with a 10 mm PA-SEX probe at 393 K. A volume mixture of o-$C_6H_4Cl_2$ (90%) and p-$C_6D_4Cl_2$ (10%) was used as solvent. Chemical shifts were measured in ppm using the resonance of polyethylene as internal reference at 30 ppm.

Crystallization Elution Fractionation (CEF) analysis were performed using a TGIC/CEF Polymer Char instrument. Samples were dissolved in TCB at a concentration of 2 mg.mL^{-1} during 60 minutes at 160°C. 200 µL of the sample solution were loaded in the column at high temperature (150°C). Then a cooling ramp was applied at a rate of 2.0 °C.min^{-1}, with a crystallization flow of 0.05 mL.min^{-1}. After the crystallization step, an elution flow was applied at 1.00 mL.min^{-1}, and the temperature was increased up to 130 °C via a heating ramp of 4.0 °C.min^{-1}. Eluted fractions were analysed with a dual integrated infrared IR5 MCT spectrometer coupled to a viscometer detector in order to measure the chemical composition distribution (CCD). The IR5 MCT spectrometer measures the CH_3/1000C content via direct analysis, and the 1-hexene content via a calibration curves, constructed with narrow CCD home-made ethylene/1-hexene copolymer standards. The viscometer detector measures the intrinsic viscosity relied to the molar mass.

SEM images have been observed on a FEI Quanta 250 FEG microscope, after metallization of the samples by a carbon plait evaporation on a Balzers MED010 apparatus. The SEM-EDX of catalyst samples were observed after inclusion of the samples into an EpoFix resin. The surfacing of the resin block was carried on by a “Diatome Ultra 45” diamond knife performed on a Reichert Ultracut S ultramicrotome.

3. Results & Discussion

3.1. Pore structure of silica supports and catalyst particles

Commercial silica used in this work were analysed by mercury intrusion and nitrogen porosimetery. Both of these techniques provide unique information about the pore sizes and their distribution. **Figure 1** shows mercury intrusion porosimetery of the three silicas as received. It can be seen that the intrusion curves of the samples display a first intrusion from a relatively low pressure of 0.01 MPa up to ~0.5 MPa where a plateau is reached (see **Figure 1a**). This first intrusion occurs over a narrow pressure range at slightly different pressures for each of the samples (i.e., at ~0.05 MPa for PQMS 1732 silica, at ~0.08 MPa for Grace 948 silica and at ~0.1 MPa for sample PQMS 3040 silica). This first intrusion is typically attributed to the rearrangement of the particles and filling of the inter-particle porosity. The inter-particle characteristic size of the interparticle voids is on the same order of size as the smallest particles in the batch.

A second intrusion step over a relatively broad pressure range can be seen for all three samples. This step spans from ~10 to 220 MPa for PQMS 1732 silica and from ~1 to ~220 MPa for the two other silica. Interestingly, the slope of this high-pressure intrusion step changes for Grace 948 silica at about 120 MPa, after which the onset of a plateau can be observed. For the two PQ silica samples, a plateau was not achieved at the maximum pressure. This second intrusion should be attributed to the filling of intra-particle porosity. PQMS 1732 silica has only small pores (high-pressure intrusion), whereas PQMS 3040 and Grace 948 contain smaller as well as bigger pores (lower-pressure intrusion). The second plateau in the case of Grace 948 silica suggests that porosity < 6 nm is not (or only slightly) present in this silica, and most of the porosity has been adequately assessed. On the other hand, the absence of such a plateau in the two PQ silica samples is an indication that pores of diameter < 6 nm are present in these samples and not all porosity has been adequately assessed. In agreement with the supplier data shown in **Table 1** of the previous section, **Figure 1a** also shows that the intruded volume of PQMS 3040 silica is the highest, whereas the lowest intruded volume is of PQMS 1732 silica. Quantitative information on the total pore volume and the derived porosity for the samples are summarized in **Table 2** which indicates that Grace 948 has the highest porosity while PQMS 1732 is the least porous among the studied series. The difference in values of the pore volumes of the silicas shown in **Table 1** and **Table 2** can be attributed to the difference in both the analytical techniques. Highest weight loss of PQMS 1732 upon pre-treatment (at 200 °C for 16 h) can be attributed to its highest surface area due to which it may had the highest amount of adsorbed water and other gases.

a

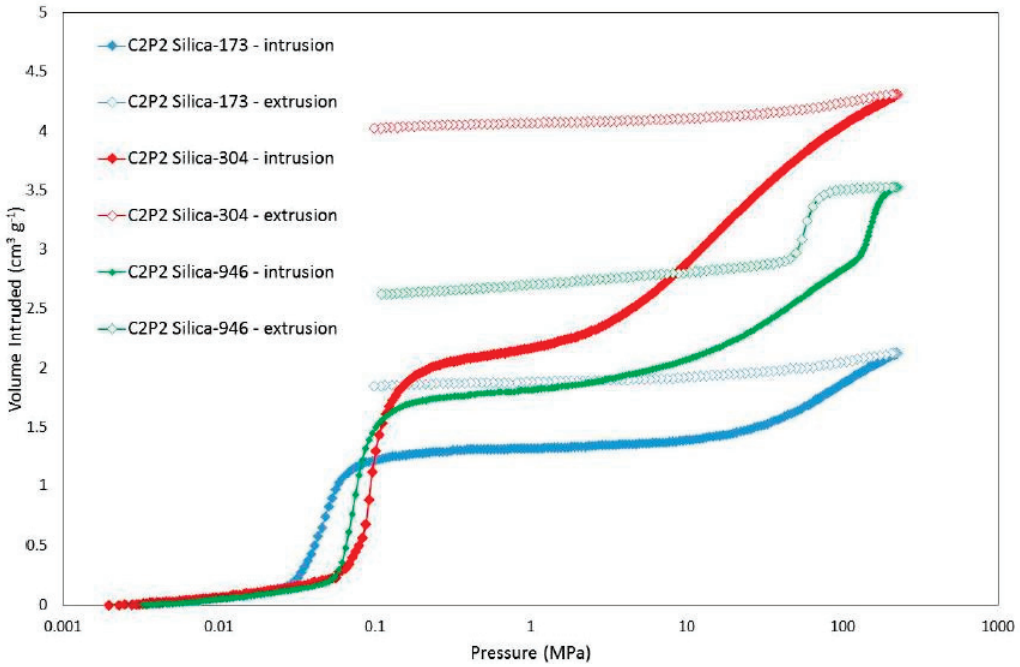

b

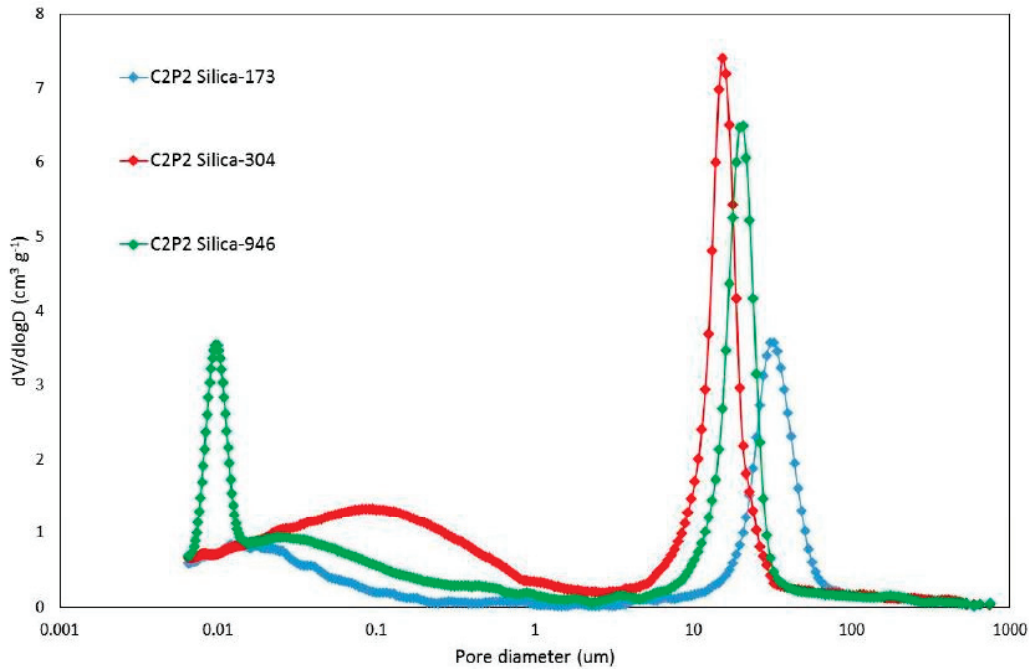

Figure 1. (a) Mercury intrusion and extrusion curves over the three as received silica samples where closed symbols denote intrusion and open symbols denote extrusion. (b) Differential pore size distributions of the three as received silica samples derived from the intrusion curves shown in (a). 173 stands for PQMS 1732 silica, 304 stands for PQMS 3040 and 946 stands for Grace 948 silica.

Table 2. Physical properties of the three commercial silica samples investigated by mercury porosimetery.

Silica Name	Weight loss (wt%)	$P_{v,total}$ ($cm^3.g^{-1}$)	Porosity %	$\rho_{apparent}$ $g.cm^{-3}$
PQMS 1732	7.4	2.13	68	1.02
PQMS 3040	6.5	4.31	81	1.01
Grace 948	4.6	3.53	85	1.62

Mercury intrusion experiments also allows the estimation of the so-called apparent density for the solid samples. Interestingly, the two PQ silica samples for which no plateau was achieved display rather similar apparent density values despite their rather different "porous properties", and have much lower apparent densities compared to Grace 948 silica, which appeared to have reached a plateau. However, none of the measured densities match with the true density of silica, which varies from 2.196 – 2.648 g cm^{-3}, depending on the type of silica. This is again an indication that not all porosity has been adequately assessed and that pores < 6 nm, the lower limit of the mercury intrusion technique, are present in all of the samples.

The pore size distributions derived from the intrusion curves are plotted in **Figure 1b**. The pore size distributions of the samples indeed show two contributions of porosity, namely a first narrow contribution from ~5 – 100 μm corresponding to inter-particle porosity and a second broad contribution ranging from approx. 0.006 – 1 μm (intra-particle porosity). The inter-particle contribution of PQMS 3040 silica is the smallest, with a maximum intensity around 15 μm suggesting the smallest particles, while the inter-particle contribution of PQMS 1732 silica the largest, with a maximum intensity around 30 μm, suggesting the largest particles. Once again these estimations are in excellent agreement with the Master Sizer data shown in **Table 1** of the previous section. The pore size distributions also display that PQMS 1732 silica does not possess the larger intra-particle pores ranging from 0.1 – 1 μm and that the other two samples do possess these pores. The presence of these pores may play a significant role in the dispersion of metallocene/MAO solution throughout the silica particles as we shall see in the coming sections of this chapter where SEM-EDX images of the supported catalyst particles are shown. A high contribution of very small pores of ~0.01 μm should also be noted in the pore size distribution of Grace 948 silica, correlating nicely with the slope change in the intrusion curve.

All three distributions have not yet returned to baseline level around 0.006 μm (6 nm), which is again an indication that porosity < 0.006 μm is present and that not all porosity has been adequately assessed, explaining the relatively low apparent density values in **Table 2**.

Nitrogen porosimetery results obtained for $(n\text{-}BuCp)_2ZrCl_2$/MAO catalyst supported on the full batches of three commercial silica are shown in **Figure 2** which are in good agreement with those obtained from mercury porosimetery. Both types of porosimetery techniques confirm that these three commercial silica are mesoporous, and that PQMS 3040 has the highest pore volume and PQMS 1732 has the least pore space. Grace 948 silica supported catalyst has a pore volume which is not very different from that supported on PQMS 1732 silica. Due to the presence of both small and large pores in PQMS 3040 and Grace 948 silica, the exponential rise in the quantity of nitrogen adsorbed occurs more or less at the same relative pressure of about 0.8, whereas in the case of PQMS 1732 silica supported catalyst only small pores are present as indicated by the smooth rise in adsorption isotherm (see **Figure 2a**).

Differential pore size distributions of the final supported catalysts are also in good agreement with those measured with mercury porosimetery (i.e., both the techniques show that the pore diameters of the three silica are in the order; PQMS 3040 > Grace 948 > PQMS 1732) and indicates some amount of pores below < 6 nm (see **Figure 2b**). Such porosity was also noticed in the nitrogen porosimetery of untreated silica.

The impact of immobilizing $(n\text{-}BuCp)_2ZrCl_2$/MAO catalyst on the porosity of the particles is shown in **Figure 3 - Figure** 5 for PQMS 1732, Grace 948 and PQMS 3040 respectively. In the case of PQMS 1732, it can be seen from **Figure 3** that the average pore size of the particle decreased, but that secondary porosity with pores smaller than 3 - 4 nm was found to increase slightly after immobilization. As discussed above this secondary porosity is generally attributed to the pores created once the MAO solution used to prepare the catalyst dries out. Build-up of a pore structure by MAO after its immobilization on silica supports has also been evidenced by Fink et al.,[4] who reported that the loss of surface area by MAO deposition in larger pores of 10 – 40 nm radii is compensated by the formation of smaller pores in the range of 1 – 5 nm. Similarly, Turunen et al.,[5] attributed the formation of these micropores to a slight decrease in the average pore size due to the deposition of MAO in the original silica structure. It is important to mention here that the pore size distribution of the final catalyst showed slight bimodality, and this was seen only in the case of PQMS 1732 silica. It is possible that this

observation might be attributable to the uneven deposition of bulky MAO (as we shall see in the coming sections) which can have its own pore structure upon drying.

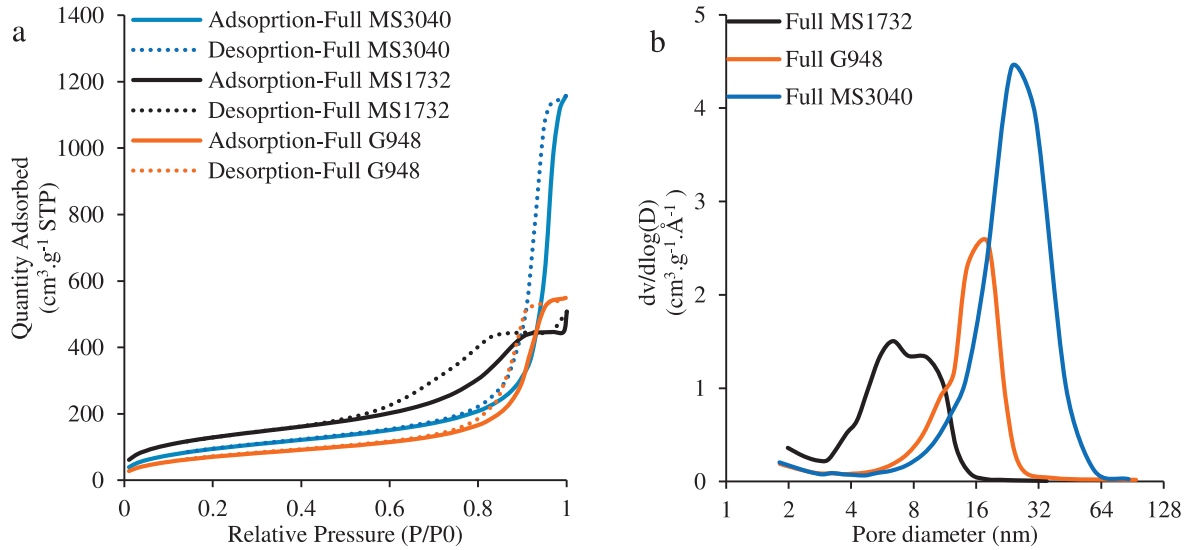

Figure 2. (a, b) Comparison of nitrogen adsorption/desorption isotherms and pore size distribution of catalysts supported on full batches of three commercial silica used in this work.

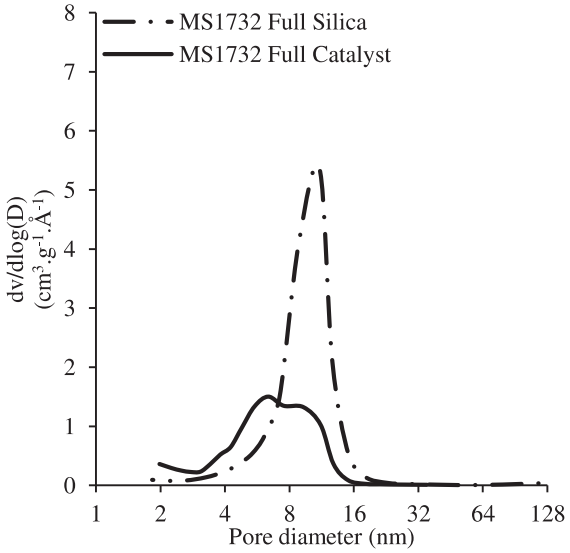

Figure 3. Comparison of pore volume distribution before and after immobilization of metallocene/MAO on full batch of PQMS 1732 silica.

Figure 4a and **b** compare the nitrogen adsorption/desorption isotherms and pore size distribution of dehydroxylated fraction of Grace 948 silica which was obtained on 45 µm sieve with that of the final catalyst supported on it. It can be noticed that, despite decrease in pore size due to the deposition of bulky MAO, the overall shape of the isotherms remains very similar before and after impregnation of the support with $(n\text{-BuCp})_2ZrCl_2$/MAO solution which indicates that the original support pore structure remained intact during the catalyst immobilization step. This is a bit different from what we saw in **Figure 3**, where the PQMS1732 system showed a certain bimodality. In addition, it is interesting to note that the decrease in pore size of the Grace 948 is very different from that of the PQMS 1732. Immobilization of the catalyst on the Grace support lead to a "shifting" of the unimodal distribution from one centred on 30 – 32 nm, to a new one centred at 14 - 15 nm. In the PQMS 1732 case, the average pore size dropped from a unimodal distribution with a peak at 11 nm, to a broad/bimodal distribution with the peak spread from 5 - 9 nm. This is evidence that the overall pore structure of the 2 supports is quite different. Furthermore, the BET calculated surface area of the catalyst slightly increased as compared to that of the dehydroxylated silica. Once again it is possible that this can be attributed to the generation of additional microporosity due to dried MAO. The sharp rise in nitrogen quantity adsorbed by the catalyst sample at the saturation pressure as well as the increased area under the curve of pore size distribution below 4 nm pore diameter (see **Figure 4a** and **b**) is an indication of this. In addition, sieving operation does not seem to influences the pore structure and pore size distribution of the supported catalysts as shown by **Figure 4c** and **d**. Overall, it can be seen that the pore dimensions and distributions of all the catalysts based upon Grace 948 silica are identical.

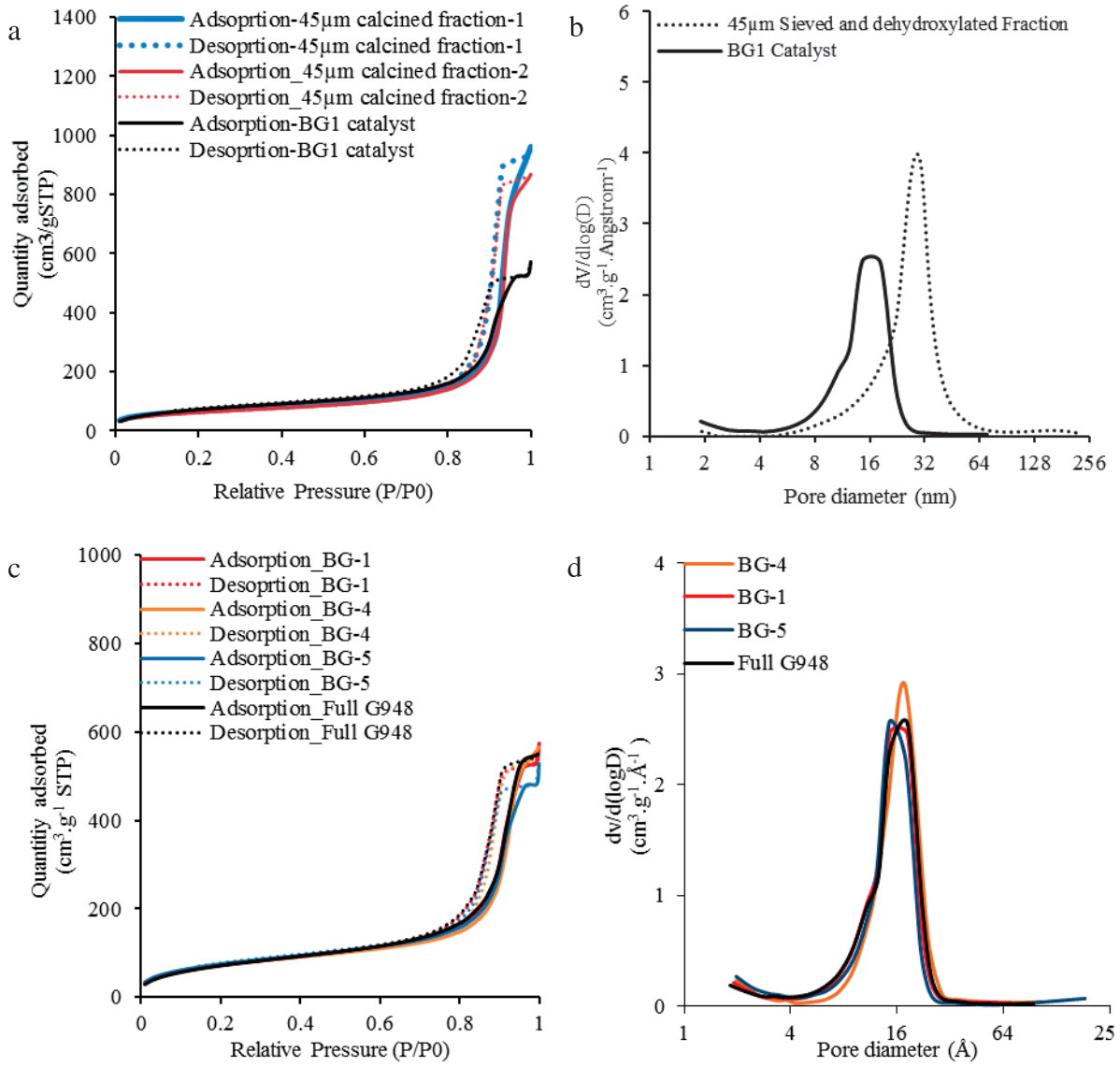

Figure 4. (a, b) Comparison of nitrogen adsorption/desorption isotherms and pore volume distribution of BG-1 catalyst with the its dehydroxylated support (i.e., the 45 µm fraction of Grace 948 silica). (c, d) Comparison of nitrogen adsorption/desorption isotherms and pore volume distribution of different catalysts prepared from sieved fractions of Grace 948 silica. Full G948 refers to the catalyst supported on full batch of Grace 948 silica.

Similar observations can also be made for all the supported catalysts prepared with PQMS 3040 and PQMS 1732 silica, as shown in **Figure 5**. A slight bimodality in the pore size distributions of the catalysts supported on PQMS 1732 silica can be attributed to the core-shell distribution of MAO in these catalysts (as we shall see in the coming sections) probably due to the presence of only small pores in this silica as shown by nitrogen and mercury porosimetery results (whereas the two other silica have both small and large pores). **Table 3 - Table** 5 provides the numerical data of surface area, average pore diameter and pore volume of the supported catalysts prepared from full batches of these three silica and from their sieved fractions along with aluminium (Al) and zirconium (Zr) contents. It can be noticed that catalysts obtained with

Grace 948 silica possess the lowest surface area, whereas the catalysts prepared with the two PQ silica have very similar surface area. Pore diameters and pore volumes of the final catalysts seem very similar for Grace 948 and PQMS 3040 catalysts while the catalysts prepared with PQMS 1732 silica have lowest values of pore volume and pore diameter. Chemical composition of all the catalysts also looks very similar as indicated by their ICP-AES analysis. Note that all the values of BET surface area, pore volume and pore diameter are average of at least two measurements.

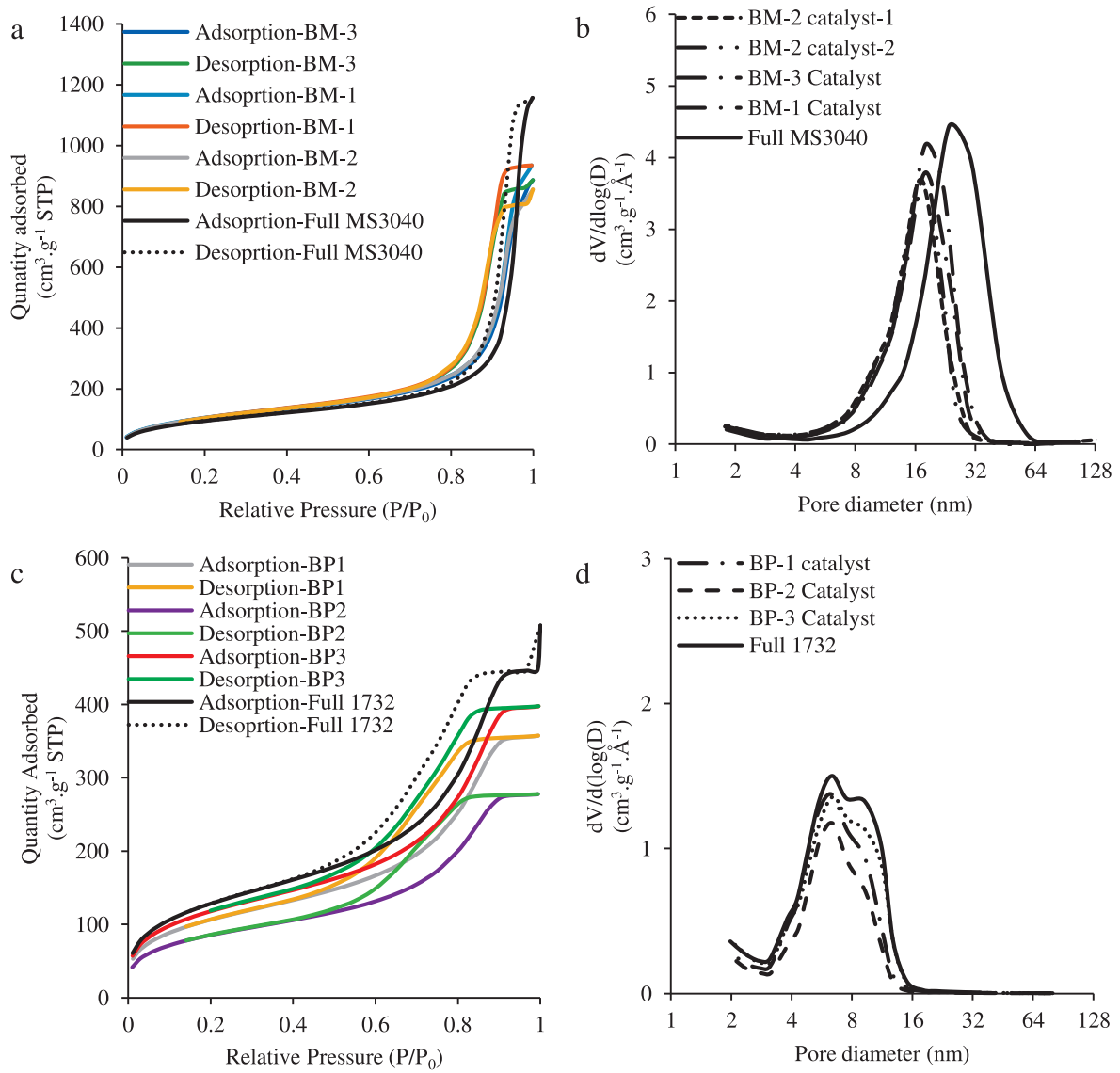

Figure 5. Comparison of nitrogen adsorption/desorption isotherms and pore volume distribution of catalysts supported on a full batch and sieved fractions of PQMS 3040 silica (a, b) and full silica batch and sieved fractions of PQMS 1732 silica (c, d). The term 'Full' refers to full silica based catalyst.

Table 3. BET and ICP-AES analysis of the catalysts prepared by using different sieved fractions and full batch of Grace 948 silica. A_s = Specific surface area, P_v = pore volume, P_d = pore diameter.

Cut Number	Sieve opening (µm)	Catalyst Name	A_s (m^2/g)	P_v (cm^3/g)	P_d (nm)	Zr (Wt%)	Al (Wt%)
1	Pan	BG-4	265	0.81	11.6	0.21	14.3
2	36	BG-2	284	0.81	10.9	0.19	12.4
3	45	BG-1	273	0.82	11.2	0.19	12.5
4	63	BG-3	269	0.75	10.8	0.18	12.5
5	80	BG-5	289	0.80	10.8	0.20	15.6
6	Full Batch	Bu/M/G948	270	0.85	11.1	0.31	14.0
-	Full Batch	Full As received silica	290	1.7	23.2	-	-

Table 4. BET and ICP-AES analysis of the catalysts prepared by using different sieved fractions and full batch of PQMS3040 silica. A_s = Specific surface area, P_v = pore volume, P_d = pore diameter.

Cut Number	Sieve opening (µm)	Catalyst Name	A_s (m^2/g)	P_v (cm^3/g)	P_d (nm)	Zr (Wt%)	Al (Wt%)
1	Pan	BM-4	395	1.31	10.7	0.23	15.8
2	36	BM-2	401	1.31	11.1	0.17	14.3
3	45	BM-3	375	1.30	11.9	0.18	13.4
4	63	BM-1	390	1.46	12.4	0.19	11.8
5	Full Batch	Bu/M/MS3040	412	2.04	16.9	0.29	12.3
-	Full Batch	As received silica	420	3.0	28.5	-	-

Table 5. BET and ICP-AES analysis of the catalysts prepared by using different sieved fractions and full batch of PQMS1732 silica. A_s = Specific surface area, P_v = pore volume, P_d = pore diameter.

Cut Number	Sieve opening (µm)	Catalyst Name	A_s (m^2/g)	P_v (cm^3/g)	P_d (nm)	Zr (Wt%)	Al (Wt%)
1	63	BP-1	389	0.57	5.5	0.23	13.59
2	80	BP-2	311	0.45	5.5	0.19	17.50
3	125	BP-3	417	0.66	5.4	0.22	18.80
4	Full Batch	Bu/M/MS1732	471	0.71	5.6	0.21	12.4
-	Full Batch	Pure silica calcined	507	1.32	8.8	-	-
-	Full Batch	Pure As received silica	536	1.4	10.1	-	-

This analysis shows a number of important points, not the least of which are the fact that: (1) the 3 supports considered here appear to have different physical structures in the sense that the pore size and pore size distributions are quite different; (2) the immobilisation of the catalyst on the support changes the morphology; (3) there is an observable difference between the morphologies of the supported catalysts before polymerization, indicating that components like MAO do not necessarily distribute evenly and in the same manner in the different supports.

3.1. Slurry Phase Ethylene Homopolymerisations and Ethylene/1-Hexene Copolymerisations with Reference Full Batch Catalysts

Figure 6 shows a comparison of kinetic profiles obtained using the full reference batches of catalyst supported on each of the three different commercial silica in ethylene homopolymerisations at 8 and 10 bar monomer pressure, 2 mmole.L^{-1} TIBA concentration (i.e., 1 mmole of TIBA in 0.5 L of heptane) and with MSP-2. At both the monomer pressures, the catalyst prepared with the full batch of Grace 948 silica shows higher instantaneous activity over the whole reaction period than those prepared by PQMS 1732 and PQMS 3040 silica. The activation rate of the reference catalysts prepared with Grace 948 and PQMS 1732 seems rapid at short times, with the latter showing more deactivation after about 5 minutes of reaction time. The activation and deactivation rate of the catalyst prepared with PQMS 3040 silica is lowest among the three reference catalysts. The effect of increasing ethylene pressure seems to impact significantly the productivities of catalysts supported on Grace 948 and PQMS 3040 silicas (whose one hour productivities increase by about 43 %, and 56 %, respectively) in comparison to its effect on the productivity of PQMS 1732 supported catalyst which on average increased

by about 20 % after 2 bar increase in ethylene pressure. Good reproducibility of these experiments is evident from the overlap of kinetic profiles of the reactions conducted with Grace 948 and PQMS 1732 based reference catalysts (see **Figure 6a** and **b)**.

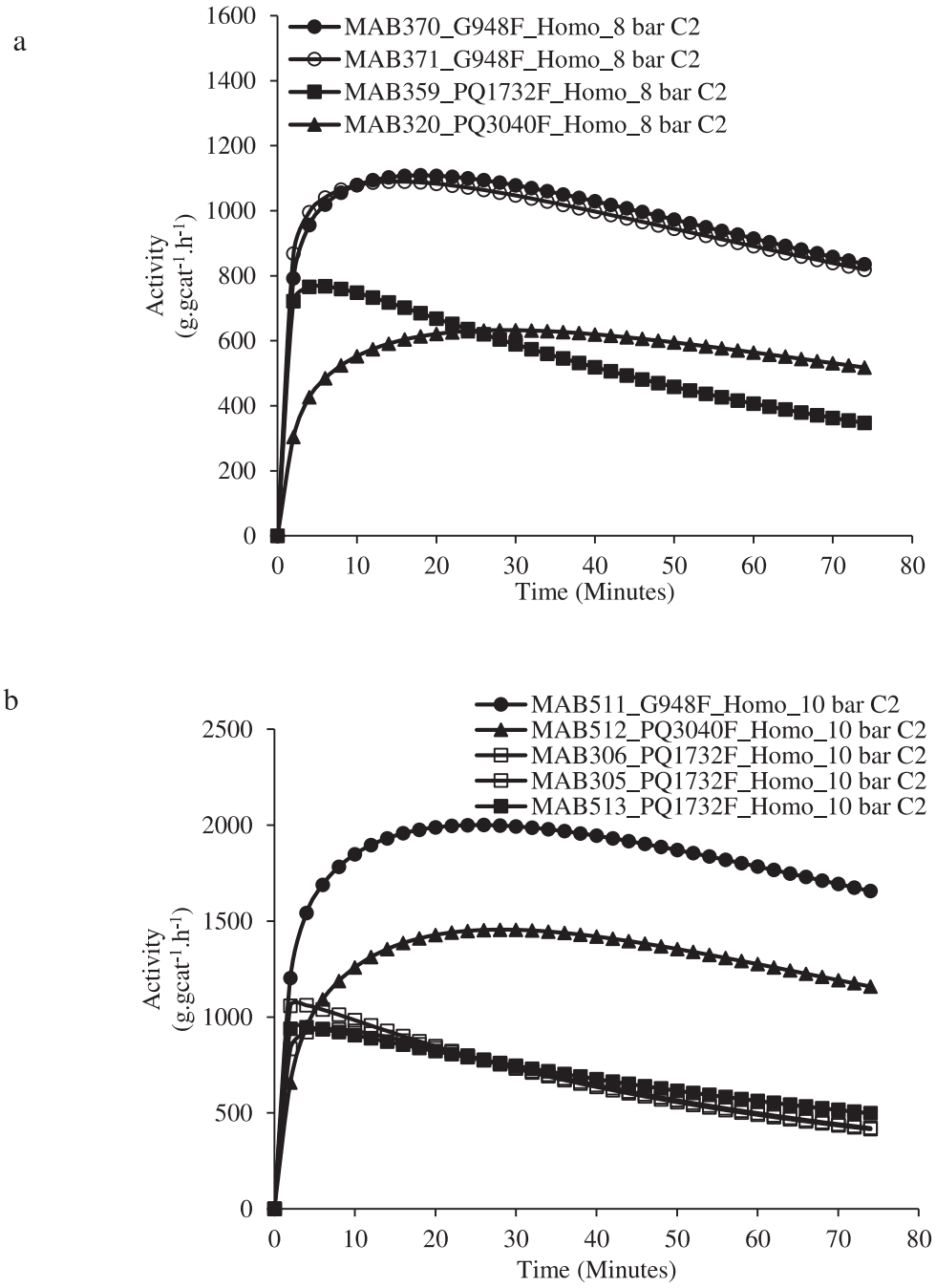

Figure 6. Comparison of kinetic profiles obtained by three reference catalysts prepared by using full batch of each commercial silica.

Similarity in the activation behaviour of the reference catalysts supported on Grace 948 and PQMS 1732 silica might be attributable to similar pore volumes of these catalysts, whereas, the slow activation behaviour of PQMS 3040 based reference catalyst can be attributed to its higher pore volume which is almost twice the pore volume of the other two supported catalysts (compare catalyst pore volumes in **Table 3** to **Table 5**). The most probable explanation for this behaviour seems to be the difference in fragmentation step of these catalysts. In low pore volume catalysts (i.e., Grace 948 and PQMS 1732 silica based catalysts), the fragmentation step probably occurs earlier than in the case of high pore volume catalyst and therefore, allows better monomer access to the active sites as well as exposes those active sites which were initially buried under the polymer layer. Another explanation to this behaviour could be the fact that since each catalyst was dipped in 5 mL heptane prior to injection in the reactor (see MSP-2 in polymerization procedure of this chapter) the volume of heptane present in high pore volume catalyst will be higher than that in the case of low pore volume catalysts and therefore, mass transfer resistance should be higher in the former case than in latter case.

The activity of these catalysts was also evaluated in slurry phase ethylene/1-hexene copolymerisations at 80 °C by adding 3 mL of liquid 1-hexene in the reaction milieu at room temperature at polymerization start-up. **Figure 7** shows the kinetic profiles of copolymerisations where, once again, the reference catalyst prepared with Grace 948 silica showed higher instantaneous activity than the other two supported catalysts. It is worth mentioning that the activation and deactivation behaviour of PQMS 1732-supported catalyst in the presence of 1-hexene has changed significantly in such a way that both the activation and deactivation rates of this catalyst are reduced in comparison to homopolymerisation, and the deactivation rate seems to be more influenced than the activation rate of this catalyst. In gas phase process it has been shown by Kumkaew et al.,[6] that the presence of 1-hexene in the reactor reduces the initial polymerization rate of silica supported $(n\text{-BuCp})_2ZrCl_2$ catalysts as compared to their initial reaction rate in homopolymerizations but after certain time of reaction start-up the instantaneous activities in copolymerizations become higher than those in homopolymerizations. They suggest that the behaviour of active sites is changed by the presence of comonomer, and that this is accompanied by the changes in fragmentation behaviour of the supported catalysts because the incorporation of 1-hexene into the polymer chains reduces the crystalline fraction and brittleness of polyethylene which enables better control on the fragmentation of the growing particles. As we go through this chapter and the following one, we will see that it appears that the fragmentation of the catalyst has a longer

lasting effect on the observed activity than one might think. We will return to this point from time to time.

For PQMS 3040-supported catalyst, it can be seen that at both the pressures the instantaneous activity grows up to first 40 minutes after which it starts to decrease slightly. On the other hand, the reference catalysts supported on Grace 948 and PQMS 1732 silica achieve their peak activities in approximately 30 minutes after which they start to decay. This is in agreement with the observations made in homopolymerisations with these catalysts where the catalyst supported on PQMS 3040 took longest time to achieve its peak activity in comparison to the times taken by the other two reference catalysts (see **Figure 6**). Therefore, it can be suggested that the lower the pore volume of the supported metallocene the lower the time it takes to achieve its peak activity. The overall low activity of PQMS 1732-supported reference catalyst is possibly a consequence of its biggest particle size (d_{50} = 128 µm), and slightly lower Zr content as compared to the other two reference catalysts which have very similar particle size (d_{50} of Grace 948 = 59 µm and d_{50} of PQMS 3040 = 45 µm) and Zr loadings.

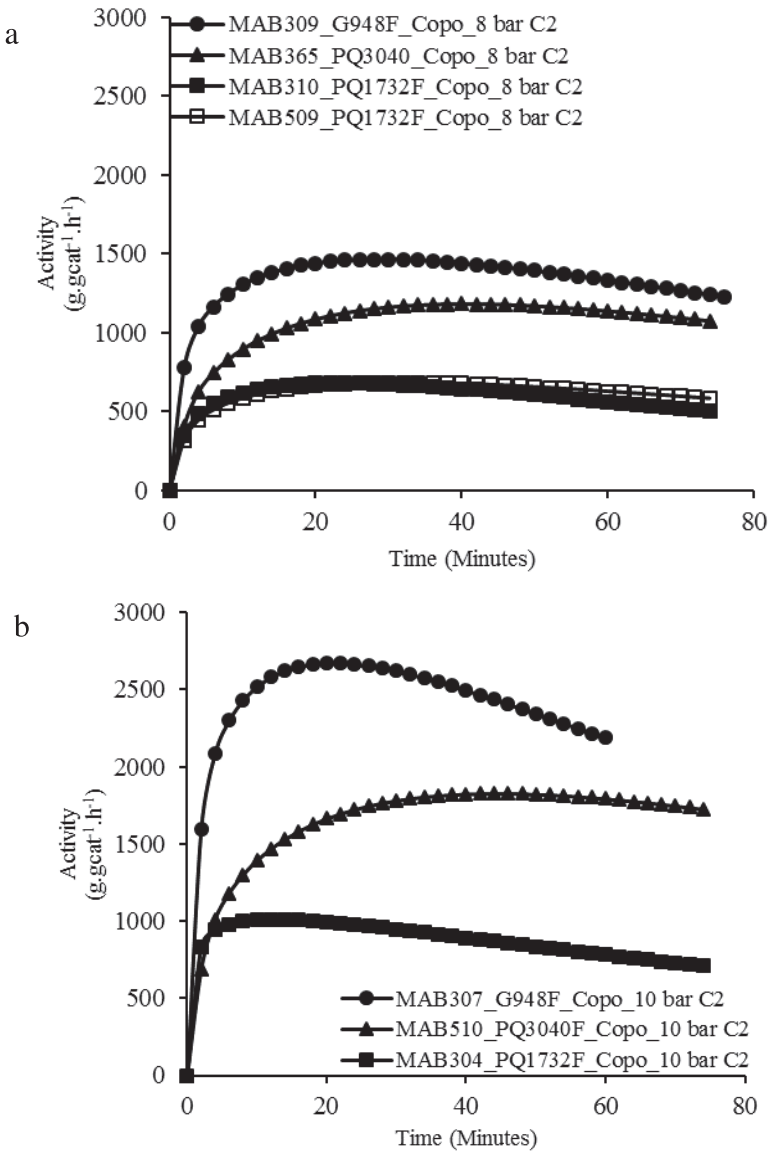

Figure 7. Comparison of ethylene/1-hexene slurry phase copolymerisation kinetic profiles obtained by the reference catalysts prepared by using full batch of each commercial silica at (a) 8 bar and (b) 10 bar ethylene pressure. 1-hexene added at the reaction start-up = 3 mL.

Molecular weight distribution (MWD) curves of these homo- and copolymer samples are compared in **Figure 8** which shows that all the supported catalysts produced polyethylenes with narrow MWD, and that the copolymers have lower molar masses than the corresponding homopolymers (as expected). Molar mass dispersity (Đ) of all the polyethylene samples is below 3 (see **Table 6**), indicating that the active species formed on all the three catalysts was similar and single-site nature of the zirconocene was preserved. Change of ethylene pressure inside the reactor does not impact the MWD of the respective homo- or copolymers, which suggests that the chain transfer with $(n\text{-BuCp})_2ZrCl_2$/MAO catalyst is assisted by the monomer. This observation is in agreement with the work of Soares et al.,[7] on soluble metallocene/MAO systems who suggested that, although the polymerization rates increase significantly by

increasing ethylene pressure, the MWD of the polyethylene samples produced by employing zirconocene catalysts does not change significantly and therefore, transfer to monomer is the dominant chain transfer mechanism in such polymerization. However, we shall see in the coming sections that this is not true for 'all' the zirconocenes as suggested by Soares et al.,[7]. The values of weight average molar mass (M_w), dispersity of molar mass (Đ) and melting temperature (T_m) of each polymer sample are shown in **Table 6** where it can be seen that the all of these values are identical for the polymers produced with the catalysts supported on Grace 948 and PQMS 3040 silicas, whereas the M_w values of the polyethylene samples produced by using PQMS 1732-supported catalyst are higher (see also **Figure 9**).

Table 6. M_w, Đ and T_m values of each HDPE sample produced in slurry phase homopolymerisations with three full silica based reference catalysts. x_{NMR} and x_{CEF} means comonomer content estimated by using 13C NMR and CEF, respectively.

Catalyst support	Sample Name	Ethylene Pressure (bar)	1-hexene used (ml)	Mw (g/mol)	Đ	T_m (°C)	x_{NMR} mol%	x_{CEF} mol%
Grace 948	MAB370	8	-	175000	2.4	136.0	-	
Grace 948	MAB371	8	-	150000	2.7	135.8	-	
Grace 948	MAB309	8	3	106000	2.3	128.7	-	0.9
Grace 948	MAB511	10	-	149000	2.5	-	-	
Grace 948	MAB307	10	3	103000	2.0	130.0	-	0.6
PQMS1732	MAB359	8	-	190000	2.6	135.1	-	
PQMS1732	MAB310	8	3	126000	2.4	130.5	-	0.6
PQMS1732	MAB509	8	3	114000	2.6	129.2	-	0.6
PQMS1732	MAB305	10	-	190000	2.3	137.3	-	
PQMS1732	MAB306	10	-	190000	2.7	135.1	-	
PQMS1732	MAB513	10	-	171000	2.5	137.0	-	
PQMS1732	MAB304	10	3	138000	2.3	129.0	-	0.4
PQMS3040	MAB320	8	-	148000	2.4	134.6	-	
PQMS3040	MAB365	8	3	90000	2.2	129.7	-	0.7
PQMS3040	MAB512	10	-	135000	2.1	136.8	-	-
PQMS3040	MAB510	10	3	94000	2.1	129.5	0.5	0.7

Since the molar mass dispersity of all the samples is very similar, indicating the formation of similar active species on the three reference catalysts independent of the support, the most

probable explanation for such a difference in MWDs can be attributed to the fact that hydrogen can be generated in-situ during ethylene (co)-polymerizations with metallocene/MAO catalysts,[8-11] and due to low activity of PQMS 1732-supported catalyst ,the amount of hydrogen generated inside the reactor was lower than in the other cases. This consequently led to higher molar masses of the polyethylenes produced with this catalyst. In simple words, all the mechanisms proposed for in-situ hydrogen generation involve interaction of the metal atom (i.e., zirconium in the present case) with the growing polymer chain leading to allylic activation.[8-11] As the catalyst supported on PQMS 1732 has the lowest activity, it is not unreasonable to assume that less zirconium interacted with the growing polymer chains as compared to the other two reference catalysts (which indirectly means that less allylic activation was there in the case of polymerizations done with the reference catalyst of PQMS 1732 silica) leading to low amount of in-situ hydrogen generated and therefore, higher molar mass polyethylenes. We will present the related proof of in-situ hydrogen generation in the next chapter. It should be noted that two types of chain transfer reactions seem to have occurred during these polymerizations; i) chain transfer assisted by the monomer whose confirmation comes from insensitivity of MWD to changes in ethylene pressure and ii) chain transfer to hydrogen due to in-situ hydrogen generation which acts as a chain transfer agent.

Such differences in MWDs of the resulting polyethylenes can also be explained by considering the physical properties of the final catalysts. In this regard, pore confinement effect leading to extrusion polymerization[12] can also be considered as a reason for the higher molar mass of the polyethylenes produced with PQMS 1732 supported reference catalyst since the pore width of this reference catalyst is the least among the series of three where the other two supported catalysts possess very similar pore diameter (see **Table 3** to **Table 5**).

a

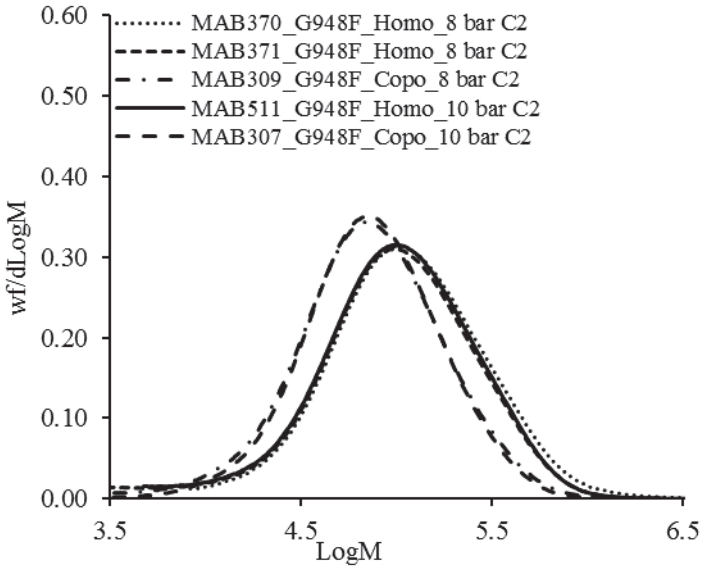

b

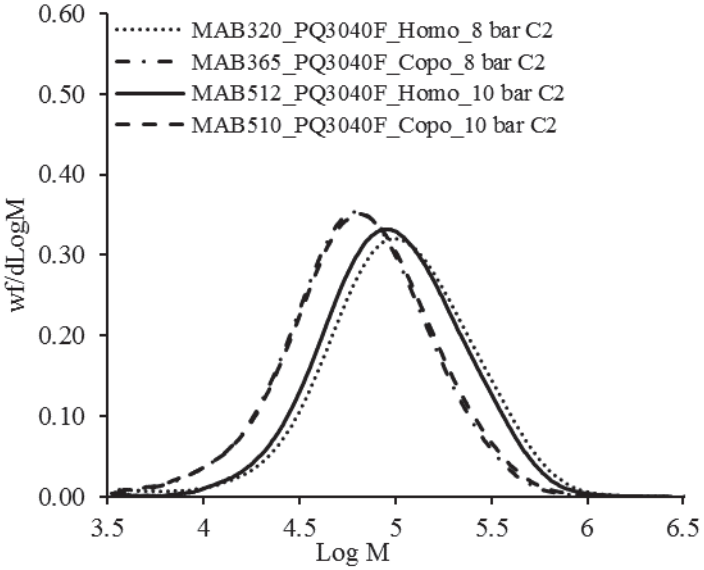

c

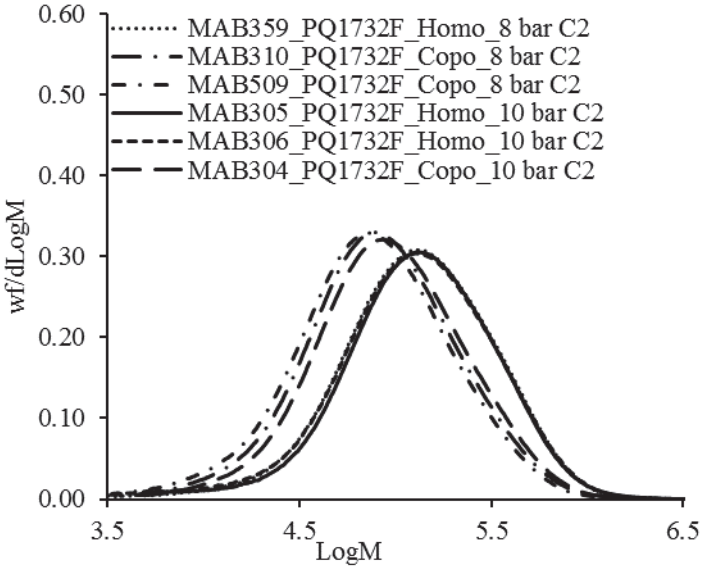

Figure 8. MWD of the homo- and copolymer produced in slurry polymerisations with three reference catalysts.

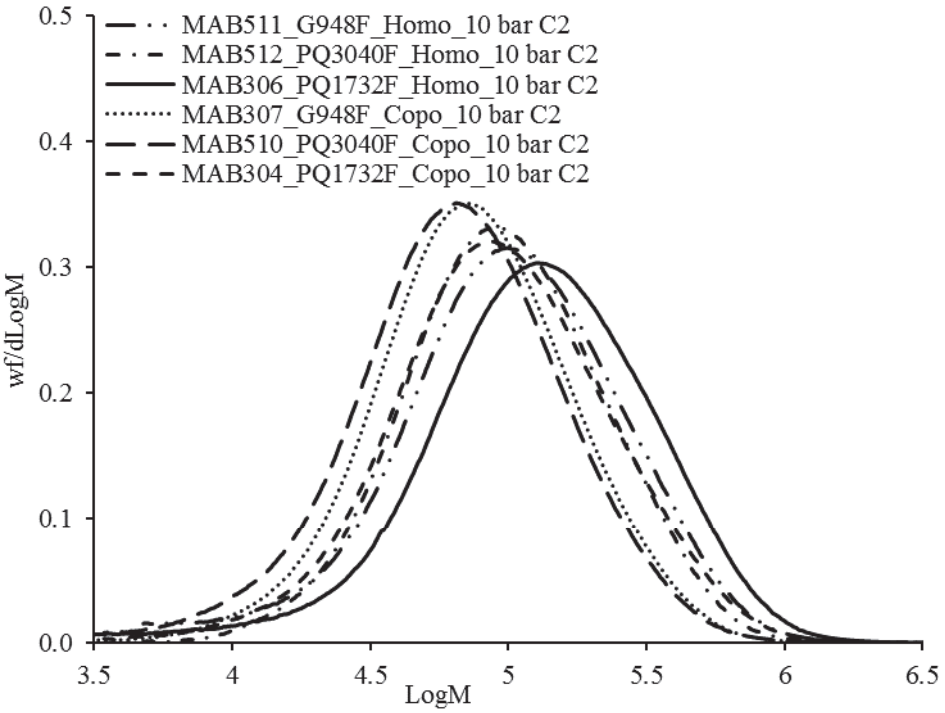

Figure 9. Comparison of the MWD of homo- and copolymers produced with three silica supported $(n\text{-BuCp})_2ZrCl_2$/MAO catalysts in ethylene slurry phase polymerizations at 10 bar ethylene pressure.

The particle size distribution (PSD) of the polymer samples replicated the corresponding silica support morphology, as expected (see **Figure S1** of **Appendix 1** of this chapter).

The external and internal morphology of the three commercial silica supports is shown in **Figure 10**. All the silica particles have spherical geometry. Grace 948 silica has cracks on its surface, whereas the other two commercial silica appear to have smooth particle surfaces (possibly corresponding to the presence of well-connected pores). The cracks are possibly a fractional part of the ones which the mercury porosimetery detected in Grace 948 silica as the pores above 10 nm (see **Figure 1**). Cross-sectional images of each silica show that the internal morphology of both the PQMS silica is very similar, showing uniform structures, whereas Grace 948 silica shows a very different internal morphology from that of both the PQMS silica. Water glass and silica granulates are obvious only in the cross-sectional image of Grace 948 particle which indicates that spray-drying process was employed in the synthesis of this silica in contrast to the emulsion process which was, probably, employed for the synthesis of PQMS silicas. Water glass is an alkali metal silicate which serves the purpose of cement or glue for silica granulates. The void space between the granulates is called interstitial void space which starts from the surface of the particle and penetrates up to the centre of the particle which is

evident in **Figure 10b** and **Figure 10c**.[4] Such interstitial voids definitely facilitate the metallocene/MAO transport during catalyst synthesis and monomer transport during early stages of polymerization to the catalyst particle centre. In the case of each PQMS silica no such voids are present neither on the surface nor in the particle interior.

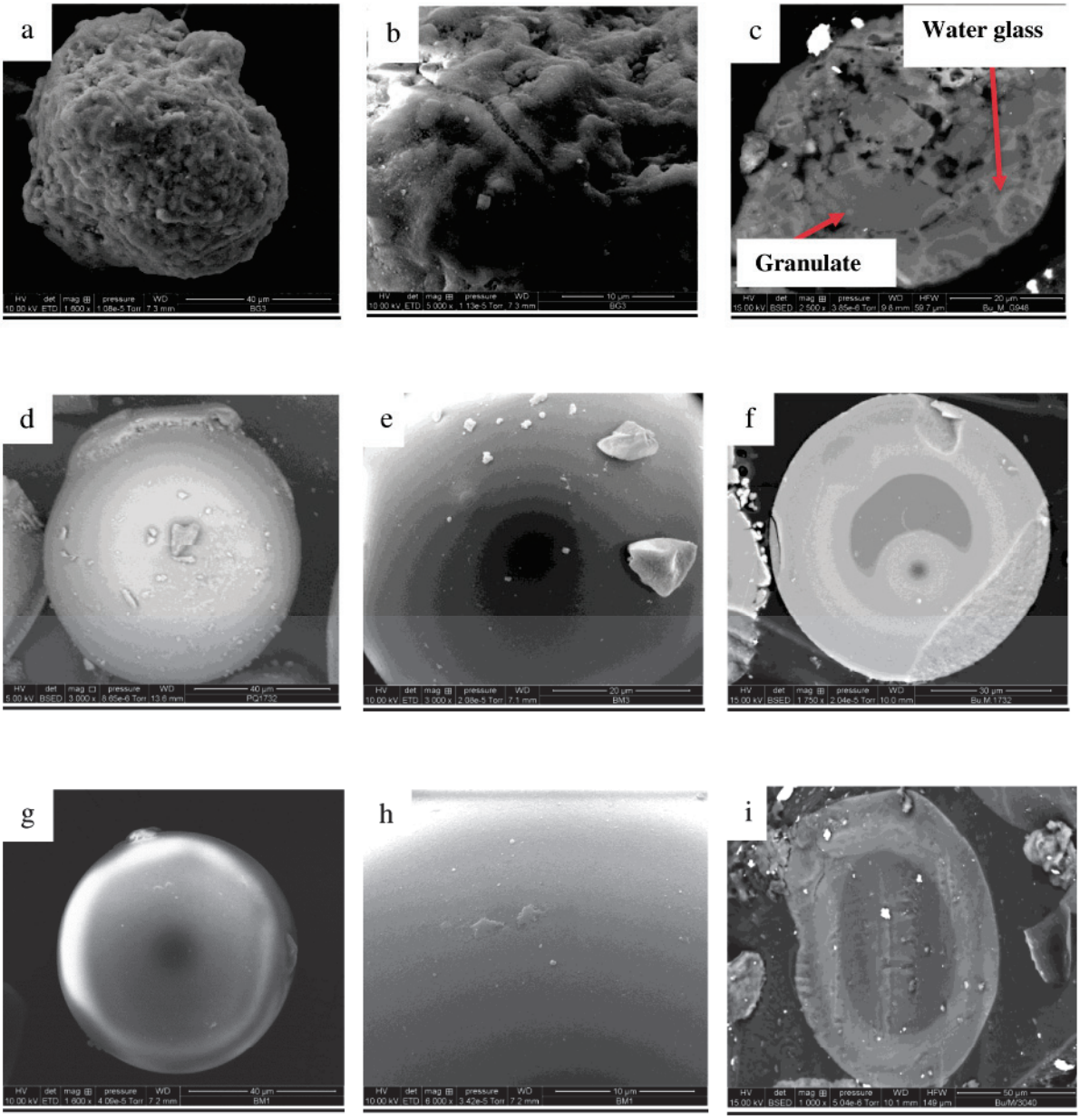

Figure 10. SEM micrographs of three commercial silica showing external and internal morphology of the particles. Grace 948 (a to c), PQMS1732 (e to f), PQMS3040 (g to i). Last image of each series show cross-section of one of the particles from the respective silica.

More discussion about the distribution of Al on these silica supports in correlation with their morphology will be made in the coming sections of this chapter. For the current section, we can use this morphological information and BET measurements to explain the differences in

the activation of (n-BuCp)$_2$ZrCl$_2$/MAO supported on these three silica as shown in **Figure 10**. Keeping in mind that all the thermodynamic effects (due to sorption etc.) and chemical effects (due to TIBA etc.) were similar due to the same reaction conditions, faster activation of Grace 948- and PQMS 1732-supported catalysts than the one supported on PQMS 3040 silica can be attributed to the lower pore volumes of the two former supports (1.7 mL.g^{-1} for Grace 948 and 1.4 mL.g^{-1} for PQMS 1732 silica) than the latter (3.0 mL.g^{-1} for PQMS 3040 silica). Catalyst particle fragmentation step starts (and completes) early when the pore volume of the particle is low leading to faster exposure (not generation) of the active sites present inside the catalyst particle and therefore, the catalyst particles with lower pore volume activates faster than those with higher pore volumes.

A drop in the rate of polymerization can obviously have many causes, one of which might be physical. One reason that PQMS 1732 silica-supported catalyst does not reach the same levels of activity as the Grace 948 supported catalyst might be attributable to the fact that the PQMS support is more uniform and might break up into small fragments with no/little porosity, whereas the Grace on the other had has macroporosity to begin with, and this does not totally disappear. As we shall see in the coming sections also, deactivation rate of the catalyst supported on PQMS 1732 silica is significantly less in copolymerizations as compared to its deactivation rate in homopolymeriztaions which can be attributed to reduced polymer crystallinity in copolymerizations due to comonomer incorporation.

3.2. Effect of Silica Support Particle Size in Slurry Phase Ethylene Homopolymerisations and Ethylene/1-Hexene Copolymerisation

The effect of silica support particle size on the reaction kinetics of ethylene (co)-polymerization(s) was analysed by using catalysts supported on different sieved fractions of each commercial silica. The benefit of sieving the full batch of a given silica is that one can obtain fractions of various particle sizes with the other physical properties (like pore diameter, pore volume and surface area) very similar. Metal loadings of these catalysts and their physical properties, shown in **Table 3** to **Table 5**, will be used to explain the observed results. Discussing the results obtained for each silica separately will be helpful for better understanding.

3.2.1. Effect of Particle Size studied with Grace 948 Silica Based Catalysts

As discussed in the previous **Chapter 3**, that polymerization protocol can have a significant impact on the slurry phase polymerizations due to the leaching of catalyst from the support upon pre-contact with an alkyl aluminium like TIBA, it is important to start this section with the demonstration of the impact of this phenomenon on ethylene polymerization kinetic profiles obtained by using catalysts of different sizes obtained by sieving Grace 948 silica. A comparison of the kinetic profiles obtained by the polymerization protocols MSP-1 (involving pre-contact between supported catalyst and TIBA) and MSP-2 (involving no pre-contact between supported catalyst and TIBA) for three catalysts of different sizes is shown in **Figure 11** and **Figure 12**, respectively. It is obvious that with MSP-1 all the catalysts show higher instantaneous activities and rapid deactivation after achieving the maximum polymerization rate as compared to those obtained via MSP-2. It can also be seen that when MSP-1 was used, the activation of 63 µm fraction based catalyst (i.e., BG-3) is actually faster than the other two catalysts of smaller size and for the first 18 minutes of reaction time.

On the other hand, when polymerizations were conducted with the same catalysts by following MSP-2 protocol, the instantaneous reaction rate was found to be clearly dependent on the silica particle size, witth the bigger catalyst particles showing lower activity then the smaller ones. In addition, with MSP-2 all the catalysts showed similar activation and deactivation behaviour (compare **Figure 11** and **Figure 12**). The morphology of the HDPE samples produced with both polymerization protocols is shown in **Figure 13**, which shows that spherical polymer particles were produced with MSP-2 protocol, whereas HDPE film (covering the reactor walls and stirrer) was produced with MSP-1 polymerization protocol. The same morphology

difference was also noticed for the other HDPE samples produced with the two polymerization protocols but are not shown here.

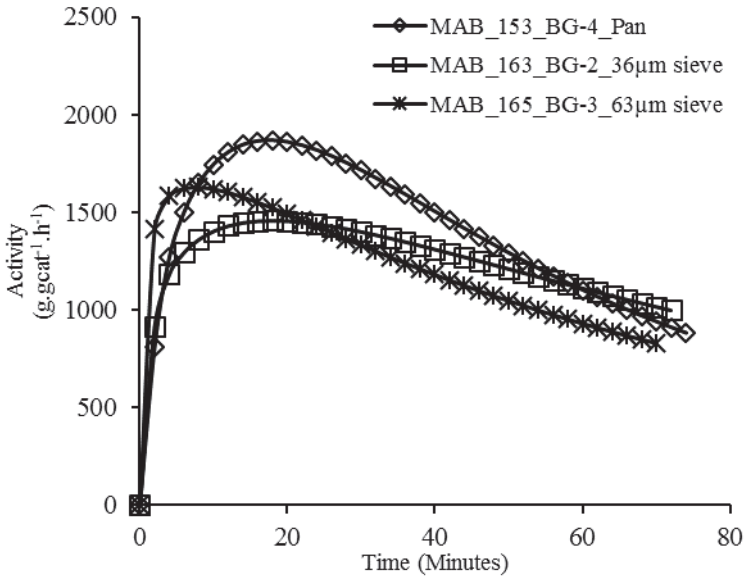

Figure 11. Ethylene polymerisation kinetic profiles obtained by using Grace 948 based catalysts of different sizes via MSP-1.

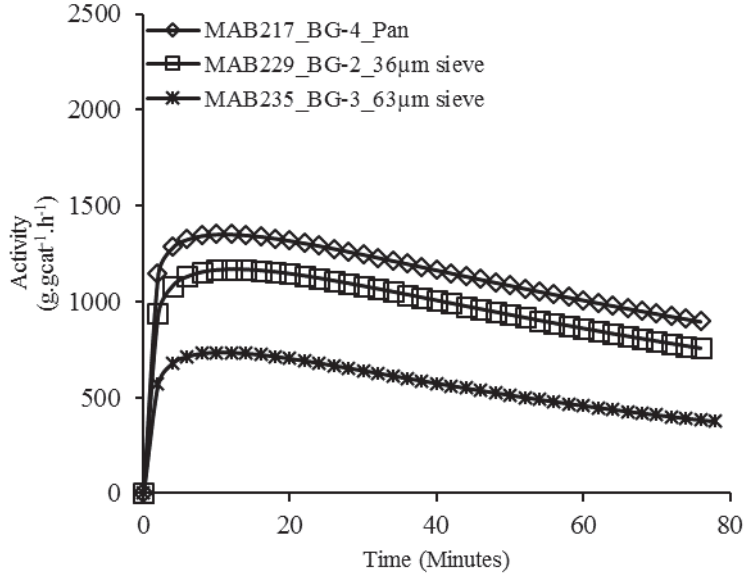

Figure 12. Ethylene polymerisation kinetic profiles obtained by using Grace 948 based catalysts of different sizes via MSP-2.

Figure 13. Morphology of the HDPE samples produced by using MSP-1 protocol (a) and MSP-2 protocol (b). Catalyst used for both polymerizations was BG-4.

Fast activation and rapid deactivation of the catalysts after achieving maximum instantaneous reaction rate along with film like polymer morphology of the samples produced via MSP-1 clearly shows the occurrence of catalyst leaching from the silica support when there is a pre-contact between the supported metallocene catalysts and TIBA as discussed in the previous chapter. On the other hand, in MSP-2 similar activation and slight deactivation after achieving the maximum instantaneous reaction rate with spherical polymer particles indicates no sign of catalyst leaching from the silica support. Here, it will be important to highlight that: i) for Grace 948 silica the bigger particles seem to leach more than the smaller ones due to faster activation of BG-3 catalyst as compared to the smaller sized catalysts which appear to activate similarly (see **Figure 11**); and ii) with MSP-1 or (the case where the aluminium alkyl scavenger get in contact with supported metallocene), it is not possible to see the impact of physical properties of silica support on the reaction kinetics and morphology due to catalyst leaching. In case of leaching, the faster activation can be attributed to the presence of desorbed metallocene/MAO (or metallocene/MMAO) in the diluent.[13] The crystallinity and MWD of the HDPE samples showed similar values and therefore, they are not shown here.

Based on these results, MSP-2 was selected for the rest of the polymerization unless otherwise mentioned. **Figure 14** shows the effect of silica support particle size on the instantaneous activity of $(n\text{-BuCp})_2ZrCl_2$/MAO supported catalyst in homo- and copolymerisations at 8 bar ethylene pressure. It should be noted that 3 mL of 1-hexene were used for copolymerisation reactions. A decrease in catalytic activity with increasing silica particle size is evident in both polymerization types, with the activity of full-silica-batch based catalyst laying close to the catalyst prepared with 36µm sieve fraction (i.e., BG-2 catalyst). In case of copolymerisations, productivity boost was observed to be the highest for the catalyst with the smallest particle size

(i.e., BG-4) while the other catalysts showed a productivity increase of approximately 20% (productivities are not shown here for the sake of brevity).

a

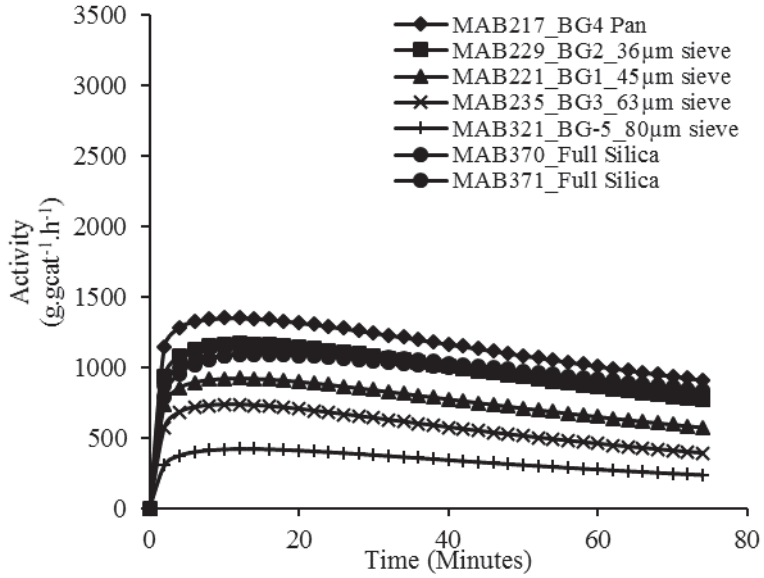

b

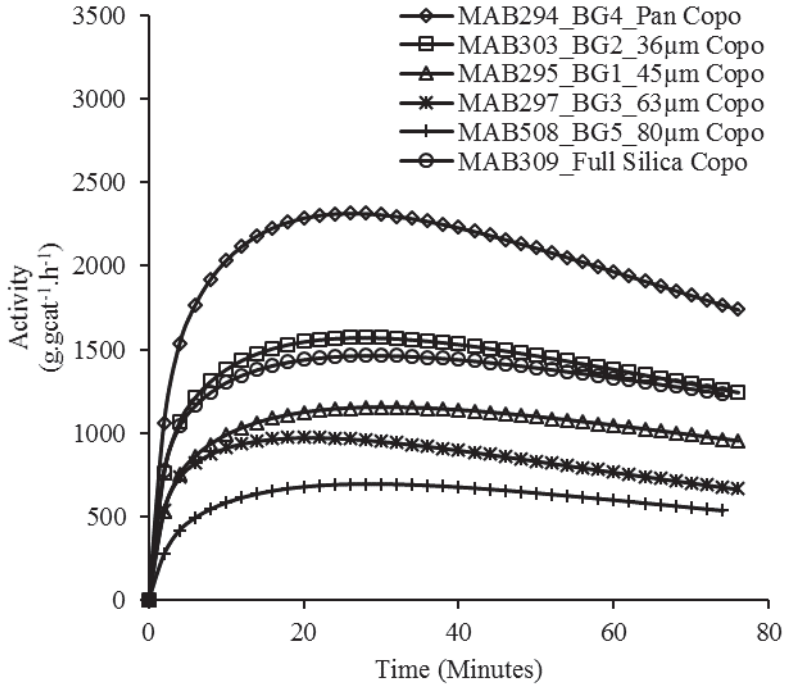

Figure 14. Effect of catalyst particle size on the instantaneous activity of each catalyst in a) homopolymerisations at 8 bar ethylene pressure and b) copolymerisations at 8 bar ethylene pressure and 3 mL 1-hexene.

Addition of 1-hexene altered the activation behaviour of the catalysts in such a way that during the initial instants of reaction start-up, all the catalysts showed less productivity (and consequently activity) as compared to their productivities in corresponding

homopolymerisations which is agreement with the results obtained by Ystenes et al.,[14] who conducted slurry phase ethylene copolymerisations with various comonomers by using Ziegler-Natta catalysts and Kumkaew et al.,[6,15] who used silica supported (n-BuCp)$_2$ZrCl$_2$/MAO catalysts in gas phase ethylene/1-hexene copolymerisations. No specific trend could be established between the catalyst particle size and the time it took in achieving an activity higher than then its activity in homopolymerisations. This time increased from 2 to 14 minutes as the catalyst particle size increased from pan fraction to 45 µm fraction, whereas, the catalysts made from 63 µm and 80 µm fractions took 2 only minutes to achieve activities higher than in corresponding homopolymerisations. It can be suggested that the activities of 63 µm and 80 µm fractions based catalysts (i.e., BG-3 and BG-5, respectively) in homopolymerisations were significantly less than those of smaller sized catalysts which allowed these bigger sized catalyst particles to achieve activities higher than those in homopolymerisations in just over 2 minutes of reaction start-up.

The dependence of the MWD of each homo- and copolymer on the catalyst particle size is shown in **Figure 15** which does not show any significant impact of support particle size on the MWD of the polymer samples. MWD of the copolymers seems to be narrower than that of the corresponding homopolymers and the Đ value of all the samples is below 3 (see **Table 7**) indicating that the single-site behaviour of (n-BuCp)$_2$ZrCl$_2$/MAO catalyst system and the active site type is not affected by particle size of the silica support. However, a minute difference can be seen between the MWD of homo- and copolymers produced with BG-3 (63 µm fraction) and BG-5 (80 µm fraction) catalysts and those of the polymers produced with smaller sized catalysts (i.e., BG-4, BG-2 and BG-1) i.e., the molar mass of polyethylene samples produced with bigger (but less active) catalyst particles (i.e., BG-3 and BG-5) are slightly higher than the molar mass of the polyethylenes produced with smaller in size (but more active) catalysts (compare MWDs in **Figure 15a** and **b**). This observation is coherent with the one made in the previous section where MWD of the polyethylene samples produced with the catalysts supported on full batches of three commercial silica were compared (i.e., **Figure 8** and **Figure 9**) and it was noticed that the molar mass of the polymer produced with the catalyst supported on largest particle size silica (i.e., PQMS 1732) was higher than that of the others produced with relatively smaller particles (i.e., the catalysts supported on Grace 948 silica and PQMS 3040 silicas).

a

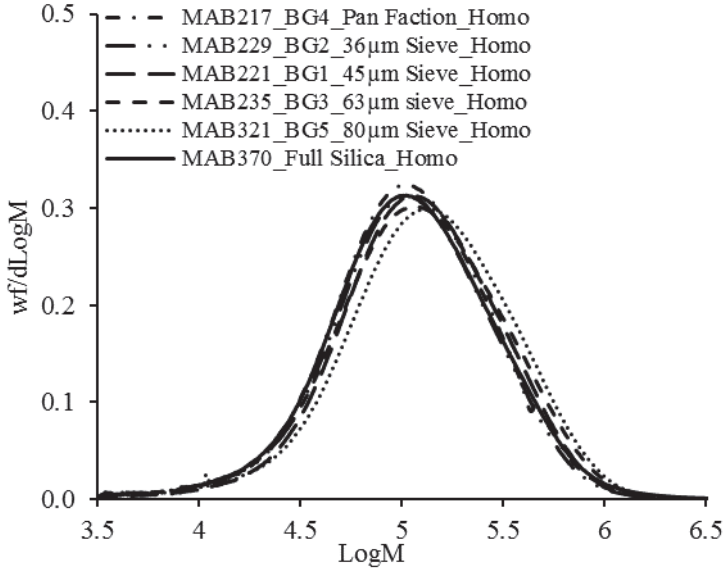

b

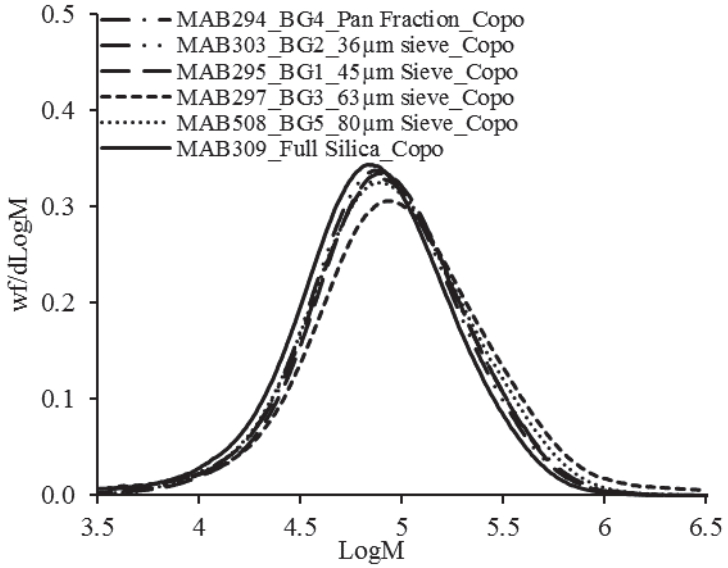

Figure 15. Effect of catalyst particle size on the MWD of (a) homopolymers and (b) copolymers produced in slurry phase polymerisations. Catalyst supported on different fractions and full batch of Grace 948 silica.

Table 7. M_w, Đ and T_m values of each HDPE sample produced in slurry phase homopolymerisations with the catalysts based upon Grace 948 Silica. P_{C2} refers to ethylene pressure, $A_{1\text{-hexene}}$ refers to the initial amounts of 1-hexene injected into the reactor, respectively. x_{NMR} and x_{CEF} means comonomer content estimated by using ^{13}C NMR and CEF, respectively. FS means full silica.

Catalyst Name	Particle size (µm)	Sample Name	P_{C2} (bar)	$A_{1\text{-hexene}}$ (ml)	M_w (g/mol)	Đ	T_m (°C)	x_{NMR} mol%	x_{CEF} mol%
BG-4	Pan	MAB217	8	-	160000	2.4	134.5	-	-
BG-4	Pan	MAB294	8	3	125000	2.2	129.5	-	0.6
BG-2	36≤dp<45	MAB229	8	-	160000	2.4	134.5	-	-
BG-2	36≤dp<36	MAB303	8	3	120000	2.4	129.2	-	0.6
BG-1	45≤dp<63	MAB221	8	-	175000	2.5	134.8	-	-
BG-1	45≤dp<63	MAB295	8	3	120000	2.3	130.7	-	0.6
BG-3	63≤dp<80	MAB235	8	-	185000	2.6	134.5	-	-
BG-3	63≤dp<80	MAB297	8	3	170000	2.8	129.2	-	0.5
BG-5	80≤dp<100	MAB321	8	-	200000	2.7	134.7	-	-
BG-5	80≤dp<100	MAB508	8	3	130000	2.4	131.8	0.5	0.6
Bu/M/G948	FS	MAB370	8	-	175000	2.4	134.2	-	-
Bu/M/G948	FS	MAB309	8	3	110000	2.3	127.8	-	0.9

This point will be discussed in more detail in the next chapter, but we believe that this difference in MWDs can be attributed to the fact that hydrogen is generated in-situ during ethylene polymerisations catalysed by $(n\text{-BuCp})_2ZrCl_2$/MAO which can then act as a chain transfer agent, as shown by other also [8-10] for different metallocene/MAO systems. In the case of BG-3 and BG-5 catalysts it is possible that less in-situ hydrogen is generated due to their low activity. This might be what caused the MWD of the polymers produced by these catalysts to be broader than those produced with smaller sized catalysts.

Furthermore, it is possible that this difference in the MWD of polyethylenes produced by the catalyst particles of different sizes can be attributed to the presence of mass transfer resistance which is higher in bigger catalyst particles as compared to that in smaller ones. Due to the bigger particle sizes, BG-3 and BG-5 catalyst particles probably have the highest (co)-monomer(s) concentration gradient(s) within them which led to low instantaneous activity and least in-situ hydrogen concentration which, consequently, produced polyethylenes (i.e., homo-

and copolymers) with molar masses slightly higher than the molar masses of the polyethylenes produced with smaller in size catalyst particles (for which the concentration gradients were probably lower leading to higher activities and more in-situ hydrogen generation). The modelling effort of Floyd et al.,[16] also suggests that the impact of mass transfer resistance is more significant on the reaction rate profiles than on the MWD of polyethylene produced in slurry phase process using supported catalysts. Finally, in copolymerisations the shift of MWD curves towards lower molar masses is due to increased chain transfer reactions in the presence of 1-hexene (as well as due to the hydrogen generated in-situ) in the reaction mixture and its incorporation in the growing polymer chains.[17]

Table 7 shows that the melting temperature and comonomer content does not vary with changes in the catalyst particle size and that the comonomer measurements done with ^{13}C NMR (see **Figure S2** in **Appendix 1** for a typical ^{13}C NMR spectrum) are in good agreement with those performed by using CEF.

In order to analyse the distribution of active sites inside the catalyst particles of different sizes, SEM-EDX analysis was performed on the micro-tomed samples of the final catalysts. The results obtained for Grace 948-supported particles are shown in **Figure 16**. Due to zirconium (Zr) loading of these catalysts below the detection limit of SEM-EDX, aluminium (Al) mapping was only possible which also provided information about the presence of active sites throughout the particles because during the synthesis of these supported catalysts the metallocene was mixed with MAO prior to its fixation on silica. Therefore, it is reasonable to assume that Zr distribution is also similar to that of Al. It can be seen in **Figure 16** that Al distribution (and therefore, Zr distribution also) was nearly uniform throughout the catalyst particles of small and big sizes and the particles of the catalyst prepared by using full batch of silica which allows full surface participation during the reactions. In addition, it is also obvious that the internal morphology of all the catalyst particles is same showing interstitial voids which probably offers less resistance to (co)-monomer(s) and diluent diffusion during reaction. Since these catalysts were made independently, similarity in Al distribution indicates also the reproducibility of the synthesis procedure.

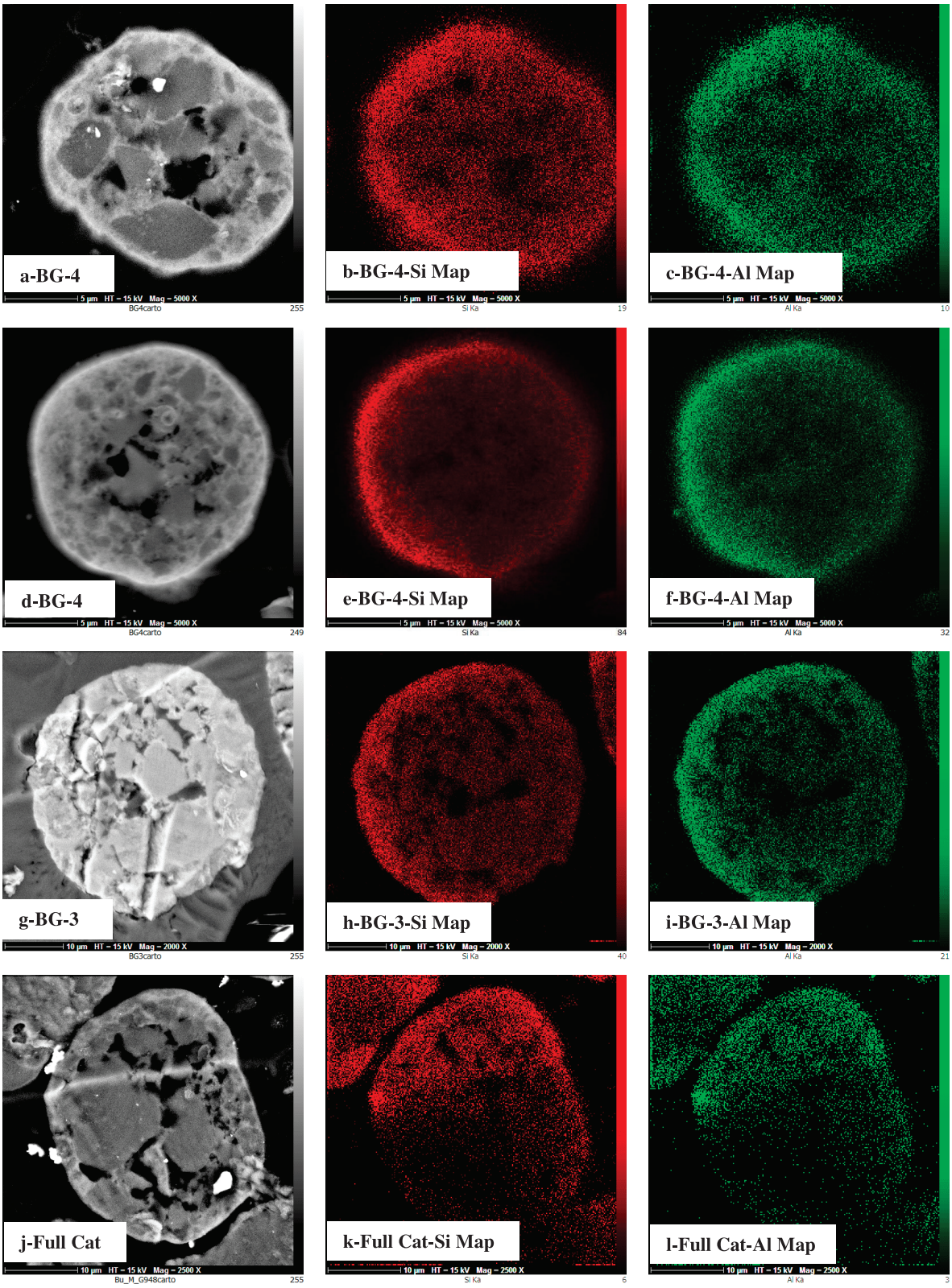

Figure 16. SEM-EDX micrographs showing Silicon (Si) and Aluminium (Al) distribution inside the particles of BG-4 (Pan fraction supported) catalyst from a to f, BG-3 (63 µm fraction supported) catalyst from g to i and full silica batch supported catalyst from j to l.

Morphology of the HDPE samples produced by BG-4 and BG-2 catalysts is shown in **Figure 17** where it can be observed that polymer particles possess nearly spherical shape. Higher magnification images (**Figure 17b** and **d**) clearly show the presence of small globules held together by fibrous polymer which, most probably, indicates that the fragments of the silica support particle were held together by the polymer being formed on it and therefore, the finally obtained polymer particles were nearly spherical in shape.

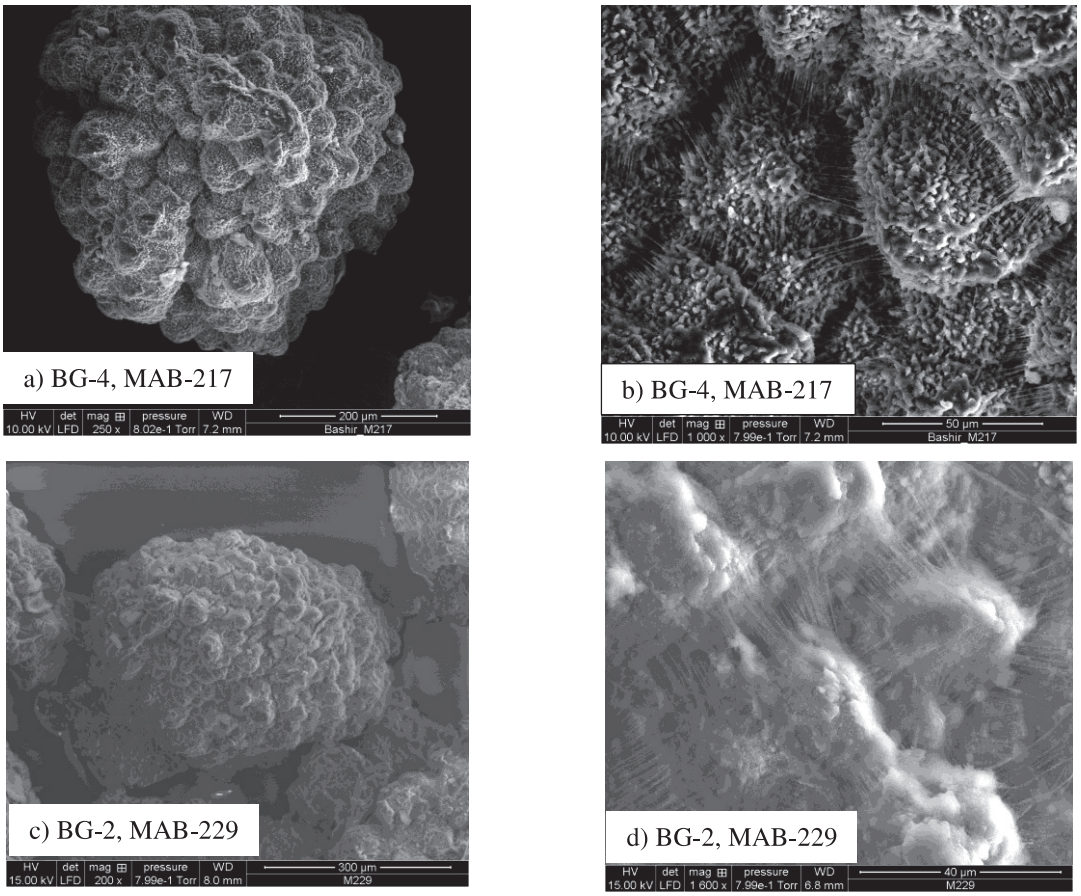

Figure 17. SEM micrographs showing morphology of the HDPE samples produced by different sized catalysts of Grace 948 silica.

3.2.2. Effect of Particle Size Studied with PQMS 1732 Silica Based Catalysts

The effect of silica support particle size on the catalytic activity of supported (n-BuCp)$_2$ZrCl$_2$/MAO catalyst system was further analysed by using three different sieved fractions of PQMS 1732 commercial silica. The instantaneous activities as a function to time and particle size in slurry phase ethylene homo- and copolymerisations at two different ethylene pressures are shown in **Figure 18** . In agreement with the results obtained with Grace

948 silica, it can be seen that decreasing the silica support particle size enhances the instantaneous activity of the supported metallocene at both monomer pressures. The activity of full batch based catalyst is very similar to the catalyst supported on 63 µm sieved fraction of PQMS 1732 silica. Besides similar shape of the kinetic profiles, an increase in catalytic activity with increasing ethylene pressure, for all the catalysts, is also obvious. In homopolymerisations, increasing ethylene pressure by 2 bar increased the productivity of BP-1 and BP-2 catalysts by very similar amount (i.e., on average 30 %), whereas this increment was about 36 % for the largest in size BP-3 catalyst and only 19 % for the catalyst supported on the full batch of silica. On the other hand, during copolymerisations equal pressure increment resulted in approximately 40 % rise in the productivity of all the catalysts which indicates that the increasing ethylene pressure has a more significant effect on the productivity of smaller catalyst particles in copolymerisations than its effect on the productivity of bigger catalyst particles.

At constant ethylene pressure (e.g., 10 bar), addition of 3 mL of 1-hexene into the reactor increased the productivity of BP-1 catalyst by 30 %, BP-2 catalyst by 24 % and BP-3 catalyst by only 17 % on average. More or less similar trend can also be observed at 8 bar ethylene pressure. Furthermore, it can be noticed that during homopolymerisations all the catalyst showed maximum instantaneous polymerization rate in the first five minutes followed by continuous deactivation until the end of reaction time. Deactivation rate of these catalysts seems to be higher than those supported on Grace 948 silica, probably due to different structural features of this silica, and possibly also linked to the particle growth and fragmentation (although this last point is difficult to prove). In copolymerisations, the activation and deactivation rates of these catalysts reduced as compared to their activation and deactivation rates in corresponding homopolymerisations, as shown for one catalyst in **Figure 19**.

The observation regarding slow activation rate in copolymerisations (not obvious in **Figure 19** but was observed while comparing other reactions) is in agreement with the one made in the previously discussed case of Grace 948 silica based catalysts and can be attributed to the presence of 1-hexene at the active sites which reduces the initial polymerisation rate of supported $(n\text{-BuCp})_2ZrCl_2$/MAO catalyst system by altering the nature of the active sites as noticed by Kumkaew et al.,[6] for the same supported catalyst in gas phase ethylene/1-hexene copolymerisations. However, the reduced deactivation rate of these supported catalysts in copolymerisations can be, probably, attributed to the reduced crystallinity due to 1-hexene

incorporation into polyethylene backbone which allows better transportation of ethylene and 1-hexene to the active sites.

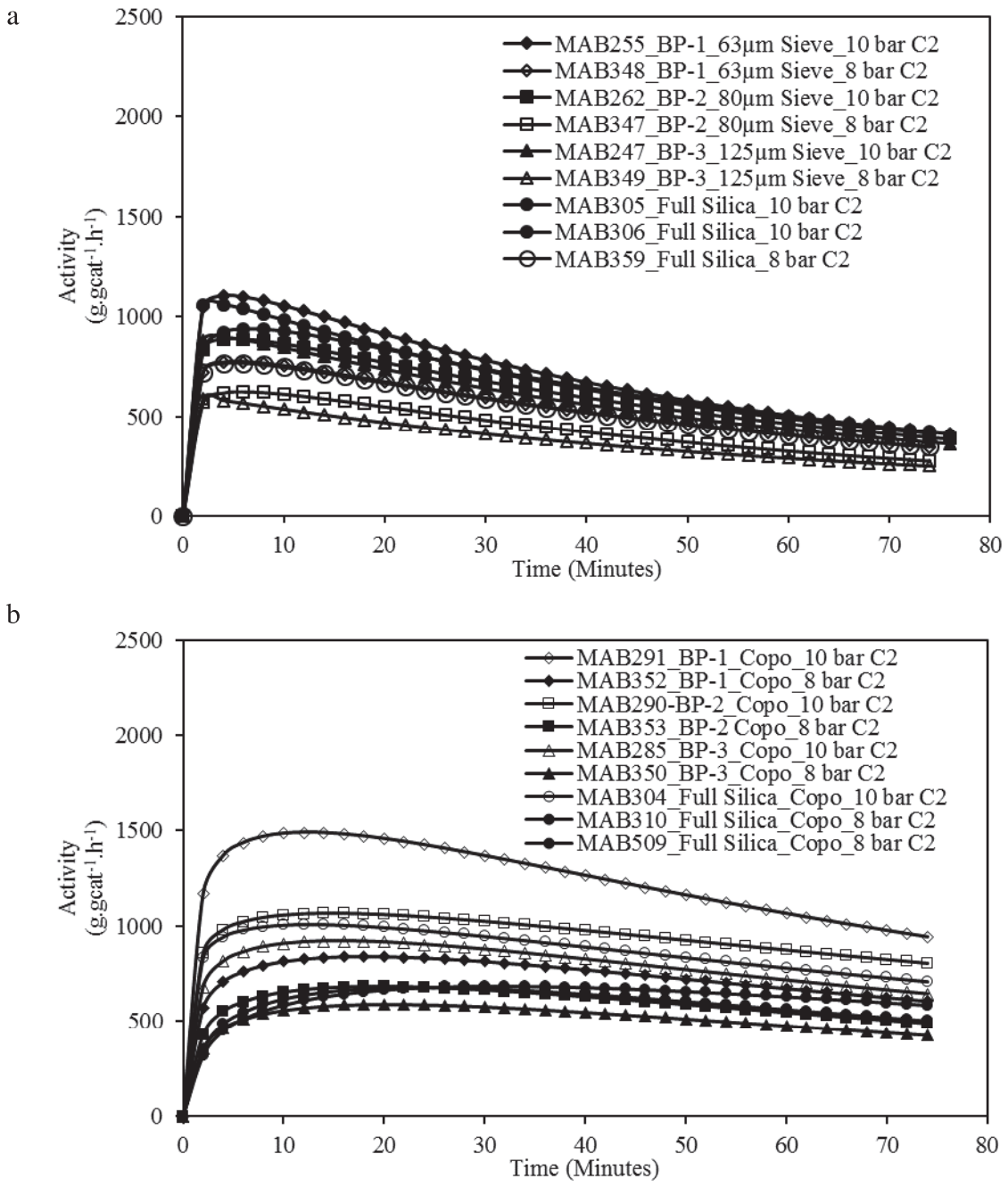

Figure 18. Effect of catalyst particle size on the instantaneous activity of each catalyst in a) homopolymerisations and b) copolymerisations at different ethylene pressures and 3 mL 1-hexene. Catalysts supported on PQMS1732 full silica and its different sieved fractions.

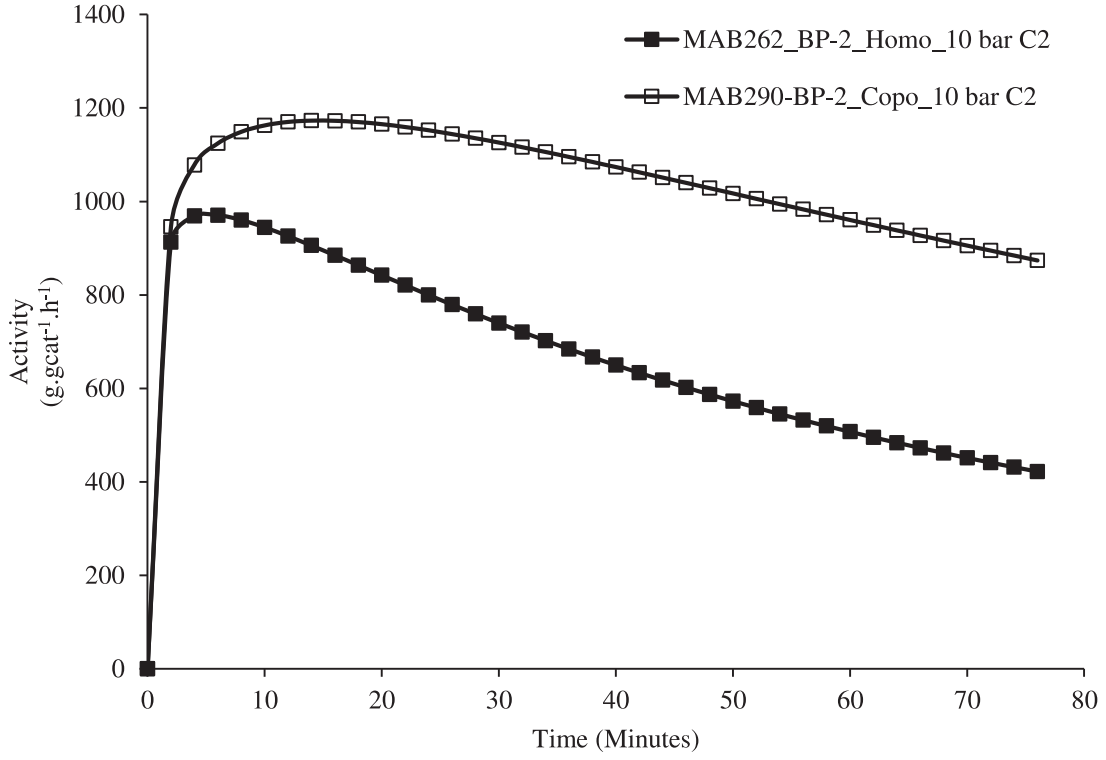

Figure 19. Comparison of ethylene homopolymerisation and ethylene/1-hexene copolymerisation kinetic profiles obtained with BP-2 catalyst at 10 bar ethylene pressure.

MWD curves of the homo- and copolymer samples produced at 8 and 10 bar of ethylene pressure are shown in **Figure 20**. For this silica, it appears that neither the support particle size, nor the reactor pressure has a significant effect on the MWD of both homo- and copolymers. The lack of pressure effect is coherent with the results discussed in the previous section where MWD curves of the polymers obtained by using full batches of silica were discussed (see **Figure 8**). Addition of 1-hexene in the reactor produces copolymer of ethylene-1-hexene with molar mass and molar mass dispersity less than the corresponding HDPE sample (see **Table 8**). This observation is in-line with the one made for Grace 948-supported catalysts and can be attributed to the fact that the presence of 1-hexene (and hydrogen generated in-situ) at the active sites enhances the chain transfer reactions and therefore, shifts the MWD of copolymers towards lower molar mass side. Once again, the molar mass dispersity value remained below 3 and very similar for all the catalysts of different sizes indicating the single-site behaviour of all the supported catalysts. Unlike the previously studied case of Grace 948 silica, the MWD curves of polyethylene samples produced with the catalysts of biggest (i.e., BP-3) and smallest

(BP-1) sizes overlap on each other despite considerable difference in their activities. Crystalline melting temperature of the HDPE and copolymer samples also seems to be unchanged by the catalyst particle size as indicated in **Table 8**. Some (not all for the sake of clarity) of the representative second heating DSC curves are shown in **Figure 21**.

a

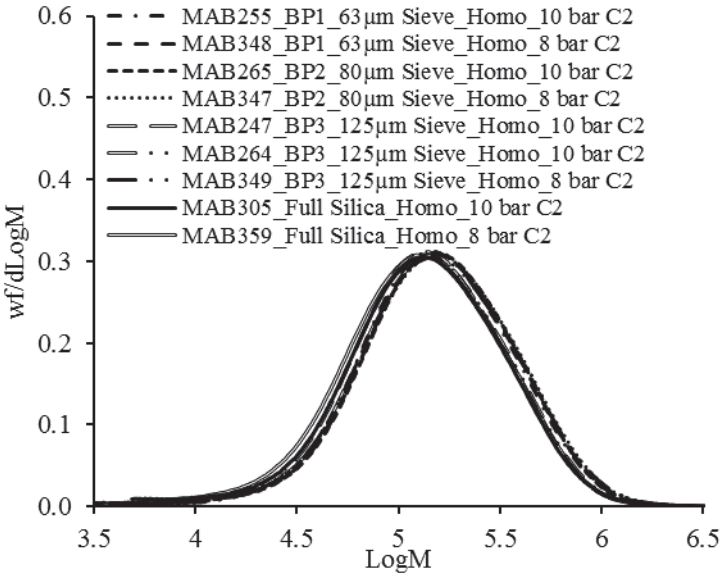

b

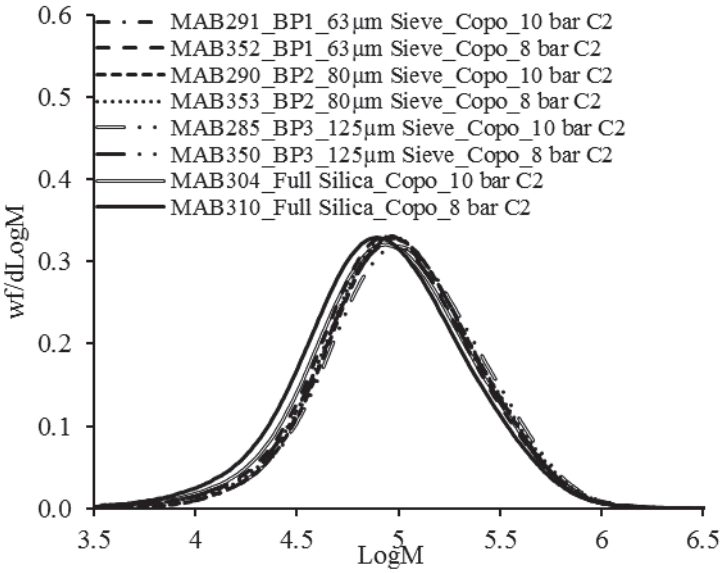

Figure 20. Effect of catalyst particle size and ethylene pressure on the MWD of (a) homopolymers and (b) copolymers produced in slurry phase polymerisations. Catalyst supported on different fractions and full batch of PQMS1732 silica.

Table 8. Weight average molar mass (M_w), dispersity of molar masses (Đ) and melting temperature (T_m) of the homo- and copolymer samples produced by using supported catalysts based on PQMS1732 silica. P_{C2} refers to ethylene pressure, $A_{1\text{-hexene}}$ refers to the initial amounts of 1-hexene injected into the reactor. x_{NMR} and x_{CEF} means comonomer content estimated by using ^{13}C NMR and CEF, respectively. FS means full silica.

Catalyst Name	Particle size (µm)	Sample Name	P_{C2} (bar)	$A_{1\text{-hexene}}$ (ml)	M_w (g/mol)	Đ	T_m (°C)	x_{NMR} mol%	x_{CEF} mol%
BP-1	63≤dp<80	MAB348	8	-	220000	2.2	135.0	-	-
BP-1	63≤dp<80	MAB352	8	3	140000	2.1	129.3	-	0.6
BP-1	63≤dp<80	MAB255	10	-	220000	2.1	136.1	-	-
BP-1	63≤dp<80	MAB291	10	3	145000	2.1	129.0	-	0.5
BP-2	80≤dp<100	MAB347	8	-	225000	2.4	135.5	-	-
BP-2	80≤dp<100	MAB353	8	3	147000	2.2	130.0	-	0.6
BP-2	80≤dp<100	MAB265	10	-	220000	2.4	136.4	-	-
BP-2	80≤dp<100	MAB290	10	3	145000	2.0	129.9	0.3	0.5
BP-3	dp≥125	MAB349	8	-	220000	2.3	135.3	-	-
BP-3	dp≥125	MAB350	8	3	141000	2.3	129.5	-	0.7
BP-3	dp≥125	MAB247	10	-	200000	2.3	135.8	-	-
BP-3	dp≥125	MAB264	10	-	205000	2.4	135.8	-	-
BP-3	dp≥125	MAB285	10	3	150000	2.3	129.6	-	0.5
Bu/M/1732	FS	MAB359	8	-	190000	2.6	135.1	-	-
Bu/M/1732	FS	MAB310	8	3	126000	2.4	130.5	-	0.6
Bu/M/1732	FS	MAB305	10	-	190000	2.3	137.3	-	-
Bu/M/1732	FS	MAB306	10	-	190000	2.7	135.1	-	-
Bu/M/1732	FS	MAB304	10	3	138000	2.3	129.0	-	0.5

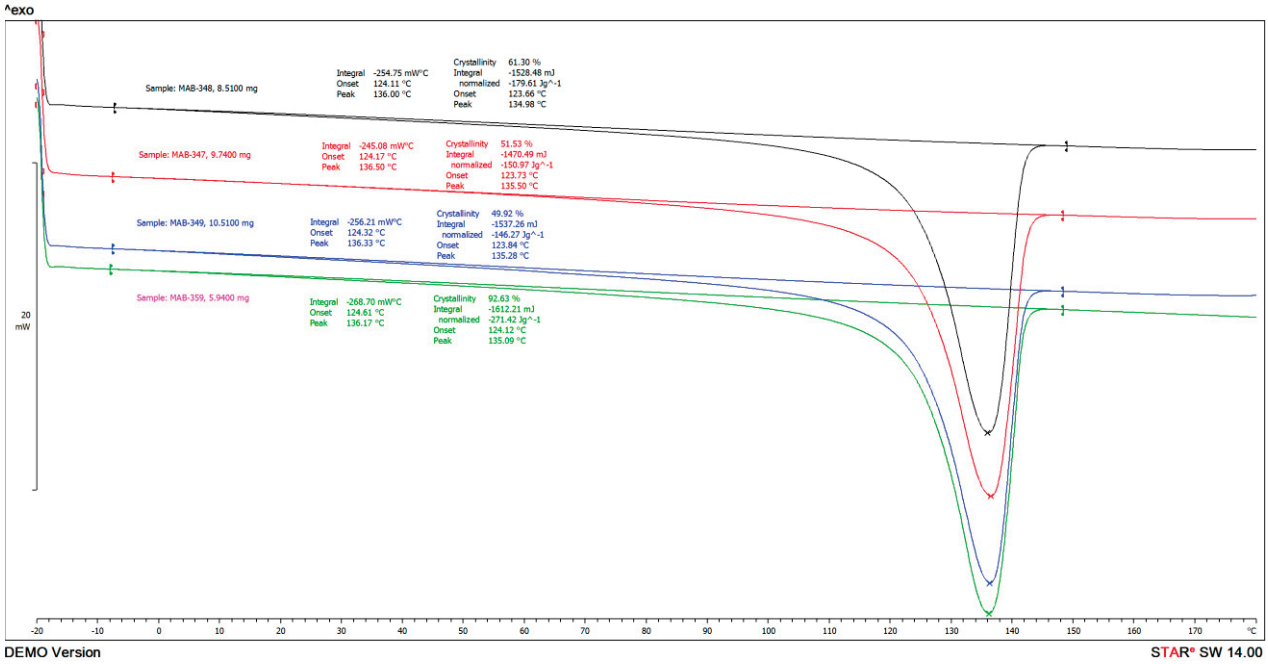

Figure 21. Second heating curves of the HDPE samples produced at 8 bar ethylene reactor pressure and by using different sized catalysts based on PQMS 1732 silica. Black line = MAB348, Red line = MAB347, Blue line =MAB349, Green Line = MAB359.

The Al distribution inside the catalyst particles of different sizes obtained from sieved fractions of PQMS 1732 commercial silica is shown in **Figure 22** where it can be observed that Al (and therefore, catalyst/co-catalyst mixture) was unable to penetrate up to the center of silica particles which led to core-shell Al distribution in all of the catalysts of different sizes prepared with PQMS 1732 silica. This core-shell Al distribution can be due to a number of factors e.g., severity of catalyst synthesis conditions (i.e., the temperature), time period of impregnation, porous structure and pore diameter of the silica support, size of MAO molecule etc. At first we should note that mercury porosimetery showed that, unlike Grace 948 silica which has a blend of small and big pores (see **Figure 1** for mercury porosimetery results and **Figure 16** for SEM-EDX images of Grace 948 silica showing macropores in it), this silica has only small pores. Micro-tomed catalyst particles provide another proof to the porosimetery measurements and show that no macropores exist in this silica and the small pores form a very well-connected porous structure. Such a uniform morphology, as well as small sized porous network (with an average pore diameter of 10 nm) is likely to be one of the various reasons for this core-shell catalyst distribution inside the particles of this silica.

Regarding size of MAO molecule, the reported average diameter of MAO molecule varies in the range of 1.0 to 1.94 ± 0.04 nm (or 10 to 19.4 ± 0.4 Å) based upon the experimental measurements done with different types of analytical techniques [18,19] and 1.4 to 1.8 nm (or 14

to 18 Å) predicted by theoretical modelling.[20] When complexed with a $(C_5H_5)_2ZrMe_2$ metallocene, Brintzinger et al.,[21] estimated the diameter of Me-MAO$^-$ counterion of the species shown in **Scheme 2** to be in the range of 2.44 to 2.88 nm (or 24.4 to 28.8 Å) depending upon the Al/Zr molar ratio. It should also be noted that MAO molecules can aggregate to form clusters having dimensions bigger than the original molecular dimensions e.g., aggregation of two associated ion pairs to an ion quadrupole would be expected to increase the effective radius by a factor of approximately $(2)^{1/3} = 1.26$. [21] Since the average pore diameter of this commercial silica is 10.1 nm (101 Å) which is not as nearly big as that of Grace 948 silica (which has 23.2 nm average pore diameter), along with a fairly uniform porous structure without any internal macroporosity (compare **Figure 22** with **Figure 16**) it is pretty likely that this core-shell Al distribution is due to plugging of certain pores by the MAO aggregates (or simply the MAO individual molecules) which have to diffuse (while the free TMA reacts with isolated silanols available) through this silica. For similar conditions of catalyst synthesis, no core-shell Al distribution was observed in Grace 948 silica based catalysts probably due to its much wider pores, and internal and external morphology where one can see macropores. This more open structure probably allows various diffusion pathways to the coordinated $(n\text{-BuCp})_2ZrCl_2$/MAO ion pair leading to its nearly uniform distribution throughout the particles of various sizes.

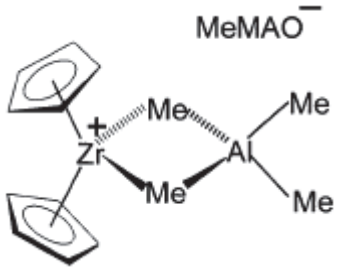

Scheme 2: Schematic representation of the ion pair formed after mixing $(C_5H_5)_2ZrMe_2$ with MAO.[21]

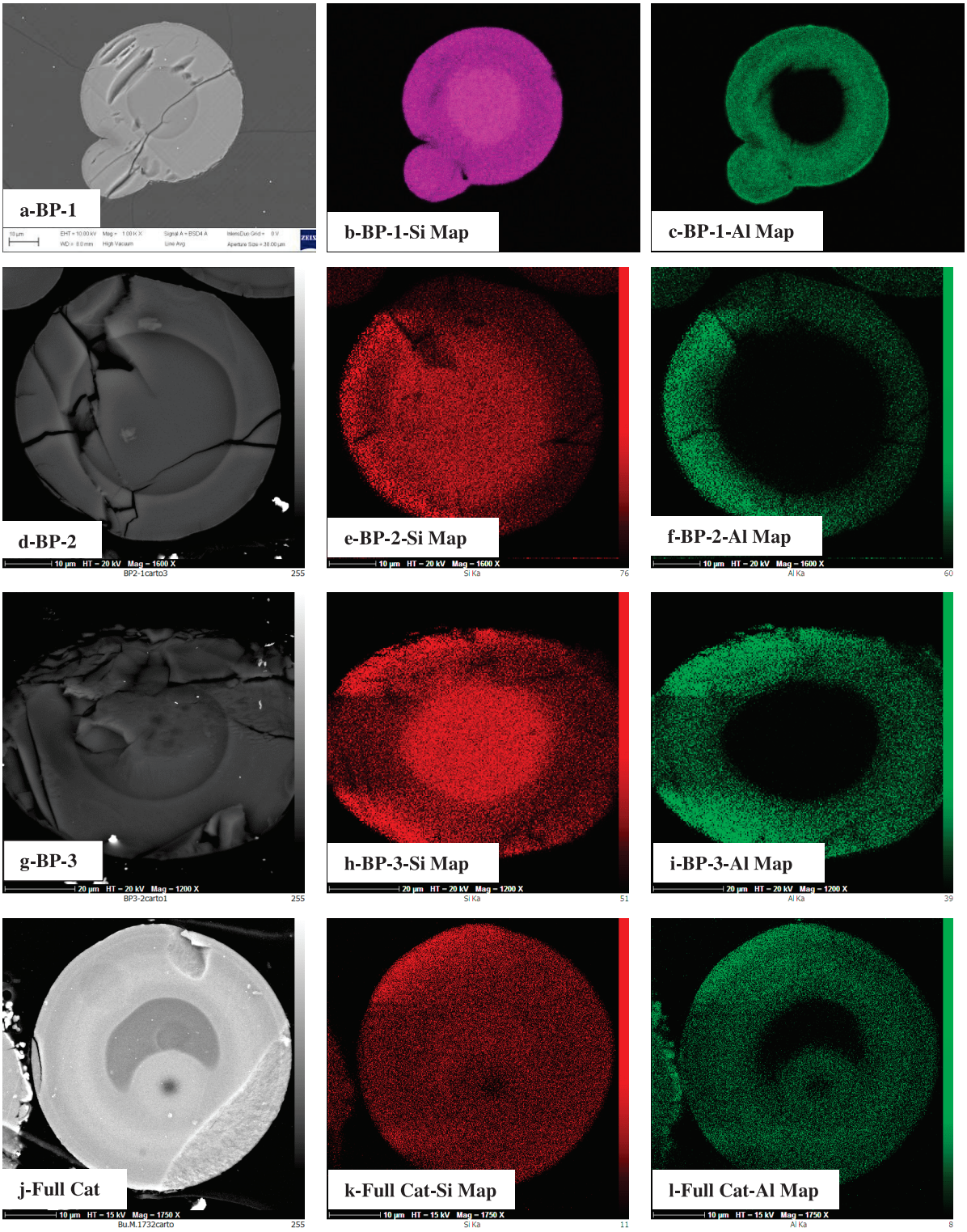

Figure 22. SEM-EDX micrographs showing Silicon (Si) and Aluminium (Al) distribution inside the particles of BP-1 (63 µm fraction supported) catalyst from a to c, BP-2 (80 µm fraction supported) catalyst from d to f, BP-3 (125 µm fraction supported) catalyst g to i and full silica batch supported catalyst from j to l.

If the problem here is one of mass transfer resistance to MAO diffusion, then increasing impregnation time should eliminate (or at least the importance of) the core-shell distribution of Al in this silica. To check this, a few more catalysts were prepared by keeping all other

parameters same but changing the impregnation time at 50 °C. For example, by using 600 °C dehydroxylated sieved fraction of 63 µm two catalysts were prepared out of which one catalyst was given an impregnation time of 3 h at 50 °C and the other one by was given an impregnation time of 6 h at the same temperature. SEM-EDX micrographs of these catalysts are shown in **Figure 23.** The same core-shell distribution is evident, even after 6 h of impregnation time. The same is also shown in **Figure 23g** to **i** for a catalyst prepared with 80 µm sieved fraction of PQMS 1732 silica and 3 h of impregnation time at 50 °C. It can therefore be concluded that uniform Al distribution in this specific commercial silica cannot be achieved by increasing the impregnation time from 1 to 6 h at 50 °C (and possibly can never be achieved if the pores "plug"). We shall see the impact of the larger pore size of the PQMS 3040 supports in the next section. The impact of increasing impregnation time on the catalytic activity will be further discussed in gas phase chapter. In this section we can rely on **Figure 24** which shows that a difference of 2 h in the impregnation time (by keeping other parameters constant) led to about 50 % rise in the instantaneous activity of the catalyst supported on 63 µm sieved fraction of PQMS 1732 silica, though, the MWD seems unaffected by increasing the impregnation time. Similar impact of longer impregnation time on catalytic activity was also made by Tisse et al.[3] Note that the Zr loading of BP1-3h catalyst was slightly less than that of BP-1 catalyst (see caption of **Figure 24**).

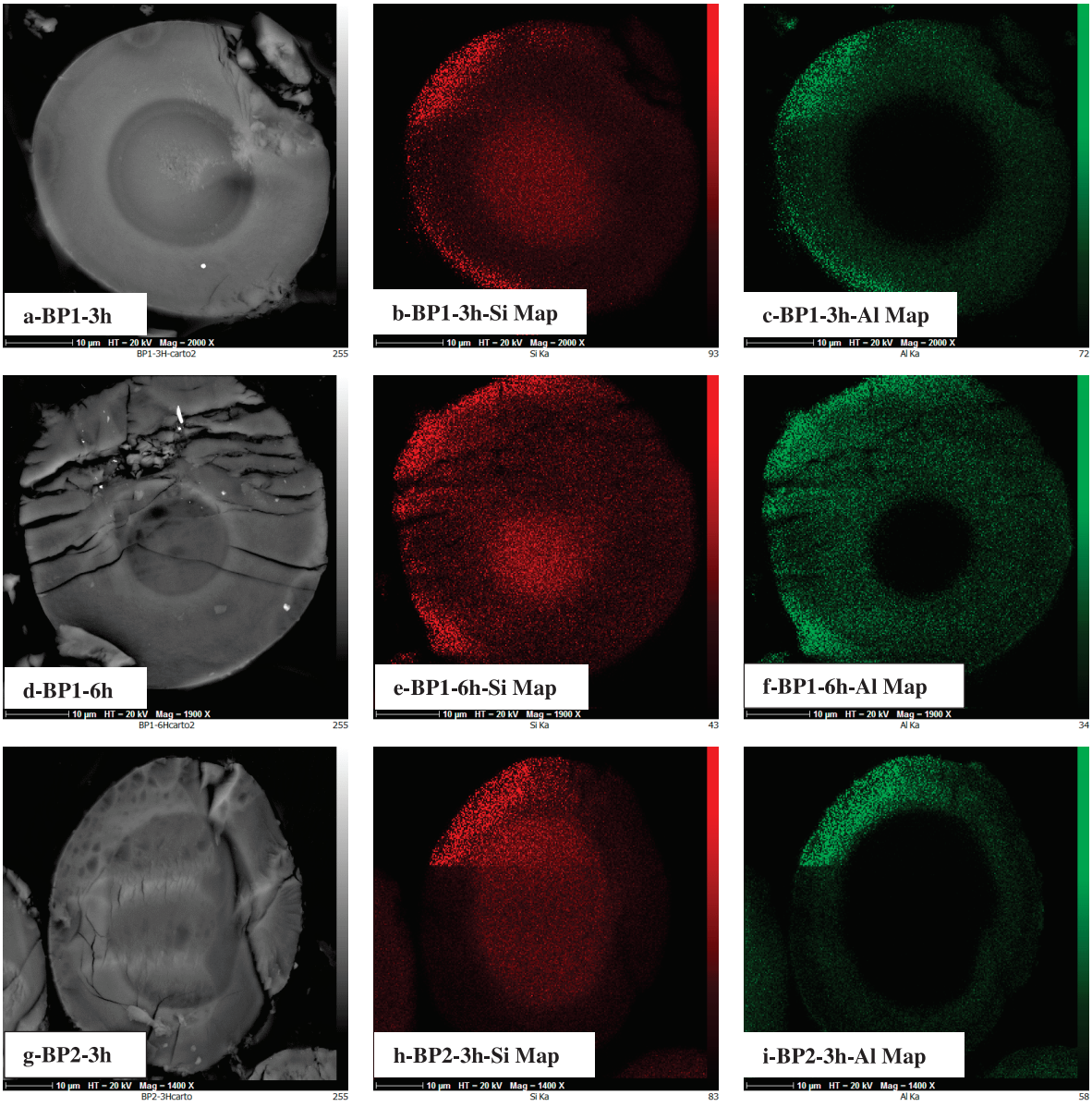

Figure 23. SEM-EDX micrographs showing Silicon (Si) and Aluminium (Al) distribution inside the particles of BP1-3h (63 µm fraction supported catalyst with impregnation time of 3 h) catalyst from a to c, BP1-6h (63 µm fraction supported catalyst with impregnation time of 6 h) catalyst from d to f and BP2-3h (80 µm fraction supported catalyst with impregnation time of 3 h) catalyst g to i.

a

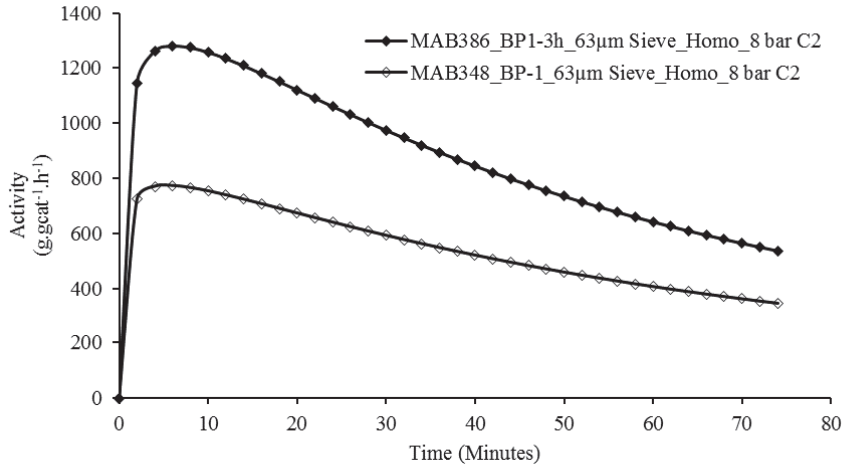

b

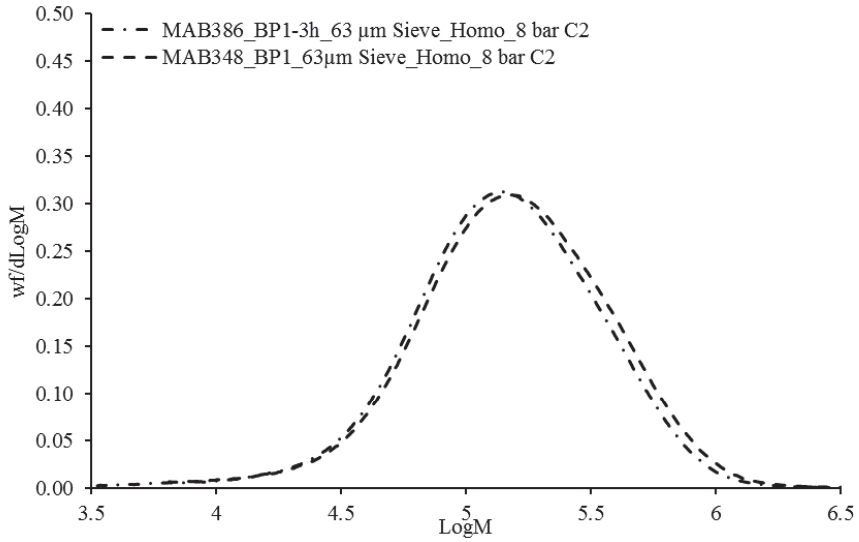

Figure 24. Effect of catalyst impregnation time on (a) the instantaneous activity in ethylene homopolymerisation at 8 bar ethylene pressure and 2 mmole.L^{-1} TIBA concentration and (b) MWD of the HDPE samples. Al content of BP-1 catalyst is 13.6 wt% and the Zr content is 0.23 wt %. Al content of BP1-3h catalyst is 16.9 wt % and the Zr content is 0.20 wt %.

Morphology of the homo- and copolymer samples analysed by SEM, presented in **Figure 25**, shows reasonably spherical polymer particles with abundant fibrous structures which seem to hold the growing catalysts fragments. This observation is in agreement to what was observed in the case of HDPE produced by Grace 948 silica based catalysts. It is important to mention that the copolymer particles seem to be more spherical with thinner and less abundant fibres as compared to those present in the homopolymer samples and suggests that the fragmentation/expansion behaviour of silica supported catalyst is less abrupt in copolymerisation which can be attributed to the reduced brittleness of polyethylene due to 1-hexene incorporation in polymer chains.

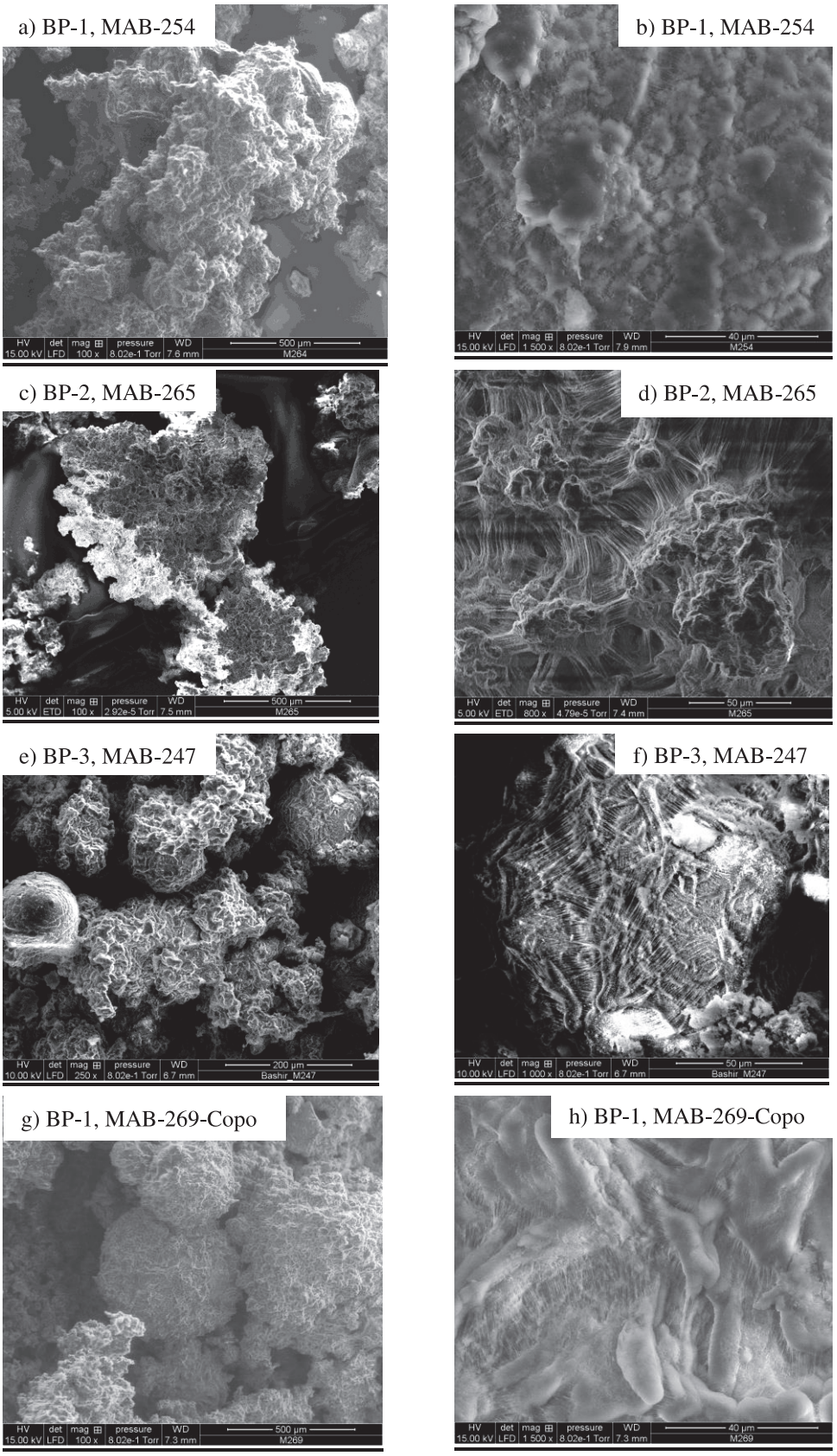

Figure 25. SEM micrographs for the comparing the morphology of the homopolymer (a to f) and copolymer (g to h) produced by using different sized catalysts based on PQMS 1732 silica.

3.2.3. Effect of Particle Studied with PQMS 3040 Silica Based Catalysts

Physical characteristics of the catalysts prepared with the different sieved fractions of this support are mentioned in **Table 4,** where it can be seen that the pore volume of each catalyst prepared with the sieved fraction of this support is higher than the pore volumes of the corresponding catalysts prepared with Grace 948 silica and PQMS1732 silica. Pore diameter of the catalysts prepared from this silica are about two times the pore diameter of the catalysts prepared from PQMS 1732 silica, and are similar to those of the catalysts prepared from Grace 948 silica. Neverthelss, the macroscopic morphology is much closer to that of the PQMS 1732 support, with a very uniform pore size distribution.

Figure 26 presents the effect of silica support particle size on the instantaneous activity of ethylene homopolymerization at two different pressures, and **Figure 27a** compares the impact of catalyst particle size on homo- and copolymerization instantaneous activities at 10 bar ethylene pressure. In agreement with the observations made for the previously discussed catalysts of different sizes, the instantaneous activity of $(n\text{-BuCp})_2ZrCl_2$/MAO supported on this silica also increases with decreasing the size of the carrier particles in both types of polymerizations and at both ethylene pressures. The range of catalyst particle sizes shown in **Figure 26a** differs from that of **Figure 26b** because the smallest size catalyst (i.e., BM-4) was consumed in previous experiments. It can be seen that the activities of the catalysts supported on 45 µm and 63 µm sieved fractions (i.e., BM-3 and BM-1 catalysts, respectively) are very similar in homopolymerizations and their behaviour remains unchanged with varying monomer pressure. In copolymerizations, the activity of these catalysts differs from each other, with BM-3 being more active than BM-1 (see **Figure 27a**). No specific reason can be given for this behaviour of these two catalysts at this point.

Good reproducibility of these reactions is shown by the two replicate runs with BM-1 catalyst as shown in **Figure 27a**. Increment of 2 bar in ethylene pressure boosted the productivity (i.e., in $g.gcat^{-1}$) of BM-2, BM-3, BM-1 and full batch supported catalyst by 15, 18, 22 and 56% on average, respectively. Surprisingly, the impact of ethylene pressure change on the productivity of the supported catalysts in homopolymerizations is highest on the full batch based catalyst. In the presence of 1-hexene, the boost in average catalytic productivity at 10 bar ethylene pressure was 28 % for BM-2 catalyst, 21 % for BM-3 catalyst and only 4 % for the biggest in size BM-1 catalyst, whereas, at the same conditions the full silica batch based catalyst showed 41 % rise in its productivity (not shown here graphically). This observation is in good agreement with the one made in the case of PQMS 1732 silica based catalysts and confirms

that the presence of 1-hexene at the active sites has a higher impact on the activity of smaller particles than on the activity of bigger catalyst particles. Furthermore, the delaying effect of 1-hexene on the activation rate of these catalysts was seen only in the case of BM-3 and BM-1 catalysts with more intense effect on the activation rate of the biggest catalyst particles (i.e., BM-1 catalyst), as can be seen in **Figure 27a**. The effect of ethylene pressure on the instantaneous activity of full batch catalyst of this silica is presented in **Figure 27b** in both polymerization types.

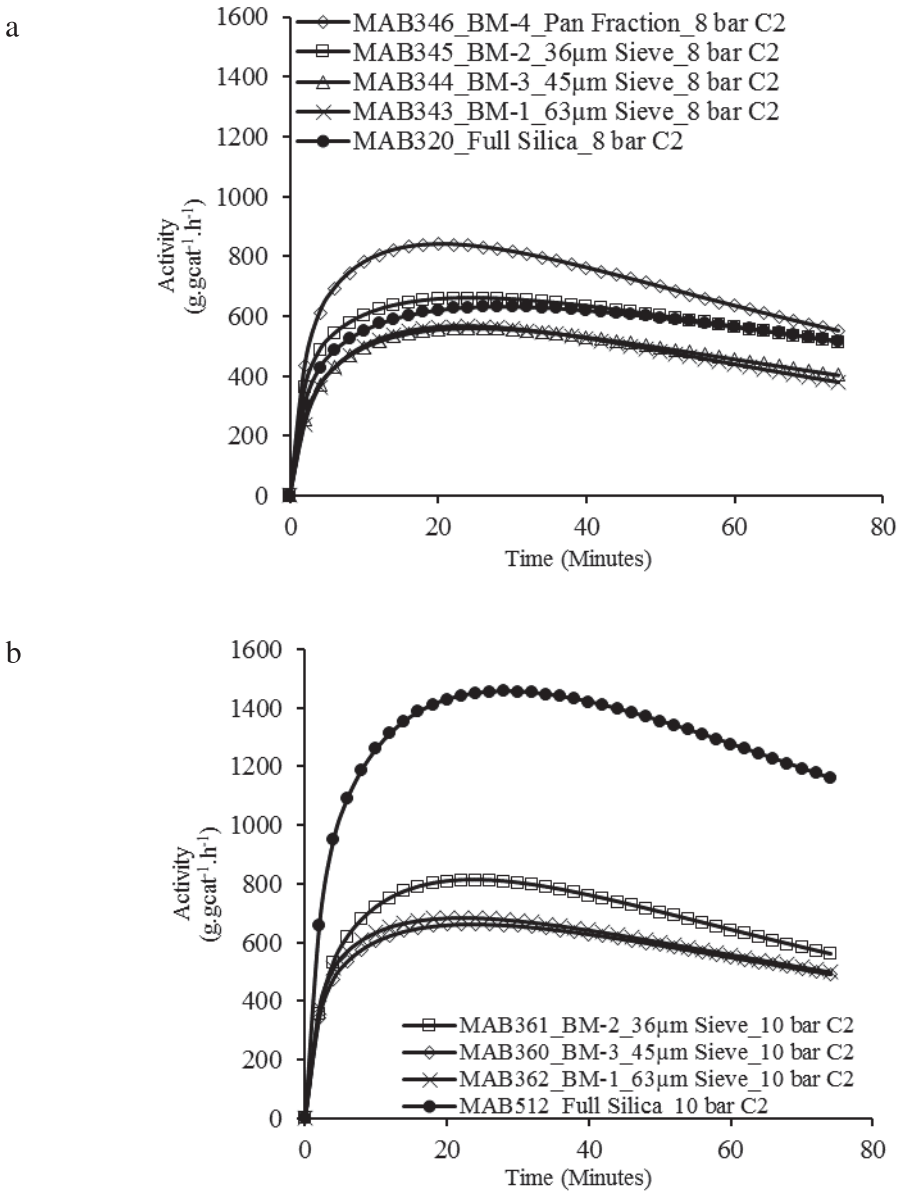

Figure 26. Effect of catalyst particle size on the instantaneous activity of each catalyst in homopolymerizations at (a) 8 bar ethylene pressure and (b) at 10 bar ethylene pressure. PQMS3040 silica used as support.

a

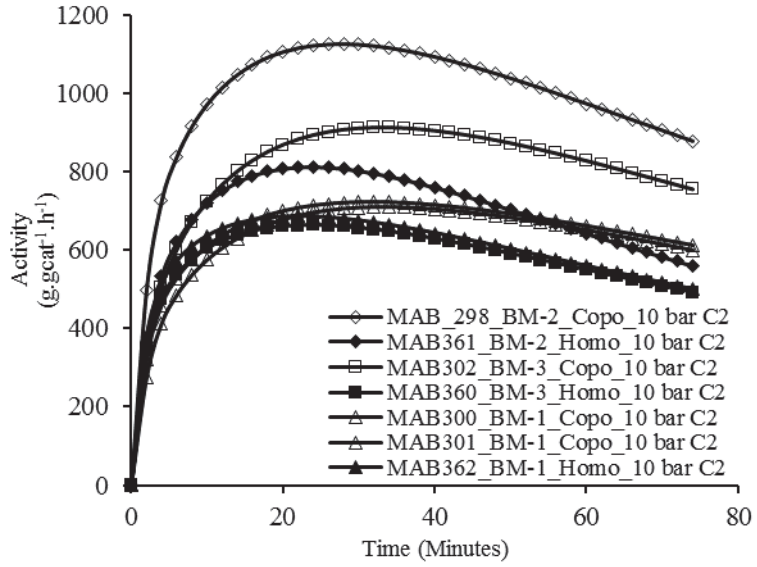

b

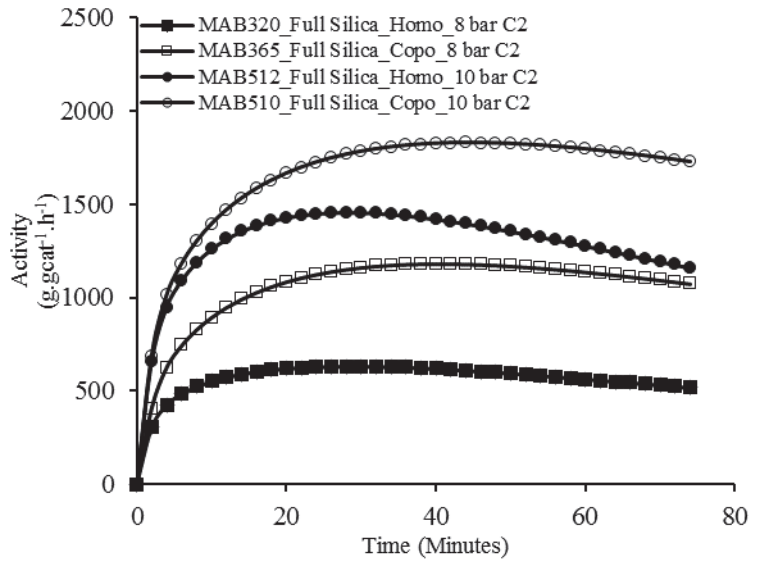

Figure 27. Comparison of the instantaneous activity of (a) different sized catalysts in homo- and copolymerizations at 10 bar ethylene pressure and (b) catalyst supported on full batch of PQMS3040 silica homo- and copolymerization at 8 and 10 bar ethylene pressure. 1-hexene used in all copolymerizations = 3 mL.

The effect of catalyst particle size on the MWD curves of the homo- and copolymers is shown in **Figure 28** which, in agreement with the results obtained for the other two silica discussed in previous sections, shows no significant impact on the polymer MWD at either ethylene pressure, (c.f. **Table 9**). No sensitivity of the MWD of the polymer samples towards change in ethylene pressure further confirms that transfer to monomer is the main chain termination mechanism with this catalyst. The response of polymer MWDs to 1-hexene presence in the reactor is also in-line with the observations made for the previous set of catalysts studied in

this work i.e., the addition of 1-hexene into the reactor causes the shift of MWD of the copolymers towards low values which can be attributed to the increased transfer reactions due to 1-hexene presence at the active sites. Regardless of the fact that MWDs are very similar we cannot exclude in-situ hydrogen which may have also contributed to the chain transfer reactions. MWDs of three copolymers produced with BM-3 catalyst at different polymerization times are compared in **Figure 29** where it is evident that the two copolymer samples produced after 75 minutes of reaction time have lower (and very similar molar masses) than the one produced after 30 minutes (for values of M_w and Đ of polymer samples see caption of **Figure 29**). Such dependence of polyethylene MWD on polymerization time can be attributed to in-situ hydrogen generation (see discussion in next chapter).

For all other samples of longer reaction times, molar mass dispersity values remained below 3 which indicates that support particle size does not impact the single-site behaviour of the catalysts and confirms the trends observed with the other supported catalysts used in this work. **Table 9** shows that the melting temperature of the homo- and copolymer samples is also unaffected by the silica support particle size. Comonomer content of the copolymers also does not show dependence on catalyst particle size.

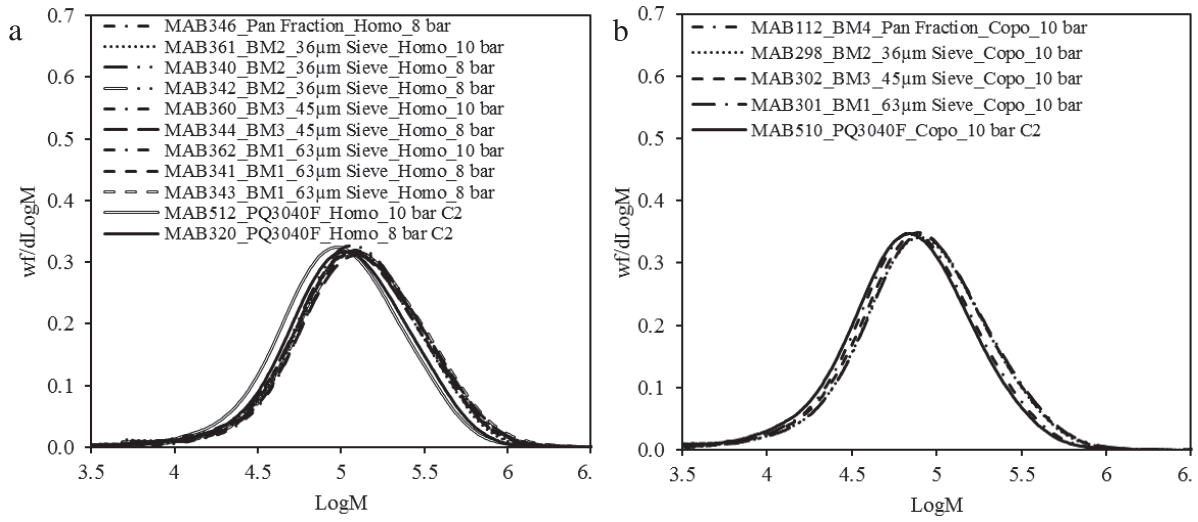

Figure 28. Effect of catalyst particle size on the MWD of (a) homopolymers and (b) copolymers produced in slurry phase polymerizations. Catalyst supported on different fractions and full batch of PQMS3040 silica.

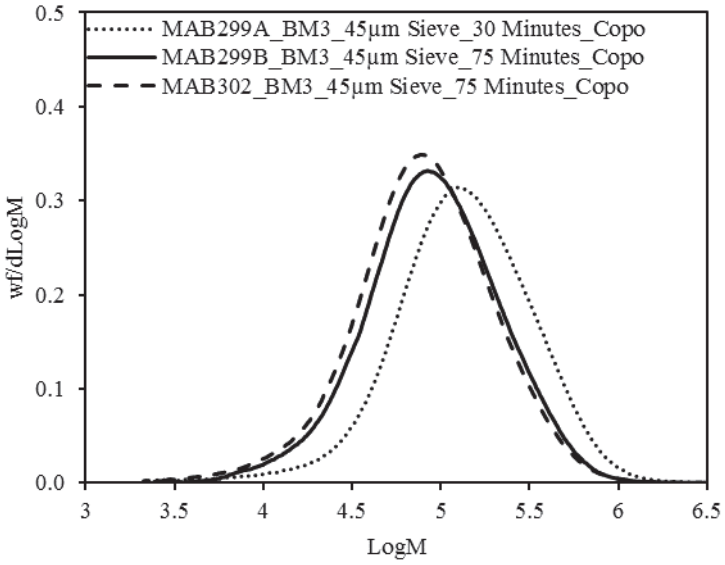

Figure 29. Comparison of the MWDs of the copolymers produced with BM-3 catalyst at different polymerization times at 80 °C, 10 bar ethylene pressure, 1-hexene = 3mL and TIBA = 2 mmole.L^{-1}. M_w = 191000 g.$mole^{-1}$, Đ = 2.4 for MAB299A and M_w = 130000 g.$mole^{-1}$, Đ = 2.2 for MAB299B.

Table 9. Weight average molar mass (M_w), dispersity of molar masses (Đ) and melting temperature (T_m) of the homopolymer and copolymer samples produced by using supported catalysts based on PQMS 3040 silica. P_{C2} refers to ethylene pressure, $A_{1\text{-hexene}}$ refers to the initial amounts of 1-hexene injected into the reactor. x_{NMR} and x_{CEF} means comonomer content estimated by using ^{13}C NMR and CEF, respectively. A1-hexene refers to the mount of 1-hexene added. FS means full silica.

Catalyst name	Particle size (µm)	P_{C2} (bar)	$A_{1\text{-hexene}}$ (mL)	Sample Name	M_w (g/mol)	Đ	T_m (°C)	x_{NMR} mol%	x_{CEF} mol%
BM-4	Pan	8	-	MAB346	176000	2.6	135.8	-	-
BM-4	Pan	10	3	MAB112	105000	2.4	129.2	-	0.6
BM-2	36≤dp<45	8	-	MAB340	175000	2.4	135.8	-	-
BM-2	36≤dp<45	8	-	MAB342	186000	2.5	135.8	-	-
BM-2	36≤dp<45	10	-	MAB361	171000	2.3	135.7	-	-
BM-2	36≤dp<45	10	3	MAB298	120000	2.3	130.0	0.3	0.6
BM-3	45≤dp<63	8	-	MAB344	190000	2.4	135.8	-	-
BM-3	45≤dp<63	10	-	MAB360	180000	2.4	136.5	-	-
BM-3	45≤dp<63	10	3	MAB302	120000	2.3	128.7	0.4	0.6
BM-1	63≤dp<80	8	-	MAB341	180000	2.6	135.5	-	-
BM-1	63≤dp<80	8	-	MAB343	195000	2.3	136.2	-	-
BM-1	63≤dp<80	10	-	MAB362	186000	2.2	135.8	-	-
BM-1	63≤dp<80	10	3	MAB300	110000	2.2	129.0	-	0.7
BM-1	63≤dp<80	10	3	MAB301	122000	2.3	129.2	-	0.6
Bu/M/MS3040	FS	8	-	MAB320	150000	2.4	134.6	-	-
Bu/M/MS3040	FS	8	3	MAB365	90000	2.2	129.7	-	0.7
Bu/M/MS3040	FS	10	-	MAB512	140000	2.1	136.8	-	-
Bu/M/MS3040	FS	10	3	MAB510	95000	2.1	129.5	0.5	0.7

Figure 30 shows the Al distribution inside the catalyst particles of different sizes prepared by using sieved fractions and full batch of PQMS 3040 silica. As with the PQMS 1732 supported catalysts, core-shell Al distribution can also be seen in these catalyst particles. This is true for all sizes with the exception of BM-4 catalyst (i.e., the smallest one which should have the shortest diffusion time). In BM-4, some of the particles contained Al distributed all the way through to the center of the particles (compare **Figure 30a** to **c** with **Figure 30d** to **f**). The three particles shown in **Figure 30g** to **i** show that there are different levels of MAO dispersion

within the particles of different diameters for 1 h impregnation at 50 °C. As above, the biggest particle (i.e., P-1) shows Al only on its boundaries, whereas the smallest in this specific series of three particles (i.e., P-3) shows relatively better Al intrusion. Since the internal morphology of PQMS 3040 silica is similar to that of PQMS 1732, but with a mixture of small and big pores, the core-shell Al distribution in PQMS 3040 silica whose pore diameter is almost double then that of PQMS 1732 clearly indicates that this silica also offer a significant diffusion resistance to the bulky MAO molecules (and eventually aggregates).

At this point it can be suggested that the (co)-monomer(s) concentration gradient(s) in (for example) a 63 µm catalyst particle of the two PQ silica(s) can be very different from the concentration gradient(s) developed in a 63 µm catalyst particle of Grace 948 silica because the active species seems to accumulate around the outer surface of PQ silica(s) supported catalysts which may not allow the development of full (co)-monomer(s) concentration gradient(s) and therefore, the MWDs of polyethylene produced with different sized PQ silica based catalysts are identical which is not the case with Grace 948 silica based catalysts where the active species seem to be nearly uniformly distributed throughout the catalyst particles (see **Figure 31**). Nevertheless, one should avoid assuming that the concentration gradients made within BM-4 catalyst and BM-1 catalyst are also similar due to similar core-shell Al distribution because the comparison of **Figure 30a** to **f** and **Figure 30g** to **i** clearly shows that Al distribution is better in small silica particle.

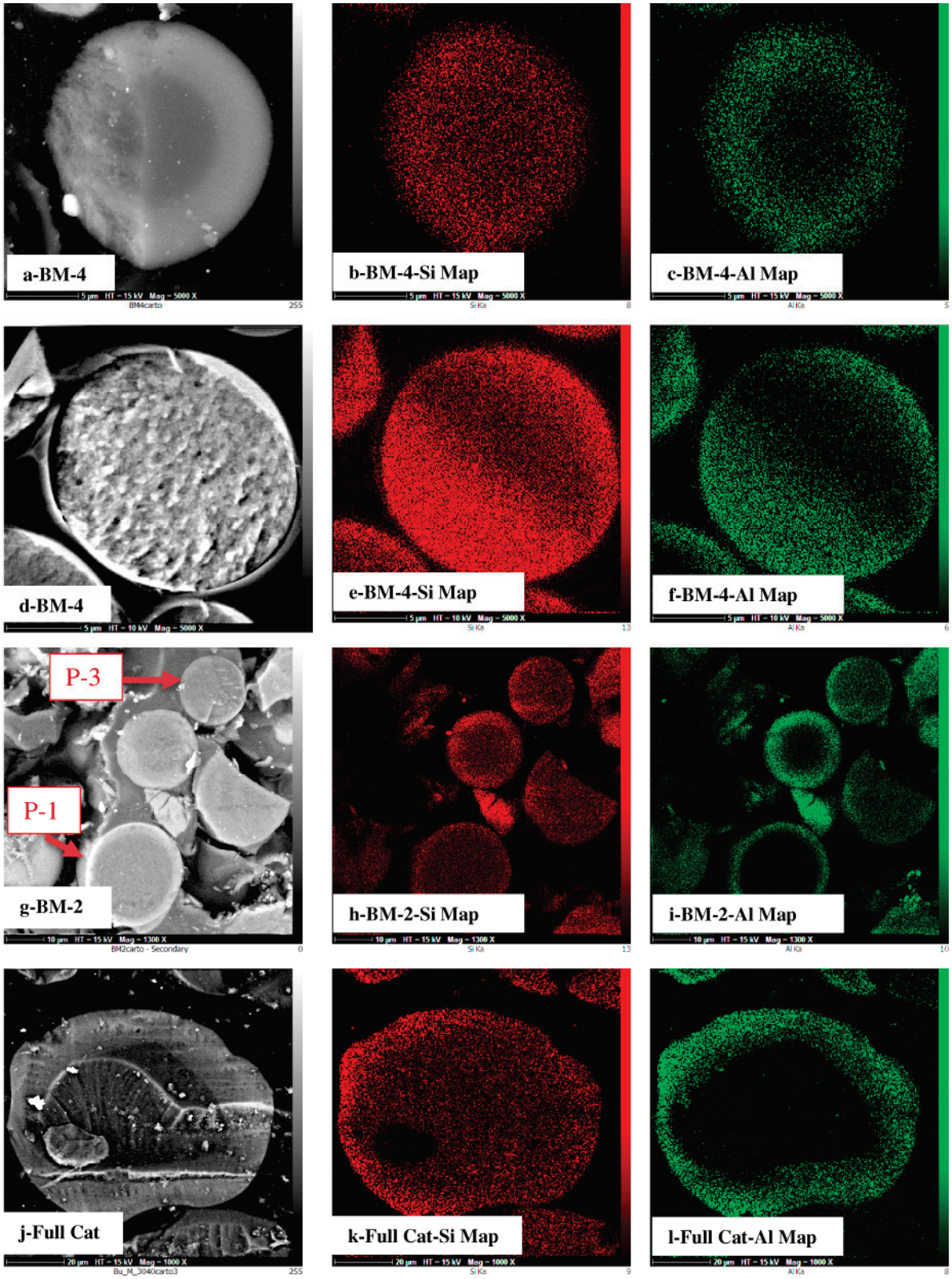

Figure 30. SEM-EDX micrographs showing Silicon (Si) and Aluminium (Al) distribution inside the particles of BM-4 (Pan fraction supported) catalyst from a to f, BM-1 (36 µm fraction supported) catalyst from g to I and full PQMS 3040 silica batch supported catalyst j to l.

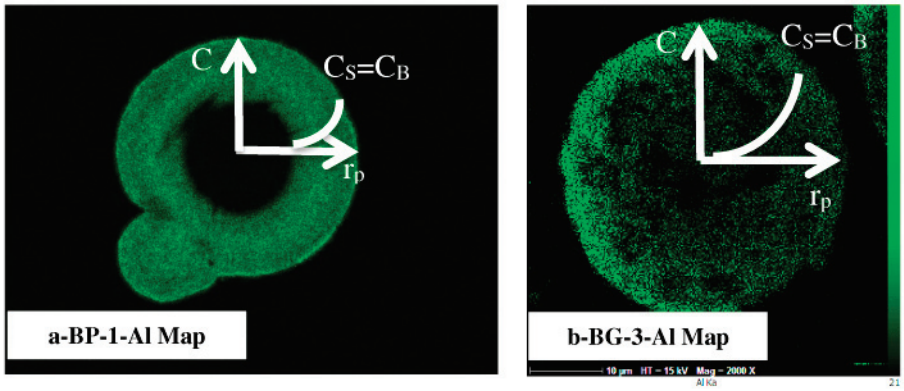

Figure 31.Graphical representation of the (co)-monomer(s) concentration(s) gradient(s) developed during the course of polymerization in slurry phase ethylene polymerization with BP-1 and BG-1 catalysts. C= monomer concentration at any position inside the catalyst, C_s = monomer concentration at the catalyst surface, C_B = bulk monomer concentration, r_p = particle radius.

In order to analyse the effect of increasing catalyst impregnation time on Al distribution within the particles of this silica, one supported catalyst was prepared by using 63 µm sieved fraction of PQMS 3040 silica and the toluene solution of $(n\text{-}BuCp)_2ZrCl_2$/MAO was allowed to react with 600 °C dehydroxylated silica fraction for 3 h at 50 °C followed by drying under vacuum at 75 °C for a few hours. The cross-sectional SEM-EDX images of that catalyst, named as BM1-3h, are shown in **Figure 32** which clearly show that after 3 h of impregnation time, Al is distributed throughout the silica particles and no particle with core-shell distribution can be seen in a number of particles shown in **Figure 32d** to **f**. In addition, the particle shown in **Figure 32a** to **c** is cut from two sides none of which show signs of core-shell Al distribution. It should be recalled that with the same sized fraction of PQMS 1732 silica it was not possible to eliminate the core-shell Al distribution even after 6 h of impregnation time which allows us to conclude that for the silicas of same pore structure, it is, most probably, the pore diameter of the silica (at a given catalyst impregnation temperature and time) which is critically important in determining the distribution of MAO (and therefore, the active sites with this method of supported metallocene synthesis) inside the catalyst particles.

The effect of higher impregnation time on the instantaneous activity of BM-1 and BM-1-3h catalysts is shown in **Figure 33** where an increase of about 50 % in polymerization rate is obvious upon increased impregnation time. This result is good agreement with the results shown in the previous section of PQMS 1732 silica (see **Figure 24a**).

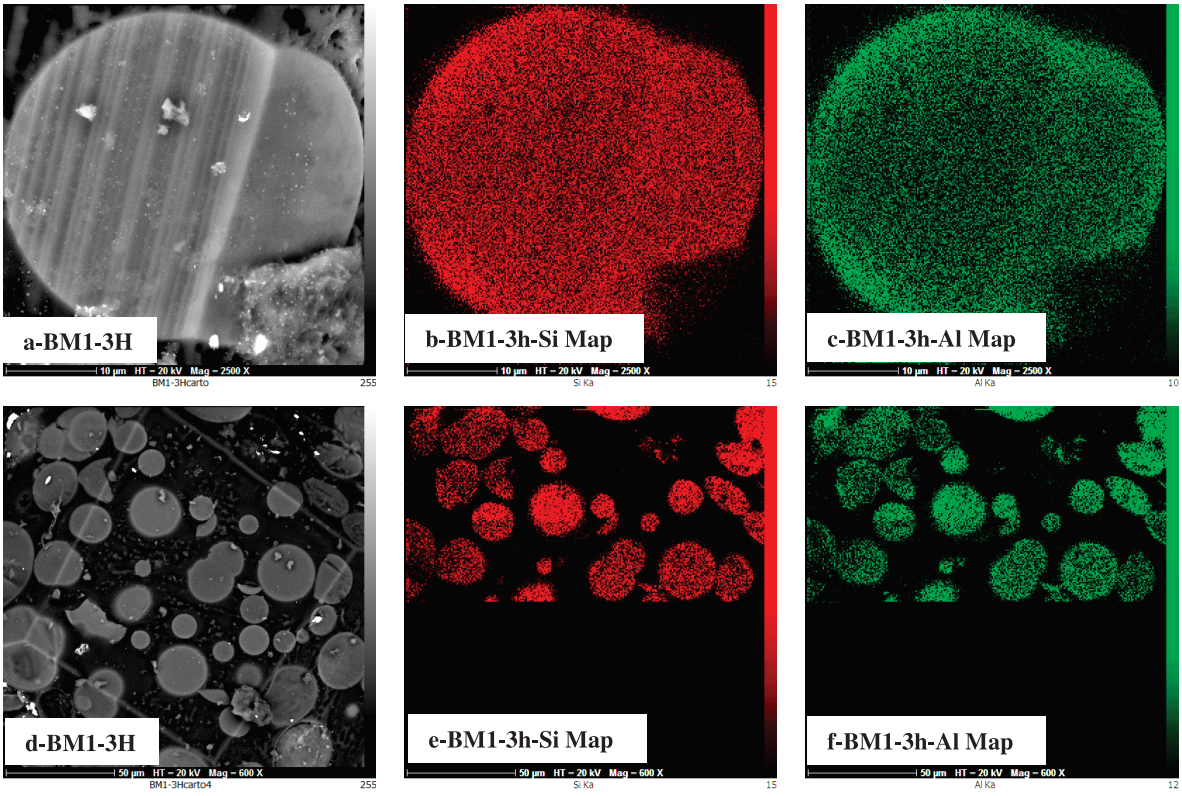

Figure 32. SEM-EDX micrographs showing Silicon (Si) and Aluminium (Al) distribution inside the particles of BM1-3h (63µm fraction supported) catalyst from a to f. The image 'e' and 'f' were not completed due to problem with the SEM-EDX software.

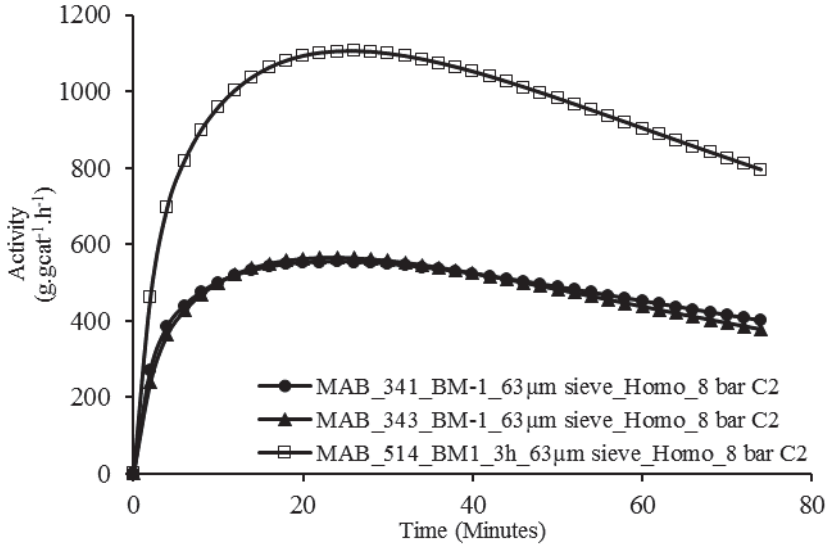

Figure 33. Effect of catalyst impregnation time on the instantaneous activity in ethylene homopolymerization at 8 bar ethylene pressure and 2 mmole.L^{-1} TIBA concentration. Al content of BM-1 catalyst is 11.8 wt% and the Zr content is 0.19 wt %. Al content of BM1-3h catalyst is 17.7 wt % and the Zr content is 0.22 wt %.

3.3. Slurry Phase Ethylene Polymerizations with Silica Supported THI/MAO catalyst

As it has been shown in the previous section that, although the activity of the silica supported (n-BuCp)$_2$ZrCl$_2$/MAO catalysts shows a clear dependence on the support particle size, the MWD of the obtained homo- and copolymers from such catalysts of varying particle sizes does not show clear differences. One might expect that if the explanation for the activity differences were due to monomer mass transfer resistance in the larger particles, there would be an impact on the MWD. However, the fact that the MWDs of the polyethylenes produced at 8 and 10 bar ethylene reactor pressure by using the same catalysts are very similar indicates that the MWD is "independent" of the monomer concentration, and that chain transfer assisted by the monomer is the main termination mechanism in (n-BuCp)$_2$ZrCl$_2$/MAO catalysed ethylene homopolymerizations. In-situ hydrogen generation with this catalyst further complicated the analysis of polymer MWDs. This insensitivity of polymer MWD to changes in ethylene reactor concentration is an obstacle to definitely attributing the observed differences in reaction kinetics of supported (n-BuCp)$_2$ZrCl$_2$/MAO catalysts to their different particle diameters and, consequently, to the existence of diffusion resistance.

In order to further confirm chain transfer assisted by the monomer as the dominant chain termination mechanism with silica supported (n-BuCp)$_2$ZrCl$_2$/MAO catalyst, ethylene homopolymerizations were conducted at different ethylene pressures by using the catalyst supported on full batch of Grace 948 silica. This catalyst was selected because it exhibits no core-shell Al distribution. The obtained reaction rate profiles and MWD of the respective HDPE samples are shown in **Figure 34a** and **b**, respectively. It is obvious that the reaction rate profile of this supported catalyst is a strong function of ethylene pressure inside the reactor, but the MWD of HDPE appears to be insensitive to such changes of ethylene concentration in the reactor.

Therefore, a different metallocene, rac-ethylenebis(4,5,6,7-tetrahydro-1-indenyl)zirconium dichloride or THI, for which transfer to monomer is not the dominant chain termination mechanism was supported on full batch of Grace 948 silica and used to study the effect of ethylene concentration on MWD of polyethylene. The synthesis procedure for this catalyst was exactly the same as that used for supporting (n-BuCp)$_2$ZrCl$_2$/MAO catalysts on different silicas. However, reactor fouling was observed when ethylene homopolymerizations were conducted using the MSP-2 polymerization protocol in which there was no pre-contact between the Grace 948 silica supported THI/MAO catalyst (referred to hereafter as THI/MAO/G948F catalyst) and the TIBA, as shown in **Figure 35**. It can be noticed that the reaction rate profiles

of the two homopolymerization runs are very different which can be attributed to the amount of catalyst used in both the polymerizations, as shown in **Figure 35b** & **c**.

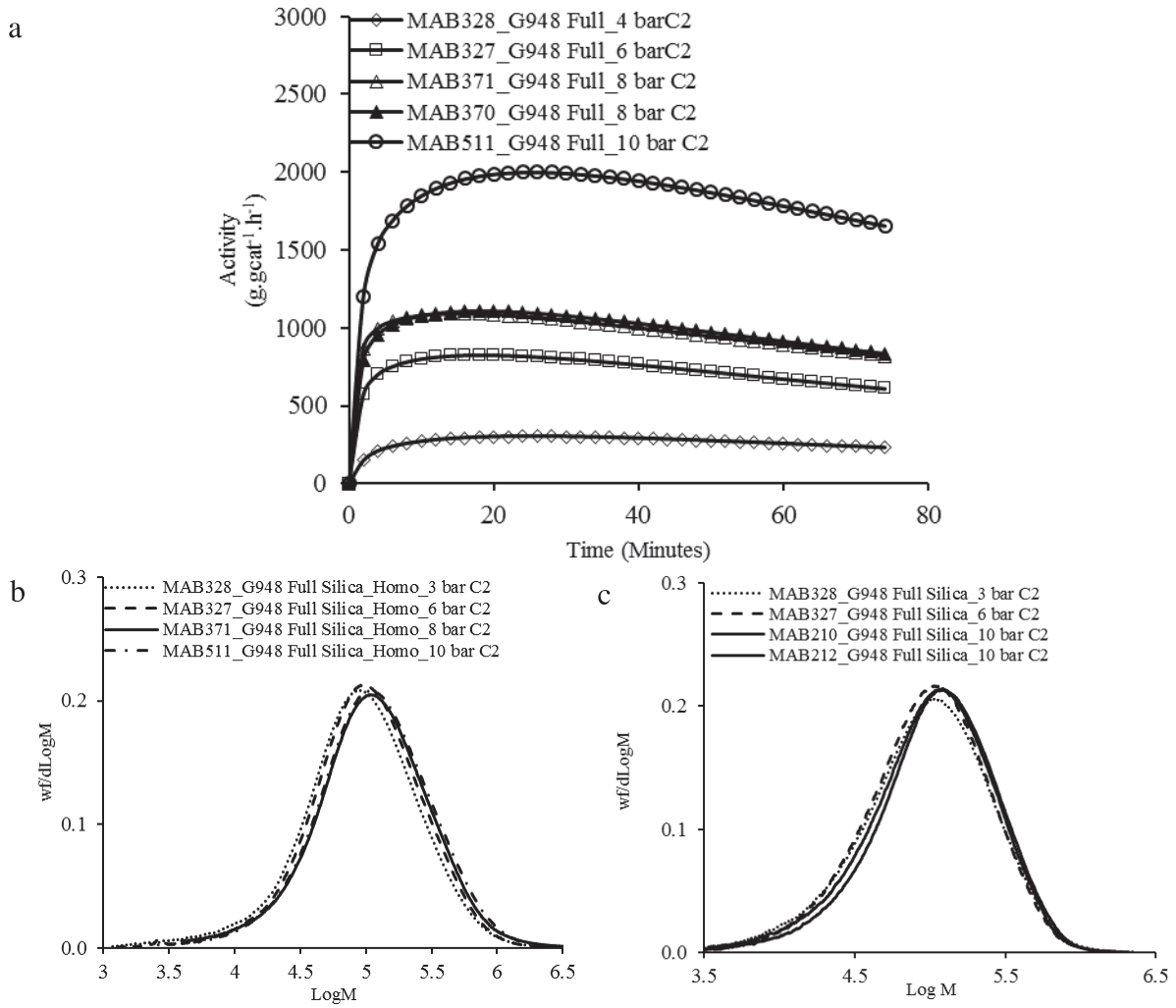

Figure 34. Effect of ethylene rector pressure on the (a) reaction rate profile of (n-BuCp)$_2$ZrCl$_2$/MAO supported on full batch of Grace 948 silica in ethylene homopolymerization (b) MWD of HDPE measured with new set of HT-SEC columns and (c) MWD of HDPE measured with previous set of HT-SEC columns.

In the first run, named as MAB407, it seems that more catalyst dissolved in the diluent leading to a kinetic profile similar to that of typical homogeneous polymerizations i.e., fast activation followed by rapid deactivation of the metallocene/MAO catalyst. In contrast, if a lower quantity of catalyst is injected into the reactor then less catalyst/MAO mixture leaches out of the supports and the reaction rate grows over the period of reaction time in second run named MAB409. This result was surprising since this MSP-2 polymerization protocol has been shown

to yield no reactor fouling with any of the silica supported (n-BuCp)$_2$ZrCl$_2$/MAO catalysts discussed in the previous sections of this chapter and the ones used in the previous **Chapter 3**.

a

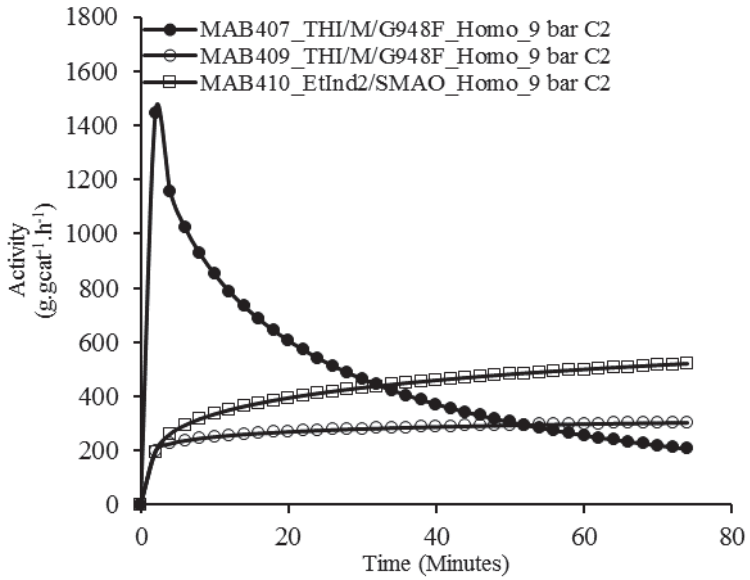

b-MAB407-32 mg of catalyst used

c-MAB409-20 mg of catalyst used

d-MAB410-21 mg of catalyst used

Figure 35. (a) Reaction rate profiles of ethylene homopolymerizations with THI/MAO/G948F and EtInd2/SMAO catalysts, (b & c) reactor condition at the end of polymerizations THI/MAO/G948F and (d) reactor condition at the end of polymerizations with EtInd2/SMAO catalyst. Polymerization protocol used = MSP-2, Reactor diluent = n-heptane, TIBA concentration = 2 mmole.L^{-1}, ethylene pressure = 9 bar, Reaction time = 75 minutes.

In order to investigate that whether leaching of THI/MAO catalyst from Grace 948 happened due to the nature of metallocene or the catalyst synthesis procedure is responsible for this behaviour, another catalyst of the same indenyl family, named as rac-ethylenebis(indenyl)zirconium (rac-Et(Ind)$_2$ZrCl$_2$) dichloride, was prepared by supporting it on Grace 948 silica impregnated with MAO (SMAO) whose synthesis method is described in **Chapter 2**. rac-Et(Ind)$_2$ZrCl$_2$ was supported on SMAO by adding 2 g of SMAO to a three necked round bottom flask and adding a 10 mL solution of metallocene in toluene drop-wise at room temperature under argon in order to obtain an Al/Zr molar ratio of 150 in the final catalyst. The volume of toluene solution was about 150% higher than the pore volume of the used silica in order to completely fill the pores. The slurry was then heated for 1 h at 50 °C followed by one heptane wash and vacuum drying at 50 °C for few hours. The final catalyst was a free flowing powder and named hereafter as EtInd2/SMAO. It should be noted that in this catalyst synthesis method washing step was employed at the end of SMAO synthesis in addition to one wash applied before vacuum drying, whereas no washing was done while preparing THI/MAO/G948F catalyst. Metal loadings of EtInd2/SMAO and THI/MAO/G948F catalysts are shown in **Table 10** (along with loadings from two other catalysts that will be discussed below). Both the catalysts show very different metal loadings and therefore, the Al/Zr molar ratios.

Table 10. Elemental characterization of THI/MAO catalysts and EtInd2/SMAO catalyst by ICP-AES. Silica support used for all of these catalyst is Grace 948 dehydroxylated at 600°C.

Catalyst	**Al (wt%)**	**Zr (wt%)**	**Al/Zr Molar ratio**
THI/36	13.4	0.24	189
THI/80	14.2	0.22	218
THI/MAO/Grace 948F	17.7	0.19	315
EtInd2/SMAO	14.7	0.41	121

Reaction rate profile of ethylene homopolymerization with EtInd2/SMAO catalyst is similar in shape to the one of THI/MAO/G948F catalyst where similar amount of the later catalyst was used (see **Figure 35a**) i.e., both the catalysts show slow rise in catalytic activity over the whole reaction period without any deactivation. Such profiles were designated by Floyd et al.,[16] as acceleration-type, and can be either due to a slow activation of the catalyst or due to severe mass transfer resistance. As shown in **Figure 35c**, the milky colour of reactor diluent at the end

of reaction shows that significant amount of polyethylene was formed by homogeneous catalysis due to the leaching of EtInd2/SMAO catalyst from the support into heptane and therefore, the resistance to monomer transport to the active sites located on the support particles should have been high leading to acceleration-type rate profiles for both the catalysts (besides milky colour solid polymer particles were also obtained in this reaction). Furthermore, leaching of EtInd2/SMAO catalyst (which was prepared with a different method including washing steps) further supports the rough assumption that the interaction of indenyl based catalysts (like $Et(Ind)_2ZrCl_2$ and THI) with TIBA (and/or other aluminium alkyls) are different from that of cyclopentadienyl (like $(n\text{-}BuCp)_2ZrCl_2$) catalysts. However, further investigation on this subject is beyond the scope of the present work.

Two additional THI/MAO supported catalysts of different sizes were prepared by using 36 µm and 80 µm sieved fractions of Grace 948 silica by employing two washing steps during their synthesis to avoid leaching. These two fractions of Grace 948 silica were selected because of their considerable size difference and due to the absence of any core-shell Al distribution in this silica supported catalysts, as shown in the previous sections. The catalysts were prepared by adding a weighed amount of 600 ºC dehydroxylated silica (i.e., either 36 µm or 80 µm sieved fraction) into a round bottom flask inside the glove box. Then the amounts of THI and MAO (30 wt% solution in Toluene from Albemarle) required to achieve an Al/Zr molar ratio of 150 (by targeting 14-16 wt% of Al in the final catalysts) were mixed in toluene whose volume was about 150 % in excess of the pore volume of the used silica. This activated catalyst/co-catalyst (i.e., THI/MAO/toluene) mixture was then poured onto the silica drop wise followed by heating at 50 ºC for one hour without any stirring under argon and condenser arrangement in order to reflux the evaporating toluene. After 1 h of impregnation time, the slurry was allowed to settle down and then the supernatant layer was removed first, followed by two washes with n-heptane whose volume was equivalent to the supernatant removed each time. Last step was to vacuum dry the catalyst at 75 ºC for few hours after which a free flowing catalyst was obtained in all cases. The catalyst supported on 36 µm sieved fraction was named as THI/36 whereas the one supported on 80 µm fraction was named as THI/80. ICP-AES characterization of THI/36 and THI/80 catalysts is shown in **Table 10** where it can be seen that the metal loadings of both the different sized catalysts is very similar and the Al/Zr molar ratio is less than that of THI/MAO/G948F catalysts probably due to the applied washing steps.

Slurry phase ethylene homopolymerizations at two different pressures were conducted using THI/36 catalyst in order to analyse the effect of ethylene pressure on reaction rate profile,

polyethylene MWD and the presence of leaching. **Figure 36a** and **d** compare the effect of ethylene pressure on reaction rate profile of THI/36 catalyst and on the MWD of HDPE samples produced by using MSP-2, respectively. An increase in reaction rate and in molar mass of the final HDPE is evident with increasing ethylene concentration inside the reactor. A very thin polymer film was observed around the reactor wall and some haziness in the reactor diluent indicative of some dissolved polyethylene (see **Figure 36b**) at the end of the reaction with 2 mmole.L^{-1} concentration of TEA, whereas no such thing was observed when TEA concentration was reduced to 1 mmole.L^{-1} as shown in **Figure 36c**. M_w of the HDPE samples were found to be 120,000 g.$mole^{-1}$ (Đ = 3.4) and 210,000 g.$mole^{-1}$ (Đ = 3.5) at 8 and 11 bar, respectively, which indicates that transfer assisted by the monomer is not the dominant chain transfer mechanism with this zirconocene. The obtained Đ values are slightly higher than 3 which are in close agreement with the work of Collins et al.,[22] whose polypropylene samples produced on silica supported THI/TMA catalyst showed Đ values of 2.8. Similarly, Soga et al.,[23] obtained polypropylene samples with a Đ value of 4 to 4.8 by $MgCl_2$-supported-THI catalyst. It should be noted that low TEA concentration used at higher ethylene pressure probably did not impact the MWD because in the previous **Chapter 3** it has been shown that changes in TEA concentration does not impact the MWD of HDPE produced with silica supported (n-BuCp)$_2$$ZrCl_2$/MAO metallocene system.

In contrast to the results obtained with TEA as scavenger, huge reactor fouling was observed when TIBA was used as the scavenger for the homopolymerization conducted with THI/36 catalyst under identical conditions with the same polymerization protocol i.e., MSP-2, as shown in **Figure 36e**. This observation further supports the previous results that the interaction of indenyl metallocenes with TIBA seems to be very different from that of cyclopentadienyl ring based metallocenes because even after two washes during the synthesis of THI/36 catalyst, it showed leaching when TIBA was present as scavenger in the reactor diluent. Therefore, it was decided to evaluate these catalysts in gas phase polymerizations because of no leaching problem in gas phase process. Nevertheless, reaction rate profiles of two homopolymerizations conducted with THI/80 catalyst at 11 bar ethylene pressure and 1 mmole.L^{-1} concentration of TEA in heptane are compared with the profiles of THI/36 catalyst in **Figure 37** which shows that, in agreement with the results obtained for silica supported (n-BuCp)$_2$$ZrCl_2$/MAO catalysts of the same size, the bigger the catalyst particles the lower is the instantaneous polymerization rate. Despite the leaching, the polymerisation rate found with the THI/80 catalyst is quite reproducible.

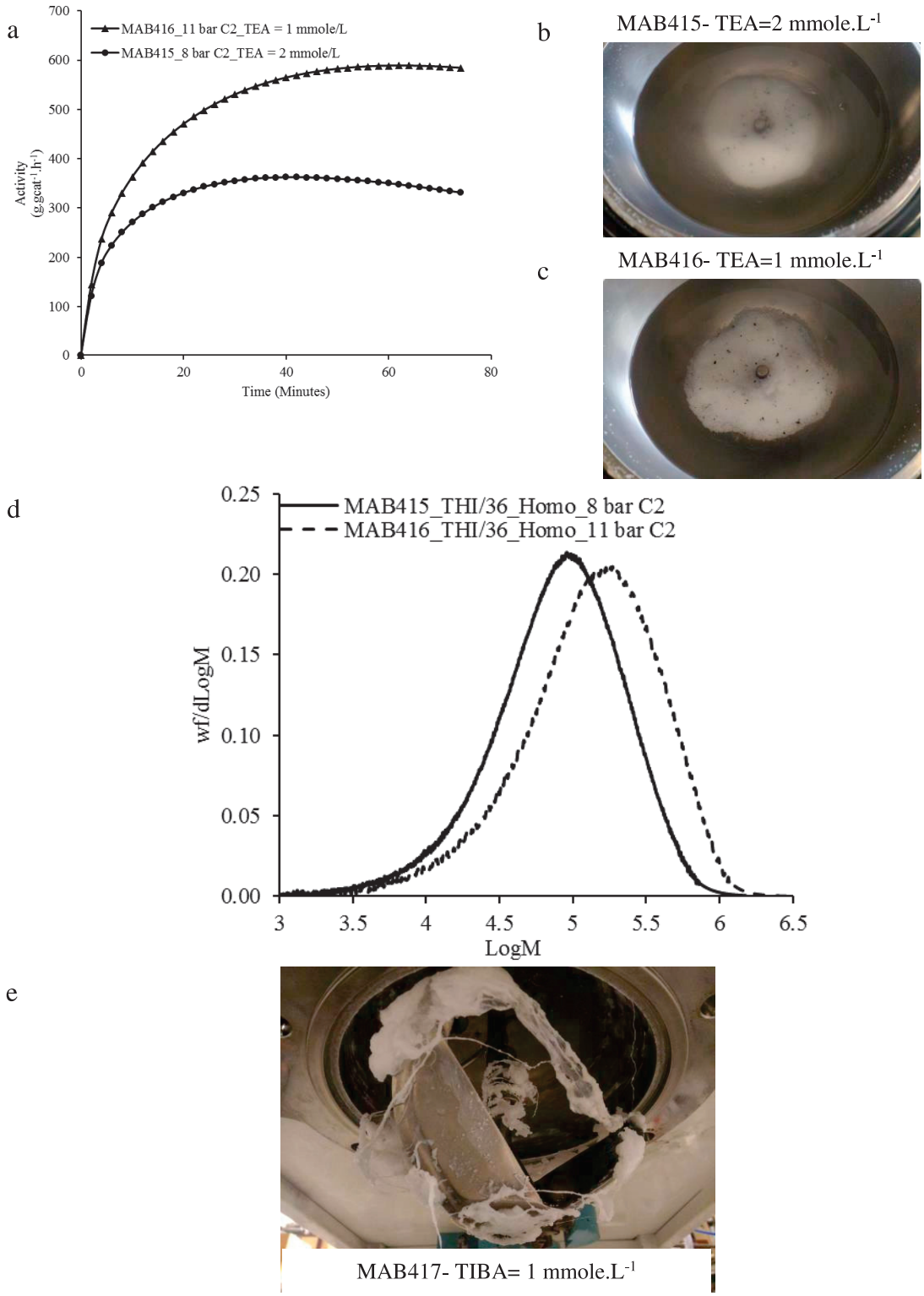

Figure 36. Effect of ethylene pressure on (a) reaction rate profile of THI/36 catalyst, (b,c) reactor condition at the end of MAB415 and MAB416, respectively (d) MWD of HDPE produced with THI/36 catalyst and (e) reactor condition at the end of homopolymerization with THI/36 catalyst using TIBA as scavenger in the concentration of 1 mmole.L^{-1}.

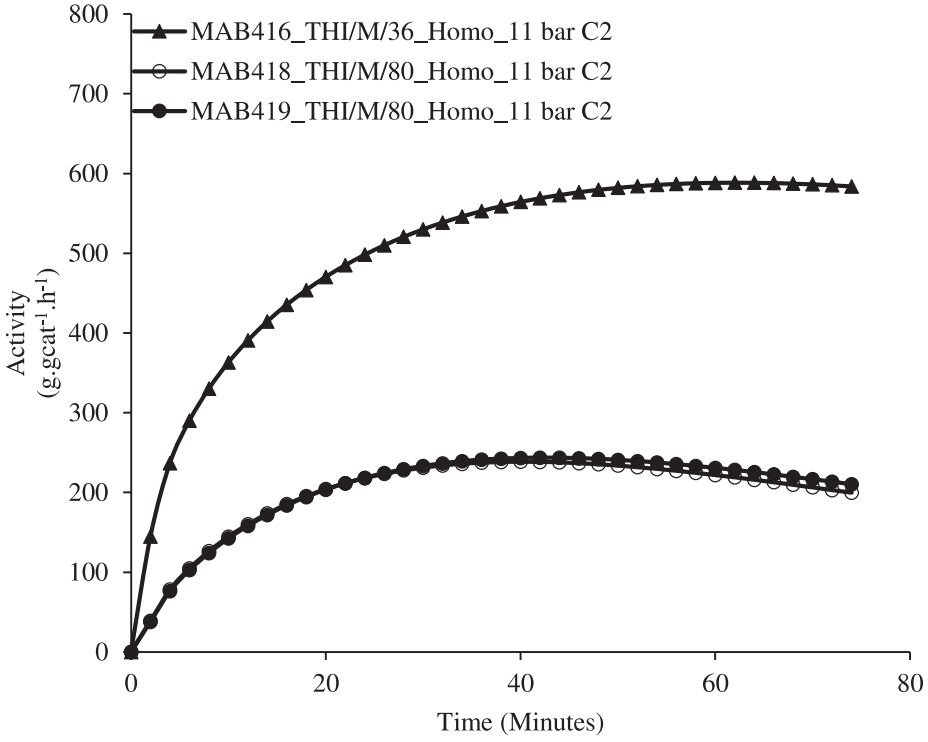

Figure 37. Effect of silica support particle size on (a) reaction rate of silica supported THI/MAO catalyst in slurry phase ethylene homopolymerizations with TEA (=1mmole.L^{-1}) as scavenger.

3.4. Conclusion from Particle Size Study

The particle size of silica supported metallocene/MAO catalysts is an important physical property which can impact the kinetic behaviour of single-site catalysts significantly in slurry phase ethylene homo- and ethylene/1-hexene copolymerizations under conditions of industrial relevance. If other physical properties like pore volume, pore diameter and surface area of the silica supported metallocene/MAO catalysts are kept similar (as achieved in this work by sieving the full batch of commercial silicas), along with the metal loadings, the smaller catalyst particles are more active than their bigger counterparts. This effect of supported catalyst's particle size on its instantaneous activity seems to be the same at different monomer pressures and in the presence and absence of a comonomer (like 1-hexene). The most obvious explanation for this dependence of catalytic activity on its particle size is the existence of intraparticle (co)-monomer diffusion resistance, which is expected to be higher in the case of bigger supported catalyst particles than for smaller catalyst particles.

Our results are in good agreement with the modelling effort of Floyd et al.,[24] whose detailed work on slurry phase ethylene polymerizations with low to high activity heterogeneous catalysts suggest that the effect of intraparticle mass transfer resistance is more visible on the reaction rate profiles than on the MWDs of the obtained polyolefins. The results presented in this work are partially complicated by the in-situ hydrogen generation by the catalyst which can have a significant effect on the MWD of the final polymer. Nevertheless, the MWDs of the polymers obtained with Grace 948 silica based catalysts clearly show that the bigger catalyst particles produced polyethylene with a slightly higher molar mass than the molar mass of the polyethylenes produced with more active smaller catalyst particles. A similar trend was also observed when the MWDs of the polyethylenes produced with the reference catalysts supported on full batches of three silicas were compared. Therefore, it can be suggested that less in-situ hydrogen was generated due to low activity of bigger catalyst particles which finally led to polyethylenes with higher molar masses as compared to the polyethylene produced with more active smaller catalyst particles (where higher in-situ hydrogen concentrations would be expected). This provides an indirect but somewhat valid proof for the existence of higher mass transfer resistance levels in catalysts of bigger particle sizes than in the smaller ones. We will return to this point in the next chapter.

Distribution of MAO inside the used silica support particles was found to be a strong function of particle size depending upon the internal and external pore structure of the silica under consideration. It was found by SEM-EDX analysis that smaller catalyst particles can have a

better inner MAO distribution than the bigger ones where core-shell Al distribution was observed at low impregnation times during catalyst synthesis, if the silica support has a well-connected internal and external pore structure without any macropores or interstitial voids e.g., in the case of PQ silicas used in this work. On the other hand, if the silica has interstitial voids (like Grace 948 silica made from spray drying process) the distribution of MAO seems to be independent of particle size which can probably be attributed to the numerous diffusion paths offered by the interstitial voids present internally and externally on silica surface. Such differences in MAO distribution inside the catalyst particles can lead to significantly different monomer concentration gradient inside the catalyst particles during the course of polymerization

3.5. Effect of Pore Volume, Pore Diameter and Surface Area of the Silica Supports on the Catalytic Activity, Molecular Properties and Physical Properties of Polyethylene

In the previous section, the effect of silica support particle size on the reaction kinetics of supported metallocene/MAO system was analysed by supporting $(n\text{-BuCp})_2ZrCl_2$/MAO and THI/MAO catalysts on sieved fractions of three commercial silicas. The benefit of sieving the full batch of each silica is that the obtained fractions of each silica have other physical properties (like pore volume, pore diameter and surface area) that remain the same from size cut to size cut. This allowed us to attribute all the observed differences in the i) reactions kinetics of the catalysts ii) molecular properties like MWD of the homo- and copolymers produced and iii) physical properties of these polymer samples to the silica support particle size. Furthermore, the distribution of Al (and active sites due to pre-activated catalysts) was also attributed, partially, to the difference in particle size of the support. Therefore, the effect of pore volume (P_v), pore diameter (P_d) and surface area (A_s) of the silica supports (used in this work) on the reactions kinetics of silica supported $(n\text{-BuCp})_2ZrCl_2$/MAO catalyst and different polymer properties can be better assessed by keeping the particle size constant (or very similar).

For this purpose, the PSD of the sieved fractions of each silica was measured and their comparison shows that the sieving operation provided the particles of different silica with very similar PSDs, as shown in **Figure 38**. The PSD span of the sieved fractions of each silica are compared in **Table 11** which indicates more or less the same breadth of the PSD curves of all the sieved fractions and further supports the good separation level achieved by the sieving operation. This similarity in the PSDs of the sieved fractions of different silicas (and therefore, the supported catalysts) allows us to assign the observed difference in their kinetic profiles in slurry phase ethylene homo- and copolymerizations with 1-hexene to their different P_v, P_d and A_s.

Along the same lines, we will attempt to correlate any differences in the MWDs, melting temperatures and comonomer contents of the polyethylene samples to these physical properties. Once again, it is important to mention that since no stirring was used during any step of the supported catalysts synthesis, each catalyst should inherit the corresponding silica fraction PSD shown in **Figure 38** (e.g., the PSD of BG-4 catalyst should be the same as that of the pan fraction of Grace 948 silica shown in **Figure 38a**). Moreover, the used silica are commercial ones so it was not possible to vary only one physical property while keeping all others constant. Therefore, in this section it may not be easy to separate completely the effects

of, for example, catalyst surface area from those of pore volumes by just keeping the particle size constant.

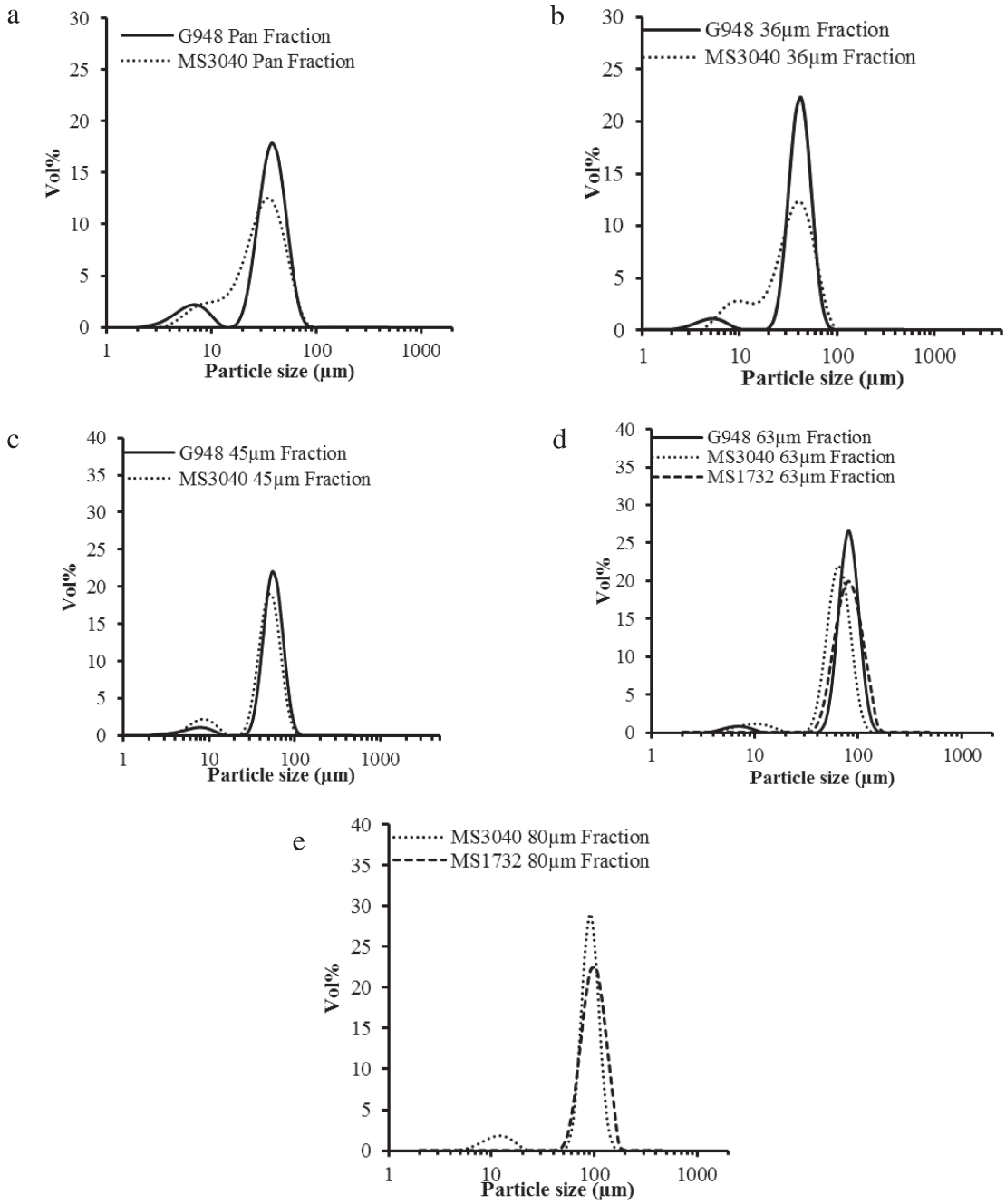

Figure 38. Comparison of the PSD of sieved fractions of each silica used in this work. 80µm fraction of Grace 948 fraction was completely used for catalyst synthesis and therefore, PSD of silica was not measured.

Table 11. Comparison of d_{10}, d_{50}, d_{90} and span of the different sieved fractions of three commercial silica used in this work.

No.	Sieve opening (µm)	Catalyst Name	Support Name	d_{10} (µm)	d_{50} (µm)	d_{90} (µm)	Span
1	Pan	BG-4	Grace 948	8.2	35.9	53.3	1.26
2	Pan	BM-4	PQMS3040	10.4	30.1	51.7	1.37
3	36	BG-2	Grace 948	27.6	40.9	56.9	0.72
4	36	BM-2	PQMS3040	10.1	34.4	59.4	1.43
5	45	BG-1	Grace 948	35.9	55.1	76.4	0.74
6	45	BM-3	PQMS3040	11.1	48.9	71.1	1.23
7	63	BG-3	Grace 948	58.9	79.9	106.0	0.59
8	63	BM-1	PQMS3040	40.3	63.0	87.2	0.74
9	63	BP-1	PQMS1732	55.2	80.5	117.0	0.77
10	80	BG-5	Grace 948	-	-	-	-
11	80	BP-2	PQMS1732	70.0	98.0	135.0	0.66
12	125	BP-3	PQMS1732	113.0	167.0	246.0	0.80

A comparison of the metal loadings, P_v, P_d and A_s of supported catalysts prepared with the same sized fraction of each silica is presented in **Table 12**. The ICP-AES elemental characterization shows that the Al/Zr molar ratio of all the catalysts vary in the range of 199 to 284 which is not extremely broad and the variations can be attributed to the fact that each catalyst was made independently. Among these catalysts, pore volumes of the ones prepared with the fractions of PQMS 3040 are the highest (as they are in the range of 1.30 to 1.46 $cm^3.g^{-1}$), whereas those of the catalysts prepared with Grace 948 fractions can be considered as intermediate (as they are in the range of 0.68 to 0.81 $cm^3.g^{-1}$) if we consider the P_v of the catalysts prepared from PQMS 1732 silica as the lowest (as they are in the range of 0.45 to 0.66 $cm^3.g^{-1}$). P_d of the catalysts supported on the fractions of Grace 948 and PQMS 3040 silica are very similar, whereas the pore diameter of the catalysts based on PQMS 1732 fractions are about half the value of those based on the Grace 948 and PQMS 3040 silica fractions. With respect to surface area, the catalysts based on the fractions of PQMS 3040 and PQMS 1732 silica are very similar but higher than the surface area of those supported on Grace 948 fractions. These results are very much in-line with those observed for the supported catalysts prepared with full batches of these silica (see **Table 3**, **Table 4** and **Table 5**).

Table 12. BET and ICP-AES analysis of the catalysts prepared by using different sieved fractions of different silica used in this work. A_s = surface area of the catalyst measured by BET, P_v = BJH desorption Pore volume of the catalyst measured by BET, P_d = Pore diameter of the catalyst measured by BET.

No.	Sieve opening (µm)	Catalyst Name	Support Name	A_s (m^2/g)	P_v (cm^3/g)	P_d (nm)	Zr (Wt%)	Al (Wt%)	Al/Zr Molar Ratio
1	Pan	BG-4	Grace 948	265	0.81	11.6	0.21	14.3	230
2	Pan	BM-4	PQMS3040	395	1.31	10.7	0.23	15.8	232
3	36	BG-2	Grace 948	284	0.81	10.9	0.19	12.4	220
4	36	BM-2	PQMS3040	401	1.31	11.1	0.17	14.3	284
5	45	BG-1	Grace 948	230	0.68	10.7	0.19	12.5	222
6	45	BM-3	PQMS3040	375	1.30	11.9	0.18	13.4	251
7	63	BG-3	Grace 948	269	0.75	10.8	0.18	12.5	234
8	63	BM-1	PQMS3040	390	1.46	12.4	0.19	11.8	209
9	63	BP-1	PQMS1732	389	0.57	5.5	0.23	13.6	199
10	80	BG-5	Grace 948	289	0.80	10.8	0.20	15.6	263
11	80	BP-2	PQMS1732	311	0.45	5.5	0.19	14.9	265
12	125	BP-3	PQMS1732	417	0.66	5.4	0.22	14.4	221

As shown in the previous sections that the internal and external particle surface and macroscopic morphology of the two PQ silica used in this work are very similar, but their pore dimensions are significantly different. It will be beneficial for the sake of understanding to start analysing the results from the catalysts prepared with the sieved fractions of these silica. **Figure 39 a** and **b** presents a comparison of kinetic profiles of BP-1 (i.e., the catalyst supported on 63 µm sieved fraction of PQMS 1732) and BM-1 (i.e., the catalyst supported on 63 µm sieved fraction of PQMS 3040) catalysts in ethylene homo- and copolymerizations, respectively. It can be seen that BP-1 catalyst activates faster than BM-1 in both homo- and copolymerizations, and reaches a higher activity.

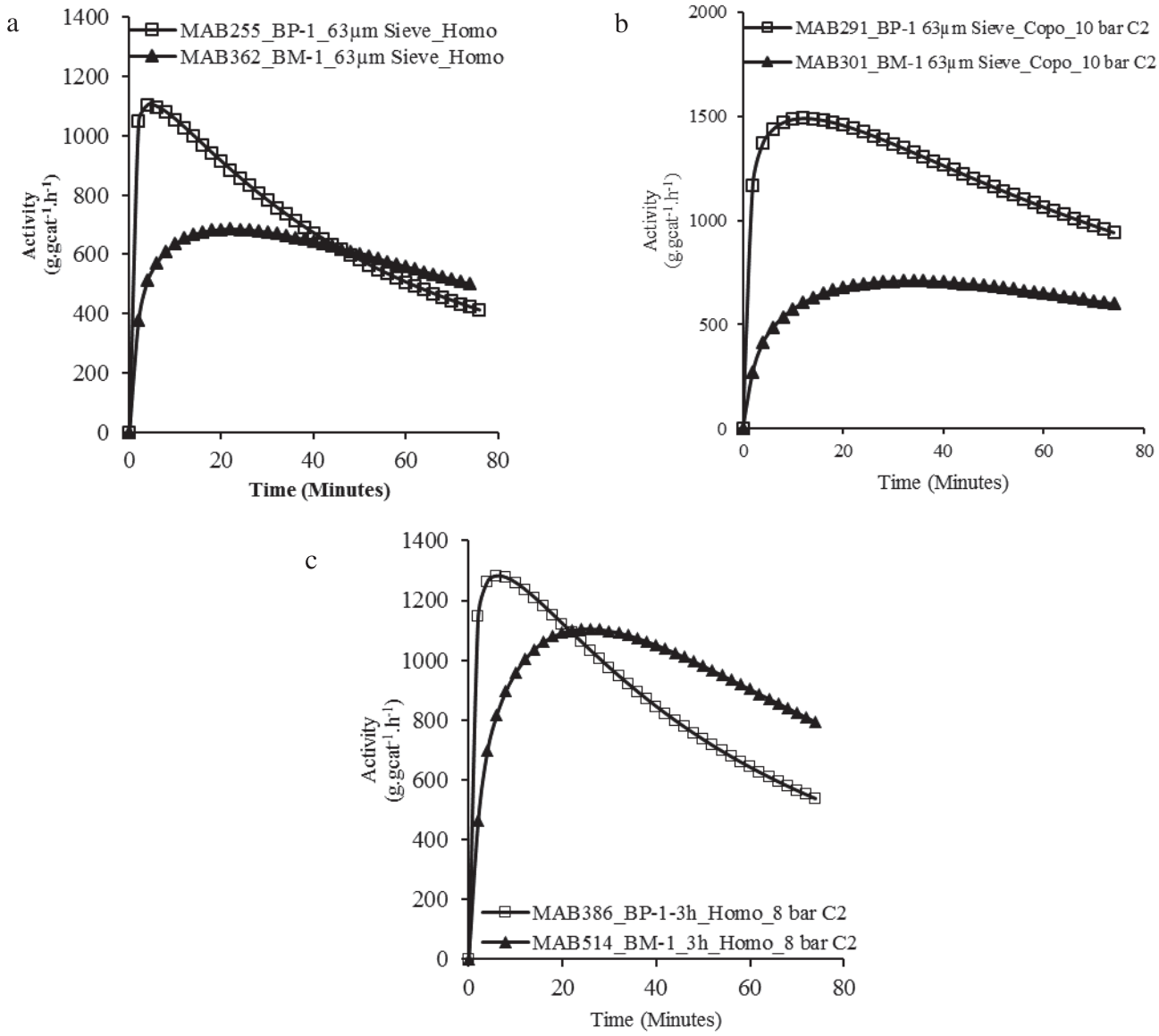

Figure 39. Comparison of the kinetic profiles of BP-1 and BM-1 catalysts in slurry phase ethylene homo- and copolymerisations (a, b). Comparison of kinetic profiles of BP-1-3h and BM-1-3h catalysts in ethylene homopolymerisation.

Table 12 shows that both the catalysts bear similar Al/Zr molar ratios and **Figure 38d** tells us that the particle sizes of these two catalysts also quite similar. Their macroscopic morphologies are very similar (especially in terms of uniformity and lack of visible macropores), and they come from the same manufacturer so it is reasonable to suppose that their chemical compositions are similar. Thus, the differences in their kinetic profiles can most likely be attributed to the differences in their pore volumes and pore diameters.

A look on the pore volume and pore diameter of these catalysts shown in **Table 12** reveals that BP-1 catalyst has pore volume and pore diameter values which are 60 % and 55 %, respectively,

less than those of BM-1 catalyst. The time taken by BP-1 catalyst to reach the peak activity in homopolymerization is 82% higher than the time taken by BM-1 catalyst to achieve its peak activity, and the difference is similar in copolymerization. Therefore, the faster activation of BP-1 catalyst than BM-1 catalyst, in both types of the reactions seems to be correlated with smaller P_d and P_v values. It is possible that the amount of the polymer required to fill the pore volume of the growing BP-1 catalyst/polymer particles will be 60% less than that required to fill the pore volume of BM-1 catalyst which leads to faster fragmentation of the BP-1 catalyst particles than that of BM-1 catalyst particles and therefore causes difference in the activation of these catalysts. It should also be noted that all things being equal, larger pore volumes correspond to more friable supports. It is not entirely clear what role this plays in terms of the observed activity profiles. Regardless, it is important to note that even if the fragmentation explanation given above can explain the rapid activation of the BP catalysts, it does not explain the overall different shapes and the fact that occasionally it seems to take a much longer time for BM to reach activities on the order of those seen for BP. Perhaps if the supports fragment differently, the micrograins of the BP catalyst are more deeply buried in layers of polymer, meaning that mass transfer resistance to diffusion of monomer through the polymer controls the rate more in this case than in the other.

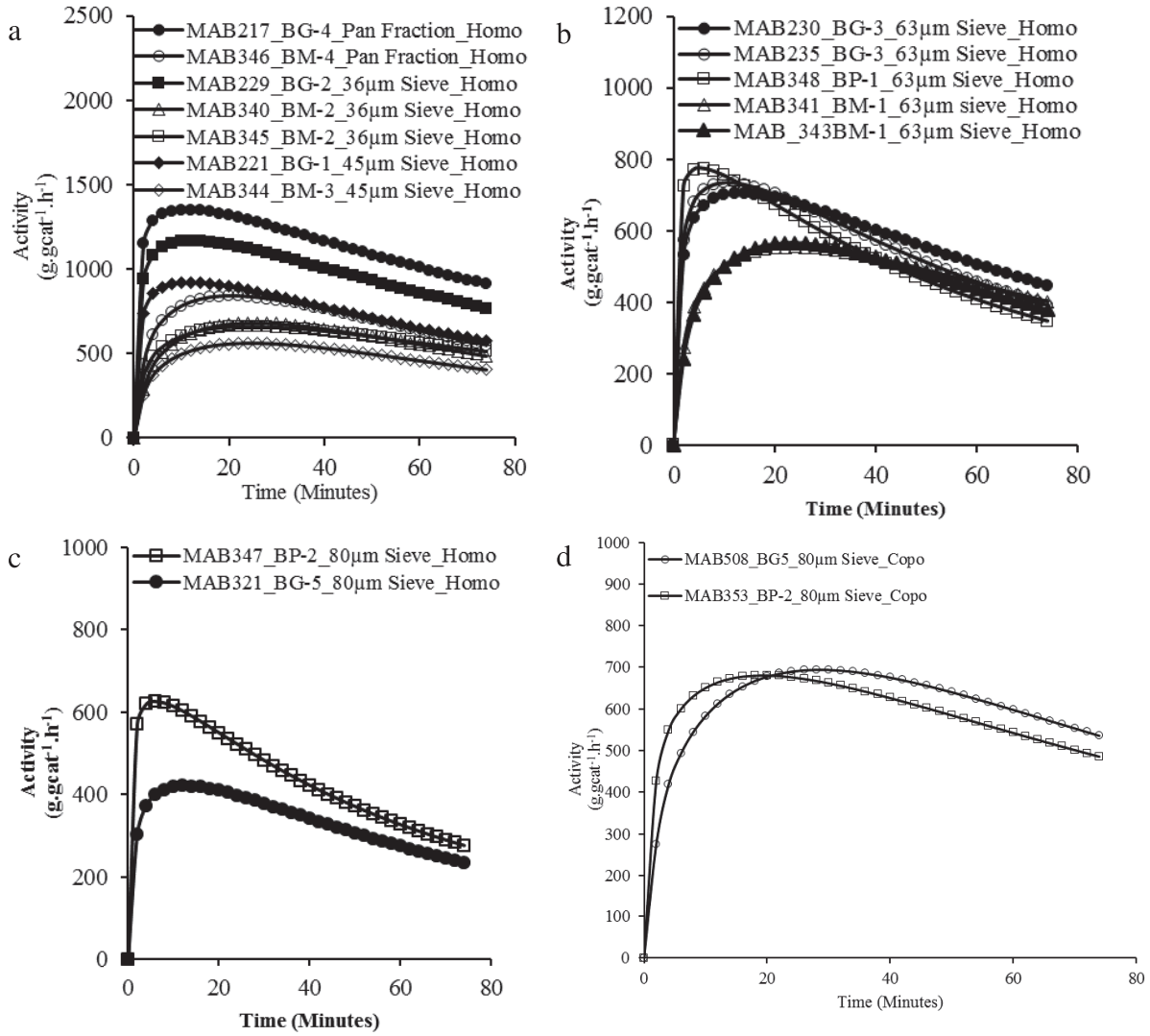

Figure 40. Comparison of slurry phase homopolymerization kinetic profiles (a - c) and (d) copolymerization activity profiles of the silica supported catalysts prepared from same sized fractions of different commercial silica.

A comparison of the BG, BM and BP activity profiles for different cuts and for homo- and copolymerization runs are shown in **Figure 40**. Further confirmation of the effect of P_v and P_d on the reaction kinetics can be obtained by comparing the kinetic profiles of the BG and BM cuts in **Figure 40a**. It can be seen that the BG catalysts with the smaller pore volume has consistently higher activities than the BM catalysts of the same size. In **Figure 40b**, activity profiles found with BG-3 (i.e., the catalyst supported on 63 µm fraction of Grace 948 silica with the intermediate pore volume, but closer to BP) are compared with those of BP-1 and BM-1 (same size, different P_v). BG-3 activates more quickly than BM-1, and at a rate similar to that of BP-1. The results in **Figure 39** and **Figure 40** allow us to arrange these three catalysts in the order BP-1 > BG-3 > BM-1 on the basis of the time required to achieve peak activity. Keeping

in view that the metal loadings of BG catalysts are also very similar to the other two catalysts, it can now be suggested with reasonable confidence that the lower the pore volume of the silica supported catalyst the higher is the activation rate. One explanation for this is that the lower pore volume might correspond to a more rapid fragmentation of growing macroparticles, which leads to faster exposure of the hidden active sites in the particle interior as compared to the catalyst particle with bigger pore volume. In addition, the amount of the injection liquid (heptane in this case) present in the pores of the catalyst will be higher for a higher pore volume catalyst which can pose additional resistance to (co)-monomer(s) transport at the active sites leading to low activation rates of high pore volume silica supported metallocene/MAO catalysts. Note that heat transfer effects are less significant in slurry phase than in gas phase polymerizations, and since the particle size is kept constant for these catalysts the effects of heat transfer, if any, should be similar for all of the considered catalysts. The same reasoning can be used to explain the differences in the catalytic activities of BP-2 and BG-5 catalysts (i.e., the catalysts supported on 80 µm sieved fractions of PQMS 1732 and Grace 948 silica, respectively) shown above (see **Figure 40c**) which allows us to further conclude that, despite the differences in the silica morphology, the pore volume and pore diameter of the silica supported catalyst are the most important physical properties provided that the particle size is kept constant.

With respect to surface area, it appears difficult to conclude since the BP catalysts have specific surface areas comparable to those of BM catalysts and show higher activities than the latter ones. On the other hand, BG catalysts have lower surface areas than BM catalysts but show higher activities than BM catalysts. Therefore, it can be suggested that the effect of specific surface area of these catalysts is dominated by the effects of their pore volumes and pore diameters.

The effect of catalyst P_v and P_d on the MWD of the slurry phase homo- and copolymers is shown in **Figure 41**, whereas **Table 13** compares the M_w, molar mass dispersity (Đ) and melting temperature (T_m) of the same samples. MWDs of the HDPE samples produced with the catalysts supported on pan fraction, 36 µm and 45 µm fractions of Grace 948 and PQMS 3040 silicas overlap each other despite significant differences in the activities of the catalysts from which they originated (**Figure 41a**), and the same can be noticed for the Đ values of the respective samples shown in **Table 13**.

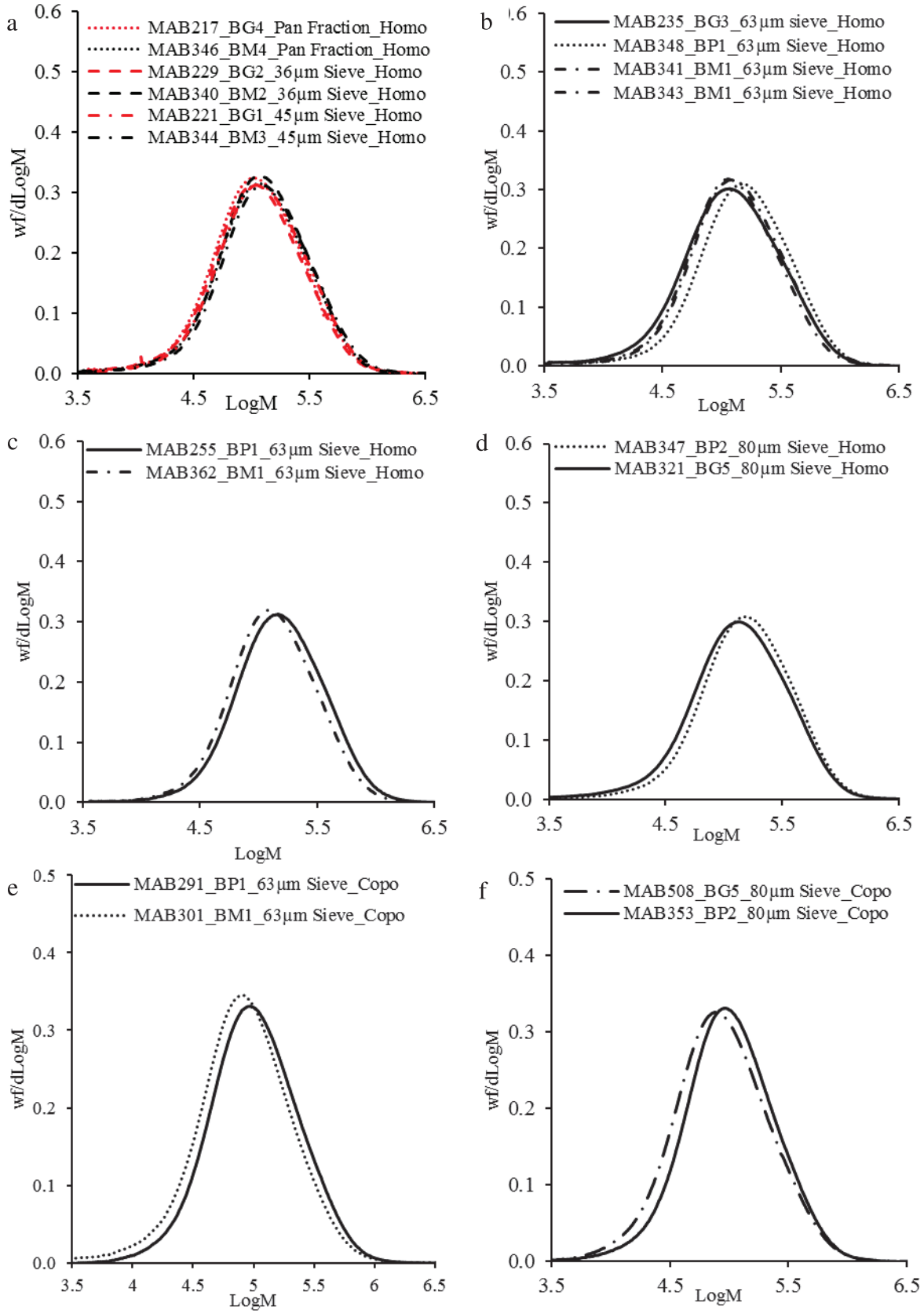

Figure 41. Comparison of the MWD of slurry phase homopolymer samples (a to d) and copolymer samples (e, f) produced with the silica supported catalysts prepared from same sized fractions of three different commercial silica.

Single-site nature of (n-BuCp)$_2$ZrCl$_2$/MAO catalyst seems to be unchanged by the variations in different physical properties of the silica supports as the molar mass dispersity of each sample is close to 2. However, as we move on to compare the MWDs of the polyethylene samples produced with catalyst supported on fractions of PQMS 1732 silica with the MWDs of the polymers produced with the catalysts supported on PQMS 3040 and Grace 948 silica fractions of equivalent size some clear differences become visible as shown in **Figure 41b** to **f.** The molar mass of the samples produced with all the catalysts supported on PQMS 1732 silica fractions seem to be (slightly) higher than that of the samples produced with the catalysts supported on the other two silicas used in this work as shown by M_w values also (see **Table 13**).

This behaviour can be better explained based upon pore confinement effect rather than in-situ hydrogen generation effect. It should be noted that BP catalysts showed higher activities and therefore, may have generated more in-situ hydrogen as compared to BG and BM catalysts which should have led to low molar masses of the polyethylenes produced with the BP catalysts. dos Santos et al.,[25] observed similar dependence of the M_w of polyethylene on the catalyst pore diameter i.e., the samples produced with smaller pore diameter catalysts showed higher M_w as compared to those produced with wider pore catalysts and attributed it to the pore confinement effect of smaller pores due to which the formed polymer chains are extruded out, as described by the extrusion polymerization mechanism of Aida et al.,[12] who used mesoporous nanofibrous silica (MSF) of pore diameter equal to 2.7 nm (27 Å) as a support for Cp$_2$Ti/MAO catalyst. They showed that ultra-high molecular weight polyethylene can be produced at 10 bar ethylene pressure and 20 °C by using this supported catalyst of very small pore dimensions. On the other hand, the same catalyst supported on an amorphous silica gave polyethylene of ordinary characteristics which allowed Aida et al.,[12] to attribute the very high molar mass and linear nature of the produced polyethylene to the pore confinement effect of the used support. In the present work, same effect can be considered responsible for the differences in the MWDs of the polyethylenes (i.e., either HDPE or copolymer) produced with the catalysts supported on PQMS 1732 and the two other silicas. No differences in **Figure 41a** can be seen which is probably due to the fact that the pore diameters of all the catalysts are very similar as shown in **Table 12** and therefore, the level of extrusion polymerization, if exists, is similar in all the catalysts supported on these two silicas. However, 50% smaller pore diameter values for all the catalysts based on PQMS 1732 silica (see **Table 12**) indicates that the extrusion polymerization

mechanism happening in the pores of PQMS 1732 based catalysts should be different from that happening in the supported catalysts of Grace 948 and PQMS 3040 silicas.

This allows us to attribute the higher molar masses of both homo- and copolymer samples produced with low pore diameter catalysts (i.e., BP-1 and BP-2) as compared to the molar masses of polymers produced with higher pore diameter catalysts (i.e., BG-3, BM-1 and BG-5) to the different level of extrusion polymerization mechanism in the former catalysts than that in the latter ones. In order to confirm that the observed differences are not due to HT-SEC related reproducibility issues, MWD measurements of some of the samples done with the another set of HT-SEC columns is presented in **Figure 42** which supports the trends shown in **Figure 41a**.

Comonomer contents and melting temperatures of the obtained homo- and copolymers seem to be independent of pore volume, pore diameter and surface area of these catalysts as shown in **Figure 43** (for some of the samples) and **Table 13**.

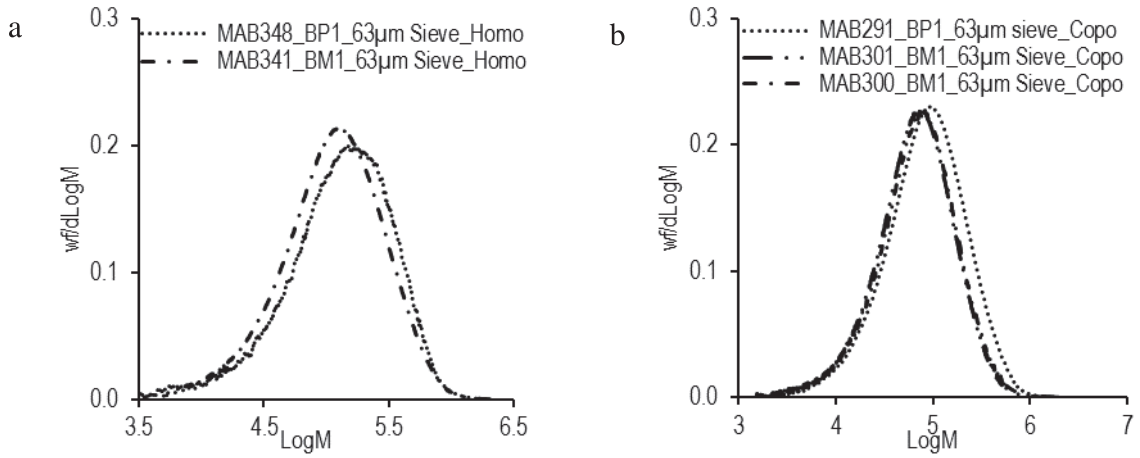

Figure 42. MWD measurement of homo- and copolymer samples produced with BP-1 and BM-1 catalysts with another set of HT-SEC columns.

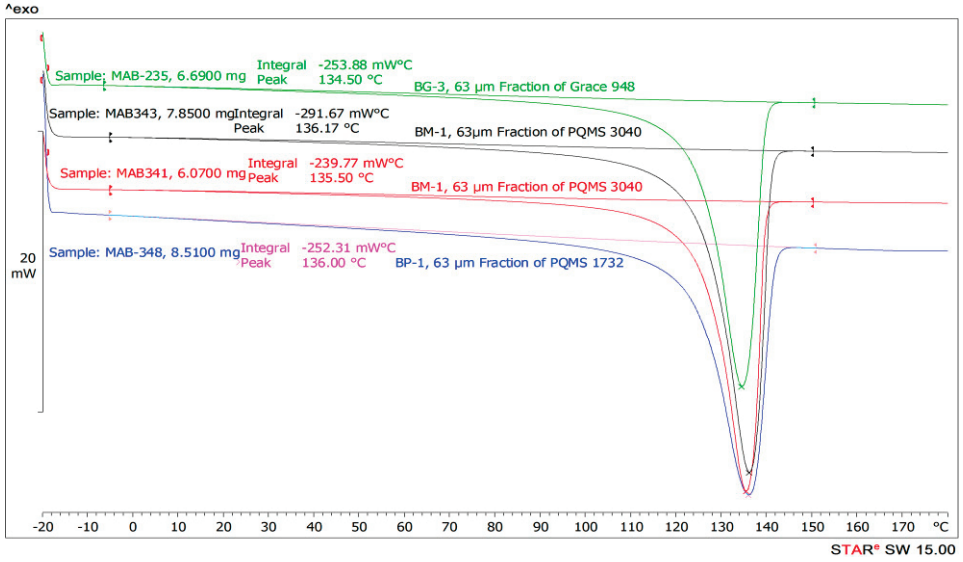

Figure 43. Comparison of second heating of the HDPE samples produced with BG-3, BM-1 and BP-1 catalysts.

Table 13. Mw, Đ, T_m and comonomer content (x%) of the homo and copolymer samples produced with the same sized fractions of the three different commercial silica. $A_{1\text{-hexene}}$ indicates the amount of 1-hexene used in copolymerizations. x_{NMR} and x_{CEF} means co-monomer estimation with ^{13}C NMR and CEF, respectively. G948 = Grace 948, PQ3040 = PQMS 3040, PQ1732 = PQMS 1732.

No.	Sieve opening (µm)	Catalyst Name	Support Name	Sample Name	$A_{1\text{-hexene}}$ (ml)	M_w (g.mol^{-1})	Đ	T_m (°C)	x_{NMR} (mol%)	x_{CEF} (mol%)
1	Pan	BG-4	G948	MAB217	-	160000	2.4	134.5	-	-
2	Pan	BM-4	P3040	MAB346	-	176000	2.6	135.8	-	-
3	36	BG-2	G948	MAB229	-	160000	2.4	134.5	-	-
4	36	BM-2	P3040	MAB340	-	175000	2.4	135.8	-	-
5	45	BG-1	G948	MAB221	-	175000	2.5	134.8	-	-
6	45	BM-3	P3040	MAB344	-	190000	2.4	135.8	-	-
7	63	BG-3	G948	MAB235	-	185000	2.6	134.5	-	-
8	63	BM-1	P3040	MAB341	-	180000	2.6	135.5	-	-
9	63	BP-1	P1732	MAB348	-	220000	2.2	135.0	-	-
10	63	BP-1	P1732	MAB255	-	220000	2.1	136.1	-	-
11	80	BG-5	G948	MAB321	-	200000	2.7	134.7	-	-
12	80	BP-2	P1732	MAB347	-	225000	2.4	135.5	-	-
13	63	BG-3	G948	MAB297	3	170000	2.8	129.2	-	0.5
14	63	BP-1	P1732	MAB352	3	140000	2.1	129.3	-	0.6
15	63	BM-1	P3040	MAB301	3	120000	2.3	128.7	-	0.6
16	63	BP-1	P1732	MAB291	3	145000	2.1	129.0	-	0.5
17	80	BG-5	G948	MAB508	3	130000	2.4	131.8	0.5	0.6
18	80	BP-2	P1732	MAB353	3	150000	2.2	130.0	-	0.6

3.6. Conclusion from the Effect of Porosity Study

Silica supported (n-BuCp)$_2$ZrCl$_2$/MAO catalysts of equal sizes but different pore volumes, pore diameters and surface areas evaluated in slurry phase ethylene homo- and ethylene/1-hexene copolymerizations reveal that pore diameter and pore volume seem to impact significantly the instantaneous activity of the catalyst in both types of polymerizations. Higher activation rates were observed for the supported catalysts of lower pore volume when the internal and external morphology of the catalyst particles was kept similar along with constant particle size (i.e., PQMS 1732 and PQMS 3040 supported catalysts). Since the level of mass transfer resistance can be assumed to be constant due to same particle sizes, this observation can be attributed to the delayed fragmentation of the supported catalyst with higher pore volume as compared to that with lower pore volume. The same effect of difference in pore volumes was noticed when two silica supported catalysts having different external and internal morphologies were evaluated in slurry phase ethylene (co)-polymerizations (i.e., Grace 948 and PQMS 3040 supported catalysts).

Pore diameter of the supported catalysts showed its influence on the MWD of the obtained polyethylenes in a way that those samples which were produced by using low pore diameter catalysts possessed somewhat higher molar masses than those produced with the catalysts of wider pores under identical conditions. Such an effect of pore diameter on the MWD of the produced polyethylenes can be attributed to pore confinement effect. Among the catalyst particles of same external and internal morphologies those with higher surface area (i.e., PQMS 1732 silica supported catalysts) showed higher instantaneous activity, however, this effect was reversed when the supported catalysts of Grace 948 silica and PQMS 3040 silica (which have different morphologies) were compared.

4. References

1. Soares, J B P, McKenna, T F L., Polyolefin Reactors and Processes, In Polyolefin Reaction Engineering, Wiley-VCH Verlag GmbH & Co. KGaA, **2012**.

2. Floyd, S, Choi, K Y, Taylor, T W, Ray, W H, Polymerization of olefins through heterogeneous catalysis. III. Polymer particle modelling with an analysis of intraparticle heat and mass transfer effects, J. Appl. Polym. Sci., **1986**, 32, 2935-2960.

3. Tisse, V F, Prades, F, Briquel, R, Boisson, C, McKenna, T F L, Role of Silica Properties in the Polymerisation of Ethylene Using Supported Metallocene Catalysts, Macromol. Chem. Phys., **2010**, 211, 91-102.

4. Fink, G, Steinmetz, B, Zechlin, J, Przybyla, C, Tesche, B, Propene Polymerization with Silica-Supported Metallocene/MAO Catalysts, Chem. Rev., **2000**, 100, 1377-1390.

5. Turunen, J P J, Venäläinen, T, Suvanto, S, Pakkanen, T T, Novel use of mesoporous aluminas as supports for Cp2ZrCl2 and Cp*ZrMe3: Ethylene polymerization and formation of polyethylene nanofibers, J. Polym. Sci. A Polym. Chem., **2007**, 45, 4002-4012.

6. Kumkaew, P, Wu, L, Praserthdam, P, Wanke, S E, Rates and product properties of polyethylene produced by copolymerization of 1-hexene and ethylene in the gas phase with (n-BuCp)2ZrCl2 on supports with different pore sizes, Polymer., **2003**, 44, 4791-4803.

7. D'Agnillo, L, Soares, J B P, Penlidis, A, Effect of operating conditions on the molecular weight distribution of polyethylene synthesized by soluble metallocene/methylaluminoxane catalysts, Macromol. Chem. Phys., **1998**, 199, 955-962.

8. Folie, B, Ruff, C J, High-pressure polymerization of ethylene and 1-butene with metallocenes: kinetic mechanism inferred from unsaturation, Polymer Preprints(USA)., **1998**, 39, 201-202.

9. Hasegawa, S, Sone, M, Tanabiki, M, Sato, M, Yano, A, High-temperature ethylene/α-olefin copolymerization with a zirconocene catalyst: Effects of the zirconocene ligand and polymerization conditions on copolymerization behavior, J. Polym. Sci. A Polym. Chem., **2000**, 38, 4641-4648.

10. Wasserman, E, Hsi, E, Young, W T, Studies on dihydrogen generation by a bridged metallocene polyethylene catalyst, Polymer Preprints(USA)., **1998**, 39, 425-426.

11. Richardson, D E, Alameddin, N G, Ryan, M F, Hayes, T, Eyler, J R, Siedle, A R, Intrinsic Ancillary Ligand Effects in Cationic Zirconium Polymerization Catalysts: Gas-Phase Reactions of [L2ZrCH3]+ Cations with Alkenes, J. Am. Chem. Soc., **1996**, 118, 11244-11253.

12. Keisuke Kageyama, Jun-ichi Tamazawa, Takuzo Aida, Extrusion Polymerization: Catalyzed Synthesis of Crystalline Linear Polyethylene Nanofibers Within a Mesoporous Silica, Science., **1999**, 285, 2113-2115.

13. Panchenko, V N, Echevkaya, L G, Zakharov, V A, Matsko, M A, Influence of triisobutylaluminum on the polymerization of ethylene by SiO2-supported ansa-zirconocene catalysts, Applied Catalysis A: General., **2011**, 404, 47-53.

14. Wester, T S, Ystenes, M, Kinetic studies of the injection of comonomers during polymerization of ethene and propene with MgCl2-supported Ziegler-Natta catalysts, Macromol. Chem. Phys., **1997**, 198, 1623-1648.

15. Kumkaew, P, Wanke, S E, Praserthdam, P, Danumah, C, Kaliaguine, S, Gas-phase ethylene polymerization using zirconocene supported on mesoporous molecular sieves, J. Appl. Polym. Sci., **2003**, 87, 1161-1177.

16. Floyd, S, Heiskanen, T, Taylor, T W, Mann, G E, Ray, W H, Polymerization of olefins through heterogeneous catalysis. VI. Effect of particle heat and mass transfer on polymerization behavior and polymer properties, J. Appl. Polym. Sci., **1987**, 33, 1021-1065.

17. Bruaseth, I, Bahr, M, Gerhard, D, Rytter, E, Pressure and trimethylaluminum effects on ethene/1-hexene copolymerization with methylaluminoxane-activated (1,2,4-Me3Cp)2ZrCl2: Trimethylaluminum suppression of standard termination reactions after 1-hexene insertion, J. Polym. Sci. A Polym. Chem., **2005**, 43, 2584-2597.

18. Hansen, E W, Blom, R, Kvernberg, P O, Diffusion of Methylaluminoxane (MAO) in Toluene Probed by 1H NMR Spin-Lattice Relaxation Time, Macromol. Chem. Phys., **2001**, 202, 2880-2889.

19. Babushkin, D E, Semikolenova, N V, Panchenko, V N, Sobolev, A P, Zakharov, V A, Talsi, E P, Multinuclear NMR investigation of methylaluminoxane, Macromol. Chem. Phys., **1997**, 198, 3845-3854.

20. Tritto, I, Sacchi, M C, Locatelli, P, Li, S X, Low-temperature 1H and 13C NMR investigation of trimethylaluminium contained in methylaluminoxane cocatalyst for metallocene-based catalysts in olefin polymerization, Macromol. Chem. Phys., **1996**, 197, 1537-1544.

21. Babushkin, D E, Brintzinger, H H, Activation of Dimethyl Zirconocene by Methylaluminoxane (MAO)Size Estimate for Me-MAO- Anions by Pulsed Field-Gradient NMR, J. Am. Chem. Soc., **2002**, 124, 12869-12873.

22. Collins, S, Kelly, W M, Holden, D A, Polymerization of propylene using supported, chiral, ansa-metallocene catalysts: production of polypropylene with narrow molecular weight distributions, Macromolecules., **1992**, 25, 1780-1785.

23. Kaminaka, M, Soga, K, Polymerization of propene with the catalyst systems composed of Al2O3- or MgCl2-supported Et[IndH4]2ZrCl2 and AlR3 (R = CH3, C2H5), Makromol. Chem. , Rapid Commun., **1991**, 12, 367-372.

24. Floyd, S, Choi, K Y, Taylor, T W, Ray, W H, Polymerization of olefines through heterogeneous catalysis IV. Modeling of heat and mass transfer resistance in the polymer particle boundary layer, J. Appl. Polym. Sci., **1986**, 31, 2231-2265.

25. Silveira, F, Pires, G P, Petry, C F, Pozebon, D, Stedile, F C, dos Santos, J H Z, Rigacci, A, Effect of the silica texture on grafting metallocene catalysts, Journal of Molecular Catalysis A: Chemical., **2007**, 265, 167-176.

APPENDIX-1
CHAPTER 4

a

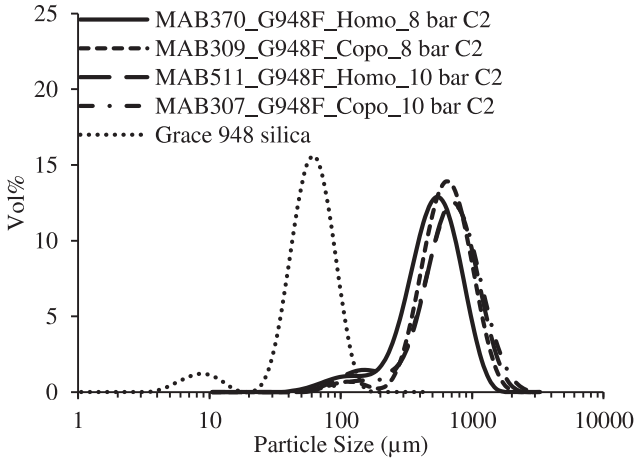

b

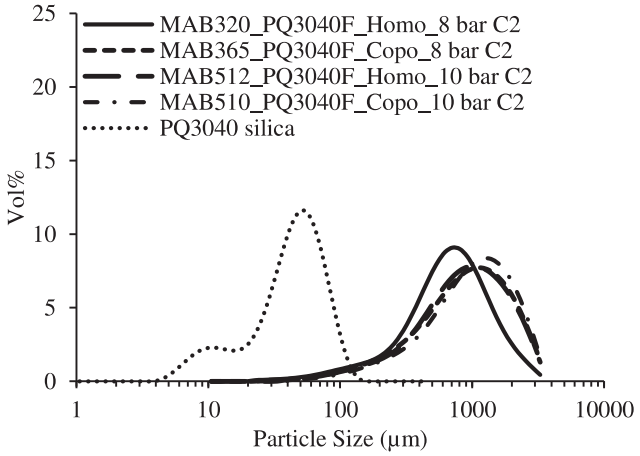

c

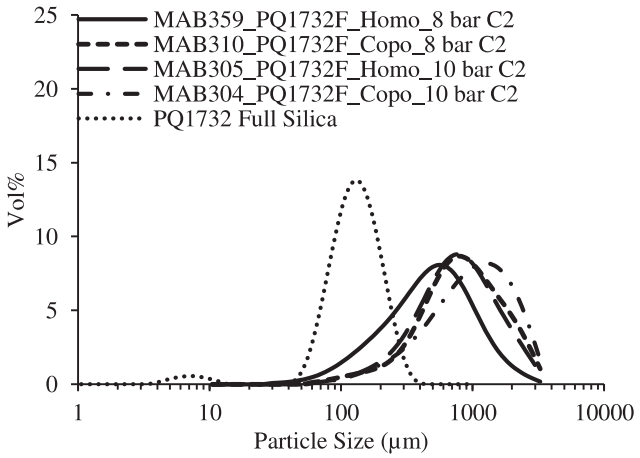

Figure S1. Comparison of pure silica and polyethylene particle size distribution produced with the catalyst supported on corresponding silica support.

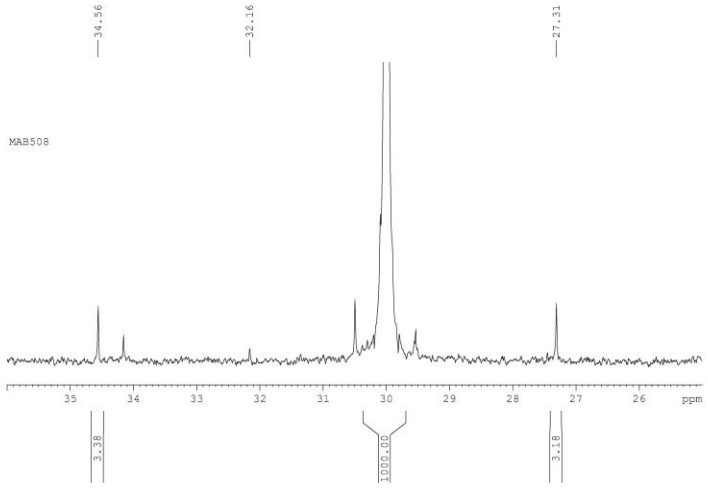

Figure S2. ^{13}C NMR Spectrum of MAB508

CHAPTER 5

The Effect of Particle Size and Porosity of Silica Supported Metallocene/MAO Catalysts on their Gas Phase Ethylene Polymerization Kinetics and Polymer Properties

Contents

1. Introduction 271

2. Experimental Section 272

2.1. Polymerization Protocol 272

3. Results and Discussion 273

3.1. Gas Phase Ethylene Homopolymerizations and Ethylene/1-Hexene Copolymerizations with Reference Catalysts Supported on Full Batch of Silica 273

3.2. Effect of Silica Support Particle Size in Gas Phase Ethylene Homopolymerizations and Ethylene/1-Hexene Copolymerizations 282

3.2.1. Effect of Catalyst Particle Size Studied with Grace 948 Silica 282

3.2.2. Effect of Catalyst Particle Size Studied with PQMS 3040 Silica 288

3.2.3. Effect of Catalyst Particle Size Studied with PQMS 1732 Silica 292

3.2.4. Effect of Catalyst Particle Size Studied with THI/MAO and $(n\text{-BuCp})_2ZrCl_2$/MAO Supported Catalysts 298

3.3 Conclusion from the Catalyst Particle Size Study in Gas Phase Polymerizations 322

3.4. Effect of Porosity of Silica Supported Metallocene/MAO Catalysts on their Activity, Molecular and Physical Properties of Polyethylene 324

3.5. Conclusions from the Effect of Porosity of the Supported Metallocene/MAO Catalysts on their Activity, Molecular and Physical Properties of Polyethylene 333

4. References 335

APPENDIX 1 337

1. Introduction

A significant amount of polyolefins available in the market comes from commercial plants whose one or more reactors operate in gas phase mode. For the case of polyethylene, commercial gas phase reactors are exclusively fluidized bed reactors (FBRs). The gas phase ethylene (co)-polymerization process is industrially attractive because of its low costs (capital and operating expenditure) and the possibility to produce an extended range of products in comparison to slurry or solution processes, where solubility related issues do not permit the production of low (or very low) molar mass and/or crystallinity grades. The issue with gas phase process is heat transfer which at first reduces the 'per pass' conversion of the process, and if controlled poorly can lead to off-spec product since almost all the molecular properties of polyethylene (and its various grades) are temperature sensitive. In addition, thermal run away is not an unheard term at such plants in the case of poor heat transfer control.[1]

As discussed in **Chapter 1**, there are few studies available in the open literature which employed gas phase ethylene polymerization process to systematically investigate the impact of physical properties of silica supported metallocene/MAO catalysts on their ethylene polymerization kinetics and on the properties of the obtained polyethylene. For example, in the work of Kumkaew et al.,[2,3] silica particle size has not been kept similar while studying the impact of support pore diameter on the reaction kinetics of the final supported catalysts and on polyethylene properties.

Therefore, in the present work, the aim is to explore the impact the of particle size, pore volume, pore diameter and surface area of silica supported metallocene/MAO catalysts on their ethylene homo- and ethylene/1-hexene copolymerization kinetics in the gas phase process. Molecular and physical properties of the obtained HDPE and copolymer samples are also analyzed in order to investigate whether the said physical properties of the supported catalysts influence these properties or not. All the supported catalysts used in this chapter are essentially those utilized in **Chapter 4** and the current chapter is also divided in two sections. The first section is devoted to the effect of catalyst particle size on; i) the reaction kinetics in the gas phase process and ii) polyethylene properties, whereas the second section describes the effect of catalyst porosity (i.e., pore volume, pore diameter and surface area) by fixing its particle size on the reaction kinetics as well as on the properties of polyethylene produced in the gas phase process.

2. Experimental Section

All the chemicals, catalysts, characterization methods used in this section are essentially the same and therefore, the relevant details can be found in the experimental section of **Chapter 4**.

2.1. Polymerization Protocol

In the gas phase polymerizations, 15 to 20 mg of the catalyst was mixed with 25 to 30 g of NaCl (dried at 400 °C) in an injection cartridge inside a glove box which was then attached to the reactor. Afterwards, the reactor was purged with argon followed by vacuum. 1 mL of 1 M scavenger solution (and 3 mL 1-hexene during copolymerizations unless otherwise mentioned) was then injected into the reactor under argon flow at room temperature. The reactor was then heated and once the temperature reached at 80 °C, catalyst + salt mixture was injected into the reactor under ethylene pressure and constant stirring at 400 rpm. This way of injection allows no pre-contact between the catalyst and the scavenger. Ethylene pressure was then maintained at 11 bar for 1 h and 15 minutes unless otherwise mentioned after which the reaction was stopped. The obtained polymer + salt mixture was added into water and stirred for few hours in order to dissolve all the salt in water. Afterwards, the polymer was separated by filtration followed by drying at 50 °C under vacuum for few hours.

3. Results and Discussion

3.1. Gas Phase Ethylene Homopolymerizations and Ethylene/1-Hexene Copolymerizations with Reference Catalysts Supported on Full Batch of Silica

Before starting detailed discussion about the effect of silica support properties (and therefore, the final supported catalysts) on the catalytic activity, molecular and physical properties of the produced polyethylene grade (i.e., either HDPE or ethylene/1-hexene copolymer) with silica supported (n-BuCp)$_2$ZrCl$_2$/MAO catalyst in gas phase process, it is important to compare the catalytic performance of the reference catalysts supported on the full batch of each commercial silica used in this work. As was observed in **Chapter 4**, the particle size, pore volume, pore diameter and surface area of the three full silica batches, and the different pre-catalysts supported on them all show some different behaviours in ethylene polymerization rate profiles, and in particular show significant differences during activation and deactivation steps.

For the ease of the reader, **Table 1** presents the physical and chemical characterization of the (n-BuCp)$_2$ZrCl$_2$/MAO catalysts supported on full silica batches of three different commercial silica. It is important to mention here that the no stirring was used during the synthesis of these catalysts and therefore, d_{50} of the silica support can also be used as the representative value of final catalyst particle size. Based on the particle size, catalyst particles based upon PQMS 1732 are the largest, whereas those supported on PQMS 3040 silica have the smallest particles. Surface areas of the catalysts prepared with PQ supports are not very different, whereas that of the one supported on Grace 948 has the lowest surface area. With respect to the pore volume, the catalyst supported on PQMS 3040 silica offers the highest value of 2.04 $cm^3.g^{-1}$ which is about 58% and 65% higher than the pore volumes of the catalysts supported on Grace 948 and PQMS 1732 silica, respectively. The same trend in pore diameters of these catalysts can also be noticed qualitatively but quantitatively the pore diameter of PQMS 3040 based catalyst is 34% higher than that based on Grace 948 silica, whereas it is 66% higher than the catalyst supported on PQMS 1732 silica. Among all the catalysts, the one supported on PQMS 1732 offers lowest pore volume and pore diameter.

Finally, metal loadings of the catalysts supported on Grace 948 and PQMS 3040 silica are very similar, whereas Zr loading of the catalyst prepared with PQMS 1732 silica is slightly lower than the other two catalysts which leads to higher Al/Zr molar ratio of this catalyst in comparison to the other two catalysts. In the coming paragraphs we will try to correlate the observed differences in

the reaction kinetics of these catalysts in gas phase homo- and ethylene/1-hexene copolymerizations to the physical and chemical features of the catalysts mentioned in **Table 1**.

Table 1. ICP-AES, BET characterization and particle size (d_{50}) of the catalysts prepared with full silica batches of three different commercial supports. A_s = specific surface area, P_v = pore volume, P_d = pore diameter.

Catalyst Name	**Particle size (d_{50}) µm**	**A_s (m^2/g)**	**P_v (cm^3/g)**	**P_d (nm)**	**Zr (Wt%)**	**Al (Wt%)**	**Al/Zr Molar ratio**
Bu/M/MS3040	45	412	2.04	16.9	0.29	12.3	143
Bu/M/G948	60	270	0.85	11.1	0.31	14.0	153
Bu/M/MS1732	128	471	0.71	5.6	0.21	12.4	200

Figure 1 shows the instantaneous activity of the three catalysts in gas phase ethylene homopolymerization at 1 mmole initial TIBA content and ethylene/1-hexene copolymerizations with 0.5 mmole initial TIBA at 11 bar ethylene pressure. The reason for the different shapes of the kinetic profile of Grace 948 based catalyst is not immediately clear. It is entirely possible that the physical properties of the different supports come into play here. The higher specific surfaces of the PQ supports could make them more friable than the Grace 948 (reputed to be a "harder" support). This means that they might fragment more rapidly, which might explain the rapid activation. However, this is very difficult to verify with the equipment available in our laboratory. In addition, the presence of macropores in Grace 948 silica may have allowed better TIBA diffusion leading to higher local concentration of TIBA and consequently slower activation as well as increasing activity over the whole reaction time in comparison to the other two reference catalysts. Different studies have shown that increased TIBA content can lead to slow activation of silica supported (n-BuCp)$_2$ZrCl$_2$/MAO catalyst in gas phase process.[4,5,6] Gas phase copolymerizations performed at a lower TIBA content provided similar kinetic profiles with all the three reference catalysts as shown in **Figure 1b** which partially supports the previous argument.

With respect to silica support particle size, **Figure 1** shows that the activity order of these catalysts is Grace948 > PQMS1732 ≥ PQMS3040 which is partially in agreement to what was expected. Reference catalyst supported on Grace 948 and PQMS 1732 have similar pore volume and pore diameters but different surface areas and particle sizes. Smaller particle size of Grace 948 silica supported catalyst than that of PQMS 1732 silica supported catalyst seems to be the most probable

reason for higher activity of the former reference catalyst, especially in copolymerizations (see **Figure 1b**). Note that the Zr loading of the catalyst supported on PQMS 1732 is lower than the Zr loading on PQMS 3040 catalyst, so the fact that the activity in terms of grams PE per gram of support per unit time is higher implies that the difference between the Grace and PQ supported particle activity profiles is most probably coming from the physical differences in the morphology of these supported catalysts, rather than chemical differences. It also worth mentioning here that the same observations were also made when these catalysts were used in slurry polymerizations.

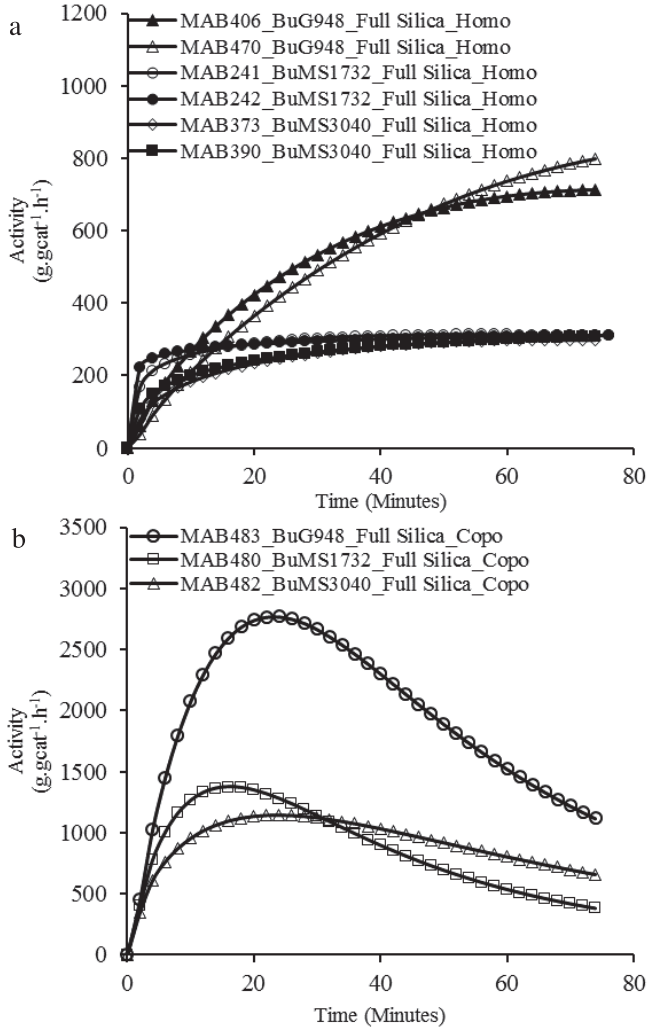

Figure 1. Comparison of the instantaneous activity of the $(n\text{-}BuCp)_2ZrCl_2$/MAO catalyst supported on full batches of three commercial silica in (a) ethylene homopolymerizations at 11 bar ethylene pressure and 1 mmole initial TIBA concentration and (b) ethylene/1-hexene copolymerizations at 11 bar ethylene pressure and 0.5 mmole initial TIBA concentration.

Despite some of the uncertainties as to why we see different rates here, this observation suggests that the average particle size is clearly not the only property which impacts the catalytic activity. Let us consider the external and internal morphologies of the different supports shown in **Figure 2**. The PQ supports show a very similar overall morphology in terms of shape, texture and uniformity, whereas the Grace support is far less homogeneous, containing marcropores and granulates, as well as what appears to be a slightly different morphology in the outer and inner portions of the particle.

However, even if we consider only the 2 PQ catalysts, **Figure 1** shows that the PQMS1732 activates more quickly and to a higher maximum value than PQMS 3040 in both homo- and copolymerization. If particle sizes were the most important factor, we would expect exactly the opposite behaviour, with the big particles activating more slowly than the small ones if the overall geometry is the same. Thus, the difference in the activation rates of these two catalysts is probably related to differences in their pore volumes and pore diameters. PQMS 1732 silica supported catalyst has pore volume and pore diameter values which are almost 70% lower than that of the catalyst supported on PQMS 3040 which probably leads to rapid particle fragmentation of PQMS 1732 catalyst/polymer particles and, consequently, faster activation of this catalyst as compared to the one supported on PQMS 3040 silica.

MWDs of the homo- and copolymers produced with these reference catalysts are compared in **Figure 3**. HDPE produced with the reference catalyst supported on Grace 948 showed higher molar mass than that of the HDPEs produced with the other two reference catalysts which have similar MWDs (**see Figure 3a**). On the other hand, the copolymer produced with the reference catalyst supported on PQMS 1732 silica show relatively higher molar mass than the other two copolymers (see **Figure 3b**). Most probably, in-situ hydrogen generation [7-10] seems to be the reason for this behaviour of MWDs. We will present proof for in-situ hydrogen generation in the coming parts of this chapter. It has been shown by Hasegawa et al.[8] that the quantity of in-situ hydrogen increases with increasing the reactor temperature as well as it depends upon the type of metallocene used. Furthermore, the work of Kumkaew et al.,[2] with the same silica supported catalyst shows that at higher reactor temperature during gas phase copolymerizations, the molar mass of the produced copolymers decreases indicating higher activation energies of chain transfer reactions.

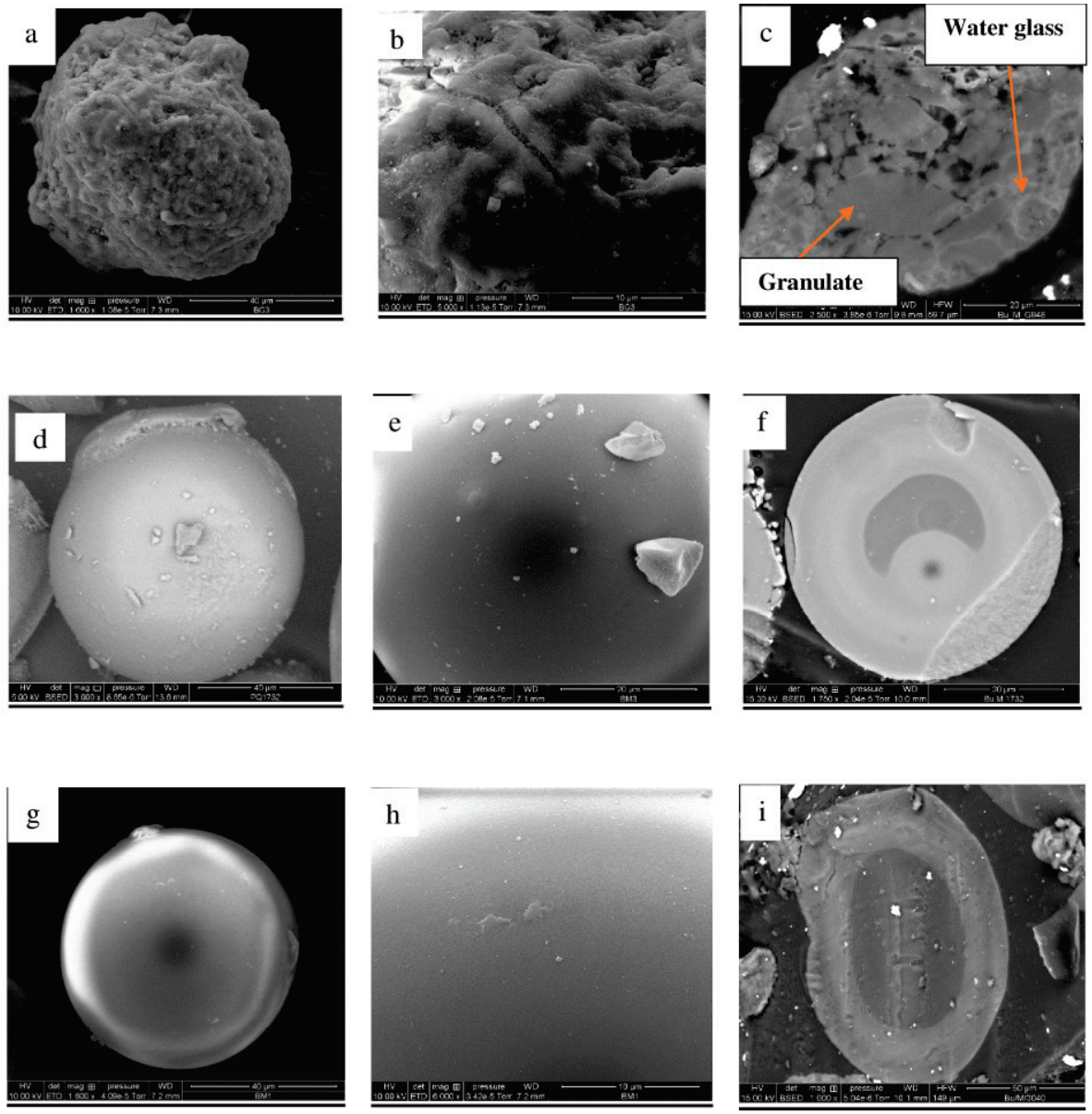

Figure 2. SEM micrographs of three commercial silica showing external and internal morphology of the particles. Grace 948 (a to c), PQMS1732 (e to f), PQMS3040 (g to h). Last image of each series show cross-section of one of the particles from the respective silica.

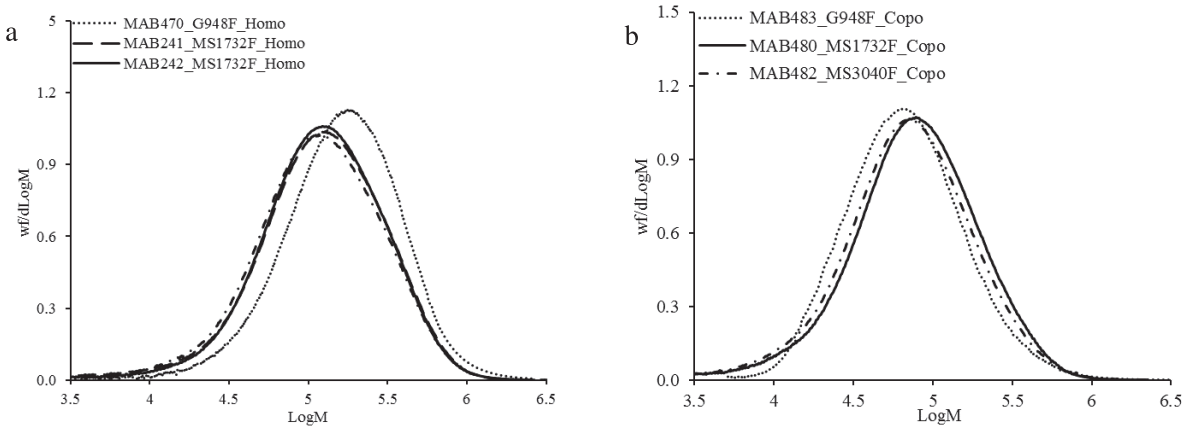

Figure 3. MWD of (a) the homopolymers and (b) copolymers produced with (n-BuCp)$_2$ZrCl$_2$/MAO supported on full batches of three commercial silicas used in this work. 'F' indicates full silica.

Since these samples were produced in the gas phase process which is known for its poor heat transfer, the higher molar mass of the HDPE sample produced with the reference catalyst of Grace 948 silica can, most probably, be attributed to it slow activation and rise in activity due to which the temperature of growing catalyst/polymer particles may have been lower as compared to that of the two PQ silica based catalyst/polymer particles. As a result, less in-situ hydrogen generated (and therefore, consumed) may have produced HDPE with relatively higher molar mass. On the other hand, in gas phase copolymerizations, we can see that the Grace 948 catalyst showed activation similar to the other two reference catalysts but with significantly higher activity which may have led to higher local temperature of the growing particles and therefore, higher in-situ hydrogen concentration which produced a copolymer with lowest molar mass (see **Figure 3b** and **Table 2**).

However, we will discuss these observations in the coming sections of this chapter where the physical properties of the catalysts are varied in a systematic way which will provide a better insight into this dependence of MWD on the support type used for (n-BuCp)$_2$ZrCl$_2$/MAO catalyst. Molar mass dispersity (Đ) for all the polymers is well below 3 indicating single-site nature of all the catalysts independent of the support used. **Table 2** shows that the melting temperature of HDPE samples does not change with the support type but that of the copolymer produced with Grace 948 based reference catalyst was higher than the other two samples which can be attributed to the difference in the comonomer contents of these samples. Grace 948 silica based reference catalyst showed considerably higher activity than the other two catalysts and therefore, different levels of

composition drift in these reactions can be considered as a reason for the variations in the comonomer contents of the obtained copolymers.

Table 2. Comparison of weight average molar mass (M_w), dispersity of molar mass (Đ), melting temperature (T_m) of the homo- and copolymers produced with the reference catalysts supported on Grace 948, PQMS 1732 and PQMS 3040 silicas. A_{TIBA} and $A_{1\text{-hexene}}$ refers to the initial amounts of TIBA and 1-hexene added to the reactor, respectively. x_{CEF} refers to comonomer content measured with CEF. All HT-SEC measurements with new set of columns.

Sample Name	Catalyst name	A_{TIBA} (mmole)	$A_{1\text{-hexene}}$ used(ml)	M_w	Đ	T_m (°C)	x_{CEF} (mol%)
MAB406	Bu/M/G948	1.0	0	-	-	135.8	-
MAB470	Bu/M/G948	1.0	0	225000	2.2	136.8	-
MAB241	Bu/M/MS1732	1.0	0	176000	2.6	136.0	-
MAB242	Bu/M/MS1732	1.0	0	175000	2.4	136.7	-
MAB390	Bu/M/MS3040	1.0	0	185000	2.8	135.8	-
MAB483	Bu/M/G948	0.5	3	95000	2.2	125.0	1.2
MAB480	Bu/M/MS1732	0.5	3	115000	2.3	120.5	1.7
MAB482	Bu/M/MS3040	0.5	3	105000	2.4	121.5	1.7

Particle size distribution (PSD) of the polymer samples produced with three reference catalysts are compared with the corresponding silica PSDs in **Figure 4** where, overall, a good replication of the original catalyst support by the polyethylene particles can be observed. Copolymer particles possessed bigger sizes than the corresponding homopolymers because of higher activity of each catalyst in the copolymerizations. PSD of the homopolymer produced with Grace 948 supported reference catalyst does not show any presence of fine particles in comparison to the PSDs of the HDPE samples produced with two other reference catalysts (see **Figure 4d**) which may be attributed to the different fragility of these supports and the differences in their activation during polymerization. On the other hand, in copolymer PSDs of **Figure 4e** one can see a small peak showing the presence of fine particles in all the samples which can be attributed to similar activation of all the reference catalysts. The overlap between the PSDs of the copolymers produced with the reference catalysts of two PQ silica (see **Figure 4e**) is caused by the fact that some of the polymer particles of the sample MAB480 (i.e., the one produced with PQMS 1732 supported catalyst) were not able to pass through the sieve of the Master Sizer and therefore, those particles are not included in this PSD. From **Figure 4d** it can be concluded that the bigger the support particle size the bigger the polymer particle size is, despite low activity of the catalyst supported on bigger silica particles.

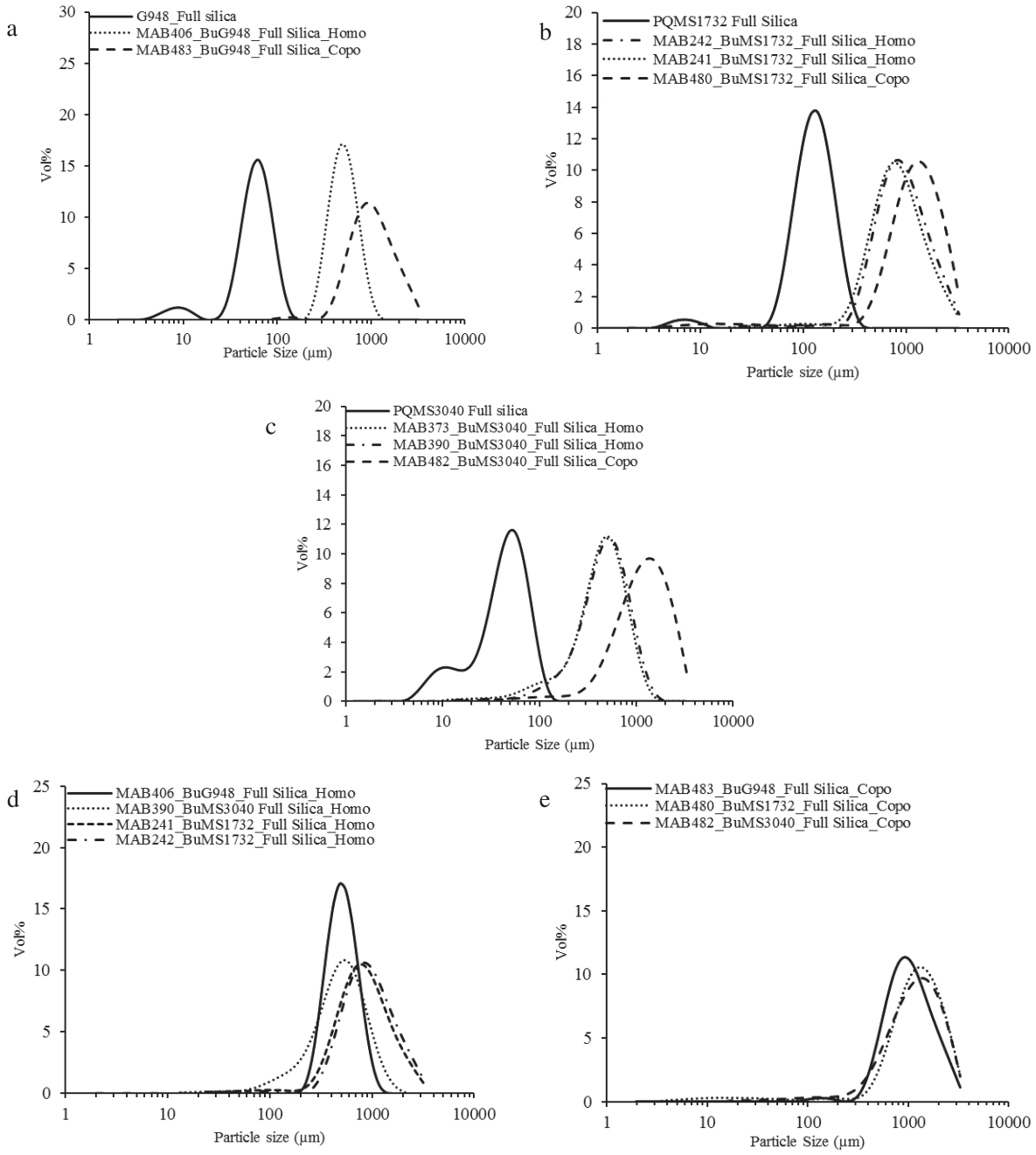

Figure 4. Comparison of pure silica and polyethylene particle size distribution produced with the catalyst supported on corresponding silica support.

The results obtained from these reference catalysts suggests that;

i) For two silica produced with the same synthesis method having identical internal and external particle morphology but different particles sizes (e.g., PQMS 3040 and PQMS 1732), the dominant physical properties which control ethylene polymerization kinetics

of a metallocene supported appear to be the pore volume and pore diameter of the final silica supported catalyst. The catalyst which is supported on the silica with lower pore volume achieves higher activation rate despite its larger particle size as compared to the activation rate of the same catalyst supported on the silica with smaller particle size and larger pore volume.

ii) It can be seen that two silica prepared with different methods (e.g., Grace 948 made with spray-drying method and PQMS 1732 prepared with emulsion process) but with comparable pore volumes and/or pore diameters behave quite differently. The Grace 948 has lower specific surface and comparable pore volume with respect to PQMS 1732 yet is far more active. PQMS 1732 is larger than PQMS 3040, and has much smaller pore volumes leading to the speculatation that pore volume is a factor if all else is the same.

iii) With respect to surface area of the silica support and the final catalysts, the activation rate of the catalyst with higher surface area is faster than the activation rate of the catalyst with lower surface area, provided that both the silica have similar external and internal particle morphology (e.g., PQMS 3040 and PQMS 1732 silica supported catalysts in this work show this trend).

~~iv)~~ Considering the copolymerizations where activation and deactivation behaviour of all the catalysts was very similar, the molar mass of the copolymer produced with the reference supported catalyst of lowest pore diameter (i.e., Bu/M/MS1732 catalyst) seems to be higher than those of the samples produced with the reference supported catalysts of larger pore diameters despite low activity of the former reference catalyst as compared to the latter ones. This effect cannot be concluded in this section with enough confidence because the particle sizes of the reference catalysts were very different and the low activity of the smallest pore diameter catalyst might have been due to its biggest particle size. Furthermore, in-situ hydrogen generation linked with catalyst activity and particle temperature in gas phase process further complicates the discussion about MWDs and therefore, it is of importance to fix other physical properties of the supported metallocene/MAO catalysts while studying the effect of one specific physical property and this approach will be applied in the next sections of the current chapter to study the effect of physical properties of supported metallocene/MAO

catalysts on the reaction kinetics, molecular and physical properties of the obtained HDPE and ethylene/1-hexene copolymers.

3.2. Effect of Silica Support Particle Size in Gas Phase Ethylene Homopolymerizations and Ethylene/1-Hexene Copolymerizations

In the previous section we observed that the particle size was not the sole determining factor in how fast the catalysts activate. However, this does not mean that the catalyst size has no impact on the rate of reaction. In this section we will begin by looking at the impact of the size of the catalyst particles in gas phase polymerizations, keeping all other parameters constant.

3.2.1. Effect of Catalyst Particle Size Studied with Grace 948 Silica

The catalysts used in the study are those used in **Chapter 4** dealing with slurry phase polymerizations and the details regarding the synthesis procedure of these catalysts can be found therein. For the ease of reading, **Table 3** reproduces the ICP-AES elemental analysis of these catalysts which indicates similar metal content on each catalyst and that all physical properties other than the particle size of these catalysts are very similar.

Table 3. BET and ICP-AES analysis of the catalysts prepared by using different sieved fractions of Grace 948 silica and full batch of Grace 948 silica. A_s = specific surface area, P_v = pore volume, and P_d = pore diameter.

Cut Number	Sieve opening (µm)	Catalyst Name	A_s (m^2/g)	P_v (cm^3/g)	P_d (nm)	Zr (Wt%)	Al (Wt%)
1	Pan	BG-4	265	0.81	11.6	0.21	14.3
2	36	BG-2	284	0.81	10.9	0.19	12.4
3	45	BG-1	230	0.68	10.7	0.19	12.5
4	63	BG-3	269	0.75	10.8	0.18	12.5
5	80	BG-5	289	0.80	10.8	0.20	15.6
6	Full Batch	Bu/M/G948	270	0.85	11.1	0.31	14.0
	Full Batch	Full As received silica	290	1.7	23.2	-	-

The effect of Grace 948 silica support particle size on the instantaneous activity (and calculated productivity) of supported $(n\text{-BuCp})_2ZrCl_2$/MAO catalysts in gas phase ethylene homo- and ethylene/1-hexene copolymerizations is shown **Figure 5** and **Figure 6**, respectively. The effect of catalyst particle size on the observed instantaneous rate of gas phase homo- and copolymerization

is quite pronounced i.e., the smaller catalyst particles show higher activities than their bigger analogs with similar metal loadings. The effect of TIBA concentration inside the reactor on the instantaneous activity of each catalyst of different particle size is demonstrated in **Figure 6**. As one would expect, the gas phase copolymerizations done with 1 mmole (**Figure 6a**) and 0.5 mmole (**Figure 6b**) TIBA injected at the start of the reaction behave much as the full silica catalysts did in the previous section. An example for this comparison is presented in **Figure 6c**.

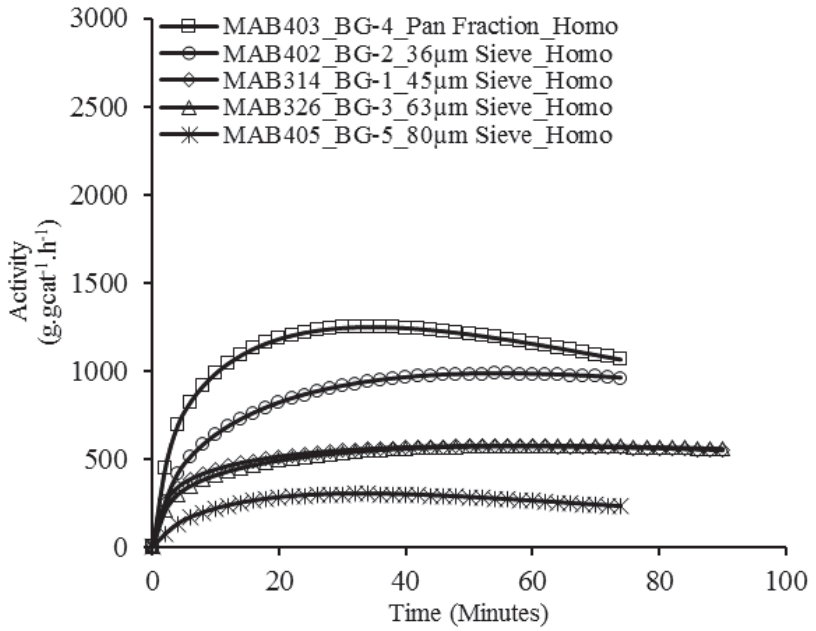

Figure 5. Effect of Grace 948 silica support particle size on the instantaneous activity of supported $(n\text{-BuCp})_2ZrCl_2$/MAO catalyst in ethylene homopolymerization at 11 bar ethylene pressure.

Therefore, it can be concluded that the effect of silica support particle size (or the final catalyst particle size) on its rate of polymerization is independent of TIBA concentration, and that the differences in the kinetic profiles of supported catalysts with varying sizes but similar metal loadings appear due to reasons other than those attributable to the active sites e.g., resistance to (co)-monomer(s) transport at the active sites which is higher in bigger catalyst particles than in the smaller ones. We will return to the discussion about mass transfer resistance below. Surprisingly, the catalysts made from the silica fractions obtained on 45 µm and 63 µm sieves (i.e., BG-1 and BG-3 catalysts, respectively) behaved very similarly in homopolymerizations but in copolymerizations, BG-1 was found to be more active than BG-3, as indicated by **Figure 6b**. The

instantaneous activity of full silica batch based catalyst in gas phase copolymerizations seems to be very similar to that of the catalysts supported on 36 µm and pan fractions of Grace 948 silica, as shown in **Figure 6b**, which is in full agreement with the results obtained in slurry phase reactions with the same catalysts.

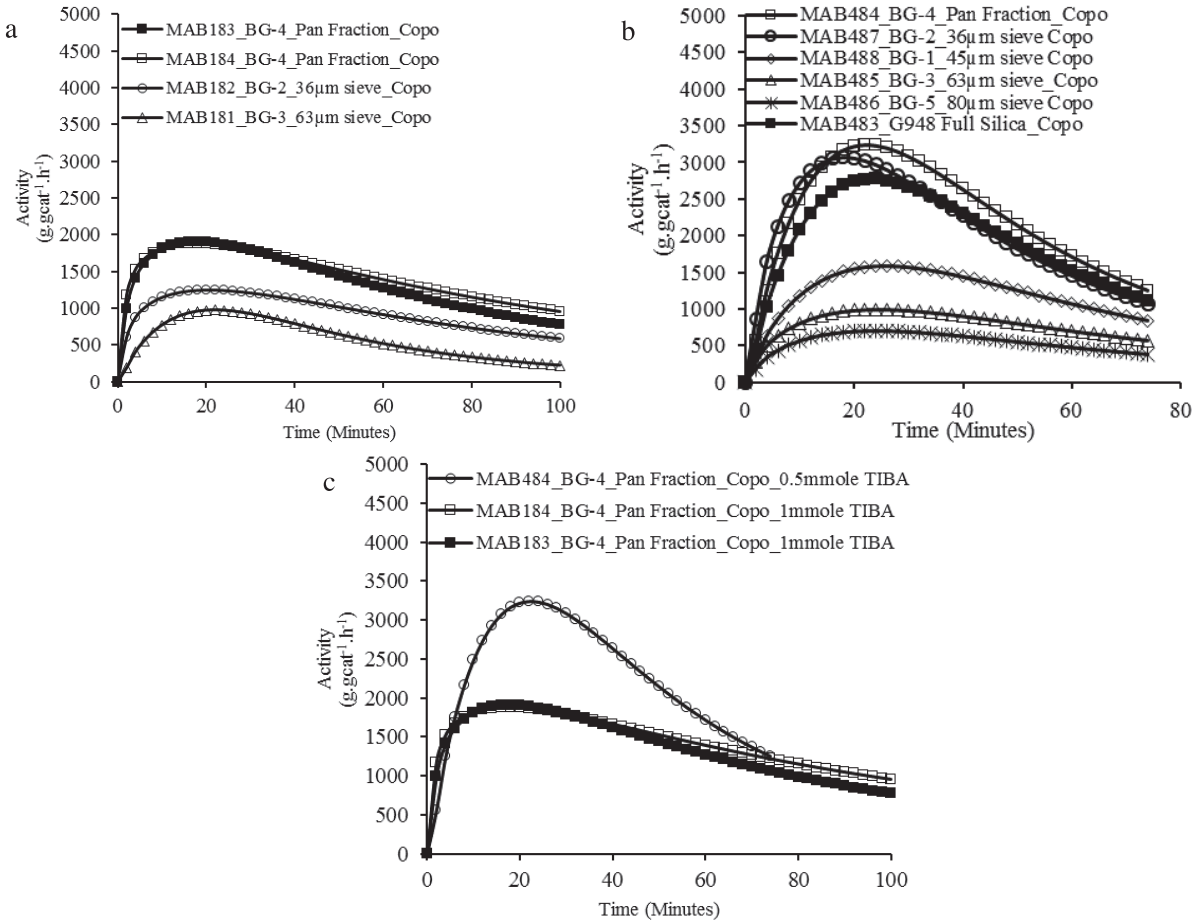

Figure 6. Effect of Grace 948 silica support particle size on the instantaneous activity of supported $(n\text{-BuCp})_2ZrCl_2$/MAO catalyst in ethylene/1-hexene copolymerizations at (a) 1.0 mmole TIBA added into the reactor, (b) 0.5 mmole TIBA added into the reactor. (c) Comparison of the kinetic profiles of BG-4 catalyst at two TIBA amounts injected at the reaction start-up.

MWDs of the obtained homo- and copolymer samples is presented in **Figure 7** which basically does not show any significant impact of catalyst particle size on the MWD of polyethylenes, despite the noticeable difference in the polymerization rates. **Table 4** indicates that the molar mass dispersity (Đ) of all the samples remained close to 2 despite considerable differences in the activities of the catalysts, which indicates that particle size of the support does not alter the active

site type. Copolymers had (as expected) lower molar masses than the homopolymers due to the increased chain transfer reactions in the presence of 1-hexene at the active sites during copolymerizations. The role of in-situ hydrogen generated in the MWDs can be kept aside at present.

One noticeable trend shown graphically in **Figure 7** and numerically in **Table 4** is that the molar mass of the homo- and copolymers produced with bigger in size but less active BG-3 and BG-5 catalysts is slightly, but consistently, higher than the molar mass of the samples produced with more active but smaller in size catalysts (i.e., BG-4, BG-2). This is in agreement with the observations made in the MWDs of the polyethylenes produced with the same catalysts in slurry phase reactions (see **Chapter 4**). This difference in M_w values appears to be more systematic in the copolymers produced with 0.5 mmole TIBA content inside the reactor. We will address this difference in MWDs of the homo- and copolymers in the later sections of this chapters because it may be linked with the amount of in-situ hydrogen generated by these catalysts. As a remark, it is worth mentioning here that the proposed mechanisms of in-situ hydrogen generation are linked with active zirconium and therefore, it might not be unreasonable to assume that the bigger but less active catalyst particles produce less in-situ hydrogen and consequently, copolymers with slightly high molar masses even after reasonably long reaction times. In addition to particle size effect, **Figure 7b** shows that the amount of TIBA injected at the reaction start-up has no impact on the MWD of the produced polyethylenes. This observation needs to be considered carefully since the reaction times of high and low TIBA content polymerizations (compare **Figure 6a** and **b**) are different along with deactivation rates of the same catalysts. Polymerization time can also have a significant impact on the MWDs of polymers produced with this metallocene/MAO system, as will be shown in the coming sections.

Melting temperature of the homopolymers seem to be insensitive to particle size of the catalyst as shown in **Table 4**. Copolymers produced with less active but bigger catalyst particles showed higher comonomer content (and lower melting temperature) than that of the copolymers produced with smaller but more active catalysts. This observation can be attributed to higher level of composition drift in the case of copolymers produced with smaller catalyst particles as compared to that during polymerizations with bigger ones.

PSD of the sieved silica fractions and polymer samples produced with the corresponding final supported catalysts are shown in **Appendix 1** (**Figures S1** and **S2**). In principle, all the polymers replicated the original silica support morphology. The smaller catalyst particles produced smaller polymer particles despite their significantly higher activities than the bigger catalyst particles. The results are summarized in **Table 5**.

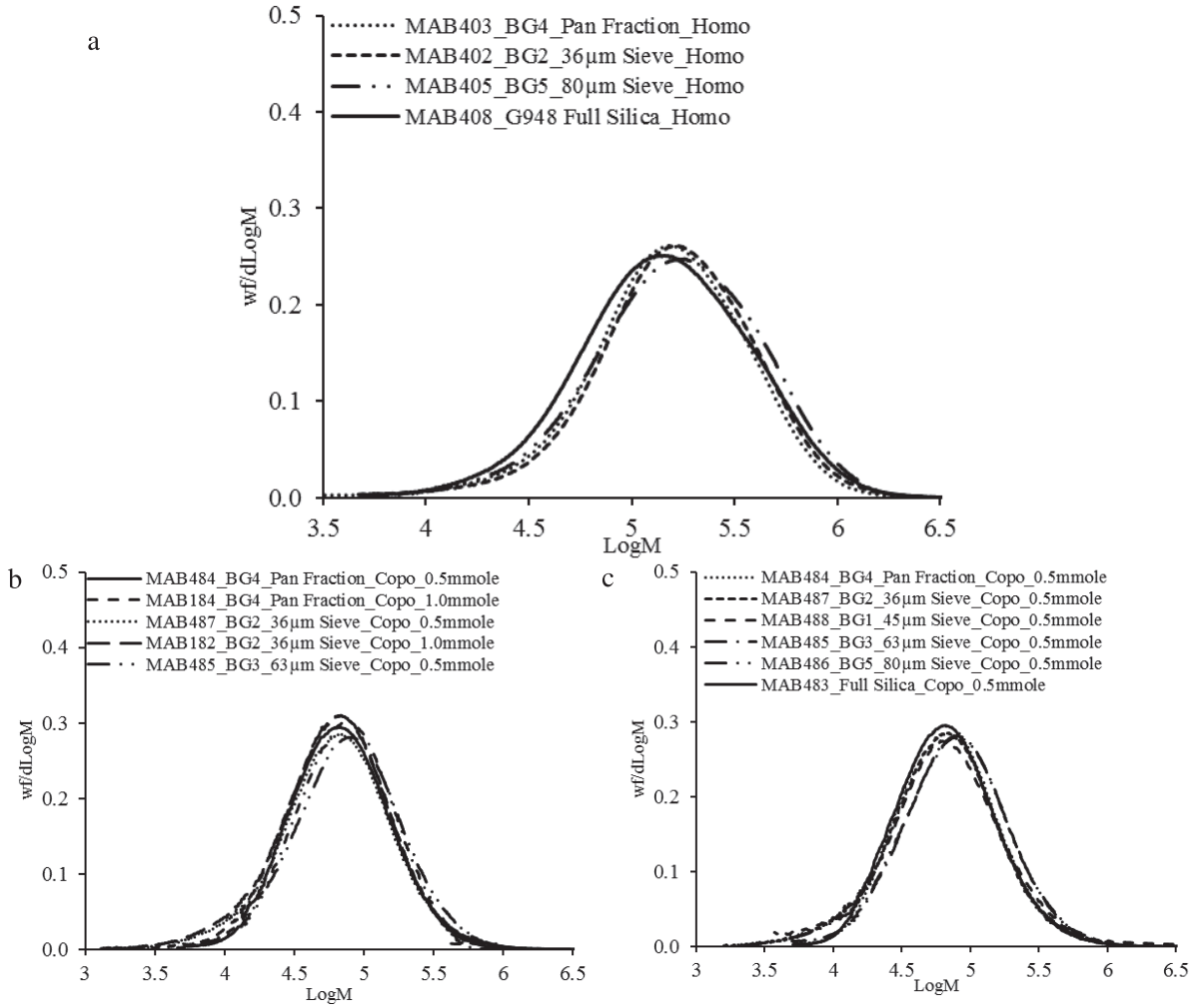

Figure 7. Effect of silica support particle size on (a) the MWD of HDPE, (b) the MWD of ethylene/1-hexene copolymer at different TIBA amounts inside the reactor and (c) MWD of ethylene/1-hexene copolymers produced at fixed TIBA amount in the reactor.

Table 4. Comparison of weight average molar mass (M_w), dispersity of molar mass (Đ), melting temperature (T_m) and 1-hexene content (x) of the polymers produced with different sized catalysts of Grace948 silica. A_{TIBA} and $A_{1\text{-hexene}}$ refer to TIBA and 1-hexene initial amounts added into the reactor. x_{NMR} and x_{CEF} refer to the comonomer contents estimated by NMR and CEF, respectively.

Sample Name	Catalyst name	A_{TIBA} (mmole)	$A_{1\text{-hexene}}$ (ml)	M_w	Đ	T_m (°C)	x_{NMR} (mol%)	x_{CEF} (mol%)
MAB403	BG-4 (Pan)	1.0	0	210000	2.4	134.7	-	-
MAB484	BG-4 (Pan)	0.5	3	95000	2.2	124.2	-	1.1
MAB184	BG-4 (Pan)	1.0	3	95000	2.3	125.8	1.1	1.0
MAB402	BG-2 (36µm)	1.0	0	230000	2.3	135.7	-	-
MAB487	BG-2 (36µm)	0.5	3	90000	2.3	123.5	-	1.2
MAB182	BG-2 (36µm)	1.0	3	165000	2.6	124.5	1.4	1.2
MAB314	BG-1 (45µm)	1.0	0	200000	2.3	135.2	-	-
MAB488	BG-1 (45µm)	0.5	3	90000	2.3	121.5	-	1.5
MAB326	BG-3 (63µm)	1.0	0	175000	2.4	135.5	-	-
MAB181	BG-3 (63µm)	1.0	3	100000	2.1	121.8	2.2	1.4
MAB485	BG-3 (63µm)	0.5	3	100000	2.1	118.3	-	2.2
MAB405	BG-5 (80µm)	1.0	0	245000	2.5	136.0	-	-
MAB486	BG-5 (80µm)	0.5	3	115000	2.5	117.2	-	2.4
MAB408	Full batch	0.5	0	220000	2.5	134.6	-	-
MAB483	Full batch	0.5	3	95000	2.2	125.0	-	1.2

Table 5. Comparison of d_{10}, d_{50}, d_{90} and span of the homo- and copolymers produced with different sized catalysts of Grace 948 silica. A_{TIBA} and $A_{1\text{-hexene}}$ refer to TIBA and 1-hexene initial amounts added into the reactor.

Sample Name	Catalyst name	A_{TIBA} (mmole)	$A_{1\text{-hexene}}$ (ml)	d_{10}	d_{50}	d_{90}	Span
MAB403	BG-4 (Pan)	1.0	0	242	398	625	0.96
MAB484	BG-4 (Pan)	0.5	3	360	524	760	0.76
MAB184	BG-4 (Pan)	1.0	3	183	466	811	1.35
MAB402	BG-2 (36µm)	1.0	0	261	445	720	1.03
MAB487	BG-2 (36µm)	0.5	3	436	641	934	0.78
MAB182	BG-2 (36µm)	1.0	3	362	621	1010	1.04
MAB488	BG-1 (45µm)	0.5	3	536	750	1070	0.71
MAB326	BG-3 (63µm)	1.0	0	523	749	1100	0.77
MAB181	BG-3 (63µm)	1.0	3	592	977	1800	1.24
MAB485	BG-3 (63µm)	0.5	0	618	938	1550	0.99
MAB405	BG-5 (80µm)	1.0	0	385	605	972	0.97
MAB486	BG-5 (80µm)	0.5	3	693	1167	2193	1.29
MAB408	Full batch	0.5	0	278	467	774	1.06
MAB483	Full batch	0.5	3	508	966	1980	1.52

3.2.2. Effect of Catalyst Particle Size Studied with PQMS 3040 Silica

Table 6, which is essentially the same table presented as **Table 2** in the **Chapter 4**, shows the physical characterization by BET and chemical characterization by ICP-AES of all the supported catalysts prepared by using different sieved fractions of PQMS 3040 silica. These catalysts were also evaluated in gas phase ethylene homo- and ethylene/1-hexene copolymerizations to investigate the impact of catalyst particle size on its activity and polyethylene properties. Once again, it can be seen that all of the catalysts possess very similar metal loadings. The catalyst prepared with the full silica batch appears to have slightly higher Zr content, but the Al content remained similar to the catalysts prepared by using sieved silica fractions. The most probable reason for this difference is that this reference catalyst was prepared by an industrial partner, and small variations in the synthesis method could explain these differences.

Table 6. BET and ICP-AES analysis of the catalysts prepared by using different sieved fractions of PQMS 3040 silica and full batch of the said silica. A_s = surface area of the catalyst measured by BET, P_v = BJH desorption Pore volume of the catalyst measured by BET, P_d = Pore diameter of the catalyst measured by BET.

Cut Number	Sieve opening (µm)	Catalyst Name	A_s (m^2/g)	P_v (cm^3/g)	P_d (nm)	Zr (Wt%)	Al (Wt%)
1	Pan	BM-4	395	1.31	10.7	0.23	15.8
2	36	BM-2	401	1.31	11.1	0.17	14.3
3	45	BM-3	375	1.30	11.9	0.18	13.4
4	63	BM-1	390	1.46	12.4	0.19	11.8
5	Full Batch	Bu/M/MS3040	412	2.04	16.9	0.29	12.3
-	Full Batch	As received silica	420	3.0	28.5	-	-

Figure 8 and **Figure 9** show that the effect of catalyst particle size on the reaction kinetics of (n-BuCp)$_2$ZrCl$_2$/MAO system supported on different sieved fractions of PQMS 3040 silica is the same for homo- and copolymerization, respectively, as was observed in the case of Grace 948 silica based catalysts; i.e., the smaller catalyst particles show higher activities than the bigger ones bearing similar active metal loadings. In addition, the impact of initial TIBA content on the kinetic profiles of these catalysts is also similar to that observed for Grace 948 silica based catalysts i.e., the lower the TIBA content the faster the activation and deactivation rates of the corresponding catalyst (see **Figure 9c**).

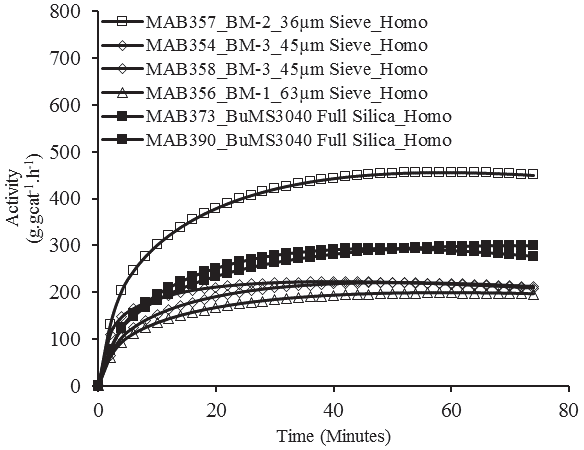

Figure 8. Effect of PQMS 3040 silica support particle size on the instantaneous activity of supported (n-BuCp)$_2$ZrCl$_2$/MAO catalyst in ethylene homopolymerizations (TIBA = 1mmole).

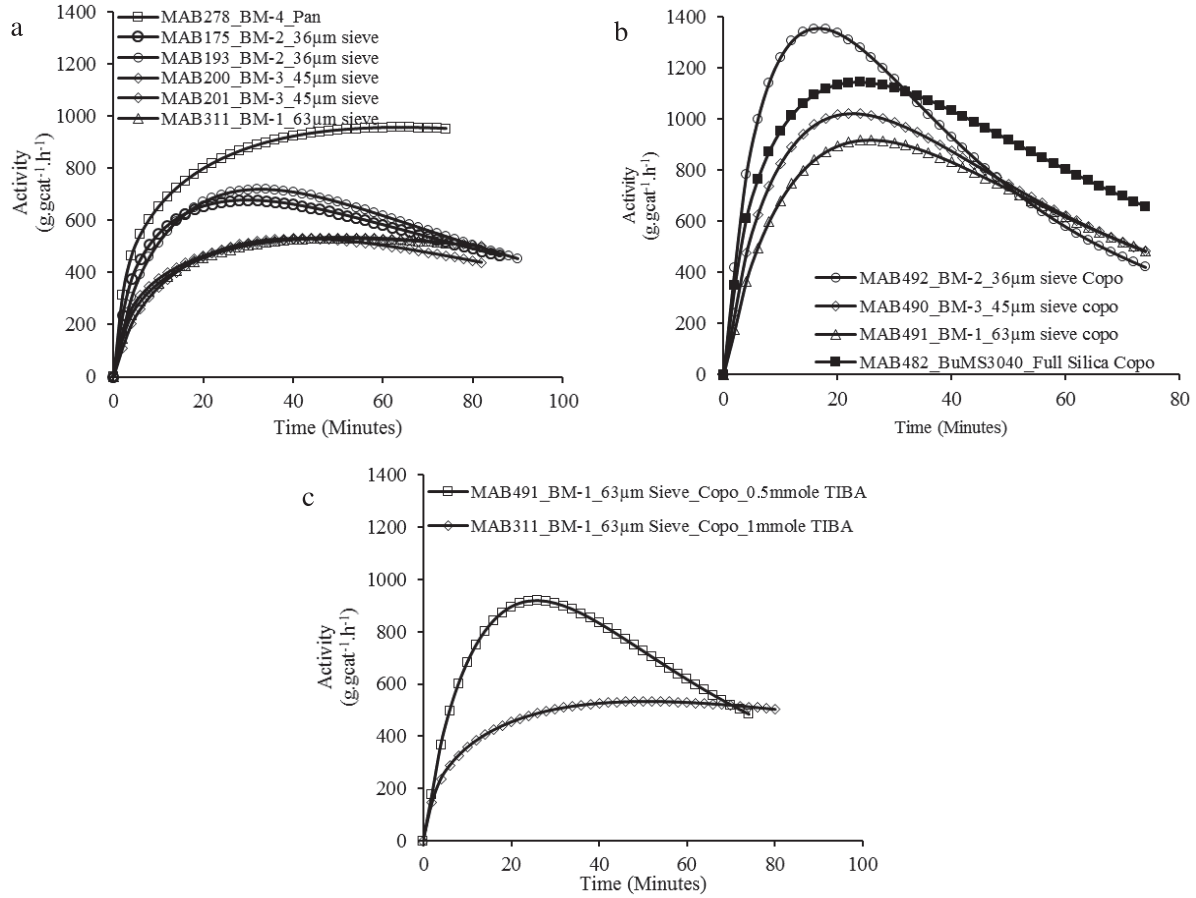

Figure 9. Effect of PQMS 3040 silica support particle size on the instantaneous activity of supported (n-BuCp)$_2$ZrCl$_2$/MAO catalyst in ethylene/1-hexene copolymerizations at (a) 1.0 mmole TIBA added into the reactor, (b) 0.5 mmole TIBA added into the reactor. Comparison of the kinetic profiles of BM-1 catalyst at two TIBA amounts injected at the reaction start-up (c).

The effect of catalyst particle size on the MWD, Đ values and polymer melting temperature is shown in **Figure 10a** and **Table 7** which indicates that the there is no significant effect of changes in the particle size of the catalyst on these molecular and physical properties of the produced HDPE samples. This observation is in agreement with the one made in the case of Grace 948 silica base catalysts. Slightly broader MWD were observed for the HDPE samples produced with bigger catalysts particles which led to somewhat higher Đ values for the HDPE samples, as can be seen in **Table 7**. Just like the MWDs of the homopolymers, no differences can be detected in the MWDs of the copolymers produced with silica supported (n-BuCp)$_2$ZrCl$_2$/MAO catalysts of different sizes except that the bigger catalyst particles produced copolymers of slightly higher molar masses, especially at lower TIBA content (see **Figure 10b** and **Table 7** for values). T_m of the copolymers shows slight variation with catalyst particle size which can be attributed to variations in their comonomer contents. As seen in the previously discussed case of Grace 948 silica based catalysts, bigger catalyst particles of this silica also incorporated more 1-hexene as compared to their smaller but more active analogs (e.g., compare x values at 1 mmole TIBA content in **Table 7**). This behaviour can be, once again, attributed to different levels of 1-hexene composition drift during copolymerizations.

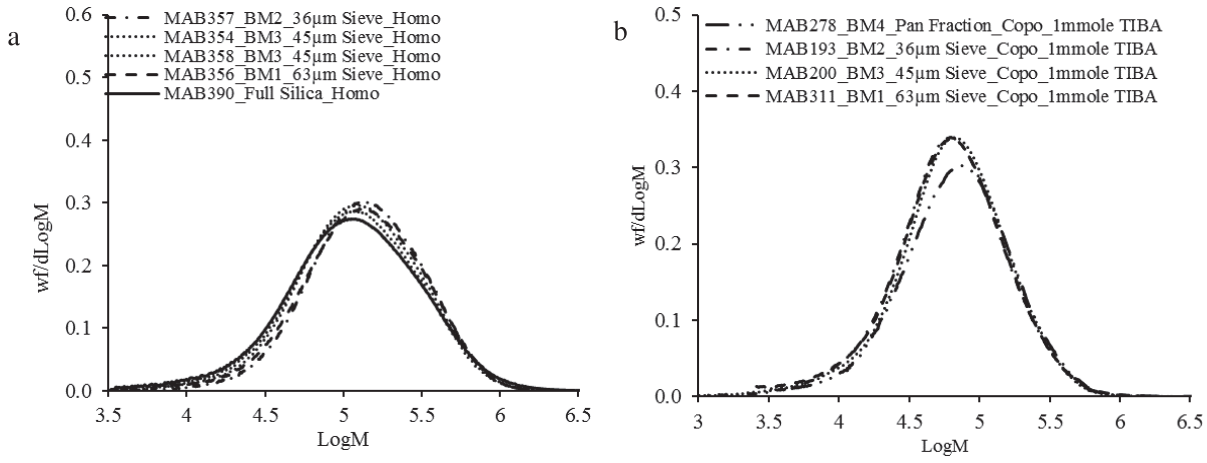

Figure 10. Effect of catalyst particle size on the MWD of (a) HDPE and (b) copolymers.

Table 7. Comparison of weight average molar mass (M_w), dispersity of molar mass (Đ), melting temperature (T_m) and 1-hexene content (x) of the polymers produced with different sized catalysts of PQMS 3040 silica. A_{TIBA} and $A_{1\text{-hexene}}$ refer to the initial amounts of TIBA and 1-hexene, respectively. x_{NMR} and x_{CEF} refer to the comonomer contents estimated by NMR and CEF, respectively.

Sample Name	Catalyst name	A_{TIBA} (mmole)	$A_{1\text{-hexene}}$ (ml)	M_w	Đ	T_m (°C)	x_{NMR} (mol%)	x_{CEF} (mol%)
-	BM-4 (Pan)	-	0	-	-	-	-	-
MAB278	BM-4 (Pan)	1.0	3	110000	2.3	121.3	-	1.4
MAB357	BM-2 (36µm)	1.0	0	190000	2.3	135.7	-	-
MAB175	BM-2 (36µm)	1.0	3	90000	2.3	119.3	-	2.1
MAB193	BM-2 (36µm)	1.0	3	90000	2.2	120.0	-	-
MAB489	BM-2 (36µm)	0.5	3	105000	2.2	121.2	-	1.7
MAB492	BM-2 (36µm)	0.5	3	110000	2.3	120.7	-	1.9
MAB354	BM-3 (45µm)	1.0	0	180000	2.4	135.5	-	-
MAB358	BM-3 (45µm)	1.0	0	175000	2.4	135.5	-	-
MAB200	BM-3 (45µm)	1.0	3	90000	2.4	120.8	-	1.6
MAB201	BM-3 (45µm)	1.0	3	90000	2.2	120.5	-	1.5
MAB490	BM-3 (45µm)	0.5	3	115000	2.1	119.3	-	2.1
MAB356	BM-1 (63µm)	1.0	0	190000	2.3	135.8	-	-
MAB311	BM-1 (63µm)	1.0	3	90000	2.1	120.8	-	1.6
MAB491	BM-1 (63µm)	0.5	3	120000	2.4	121.7	-	1.6
MAB373	Full batch	1.0	0	200000	2.6	135.5	-	-
MAB390	Full batch	1.0	0	185000	2.8	135.8	-	-
MAB482	Full batch	0.5	3	105000	2.4	121.5	-	1.7

The PSDs of both the homo- and copolymerization runs evolved as expected. The results are shown in **Appendix 1** (**Figures S3**) along with the PSD of each sieved fraction, and summarized in **Table 8**. d_{10}, d_{50}, d_{90} and span of the homo- and copolymers produced with different sized catalysts of PQMS 3040 are shown in **Table 8** which indicates that, overall, the copolymer samples have span values lower than that of HDPE samples. In addition, it can be noticed that at lower TIBA concentration the span of the copolymer PSDs are lower than their span values at higher TIBA concentration. It is possible that 1-hexene incorporation into polyethylene chains reduce the brittleness of the polymer which in turn reduces the fracture of the growing polymer particles due to the stresses generated by polymer accumulation within the growing particle and, therefore, leads to reduced generation of fine particles and compact morphology of the polymer particles.

Table 8. Comparison of d_{10}, d_{50}, d_{90} and span of the homo and copolymers produced with different sized catalysts of PQMS 3040. A_{TIBA} and $A_{1\text{-hexene}}$ refer to TIBA and 1-hexene initial amounts added into the reactor.

Sample Name	Catalyst name	A_{TIBA} (mmole)	$A_{1\text{-hexene}}$ (ml)	d_{10}	d_{50}	d_{90}	Span
MAB278	BM-4 (Pan)	1.0	3	135	268	467	1.24
MAB357	BM-2 (36µm)	1.0	0	82	235	458	1.59
MAB193	BM-2 (36µm)	1.0	3	215	370	600	1.04
MAB492	BM-2 (36µm)	0.5	3	240	352	513	0.77
MAB200	BM-3 (45µm)	1.0	3	246	450	744	1.11
MAB201	BM-3 (45µm)	1.0	3	244	438	725	1.10
MAB490	BM-3 (45µm)	0.5	3	327	485	721	0.81
MAB311	BM-1 (63µm)	1.0	3	274	512	887	1.20
MAB491	BM-1 (63µm)	0.5	3	321	565	967	1.14
MAB373	Full batch	1.0	0	159	438	819	1.50
MAB390	Full batch	1.0	0	212	504	960	1.48
MAB482	Full batch	0.5	3	468	1180	2350	1.59

3.2.3. Effect of Catalyst Particle Size Studied with PQMS 1732 Silica

The third silica used to study the impact of support particle size on ethylene polymerization kinetics is PQMS 1732. This silica was also sieved and different fractions were obtained which were then dehydroxylated at 600°C and used to support $(n\text{-BuCp})_2ZrCl_2$/MAO catalyst in the way similar to that used for the preparation of catalysts discussed in the previous sections. However, it should be noted that this commercial silica has a d_{50} value of 128 µm which is more than twice the d_{50} values of Grace 948 and PQMS 3040 silica (i.e., 60 µm and 45 µm, respectively) and therefore, while sieving this silica the smallest fraction obtained was on 45 µm sieve (meaning that no particles were obtained on 36 µm sieve and pan). Consequently, three fractions selected to prepare the supported catalysts were those obtained on 63 µm, 80 µm and 125 µm. This will allow us to compare the catalysts prepared from 63 and 80 µm sieved fractions to the ones supported on the same fractions of Grace 948 silica and PQMS 3040 silica. BET and elemental characterization of the catalysts by ICP-AES for this silica support is shown in **Table 9**. For all the catalysts prepared with this support, Al loading varied in a very close range of 12.4 to 14.9 wt%, whereas the Zr content remained in the narrow range of 0.19 to 0.23 wt% which shows the good reproducibility of the catalyst synthesis procedure since all catalysts were prepared separately. In addition, the pore volumes of these catalysts are not very different from those of Grace 948 based silica based catalysts but they are more 2 times less than the pore volumes of the catalysts prepared with PQMS 3040 silica (e.g., BP-1 has a pore volume of 0.57 $cm^3.g^{-1}$, whereas, BM-1 catalysts (prepared with

63 µm fraction of PQMS 3040 silica) has a pore volume of 1.46 $cm^3.g^{-1}$). Similarly, the pore diameters of these catalysts are almost half the pore diameters of Grace 948 and PQMS 3040 silica based catalysts. The surface areas of these catalysts are higher than those based on Grace 948 silica, but comparable with those made from PQMS 3040 based silica.

Table 9. BET and ICP-AES analysis of the catalysts prepared by using different sieved fractions and full batch of PQMS 1732 silica. A_s = surface area of the catalyst measured by BET, P_v = BJH desorption Pore volume of the catalyst measured by BET, P_d = Pore diameter of the catalyst measured by BET.

Cut Number	Sieve opening (µm)	Catalyst Name	A_s (m^2/g)	P_v (cm^3/g)	P_d (nm)	Zr (Wt%)	Al (Wt%)
1	63	BP-1	389	0.57	5.5	0.23	13.6
2	80	BP-2	311	0.45	5.5	0.19	14.9
3	125	BP-3	417	0.66	5.4	0.22	14.4
4	Full Batch	Bu/M/MS1732	471	0.71	5.6	0.21	12.4
-	Full Batch	Pure silica calcined	507	1.32	8.8	-	-
-	Full Batch	Pure As received silica	536	1.4	10.1	-	-

These catalysts were evaluated under the polymerization conditions of the previous ones unless otherwise mentioned. The instantaneous activity of three different sized catalysts based on PQMS 1732 silica is shown in **Figure 11** for homopolymerization, and in **Figure 12** for copolymerization. In agreement with the results obtained for the previous two silicas, the catalyst particles of smaller size are more active than their bigger counterparts despite very similar active metal loadings. It is important to mention here that a 100 µm sieve was present between the 80 µm sieve and 125 µm sieve which means that the catalyst particles obtained from the 80 µm sieved silica fraction have sizes in the range of 80 to 100 µm and not in the range the range of 80 µm to 125 µm. In addition, no particles were obtained on the top most 250 µm sieve which means that the particles obtained on 125 µm sieve may possess the PSD of a full batch of PQMS 1732 silica. Due to this reason the activity profiles of BP-3 catalyst and full batch based reference catalyst look very similar (see **Figure 11**).

BP-1 (catalyst supported on silica fraction obtained on 63 µm sieve) and BP-2 (catalyst supported on silica fraction obtained on 80 µm sieve) catalysts showed very fast activation as compared to the activation of BP-3 (supported on silica obtained on 125 µm sieve) catalyst which took

approximately 50 minutes to reach the peak activity. This behavior can most likely be attributed to the significantly bigger particle size of BP-3 catalyst which offers higher resistance to monomer transport at the active sites within the catalyst particle and therefore, acceleration-type kinetic profiles[11] were observed in the reactions done with this catalyst. In gas phase homopolymerizations, all the catalysts based on PQMS 1732 silica show either negligible or no deactivation over the whole reaction period, whereas, in the slurry polymerizations these catalysts showed faster deactivation after rapid activation (see **Chapter 4**).

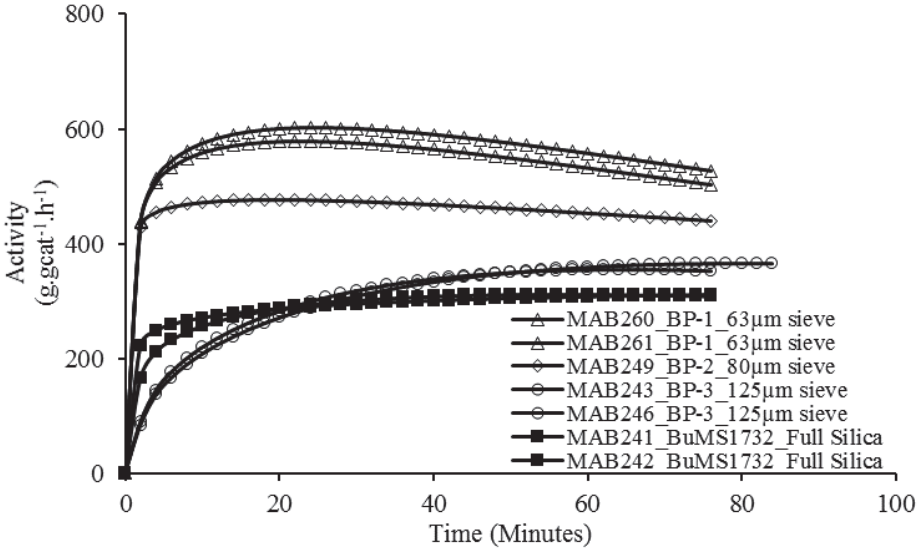

Figure 11. Effect of PQMS1732 silica particle size on the instantaneous activity ethylene homopolymerization. Ethylene pressure = 11 bar, TIBA added = 1 mmole.

Same effect of catalyst particle size on the instantaneous activity and productivity profiles of these catalysts in gas phase ethylene/1-hexene copolymerizations at 11 bar ethylene pressure and two initial amounts of TIBA can be seen in **Figure 12**. The amount of 1-hexene used in these copolymerizations was kept similar to that used for the previously discussed catalysts i.e., 3 mL. On average, the boosts in catalytic activity of BP-1, BP-2 and BP-3 catalysts is 50%, 43% and 52%, respectively, at TIBA concentration of 1 mmole. Reducing the TIBA concentration by 0.5 mmole gave a further increase of about 20% in the activity of BP-1 catalyst but no significant

activity rise was observed in the case of BP-2 catalysts (compare **Figure 12a** and **b**). At lower scavenger amount, BP-1 and BP-2 catalysts deactivated relatively faster than in the case of higher scavenger concentration which is in agreement with the observations made in the previous sections and can be attributed to faster consumption of TIBA during the reaction. Another notable difference in the gas phase copolymerization kinetic profiles of BP-1 and BP-2 catalysts is that their activation rate in the presence of 1-hexene is slower than that during the homopolymerizations (compare **Figure 12** with **Figure 11**) which can be attributed to the change of active site behavior due to the presence of 1-hexene as noted by Kumkaew et al.,[2] also who showed that the activation of silica supported $(n\text{-BuCp})_2ZrCl_2$/MAO catalysts can be delayed due to 1-hexene presence but the overall catalytic activity is higher in copolymerizations than in the homopolymerizations.

All of these supported catalysts showed very similar deactivation trend which can be attributed to higher catalytic activities in copolymerization reactions leading to faster consumption of scavenger. In addition, such deactivation of the catalysts can also be attributed to the impurities present in the 1-hexene batch used. Nevertheless, the overall dependence of the instantaneous catalytic activity of the silica supported $(n\text{-BuCp})_2ZrCl_2$/MAO on its particle size remains the same.

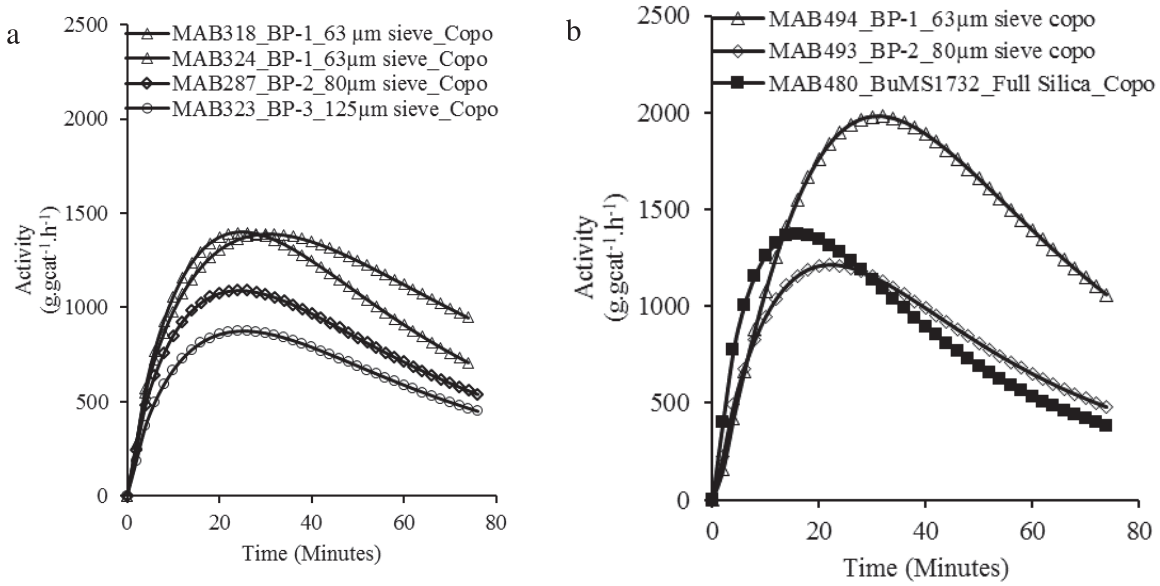

Figure 12. Effect of PQMS 1732 silica support particle size on the instantaneous activity of ethylene/1-hexene copolymerization in gas phase process using (a) 1 mmole of TIBA and (b) 0.5 mmole of TIBA.

As with the other supports, the MWDs of the homo- and copolymers shown in **Figure 13** seem to be unchanged by the variations in the catalyst particle size. As shown in **Table 10**, the dispersity of molar masses for all the polymer samples is between 2 and 3 indicating that all the catalysts behaved like a single-site catalyst and that the variations in particle size of silica supported (n-BuCp)$_2$ZrCl$_2$/MAO catalyst do not impact significantly the nature of the active species. For the copolymers produced with these catalysts, the molar mass and Đ values decreased with the incorporation of 1-hexene into the polymer chains which is also as expected. However, once again, it can be noticed that the copolymers produced with bigger catalyst particles have slightly higher molar masses, especially at lower initial TIBA content (compare M_w values in **Table 10**). The comonomer content and melting temperatures of the polymers also behaved similarly (see **Table 10**).

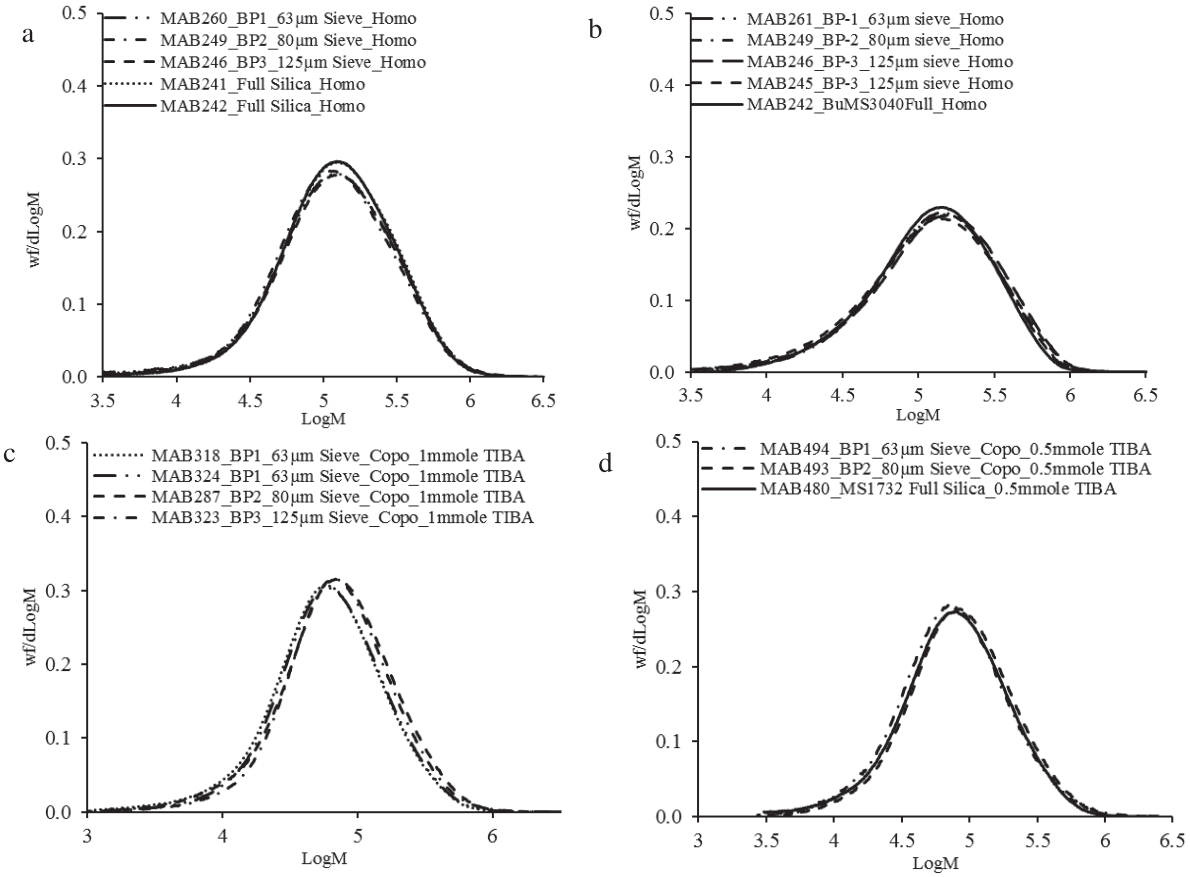

Figure 13. Effect of catalyst particle size on (a) the MWDs of homopolymers with new set HT-SEC columns, (b) the MWDs of homopolymers with previous set HT-SEC columns, (c) the MWDs of copolymers produced with 1.0 mmole TIBA done with new set HT-SEC columns and (d) the MWDs of copolymers produced with 0.5 mmole TIBA.

The PSD of the obtained homo- and copolymer samples with the catalysts of different sizes based upon PQMS 1732 silica evolved as expected and are shown in **Appendix 1** (**Figure S4**). All the polymer samples replicate the corresponding supported catalyst's morphology and the bigger catalyst particles produced bigger polymer particles despite their lower activities. Variations in TIBA content also impacted the polymer PSDs in a fashion which is similar to that observed in the previously discussed cases i.e., at higher TIBA content the polymer particles showed bigger sizes probably due to relatively low catalyst deactivation. PSDs of polymers produced with BP-3 catalyst were not measured because the polymer particle size was beyond the maximum limit (i.e., 3 mm) of Malvern Master Sizer. The results are summarized in **Table 11**.

Table 10. Comparison of weight average molar mass (M_w), dispersity of molar mass (Đ), melting temperature (T_m) and 1-hexene content (x) of the polymers produced with different sized catalysts of PQMS1732 silica. A_{TIBA} and $A_{1\text{-hexene}}$ refers to amounts of TIBA and 1-hexene added into the reactor at the reaction startup. x_{NMR} and x_{CEF} refers to comonomer estimated from ^{13}C NMR and CEF, respectively.

Sample Name	Catalyst name	A_{TIBA} (mmole)	$A_{1\text{-hexene}}$ (ml)	M_w	Đ	T_m (°C)	x_{NMR} (mol%)	x_{CEF} mol%
MAB260	BP-1 (63µm)	1.0	0	175000	2.6	134.8	-	-
MAB318	BP-1 (63µm)	1.0	3	90000	2.5	121.5	-	1.6
MAB324	BP-1 (63µm)	1.0	3	90000	2.1	121.2	-	1.5
MAB494	BP-1 (63µm)	0.5	3	105000	2.4	123.5	-	1.3
MAB249	BP-2 (80µm)	1.0	0	165000	2.6	135.2	-	-
MAB287	BP-2 (80µm)	1.0	3	105000	2.5	120.1	-	1.7
MAB493	BP-2 (80µm)	0.5	3	115000	2.6	118.8	-	1.9
MAB246	BP-3 (125µm)	1.0	0	180000	2.5	136.0	-	-
MAB323	BP-3 (125µm)	1.0	3	105000	2.4	121.3	-	1.6
MAB241	Full batch	1.0	0	176000	2.6	136.0	-	-
MAB242	Full batch	1.0	0	175000	2.4	136.7	-	-
MAB480	Full batch	0.5	3	115000	2.3	120.5	-	1.7

Table 11. Comparison of d_{10}, d_{50}, d_{90} and span of the homo- and copolymers produced with different sized catalysts of PQMS 1732 and the reference catalyst supported on full batch of PQMS 1732 silica. A_{TIBA} and $A_{1\text{-hexene}}$ indicate the initial amounts of TIBA and 1-hexene added into the reactor.

Sample Name	Catalyst name	A_{TIBA} (mmole)	$A_{1\text{-hexene}}$ (ml)	d_{10}	d_{50}	d_{90}	Span
MAB260	BP-1 (63µm)	1.0	0	57	555	975	1.65
MAB324	BP-1 (63µm)	1.0	3	663	1180	2260	1.35
MAB494	BP-1 (63µm)	0.5	3	555	948	1755	1.27
MAB249	BP-2 (80µm)	1.0	0	391	715	1200	1.13
MAB287	BP-2 (80µm)	1.0	3	771	1400	2490	1.23
MAB493	BP-2 (80µm)	0.5	3	654	1180	2270	1.37
MAB245	BP-3 (125µm)	1.0	0	414	968	2060	1.70
MAB323	BP-3 (125µm)	1.0	3	-	-	-	-
MAB241	Full batch	1.0	0	379	802	1760	1.72
MAB242	Full batch	1.0	0	444	889	1920	1.66
MAB480	Full batch	0.5	3	521	1205	2350	1.52

3.2.4. Effect of Catalyst Particle Size Studied with THI/MAO and (n-BuCp)$_2$ZrCl$_2$/MAO Supported Catalysts

The results discussed in the previous sections along with those presented in the **Chapter 4** where the same supported catalysts were evaluated in slurry phase homo- and copolymerizations show that while the particle size of the final silica supported (n-BuCp)$_2$ZrCl$_2$/MAO catalyst has a strong influence on its instantaneous activity in ethylene polymerization the MWDs of the obtained HDPE or ethylene/1-hexene copolymers from catalysts of various sizes does not show any correlation with the catalyst particle size and/or its instantaneous activity. Given that the activities were a strong function of the particle size for all of the supports – regardless of their macroscopic morphologies – and that metal loadings appeared to be independent of particle size, the most logical explanation for the size-dependency of the activity would be mass transfer resistance. It is quite logical to expect that larger particles offer greater mass transfer resistance to monomer, and thus one would expect lower activities that correspond to lower monomer concentrations. On the other hand, one would also expect the average M_w to be lower, and the polydispersity to be greater in larger particles for exactly the same reason. However, given the fact that chain transfer to monomer is the dominant mechanism in terms of M_w control with (n-BuCp)$_2$ZrCl$_2$ metallocene, we decided to repeat the experiments using a different metallocene precursor, THI, that is known to produce polymers whose M_w is sensitive to monomer concentrations in order to test this theory.

One of the difficulties in visualizing such differences in the MWDs of the polyethylene samples (i.e., either HDPE or copolymers) is the dominance of chain transfer to monomer as the main chain termination mechanism with (n-BuCp)$_2$ZrCl$_2$/MAO supported catalysts as shown in the previous chapter with several reactions at different pressures. In order to probe more deeply into this point and hopefully find stronger evidence for the difference in reaction rates as a function of particle size, rac-ethylenebis(4,5,6,7-tetrahydro-1-indenyl)zirconium dichloride (THI) was selected as a second catalyst since transfer to monomer is not the major chain termination mechanism with this metallocene. We should, therefore, be able to see increments in polyethylene molar mass with increasing ethylene pressure inside the reactor and vice versa.

The synthesis procedure of silica supported THI/MAO catalysts is explained in **Chapter 4**. The metal loadings of the final catalysts are compared in **Table 12** with those of the same sized (n-BuCp)$_2$ZrCl$_2$/MAO supported catalyst. It is important to mention that Grace 948 silica was used only for supporting THI/MAO catalysts because it allowed MAO (and therefore, the active species due to the used catalyst synthesis procedure) to distribute throughout the silica particles as shown by SEM-EDX analysis of the catalysts in the previous chapter. Metal loadings and Al/Zr molar ratios of the two THI/MAO catalysts vary in a narrow range just like those of the BG-2 and BG-5 catalysts. Hereafter, we will refer to THI/MAO supported on 36 µm and 80 µm silica fraction as THI/36 and THI/80, respectively. THI/36 and THI/80 catalysts differ from BG-2 and BG-5 in a sense that washing was applied at the end of the former catalysts while the latter were not washed due to the catalyst leaching problem discussed in the previous chapter.

Gas phase ethylene/1-hexene copolymerizations were conducted at very low TIBA and 1-hexene concentrations in order to enhance the rate of reaction and thus create conditions where mass transfer resistance is potentially highest.[2,3,5] In addition, the polymerizations were stopped at different reactions times and polymer samples were collected to study the evolution of MWD with polymerization time since it is well known that the mass transfer resistance will be highest during the reaction start-up and can eventually become less important with the passage of time.[14] All the polymerizations were conducted by adding 1 mL of 0.33 M 1-hexene (giving 0.13 mmole TIBA per liter of reactor volume and 1-hexene concentration of 7.9 mmole at RTP) into the empty pre-conditioned reactor at room temperature followed by heating to 80 °C and catalyst + salt mixture injection at the reaction temperature with an injection cartridge under ethylene pressure.

Table 12. ICP-AES analysis of the catalysts prepared by using different sieved fractions of Grace 948 silica and full batch of Grace 948 silica. * indicates absence of washing step during synthesis.

Cut Number	Sieve opening (μm)	Metallocene	Catalyst Name	Al (Wt%)	Zr (Wt%)	Al/Zr Molar ratio
1	36	THI	THI/36	13.4	0.24	189
2	80	THI	THI/80	14.2	0.22	218
3	Full Batch	THI	THI/M/G948F*	17.7	0.19	315
4	36	n-BuCp	BG-2*	12.4	0.19	221
5	80	n-BuCp	BG-5*	15.6	0.20	264
6	Full Batch	n-BuCp	Bu/M/G948F*	14.0	0.31	153

The effect of ethylene pressure on the reaction rate profile, catalyst productivity and MWD of the polyethylene samples obtained by using THI/36 and THI/80 catalysts is shown in **Figure 14**. An increase in catalytic activity, productivity and molar mass of the produced polymer with increasing ethylene pressure is obvious for both the catalysts. The shift of MWD curve towards higher molar mass with increasing ethylene reactor concentration is an evidence for the absence of the chain transfer to monomer during ethylene/1-hexene copolymerization with silica supported THI/MAO catalyst, and suggests that it is unlikely that a significant amount of chain termination occurs by β-hydrogen transfer to the metal. **Table 13** shows the values of M_w, M_n, dispersity of molar masses (Đ) and melting temperature of the copolymer samples produced. It can be noticed that Đ has a value much higher than 2 (and higher than the catalyst presented in the previous section) which indicates that there is either more than one type of active site, or that there is significant mass transfer resistance throughout the polymerizations.

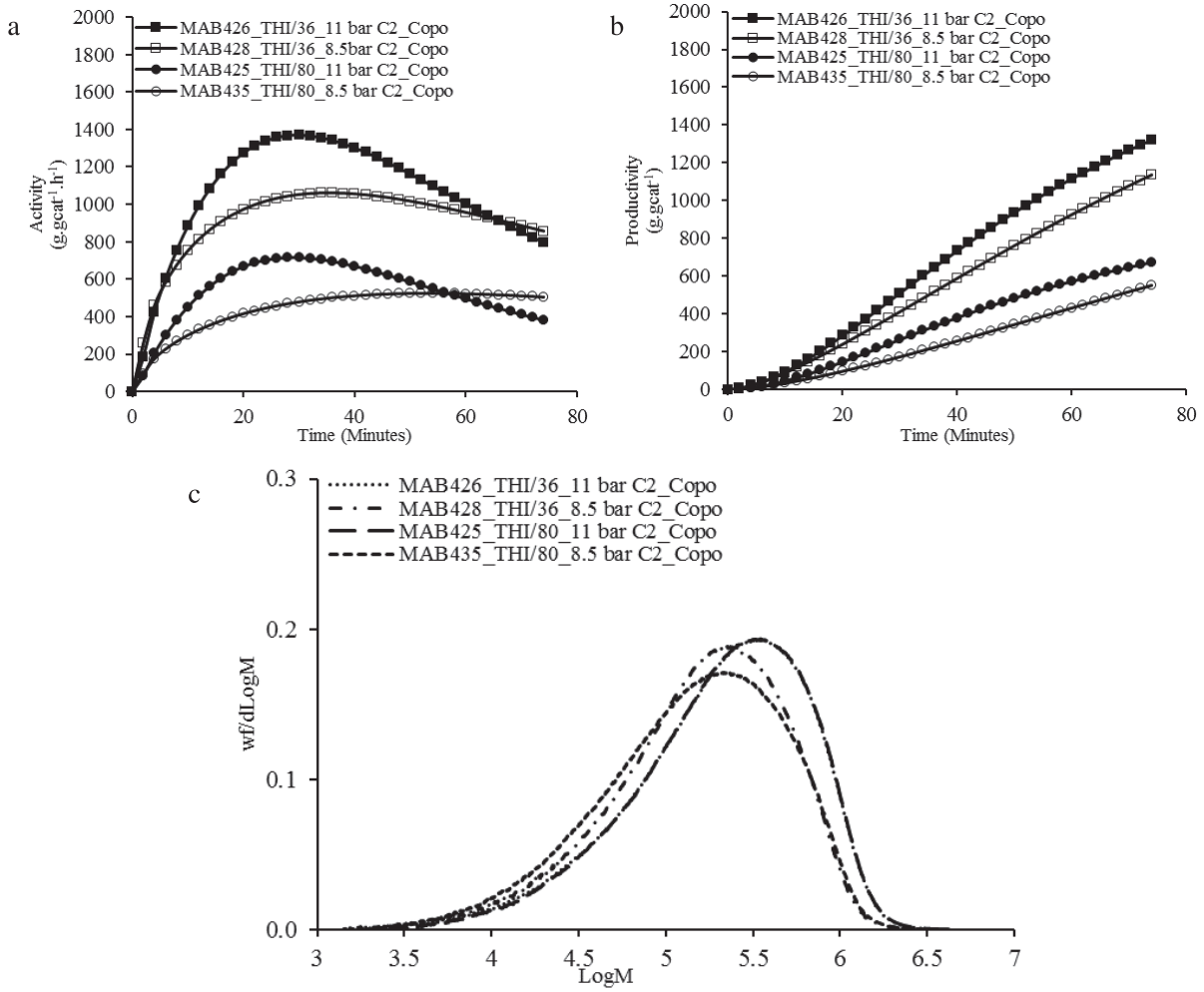

Figure 14. Comparison of (a) instantaneous activity, (b) productivity of THI/36 and THI/80 catalyst in gas phase ethylene/1-hexene copolymerization at 80°C and two different pressures and (c) MWDs of the obtained copolymers.

Table 13. M_w, M_n, dispersity of molar mass (Đ) and melting temperature (T_m) of the polyethylene samples produced with THI/36 and THI/80 catalysts.

Cut Number	Catalyst Name	P_{C2} (bar)	M_w (g/mole)	M_n (g/mole)	Đ	T_m (°C)
MAB428	THI/36	8.5	256 300	67 200	3.8	121.7
MAB426	THI/36	11.0	336 500	83 200	4.0	121.8
MAB435	THI/80	8.5	252 000	61 600	4.1	119.3
MAB425	THI/80	11	341 000	88 600	3.7	122.3

Regarding differences in the MWD of the copolymer samples shown in **Figure 14**, it appears that the major difference between the curves is due to the reactor pressure more than anything else. The two curves obtained for the 11 bar runs overlap each other almost perfectly, and despite some small

differences, the 2 curves for the 8.5 bar runs are very similar as well. In terms of the influence of particle size on activity, these results support the observations made with (n-BuCp)$_2$ZrCl$_2$/MAO. On the other hand, it is very difficult to use the 75 minute results to determine whether or not mass transfer resistance has occurred in the particles

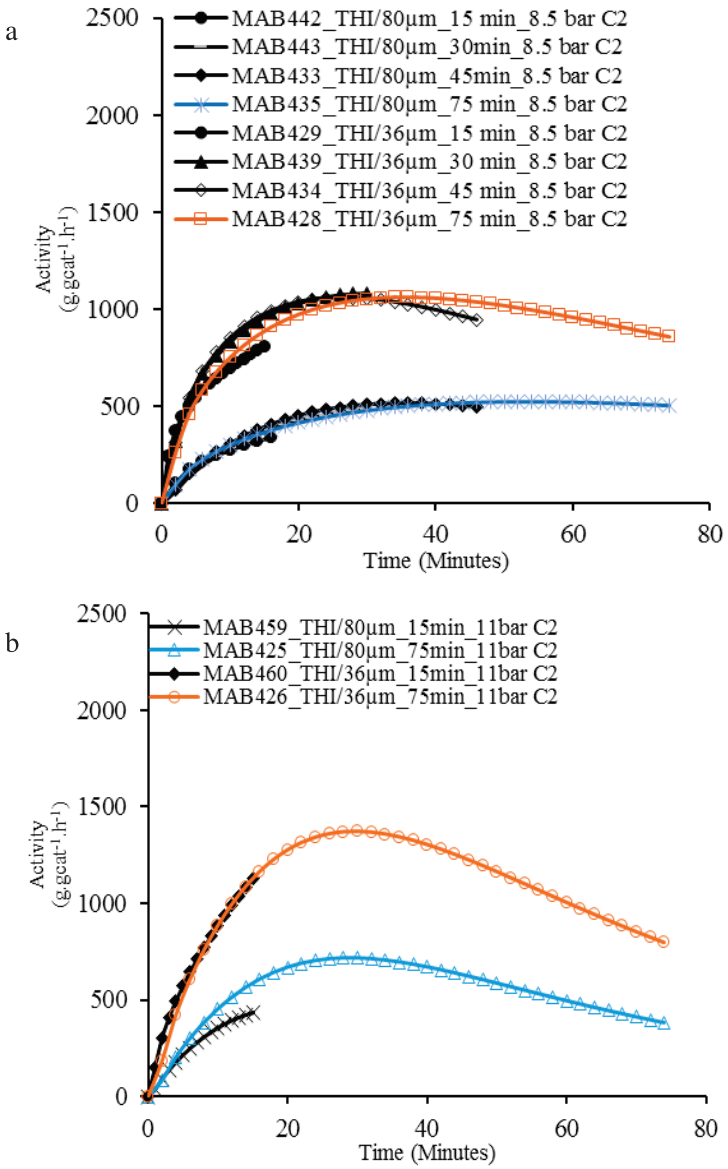

Figure 15. Comparison of instantaneous activity and productivity of THI/36 and THI/80 catalysts in gas phase copolymerizations conducted at different reaction times at (a,c) 8.5 bar ethylene pressure and (b,d) at 11 bar ethylene pressure.

The next step is to conduct the gas phase polymerizations of shorter reaction times and analyze the evolution of polymer MWDs with reaction time to see whether they show some differences or not.

Figure 15 presents the instantaneous activity of THI/36 and THI/80 catalysts in gas phase copolymerizations at two ethylene pressures and different reaction times at 80 °C. It is important to mention that the concentration of TIBA and 1-hexene were kept constant in all of these reactions as mentioned before. Good reproducibility of the reactions is evident in **Figure 15** since all the activity profiles overlap each other.

MWD curves of these copolymer samples are shown in **Figure 16** which clearly show that low molecular weight polyethylene is produced during the first 15 minutes of the reaction with both the catalysts at 8.5 bars. After this point it increases until after 30 minutes of polymerization it is hard to differentiate between the distributions of the polymer produced with the smaller catalyst particles. The same general behavior is seen for the larger particles, but it takes at least 45 minutes for the change in MWD to become less apparent. This shows that the molar masses develop at different rates if the particle size of the supported metallocene/MAO catalyst is different and after a certain time it may not be possible to see any visible differences in the MWDs of the polymers under question.

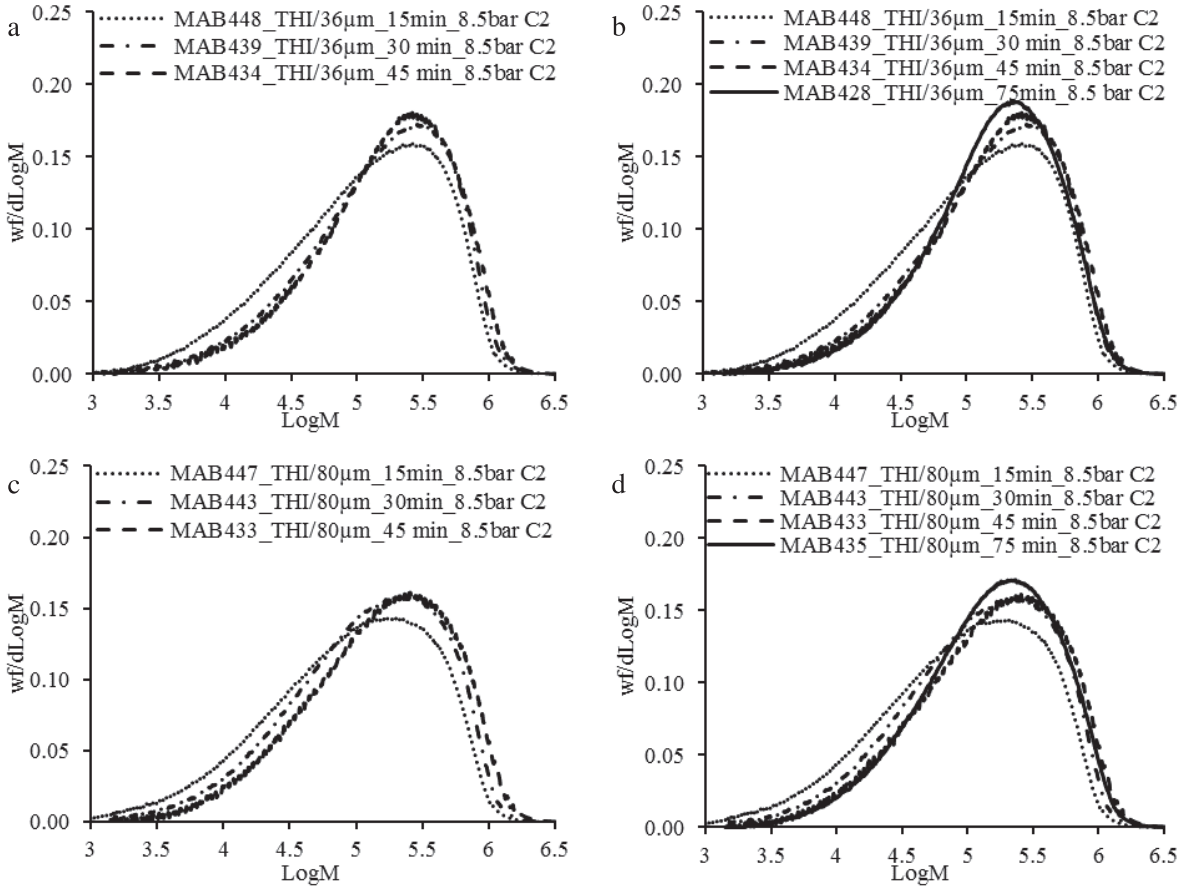

Figure 16. Evolution of MWD of the copolymers produced with (a,b) THI/36 catalyst and (c,d) THI/80 catalyst at 8.5 bar ethylene pressure.

If we replot these data comparing the MWD of polymer produced on the large and small particles at the same times, we can see from **Figure 17** that at least for the first 30 minutes of the polymerization time the MWD curve of the copolymer produced with less active THI/80 catalyst is shifting more toward the lower end of the range than that of the copolymer produced with more active THI/36 catalyst. This trend is even more clear in **Figure 18**, where we can see the net differences in the number and weight average molecular weights for the 2 different sized catalysts as a function of reaction time, along with the values of the molar mass dispersity (Đ). The evolution of Đ in **Figure 18c** is particularly interesting as the values decrease sharply as a function of time. During the first 30 minutes of the reaction, Đ values were higher for the copolymers produced with THI/80 catalyst than those for those produced with THI/36 catalyst. High dispersities are indicative of non-negligible mass transfer resistance

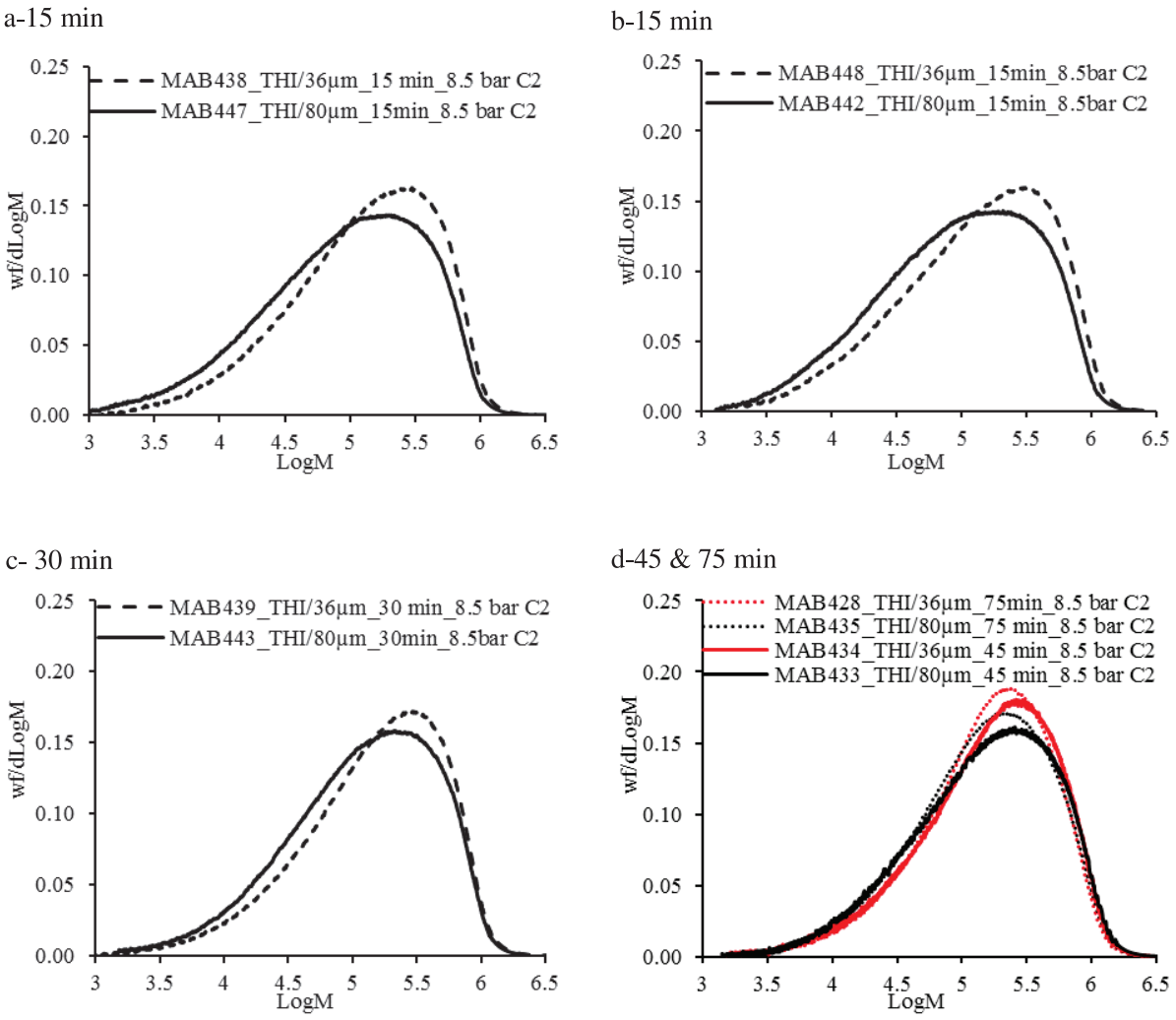

Figure 17. Comparison of the MWD of copolymer samples produced with THI/36 and THI/80 catalysts at 15 min of reaction time (a & b), at 30 min of reaction time (c) and at 45 and 75 min of reaction time (d).

According to Floyd et al.,[11,12] intraparticle diffusion resistance can be significant for large particles having moderate to very high activity in ethylene polymerization during the initial moments of particle growth. As the polymer particle grows with time, the intraparticle concentration gradients are vanished due to increase in external particle surface area. It seems therefore quite reasonable that the observed differences in the instantaneous activities (and changes in the MWD) can be attributed to the higher level of intraparticle diffusion resistance in bigger catalyst particles than

that in the smaller ones during the initial reaction instants, and as the reaction proceeds this effect disappears. In our case the overall activities are not particularly high, so the bulk of the polymer is produced under conditions where no mass transfer resistance seems to be observable, and the final, long time MWDs are similar (depending more on the reactor pressure than anything else).

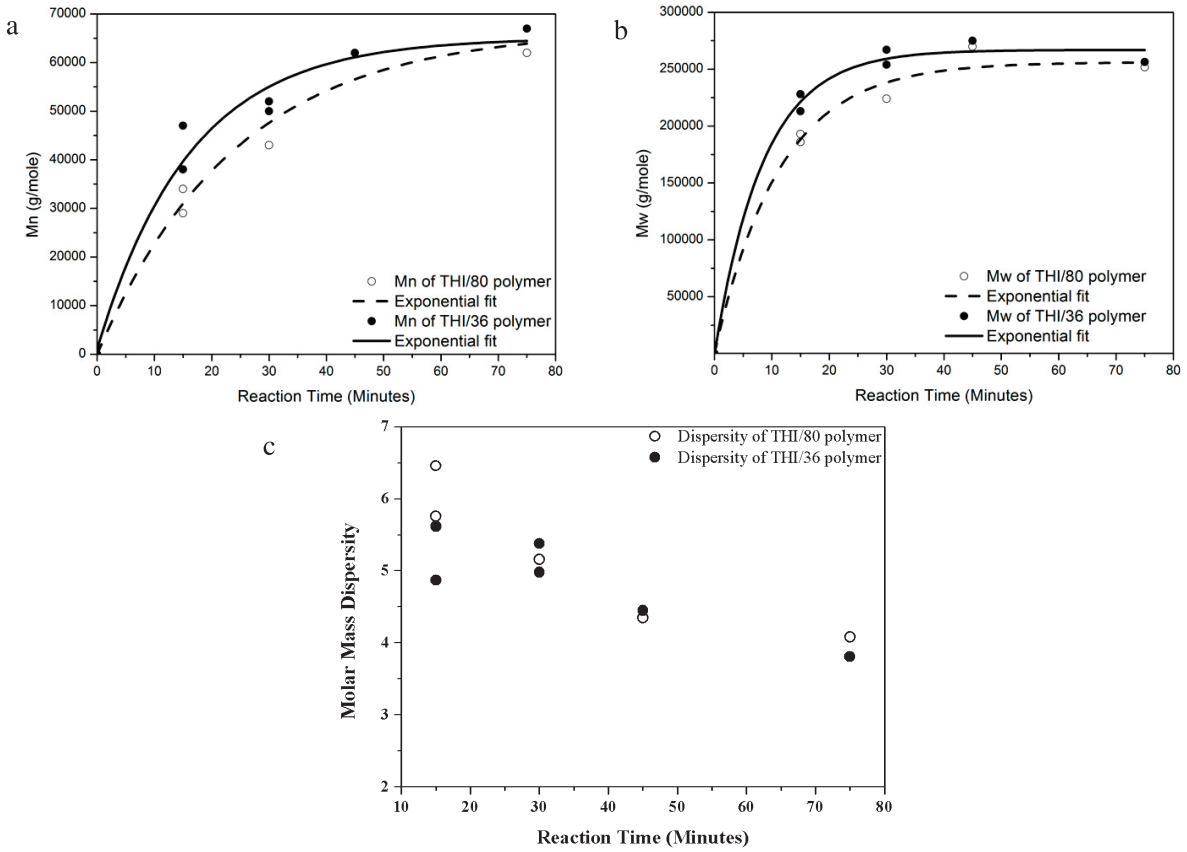

Figure 18. Evolution of M_w, M_n and polydispersity index (Đ) of the copolymer with time and its dependence on support particle size.

Further investigation of the above mentioned copolymer samples was carried out by Crystallization Elution Fractionation (CEF) technique which provides information about the comonomer content, comonomer distribution in the polymer and intrinsic viscosity of the polymer samples. Since the copolymer samples (those discussed in this section) have been produced at different time intervals, it is of interest to analyze time evolution of comonomer content, long chain branching (LCB) and intrinsic viscosity (IV) of the polymer samples produced with THI/MAO catalyst supported on

silica. **Figure 19** shows that the bigger the catalyst particles are, the higher is the 1-hexene content and number of CH_3 groups per 1000 carbon atoms, and the lower the intrinsic viscosity and the melting temperature of the produced copolymer. It is important to highlight that intrinsic viscosity is a measure of the molar mass of the polymer and the trend of intrinsic viscosity, measured with CEF perfectly matches with that of M_w and M_n trends shown in **Figure 18** which were measured with HT-SEC. Melting temperatures of the copolymer samples (see **Figure 19d**) also correspond with the comonomer content indicating that the due to higher comonomer content of the copolymer produced with larger catalyst particles their melting temperatures are lower than those samples produced with smaller catalyst particles.

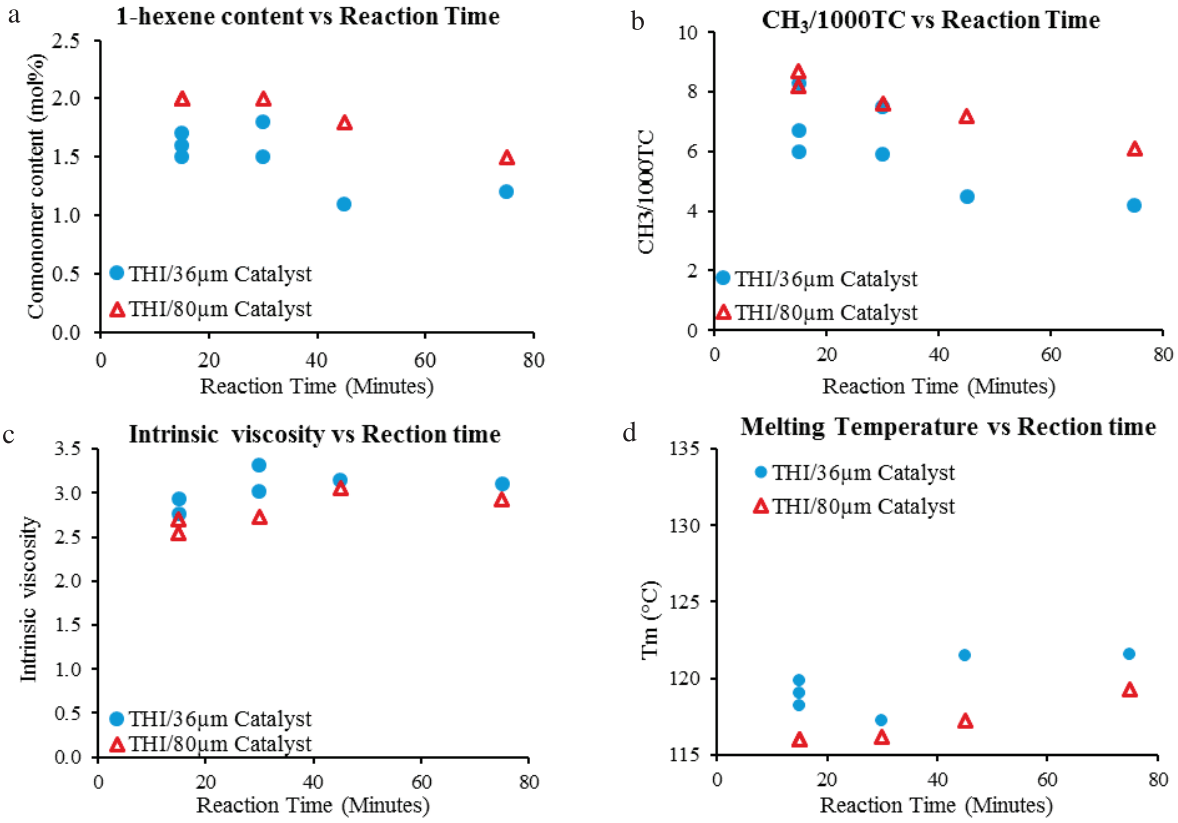

Figure 19. Time evolution of 1-hexene content, CH_3/1000C, intrinsic viscosity and melting temperature (T_m) of the copolymer samples produced with THI/36 and THI/80 catalysts. Melting temperature was measured with DSC.

Proton NMR (^1H) spectra of two copolymer samples produced with THI/36 and THI/80 are compared in **Figure 20**. Most probably, the peak at 5.43 ppm observed for both the samples can be

assigned to vinylene structures Vy1-cis or Vy1-trans based upon the assignments of Redwine et al.,[13] who proposed that these structures correspond to10 - 30% of internal unsaturations depending upon the catalyst type used to produce the copolymer. The signals between 5.19 to 5.17 show a multiplet, which is probably an overlapping of the signals corresponding to two trisubstituted structures, namely (Z)T2 and (E)T2, both of which have very close chemical shifts (i.e., 5.11 and 5.09 ppm, respectively).[14] Further confirmation about these structures can come from the region of 2.00 to 1.50[14] ppm but due to significant noise in that region it is difficult to conclude about which specific type of trisubstituted group it is. The singlet at 4.71 ppm in the ^{1}H NMR spectra of **Figure 20** can be attributed to terminal Vd2 structure.[13,14]

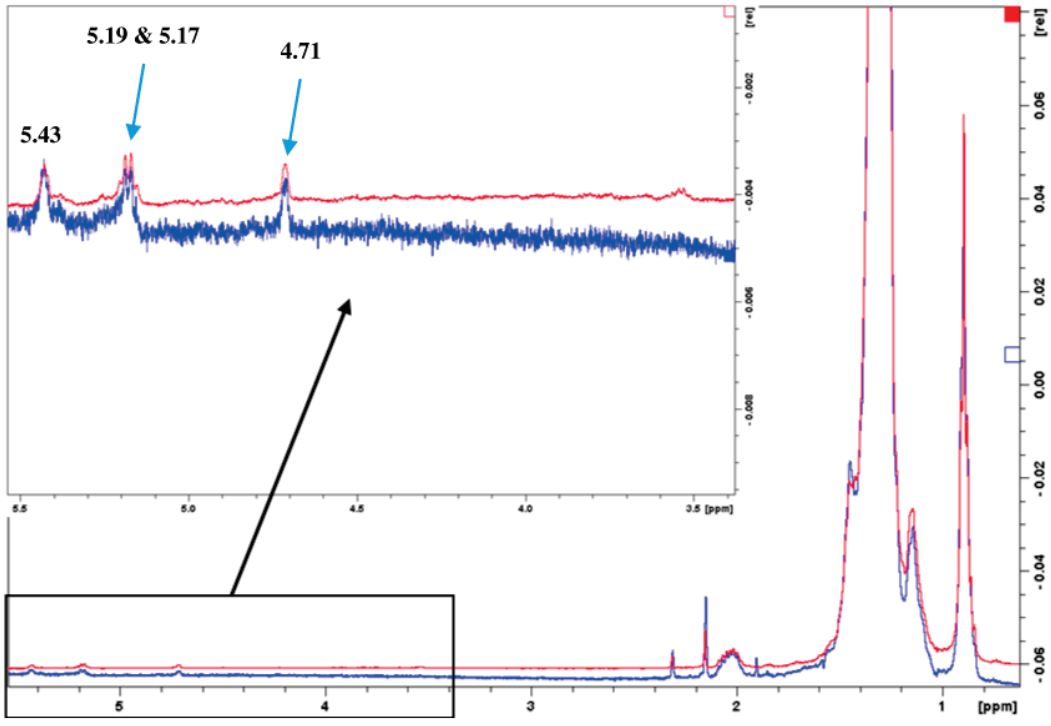

Figure 20. ^{1}H NMR spectra of MAB442 (blue) produced with THI/80 and MAB443 (red) produced with THI/36 catalyst. THI/MAO/silica catalyst based copolymers.

According to Busico et al.,[14] there are two reaction mechanisms by which Vy1-cis can be formed. The first mechanism is by allyl activation, whereas the second one is by olefin isomerization. As the molar masses of the copolymers produced with THI/MAO catalysts increase with increasing ethylene pressure and polymerization time it seems that allyl activation (by which hydrogen is

produced) is not the most probable mechanism for the formation of Vy1-cis or Vy1-trans structures. Therefore, the mechanisms shown in **Figure 21** and **Figure 22** can be proposed for the formation of Vy1-cis, trans and (Z)T2, (E)T2 structures, respectively, in the copolymers produced with silica supported THI/MAO catalysts.[14]

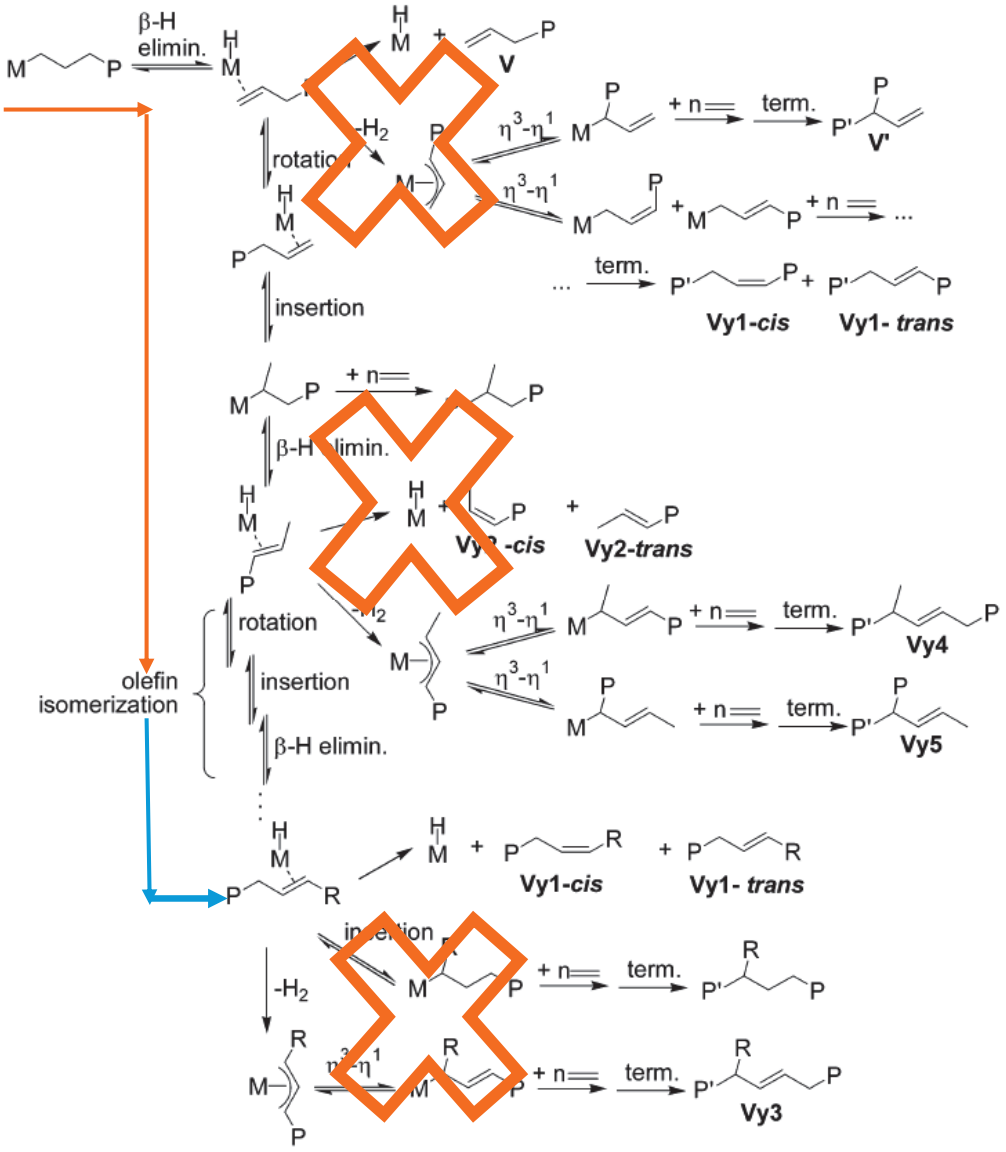

Figure 21. Possible Paths Leading to Chain Unsaturation for a Polymeryl with a Last-Inserted Ethene Unit. Reproduced from Busico et al.,[14] with Permission. Cross (added in this work) indicates that these mechanisms are probably not possible.

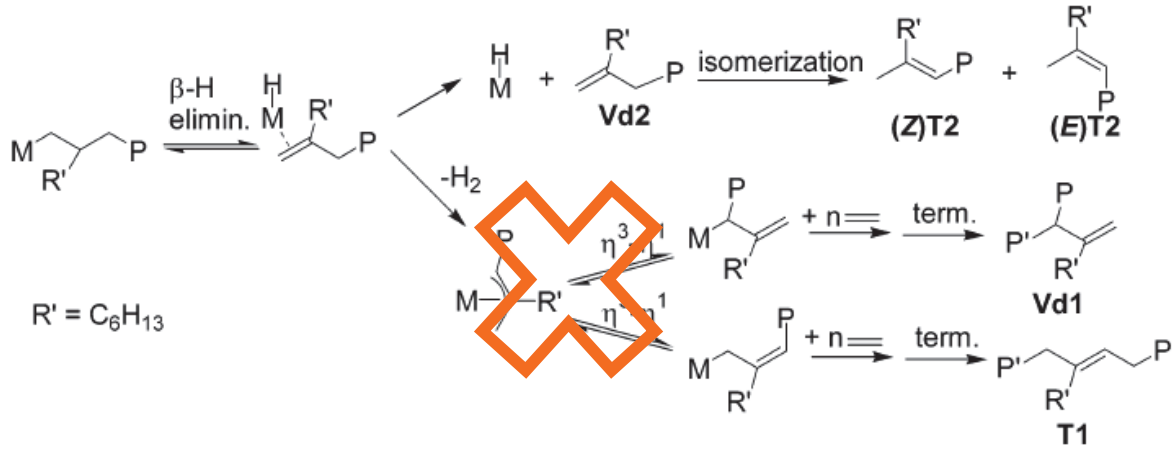

Figure 22. Possible Paths Leading to Chain Unsaturation for a Polymeryl with a Last-Inserted Octene Unit. Reproduced from Busico et al.,[14] with Permission. Cross (added in this work) indicates that these mechanisms are probably not possible.

The results obtained with THI/36 and THI/80 catalysts show that the mass transfer resistance manifests itself during the early stages of ethylene polymerization and therefore, it is of interest to confirm this observation with $(n\text{-BuCp})_2ZrCl_2$/MAO catalyst supported on 36 µm and 80µm fractions of Grace 948 silica i.e., BG-2 and BG-5 catalysts. Gas phase copolymerizations were stopped at different time intervals and all the conditions were kept strictly similar to those used with THI/MAO supported catalysts i.e., T = 80 °C, TIBA = 0.13 mmole.L^{-1}, 1-hexene = 7.9 mmoles. Instantaneous activities and productivities of both the catalysts at different time intervals are compared in **Figure 23** for BG-2 and BG-5 catalysts where, in agreement with the previous results, the former (smaller in size catalyst) is more active and productive than the bigger in size BG-5 catalyst under identical conditions. Despite the catalyst deactivation in 75 minute reactions, $(n\text{-BuCp})_2ZrCl_2$/MAO supported on silica are more active than the THI/MAO catalyst supported on exactly the same silica supports under identical polymerization conditions (compare **Figure 23a** with **Figure 15a**).

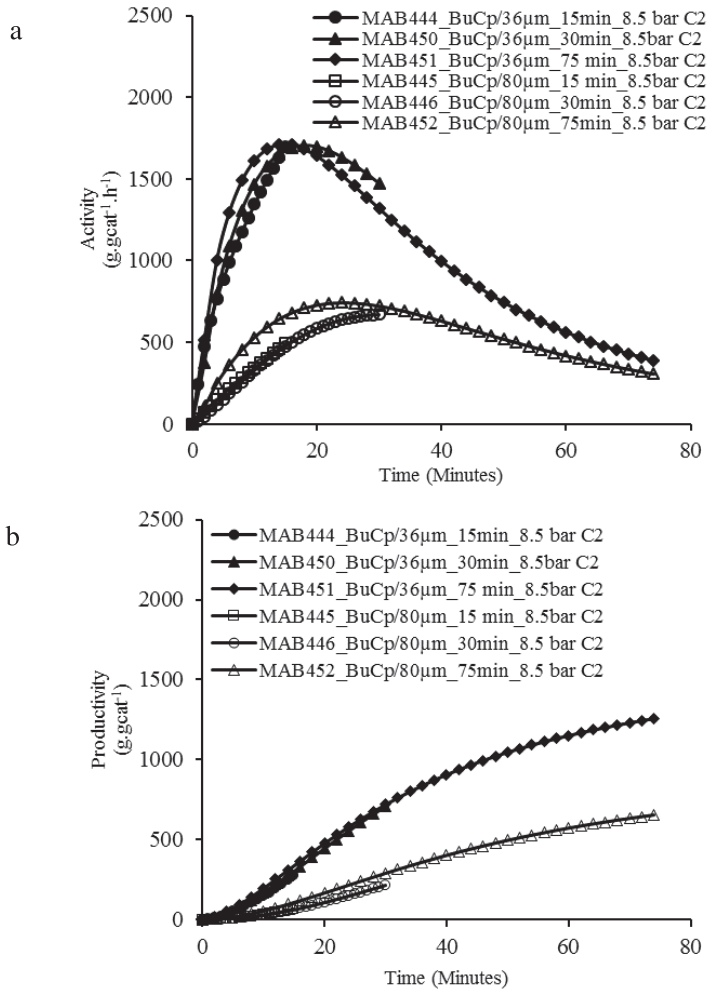

Figure 23. Comparison of instantaneous activity and productivity of BG-2 and BG-5 catalysts in gas phase copolymerizations conducted at 8.5 bar ethylene pressure.

MWD development of these copolymers samples with reaction time is shown in **Figure 24**. It is obvious that for the copolymers, the evolution of MWD with time is opposite to what was observed in the case of copolymers produced with THI/36 and THI/80 catalysts i.e., the copolymers produced with (n-BuCp)$_2$ZrCl$_2$/MAO supported catalyst have higher molar mass at short reaction times and as the polymerization time increases the copolymers attain lower molar masses before stabilizing at a certain value, whereas, in the case of THI/MAO catalyst the molar mass of the copolymers increased with increasing reaction time before becoming constant at higher reaction times under the same polymerization conditions (compare **Figure 24** with **Figure 16**). These results also support those shown in **Chapter 4** with BM-1 catalyst.

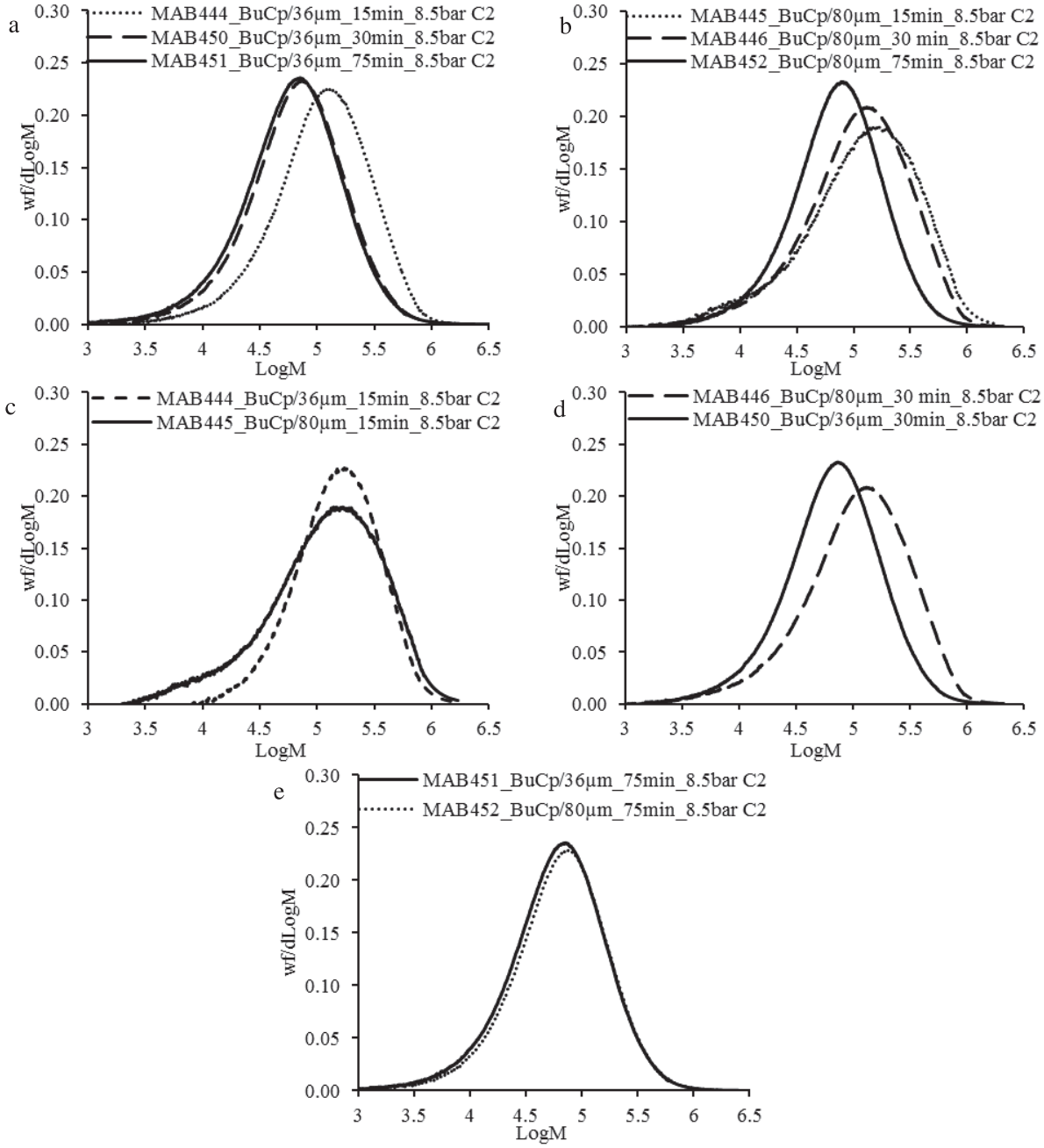

Figure 24. MWD evolution with time for (n-BuCp)$_2$ZrCl$_2$/MAO catalyst supported on 36 µm (BG-2) and 80 µm (BG-5) sieved fractions of Grace 948 silica in gas phase ethylene/1-hexene copolymerization.

Such a decrease in polymer molar mass with increasing reaction time before achieving a steady state value indicates the generation of hydrogen in-situ during (n-BuCp)$_2$ZrCl$_2$/MAO catalyzed ethylene/1-hexene copolymerizations which has also been reported by various authors[8,10,15,16] using other homogeneous and heterogeneous metallocene catalyst systems under different conditions of

temperature, pressure and comonomer concentration. As an example, **Table 14** shows some of the data reported by Masion et al.[16] about in-situ hydrogen generated during slurry phase ethylene homo- and ethylene/1-hexene copolymerization, as well as the consumption of externally added hydrogen by different bridged and unbridged zirconcene and titanocenes (see **Figure 25** for chemical structures of the metallocenes). In all of these examples, the authors used sulfated alumina as the support for the metallocene and TIBA as scavenger. Reactor temperature was either 95 or 80 °C. The first four entries of **Table 14** show that in-situ hydrogen can be generated in ethylene homo- and copolymerizations, and that unbridged zirconocenes produce less hydrogen then the bridged ones under identical conditions. The last three entries of **Table 14** show that unbridged titanocenes consume hydrogen faster as compared to the bridged ones. Comparison of zirconocene with titanocene, both of which have a similar ligand framework, shows that the former has a far better hydrogen response than the latter one (compare fifth entry with the eighth one). We can also see that unbridged titanocene with two Cp rings seems to be a better hydrogen consumer than that having one Cp ring as shown by the sixth and seventh entries of **Table 14**. Masion et al.[16] have provided numerous examples and the interested reader is suggested to consult their work for further details.

Table 14. Comparison of hydrogen generated and consumed by different bridged and unbridged metallocenes as shown by Masion et al.[16] $A_{1\text{-hexene}}$ refers to the amount of 1-hexene.

Example	Metallocene	Reaction time (min)	$A_{1\text{-hexene}}$ (g)	Reactor Temperature (°C)	H_2 added at Reaction startup (ppm)	H_2 at the end of reaction time (ppm)
3	MET-I-A	60	0	95	0	213
4	MET-I-A	60	5	95	0	287
10	MET-II-A	60	0	95	0	30
11	MET-II-A	60	5	95	0	38
24	MET-I-A	30	45	80	1800	0
31	MET-II-F	30	45	80	1800	<1
32	MET-II-G	30	45	80	1800	13
33	MET-II-H	30	45	80	1800	78

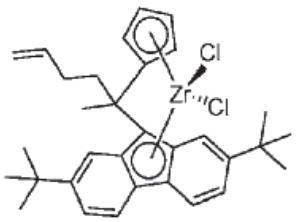

MET-I-A

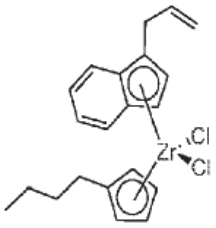

MET-II-A

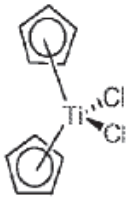

MET-II-F

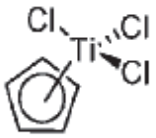

MET-II-G

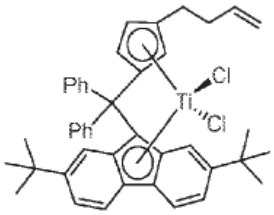

MET-II-H

Figure 25. Chemical structures of difference metallocenes used in by Masion et al.[16]

Our results combined with those discussed in the previous paragraph lead us to propose that silica supported (n-BuCp)$_2$ZrCl$_2$/MAO generates in-situ hydrogen during ethylene/1-hexene copolymerization. Ziegler et al.,[9] proposed that such a hydrogen molecule is liberated by the allylic activation which refers to the generation of an unstable intermediate formed after the unimolecular β-hydrogen transfer to the metal i.e., the unsaturated chain end of the polymer coordinated with the metallocene hydride complex (see **Scheme 1**). A similar mechanism has been proposed by Wasserman et al.,[10] and Folie et al.,[7] for ethylene polymerization with metallocene at different conditions. Since metallocenes are usually very sensitive to hydrogen, and Hasegawa et al.[8] showed that the amount of in-situ hydrogen generated during ethylene polymerization is a function of temperature (i.e., more in-situ hydrogen generation as the reactor temperature is raised), it can be

anticipated that at short reaction times the amount of hydrogen produced and consumed by supported (n-BuCp)$_2$ZrCl$_2$/MAO was low which led to higher molar masses of the corresponding copolymers. On the other hand, as the reaction continues for longer time the amount of in-situ hydrogen increases and finally achieves some equilibrium value giving polymers of constant molar masses.

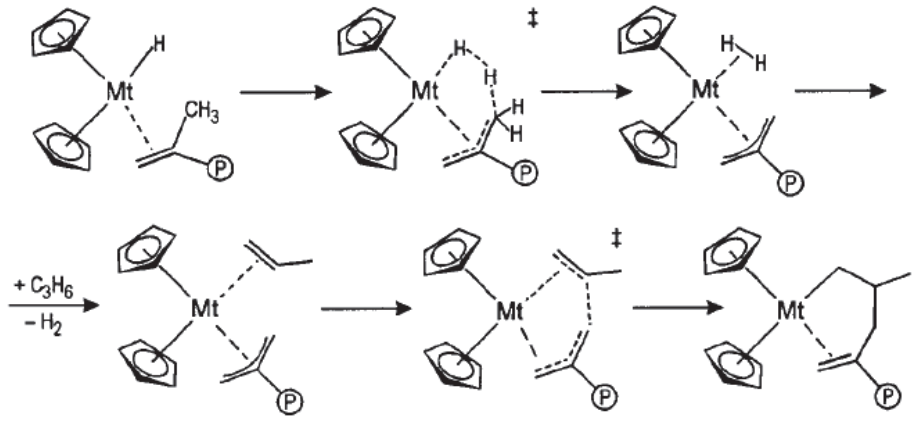

Scheme 1. Mechanism of hydrogen generation by allylic activation process proposed by Ziegler et al., during olefin polymerization with metallocenes.

Comparison of **Figure 24c, d** and **e** clearly shows for at least the first 30 minutes of reaction, the polymers produced with bigger but less active BG-5 catalyst possess higher molar mass than the polyethylene produced with smaller in size but more active BG-2 catalyst, and this difference in the polymer molar masses has vanished after 75 minutes of polymerization. The most probable reason for this observation might be that due to higher monomer concentration gradients in BG-5 catalyst particles leading to their low activity, the amount of in-situ hydrogen generated during the first 30 minutes of reaction time was lower than that generated during polymerization with BG-2 catalyst, consequently providing higher molar mass of the copolymers produced with BG-5 catalyst than that of the samples produced with BG-2 catalyst.

From **Scheme 1**, it can also be seen that for the generation of hydrogen the active metal center has to interact with the growing polymer chain. Therefore, due to higher concentration gradients in bigger catalyst particles one should expect low amount of growing polymer chains if we assume that the amount of the active metal is similar on catalyst particles of different sizes. This low amount of growing polymer chains will generate less hydrogen and therefore, the molar mass of the copolymer produced with BG-5 catalyst is higher than that of the polymer produced with BG-

2 catalyst during the first 30 minutes of reaction time. As the diffusion resistance decreases with time, at longer reaction periods the amount hydrogen generated and consumed by the polymer particles grown up from BG-5 catalyst increases which provides the copolymers of MWDs similar to those produced with BG-2 catalyst (see **Figure 24e**).

It is important to note that the MWD of the copolymer produced with smaller in size but more active BG-2 catalyst achieves its stable value after 30 minutes of reaction time and does not changes significantly by further increase in the reaction time, as shown in **Figure 24a**. At this point it should also be highlighted that smaller catalyst particles are more active and therefore, they should be hotter (at least by few degrees) than their bigger less active counterparts (although it is more difficult to take heat out of the bigger ones than the smaller one) which might have led to more generation of in-situ hydrogen in agreement with the work of Hasegawa et al.,[8] according to which the hydrogen generation increases with increasing reactor temperature during ethylene polymerizations with metallocenes. Molar mass dispersity values also show that during the first 30 minutes, nature of the active sites producing copolymers on BG-5 catalyst is different from the nature of active sites on BG-2 catalyst (see **Figure 26b**) which is again a proof for the existence of more diffusion resistance in bigger catalyst particles during early stages of ethylene polymerization.

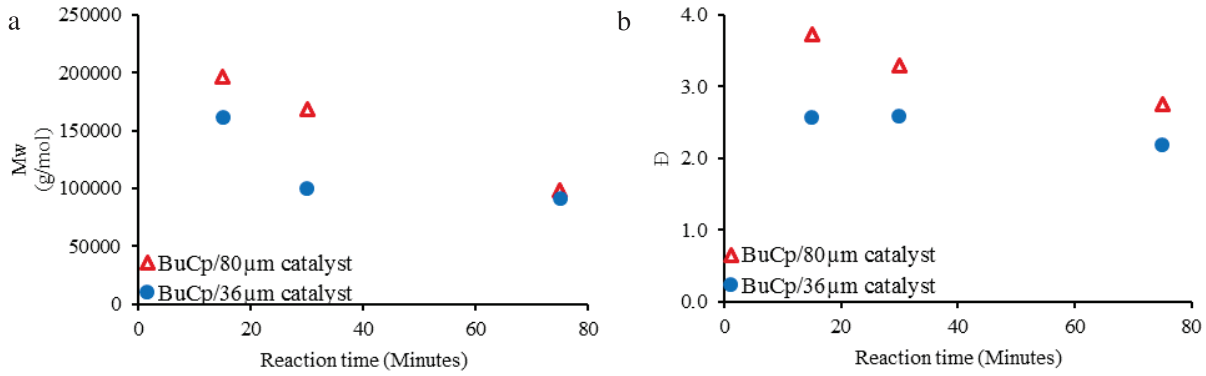

Figure 26. Evolution of (a) M_w and (b) molar mass dispersity (Đ) of the copolymers produced with BG-2 and BG-5 catalyst in gas phase ethylene/1-hexene copolymerization with reaction time.

Proton NMR was also performed on some of these copolymers to obtain the proof for in-situ hydrogen generation, as suggested by the MWD evolution with time. **Figure 27** compares proton NMR spectra of two copolymer samples produced with BG-2 and BG-5 catalysts which show two

doublets in the range of 4.97 to 4.87 ppm attributable to terminal vinyls according to Busico et al.[14] Due to significant noise after 5.5 ppm it was not possible to see the second peak at 5.81 ppm designated to terminal vinyls. Other peak assignments in **Figure 27** are basically similar to those made for the proton spectra of copolymers produced with THI/MAO catalysts (see **Figure 20)** and show internal unsaturations indicating the generation of in-situ hydrogen with the exception that since this catalyst does not favor isomerization the multiplet in the range of 5.19 to 5.17 can be attributed to T1 structure (see **Figure 29**). Although the presence of terminal vinyls indicate that polymer chains produced with $(n\text{-BuCp})_2ZrCl_2$/MAO catalyst can terminate via β-hydride elimination, the low intensity of these peaks in comparison to those of internal unsaturations along with the evolution of polymer MWD with polymerization time shown in the previous paragraphs indicate that β-hydride elimination is not the dominant chain termination mechanism.

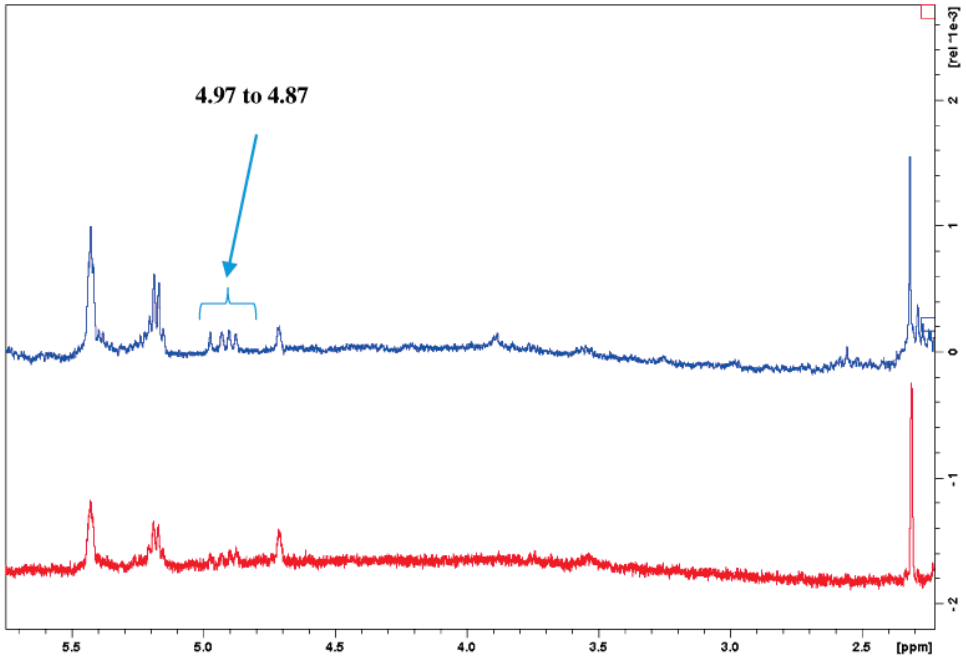

Figure 27. ^1H NMR of MAB450 (blue line) produced with BG-2 and MAB446 (red line) produced with BG-5 after 30 minutes of polymerization time. $(n\text{-BuCp})_2ZrCl_2$/MAO/silica catalyst based copolymers.

Therefore, in-situ hydrogen was produced due to allyl activation which allows us to propose that BG-2 and BG-5 along with other silica supported $(n\text{-BuCp})_2ZrCl_2$/MAO catalysts may have terminated dominantly according to the mechanisms proposed in **Figure 28** and **Figure 29**.

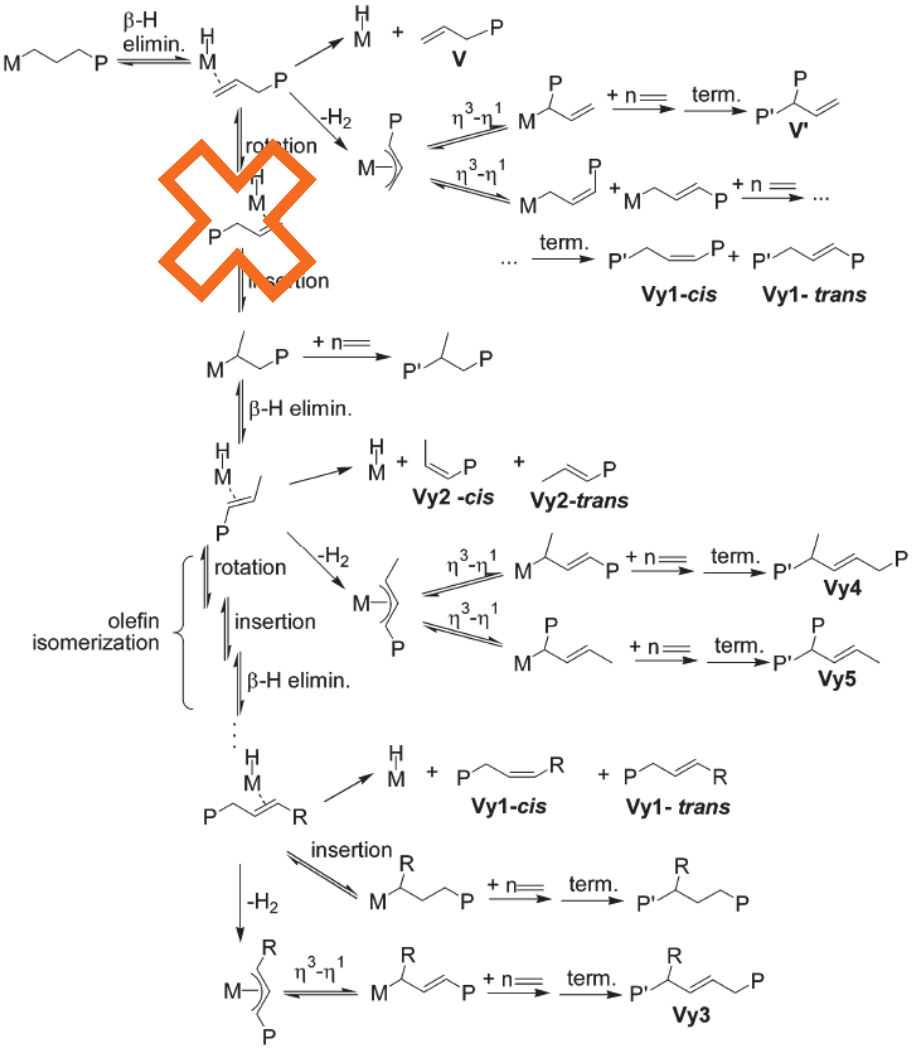

Figure 28. Possible paths leading to chain unsaturation for a polymeryl with a last-inserted ethylene unit. Reproduced from Busico et al.,[14] with permission. Cross (added in this work) indicates that these mechanisms are probably not possible.

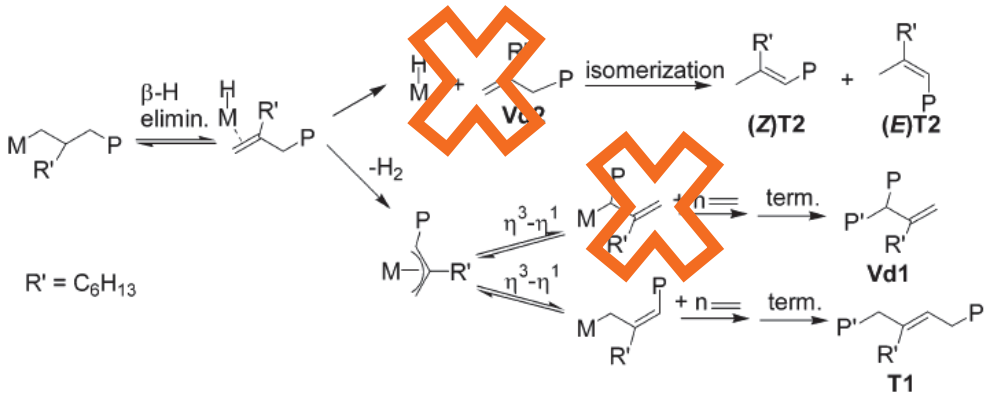

Figure 29. Possible paths leading to chain unsaturation for a polymeryl with a last-inserted octene unit. Reproduced from Busico et al.,[14] with permission. Cross (added in this work) indicates that these mechanisms are probably not possible.

Evolution of comonomer content, CH_3/1000 carbon atoms, intrinsic viscosity and melting temperature with reaction time of the copolymers produced by using (n-BuCp)$_2$ZrCl$_2$/MAO and THI/MAO catalysts is compared in **Figure 30**. (n-BuCp)$_2$ZrCl$_2$/MAO supported catalysts incorporate less 1-hexene as compared to their THI/MAO counterparts and therefore, CH_3 groups per 1000 carbon atoms is also lower in the copolymers produced with the former catalysts than that in the copolymers produced with the later catalysts (**Figure 30a,b**). The melting temperature of the copolymers produced with (n-BuCp)$_2$ZrCl$_2$/MAO supported catalysts is also higher than that of copolymers produced with THI/MAO catalysts. Intrinsic viscosities of the copolymer produced with (n-BuCp)$_2$ZrCl$_2$/MAO supported catalysts are lower than that of the copolymers produced with THI/MAO catalysts because the copolymers produced with THI/MAO catalysts have significantly higher molar masses than the molar masses of copolymers produced with (n-BuCp)$_2$ZrCl$_2$/MAO supported catalysts, under the identical conditions.

Coming back to the effect of particle size, it can be noticed that once again the bigger particles have a higher comonomer content and number of CH_3/1000 carbon atoms. Furthermore, the intrinsic viscosity of copolymers produced with BG-5 catalyst is higher than that of the copolymers produced with BG-2 catalyst, which is coherent with the HT-SEC measurements of MWD (compare **Figure 30c** with **Figure 24**). Due to higher comonomer incorporation, the melting temperature of the copolymers produced with BG-5 catalyst is lower than the melting temperature of the copolymers produced with BG-2 catalyst. These results are in agreement with those observed in the case of THI/MAO catalysts, and help to present an acceptable experimental proof for the

existence of intraparticle diffusion resistance during the early stages of ethylene polymerization on silica supported metallocene/MAO catalysts.

Based on the results obtained with BG-2 and BG-5 catalysts in gas phase copolymerization reactions of different times, it can now be concluded that the effect of catalyst particle size and the resulting diffusion resistance to monomer(s) transport at the active sites on the MWD of the copolymers can be better seen at short reaction times, typically below 30 minutes, and the bigger the particle size of silica supported $(n\text{-}BuCp)_2ZrCl_2$/MAO catalyst the higher the diffusion resistance leading to lower instantaneous activity and in-situ hydrogen production which causes the molar mass of the polyethylene samples to be higher than or similar to those polyethylenes which are produced with smaller in size but more active $(n\text{-}BuCp)_2ZrCl_2$/MAO catalyst under identical polymerization conditions. This statement allows us to attribute the slightly higher molar masses of the polyethylenes produced with bigger catalysts particles of Grace 948 silica (see **Figure 7**), PQMS 3040 silica (see **Figure 10**) and PQMS 1732 silica (see **Figure 13**) to the lower quantity of in-situ hydrogen generated and consumed by the respective polymer. In addition, one can also explain the observed differences in the MWDs of the polyethylene samples produced with $(n\text{-}BuCp)_2ZrCl_2$/MAO supported on full batches of three different silica employed in this work by using the same proposal. Similar reasoning can also be used as an explanation for the differences in the MWDs of the homo- and copolymers produced with the said catalysts in slurry phase polymerizations (see **Chapter 4**).

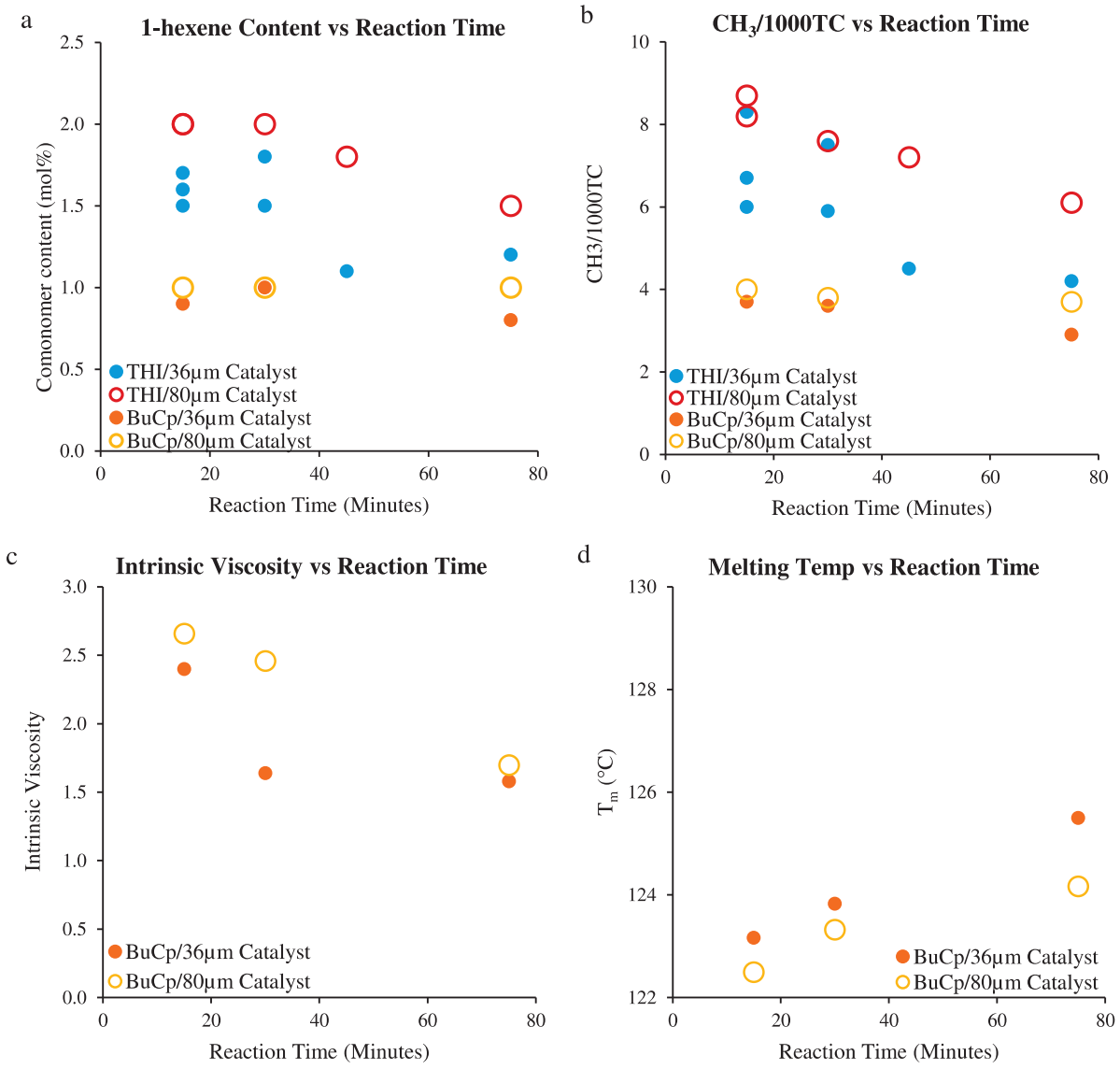

Figure 30. Comparison of 1-hexene content (a) and CH_3/1000C (b) of the copolymers produced with two different metallocene/MAO systems supported on same sized fractions of silica. Comparison of intrinsic viscosity (c) and melting temperature (d) of the copolymer samples produced with BG-2 and BG-5 catalysts at different reaction times. Melting temperature was measured with DSC.

3.3 Conclusion from the Catalyst Particle Size Study in Gas Phase Polymerizations

In this section, the effect of particle size of silica supported metallocene/MAO catalysts has been analyzed in gas phase ethylene homo- and ethylene/1-hexene copolymerizations. The metallocenes used are $(n\text{-BuCp})_2ZrCl_2$ and, to a lesser extent, rac-ethylenebis(4,5,6,7-tetrahydro-1-indenyl)zirconium dichloride (THI). Sieved fractions of different sizes of three commercial silica were used as the supports. It was shown that the smaller silica-supported metallocene/MAO catalyst particles are clearly more active than the bigger ones, provided that the active metal loadings as well as other physical properties of the final supported catalyst are kept similar. This statement has been shown to be valid at two TIBA concentrations. Melting temperatures of the HDPE samples do not show any dependence on the particle size of the silica supported metallocence/MAO catalyst. However, comonomer content appears to be a function of catalyst particle size as the obtained results indicate that bigger catalyst particles incorporate higher 1-hexene as compared to that incorporated by the more active smaller catalyst particles.

Furthermore, in so far as we know, this work provides the first experimental evidence for the existence of mass transfer resistance during early stages of ethylene polymerization with silica supported metallocene/MAO catalysts. This was shown by performing gas phase ethylene/1-hexene copolymerizations of different time periods with the above mentioned two different metallocene/MAO catalysts supported on two significantly different sized fractions of Grace 948 silica. The evolution of the molecular weight distribution (MWD) with time clearly indicated that the molar mass of the copolymers produced with smaller in size but more active silica supported THI/MAO catalyst was higher than that of the copolymers produced with its bigger but less active analog up to first 30 minutes of the polymerization time. As the reaction times exceeded 30 minutes, it was hard to distinguish between the MWDs of the obtained copolymers obtained from small and big catalyst particles. During the first 30 minutes, molar mass dispersity was found to be high for the copolymers obtained with bigger catalyst particles as compared to that of the copolymers obtained from the smaller catalyst particles and as the polymerization time was increased the dispersities of the copolymers produced from bigger and smaller catalyst particles became very similar. Silica supported $(n\text{-BuCp})_2ZrCl_2$/MAO catalysts of different sizes also showed the same dependence of molar mass dispersity on the polymerization time.

However, evolution of the copolymer MWDs produced with small and big particles of silica supported $(n\text{-BuCp})_2ZrCl_2$/MAO catalysts with polymerization time was completely opposite to that observed for the copolymers produced with the THI/MAO supported analogs. ^1H proton NMR analysis of the copolymers in conjunction with the MWD results suggested that in-situ hydrogen was produced during the copolymerizations with silica supported $(n\text{-BuCp})_2ZrCl_2$/MAO catalysts, whereas the chain termination mechanism with silica supported THI/MAO catalysts probably does not allow in-situ hydrogen generation. Therefore, in-situ hydrogen generation has been proposed as the reason for the observed differences in the MWD evolution of copolymers produced with these two silica supported metallocene/MAO catalysts. Nevertheless, the evolution of copolymer MWDs with polymerization in both the cases provide considerable evidence for the existence of mass transfer resistance during early stages of ethylene polymerization with silica supported metallocene/MAO catalysts. Perhaps, this work also provides the first experimental evidence of the effect of in-situ hydrogen on evolution of MWDs of the copolymers produced with silica supported $(n\text{-BuCp})_2ZrCl_2$/MAO catalysts in gas phase process.

3.4. Effect of Porosity of Silica Supported Metallocene/MAO Catalysts on their Activity, Molecular and Physical Properties of Polyethylene

In this section, the aim is to investigate the effect of pore volume (P_v), pore diameter (P_d) and surface area (A_S) of the final silica supported catalyst on its ethylene polymerization kinetics as well as on the properties of polyethylene produced in gas phase process. The particle size of each silica supported catalyst used in this section was kept constant by supporting it on a sieved fraction of the commercial silica used in this work. In addition, the PSDs of different sieved fractions of the three commercial silica used in this work are shown to be very similar. As a result, the observed differences in ethylene (co)-polymerization kinetics of the catalysts obtained from such supported catalysts which have same particle sizes can be attributed to their different P_v, P_d and A_s. Similarly, any differences in the properties of the corresponding polyethylenes can also be ascribed to differences in catalyst porosities. For the ease of reader, **Table 15** is once again presented here which shows the comparison of all the catalysts supported on the sieved fractions of the three commercial silica used in this work. Like the previous chapter, it may be helpful for understanding if we first start the discussion from the two PQMS silica due to their very similar external and internal particle morphology as they seem to have been produced with the same procedure.

Table 15. BET and ICP-AES analysis of the catalysts prepared by using different sieved fractions of different silica. A_s = surface area of the catalyst measured by BET, P_v = BJH desorption Pore volume of the catalyst measured by BET, P_d = Pore diameter of the catalyst measured by BET.

No.	Sieve opening (µm)	Catalyst Name	Support Name	A_s (m^2/g)	P_v (cm^3/g)	P_d (nm)	Zr (Wt%)	Al (Wt%)	Al/Zr Molar Ratio
1	Pan	BG-4	Grace 948	265	0.81	11.6	0.21	14.3	230
2	Pan	BM-4	PQMS3040	395	1.31	10.7	0.23	15.8	232
3	36	BG-2	Grace 948	284	0.81	10.9	0.19	12.4	220
4	36	BM-2	PQMS3040	401	1.31	11.1	0.17	14.3	284
5	45	BG-1	Grace 948	230	0.68	10.7	0.19	12.5	222
6	45	BM-3	PQMS3040	375	1.30	11.9	0.18	13.4	251
7	63	BG-3	Grace 948	269	0.75	10.8	0.18	12.5	234
8	63	BM-1	PQMS3040	390	1.46	12.4	0.19	11.8	209
9	63	BP-1	PQMS1732	389	0.57	5.5	0.23	13.6	199
10	80	BG-5	Grace 948	289	0.80	10.8	0.20	15.6	263
11	80	BP-2	PQMS1732	311	0.45	5.5	0.19	14.9	265

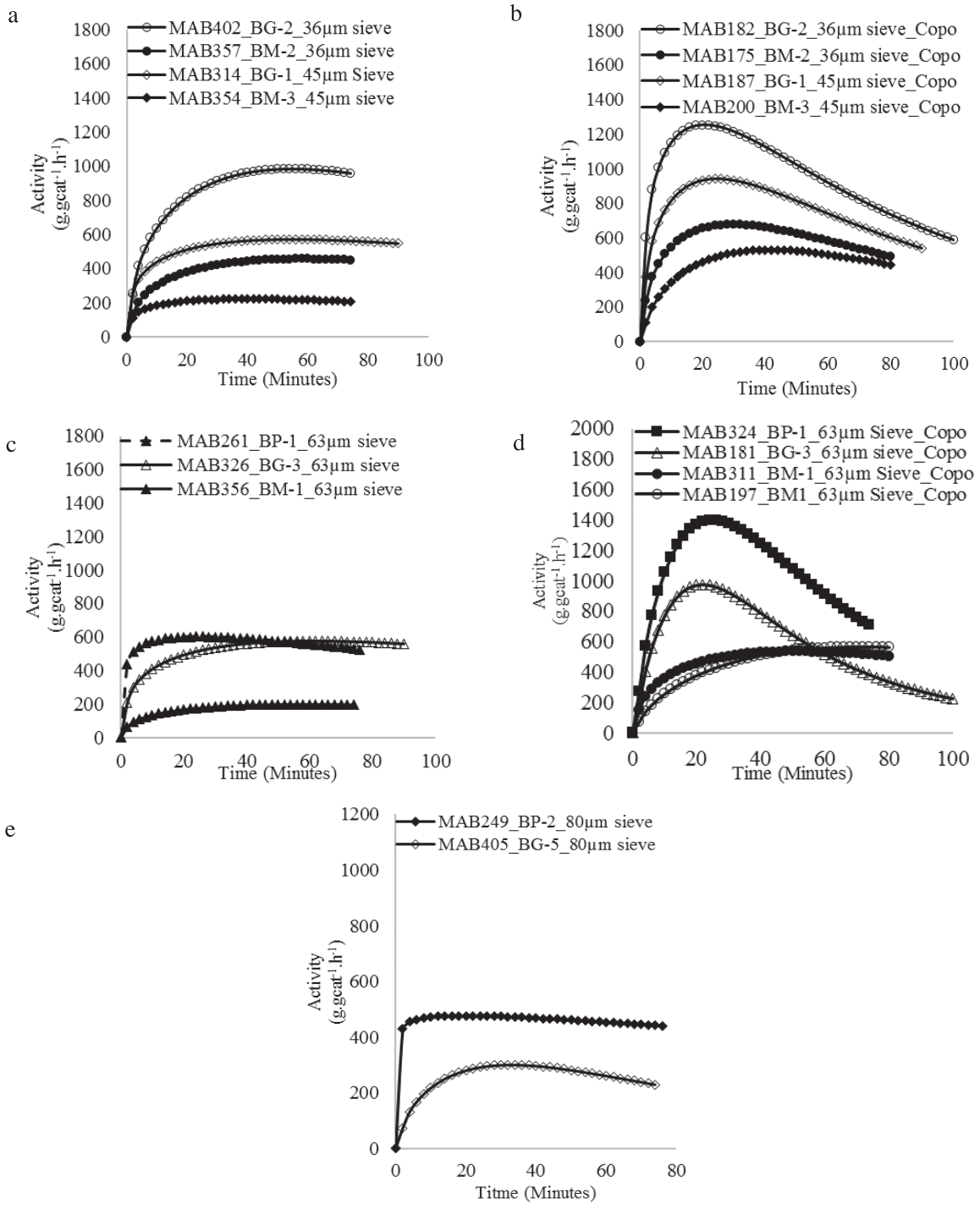

Figure 31. Comparison of the instantaneous activity of the $(n\text{-}BuCp)_2ZrCl_2$/MAO catalyst in ethylene homo & copolymerizations supported on the fractions of Grace 948, PQMS3040 and PQMS1732 silica obtained on 36 µm, 45 µm (a,b), 63 µm (c,d) and 80 µm (e,f) mesh sieves. For all the reactions initial TIBA amount = 1 mmole.

Instantaneous activity profiles of the catalysts based on 63µm sieve fraction of PQMS 1732 and PQMS 3040 silica in gas phase homo- and copolymerizations are compared in **Figure 31c** and **d**, respectively. In both polymerization types it is obvious that the activation rate of BP-1 catalyst is higher than BM-1 catalyst and reaches its peak activity earlier than BM-1; BP-1 took 26 minutes to reach its maximum value in contrast to the 58 minutes taken by the BM-1 catalyst. The same trend can also be noticed in copolymerizations where BM-1 catalyst does not show deactivation. The Al/Zr ratio of these two catalysts are not very different (cf **Table 15**; the Al and Zr contents of BP-1 are 13.6% and 0.23%, vs 11.8 and 0.19% for BM-1 respectively), and certainly not different enough to explain the average difference in the instantaneous activities of BP-1 and BM-1. On the other hand, it appears that the differences in average gas phase homo- and copolymerization rates are 68 % and 50 %, respectively, which corresponds closely to the differences in the pore volume (i.e., BM-1 has 60 % more pore volume than BP-1) and pore diameter of the two catalysts (i.e., BM-1 has 55 % more pore diameter than BP-1) rather than the chemical or surface area differences in the two catalysts.

At lower initial TIBA amount of 0.5 mmole, similar differences in the instantaneous activities of BP-1 and BM-1 catalysts are shown in **Figure 32b** for ethylene/1-hexene copolymerization. However, the change in the activation and deactivation behavior of BM-1 at low initial TIBA concentrations with respect to the same behavior at 1 mmole of TIBA can be attributed to the reasons discussed in the previous sections of this chapter i.e., i) the formation of dormant heterobimetalic species whose concentration should be higher at higher initial TIBA amounts inside the reactor and therefore, causes slow activation of BM-1 catalyst, ii) faster consumption of TIBA leads to earlier and rapid catalyst deactivation.

These results are in good agreement with those discussed in **Chapter 4** where BP-1 and BM-1 catalysts were evaluated in slurry phase reactions. Therefore, it can be suggested that when the particle size of the two different silica supports is kept constant along with their external and internal morphology, the metallocene/MAO catalyst supported on the silica with lower pore volume and pore diameter appear to show higher ethylene (co)-polymerization activities than the one which is supported on the silica with higher pore volume and pore diameter. This behavior can be attributed to the fact that the fragmentation of the growing catalyst/polymer particle with lower pore volume will be faster than the fragmentation of the same catalyst/polymer particle with higher

pore volume because the latter will need more polymer to be formed inside the pores before enough stresses are generated which can fragment the particle. Furthermore, **Figure 31c** and **d** also show that activation rate of the catalyst with lower pore volume is higher than the one with higher pore volume and the same trend was also noticed for full batch catalysts of these same silica (see **Figure 1**).

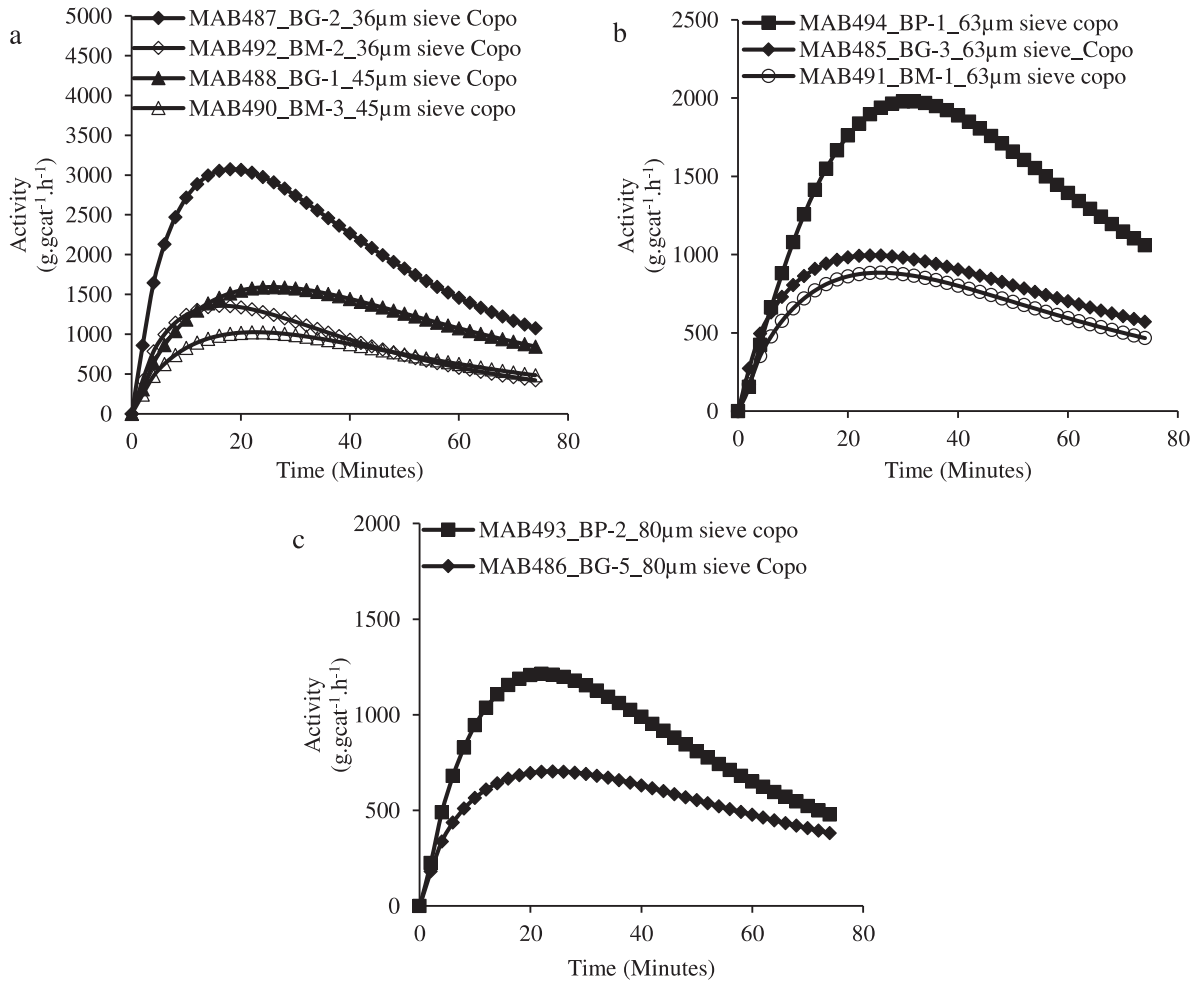

Figure 32. Comparison of the instantaneous activity of the (n-BuCp)$_2$ZrCl$_2$/MAO catalyst supported on the fractions of Grace 948, PQMS3040 and PQMS1732 silica obtained on 36 µm, 45 µm (a), 63 µm (b) and 80 µm (c) mesh sieves in gas phase ethylene/1-hexene copolymerizations at 0.5 mmole initial TIBA amount.

In addition, this trend can be further verified by comparing the activation rate and activity of BP-1 catalyst with that of BG-3 catalyst which was prepared by using 63 µm fraction of Grace 948 silica (see **Figure 31c** and **d**). Homopolymerization activity of BP-1 and BG-3 catalysts look similar with the only difference that BP-1 activates slightly faster than BG-3 but in copolymerization BP-1 catalyst showed (on average) 36 % higher instantaneous activity than that of BG-3 catalyst with once again slightly faster activation. BP-1 catalyst has 24 % lower pore volume, about 50% lower pore diameter and 30% higher surface area than that of BG-3 catalyst which confirms that for a silica supported catalyst with higher surface area, lower pore volume and pore diameter, the activation is faster (or it's activation rate is higher) than the one with lower surface area, higher pore volume and pore diameter, provided that the particle sizes are kept similar. On the other hand, if one compares the activity profiles of BM-1 catalyst and BG-3 catalysts on the basis of surface area, it can be suggested that the effect of catalyst surface area is dominated by the effects of P_d and P_v because these two physical parameters are clearly linked with the fragmentation of the growing catalyst/polymer particles and therefore, the catalyst with lower P_v and lower A_s (i.e., BG-3 catalyst) has higher activity than the catalyst with the higher P_v and higher A_s (i.e., BM-1 catalyst). At lower initial TIBA amount, the observations related to catalyst activity remain the same qualitatively despite the fact that BM-1 catalyst showed significant improvement in its activity as compared to its activity at higher initial TIBA amount inside the reactor (see **Figure 32b**).

With respect to P_d and P_v, the same observations can be made in **Figure 31e** and **Figure 32d** where the instantaneous activity of the catalysts prepared with 80 µm fractions of PQMS 1732 (i.e., BP-2 catalyst) and Grace 948 (i.e., BG-5 catalyst) silica are compared at two different initial TIBA amounts in the reactor. The average difference in the activity of BP-2 and BG-5 catalysts in homopolymerizations is 44%, whereas, in the copolymerizations this difference amounts to 34% (at both TIBA levels) which is in close agreement to the differences in the pore volumes and pore diameters of these two catalysts (compare entry 10 and 11 in **Table 15**) because the surface area of these two catalysts are not very different.

It appears from the previous paragraph that the P_d and P_v of the final catalysts (with the same particle size distribution) influence the ethylene polymerization activity of a silica supported

metallocene in an identical manner and this effect seems to be independent of the silica synthesis procedure.

According to **Figure 31a** and **b**, both the catalysts based on Grace 948 silica (i.e., BG-2 and BG-1) are about 50% more active than their counterparts based on PQMS 3040 silica (i.e., BM-2 and BM-3). At 0.5 mmole initial TIBA amount, numerical differences in the activities of these catalysts remain almost unchanged as can be noticed from **Figure 32a**. Metal loadings and P_d values of these catalysts are very similar (compare entries 3 - 6 in **Table 15**) which indicates that the differences in the catalytic activities are most likely the consequences of the differences in their pore volumes.

The effect of prolonged catalyst impregnation time on the instantaneous activity and productivity of the supported catalysts prepared from 63 µm sieved fractions of PQMS 1732 and PQMS 3040 in gas phase copolymerizations at 0.5 mmole initial TIBA content is shown in **Figure 33** where no significant effect on the shape of the kinetic profiles of BP-1-3h and BP-1-6h catalysts can be noticed. The suffix 3h and 6h indicates 3 h and 6 h of impregnation time during catalyst synthesis, as discussed in the previous **Chapter 4**. However, the activation rate of the BM-1-3h catalyst seems to be improved as compared to BM-1 catalyst (see **Figure 33c**) which can be attributed to better MAO distribution throughout the silica particles. In contrast, core-shell Al distribution was noticed for the same sized catalyst prepared from 63 µm fraction of PQMS 1732 silica (i.e., BP-1-6h catalyst) even after 6 h of impregnation time, as shown in **Chapter 4**. Nevertheless, instantaneous activity of BP-1-3h catalyst when compared with BM-1-3h catalyst still remained higher supporting the results shown in **Figure 31d**. Note that the presence of core-shell distribution further decreases the active P_d and P_v values of the supported catalyst since the uncoated core of the catalyst particles does not participate in the polymerization process. These gas phase instantaneous activity results are in full agreement with those shown in the previous slurry phase **Chapter 4** with the same catalysts implying that the reaction phase cannot impact ethylene polymerization kinetics of these catalysts significantly.

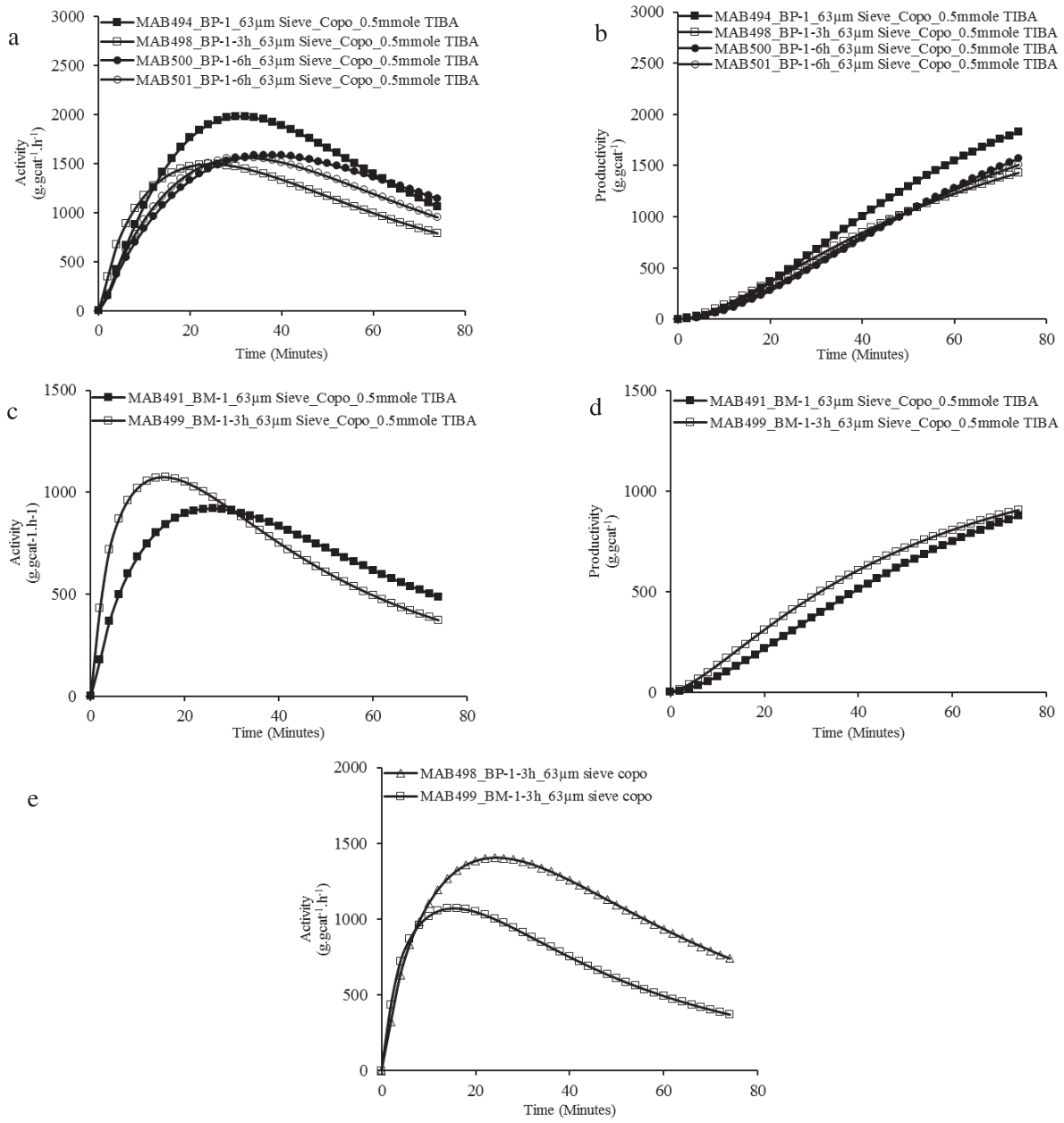

Figure 33. Effect of longer impregnation times during catalyst synthesis on the instantaneous activity and productivity of the catalysts prepared with 63 µm sieved fractions of PQMS 1732 silica and PQMS 3040 silica (a-d). Comparison of the instantaneous activity of BP-1-3h an BM-1-3h catalysts (e). All reactions done at 0.5 mmole TIBA, 3mL 1-hexene, 11 bar ethylene pressure and 80 °C.

Some of the kinetic profiles shown in **Figure 31** are of longer reaction time. As we have seen in the previous section of this chapter that the polymerization time can have an effect on the MWDs of polyethylene produced with silica supported (n-BuCp)$_2$ZrCl$_2$/MAO catalyst, it will be helpful to compare the MWDs of those polyethylenes which were produced at equal reaction time i.e., 75 minutes. **Figure 34** compares the MWDs of some of the selected HDPE and ethylene/1-hexene copolymers produced with the catalysts of same size but different porosities. A general trend is that the polyethylenes produced with low pore volume (i.e., more active) catalysts showed somewhat lower molar mass than the molar mass of the polyethylenes produced with higher pore volume (i.e., less active) catalysts.

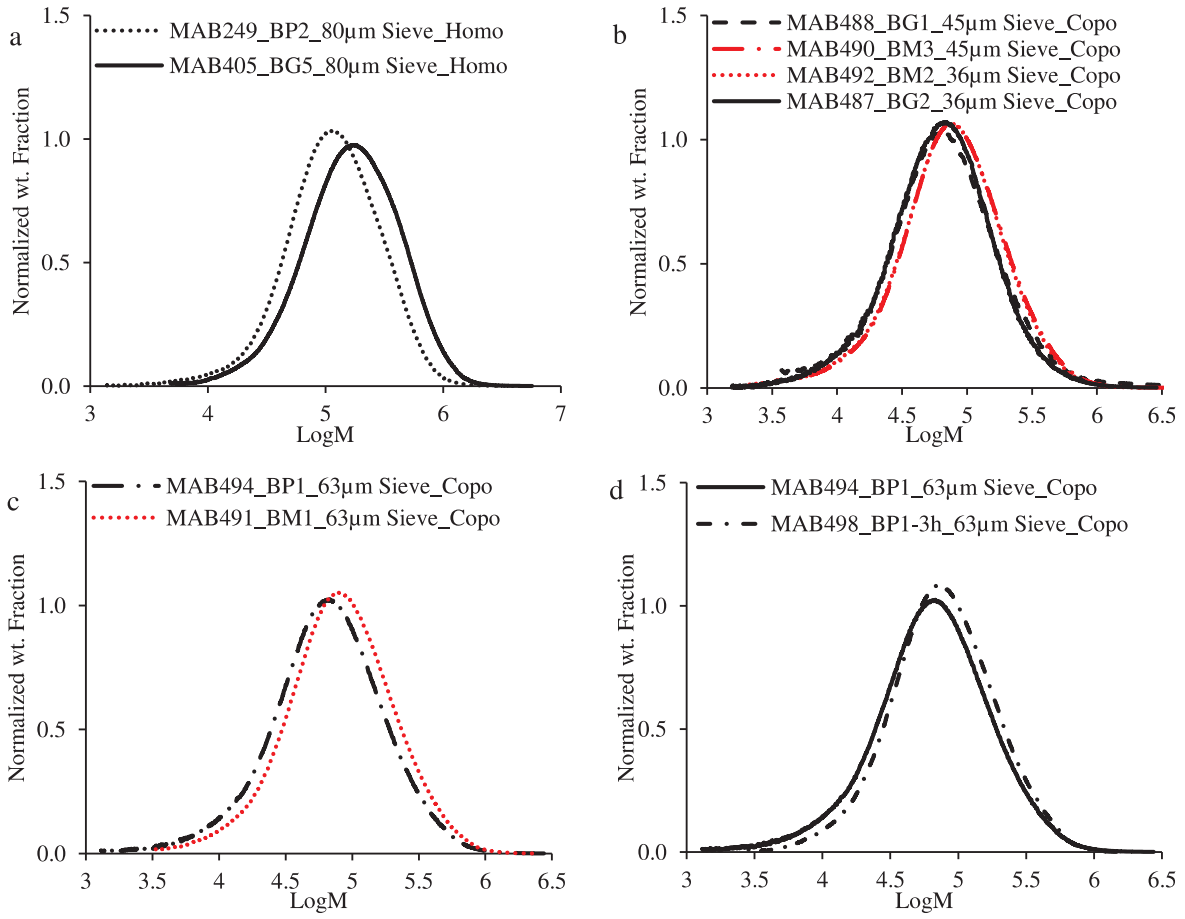

Figure 34. Comparison of the MWDs of HDPE (a) and ethylene/1-hexene copolymers (b-d) produced in gas phase process. All MWDs normalized according to Soares et al.[17]

These results are opposite to those observed in the previous chapter of slurry phase polymerizations with the same catalysts where the observed differences were attributed to the differences in pore diameters of the final supported catalysts. Since these polyethylenes were produced in the gas phase

process and the gas phase process is known for its poor heat transfer capabilities in comparison to slurry process, it appears that the observed differences in MWDs can be attributed to differences in particle temperatures (or heat transfer phenomenon) rather than the differences in pore diameters of the supported catalysts. The more active catalysts may have generated more in-situ hydrogen due to higher local temperatures at the particle level and therefore, the molar masses are observed to be relatively lower than those polyethylenes produced with less active catalysts. Hasegawa et al.,[8] showed that in-situ hydrogen generation with metallocenes increases with increase in reaction temperature. It is worth mentioning here that Kumkaew et al.,[2] showed that by increasing reactor temperature the activity of silica supported $(n\text{-}BuCp)_2ZrCl_2$ catalyst and the molar mass of the copolymers produced thereof in gas phase ethylene/1-hexene copolymerization decreases. Their results indicate that the activation energy of transfer reaction(s) is higher than the activation energy of propagation reaction and therefore, the molar mass of the polyethylene reduces at higher reactor temperature. Therefore, the explanation provided above for the observed differences in MWDs of the polyethylenes seems reasonable. Unlike the results shown in the previous chapter of slurry phase reactions, in the gas phase process it appears difficult to separate the effects of particle temperature from those of the physical properties of the catalyst particle (like P_d, P_v, A_s) on the MWDs of the obtained polyethylene samples.

Table 16 compares the numerical values of M_w and Đ values of the polyethylenes produced with catalysts of similar sizes but different P_d, P_v and A_s. Melting temperatures of the HDPE samples do not seem to be effected by the P_d, P_v and A_s of the supported catalysts, as shown in **Table 16**. However, it appears that during copolymerizations the polymer produced with bigger pore diameter and pore volume shows slightly lower melting temperature which can be attributed to the higher comonomer incorporation. This result is in good agreement with observations reported by Kumkaew et al.,[3] who used the same metallocene supported on SMAO with different pore diameters. Based on this observation, it can be suggested that higher pore volume catalysts show lower activity probably due to the reason that local 1-hexene concentration at the active sites in such catalysts is higher than the local concentration of 1-hexene in low pore volume catalysts which probably changes the behavior of the active sites. It has been shown by Kumkaew et al.,[3] that higher levels of 1-hexene inside the reactor can significantly reduce the catalytic activity of $(n\text{-}BuCp)_2ZrCl_2$/SMAO catalysts. On the other hand, due to low activity of high pore volume catalysts

the composition drift in 1-hexene may have been less pronounced than in the case of low pore volume but high activity catalysts which can also be considered as another reason for more comonomer incorporation by the former catalysts.

Table 16. M_w, Đ, T_m and comonomer content (x_{CEF}) of the homo- and copolymer samples produced in gas phase polymerizations with the same sized fractions of the three different commercial silica. $A_{1\text{-hexene}}$ refers to amounts of 1-hexene added into the reactor at the reaction startup. x_{CEF} refers to comonomer content estimated from CEF.

No.	Sieve opening (μm)	Catalyst Name	Support Name	Sample Name	$A_{1\text{-hexene}}$ (mL)	M_w (g.mol^{-1})	Đ	T_m (°C)	x_{CEF} (mol%)
1	36	BG-2	Grace 948	MAB402	-	230000	2.3	135.7	-
2	36	BM-2	PQMS3040	MAB357	-	190000	2.2	135.7	-
3	45	BG-1	Grace 948	MAB314	-	200000	2.3	135.2	-
4	45	BM-3	PQMS3040	MAB354	-	180000	2.4	135.5	-
5	63	BG-3	Grace 948	MAB326	-	175000	2.4	135.5	-
6	63	BM-1	PQMS3040	MAB356	-	190000	2.3	135.8	-
7	63	BP-1	PQMS1732	MAB260	-	175000	2.6	134.8	-
8	80	BG-5	Grace 948	MAB405	-	245000	2.5	136.0	-
9	80	BP-2	PQMS1732	MAB249	-	165000	2.6	135.2	-
10	36	BG-2	Grace 948	MAB487	3	90000	2.3	123.5	1.2
11	36	BM-2	PQMS 3040	MAB492	3	110000	2.3	120.7	1.9
12	45	BG-1	Grace 948	MAB488	3	90000	2.3	121.5	1.5
13	45	BM-1	PQMS 3040	MAB490	3	115000	2.1	119.3	2.1
14	63	BM-1	PQMS3040	MAB491	3	120000	2.4	121.7	1.6
15	63	BP-1	PQMS1732	MAB494	3	100000	2.7	123.5	1.3
16	80	BG-5	Grace 948	MAB486	3	115000	2.5	117.2	2.4
17	80	BP-2	PQMS1732	MAB493	3	115000	2.5	118.8	1.9

3.5. Conclusions from the Effect of Porosity of the Supported Metallocene/MAO Catalysts on their Activity, Molecular and Physical Properties of Polyethylene

Pore volume, pore diameter and surface area of the used silica supports and the resulting supported metallocene/MAO catalysts are very important physical properties and have a significant effect on their gas phase ethylene homo- and ethylene/1-hexene copolymerization kinetics provided that the particle size (or the particle size distribution) of these catalysts is kept similar. Among the two silica supported $(nBuCp)_2ZrCl_2$/MAO catalyst particles of the same size, internal pore structure, surface area but different pore diameters and pore volumes, higher instantaneous activities have been observed with the one with lower pore diameter and pore volume in ethylene homo- and

ethylene/1-hexene copolymerizations. More importantly, it appears that the catalyst with smaller pore diameter and low pore volume activates rapidly probably due to its earlier (or, in other words, faster) fragmentation than the one with wider pores and higher pore volume. When compared with a catalyst having similar pore volume but higher pore diameter with a different internal morphology (i.e., the Grace 948 based catalysts), the one with smaller pore diameter (i.e., PQMS 1732 based catalysts) showed higher instantaneous activities. Since the surface areas of the catalysts used in this work are not very different it was difficult to see any clear impact of this physical property on the reaction kinetics of the supported catalyst.

Molecular weight distribution (MWD) of the polyethylene samples seems to be more effected by the local temperature of the growing polymer particles and in-situ hydrogen generated. The polyethylene samples produced with low pore diameter and pore volume but more active catalysts showed slightly lower molar masses as compared to those of the samples produced with higher pore diameter and pore volume but less active catalyst particles. This observation has been attributed to the fact that due to poor heat transfer control in gas phase process, the growing particles of more active catalysts should be hotter leading to higher in-situ hydrogen generation and, consequently, lower molar mass of the resulting polyethylene samples.

Comonomer incorporation appears to be slightly higher for the catalyst particles of higher pore volume and pore diameters attributable to different levels of composition drifts during the course of polymerizations, whereas the melting temperatures of the homopolymers do not show any dependence on the pore volume, pore diameter or surface area of the catalyst.

4. References

1. Soares, J B P, McKenna, T F L., Polyolefin Reactors and Processes, In Polyolefin Reaction Engineering, Wiley-VCH Verlag GmbH & Co. KGaA, **2012**.

2. Kumkaew, P, Wanke, S E, Praserthdam, P, Danumah, C, Kaliaguine, S, Gas-phase ethylene polymerisation using zirconocene supported on mesoporous molecular sieves, J. Appl. Polym. Sci., **2003**, 87, 1161-1177.

3. Kumkaew, P, Wu, L, Praserthdam, P, Wanke, S E, Rates and product properties of polyethylene produced by copolymerisation of 1-hexene and ethylene in the gas phase with (n-BuCp)2ZrCl2 on supports with different pore sizes, Polymer., **2003**, 44, 4791-4803.

4. Hammawa, H, Mannan, T M, Lynch, D T, Wanke, S E, Effects of aluminum alkyls on ethylene/1-hexene polymerization with supported metallocene/MAO catalysts in the gas phase, J. Appl. Polym. Sci., **2004**, 92, 3549-3560.

5. Kou, B, McAuley, K B, Hsu, C C, Bacon, D W, Yao, K Z, Mathematical Model and Parameter Estimation for Gas-Phase Ethylene Homopolymerization with Supported Metallocene Catalyst, Ind. Eng. Chem. Res., **2005**, 44, 2428-2442.

6. Kou, B, McAuley, K B, Hsu, C C, Bacon, D W, Yao, K Z, Gas-Phase Ethylene/Hexene Copolymerization with Metallocene Catalyst in a Laboratory-Scale Reactor, Ind. Eng. Chem. Res., **2005**, 44, 2443-2450.

7. Folie, B, Ruff, C J, High-pressure polymerization of ethylene and 1-butene with metallocenes: kinetic mechanism inferred from unsaturation, Polymer Preprints(USA)., **1998**, 39, 201-202.

8. Hasegawa, S, Sone, M, Tanabiki, M, Sato, M, Yano, A, High-temperature ethylene/α-olefin copolymerization with a zirconocene catalyst: Effects of the zirconocene ligand and polymerization conditions on copolymerization behavior, J. Polym. Sci. A Polym. Chem., **2000**, 38, 4641-4648.

9. Margl, P M, Woo, T K, Ziegler, T, Potential Catalyst Deactivation Reaction in Homogeneous Ziegler-Natta Polymerization of Olefins: Formation of an Allyl Intermediate, Organometallics., **1998**, 17, 4997-5002.

10. Wasserman, E, Hsi, E, Young, W T, Studies on dihydrogen generation by a bridged metallocene polyethylene catalyst, Polymer Preprints(USA)., **1998**, 39, 425-426.

11. Floyd, S, Heiskanen, T, Taylor, T W, Mann, G E, Ray, W H, Polymerization of olefins through heterogeneous catalysis. VI. Effect of particle heat and mass transfer on polymerization behavior and polymer properties, J. Appl. Polym. Sci., **1987**, 33, 1021-1065.

12. Floyd, S, Choi, K Y, Taylor, T W, Ray, W H, Polymerization of olefins through heterogeneous catalysis. III. Polymer particle modelling with an analysis of intraparticle heat and mass transfer effects, J. Appl. Polym. Sci., **1986**, 32, 2935-2960.

13. He, Y, Qiu, X, Klosin, J, Cong, R, Roof, G R, Redwine, D, Terminal and Internal Unsaturations in Poly(ethylene-co-1-octene), Macromolecules., **2014**, 47, 3782-3790.

14. Busico, V, Cipullo, R, Friederichs, N, Linssen, H, Segre, A, Van Axel Castelli, V, van der Velden, G, H NMR Analysis of Chain Unsaturations in Ethene/1-Octene Copolymers Prepared with Metallocene Catalysts at High Temperature, Macromolecules., **2005**, 38, 6988-6996.

15. Frederick J.Karol, Sun-Chueh Kao, Eric P.Wasserman, Zhengtian Yu., Features of cyclopentadienyl metal catalysts for ethylene copolymerization in gas and liquid phase, In Metalorganic Catalysts for Synthesis and Polymerization, Eds. Walter Kaminsky., Springer-Verlag Berlin Heidelberg, Heidelberg, **1999**.

16. Masino, A. P.; Murray, R. E.; Yang, Q.; Secora, S. J.; Jayaratne, K. C.; Beaulieu, W. B.; Ding, E.; Glass, G. L.; Solenberger, A. L.; Cymbaluk, T. H. Dual Metallocene Catalyst Systems for Decreasing Melt Index and Increasing Polymer Production Rates. US2013/0079477A1, **2013**.

17. Soares, J B P, McKenna, T F L., Polyolefin Microstructural Characterization, In Polyolefin Reaction Engineering, Wiley-VCH Verlag GmbH & Co. KGaA, **2012**.

APPENDIX 1

Chapter 5

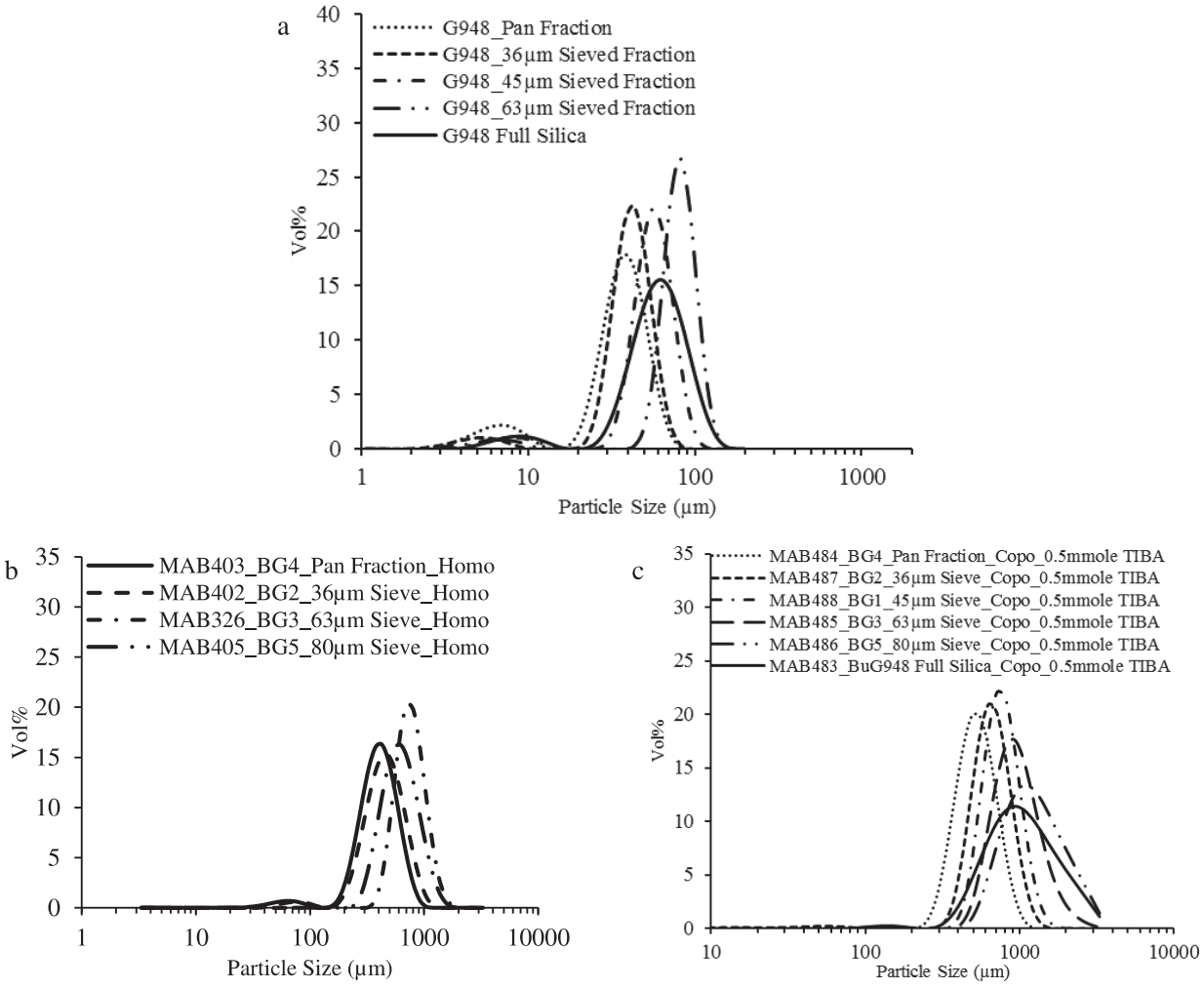

Figure S1. Effect of catalyst PSD and polymerization protocol on the polymer PSD.

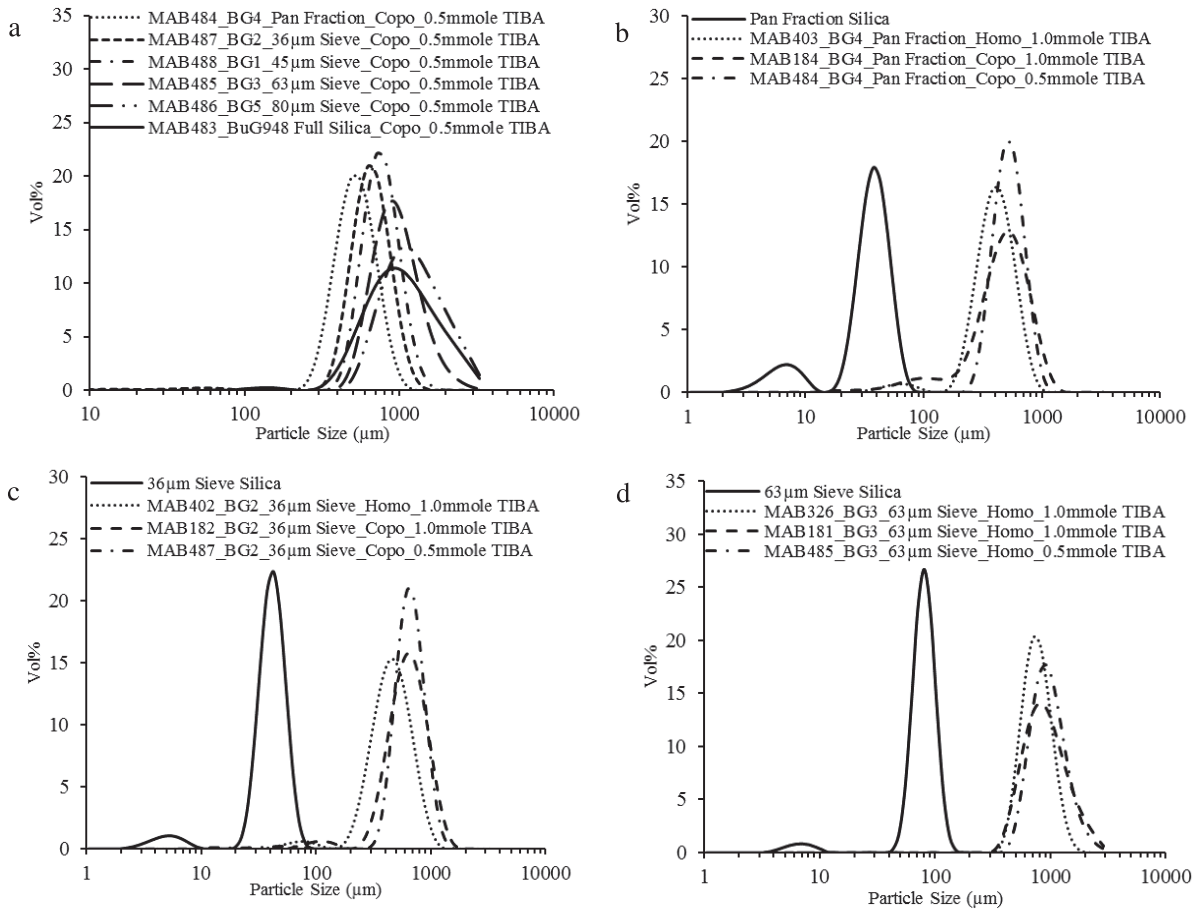

Figure S2. Comparison of copolymer PSD with the catalyst and HDPE PSD. Grace 948 silica used as catalyst support.

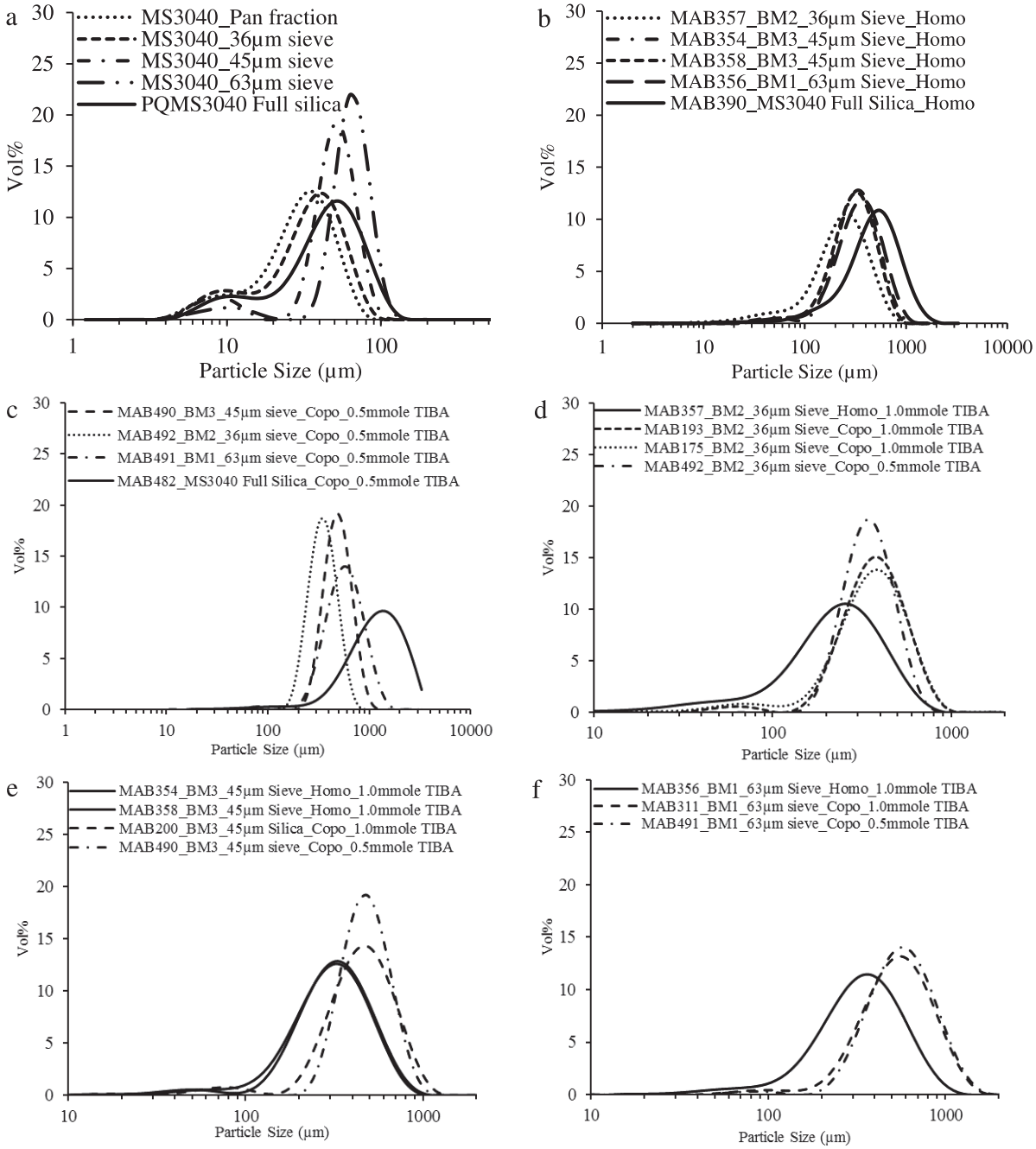

Figure S3. Comparison of the PSD of (a) full silica and the sieved fractions of PQMS 3040 silica, (b) HDPE samples, (c) copolymers produced with 0.5 mmole TIBA content and (d-f) HDPE and copolymer samples produced with the same catalyst.

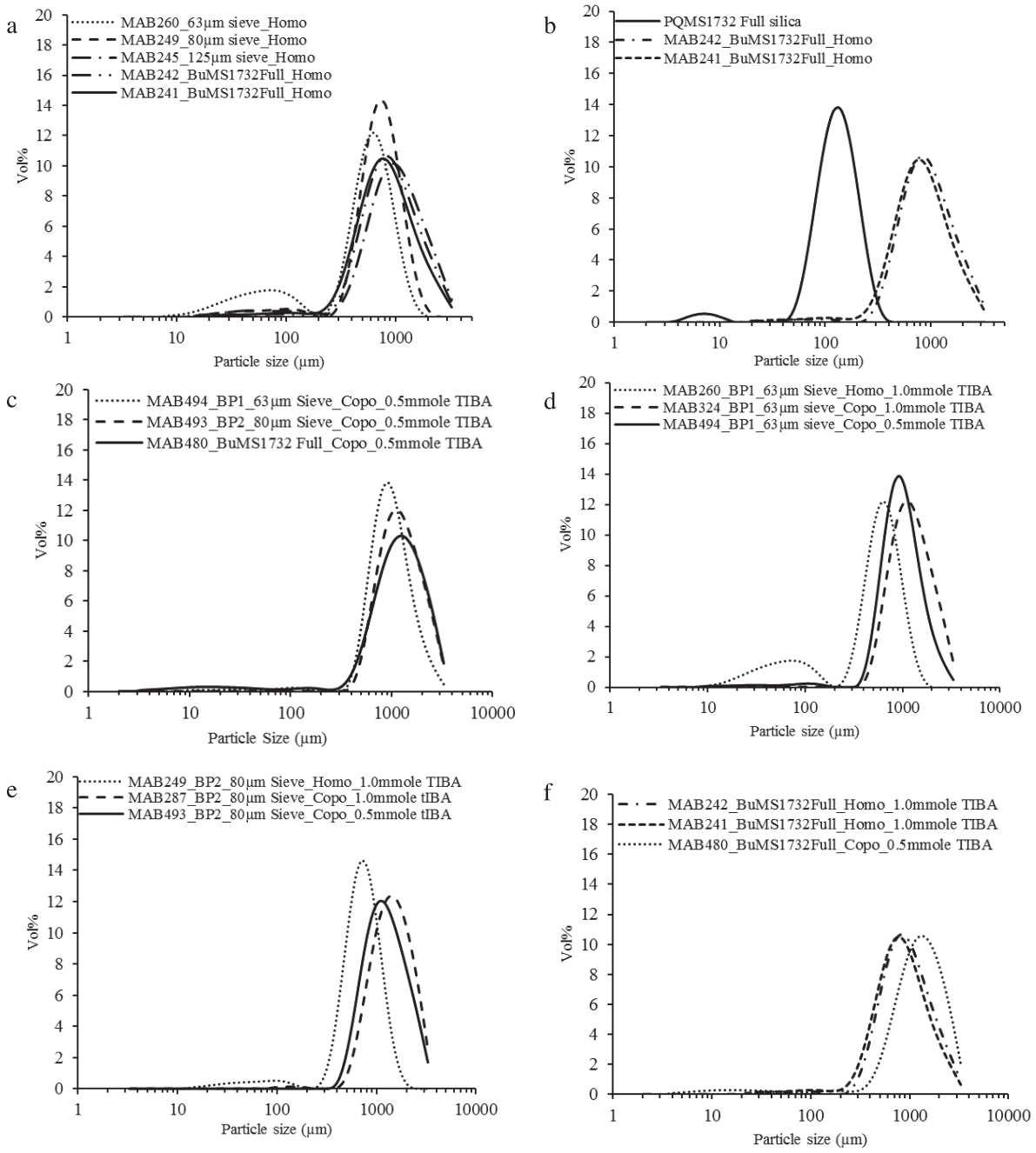

Figure S4. Comparison of the PSD of HDPE and copolymers produced with different sized catalysts of PQMS1732 silica.

Conclusions and Perspectives

The current PhD dissertation shows an experimental investigation focused on analyzing the effects of physical properties of silica supported metallocenes on their ethylene polymerization kinetics in slurry and gas phase processes. Keeping the reaction kinetics aside, the impact of physical properties of silica supported metallocenes on the molecular and physical properties of the polyethylene grades is also analyzed. In addition, finding the reason why particles of silica supported metallocenes with different sizes, pore diameters, pore volumes, surface areas etc., behave differently in the same reactor under identical conditions is another objective of the present work.

For such a study where one aims to study role of physical properties of the silica supports on the catalytic performance of the final supported metallocenes, the surface chemistry needs to be fixed initially as it has a significant effect on the performance of these catalysts in ethylene polymerization. It was desired to prepare catalysts of reasonable activities since the mass transfer effects are assumed to be easily seen at high catalytic activities (nevertheless, low activity catalysts are not immune to such effects). Literature review provided a mixed opinion about the impact of silica dehydroxylation temperature on the catalytic activities of supported metallocenes as for some single-site catalysts the activity was found to increase with decreasing silanol concentration, whereas for others the opposite was found to be true. Therefore, a detailed study encompassing the mostly used silica dehydroxylation temperature range of 200 °C to 600 °C was conducted by using Grace 948 silica as a model support. Methylalumnioxane (MAO) was first grafted on these silica samples dehydroxylated at three different temperatures followed by the fixation of $(n\text{-BuCp})_2ZrCl_2$ zirconocene at 80 °C. Evaluation of these catalysts in slurry and gas phase ethylene homopolymerizations clearly showed that, for this metallocene/MAO catalytic system, reasonable activities can be obtained when silica is dehydroxylated at 600 °C. Solid-state NMR studies of silica impregnated with MAO (SMAO) samples allowed us to show experimentally the generation of Si-Me bonds for the silica dehydroxylated above 400 °C which proved that strained siloxane (-Si-O-Si-) bonds are only produced on silica surface when it is thermally treated above 200 °C. Furthermore, in the same study it was observed that TIBA is a better scavenger than TEA since the activities in slurry phase polymerizaitons employing TIBA as scavenger were higher than those conducted with TEA as scavenger. Based on the results of this study, it was decided to proceed with 600 °C as the standard silica dehydroxylation temperature in this study.

In addition to silica dehydroxylation temperature, the method used to support metallocene and MAO on silica can impact the catalytic activity in ethylene polymerization. Impregnating the silica with MAO prior to metallocene fixation is a two-step method with washings in between these steps and, consequently, it does not seem to be a method of choice for making numerous catalysts. In addition, the literature also suggest that the activity of silica supported metallocenes produced with this method is lower than the activity of the supported metallocenes prepared by mixing the metallocene and MAO together prior to the addition of this catalyst/co-catalyst solution on to the silica support. This second method (termed hereafter as activated catalyst method) also reduces the time and amount of solvents used. Therefore, it was decided to prepare all the (n-BuCp)$_2$ZrCl$_2$/MAO silica supported catalysts with activated catalyst method. Silica particles of different sizes were obtained by sieving full batches of three commercial silica which were then dehydroxylated at 600 °C. Sieving the full batch of silica provides catalysts of different particle sizes with constant pore volume, pore diameter and surface area.

After preparing silica supported (n-BuCp)$_2$ZrCl$_2$/MAO catalysts of varying sizes but similar Al/Zr molar ratio, slurry phase ethylene polymerizations were conducted at different ethylene pressures to study the impact of catalyst particle size on its instantaneous activity and the final polymer properties. These experiments were hampered by reactor fouling due to catalyst leaching and soon it was discovered that polymerization protocol was to be blamed for this. Pro-longed contact between TIBA and supported metallocene/MAO catalysts caused catalyst leaching. Therefore, a detailed study was conducted in order to minimize the contact time between TIBA and the supported metallocenes so that the problem of catalyst leaching can be avoided because one cannot assure purely heterogeneous catalysis if the catalyst desorbs from the support. In this study, other scavengers (i.e., TEA and ToA) were also used at different concentrations. The results of this study indicated that injecting the catalyst into the reactor containing diluent plus scavenger at the desired polymerization temperature can help to avoid catalyst leaching which is probably due to the reduced contact time between the scavenger and the supported metallocene.

Once the protocol for slurry phase polymerization was fixed, experiments conducted with silica supported (n-BuCp)$_2$ZrCl$_2$/MAO catalysts of different sizes showed that the smaller particles have significantly higher activities than their bigger counterparts under identical conditions. This dependence of catalytic activity on the particle size was confirmed at different ethylene pressures

in homo- and copolymerizations with 1-hexene. However, the molar mass distribution (MWD) of the polymers remained insensitive to the catalyst particle size which was expected to be different depending upon the catalyst particle size because if (co)-monomer(s) diffusion resistance is responsible for different polymerization rates of big and small catalyst particles then MWDs of the resulting polymers should also be different. On the other hand, the molar mass dispersities of the polymers were also very similar which showed that the active sites formed on the supported catalysts were also independent of the particle size.

In order to investigate this further, slurry phase ethylene homopolymerizations were conducted with supported $(n\text{-BuCp})_2ZrCl_2$/MAO catalyst by varying monomer pressure from 3 to 10 bar. The MWDs of the obtained polyethylene samples showed no dependence on monomer pressure which allowed us to conclude that chain transfer to monomer is the dominant chain termination mechanism with this catalyst. Other physical properties like melting temperature and crystallinity of the polymer samples also remained unchanged by the changes in catalyst particle size. SEM-EDX analysis of the catalyst particles of different sizes and different silica types showed even distribution of $(n\text{-BuCp})_2ZrCl_2$/MAO throughout the particles of Grace 948 silica and core-shell distribution in the case of PQMS 3040 and PQMS 1732 silica. Since this core-shell distribution was present in almost all particle of PQ silicas, it cannot be considered as the absolute reason for the differences in catalytic activities of big and small catalyst particles. In order to mitigate this core-shell distribution problem, few more catalysts of different sizes were prepared with PQMS 1732 and PQMS 3040 silica by increasing the impregnation time from 3 to 6 hours during catalyst synthesis. By SEM-EDX analysis of these catalysts, it was concluded that for PQMS 3040 silica based catalysts core-shell distribution of $(n\text{-BuCp})_2ZrCl_2$/MAO can be avoided by increasing the impregnation time upto 3 hours, whereas for the other silica it was not possible to achieve uniform distribution of active species even after 6 hours of impregnation time at 50 °C. These observations were attributed to the differences in the pore diameters of these silica since PQMS 3040 silica has a pore volume of 29 nm while that of PQMS 1732 is only 10 nm.

rac-ethylenebis(4,5,6,7-tetrahydro-1-indenyl)zirconium dichloride (THI) was then supported on full batch of Grace 948 silica as well as on 36 µm and 80 µm sieved fractions of the same silica since no core-shell distribution of $(n\text{-BuCp})_2ZrCl_2$/MAO catalyst was observed for this silica. Unfortunately, this catalyst showed significant leaching and, consequently, reactor fouling even

with the polymerization protocol which was shown to cause no leaching for silica supported (n-BuCp)$_2$ZrCl$_2$/MAO catalysts. Similar type of catalyst leaching was observed when rac-Et(Ind)$_2$ZrCl$_2$ supported on SMAO was used in ethylene homopolymerizations with the same polymerization protocol under identical conditions. This observation indicates that the interaction of indenyl based metallocenes with TIBA is different from that of cyclopentadienyl based metallocenes. Due to catalyst leaching problems, these catalysts were further investigated in gas phase polymerizaitons.

Gas phase ethylene homo- and ethylene/1-hexene copolymerizations of (n-BuCp)$_2$ZrCl$_2$/MAO catalysts of different particle sizes confirmed the trends observed in the slurry phase polymerizations i.e., the smaller the catalyst particle the higher the activity but the MWD remains independent of the catalyst particle size. Other polymer properties also showed no significant dependence on catalyst particle size. THI/MAO catalysts were then evaluated at two different pressures and the obtained polyethylenes showed clear difference in their molar masses which indicated that this catalyst is not sensitive to chain transfer to monomer and probably β-H elimination is the main chain termination mechanism. Afterwards, short and long time ethylene/1-hexene copolymerizations with THI/MAO catalysts of two different particle sizes (i.e., 36 µm and 80 µm) conducted at 8 and 11 bar ethylene pressure clearly showed that the MWD of the copolymers depends upon the catalyst particle size during initial 30 minutes of the reaction time after which it is difficult to see any clear differences in the MWDs of the polymers. This observation was attributed to the fact that the mass transfer resistance is high during the initial stages of heterogeneous olefin polymerization and as the polymerization proceeds the resistance to monomer transport decays. Therefore, the bigger catalyst particles (which have higher mass transfer resistance) should produce polyethylene of lower molar mass and broader distribution as compared to that produced with smaller catalyst particles (which have lower mass transfer resistance). The MWDs of the polyethylene samples (and dispersity of the MWDs) produced with THI/MAO catalysts of different sizes showed exactly similar dependence on catalyst particle size i.e., polyethylene produced with THI/80 catalyst particles showed lower molar mass (and broader MWDs) as compared to that of the polyethylene produced with THI/36 catalyst particles and as the polymerization time exceeded 30 minutes the molar mass of polyethylene became independent of the catalyst particle size. This results allowed us to conclude that the mass transfer resistance exists but only during the initial stages of ethylene polymerization. Comonomer content of the bigger

polymer particles (which came from bigger catalyst particles) was found to be higher than that of the smaller polymer particles (which came from bigger catalyst particles) which led to lower crystallinity of bigger polymer particles as compared to their smaller analogs.

Using the same polymerization times and conditions, (n-BuCp)$_2$ZrCl$_2$/MAO supported on 36 µm and 80 µm sieved fractions of Grace 948 silica was evaluated in gas phase ethylene/1-hexene copolymerizations. MWDs of the obtained polyethylene samples decreased with increasing polymerization time which is completely opposite to the results obtained with THI/MAO silica supported catalysts of the same size (i.e., in the case of THI/MAO catalysts of different sizes the MWDs of the obtained polymer samples increased with increasing reaction time). This observation was attributed to the in-situ hydrogen generation during the course of polymerization as observed by other authors also who used other metallocene/MAO catalysts in ethylene polymerization. Nevertheless, clear differences in the MWDs of the copolymers produced with small and big (n-BuCp)$_2$ZrCl$_2$/MAO catalyst particles were visible up to first 30 minutes of reaction time which vanished after 75 minutes of polymerization time i.e., until the first 30 minutes of polymerization the polymer produced with bigger catalyst particles showed higher molar mass as compared to that of the polymer produced with smaller catalysts particle, whereas after 75 minutes of the reaction time it was hard to distinguish between their MWDs. Molar mass dispersities were also found to be higher for the polyethylenes produced with 80 µm catalyst particles as compared to those of the samples produced with 36 µm catalyst particles during the first 30 minutes of reaction time which converged after 75 minutes of polymerization. The comonomer content of the polymers showed dependence on the catalyst particle size which was similar to that shown by the polymers produced with THI/MAO catalysts of different sizes.

These results once again confirmed that the mass transfer resistance was significant during the first 30 to 40 minutes of polymerization time after which the concentration gradients inside the growing polymer particles probably level out and therefore, the MWDs of the polyethylenes produced at longer times does not show any significant differences. Furthermore, smaller silica supported (n-BuCp)$_2$ZrCl$_2$/MAO particles may have generated higher concentration of in-situ hydrogen during first 30 minutes of reaction time due to their higher activities as compared to their bigger counter parts which led to lower molar mass of the polyethylenes produced with smaller catalyst particles in comparison with the molar mass of the polyethylene produced with bigger catalyst particles.

After a certain polymerization time, in-situ hydrogen generation reaches the equilibrium value for both the catalysts of different sizes which causes the final MWDs of the polymers to overlap each other.

It is of high interest to use the same strategy in slurry phase ethylene polymerizations where the mass transfer resistance is significantly higher as compared to that in gas phase reactions and study the impact of catalyst particle size and polymerization time on the evolution of polyethylene MWD. Furthermore, higher comonomer contents used during polymerization will provide further insights into the mass transfer phenomenon during early stages of heterogeneous olefin polymerization.

Other interesting results are disseminated in this work by comparing silica supported (n-BuCp)$_2$ZrCl$_2$/MAO catalyst particles of the same size but different pore diameter, pore volume and surface area. With respect to surface area, no clear conclusion was made probably due to different synthesis methods of the silica supports used. However, low pore diameter and low pore volume seem to help in faster activation of the silica supported (n-BuCp)$_2$ZrCl$_2$/MAO as compared to the activation (n-BuCp)$_2$ZrCl$_2$/MAO supported on silica particles of bigger pores. This result was attributed to faster fragmentation of the low pore volume catalysts as compared to the higher pore volume catalysts. Furthermore, the polyethylene samples produced by using low pore diameter catalysts showed slightly higher molar mass then those produced with the bigger pore diameter catalysts which was attributed to the phenomenon of extrusion polymerization and pore confinement effect of the former catalysts.

It was also noticed in this work that the catalysts supported on PQMS 1732 silica showed higher deactivation rates during slurry phase ethylene homopolymerizaitons which was reduced by the addition of 1-hexene into the reaction milieu i.e., in copolymerizaitons under identical conditions. For the other two supports this behavior was not noticed. Detailed investigations should be carried out by using PQMS 1732 silica support in order to further investigate the higher deactivation rates of the catalysts supported on it since this silica has a uniform pore structure and nearly perfect spherical geometry which gives polyethylene of very good morphology.

Gas phase stop flow reactions of very short time with silica supported catalysts of different sizes can further shed light on particle overheating during initial instants of polymerization which might be helpful in explaining the differences observed in the catalytic activities of small and big particles.